

BIOLOGICAL MONITORING OF OXYGEN AND NITRIC OXIDE: THE DEVELOPMENT AND CHARACTERISATION OF REAL-TIME MICROELECTROCHEMICAL SENSORS

A thesis submitted by

Andrea. M. Wynne B.Sc. (Hons.)

to the

National University of Ireland, Maynooth

For the degree of Doctor of Philosophy



NUI MAYNOOTH

Ollscoil na hÉireann Má Nuad

Based on the research carried out in the
Department of Chemistry, Faculty of Science and Engineering,

National University of Ireland, Maynooth

under the supervision and direction of

Prof. John P. Lowry and Dr. Niall J. Finnerty

February 2014

Contents

1. Introduction

1.1	The Brain	2
1.2	Micro-electrochemical O ₂ Sensors.....	3
1.2.1	Carbon Paste Electrodes (CPEs).....	4
1.2.2	Real-Time Clinical Monitoring of O ₂	5
1.3	Micro-electrochemical Nitric Oxide (NO) Sensors	7
1.4	Biosynthesis of NO	9
1.5	Neurovascular coupling.....	10
1.6	eNOS, blood flow and O ₂	12
1.7	NMDA receptor.....	13
1.8	Overview of thesis	15
1.9	References	17

2. Theory

2.1	Introduction.....	25
2.2	Mass Transport	27
2.2.1	Migration	27
2.2.2	Diffusion.....	27
2.2.3	Convection	31
2.3	Cyclic Voltammetry (CV).....	31
2.4	Constant Potential Amperometry (CPA).....	34
2.5	Measurement of dissolved O ₂	35
2.6	Polymerisation of Methyl methacrylate (MMA)	36
2.7	Electropolymerisation of <i>o</i> -Phenylenediamine (<i>o</i> -PD)	38
2.8	Ascorbic acid (AA)	40
2.9	Data Analysis	41
2.9.1	Linear Regression	41
2.9.2	Statistical Analysis	41
2.10	References	43

3. Experimental

3.1	Introduction.....	46
3.2	Computer Based Instrumentation and Computer Programs	47
3.2.1	The Computer	48
3.2.1.1	<i>In-Vitro</i> data:	48
3.2.1.2	<i>In-Vivo</i> data:	48
3.2.2	The Interface	49
3.2.3	The Potentiostat.....	49
3.2.4	Movement Meter	50
3.3	Chemicals and Solutions.....	51
3.3.1	Chemicals.....	51
3.3.1.1	<i>In-Vitro</i> Chemicals	51
3.3.1.2	<i>In-Vivo</i> Chemicals.....	52
3.3.2	Solutions.....	53
3.3.2.1	<i>In-Vitro</i> Solutions	53
3.3.2.2	Interferent Solutions.....	55
3.3.2.3	<i>In-Vivo</i> Solutions.....	56
3.4	Electrode Preparation.....	58
3.4.1	Carbon Paste Electrode (CPE)	58
3.4.2	Methyl Methacrylate Modified CPE (MMCPE)	59
3.4.3	Styrene Modified CPE (SMCPE)	59
3.4.4	Platinum (Pt) Working Electrodes	60
3.4.5	Nitric Oxide (NO) Sensors.....	61
3.4.5.1	The Nafion [®] Pre-Coat Application	61
3.4.5.2	Application of o-PD.....	62
3.4.5.3	Type 1 NO Sensor.....	62
3.4.5.4	Type 2 NO Sensor.....	63
3.4.5.5	Type 3 NO Sensor.....	64
3.5	Electrode Modification	65
3.5.1	Monomer Modified CPEs (Sty and MMA).....	65
3.5.2	PPD and Nafion [®] Modified NO Sensors	65
3.6	Electrode Treatments	66
3.6.1	BSA Treated Sensors	66

3.6.2	PEA Treated Sensors	67
3.6.3	Triton® X-100 Treated Sensors	67
3.6.4	BT Treated Sensors	67
3.6.5	Long-Term Stability Studies	67
3.6.6	Post-Implanted Sensors	67
3.7	Electrochemical Experiments	68
3.7.1	Electrochemical Cell Set-Up	68
3.7.2	Experimental Techniques	69
3.7.2.1	AA Calibrations	69
3.7.2.2	Oxygen Calibrations	70
3.7.2.3	NO Calibrations	71
3.7.2.4	Post-Implanted Calibrations	71
3.8	<i>In-Vivo</i> Experiments	72
3.8.1	Subjects	72
3.8.2	Surgical Protocol	73
3.8.3	<i>In-Vivo</i> Reference and Auxiliary Electrodes	75
3.8.4	Physiological Stimuli	76
3.8.4.1	Tail Pinch	76
3.8.4.2	Restraint Test	77
3.8.5	<i>In-Vivo</i> Injections	77
3.8.5.1	Intraperitoneal Injection (i.p)	77
3.8.5.2	Subcutaneous Injection (s.c)	77
3.9	Scanning Electron Microscopy (SEM)	78
3.10	NO synthesis and UV Spectroscopy	78
3.11	Additional equipment	80
3.12	References	82

4. In-Vitro Development of Carbon Based Sensors Suitable for the Detection of Oxygen in the Clinical Environment

4.1	Introduction	84
4.2	Experimental	87
4.3	Results and Discussion	88
4.3.1	Detection of O ₂ utilising CPEs	88
4.3.1.1	Biocompatibility studies	90

4.3.1.1.1 BSA-treated CPEs	91
4.3.1.1.2 PEA-treated CPEs.....	92
4.3.1.1.3 BT treated CPEs.....	93
4.3.1.1.4 BT treated CPEs (28 days)	95
4.3.1.1.5 Triton [®] X-100 (10%) treated CPEs	96
4.3.1.1.6 SEM images	97
4.3.2 Sty modified CPE (SMCPE).....	98
4.3.2.1 Treatments on SMCPE (ON) with Triton [®] X (10%).....	100
4.3.2.2 Optimisation of SMCPE surface.....	102
4.3.2.3 UV light on SMCPE	104
4.3.2.4 Optimum potential profile of SMCPE.....	107
4.3.2.5 CV of SMCPE.....	108
4.3.2.6 Validation of the final SMCPE design.....	108
4.3.3 MMA modified CPE (MMCPE)	110
4.3.3.1 Treatments on MMCPE (ON) with Triton [®] X (10%).....	112
4.3.3.2 Optimisation of MMCPE surface	113
4.3.3.3 UV light on MMCPE.....	115
4.3.3.4 Optimum potential profile of MMCPE	117
4.3.3.5 CV of MMCPE	118
4.3.3.6 Validation of the final MMCPE design	118
4.3.4 Oil free carbon based electrodes.....	120
4.3.4.1 Methyl methacrylate graphite powder electrode (MMGPE).....	120
4.3.4.2 Styrene graphite powder electrode (SMGPE).....	121
4.3.5 Biocompatibility studies	122
4.3.5.1 SMCPE-BSA (ON)	123
4.3.5.2 SMCPE-PEA (ON)	124
4.3.5.3 SMCPE-BT (ON).....	125
4.3.5.4 SMCPE-BT (3 days)	126
4.3.5.5 SMCPE-BT (28 days)	127
4.3.5.6 MMCPE-BSA (ON).....	128
4.3.5.7 MMCPE-PEA (ON).....	129
4.3.5.8 MMCPE-BT (ON)	130
4.3.5.9 MMCPE-BT (3 days).....	131
4.3.5.10 MMCPE-BT (28 days).....	132
4.3.6 Post <i>In-Vivo</i> Comparison.....	133

4.3.6.1 SMCPE Comparison	133
4.3.6.2 MMCPE Comparison.....	137
4.3.7 Long term stability studies	140
4.3.7.1 Stored at Room temperature (RT)	140
4.3.7.1.1 SMCPEs	141
4.3.7.1.2 MMCPEs.....	142
4.3.7.2 Stored in the fridge (4 °C).....	143
4.3.7.2.1 SMCPEs	144
4.3.7.2.2 MMCPEs.....	145
4.3.7.3 Stored in the freezer (-20 °C).....	146
4.3.7.3.1 SMCPEs	146
4.3.7.3.2 MMCPEs.....	147
4.3.8 Interference studies.....	148
4.3.9 pH Calibrations	149
4.3.9.1 SMCPE Repeat Calibration Experiments	150
4.3.9.2 MMCPE Repeat Calibration Experiments.....	151
4.3.10 Temperature studies	153
4.3.10.1 SMCPEs.....	153
4.3.10.2 MMCPEs	154
4.4 Conclusion	155
4.5 References.....	164

5. *In-Vivo* Characterisation of Sensors for the Neurochemical Detection of Oxygen



5.1 Introduction.....	168
5.2 Experimental	170
5.3 Results and Discussion.....	171
5.3.1 Hypoxia	171
5.3.1.1 MMCPE	172
5.3.1.2 SMCPE.....	173
5.3.1.3 Comparison.....	174
5.3.2 Hyperoxia.....	175

5.3.2.1	MMCPE	175
5.3.2.2	SMCPE.....	176
5.3.2.3	Comparison.....	178
5.3.3	Neuronal Activation.....	178
5.3.3.1	Restraint.....	179
5.3.3.1.1	MMCPE	179
5.3.3.1.2	SMCPE.....	181
5.3.3.1.3	Comparison.....	182
5.3.3.2	Tail Pinch	183
5.3.3.2.1	MMCPE	183
5.3.3.2.2	SMCPE.....	184
5.3.3.2.3	Comparison.....	185
5.3.4	Saline Administration	186
5.3.4.1	MMCPE	186
5.3.4.2	SMCPE.....	187
5.3.4.3	Comparison.....	188
5.3.5	Effect of Anaesthesia.....	189
5.3.5.1	MMCPE	189
5.3.5.2	SMCPE.....	191
5.3.5.3	Comparison.....	192
5.3.6	Acetazolamide (Diamox) Administration	193
5.3.6.1	MMCPEs.....	194
5.3.6.1.1	Diamox (DMSO) Administration.....	194
5.3.6.1.2	Diamox (Saline) Administration	196
5.3.6.1.3	DMSO (Saline) Administration.....	197
5.3.6.2	SMCPEs	199
5.3.6.2.1	Diamox (DMSO) Administration.....	199
5.3.6.2.2	Diamox (Saline) Administration	201
5.3.6.2.3	DMSO (Saline) Administration.....	202
5.3.6.2.4	Comparison.....	203
5.3.7	Stability of O ₂ sensors	204
5.3.7.1	MMCPE	205
5.3.7.2	SMCPE.....	206
5.4	Conclusion	207
5.5	References.....	210

6. *In-Vitro Characterisation of Nitric Oxide Sensors*

6.1	Introduction.....	214
6.2	Experimental	215
6.3	Results and Discussion.....	216
6.3.1	Bare Pt electrodes vs. NO sensors.....	216
6.3.1.1	AA detection at Pt Sensors	217
6.3.1.2	NO detection at Pt Sensors	218
6.3.2	Type 1 NO Sensor	219
6.3.2.1	NO detection at Type 1 NO Sensors	220
6.3.3	Type 2 NO sensor	223
6.3.3.1	NO detection at Type 2 NO sensors	223
6.3.3.2	AA detection at Type 2 NO sensors	224
6.3.4	Type 3 NO sensor	225
6.3.4.1	NO detection at Type 3 NO Sensors	226
6.3.4.2	AA detection at Type 3 NO Sensors.....	227
6.3.5	Comparison of Sensors	228
6.3.5.1	NO Detection	228
6.3.6	NO cylinder vs. NO synthesis.....	229
6.3.6.1	NO Synthesis.....	229
6.3.7	Comparison of NO Synthesis and NO Cylinder.....	230
6.3.7.1	Type 2 NO sensor (synthesis vs. cylinder).....	231
6.3.7.2	Type 3 NO sensor (synthesis vs. cylinder).....	232
6.3.8	Selectivity studies	233
6.3.8.1	Long term stability investigations on PPD layer	233
6.3.8.1.1	Pt (PPD) Sensor	234
6.3.8.2	Long term stability studies on different types of NO sensors.....	242
6.3.9	Stability of the NO sensitivity of Type 2 NO sensors over time	258
6.3.10	Stability of the NO sensitivity of Type 3 NO sensors over time	259
6.3.11	Interference studies Type 2 and Type 3 NO Sensor.....	261
6.3.12	Biocompatibility	274
6.3.13	Biocompatibility	281
6.3.14	Temperature studies on Type 2 Sensor and Type 3 NO Sensor	286
6.3.15	Post Calibrations <i>in-vivo</i> Type 2 NO Sensor.....	287
6.3.16	Post Calibrations <i>in-vivo</i> Type 3 NO Sensor.....	290

6.4	Conclusion	293
6.5	References.....	301

7. *In-Vivo Characterisation of Sensors for the Neurochemical Detection of Nitric Oxide*

7.1	Introduction.....	306
7.2	Experimental	307
7.3	Results and Discussion.....	308
7.3.1	Saline Administration	308
7.3.1.1	Type 2 NO sensor	308
7.3.1.2	Type 3 NO sensor	310
7.3.2	L-NAME Administration	311
7.3.2.1	Type 2 NO Sensor.....	312
7.3.2.2	Type 3 NO Sensor.....	313
7.3.3	L-Arginine Administration	314
7.3.3.1	Type 2 NO Sensor.....	315
7.3.3.2	Type 3 NO Sensor.....	317
7.3.4	Sodium Ascorbate Administration	318
7.3.4.1	Type 2 NO Sensor.....	319
7.3.4.2	Type 3 NO Sensor.....	321
7.3.5	Stability of the NO sensors	323
7.3.5.1	Type 2 NO sensor	324
7.3.5.2	Type 3 NO Sensor.....	325
7.4	Conclusion	327
7.5	References.....	330

8. *In-Vivo Monitoring of Oxygen and Nitric Oxide Simultaneously*

8.1	Introduction.....	334
8.2	Experimental	337
8.3	Results and Discussion.....	338

8.3.1	Baseline recordings	338
8.3.2	Hypoxia	340
8.3.3	Hyperoxia.....	342
8.3.4	Restraint stress	345
8.3.5	Tail Pinch.....	350
8.3.6	Chloral Hydrate	354
8.3.7	Diamox	358
8.3.8	L-NAME	361
8.3.9	L-Arginine	363
8.3.10	Day vs. night study	366
8.4	Conclusion	369
8.5	References.....	375

9. Conclusion

9.	Conclusion.....	381
9.1	References.....	389

Declaration

This thesis has not been submitted before, in whole or in part, to this or any other University for any degree, and except where otherwise stated, is the original work of the author.

Signed: _____

Andrea Wynne

*To Mam and Dad,
Without you, I would not be the person I am today,
This thesis, is dedicated to you*

*'When everything seems to be going against you,
remember that the airplane takes off against the wind,
not with it'*

Henry Ford (1863-1947)

Acknowledgements

Firstly, I would like to express my appreciation and thanks to my two supervisors, Prof. John Lowry and Dr. Niall Finnerty. John, thank you for giving me such a great opportunity and allowing me to be a part of such a great lab. Thank you for always being available for any queries and advice I may have had throughout this research, it was much appreciated. I would like to thank, Dr. Niall Finnerty, for your constant encouragement, support, kindness and best of all your comic relief, it was truly appreciated. I feel that without your help and support I probably would not have made it this far. I will forever be in your debt. Your knowledge and enthusiasm for not only your own work but the work of others in the lab is inspiring. During the final hurdle of writing the thesis, I will be forever grateful for all of the support, corrections (sorry for ruining your football viewing day in front of your fancy television, every weekend), and for taking the crazy train to 'Thesitis' with me (which has been defined in the urban dictionary as a mental illness by the way), because I know it affected you too, I appreciated the company! So, Dr. Niall, Nidge, Finno, Finnerty, I wholeheartedly thank you again, you are a legend.

I would like to thank Ms. Maryanne Dalton for the guidance throughout the first part of my journey in the Masters research, I will always be very grateful for the support giving to me, whenever I needed help, advice or reassurance. To everyone in the lab, firstly I would like to thank Dr. Fiachra Bolger (aka Fi B), thank you so much for your support throughout the years of my research. Without your suggestions, help and advice, especially during the first stage of the research, I don't know what would have happened. Thank you for always being just a phone call away if I needed any help during the write up process too. Thanks again for the support and for always being there to step on my shoes when you thought they were new (they were just clean Fi B). Dr. Keeley Baker, I cannot begin to thank you enough for not only the friendship, walks, advice, and endless chats, but your constant support and help throughout the writing up stage. Your visits to me in the write up room before you went home, kept me from losing the plot (although some may say, that already had happened). Thank you for the constant laughs and for always having 'my bedroom' made up for me if ever I needed somewhere to stay. You have been there for me right from the first day that I walked into the lab and I will never forget that.

Thank you Michelle for all of the chats, walks and endless laughs you gave me, especially when I needed them most. Thank you for doing all the hard work while we had our 'exam' over in the Bru, although you didn't have a choice (sorry about that, it's not my fault I have small

hands). Thank you Dr. John Kealy, 'Government of Ireland Post Doctoral Fellow', for your help and your endless supply of puns about everything and anything, (you know how I feel about them, but one or two did make me laugh). Thank you Karen for the Halloween secret stash you allowed the Lowry group to take from you, the first Halloween party you were here. You were destined to be a Lowry group member from the moment you handed over your hidden supply to us ha. I wish you all every success and happiness in everything you are doing and hope to do. I would like to thank Dr. Saidhbhe O'Riordan and Dr. Kenneth Pierce, for keeping in touch and for the constant encouragement and help throughout the writing process. Thank you Saidhbhe, for the visits to the department to make sure I was still alive and to ask if I needed any support or help, it was truly appreciated. To have a support system from not only the present lab but from others that have left the lab since I started writing is overwhelming and I can't thank you enough.

Thank you Niamh, Trish and Sam for the support, emails and encouragement throughout the research and also during the write up process too. I am so grateful to have met such thoughtful and caring people and I can't express my gratitude enough. I would like to thank the department for all of the parties and laughs throughout my years in Maynooth, I wish you all the very best in whatever you decide to do. To the academic staff, technicians, Noel, Carol and Donna, I am so grateful for all of the help and support you gave throughout my journey here in Maynooth. I do apologise Carol and Donna for the constant knocking at your office door for help (which seemed to be every single day, at least twice a day, 5 days a week, I would miss you come the weekend haha). I really appreciate the laughs and how nothing was ever a problem. Thank you Gama 'Theo', Haixin, Foxy and Wayne for putting up with the random hiccups and thank you for the laughs and chats up in the room of doom. To everyone not directly connected to Maynooth, you have all been a part of getting me to this stage. I would like to thank Emma, Natasha, Joanne, Aisling and Karina for supporting me throughout this whole process. You all have been there since school and I am so lucky to have you as friends. The constant encouragement and laughter was really needed and I won't forget it.

To Jeanette, thank you for being there for me and for making sure I had dinners and everything I needed, I appreciated it so much. Catherine, soon to be Catherine Wynne, thank you so much for being the sister I have always wanted and for helping me throughout my years in college. Antoinette, Georgina and Sean, thank you so much for taking my mind off of the work when I was stressed and for constantly bringing a smile to my face. I want to express my gratitude to the 'brady bunch' that is my family of mad uncles, aunties and cousins. Your encouragement and cheer leading will always be remembered and much appreciated. Mam

and Dad, words cannot express how grateful and thankful I am to have such amazing and wonderful parents as you. You are always there for me, supporting me and caring for me, throughout every step of the way. Without your love and support this would not have been possible. Thank you Dad for keeping my spirits up, by giving me something else other than work to focus on, such as, swapping things around in my room to cause me confusion, you got a great laugh out of that and I did too. Also Mam, thanks for asking me how my day was even though I know you were so busy with your own college work.

To my brothers Mark and Aaron, I thank you so much for your support, kindness, love, encouragement and the interest you gave to my research. Mark, our conversations about the NMDA receptor and NOS enzymes, has to be one of the nerdiest conversations I have had with a person outside of the chemistry department and your genuine interest (which sometimes seemed more than mine), was truly appreciated. Aaron, thank you for keeping me in tune with what was going on in the 'outside' world, and for providing me with many laughs with your 'thesis Christ' phrase. I can't thank you enough and I am truly lucky to have brothers like you two. Finally, I would like to say a big thank you to Chris, words cannot express how thankful and appreciative I am for all that you have done for me throughout these last few years. Your love and support along with the endless laughs about everything (thank god you on the same wavelength as me) will never be forgotten and if you hadn't of been on this journey with me, I don't think I would have got through it. So before I break out into song, I hope I have thanked everyone and if I have missed anybody in this, I will thank you in person.

Thank you

Abbreviations

AA	<i>Ascorbic acid</i>
ABG	<i>Arterial blood gas</i>
AIBN	<i>Azodiisobutyronitrile</i>
BOLD	<i>Blood oxygenation level dependant</i>
BSA	<i>Bovine serum albumin</i>
BT	<i>Brain tissue</i>
CPA	<i>Constant potential amperometry</i>
CPE	<i>Carbon paste electrode</i>
CM	<i>Compartment Syndrome</i>
CPA	<i>Constant potential amperometry</i>
CV	<i>Cyclic voltammetry</i>
DHAA	<i>Dehydroascorbic acid</i>
DPV	<i>Differential pulse voltammetry</i>
DMSO	<i>Dimethyl sulfoxide</i>
DOPAC	<i>3, 4-Dihydroxyphenylacetic acid</i>
EDRF	<i>Endothelium derived relaxing factor</i>
ECF	<i>Extracellular fluid</i>
eNOS	<i>Endothelial nitric oxide synthase</i>
FCV	<i>Fast cyclic voltammetry</i>
FAD	<i>Flavin adenine dinucleotide</i>
FMN	<i>Flavin mononucleotide</i>
fMRI	<i>Functional magnetic resonance imaging</i>
GP	<i>Graphite powder</i>
5-HIAA	<i>5-Hydroxyindoleacetic acid</i>
HVA	<i>Homovanillic acid</i>
H ₂ O ₂	<i>Hydrogen peroxide</i>
iNOS	<i>Inducible nitric oxide synthase</i>
MMA	<i>Methyl methacrylate</i>
MMCPE	<i>Methyl methacrylate modified CPE</i>
MMGPE	<i>Methyl methacrylate modified graphite powder electrode</i>

NEDD	<i>N-1-naphthyl-ethylenediamine</i>
NADPH	<i>Nicotinamide adenine dinucleotide phosphate</i>
L-NOARG	<i>N^G-nitro-L-arginine</i>
L-NAME	<i>N^G-nitro-L-arginine methyl ester</i>
nNOS	<i>Neuronal nitric oxide synthase</i>
NO	<i>Nitric oxide</i>
NOS	<i>Nitric oxide synthase</i>
NO ₂ ⁻	<i>Nitrite</i>
N ₂	<i>Nitrogen</i>
ON	<i>Overnight</i>
O ₂	<i>Oxygen</i>
ORR	<i>Oxygen reduction reaction</i>
<i>o</i> -PD	<i>o-phenylenediamine</i>
PCP	<i>Phencyclidine</i>
PBS	<i>Phosphate buffered saline</i>
PEA	<i>L-α-phosphatidylethanolamine</i>
PPD	<i>Poly (o-phenylenediamine)</i>
Pt	<i>Platinum</i>
KOH	<i>Potassium hydroxide</i>
RT	<i>Room temperature</i>
REM	<i>Rapid eye movement</i>
SEM	<i>Scanning electron microscopy</i>
5-HT	<i>Serotonin</i>
NaCl	<i>Sodium chloride</i>
NaOH	<i>Sodium hydroxide</i>
NaNO ₂	<i>Sodium Nitrite</i>
NaH ₂ PO ₄ ·H ₂ O	<i>Sodium phosphate monobasic</i>
SCE	<i>Saturated Calomel Electrode</i>
Sty	<i>Styrene</i>
SMCPE	<i>Styrene modified CPE</i>
SMGPE	<i>Styrene modified graphite powder electrode</i>
SULF	<i>Sulfanilamide</i>

H₂SO₄

Sulphuric acid

BH₄

Tetrahydrobiopterin

UA

Uric acid

UV

Ultraviolet

Abstract

The main aims of this thesis were to develop and characterise monomer modified oxygen (O₂) sensors that could withstand the harsh setting of an *in-vivo* environment, without the risk of alteration of the sensor components and the characterisation of nitric oxide (NO) sensors *in-vitro*, followed by the complete *in-vivo* characterisation under physiological conditions. The main result sought after for development of these novel O₂ sensors, was the potential utilisation in a clinical setting. Chapter 1 introduces the background behind the monitoring of NO and O₂ in the brain, the biosynthesis of NO in the brain, the biosynthesis of NO through the *N*-methyl-*D*-aspartate receptor (NMDA) and the potential role of NO in neurovascular coupling. Chapter 2 discusses the theory behind the project and Chapter 3 describes the experimental protocols utilised throughout this research.

Chapter 4 discusses the development and characterisation of the monomer modified O₂ sensors. The subsequent characterisation of the novel O₂ sensors *in-vivo* is discussed in Chapter 5. The use of various perturbations to alter the O₂ concentration for characterisation of the O₂ sensors is described. The characterisation of the NO sensor types (Type 2 and Type 3 NO sensor) is discussed in Chapter 6, with response times, sensitivity and selectivity discussed in detail. The subsequent characterisation of these sensors *in-vivo* is described in Chapter 7. Systemic and local administrations of various inducers and inhibitors of nitric oxide synthesis were carried out to determine the sensors viability in monitoring the analyte in a physiological environment.

In Chapter 8, another aspect of this research involving the simultaneous recording of the NO and O₂ analytes *in-vivo* is described, which utilises a combination of the styrene modified carbon paste electrodes (SMCPEs) and methyl methacrylate modified carbon paste electrodes (MMCPEs) for the detection of O₂ and the Type 2 and Type 3 sensors for the detection of NO. These results yield valuable information about the possible relationship between the two molecules. The final chapter (Chapter 9) details a summary of all of the chapters and concludes with a final discussion on the results attained.



1. Introduction

The focus of this thesis is the design and characterisation of microelectrochemical sensors that can reliably detect oxygen (O₂) and nitric oxide (NO) *in-vitro*, with the main goal being the neurochemical recording of these substrates *in-vivo*. The long-term aim is the *in-vivo* recording of tissue O₂ in a clinical setting which deems the *in-vitro* and *in-vivo* characterisation of this sensor vital. However, since the regulatory hurdles are so high for neurochemical recording in a clinical environment (see Section 1.2.2), the primary area of focus is peripheral tissue. NO is further back in terms of clinical uptake since most clinicians express little interest in measuring this novel marker in patients. However, the bioanalytical laboratory team believes that they will overcome this clinical inertia in the near future but as it currently stands it is out of the scope of this thesis. With this in mind, it is imperative to determine the behaviour and subsequent capabilities that these sensors may possess for recording in a very complex milieu that is the human body. The *in-vivo* characterisation of both sensor types were undertaken in the brain since this is our area of interest and expertise and it is firmly believed that the findings can translate across into peripheral tissue.



Figure 1: An image of the brain *inset*: a depiction of a neuron,

<http://scientopia.org/blogs/scicurious/2011/05/04/science-101-the-neuron/>

1.1 The Brain

Understanding the mechanisms behind how the brain functions is one of science's biggest challenges. Comprehension of the interplay between the electrical and chemical pathways responsible for behaviour, feelings or thought, is at the forefront of the science communities unanswered questions and eagerly awaited understanding. The real-time measurement of chemicals in the brain environment, utilising electrochemical sensors, is an advanced and significant technique. It allows for specific neurochemicals to be targeted and detected, giving sub-second information about how that molecule functions and what role it plays in the body, during specific experiments (O'Neill & Lowry, 2006). The brain is a very complex organ that comprises of over 12 billion neurons (see Figure 1) and 50 million glial cells. The largest part of the brain is the cerebrum and it is separated into four paired lobes; frontal, temporal, occipital and parietal. Each of these lobes control separate functions that regulate bodily processes (Baggaley *et al.*, 2001).

In order to comprehend how the brain works, an understanding of the different cells that compose this multifaceted organ needs to be gained. The cells that elicit a chemical and electrical signal are called neurons and they are the basic unit of the nervous system. These neurons function by sending and receiving messages to and from other nerve cells. The main communication points on the surface of the nerve cells are called synapses (see Figure 1.1). The transfer of messages occurs through synaptic transmission, which secretes a chemical called a neurotransmitter, which carries the message from neuron to neuron (Bloom & Lazerson, 1988). A stimulus is needed to trigger the neurons, creating nerve impulses which cause the charge on the inside of the cell membrane to alter from negative to positive. A nerve impulse then travels down to the end of the axon triggering the release of the neurotransmitters which cross the gap from the neuron to the target cell producing the response (Baggaley *et al.*, 2001). Depending on the type of neuron involved, the impulse either excites the post synaptic receptor (glutamate/dopamine) and continues on to the next neuron or inhibits the post synaptic receptors, causing the impulse to cease firing.

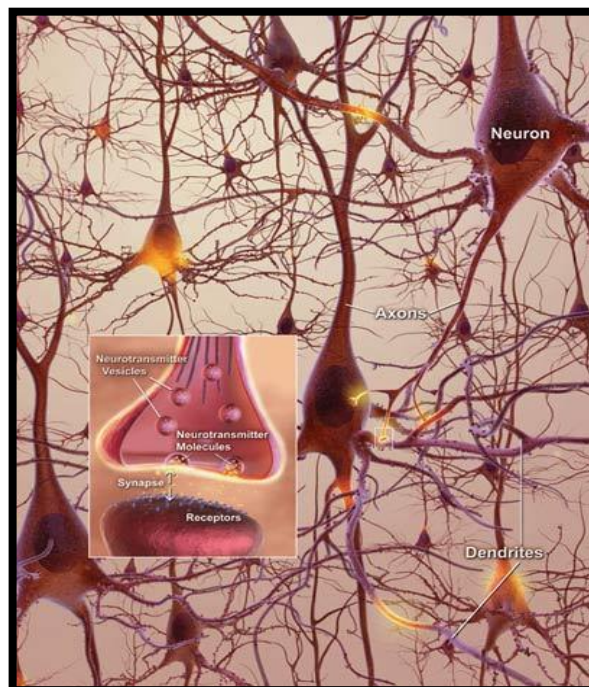


Figure 1.1: An image displaying the structure of neurons

<http://www.drugdevelopment-technology.com/projects/dimebon/dimebon3.html>

1.2 Micro-electrochemical O₂ Sensors

O₂ is the most vitally important molecule that sustains life on earth. The human body is beautifully orchestrated in receiving and delivering O₂ to the many of the uncountable cells that comprise our bodies (Lane, 2002). The brain consumes about 20% of the total amount of O₂ produced by the body and the tissue concentration is conditional on the blood supply and local utilisation of O₂ (Lowry *et al.*, 1997). The concentrations of O₂ in cerebral tissue ranges from 40 µM to 80 µM (Lowry & O'Neill, 2006). Insulated metal polarographic cathodes that continuously recorded O₂ availability in feline subjects achieved the first time O₂ recordings *in-vivo* by the technique of voltammetry using metal electrodes (Clark *et al.*, 1958). The utilisation of noble metal electrodes and carbon-based electrodes for the detection of this analyte have been extensively reported over the years (Lowry *et al.*, 1996; Luebbbers, 1996; Dittmar *et al.*, 1997; Bolger & Lowry, 2005; Lowry *et al.*, 2010; Kealy *et al.*, 2013).

1.2.1 Carbon Paste Electrodes (CPEs)

In 1958, a short one-page report that introduced the CPE, was published by Ralph Norman Adams (Adams, 1958). The preparation of a mixture of carbon powder and a binder was presented as a promising electrode material. Since that time, CPEs have undergone many developments. The modification of the CPE was attractive, due to the ease of manipulation in their production. In 1964, Kuwana and French developed the first type of CPE that contained an electroactive organic substance dissolved within the binder (Kuwana & French, 1964). In 1965, Marcoux *et al.*, prepared a modified CPE, by rubbing a modifier into the paste which enhanced the performance of the sensor (Marcoux *et al.*, 1965). Still to this day, the modification of the CPE is an attractive concept as demonstrated in recent literature (D'Souza *et al.*, 2013; Fathirad *et al.*, 2013; Soysal *et al.*, 2013; Bahrami *et al.*, 2014).

The modification of the CPE in this body of research was undertaken to try and produce a sensor that was more robust and not as easily modified when in the presence of elements that compose a biological milieu. The CPE is known to alter from a CPE to a carbon powder electrode when placed in the *in-vivo* environment. This is due to lipids and other endogenous species removing the silicone oil from the carbon paste. This characteristic of the CPEs is one that makes them so advantageous *in-vivo*, as the extraction of the oil from the carbon paste removes some of the fouling that can occur at the surface of the electrodes when placed into a complex biological setting. This then provides the sensor with long term stability *in-vivo* (Ormonde & O'Neill, 1989, 1990). CPEs are more desirable to use than metal based sensors, as they do not require protective membranes to defend against surface poisoning (Bolger & Lowry, 2005).

The utilisation of CPEs for the detection of O₂ *in-vivo* has been previously demonstrated within our research group (Lowry *et al.*, 1997; Bolger *et al.*, 2011b; Kealy *et al.*, 2013). Even though the CPEs work very efficiently in the detection of O₂ over long periods of time, more recently, the focus of our group has concentrated on the integration of electrochemical sensors into the clinical environment. For a sensor to be utilised in a clinical setting, sensitivity to interfering lipophilic ions or charged surfactants should not be an issue for the electrode (Czaban, 1985). Leeching of constituents or risk of the removal of

components from the sensors structure should not be a problem when trying to use an electrode in a clinical environment. Therefore, the CPEs would never be considered an optional sensing device for O₂ within human tissue.

In the research undertaken in this thesis, the introduction of the monomers styrene (Sty) and methyl methacrylate (MMA) into the CPE design was performed to produce a more robust and solid composite that would not be easily altered in a complex biological setting. The Sty and MMA monomers have been utilised previously in the design of sensors. The addition of Sty into the construction of carbon nanotube sensors with the goal of synthesising and characterising Sty grafted carbon nanotubes and its polystyrene nanocomposites has been demonstrated previously (Nayak *et al.*, 2007). MMA has been incorporated into the production of dental appliances, which demonstrates a compatibility with human tissue (Douglas & Bates, 1978; Murray & Darvell, 1993; Sarac *et al.*, 2006). Also a graphite/poly(MMA) sensor was designed for the detection of vitamin C (Dai *et al.*, 2008). The modification of the CPEs with the monomers MMA and Sty was successful and created a robust and solid electrode for the detection of O₂ in a complicated *in-vivo* environment (see Chapter 5).

1.2.2 Real-Time Clinical Monitoring of O₂

The O₂ sensor described within this body of work has been designed with peripheral tissue monitoring in mind, since the regulatory hurdles surrounding human brain monitoring are so high. Despite this, an extensive characterisation of the sensor was undertaken in brain extracellular fluid and described in detail in this thesis. It is predicted that the technology will translate from brain tissue to peripheral muscle tissue without any complications. Clinicians have expressed their desire for continuous real-time monitoring of vital metabolites such as O₂; however, to date such a technology is not available. The majority of techniques for measuring O₂ in hospitals suffer from low temporal resolution and have limited utility in medical emergencies. For example, blood gas analysis requires the undesirable removal of blood samples from patients resulting in slow sampling times, however, despite this limitation; it is one of the most common tests performed on patients in intensive care units.

Pulse oximetry is another standard technique utilised in intensive care units that provides an indirect reading of O₂ saturation of the patient's blood. However, unlike the electrochemical tissue O₂ sensor, pulse oximetry fails to inform the clinician about how much O₂ is actually utilised by the patient's tissue. Currently there is no electrochemical O₂ sensor utilised in peripheral tissue monitoring but the commercially available LICOX[®] probe (see Figure 1.2.2), has been extensively utilised in brain tissue monitoring (Mulvey *et al.*, 2004; Stevens, 2004; Huang & Obenaus, 2011). This probe displays a lot of similarities to the O₂ sensor described in this body of work; however, the LICOX[®] O₂ sensing component functions by diffusion of O₂ through a permeable membrane surrounding the probe and into an electrolyte solution where a signal is generated. The LICOX[®] probe is designed with brain monitoring at its core and is fixed carefully in position using a bulky housing component. The fragile membrane surrounding the probe is unsuitable for orthopaedic surgery due to risk of damage during implantation and leakage of the electrolyte into the surrounding tissue.

Despite this limitation Hansen and colleagues have reported for the first time the benefits of measuring intramuscular tissue oxygenation in the diagnosis of compartment syndrome (CS) using the LICOX[®] probe (Hansen *et al.*, 2013). CS is a very serious condition that results from increased pressure in a muscle compartment following trauma that can lead to muscle and nerve damage and a compromise in blood flow. The most common cause of CS is trauma to the muscle following extremity fractures. The pathophysiology of CS involves pressure-induced ischemia of muscle suggesting that the real-time monitoring of tissue oxygenation represents a potential method for diagnosing its onset. Ischemia is defined as being a restriction in blood supply to tissues, causing a shortage of O₂ and glucose needed for cellular metabolism. O₂ is an extremely relevant real-time indicator of CS since it is transported to the muscle via blood supply and if the blood supply is interrupted then no O₂ can reach the muscle. The use of an intramuscular sensor to directly measure the level of O₂ represents a key advancement in diagnosing tissue ischemia complications such as CS especially since the level of muscle O₂ was found to respond rapidly to ischemia and correlate with biochemical markers of muscle ischemia including ATP and pH (Hansen *et al.*, 2013).

Due to the inherent limitations of the LICOX[®] probe for intramuscular monitoring the design and development of a novel O₂ sensor has massive potential for addressing this medical emergency.

Despite the manufacturing of a sensor from biocompatible materials, the sensor assembly itself may not be suitably compatible. This leads to the need for separate testing of the sensor to determine the biocompatibility of the intact sensor design. The cytotoxic testing of implantable devices is required by all regulatory bodies and will be performed prior to any scheduled clinical studies (Koschwanez & Reichert, 2007).

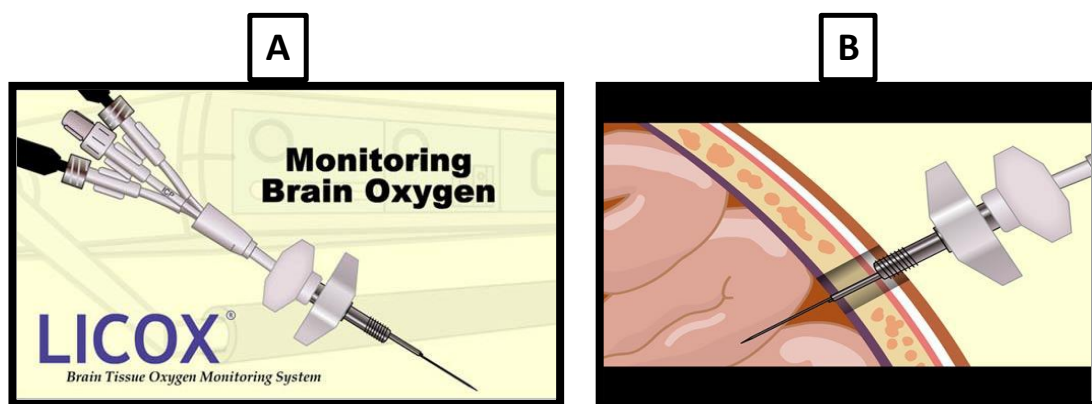


Figure 1.2.2: (A) An image displaying the LICOX[®] brain tissue monitoring probe and (B) the LICOX[®] probe inserted into brain tissue.

<http://www.digitallamb.com.au/projects/flash-animation/licox.html>

1.3 Micro-electrochemical Nitric Oxide (NO) Sensors

Detecting the free radical NO, is a very challenging task for electrochemical sensors for a variety of reasons. It has a very short half-life (typically < 10 s) due to the reactions with different molecules (Lancaster Jr, 1997). The concentration of NO *in-vivo* has been established as around 0.1 μ M (Hall & Garthwaite, 2009) and when one is trying to detect such a small and reactive molecule in the presence of a myriad of endogenous interferents, it can prove very difficult. NO has a role in the regulation of vascular tone and has been linked to a variety of diseases that include hypertension, Parkinson's disease and Alzheimer's disease (Brown *et al.*, 2005). It was characterised as the endothelium derived

relaxing factor (EDRF) in the late 80's, (Ignarro *et al.*, 1987; Palmer *et al.*, 1987). Since this discovery, many researchers have attempted to understand and unravel the various roles of NO in physiology. The production of NO occurs endogenously from L-arginine by a family of enzymes called nitric oxide synthases (NOSs) (Dinerman *et al.*, 1993; Schmidt *et al.*, 1993), which is discussed in more detail in Section 1.4.

In order for NO to be detected by electrochemical sensors, the sensors must encompass certain characteristics that enable the recording of NO *in-vivo*. These include, good selectivity and efficient discrimination between other electroactive species encountered by the sensor, good sensitivity towards the target analyte, fast response time and long term stability (Bedioui & Griveau, 2013). The first direct oxidation of NO on a platinum (Pt) electrode was reported by Shibuki *et al.*, using a miniature Clark-type electrode (Shibuki & Okada, 1991). Since then, there have been numerous reports of research groups using carbon, glassy carbon, Pt or gold electrodes covered by different types of membranes, to detect NO (Friedemann *et al.*, 1996; Pontié *et al.*, 1999; Pontié *et al.*, 2000; Ferreira *et al.*, 2005; Kato *et al.*, 2005; Ho Shim *et al.*, 2010).

The use of the polymeric ion exchanger Nafion[®], which is a perfluorinated sulfonic acid ionomer, to provide a barrier for a variety of anionic interfering species, has been successful in the detection of NO. Within our research group the detection of NO has been undertaken with a Pt-Nafion[®] sensor and a Pt-Nafion[®] sensor that incorporates a layer of *o*-phenylenediamine (*o*-PD) as an extra interference rejection layer (Brown *et al.*, 2009; Finnerty *et al.*, 2012a; Finnerty *et al.*, 2012b). These sensors provide real-time NO detection, with great sensitivity, a quick response time and great selectivity over a wide range of electroactive species *in-vivo*. NO detection *in-vivo* continues to be seen as an important objective and the more reports being produced on the monitoring of this analyte, the more we will gain a better understanding of how it functions and to what extent it is implicated in disorders like Alzheimer's disease, Parkinson's disease and hypertension.

1.4 Biosynthesis of NO

As already stated, NO is a very reactive molecule, which is synthesised by a family of enzymes, called NOS, which are located in many of the cells in the body (Guix *et al.*, 2005). There are three principle isoforms of the NOS enzyme:

- **Neuronal NOS (nNOS)**
- **Endothelial NOS (eNOS)**
- **Inducible NOS (iNOS)**

All of the NOS enzymes have similar structures and they contain both an oxygenase domain and a reductase domain. The oxygenase domain allows for the binding of L-arginine, heme and tetrahydrobiopterin (BH₄) and the reductase domain allows for flavin adenine dinucleotide (FAD), flavin mononucleotide (FMN) and nicotinamide adenine dinucleotide phosphate (NADPH). Both of these domains are connected through a binding site for calmodulin (Marletta, 1993; Alderton *et al.*, 2001). nNOS and eNOS are calcium-calmodulin dependant enzymes, that produce NO in a transient manner, whereas iNOS, is independent of calcium and calmodulin (Mungrue *et al.*, 2003). The production of NO through the iNOS enzyme occurs following immunological or inflammatory stimulation in macrophages, astrocytes and other cells. The NO produced from this stimulation lasts hours or even days (Iadecola *et al.*, 1995). It is imperative that all of the aforementioned co-factors are available for the biosynthesis of NO to proceed. (Dinerman *et al.*, 1993; Schmidt *et al.*, 1993). L-arginine, in the presence of molecular O₂ binds to its site on the NOS isozyme to produce NO and L-citrulline, Figure 1.4, displays this process by which NO is biosynthesised (Guix *et al.*, 2005).

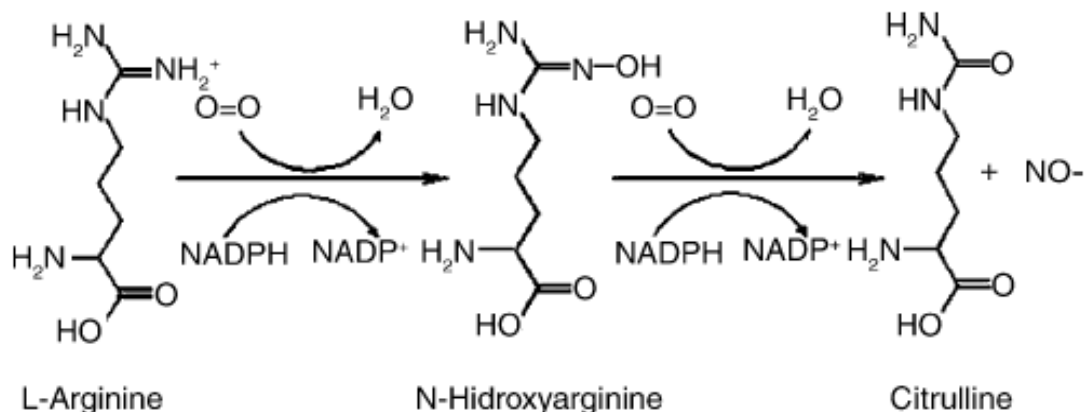


Figure 1.4: A schematic displaying the biosynthesis of NO by NOS (Guix *et al.*, 2005)

It has been observed that upon activation of the N-methyl-D-aspartate receptor (NMDA) receptors, the release of NO occurs (Garthwaite *et al.*, 1988). This is discussed in more detail in Section 1.7. It has been implicitly stated that nNOS is the main source of NO in neurons and localises to synaptic spines (Zhou & Zhu, 2009). It has also been demonstrated that in the striatum, NO is mainly produced via the nNOS enzyme (Bredt *et al.*, 1990; Bredt *et al.*, 1991), however these theories have yet to be confirmed. The release of NO from endothelial cells is believed to be an essential vasodilator mechanism that is responsible for the maintenance of vasomotor function. In both the cerebral and peripheral blood vessels, the decrease in NO production results in a major alteration of vascular function which includes vasoconstriction and increases in arteriole blood pressure (Katusic & Austin, 2013). There is clear evidence that confirms a role for NO synthesised mainly from eNOS in the regulation of vascular tone in studies undertaken by Furchgott and Zawadzki (Furchgott & Zawadzki, 1980).

1.5 Neurovascular coupling

The tight coupling between neuronal activity and the local regulation of cerebral blood flow (CBF) through intricate vasoactive mechanisms, collectively named neurovascular coupling has long been recognised (Piknova *et al.*, 2011). When there is a rise in CBF under physiological stimulation, the supply of O₂ will exceed the utilisation, resulting in a net increase in O₂ (Lowry *et al.*, 1997). CBF is fundamental to the living brain and there is an

increase in the need for more blood flow upon a rise in neuronal activity (Liao *et al.*, 2013). The principle behind neurovascular coupling is to make sure that homeostasis of the cellular environment is sustained at all times (Piknova *et al.*, 2011). This occurs through the action of neurons, glial cells and blood vessels which form the ‘neurovascular unit’ performing at the cellular level to control CBF (Iadecola, 2004; Attwell *et al.*, 2010; Cauli & Hamel, 2010). When these functions are disrupted it can lead to brain dysfunction and disease which can be observed in disorders like hypertension and Alzheimers disease (Girouard & Iadecola, 2006).

Functional neuroimaging methods utilise the mechanisms of neurovascular coupling in order to map brain activity, therefore making the understanding of how neurovascular coupling works, very important. Examples of neuroimaging methods include, functional magnetic resonance imaging (fMRI), diffuse optical imaging and positron emission tomography (Piknova *et al.*, 2011). The primary technique utilised for brain imaging carried out in humans is fMRI (Moreno *et al.*, 2013). Despite the advantages that it possesses, such as being a quick and non invasive technique, it faces challenges in a clinical setting. It does not directly calculate neuronal activation, but instead, calculates the related signals that are connected with neuronal activity. Also, not all patients fulfil the required criteria for the imaging protocols. Patients with movement disorders and patients that have difficulty with completing the tasks needed for fMRI analysis due to cognition impairments are excluded and this is a limitation of fMRI (Faro & Mohamed, 2010).

Figure 1.5, displays a redrawn summary of the basic physiological changes that link neural and vascular responses. The need for energy in the form of adenosine triphosphate (ATP) is required for the diverse cellular processes that occur within neurons. The synthesis of ATP occurs by glycolysis initially which produces a small amount of ATP. Subsequent to this, ATP is then synthesised by the oxidative glucose metabolism which needs O₂ in order to produce a large amount of ATP. A constant supply of glucose and O₂ is necessary and is maintained by CBF, which delivers these two energy substrates to neural tissue. Upon neuronal activation, an increase in the consumption of glucose and O₂ is followed by an increase in CBF. The release of by-products such as potassium (K⁺), NO, adenosine and carbon dioxide (CO₂) amongst other products may directly or indirectly alter blood flow with the constriction or vasodilation of the blood vessels. On the other hand,

neurotransmitter release of glutamate by neuronal activation could lead to the activation of the NMDA receptors which cause the NOS enzymes to produce NO through the synthesis with L-arginine (Pasley & Freeman, 2008). The results set out in Chapter 8 focuses on the theory that the production of NO is through the NMDA receptor acting on the nNOS enzyme (which is discussed in greater detail in Section 1.7).

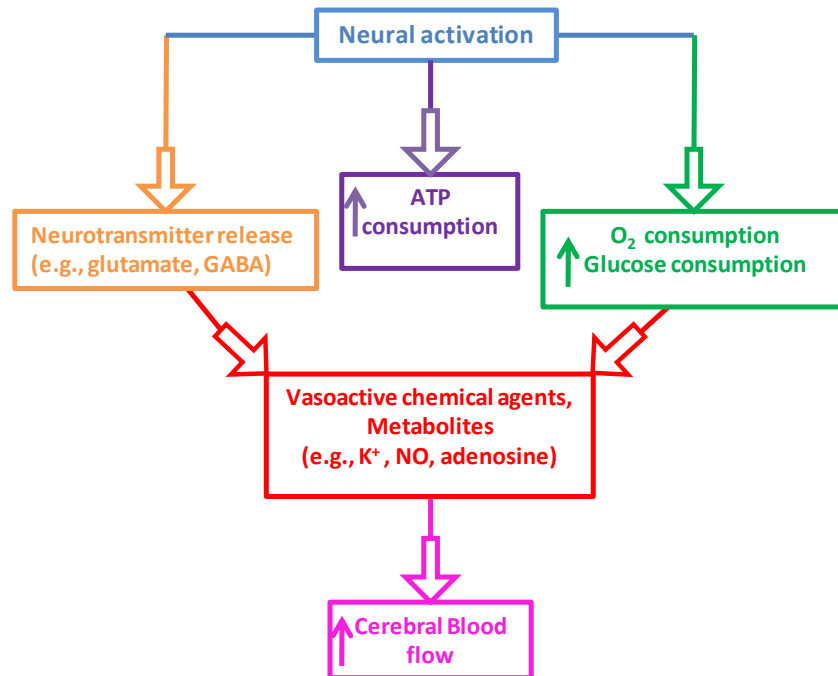


Figure 1.5: A redrawn image displaying a basic summary of the physiological changes connecting neural and vascular responses (Pasley & Freeman, 2008).

1.6 eNOS, blood flow and O₂

It is widely known that NO is an important regulator of blood flow (Rees *et al.*, 1990a; Tanaka *et al.*, 1991). The characterisation of NO as the EDRF in the 1980's was a remarkable advancement, which shed some light on the function of NO. The similarity between NO and the EDRF was indistinguishable (Ignarro *et al.*, 1987; Palmer *et al.*, 1987). Upon the production and release of the EDRF, smooth muscle relaxation is promoted (Furchgott & Zawadzki, 1980). The eNOS enzyme is the primary isoform of NOS expressed in the cardiovascular system. It is situated mostly in the vascular

endothelium and plays an important part in the maintenance of vascular tone and tissue perfusion (Mungrue *et al.*, 2003). Many variables determine the production and physiological action of endothelial NO, such as substrate availability, co-factors and the presence of NO scavengers (Chatterjee & Catravas, 2008).

N^G-nitro-L-arginine methyl ester (L-NAME) has been utilised as a means of decreasing the production of NO. It was found to be an effective inhibitor of eNOS and nNOS in the 1990's (Miilsch & Busse, 1990; Rees *et al.*, 1990b). The use of L-NAME as an NO synthesis inhibitor has been demonstrated by many research groups (Rees *et al.*, 1990b; Miller *et al.*, 1993; Losonczy *et al.*, 1996). Upon administration of L-NAME, a decrease in the NO levels can be observed, along with a concurrent decrease in O₂ (see Chapter 8, Section 8.3.8). This demonstrates a close connection between NO and O₂. Upon observing a decrease in CBF, an O₂ decrease will also be observed. It has been stated that the excellent correlation between CBF and brain tissue O₂ shows that the monitoring of brain tissue O₂ can be utilised as a true representation of CBF (Doppenberg M.D *et al.*, 1998). This has been demonstrated within our research group also (Lowry *et al.*, 1997).

1.7 NMDA receptor

Many theories behind the production of NO discussed in the scientific literature, involves NMDA receptors (Buisson *et al.*, 1992; Iadecola, 1993; Drake & Iadecola, 2007; Tonetto *et al.*, 2009). NMDA receptors are among the most strictly regulated glutamate-gated cation channels. They consist of sites for endogenous ligands that bind to the channel and increase the probability for the opening of the channel. There are two different agonist-recognition sites, one for glutamate and another for glycine/D-serine (Brady *et al.*, 2005). Glutamate binds to NMDA receptors located on interneurons that express nNOS and upon activation of the NMDA receptors, calcium channels are subsequently opened. The influx of calcium leads to the nNOS activation and subsequent NO production (Piknova *et al.*, 2011). Upon the activation of neurons, the release of glutamate is the main signal in the neurovascular response, which is then followed by a number of neurochemical pathways and the release of vasoactive chemicals like NO (Girouard & Iadecola, 2006; Attwell *et al.*, 2010; Cauli & Hamel, 2010). It has been identified that the activation of the NMDA receptor leads to the

activation of nNOS (Khaldi *et al.*, 2002) and triggering NMDA receptors increases nNOS activity which in turn produces NO (Kosenko *et al.*, 2003).

It has also been demonstrated that the use of certain drugs can affect the NMDA receptors expression and activation, thus leading to a diminished production of metabolites such as NO. The NMDA receptors have been suggested as targets of anaesthetic agents in the central nervous system and that some of the biological actions created by the anaesthetics affect the function of the receptors also. A loss of surface expressed NMDA receptors was demonstrated in a study undertaken by LacKamp *et al.*, using chloral hydrate (LacKamp *et al.*, 2009). A decrease in glutamate release and a decrease in the activation of glutamate receptors was also found after chloral hydrate administration in another study undertaken by Kreuter *et al.*, (Kreuter *et al.*, 2004). A decrease in pH has also been suggested as a potential inhibitor of the NMDA receptor activation and has been reported in the literature (Tang *et al.*, 1990; Traynelis & Cull-Candy, 1990).

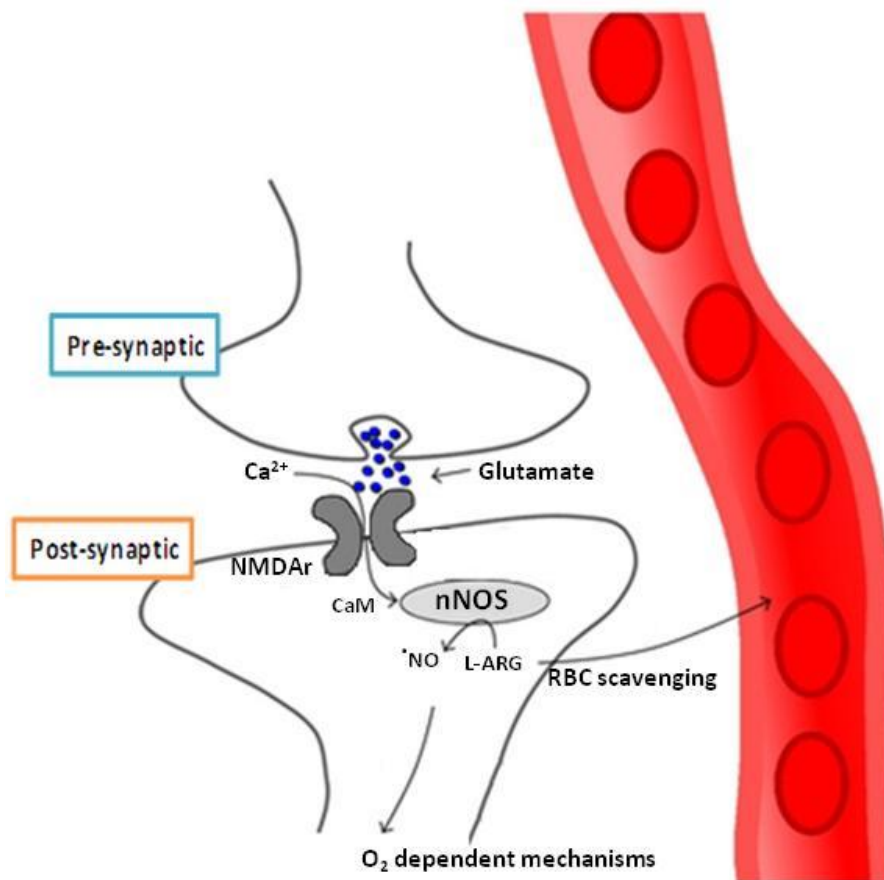


Figure 1.7: An image displaying the possible nNOS production pathways (Santos *et al.*, 2012).

Figure 1.7 displays a summary of the possible nNOS production pathways (Santos *et al.*, 2012). It summarises the synthesis of NO subsequent to the entry of calcium into the post synaptic density, following the glutamate activation of NMDA receptor. nNOS is activated by calcium through the binding of calmodulin (CaM) to the enzyme. The NO is then diffused very quickly to neighbouring tissue which inactivates it by both O₂ dependent mechanisms and through scavenging by circulating erythrocytes (RBCs) for use in vascular processes.

1.8 Overview of thesis

The brain is the most complex organ in the human body. The development and implementation of analytical instruments that can elucidate some of the most intricate mechanisms in the living brain, has been sought by many scientists around the world. Utilisation of real-time micro-sensors to try and gain knowledge of the brains specific functions and processes by targeting certain analytes is a very promising and exciting technique that gives advantages over other conventional methods. This thesis describes the *in-vitro* and *in-vivo* characterisation of monomer modified O₂ sensors with the end goal being a potential use in a clinical environment. The characterisation of the Type 2 NO sensor (see Section 3.4.5.4) and Type 3 NO sensors (see Section 3.4.5.5) *in-vitro* and *in-vivo* is also described. As the NO concentration is a vital biomarker for vasodilation and neurovascular coupling, sensors that can simultaneously and selectively measure the NO and O₂ contents in the brain can potentially answer questions about the specific NO and O₂ processes and mechanisms.

The current Chapter (Chapter 1) gives an introduction to the brain, the detection of O₂ and NO using micro-electrodes, the complex world of the clinical environment, the biosynthesis of NO and its subsequent roles in neurovascular coupling, blood flow and production through the activation of the NMDA receptor. Chapter 2 describes the background theory that is relevant to the research undertaken in this thesis, with Chapter 3 detailing the techniques and methods used in the manufacture and characterisation of the various sensor types studied throughout the course of this project. Chapter 4 introduces the beginning of the results sections with the *in-vitro* development and characterisation of the monomer

modified O₂ sensors. Chapter 5 then leads on to the characterisation of the O₂ sensors in the *in-vivo* environment. Chapter 6 describes the *in-vitro* characterisation of the NO sensor and Chapter 7 gives an account of the characterisation experiments undertaken with the NO sensors in the *in-vivo* environment.

Chapter 8 describes the implantation of the O₂ and NO sensors simultaneously *in-vivo*, in order to determine whether a correlation exists between the two molecules. It has been postulated in literature that there is a strong correlation between these two analytes, however, experiments are carried out in order to determine whether NO possesses an independent function. The final Chapter (Chapter 9) gives an overall conclusion to the thesis and discusses the main findings of the work undertaken.

1.9 References

- Adams RN. (1958). Carbon Paste Electrodes. *Analytical Chemistry* **30**, 1576-1576.
- Alderton W, Cooper C & Knowles R. (2001). Nitric oxide synthases: structure, function and inhibition. *Journal of Biochemistry* **357**, 593-615.
- Attwell D, Buchan AM, Charpak S, Lauritzen M, MacVicar BA & Newman EA. (2010). Glial and neuronal control of brain blood flow. *Nature* **468**, 232-243.
- Baggaley A, Hamilton J, Dorling Kindersley Publishing I & Perlmutter J. (2001). *The Human Body*. Dorling Kindersley Publishing, Incorporated, United Kingdom.
- Bahrami A, Besharati-Seidani A, Abbaspour A & Shamsipur M. (2014). A highly selective voltammetric sensor for sub-nanomolar detection of lead ions using a carbon paste electrode impregnated with novel ion imprinted polymeric nanobeads. *Electrochimica Acta* **118**, 92-99.
- Bedioui F & Griveau S. (2013). Electrochemical Detection of Nitric Oxide: Assessment of Twenty Years of Strategies. *Electroanalysis* **25**, 587-600.
- Bloom FE & Lazerson A. (1988). *Brain, Mind, and Behaviour*. W.H. Freeman & Company, New York, United States of America.
- Bolger F & Lowry J. (2005). Brain Tissue Oxygen: *In-Vivo* Monitoring with Carbon Paste Electrodes. *Sensors* **5**, 473-487.
- Bolger FB, McHugh SB, Bennett R, Li J, Ishiwari K, Francois J, Conway MW, Gilmour G, Bannerman DM, Fillenz M, Tricklebank M & Lowry JP. (2011). Characterisation of carbon paste electrodes for real-time amperometric monitoring of brain tissue oxygen. *Journal of Neuroscience Methods* **195**, 135-142.
- Brady S, Siegel G, Albers RW & Price D. (2005). *Basic Neurochemistry: Molecular, Cellular and Medical Aspects*. Elsevier Science, United States of America.
- Bredt DS, Glatt CE, Hwang PM, Fotuhi M, Dawson TM & Snyder SH. (1991). Nitric oxide synthase protein and mRNA are discretely localized in neuronal populations of the mammalian CNS together with NADPH diaphorase. *Neuron* **7**, 615-624.
- Bredt DS, Hwang PM & Snyder SH. (1990). Localization of nitric oxide synthase indicating a neural role for nitric oxide. *Nature* **347**, 768-770.
- Brown F, Finnerty N, Bolger F, Millar J & Lowry J. (2005). Calibration of NO sensors for *in-vivo* voltammetry: laboratory synthesis of NO and the use of UV-visible spectroscopy for determining stock concentrations. *Analytical and Bioanalytical Chemistry* **381**, 964-971.

- Brown FO, Finnerty NJ & Lowry JP. (2009). Nitric oxide monitoring in brain extracellular fluid: characterisation of Nafion[®]-modified platinum electrodes *in-vitro* and *in-vivo*. *Analyst* **134**, 2012-2020.
- Buisson A, Plotkine M & Boulu R. (1992). The neuroprotective effect of a nitric oxide inhibitor in a rat model of focal cerebral ischaemia. *British Journal of Pharmacology* **106**, 766-767.
- Cauli B & Hamel E. (2010). Revisiting the role of neurons in neurovascular coupling. *Frontiers in Neuroenergetics* **2**, 1-9.
- Chatterjee A & Catravas JD. (2008). Endothelial nitric oxide (NO) and its pathophysiologic regulation. *Vascular Pharmacology* **49**, 134-140.
- Clark LC, Misrahy G & Fox RP. (1958). Chronically implanted polarographic electrodes. *Journal of Applied Physiology* **13**, 85-91.
- Czaban JD. (1985). Electrochemical sensors in clinical chemistry. *Analytical Chemistry* **57**, 345A-356A.
- D'Souza OJ, Mascarenhas RJ, Thomas T, Namboothiri INN, Rajamathi M, Martis P & Dalhalle J. (2013). Electrochemical determination of L-Tryptophan based on a multiwall carbon nanotube/Mg–Al layered double hydroxide modified carbon paste electrode as a sensor. *Journal of Electroanalytical Chemistry* **704**, 220-226.
- Dai H, Wu X, Wang Y, Zhou W & Chen G. (2008). An electrochemiluminescent biosensor for vitamin C based on inhibition of luminol electrochemiluminescence on graphite/poly(methylmethacrylate) composite electrode. *International Society of Electrochemistry* **53**, 5113-5117.
- Dinerman JL, Lowenstein CJ & Snyder SH. (1993). Molecular mechanisms of nitric oxide regulation. Potential relevance to cardiovascular disease. *Circulation Research* **73**, 217-222.
- Dittmar A, Mangin S, Ruban C, Newman WH, Bowman HF, Dupuis V, Delhomme G, Shram NF, Cespuglio R, Jaffrezic-Renault N, Roussel P, Barbier D & Martelet C. (1997). *In-vivo* and *in-vitro* evaluation of specially designed gold and carbon fiber oxygen microelectrodes for living tissues. *Sensors and Actuators B: Chemical* **44**, 316-320.
- Doppenberg M.D EMR, Zauner M.D A, Bullock M.D PDR, Ward M.D JD, Fatouros Ph.D PP & Young M.D HF. (1998). Correlations Between Brain Tissue Oxygen Tension, Carbon Dioxide Tension, pH, and Cerebral Blood Flow—A Better Way of Monitoring The Severely Injured Brain? *Surgical Neurology* **49**, 650-654.

- Douglas WH & Bates JF. (1978). The determination of residual monomer in polymethylmethacrylate denture-base resins. *Journal of Materials Science* **13**, 2600-2604.
- Drake CT & Iadecola C. (2007). The role of neuronal signaling in controlling cerebral blood flow. *Brain and Language* **102**, 141-152.
- Faro SH & Mohamed FB. (2010). *BOLD fMRI: A Guide to Functional Imaging for Neuroscientists*. Springer, New York, United States of America.
- Fathirad F, Afzali D, Mostafavi A, Shamspur T & Fozooni S. (2013). Fabrication of a new carbon paste electrode modified with multi-walled carbon nanotube for stripping voltammetric determination of bismuth(III). *Electrochimica Acta* **103**, 206-210.
- Ferreira NR, Ledo A, Frade JG, Gerhardt GA, Laranjinha J & Barbosa RM. (2005). Electrochemical measurement of endogenously produced nitric oxide in brain slices using Nafion/*o*-phenylenediamine modified carbon fiber microelectrodes. *Analytica Chimica Acta* **535**, 1-7.
- Finnerty NJ, O'Riordan SL, Brown FO, Serra PA, O'Neill RD & Lowry JP. (2012a). *In-vivo* characterisation of a Nafion[®]-modified Pt electrode for real-time nitric oxide monitoring in brain extracellular fluid. *Analytical Methods* **4**, 550-557.
- Finnerty NJ, O'Riordan SL, Palsson E & Lowry JP. (2012b). Brain nitric oxide: Regional characterisation of a real-time microelectrochemical sensor. *Journal of Neuroscience Methods* **209**, 13-21.
- Friedemann MN, Robinson SW & Gerhardt GA. (1996). *o*-Phenylenediamine-Modified Carbon Fiber Electrodes for the Detection of Nitric Oxide. *Analytical Chemistry* **68**, 2621-2628.
- Furchgott RF & Zawadzki JV. (1980). The obligatory role of endothelial cells in the relaxation of arterial smooth muscle by acetylcholine. *Nature* **3**, 373-376.
- Garthwaite J, Charles SL & Chess-Williams R. (1988). Endothelium-derived relaxing factor release on activation of NMDA receptors suggests role as intercellular messenger in the brain. *Nature* **336**, 385-388.
- Girouard H & Iadecola C. (2006). Neurovascular coupling in the normal brain and in hypertension, stroke, and Alzheimer disease. *Journal of Applied Physiology* **100**, 328-335.
- Guix F, Uribealago I, Coma M & Munoz F. (2005). The physiology and pathophysiology of nitric oxide in the brain. *Progress in Neurobiology* **76**, 126-152.
- Hall CN & Garthwaite J. (2009). What is the real physiological NO concentration *in-vivo*? *Nitric Oxide* **21**, 92-103.

- Hansen EN, Manzano G, Kandemir U & Mok JM. (2013). Comparison of tissue oxygenation and compartment pressure following tibia fracture. *Injury* **44**, 1076-1080.
- Ho Shim J, Do H & Lee Y. (2010). Simple Fabrication of Amperometric Nitric Oxide Microsensors Based on Electropolymerized Membrane Films. *Electroanalysis* **22**, 359-366.
- Huang L & Obenaus A. (2011). Hyperbaric oxygen therapy for traumatic brain injury. *Medical Gas Research* **1**, 21-28.
- Iadecola C. (1993). Regulation of the cerebral microcirculation during neural activity: is nitric oxide the missing link? *Trends in Neurosciences* **16**, 206-214.
- Iadecola C. (2004). Neurovascular regulation in the normal brain and in Alzheimer's disease. *Nature Reviews Neuroscience* **5**, 347-360.
- Iadecola C, Zhang F, Xu S, Casey R & Ross ME. (1995). Inducible nitric oxide synthase gene expression in brain following cerebral ischemia. *Journal of Cerebral Blood Flow & Metabolism* **15**, 378-384.
- Ignarro LJ, Buga GM, Wood KS, Byrns RE & Chaudhuri G. (1987). Endothelium-derived relaxing factor produced and released from artery and vein is nitric oxide. *Proceedings of the National Academy of Sciences* **84**, 9265-9269.
- Kato D, Kunitake M, Nishizawa M, Matsue T & Mizutani F. (2005). Electrochemical nitric oxide microsensors based on two-dimensional cross-linked polymeric LB films of oligo(dimethylsiloxane) copolymer. *Electrochimica Acta* **51**, 938-942.
- Katusic ZS & Austin SA. (2013). Endothelial nitric oxide: protector of a healthy mind. *European Heart Journal* **10**, 1-7.
- Kealy J, Bennett R & Lowry JP. (2013). Simultaneous recording of hippocampal oxygen and glucose in real time using constant potential amperometry in the freely-moving rat. *Journal of Neuroscience Methods* **215**, 110-120.
- Khalidi A, Chiueh C, Bullock M & Woodward J. (2002). The significance of nitric oxide production in the brain after injury. *Annals of the New York Academy of Sciences* **962**, 53-59.
- Koschwanetz HE & Reichert WM. (2007). In vitro, in vivo and post explantation testing of glucose-detecting biosensors: current methods and recommendations. *Biomaterials* **28**, 3687-3703.

- Kosenko E, Llansola M, Montoliu C, Monfort P, Rodrigo R, Hernandez-Viadel M, Erceg S, Sánchez-Perez AM & Felipe V. (2003). Glutamine synthetase activity and glutamine content in brain: modulation by NMDA receptors and nitric oxide. *Neurochemistry International* **43**, 493-499.
- Kreuter J, Mattson B, Wang B, You Z-B & Hope B. (2004). Cocaine-induced Fos expression in rat striatum is blocked by chloral hydrate or urethane. *Neuroscience* **127**, 233-242.
- Kuwana T & French WG. (1964). Electrooxidation or Reduction of Organic Compounds into Aqueous Solutions Using Carbon Paste Electrode. *Analytical Chemistry* **36**, 241-242.
- LacKamp A, Zhang G-C, Mao L-M, Fibuch E & Wang J. (2009). Loss of surface N-methyl-D-aspartate receptor proteins in mouse cortical neurones during anaesthesia induced by chloral hydrate *in-vivo*. *British Journal of Anaesthesia* **102**, 515-522.
- Lancaster Jr JR. (1997). A Tutorial on the Diffusibility and Reactivity of Free Nitric Oxide. *Nitric Oxide* **1**, 18-30.
- Lane N. (2002). *Oxygen: The Molecule that Made the World*. Oxford University Press, New York, United States of America.
- Liao L-D, Tsytsarev V, Delgado-Martínez I, Li M-L, Erzurumlu R, Vipin A, Orellana J, Lin Y-R, Lai H-Y & Chen Y-Y. (2013). Neurovascular coupling: *in-vivo* optical techniques for functional brain imaging. *Biomedical Engineering Online* **12**, 38-57.
- Losonczy G, Mucha I, Müller V, Kriston T, Ungvári Z, Tornoci L, Rosivall L & Venuto R. (1996). The vasoconstrictor effects of L-NAME, a nitric oxide synthase inhibitor, in pregnant rabbits. *British Journal of Pharmacology* **118**, 1012-1018.
- Lowry J & O'Neill R. (2006). Neuroanalytical chemistry *in-vivo* using electrochemical sensors. In *Encyclopedia of Sensors*, pp. 501-524. American Scientific Publishers, United States of America.
- Lowry JP, Boutelle MG & Fillenz M. (1997). Measurement of brain tissue oxygen at a carbon paste electrode can serve as an index of increases in regional cerebral blood flow. *Journal of Neuroscience Methods* **71**, 177-182.
- Lowry JP, Boutelle MG, O'Neill RD & Fillenz M. (1996). Characterisation of carbon paste electrodes *in-vitro* for simultaneous amperometric measurement of changes in oxygen and ascorbic acid concentrations *in-vivo*. *Analyst* **121**, 761-766.
- Lowry JP, Griffin K, McHugh SB, Lowe AS, Tricklebank M & Sibson NR. (2010). Real-time electrochemical monitoring of brain tissue oxygen: A surrogate for functional magnetic resonance imaging in rodents. *Neuroimage* **52**, 549-555.

- Luebbers D. (1996). Oxygen electrodes and optodes and their application *in-vivo*. In *Oxygen Transport to Tissue XVII*, pp. 13-34. Springer, United States of America.
- Marcoux LS, Prater KB, Prater BG & Adams RN. (1965). A Nonaqueous Carbon Paste Electrode. *Analytical Chemistry* **37**, 1446-1447.
- Marletta MA. (1993). Nitric oxide synthase structure and mechanism. *Journal of Biological Chemistry* **268**, 12231-12234.
- Miilsch A & Busse R. (1990). NG-nitro-L-arginine (N5-[imino (nitroamino) methyl]-L-ornithine) impairs endothelium-dependent dilations by inhibiting cytosolic nitric oxide synthesis from L-arginine. *Naunyn-Schmiedeberg's Archives of Pharmacology* **341**, 143-147.
- Miller MJ, Sadowska-Krowicka H, Chotinaruemol S, Kakkis JL & Clark DA. (1993). Amelioration of chronic ileitis by nitric oxide synthase inhibition. *Journal of Pharmacology and Experimental Therapeutics* **264**, 11-16.
- Moreno A, Jago P, de la Cruz F & Canals S. (2013). Neurophysiological, metabolic and cellular compartments that drive neurovascular coupling and neuroimaging signals. *Frontiers in Neuroenergetics* **5**, 1-7.
- Mulvey JM, Dorsch NW, Mudaliar Y & Lang EW. (2004). Multimodality monitoring in severe traumatic brain injury. *Neurocritical care* **1**, 391-402.
- Mungrue IN, Bredt DS, Stewart DJ & Husain M. (2003). From molecules to mammals: what's NOS got to do with it? *Acta Physiologica Scandinavica* **179**, 123-135.
- Murray MD & Darvell BW. (1993). The evolution of the complete denture base. Theories of complete denture retention — A review. Part 3. *Australian Dental Journal* **38**, 389-393.
- Nayak RR, Lee KY, Shanmugaraj AM & Ryu SH. (2007). Synthesis and characterisation of styrene grafted carbon nanotube and its polystyrene nanocomposite. *European Polymer Journal* **43**, 4916-4923.
- O'Neill RD & Lowry JP. (2006). Voltammetry *In-Vivo* for Chemical Analysis of the Living Brain. In *Encyclopedia of Analytical Chemistry*. John Wiley & Sons, Ltd, United Kingdom.
- Ormonde DE & O'Neill RD. (1989). Altered response of carbon paste electrodes after contact with brain tissue: Implications for modified electrode use *in-vivo*. *Journal of Electroanalytical Chemistry and Interfacial Electrochemistry* **261**, 463-469.

- Ormonde DE & O'Neill RD. (1990). The oxidation of ascorbic acid at carbon paste electrodes: Modified response following contact with surfactant, lipid and brain tissue. *Journal of Electroanalytical Chemistry and Interfacial Electrochemistry* **279**, 109-121.
- Palmer RM, Ferrige AG & Moncada S. (1987). Nitric oxide release accounts for the biological activity of endothelium-derived relaxing factor. *Nature* **327**, 524-526.
- Pasley BN & Freeman RD. (2008). Neurovascular coupling. *Scholarpedia* **3**, 5340.
- Piknova B, Kocharyan A, Schechter AN & Silva AC. (2011). The role of nitrite in neurovascular coupling. *Brain Research* **1407**, 62-68.
- Pontié M, Bedioui F & Devynck J. (1999). New Composite Modified Carbon Microfibers for Sensitive and Selective Determination of Physiologically Relevant Concentrations of Nitric Oxide in Solution. *Electroanalysis* **11**, 845-850.
- Pontié M, Gobin C, Pauporté T, Bedioui F & Devynck J. (2000). Electrochemical nitric oxide microsensors: sensitivity and selectivity characterisation. *Analytica Chimica Acta* **411**, 175-185.
- Rees D, Palmer R, Schulz R, Hodson H & Moncada S. (1990a). Characterization of three inhibitors of endothelial nitric oxide synthase in vitro and in vivo. *British Journal of Pharmacology* **101**, 746-752.
- Rees DD, Palmer RMJ, Schulz R, Hodson HF & Moncada S. (1990b). Characterization of three inhibitors of endothelial nitric oxide synthase *in-vitro* and *in-vivo*. *British Journal of Pharmacology* **101**, 746-752.
- Santos RM, Lourenço CF, Ledo A, Barbosa RM & Laranjinha J. (2012). Nitric Oxide Inactivation Mechanisms in the Brain: Role in Bioenergetics and Neurodegeneration. *International Journal of Cell Biology* **2012**, 1-13.
- Sarac D, Sarac YS, Basoglu T, Yapici O & Yuzbasioglu E. (2006). The evaluation of microleakage and bond strength of a silicone-based resilient liner following denture base surface pretreatment. *The Journal of Prosthetic Dentistry* **95**, 143-151.
- Schmidt HHHW, Lohmann SM & Walter U. (1993). The nitric oxide and cGMP signal transduction system: regulation and mechanism of action. *Biochimica et Biophysica Acta (BBA) - Molecular Cell Research* **1178**, 153-175.
- Shibuki K & Okada D. (1991). Endogenous nitric oxide release required for long-term synaptic depression in the cerebellum. *Nature* **349**, 326-328.
- Soysal M, Muti M, Esen C, Gençdağ K, Aslan A, Erdem A & Karagözler AE. (2013). A Novel and Selective Methylene Blue Imprinted Polymer Modified Carbon Paste Electrode. *Electroanalysis* **25**, 1278-1285.

- Stevens WJ. (2004). Multimodal monitoring: head injury management using SjvO₂ and LICOX. *Journal of Neuroscience Nursing* **36**, 332-339.
- Tanaka K, Gotoh F, Gomi S, Takashima S, Mihara B, Shirai T, Nogawa S & Nagata E. (1991). Inhibition of nitric oxide synthesis induces a significant reduction in local cerebral blood flow in the rat. *Neuroscience Letters* **127**, 129-132.
- Tang C-M, Dichter M & Morad M. (1990). Modulation of the N-methyl-D-aspartate channel by extracellular H⁺. *Proceedings of the National Academy of Sciences* **87**, 6445-6449.
- Tonetto LL, Terzian AL, Del Bel EA, Guimarães FS & Resstel L. (2009). Inhibition of the NMDA receptor/Nitric Oxide pathway in the dorsolateral periaqueductal gray causes anxiolytic-like effects in rats submitted to the Vogel conflict test. *Behavioural and Brain Functions* **5**, 40.
- Traynelis SF & Cull-Candy SG. (1990). Proton inhibition of N-methyl-D-aspartate receptors in cerebellar neurons. *Nature* **345**, 347-350.
- Zhou L & Zhu D-Y. (2009). Neuronal nitric oxide synthase: structure, subcellular localization, regulation, and clinical implications. *Nitric Oxide* **20**, 223-230.

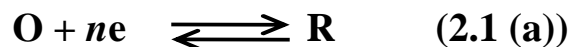


2. Theory

2.1 Introduction

The principal purpose of this thesis is the *in-vitro* characterisation and development of O₂ and NO sensors for the subsequent monitoring of O₂ and NO *in-vivo*. In order to achieve this, two voltammetric techniques were utilised throughout the course of the research, these being CV and CPA. The main technique utilised was CPA. This technique was chosen because of its high time resolution. This is of the utmost importance with regards to NO, because of the very reactive nature of the molecule and its very short half life of seconds *in-vivo* (Lancaster Jr, 1997). The two voltammetry methods are discussed in more detail in Section 2.3 and Section 2.4. The O₂ and NO sensors developed in this thesis were characterised using voltammetry, by their sensitivity (nA/μM) to the substrate, R² values and rejection of interferents.

Electrochemical analysis is based on the reactions taken place on the electrode surface. The working electrodes properties and characteristics can have a significant effect on the efficiency of the reactions that take place at the surface (Li & Miao, 2013). There are many factors affecting the electrodes reactions rate, like mass transport and electron transfer at the surface of the electrode (Bard & Faulkner, 2000). This is discussed in more detail in Section 2.2. In a general reaction at an electrode surface, a series of steps take place which cause the transformation of the dissolved oxidised species, ‘O’, to the reduced form, ‘R’ also in solution. Once all of the rates of the reaction steps in a series are equal, a steady, stable state is observed. The number of electrons is denoted as the letter *n*. Equation 2.1 (a) and Figure 2.1, display the reaction equation and pathway of reaction (Li & Miao, 2013).



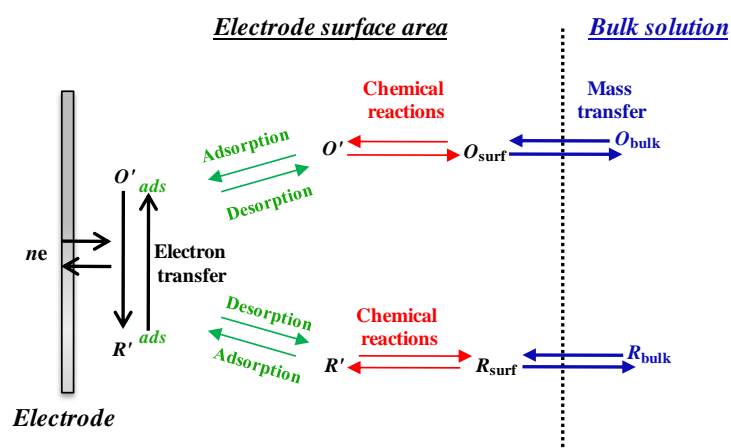


Figure 2.1: A redrawn schematic displaying the pathway of a general electrode reaction, taken from Bard *et al.*, (Bard & Faulkner, 2000).

The change in the concentration of a certain analyte in the extracellular fluid (ECF) over time is investigated in *in-vivo* voltammetry (Lowry *et al.*, 1996; Bolger *et al.*, 2011b; Finnerty *et al.*, 2012a). The Nernst equation is an essential equation formulated by Walther Nernst at the end of the nineteenth century. It is fundamental to electrochemistry and portrays the deviation of the electrode potential with the concentrations of oxidised and reduced species, [O] and [R], for an electrochemical reaction, assuming equilibrium conditions. The equation is depicted in Equation 2.1 (b), where E^* is the standard electrode potential, R, T, F and n denote the gas constant, temperature, the Faraday constant and the number of electrons, respectively (Bard *et al.*, 2012).

$$E_{eq} = E^* = \frac{RT}{nF} \ln \frac{[O]}{[R]} \quad (2.1 \text{ (b)})$$

2.2 Mass Transport

Mass transport as stated previously, is a factor that affects the rate of a reaction at the surface of an electrode. It is described as the movement of substances from one place in solution to another. It can come about due to a varying electrical or chemical potential at the two places or from movement of a volume factor of solution. Migration, diffusion and convection are the three processes involved with mass transport.

2.2.1 Migration

Migration is defined as the movement of charged species due to the presence of a gradient of electrical potential. Conversely, in these studies the presence of a large amount of background electrolyte (PBS, pH 7.4, see Section 3.7) removes the migration effects.

2.2.2 Diffusion

Diffusion takes place in all solutions and arises from the unbalanced concentrations of reagents. It is defined as the movement of molecules from an area of high concentration to a region of low concentration. The rate of the diffusion movement can be determined by Fick's first law depicted in Equation 2.2.2 (a) which states that the flux is proportional to the concentration gradient.

$$J = -D \frac{\partial c}{\partial x} \quad (2.2.2 \text{ (a)})$$

Where J denotes the diffusional flux of the species, D is the diffusion coefficient, the negative sign signifies the material moving down a concentration gradient i.e. moving from a high concentration to a low concentration and $\partial c/\partial x$ stands for the concentration gradient in direction x . However, in many experiments it is necessary to determine how the

concentration of the material differs as a function of time and that is where Fick's second law comes in. It is formulated from Fick's first law and is depicted in Equation 2.2.2 (b).

$$\frac{\partial c}{\partial t} = D \frac{\partial^2 c}{\partial x^2} \quad (2.2.2 \text{ (b)})$$

During the progression of a reaction, a concentration gradient may be created due to one of the species being consumed. However, in the case of microelectrodes that contain diameters in the 5-300 μm range (O'Neill *et al.*, 1998), currents are small and minimal substrate is consumed yielding a steady state response i.e. $\left(\frac{\partial c}{\partial t}\right) = 0$, no change in c with t .

For planar electrodes, which are equally available to species from the bulk solution, the changing current with time calculated from Fick's second law, results in the Cottrell equation (Equation 2.2.2 (c))

$$I = nFAJ = \frac{nFAD^{1/2}c_{\infty}}{(\pi t)^{1/2}} \quad (2.2.2 \text{ (c)})$$

with I the current measured at time t at the electrodes active surface of area A , being directly proportional to c_{∞} , the bulk concentration of the electroactive species. J is the flux, n is equal to the number of electrons, D is the diffusion coefficient and F is the Faraday constant.

For any coordinated system, a Laplace operator is substituted into Equation 2.2.2 (d) to determine the flux for all electrode geometries giving,

$$J = -D\nabla^2 c \quad (2.2.2 \text{ (d)})$$

and as a result, Fick's second law of diffusion for any geometry, becomes

$$\frac{\partial c}{\partial t} = D\nabla^2 c \quad (2.2.2 (e))$$

In this thesis, since all electrodes utilised had disk surfaces, the equation assigned was

$$\frac{\partial^2 c}{\partial r^2} + \frac{1}{r} \frac{\partial c}{\partial r} + \frac{\partial^2 c}{\partial z^2} \quad (2.2.2 (f))$$

The solution to all the diffusion equations requires that initial conditions (values at $t = 0$) and two boundary conditions (conditions associated with certain values of the spatial coordinates) be obeyed.

Initial conditions ($t = 0$) and boundary conditions

Initial conditions:

Prior to the beginning of experiments at time 0 ($t = 0$), homogeneity of the solution can be expressed by these conditions. If species O has a bulk concentration of C_o^* that is distributed evenly, the initial condition for all x values can be expressed as

$$C_o(x, 0) = C_o^* \quad (2.2.2 (g))$$

If R is not present initially then for all values of x

$$C_R(x, 0) = 0 \quad (2.2.2 \text{ (h)})$$

Semi-infinite boundary conditions:

The electrochemical cell walls are usually large distances away, contrasting to the diffusion path of the electrode, so one can hypothesise that the concentration reaches a constant value at large distances from the electrode at all values for t.

$$\lim_{x \rightarrow \infty} C_O(x, t) = C_O^* \quad (2.2.2 \text{ (i)})$$

As R is not present in solution at the beginning of the experiment, the equation then becomes,

$$\lim_{x \rightarrow \infty} C_R(x, t) = 0 \quad (2.2.2 \text{ (j)})$$

Boundary conditions:

When determining the diffusion limited current subsequent to a controlled potential, a current response arises when there is no electrode reaction occurring, to when all the electroactive species have reacted.

$$D_O \left[\frac{\partial C_O(x, t)}{\partial x} \right]_{x=0} + D_R \left[\frac{\partial C_R(x, t)}{\partial x} \right]_{x=0} = 0 \quad (2.2.2 (k))$$

If the current is controlled, the variation in potential is registered

$$-J_O(0, t) = \frac{i}{nFA} = D_O \left[\frac{\partial C_O(x, t)}{\partial x} \right]_{x=0} \quad (2.2.2 (l))$$

with i denoting current, n representing the number of transferred electrons, F signifying the Faraday constant and A indicative of the area of the active surface of the electrode.

2.2.3 Convection

Convection is defined as the stirring or the motion of fluid from an external source. Fluid can flow from a cause of natural convection which involves density gradients and can also occur from forced convection. These types of movement of species can be discounted from the thesis as all steady state currents were only recorded in quiescent solutions.

2.3 Cyclic Voltammetry (CV)

CV is the most broadly used measuring method in electrochemistry. It is most often the first technique utilised for attaining qualitative information regarding electrochemical reactions. It can offer information about the thermodynamics of redox processes, the kinetics of electron transfer reactions and the adsorption processes. In this thesis, CV was utilised to determine the redox potentials of the electroactive species in question (i.e. O_2). A CV is performed in a quiescent (unstirred) solution, where only diffusional transport of material influence the scan and the potential is scanned linearly using a triangular waveform, which is depicted in Figure 2.3 (a).

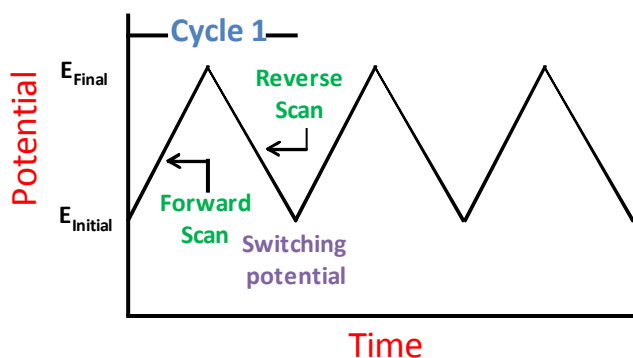


Figure 2.3 (a): Potential vs. time triangular shaped waveform signal in a CV experiment, redrawn from (Wang, 2006).

From an initial potential (E_i) where no oxidation takes place, a potential is applied using a fixed scan rate (ν) until a maximum potential (E_{\max}) is reached, where electron transfer occurs more quickly. The species that has been oxidised in the forward scan is then reduced back to the starting potential by inverting the sweep. There is generation of two types of current when operating CV called the Faradaic current (i_f) and the capacitance current (i_c). The (i_f) is produced from the electrochemical reactions that take place at the surface of the electrode at the varying potentials whilst the (i_c), otherwise known as the background current, does not involve any chemical reactions and never dissipates. It is necessary to subtract the background current from the overall current in order to determine a characteristic CV of a specific analyte in question.

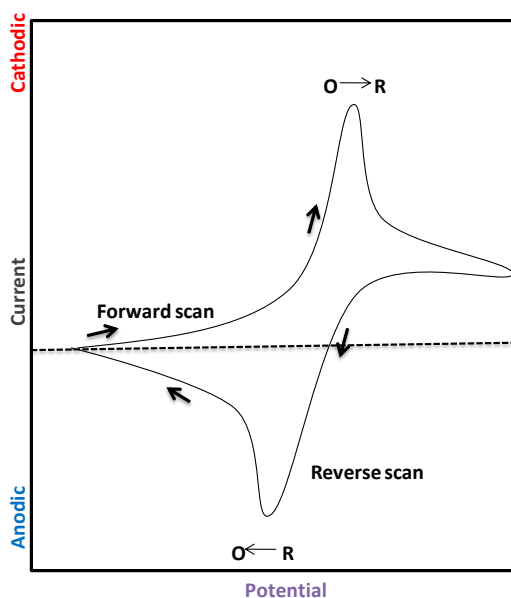


Figure 2.3 (b): Typical current-potential profile for a CV of a reversible redox species redrawn from Wang, 2006)

Figure 2.3 (b) illustrates the general response obtained for a reversible redox couple during a single potential cycle and describes the system in Equation 2.1 (a). The voltammogram begins at a value where no electron transfer takes place. As the applied potential is swept to more positive potentials, values are reached that are capable of inducing electron transfer, until a peak is reached. After traversing the potential region where the reduction process takes place, the reduced (R) molecules are reoxidised back to the oxidised (O) molecules, resulting in an anodic peak (Wang, 2006).

2.4 Constant Potential Amperometry (CPA)

During the course of this project, CPA was the most frequently employed technique. In CPA, the current is held at a constant potential that has been previously determined by CV to cause oxidation or reduction of the substance of interest at the surface of the sensor. The electroactive species that are under investigation undergo electron transfer at this potential and give rise to a current. CPA is similar to CV in that diffusion is assumed to be the only form of mass transport in the system (see Section 2.3), which leads to a steady-state diffusion-limited current. Amperometric currents can be constantly measured at the electrode, as the current due to analyte oxidation or reduction is directly proportional to the analyte concentration at all times. With CPA, high temporal resolution can be achieved and also the sampling rate can resolve signals on a sub-millisecond time scale (Hermans, 2007). All of the qualities associated with this technique make it ideal for the *in-vitro/in-vivo* experiments undertaken in this body of research.

Adsorption of reactants onto the surface of the sensor is not a concern with CPA, as the species are electrolysed rapidly when they come in contact with the electrode. Therefore adsorption processes do not hamper the response to the concentration changes of the analyte as it occurs. Amperometry can be regarded as a sweep technique where $v = 0$ and E_{\min} is at high overpotential values. With $v = 0$, the diffusion-limited current for a reversible or irreversible reaction is given by Equation 2.4 (a).

$$i_{ss} = \frac{nFACD}{r} \quad (2.4 \text{ (a)})$$

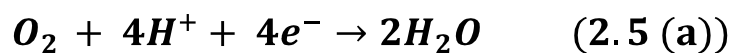
where the i_{ss} is the steady-state current, n is the number of electrons, A is the electrode area, D is the diffusion coefficient, F is the Faraday constant, C is the concentration and r is the radius. However, additional factors such as the geometry or the insulation thickness (Dayton *et al.*, 1980) of the electrode have an effect on the steady-state current and as a result a geometric factor, G , is incorporated into Equation (2.4 (b))

$$i_{ss} = \frac{GnFACD}{r} \quad (2.4 \text{ (b)})$$

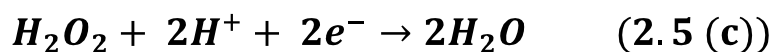
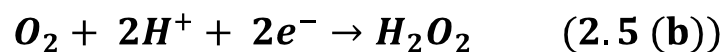
The resulting current is directly proportional to the diffusion coefficient and the substrate concentration.

2.5 Measurement of dissolved O₂

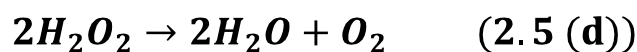
The O₂ reduction reaction (ORR) plays a vital role in life processes such as biological respiration and in energy converting systems for example, fuel cells (Song & Zhang, 2008). A number of mechanisms have been proposed for the reaction of the electrocatalytic reduction of O₂ at the surface of noble metal working electrodes; however, there is still uncertainty as to which mechanism is accurate. Originally, Damjanovic, *et al.*, proposed a four-electron transfer mechanism (Damjanovic *et al.*, 1967), which is depicted in Equation (2.5 (a)).



However, a two-step mechanism for the reduction of O₂ at the surface of a metal electrode has also been proposed also (Hoare, 1968) and they are illustrated in Equation (2.5 (b)) and (2.5 (c)).



The four-electron transfer pathway includes a number of steps where O_2 is reduced to OH^- or H_2O . A peroxide intermediate may be involved in the reduction steps which adsorbs on the surface of the electrode, however, this does not result in peroxide in the solution phase. With regards to the two electron transfer pathway, peroxide species are present in the solution phase. The resulting O_2 from the decomposition of these species (see Equation 2.5 (b)) in the solution is recycled through the reaction depicted in Equation 2.5 (c) and then the overall reaction is the four-electron pathway.



2.6 Polymerisation of Methyl methacrylate (MMA)

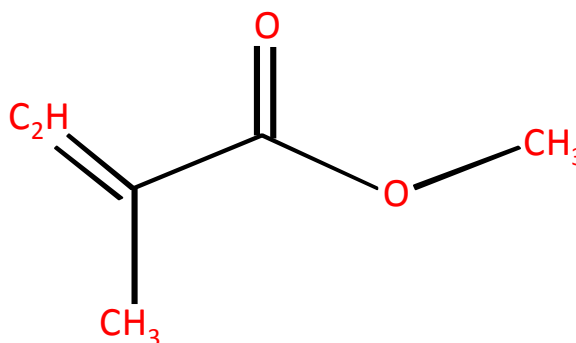


Figure 2.6 (a): Illustration of MMA molecule

The polymerisation of MMA can be produced utilising a variety of polymerisation mechanisms. The most common technique is the free radical polymerisation of MMA. The free radical polymerisation of acrylates and methacrylates is a chain polymerisation across the double bond of the monomer (Figure 2.6 (a)). Application of an initiator such as azodiisobutyronitrile (AIBN) has been demonstrated for the polymerisation of MMA and is

very common (Zhu *et al.*, 1990a; Hong *et al.*, 2002; Chen *et al.*, 2004; Yoshida, 2010). Figure 2.6 (b) displays the mechanism by which MMA is polymerised with AIBN.

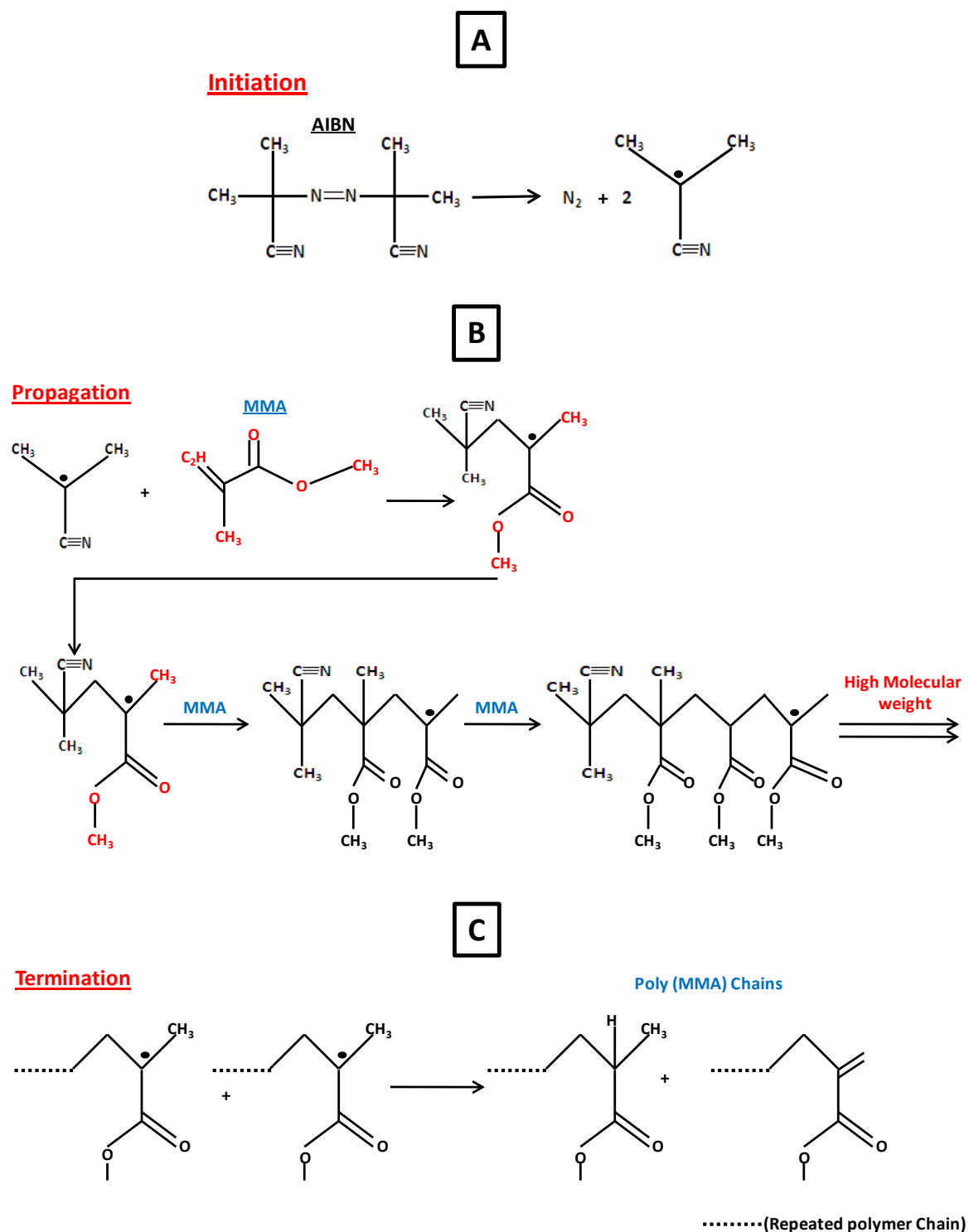


Figure 2.6 (b): Mechanism of radical polymerisation of MMA with AIBN as the initiator (A): Initiation (B): Propagation and (C): Termination.

The polymerisation of MMA can be initiated with light or δ -radiation. The photo initiation of MMA using ultraviolet (UV) or visible light can be performed independently, without the use of sensitizers. It has not yet been determined whether the photo induced polymerisation is by a free radical mechanism or by an excited state mechanism (Gruber, 1992). In this body of research, the polymerisation of MMA was undertaken to try and achieve a more solid composite within the cavity of the CPE. Thus, MMA was polymerised under UV light when manufacturing the MMA modified CPE (see Section 3.4.2).

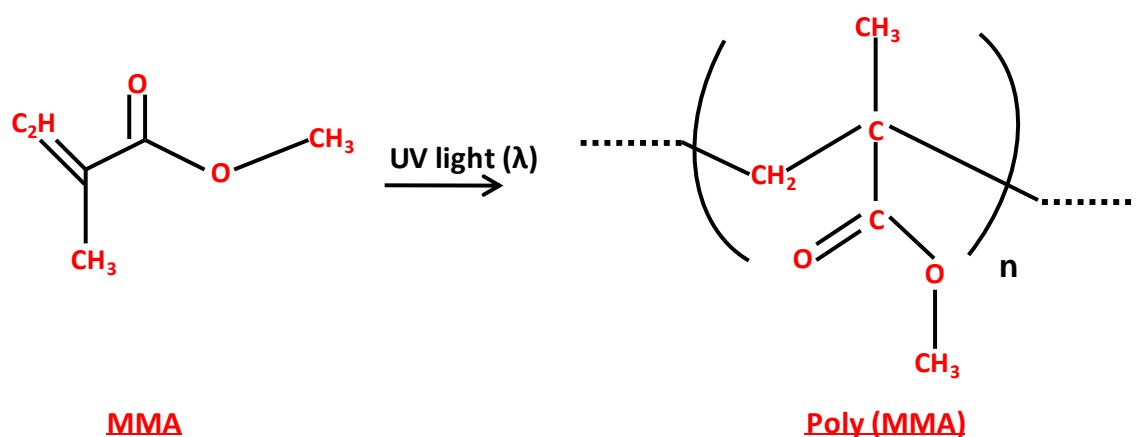


Figure 2.6 (c): The polymerisation of MMA by UV light

2.7 Electropolymerisation of *o*-Phenylenediamine (*o*-PD)

Poly-*o*-phenylenediamine (PPD) can be integrated into the design of a sensor by using it either as a conducting polymer or an insulating polymer. Ariffin *et al.*, incorporated it into a sensor design as a conducting polymer film, for the detection of H_2O_2 using Electrochemical Impedance Spectroscopy (Ariffin *et al.*, 2012). Utilising PPD as an insulating polymer layer has been demonstrated with glucose oxidase biosensors (Lowry *et al.*, 1994; Lowry & O'Neill, 1994). The NO sensors (Type 2 and Type 3 NO sensor) investigated in this body of research contain an insulating layer of PPD in their design also. The PPD layer was applied by the electropolymerisation in a neutral electrolyte (see

Section 3.4.5.2). This procedure was demonstrated by Malitesta *et al.*, (Malitesta *et al.*, 1990). This insulating layer has demonstrated the ability to block out any unwanted species that are larger than the *o*-PD monomer (Friedemann *et al.*, 1996; O'Neill *et al.*, 2008; Govindarajan *et al.*, 2013). The PPD layer was incorporated into the design of these novel sensors to allow for a reduction in the number of Nafion pre-coats annealed onto the electrode surface without compromising the selectivity of the sensor. This is important as it will decrease the thickness of the diffusion layer surrounding the electrode surface and allow for quicker response times in comparison to the extensively characterised Type 1 NO sensor.

Two different structures of the insulating form of PPD have been hypothesised, as it has not been determined what the actual structure looks like. A 'ladder' like structure where the amino groups are condensed within the benzene rings adjacent to each other along the polymer chain (Chiba *et al.*, 1987) (see Figure 2.7, structure A) and an 'open' 1,4-substituted benzenoid-quinoid structure (Yano, 1995) (see Figure 2.7, structure B) have been assumed. The speculated 'open' structure of PPD has been reported as the more dominant structure (Losito *et al.*, 2003).

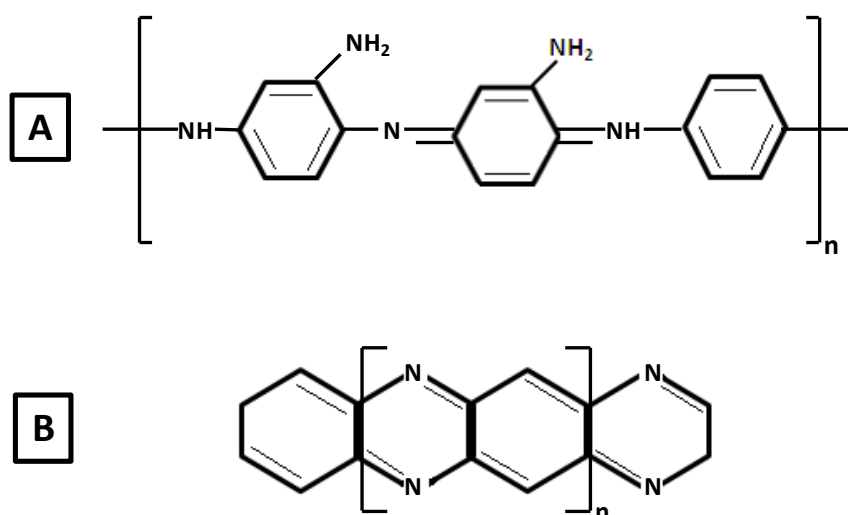


Figure 2.7: Possible structures for the polymeric form of *o*-PD

2.8 Ascorbic acid (AA)

AA is essential for normal physiological function and is vital for tissue growth and the healing of wounds (Iqbal *et al.*, 2004). It is the main electroactive compound that can inhibit an electrode's ability to detect a particular analyte of interest. It is in abundance in the ECF of the brain at a concentration of approximately 500 μM (Miele & Fillenz, 1996b). It is readily oxidised at metal electrodes having an $E_{1/2}$ between -100 to +400 mV vs. SCE (O'Neill *et al.*, 1998). A $2e^-$ process that results in the production of L-dehydroascorbic acid is the mechanism associated with the reaction of AA. An electro-inactive open chain product (L-2-3-diketogulonic acid) is formed upon hydrolyses of L-dehydroascorbic acid. The mechanism for the reaction is illustrated in Figure 2.8.

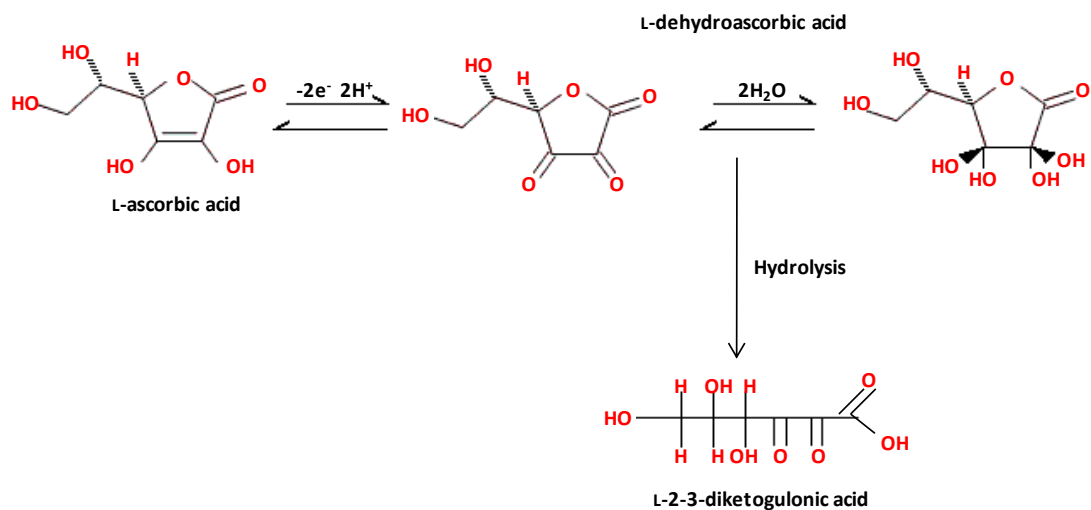


Figure 2.8: Reaction scheme for the oxidation of ascorbic acid

2.9 Data Analysis

On cessation of the experiments undertaken with CPA, the data was analysed using linear regression. The regression was applied after the average steady state current value was obtained and this value was then plotted graphically, current response against substrate concentration.

2.9.1 Linear Regression

Linear regression is effectively the plotting of the line that minimises the sum of the squares of the vertical distances of the points from the line utilising GraphPad Prism (see Section 3.2).

2.9.2 Statistical Analysis

Statistical analysis is carried out in order to determine whether two results are statistically different. The *t*-tests and one-way ANOVA tests were utilised as the method of analysis during the course of this research. The two forms of *t*-tests utilised were paired *t*-tests and unpaired *t*-tests. If the electrodes differed only by an intervention (i.e. time, as per time stability experiments) paired *t*-tests were employed. Unpaired *t*-tests were performed on electrodes that differed by their treatments (i.e. comparing electrodes with different designs or different outer membranes). One-way ANOVA was utilised when multiple comparisons needed to be carried out. These tests were performed using GraphPad Prism and yielded a resulting *P* value. Table 2.9.2, details how the *P* value correlates to how significantly different/not significantly different, a result is. This value allows one to decide whether the results observed are significantly different.

<i>P</i> value	Significance	No. of asterisks
< 0.001	Extremely significant	***
0.001 to 0.01	Very significant	**
0.01 to 0.05	Significant	*
> 0.05	Not significant	ns

Table 2.9.2: A table displaying a summary of the correspondence of the *P* value to the number of number of asterisks.

The R^2 value is a fraction between 0.0 and 1.0 that has no units. It is the measure of the goodness of fit of the data points to a line where $0 < R^2 < 1$. An R^2 value of 0 means that knowing x does not help one predict y , there is no linear relationship between x and y data values in the graph. An R^2 value of 1 indicates that all points lie exactly on the straight line with no scatter. Knowing x will allow one to predict y .

2.10 References

- Ariffin AA, O'Neill RD, Yahya M & Zain ZM. (2012). Electropolymerization of *o*-Phenylenediamine and its Use for Detection on Hydrogen Peroxide and Ascorbic Acid by Electrochemical Impedance Spectroscopy. *International Journal of Electrochemical Science* **7**, 10154-10163.
- Bard AJ & Faulkner LR. (2000). *Electrochemical Methods: Fundamentals and Applications*. Wiley, United States of America.
- Bard AJ, Inzelt G & Scholz F. (2012). *Electrochemical Dictionary*. Springer New York.
- Bolger FB, McHugh SB, Bennett R, Li J, Ishiwari K, Francois J, Conway MW, Gilmour G, Bannerman DM, Fillenz M, Tricklebank M & Lowry JP. (2011b). Characterisation of carbon paste electrodes for real-time amperometric monitoring of brain tissue oxygen. *Journal of Neuroscience Methods* **195**, 135-142.
- Chen G, Zhu X, Cheng Z, Xu W & Lu J. (2004). Controlled/"living" radical polymerization of methyl methacrylate using AIBN as the initiator under microwave irradiation. *Radiation Physics and Chemistry* **69**, 129-135.
- Chiba K, Ohsaka T, Ohnuki Y & Oyama N. (1987). Electrochemical preparation of a ladder polymer containing phenazine rings. *Journal of Electroanalytical Chemistry and Interfacial Electrochemistry* **219**, 117-124.
- Damjanovic A, Genshaw MA & Bockris JOM. (1967). The Mechanism of Oxygen Reduction at Platinum in Alkaline Solutions with Special Reference to H₂O₂. *Journal of The Electrochemical Society* **114**, 1107-1112.
- Dayton MA, Brown JC, Stutts KJ & Wightman RM. (1980). Faradaic electrochemistry at microvoltammetric electrodes. *Analytical Chemistry* **52**, 946-950.
- Finnerty NJ, O'Riordan SL, Brown FO, Serra PA, O'Neill RD & Lowry JP. (2012a). *In-vivo* characterisation of a Nafion[®]-modified Pt electrode for real-time nitric oxide monitoring in brain extracellular fluid. *Analytical Methods* **4**, 550-557.
- Friedemann MN, Robinson SW & Gerhardt GA. (1996). *o*-Phenylenediamine-Modified Carbon Fiber Electrodes for the Detection of Nitric Oxide. *Analytical Chemistry* **68**, 2621-2628.
- Govindarajan S, McNeil CJ, Lowry JP, McMahon CP & O'Neill RD. (2013). Highly selective and stable microdisc biosensors for l-glutamate monitoring. *Sensors and Actuators B: Chemical* **178**, 606-614.
- Gruber H. (1992). Photoinitiators for free radical polymerization. *Progress in polymer Science* **17**, 953-1044.

- Hermans A. (2007). *Fabrication and Applications of Dopamine-sensitive Electrodes*. ProQuest, 2007, United Kingdom.
- Hoare JP. (1968). *The electrochemistry of oxygen*. Interscience Publishers, California, United States of America.
- Hong K, Zhang H, Mays JW, Visser AE, Brazel CS, Holbrey JD, Reichert WM & Rogers RD. (2002). Conventional free radical polymerization in room temperature ionic liquids: a green approach to commodity polymers with practical advantages. *Chemical Communications* **13**, 1368-1369.
- Iqbal K, Khan A & Khattak M. (2004). Biological significance of ascorbic acid (vitamin C) in human health—a review. *Pakistan Journal of Nutrition* **3**, 5-13.
- Lancaster Jr JR. (1997). A Tutorial on the Diffusibility and Reactivity of Free Nitric Oxide. *Nitric Oxide* **1**, 18-30.
- Li G & Miao P. (2013). Theoretical Background of Electrochemical Analysis. In *Electrochemical Analysis of Proteins and Cells*, pp. 5-18. Springer Berlin Heidelberg, New York, Unites States of America.
- Losito I, Palmisano F & Zambonin PG. (2003). o-Phenylenediamine electropolymerization by cyclic voltammetry combined with electrospray ionization-ion trap mass spectrometry. *Analytical Chemistry* **75**, 4988-4995.
- Lowry JP, Boutelle MG, O'Neill RD & Fillenz M. (1996). Characterisation of carbon paste electrodes *in-vitro* for simultaneous amperometric measurement of changes in oxygen and ascorbic acid concentrations *in-vivo*. *Analyst* **121**, 761-766.
- Lowry JP, McAteer K, El Atrash SS, Duff A & O'Neill RD. (1994). Characterization of glucose oxidase-modified poly(o-phenylenediamine)-coated electrodes *in-vitro* and *in-vivo*: homogeneous interference by ascorbic acid in hydrogen peroxide detection. *Analytical Chemistry* **66**, 1754-1761.
- Lowry JP & O'Neill RD. (1994). Partial characterization *in-vitro* of glucose oxidase-modified poly(phenylenediamine)-coated electrodes for neurochemical analysis *in-vivo*. *Electroanalysis* **6**, 369-379.
- Malitesta C, Palmisano F, Torsi L & Zambonin PG. (1990). Glucose fast-response amperometric sensor based on glucose oxidase immobilized in an electropolymerized poly(o-phenylenediamine) film. *Analytical Chemistry* **62**, 2735-2740.
- Miele M & Fillenz M. (1996a). *In-vivo* determination of extracellular brain ascorbate. *Journal of Neuroscience Methods* **70**, 15-19.

- O'Neill RD, Lowry JP & Mas M. (1998). Monitoring Brain Chemistry *in-vivo*: Voltammetric Techniques, Sensors, and Behavioral Applications. *Critical Reviews™ in Neurobiology* **12**, 69-127.
- O'Neill RD, Rocchitta G, McMahon CP, Serra PA & Lowry JP. (2008). Designing sensitive and selective polymer/enzyme composite biosensors for brain monitoring *in-vivo*. *Trends in Analytical Chemistry* **27**, 78-88.
- Song C & Zhang J. (2008). Electrocatalytic oxygen reduction reaction. In *PEM fuel cell electrocatalysts and catalyst layers*, pp. 89-134. Springer, New York, United States of America.
- Wang J. (2006). *Analytical Electrochemistry*. Wiley, United States of America.
- Yano J. (1995). Electrochemical and structural studies on soluble and conducting polymer from o-phenylenediamine. *Journal of Polymer Science Part A: Polymer Chemistry* **33**, 2435-2441.
- Yoshida E. (2010). Effect of azoinitiators on nitroxide-mediated photo-living radical polymerization of methyl methacrylate. *Colloid and Polymer Science* **288**, 341-345.
- Zhu S, Tian Y, Hamielec AE & Eaton DR. (1990b). Radical trapping and termination in free-radical polymerization of methyl methacrylate. *Macromolecules* **23**, 1144-1150.



3. Experimental

3.1 Introduction

In this chapter, details of the *in-vitro* and *in-vivo* design and characterisation of both O₂ and NO sensors are described. The O₂ and NO sensors are based on CPE's (Lowry *et al.*, 1996) and platinum (Pt) electrodes (Brown & Lowry, 2003) respectively. A CPE that included the monomers styrene (Sty) or methyl methacrylate (MMA) was developed in order to prevent the removal of the pasting oil from the CPE. Ormonde and O'Neill have demonstrated that when the CPEs are in the *in-vivo* environment, lipids present, remove the oil from the CPE surface leaving a carbon powder electrode (Ormonde & O'Neill, 1990). The incorporation of MMA and Sty has been demonstrated previously in the development of sensors by other research groups, (Chatzandroulis *et al.*, 2004a; Chatzandroulis *et al.*, 2005; Xu *et al.*, 2011). To prevent the potential interference from species found in the *in-vivo* environment, an *o*-phenylenediamine (*o*-PD) layer was incorporated into the NO sensor design. It was also hoped that this would decrease the diffusion layer of the existing Type 1 NO sensor (Brown *et al.*, 2009), thus improving the response time without compromising the sensitivity and selectivity. The inclusion of an *o*-PD layer for such purposes has been previously demonstrated in the design of glucose biosensors (Malitesta *et al.*, 1990). Porterfield and co-workers have previously described use of an NO selective probe system to monitor NO release from cultured macrophages which also incorporates NO and *o*-PD in the sensor design (Porterfield *et al.*, 2001).

Section 3.2 outlines the computer based instrumentation and equipment. A description of all the chemicals and solutions that are utilised throughout this project, are represented in section 3.3. Section 3.4 describes the manufacture of the sensors and the sensor modification is depicted in Section 3.5. The treatments and *in-vitro* characterisation of the sensors are presented in sections 3.6 and 3.7 respectively. Section 3.8 gives a detailed account of the procedures followed for the utilisation of these sensors *in-vivo*. The use of scanning electron microscopy (SEM) is outlined in Section 3.9. The synthesis of NO is presented in section 3.10 and any additional equipment used throughout the project is listed in section 3.11.

3.2 Computer Based Instrumentation and Computer Programs

Throughout the project, the data was collected via three main components. These included a computer, a powerlab[®] or e-corder and the potentiostat (biostat or quadstat). Electrochemical experiments (constant potential amperometry, (CPA) and cyclic voltammetry, (CV)) utilised the software packages LabChart[®] 6 and LabChart[®] for Mac version 6.1 (ADInstruments Ltd; Dunedin, New Zealand), eDAQ chart version 5.5.15 and EChem version 2.1.12 (eDAQ Pty Ltd; Denistone East, Australia). The graphical and statistical analysis of the data was performed using Microsoft Office Excel 2007 and GraphPad Prism[®] version 5.01 (GraphPad Software Inc. CA USA). This analysis included linear regression analysis and statistical analysis including paired and unpaired *t*-tests and one-way ANOVA analysis. For the statistical analysis carried out, a *P* value was obtained, which is the probability value indicating if the results obtained are significantly different. Table 3.2 details a summary of the significance values. The individual instrumentation components are described further in this Section. An image presenting the *in-vitro* set-up is displayed in Figure 3.2.

<i>P</i> value	Significance	No. of asterisks
< 0.001	Extremely significant	***
0.001 to 0.01	Very significant	**
0.01 to 0.05	Significant	*
> 0.05	Not significant	ns

Table 3.2: A table displaying a summary of the correspondence of the *P* value to the number of asterisks.



Figure 3.2: The *in-vitro* experimental set-up.

3.2.1 The Computer

3.2.1.1 In-Vitro data: A logiQ M760TG notebook with an Intel dual core processor running at 1.8GHz was utilised in the collection of the data.

3.2.1.2 In-Vivo data: A MAC OS X with an Intel core 2 duo processor running at 2.4GHz was employed for *in-vivo* data acquisition.

3.2.2 The Interface

An eight channel powerlab[®] 8/30 from (AD instruments Ltd; Dunedin, New Zealand) or an eight channel e-corder 821 from (eDAQ Pty Ltd; Denistone East, Australia) was employed. The e-corder 821 is displayed in Figure 3.2.2 below.



Figure 3.2.2: An image displaying the e-corder 821.

3.2.3 The Potentiostat

A four channel biostat from (ACM instruments; Cumbria, UK) or a software controlled four channel quadstat from (eDAQ Pty Ltd; Denistone East, Australia), was utilised throughout the project. The four channel quadstat is displayed in Figure 3.2.3.



Figure 3.2.3: An image displaying the quadstat 164.

3.2.4 Movement Meter

The movement meter (Figure 3.2.4) was employed during the *in-vivo* experiments to correlate the real-time monitored currents with movement of the animal. It comprises of a passive infrared (PIR) detector (Elite Security Products, Unit 7, Levis Trading Estate, Station Road, Stechford, Birmingham B33 9AE, UK), which connected directly to the data acquisition system (Powerlab[®]). The PIR detector consists of pyroelectric sensors and an electronic system. The sensors convert the optical signal that is being observed into an electrical signal that is processed within its electrical compartment and then analysed in the microprocessor (Kastek *et al.*, 2008). It was modified in-house with a microprocessor to enable a greater enhancement of the sensor, thereby recording more movement per second.

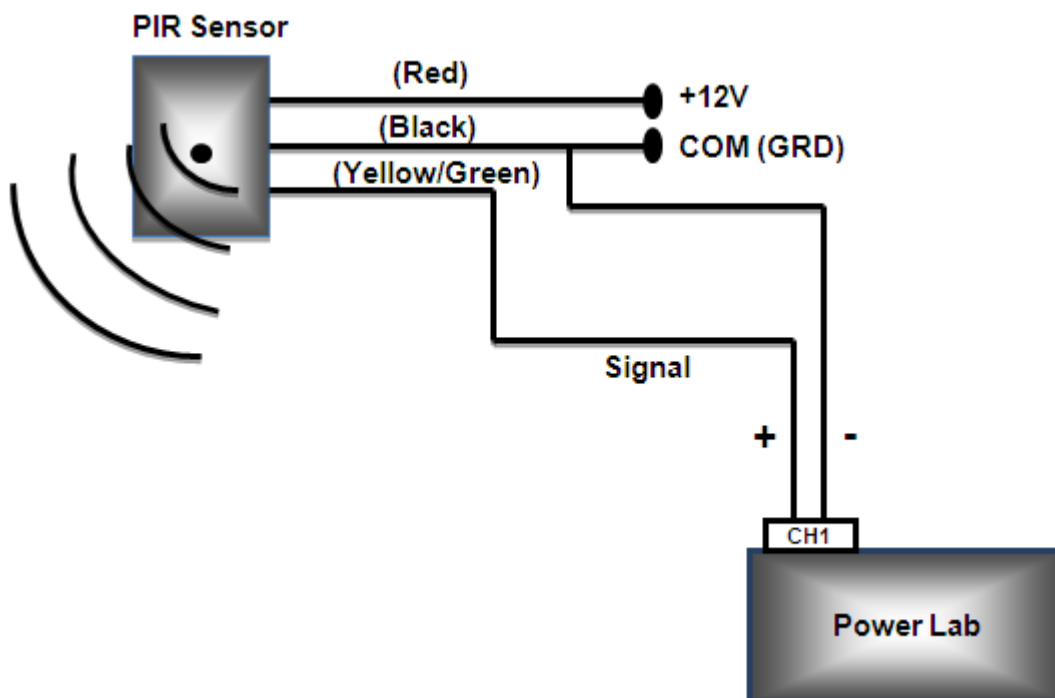


Figure 3.2.4: Schematic of the PIR Sensor.

3.3 Chemicals and Solutions

3.3.1 Chemicals

A list of *in-vitro* and *in-vivo* chemicals along with the relevant suppliers that were utilised throughout the course of the research project is shown below.

3.3.1.1 *In-Vitro* Chemicals

• Ascorbic acid	Sigma Aldrich [®] Co.
• Bovine serum albumin	Fluka Chemical Co.
• L-cysteine	Sigma Aldrich [®] Co.
• Dehydroascorbic acid	Sigma Aldrich [®] Co.
• 3, 4-Dihydroxyphenylacetic acid	Sigma Aldrich [®] Co.
• Dopamine	Sigma Aldrich [®] Co.
• L-glutathione	Sigma Aldrich [®] Co.
• Graphite powder	Sigma Aldrich [®] Co.
• Homovanillic acid	Sigma Aldrich [®] Co.
• Hydrogen peroxide 30% w/w ACS reagent	Sigma Aldrich [®] Co.
• 5-Hydroxyindoleacetic acid	Sigma Aldrich [®] Co.
• Methyl methacrylate 99 % solution	Sigma Aldrich [®] Co.
• Nafion [®] 5% in aliphatic alcohol	Sigma Aldrich [®] Co.
• N-1-naphthyl-ethylenediamine	Sigma Aldrich [®] Co.
• Nitric oxide gas	In House Synthesis
• Nitric oxide gas	BOC Gases
• Nitrogen gas	BOC Gases
• Oxygen gas	BOC Gases
• <i>o</i> -Phenylenediamine	Sigma Aldrich [®] Co.
• L- α -phosphatidylethanolamine	Sigma Aldrich [®] Co.

- Potassium hydroxide Sigma Aldrich[®] Co.
- Pyrogallol Sigma Aldrich[®] Co.
- Serotonin Sigma Aldrich[®] Co.
- Silicon oil Aldrich Chemical Co.
- Sodium chloride Sigma Aldrich[®] Co.
- Sodium hydroxide Sigma Aldrich[®] Co.
- Sodium nitrite Sigma Aldrich[®] Co.
- Sodium phosphate monobasic Sigma Aldrich[®] Co.
- Styrene ≥ 99 % solution Sigma Aldrich[®] Co.
- Sulfanilamide Sigma Aldrich[®] Co.
- Sulphuric acid (97%) Fisher Scientific
- Triton[®] X-100 Sigma Aldrich[®] Co.
- L-tryptophan Sigma Aldrich[®] Co.
- L-tyrosine Sigma Aldrich[®] Co.
- Uric acid Sigma Aldrich[®] Co.

3.3.1.2 *In-Vivo* Chemicals

- Acetazolamide (Diamox) Sigma Aldrich[®] Co.
- L-arginine Sigma Aldrich[®] Co.
- Buprenorphine hydrochloride (Temgesic[®]) Sigma Aldrich[®] Co.
- Chloral hydrate BDH Laboratory Supplies, UK
- Dentalon[®] Heraeus Kulzer GmbH
- Dimethyl sulfoxide Sigma Aldrich[®] Co.
- Isoflurane Abbott Laboratories, IRL.
- N (G)-nitro-L-arginine methyl ester Sigma Aldrich[®] Co.
- Sodium L-ascorbate Sigma Aldrich[®] Co.

3.3.2 Solutions

All solutions were prepared on the day that an experiment was carried out, unless otherwise stated. All solutions were made with deionised water denoted by H₂O, unless mentioned otherwise. The procedures for making each solution are outlined below in a separated *in-vitro* and *in-vivo* list.

3.3.2.1 In-Vitro Solutions

Bovine serum albumin (BSA)

A 10% (w/v) solution was prepared by dissolving 0.1 g in 1 mL H₂O.

Carbon paste

A solution containing 0.71 g of graphite powder and 250 µL of silicone oil was thoroughly mixed together. To ensure complete unification of the two components, a pestle and mortar were used to carry out the procedure for three hours.

Carbon (MMA) paste

A mixture of 0.0125 g of carbon paste was mixed with 10 µL of MMA (99 % solution) in order to get a uniform combination of the two components.

Carbon (Sty) paste

A solution of 0.0125g of carbon paste was mixed with 9 µL of Sty (≥ 99 % solution) to ensure full mixture of the paste and monomer.

Neutral Griess reagent

A reagent consisting of 0.4 mM N-1-naphthyl-ethylenediamine (NEDD) and 0.017 mM sulfanilamide (SULF) was prepared in air saturated 100 µM PBS, pH 7.4, containing 0.293 g SULF and 0.0104 g NEDD in 100 mL.

Nitric oxide (NO)

A stock solution of NO was prepared by bubbling it into H₂O and its subsequent concentration determined by UV spectroscopy.

o-Phenylenediamine (o-PD)

A 300 mM stock solution was made up using 0.324 g of o-PD in 10 mL of N₂ saturated phosphate buffer saline (PBS).

Phosphate buffered saline (PBS)

PBS was prepared by dissolving 8.9 g of sodium chloride (NaCl) (0.15 M), 1.76 g of sodium hydroxide (NaOH) (0.044 M) and 6.06 g of sodium phosphate (NaH₂PO₄·H₂O) (0.044 M) in 1 L of H₂O. The pH was then adjusted accordingly to 7.4.

L-α-phosphatidylethanolamine (PEA)

A 10% solution was prepared by dissolving 0.1 g in 1 mL H₂O.

Potassium hydroxide (KOH)

A 4 M KOH solution was prepared by dissolving 224 g of KOH in 1000 mL.

Pyrogallol 5% alkaline

A 5% stock solution was prepared in 4 M KOH (5 g/ 100 mL).

Sodium nitrite (NaNO₂)

A saturated stock solution of NaNO₂ was prepared in H₂O.

Sulphuric acid (H₂SO₄)

A 6 M H₂SO₄ stock solution was prepared from a 97% H₂SO₄ commercial solution. 329 mL of H₂SO₄ was added very carefully to H₂O and then made up to 1 L.

Triton[®] X-100

A 10% solution was made up by dissolving 0.1 mL in 1 mL H₂O.

3.3.2.2 Interferent Solutions

Ascorbic acid (AA)

A 0.1 M stock solution of AA was prepared by dissolving 0.176 g in 10 mL of H₂O.

L-cysteine

A 50 μM solution of L-cysteine was made up by mixing 0.024 g in 10 mL H₂O.

Dehydroascorbic acid (DHAA)

A 50 μM solution of DHAA was prepared by dissolving 0.0696 g in 10 mL H₂O.

3, 4-Dihydroxyphenylacetic acid (DOPAC)

A 100 μM solution of DOPAC was prepared by mixing 0.013 g in 10 mL H₂O.

Dopamine

A 0.05 μM solution was prepared by dissolving 0.000038 g in 10 mL H₂O.

L-glutathione

A 50 μM glutathione solution was made up by mixing 0.122 g of glutathione in 10 mL H₂O.

Homovanillic acid (HVA)

A 10 μM solution of HVA was prepared by dissolving 0.0073 g in 10 mL H₂O.

Hydrogen peroxide 30% w/w ACS reagent (H₂O₂)

A 100 mM stock solution was prepared by dissolving 0.56 g of H₂O₂ in 50 mL H₂O.

5-Hydroxyindoleacetic acid (5-HIAA)

A 50 μM solution was prepared by dissolving 0.038 g of 5-HIAA in 10 mL H₂O.

Nitrite (NO₂⁻)

A 100mM solution of NaNO₂ was prepared by mixing 0.17 g of NaNO₂ with 25 mL H₂O.

Serotonin (5-HT)

A 0.01 μM solution was made up by dissolving 0.0085 g of 5-HT in 100 mL H₂O.

L-tryptophan

A 100 μM solution was prepared using 0.082 g of L-tryptophan in 10 mL H₂O.

L-tyrosine

A 100 μM solution was prepared by dissolving 0.072 g of L-tyrosine in 10 mL H₂O.

Uric acid (UA)

A solution was prepared by mixing 0.038 g of UA in 10 mL H₂O.

3.3.2.3 In-Vivo Solutions

Acetazolamide (Diamox)

A 50 mg/kg solution was prepared by dissolving acetazolamide in a solution of 1 mL saline and 0.5 mL DMSO.

L-arginine

For systemic administration, 300 mg/kg was dissolved in 1 mL saline solution.

Buprenorphine hydrochloride (Temgesic[®])

A solution of 0.3 mg/mL Buprenorphine hydrochloride was injected in a volume of 1 mL/kg.

Chloral hydrate

A 350 mg/kg solution was prepared by dissolving chloral hydrate in 1 mL saline.

N (G)-nitro-L-arginine methyl ester (L-NAME)

For systemic administration, 30 mg/kg was made up in 1 mL saline solution.

Saline solution

A 0.9% solution was prepared by dissolving 0.9 g NaCl in 100 mL H₂O.

Sodium ascorbate

A 1 g/kg dose in a volume of 1 mL of saline was prepared. Sodium ascorbate is the preferred interferent to use, as AA can cause a significant irritation to the animal.

3.4 Electrode Preparation

3.4.1 Carbon Paste Electrode (CPE)

The construction of the CPEs involved 5 cm of Teflon[®] coated silver wire (200 μm bare diameter, 270 μm coated diameter (8T), Advent Research Materials; Oxford, UK). Using a scalpel blade, one end of the wire was carefully cut at a 90° angle. In order to solder the silver wire into a gold clip, 3 mm of Teflon[®] was taken from the opposing end of the silver wire for introduction to the clip. The gold clip provided electrical contact and rigidity for connection to the crocodile clips. The Teflon[®] was carefully pushed up the wire in order to create a 2mm cavity. The carbon paste (Section 3.3.2.1) was then packed into the compartment by intermittently dipping the electrode into a small portion of the paste and using a bare length of silver wire the carbon paste was pushed into the cavity of the electrode. This method was ceased when the paste was condensed into the cavity. Finally, a flat active surface was obtained by tapping the electrode on a hard surface. Figure 3.4.1 below displays an image of the CPE. Using a scalpel blade the two opposing ends of the wire were cut.

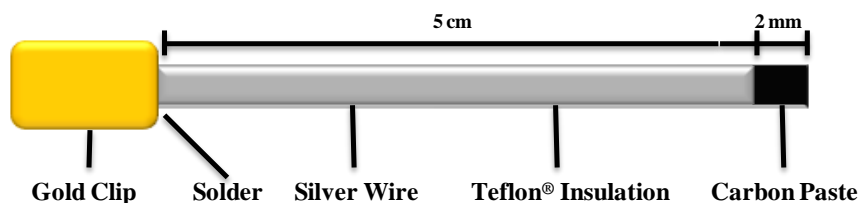


Figure 3.4.1: A schematic representation of a CPE

3.4.2 Methyl Methacrylate Modified CPE (MMCPE)

The CPE was constructed as described previously in Section 3.4.1. The CPE was then placed overnight in 2.5 mL of MMA in the fridge. Following this, the electrode was dipped into a homogenised mixture of MMA and carbon paste (Section 3.3.2.1), until it was fully compact. Finally, a flat active surface was obtained by tapping the electrode on a hard surface. Once the flat surface was obtained the electrodes were placed in an ultraviolet light (UV) cabinet (CV-006, UVItec Ltd, Cambridge, England) for thirty minutes. Below is an image representing the MMCPE (Figure 3.4.2).

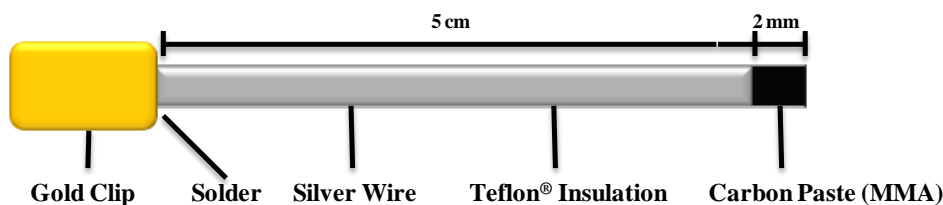


Figure 3.4.2: A schematic representation of a MMCPE.

3.4.3 Styrene Modified CPE (SMCPE)

The CPE was constructed as described previously in Section 3.4.1. The CPE was then placed overnight in 2.5 mL of Sty in the fridge. Following this, the electrode was dipped into a homogenised mixture of Sty and carbon paste (Section 3.3.2.1), until it was fully compact. Finally, a flat active surface was obtained by tapping the electrode on a hard surface. An image representing the SMCPE is depicted in Figure 3.4.3.

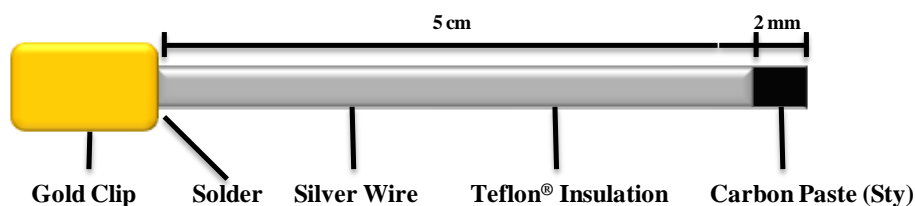


Figure 3.4.3: A schematic representing a SMCPE

3.4.4 Platinum (Pt) Working Electrodes

The platinum electrodes were constructed using 4 cm of Teflon[®] coated Pt/Ir (90%/ 10%) wire (125 μm bare diameter, 175 μm coated diameter (5T), Advent Research Materials, Oxford, UK). Using a scalpel blade, one end of the wire was carefully cut at a 90° angle to ensure an accurate flat active surface. In order to solder the wire into a gold clip, 3 mm of Teflon[®] was removed from the opposing end of the Pt wire for introduction to the clip. The gold clip provides electrical contact and rigidity for connection to the crocodile clips. The schematic of the Pt working electrode is shown in Figure 3.4.4.

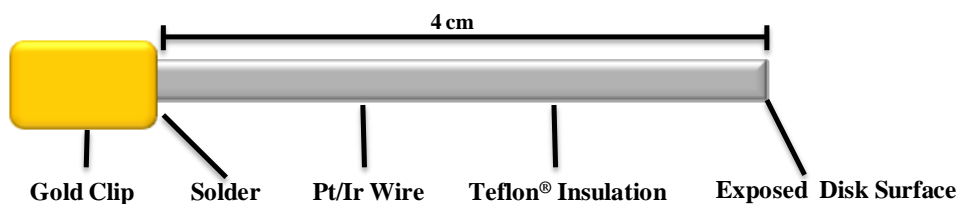


Figure 3.4.4: A schematic of a Pt electrode

3.4.5 Nitric Oxide (NO) Sensors

The NO sensors manufactured in this project were all Pt based electrodes modified by different combinations of Nafion[®] and *o*-PD. The manufacture of the Pt electrode prior to modification can be seen in Section 3.4.4. A pre-coat application method was utilised in the construction of each NO sensor, along with the modification of the electrodes with *o*-PD (see Section 3.4.5.1 and 3.4.5.2, respectively).

3.4.5.1 The Nafion[®] Pre-Coat Application

The pre-coat application method involved placing a fixed volume (5 μ L) of Nafion[®] on a clock glass using a syringe. The application of a Nafion[®] droplet was allowed to air dry at room temperature for five minutes. After solvent from the initial droplet had evaporated, further applications were placed on top of the original droplet. A concentrated layer of Nafion[®] was then formed on the clock glass. After 1-5 applications (depending on the NO sensor type) had been placed on the clock glass, a final application of Nafion[®] was placed onto the concentrated pre-coat of Nafion. The active surface of the electrode was then placed through the concentrated layer of Nafion[®] on the clock glass. The electrodes were then placed in the oven and annealed for 5 minutes at 210 °C. After the annealing process had been completed, the electrode was coated again, by using the same procedure i.e. placing another application of Nafion[®] onto the concentrated layer and then dipping the electrode through the layer to obtain a further Nafion[®] pre-coat. The modified electrode was then annealed again at 210 °C for 5 minutes.

3.4.5.2 Application of *o*-PD

The electropolymerisation of *o*-PD onto the Nafion[®] modified Pt disk electrodes, was carried out by applying a constant potential of +700 mV *vs.* SCE. A 300mM solution made up in N₂ saturated PBS was utilised. The electrodes were polymerised for 30 minutes and the electrochemical cell (Figure 3.7) was kept under a N₂ atmosphere as the monomer is readily oxidised in air. The resulting membrane that formed over the active surface was black in colour.

3.4.5.3 Type 1 NO Sensor (5 pre-coats, 2 applications of Nafion[®])

The design of this sensor was based on previous work carried out by our research group (Brown & Lowry, 2003; Brown *et al.*, 2009). The Nafion[®] modified Pt electrodes were constructed using the method for manufacturing the Pt electrodes (see Section 3.4.4). A pre-coat application method (explained in Section 3.4.5.1) was then employed to modify the surface of the Pt electrode. Once the annealing process was ceased the electrodes were placed into the gold clips. A representation of the sensor is shown in Figure 3.4.5.3.

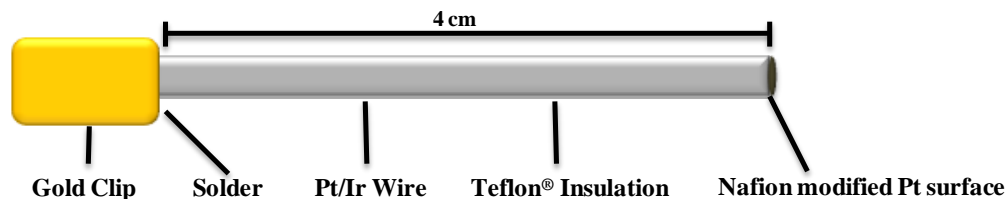


Figure 3.4.5.3: A schematic of a Type 1 NO Sensor.

3.4.5.4 Type 2 NO Sensor

(1 pre-coat, 2 applications of Nafion[®], annealed after each coat at 210 °C, followed by polymerisation with *o*-PD for 30 minutes)

This NO sensor was manufactured utilising the Pt working electrode (see Section 3.4.4). The pre-coat method was then employed (see Section 3.4.5.1). Finally, the addition of an *o*-PD layer (see Section 3.4.5.2) was utilised after the annealing process. The *o*-PD layer was incorporated after the method of annealing as it was found that the annealing temperature of 210 °C compromised the selectivity of the *o*-PD polymer in the sensors (Friedemann *et al.*, 1996). An image of the Type 2 NO sensor is displayed below (Figure 3.4.5.4).

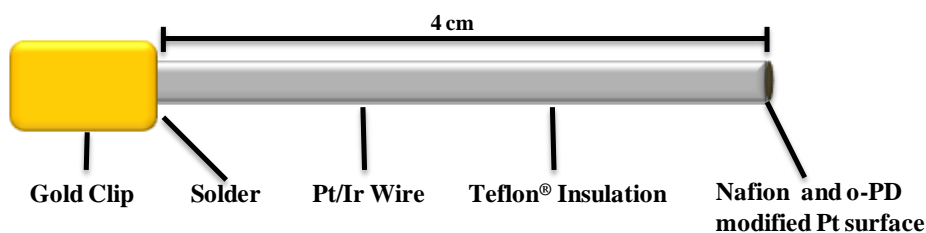


Figure 3.4.5.4: A schematic of the Type 2 NO Sensor.

3.4.5.5 Type 3 NO Sensor

(2 pre-coats, 1 application of Nafion[®], annealed at 210 °C followed by 1 dip into 5% Nafion[®] solution, annealed at 210 °C and finally polymerisation with *o*-PD for 30 minutes)

This NO sensor was manufactured utilising the Pt working electrode (see Section 3.4.4). The pre-coat method was then employed (see Section 3.4.5.1). After the first annealing of the Nafion[®] onto the electrode was completed, they were dipped in a 5% solution of Nafion[®] and annealed again. Finally an *o*-PD layer was incorporated into the design, by electropolymerisation as described in Section 3.4.5.2. Figure 3.4.5.5 below represents an image of the Type 3 NO sensor.

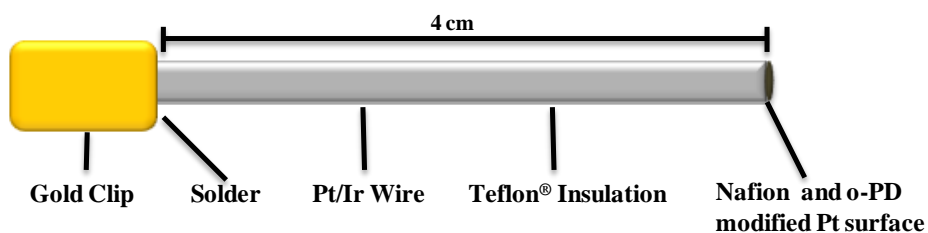


Figure 3.4.5.5: A schematic of the Type 3 NO sensor.

3.5 Electrode Modification

3.5.1 Monomer Modified CPEs (Sty and MMA)

The manufacture of modified CPEs has been demonstrated by many research groups. The first modifications of a CPE detailed the incorporation of the organic compounds, ferrocene and anthraquinone, in the liquid component of the paste (Kuwana & French, 1964). Enzymes, for example glucose oxidase, have also been introduced into the carbon paste of a CPE (Matuszewski & Trojanowicz, 1988). Monomer modified carbon paste electrodes for the trace determination of Cu (II) has also been demonstrated by Khoo and Guo (Khoo & Guo, 1999). The incorporation of Sty into the manufacture of carbon based sensors can be observed in the research carried out by Xu *et al.* (Xu *et al.*, 2011) and Nayak *et al.* (Nayak *et al.*, 2007). The inclusion of MMA in a carbon based biosensor has also been utilized for the detection of Vitamin C (Dai *et al.*, 2008). The fabrication of the two sensors (MMCPE and SMCPE) is described in Section 3.4.2 and 3.4.3, respectively.

3.5.2 PPD and Nafion[®] Modified NO Sensors

The inclusion of Nafion[®] in the manufacture of NO sensors has been demonstrated previously in our research group (Brown & Lowry, 2003). The application of the Nafion layers is discussed in Section 3.4.5.1. To combat interference from endogenous species in the *in-vivo* environment, the electropolymerisation of *o*-PD is incorporated into the design of the two types of NO sensor (see Section 3.4.5.2 for the application of the method). The electropolymerisation of *o*-PD is discussed comprehensively by O'Neill *et al.* (O'Neill *et al.*, 2008).

3.6 Electrode Treatments

To determine the effects that the components of the *in-vivo* environment may have on the sensors, biocompatibility and the stability of the sensors were investigated. These treatments were carried out on both the O₂ sensors and the NO Sensors. In order to try and mimic the *in-vivo* environment, the sensors were treated with a protein (BSA), a lipid (PEA), a surfactant (Triton[®] X-100) and then finally a homogenised sample of *ex-vivo* brain tissue (BT). The procedure followed for each treatment is further detailed in this section.

3.6.1 BSA Treated Sensors

Prior to treatment of each of the sensors, calibrations to determine the sensitivity towards O₂ (SMCPE and MMCPE) and NO (Type 1, 2 and 3 NO sensor) and selectivity against AA, were carried out on the sensors. AA was chosen for selectivity experiments, as it is the most copious analyte in the *in-vivo* environment (Agus *et al.*, 1997). Once these parameters were established, the sensors were placed in the solution of BSA. The sensors were kept in the solution of BSA, in the refrigerator at 4 °C, for a certain amount of time and once that time had elapsed, they were intermittently tested for sensitivity and selectivity.

3.6.2 PEA Treated Sensors

The sensors were treated with PEA, following the same protocol as described in Section 3.6.1.

3.6.3 Triton[®] X-100 Treated Sensors

The sensors were treated with Triton[®] X-100, in the same manner as described in Section 3.6.1.

3.6.4 BT Treated Sensors

The working electrodes were carefully placed in a homogenised solution of *ex-vivo* BT. Concurrently, the procedure outlined in Section 3.6.1 was adhered to.

3.6.5 Long-Term Stability Studies

For these studies the electrodes were placed in various storage conditions between specified time periods and intermittently tested.

3.6.6 Post-Implanted Sensors

Following implantation of the electrodes *in-vivo*, the sensors were removed and re-calibrated to further verify the long term stability of the sensor in the brain environment.

3.7 Electrochemical Experiments

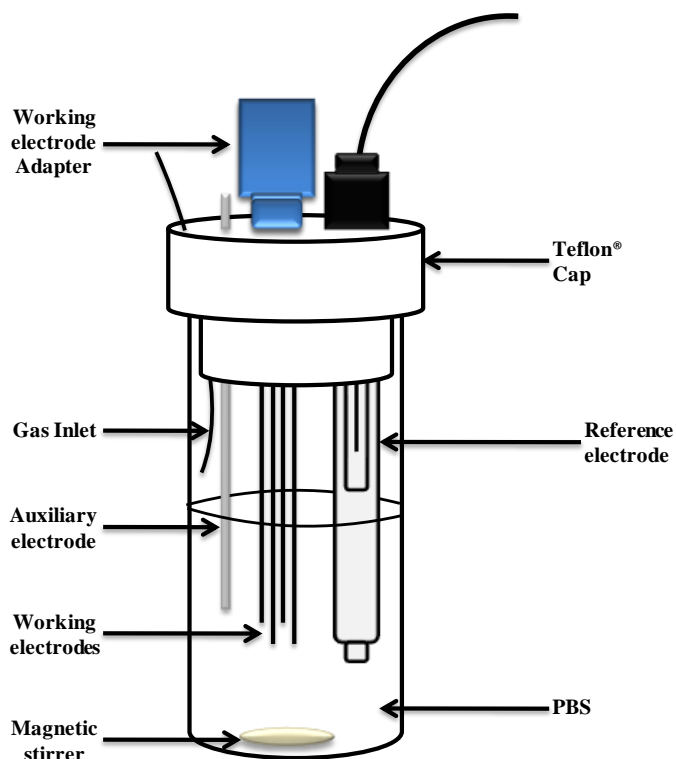


Figure 3.7: A schematic representing the experimental *in-vitro* set-up.

3.7.1 Electrochemical Cell Set-Up

The above display (Figure 3.7) represents the three electrode cell set-up. The diagram consists of a reference electrode, an auxiliary electrode and four working electrodes. The reference electrode which is a saturated calomel electrode (SCE), maintains a fixed potential against which the working electrodes can be measured. The electrochemical reactions take place at the working electrode surface and it is these changes that are analysed and investigated. The auxiliary electrode employed, acts as a source or sink for electrons. Any conducting wire where the electrochemical properties do not interfere with the reactions occurring at the working electrode can be utilised for the auxiliary. The auxiliary used in our case was a bare silver wire. A Teflon[®] cap that had individual compartments for placement of each of the electrodes and an inlet for injections and gas

was utilised. All *in-vitro* experiments were carried out in PBS and at room temperature (*ca.* 25 °C), unless otherwise stated.

3.7.2 Experimental Techniques

The main experimental technique utilised during the course of this project, was CPA. CPA involves the application of a constant potential and the subsequent observation of the change in current, as a function of time (Jiang, 2007). This experimental technique allows for real-time detection of an array of electroactive analytes. It is imperative that the sensor being designed excludes interference from other electroactive species, as the applied voltage will detect all species with oxidation/reduction potentials within the same range as the target analyte. The other technique utilised was CV (see Section 2.3). It is used for the study of redox processes and is based on varying the applied potential at a working electrode in both forward and reverse directions, while the current is monitored.

3.7.2.1 AA Calibrations

PBS (20 mL) was placed into a glass cell using a syringe. The PBS was then N₂ saturated for 30 minutes prior to experimental set-up (see Figure 3.7). Throughout the experiment N₂ was kept over the solution of PBS to retain N₂ saturation. A potential of 900 mV *vs.* SCE was then applied to the working electrodes, as generally the AA calibrations were undertaken subsequent to the NO calibrations. This potential was utilised throughout the research as it is the optimum potential for NO oxidation at the electrode. Upon application of the potential a capacitance current was instantly observed. A stable current baseline was achieved prior to the start of the calibration. In general, the more complex the sensor design was, the longer it needed for the current baseline to dissipate. AA was then introduced to the cell through the injection port in the Teflon[®] cap using pre-determined aliquots (see Table 3.7.2.1). The solution was agitated for *ca* 5 seconds by the magnetic stirrer. Intermittent injections of AA followed once the current value had reached a new steady current response.

[AA], μM
0
200
400
600
800
1000

Table 3.7.2.1: A table displaying the AA concentrations utilised in the calibration.

3.7.2.2 Oxygen Calibrations

O₂ calibrations were set up in the same manner as AA calibrations. A potential of -650 mV vs. SCE was applied to the working electrodes. Concentrations of N₂, Air, and O₂ were introduced to the cell (see Section 4.2). The concentrations are displayed below in Table 3.7.2.2.

[O ₂], μM
0
240
1200

Table 3.7.2.2: A table representing the concentrations used in the O₂ calibrations.

3.7.2.3 NO Calibrations

NO calibrations were carried out in the same manner as AA calibrations. The potential utilised for the detection of NO was +900 mV vs. SCE (Brown et al. 2009). The concentrations of NO introduced to the cell are outlined in Table 3.7.2.3.

[NO], μM
0
0.2
0.4
0.6
0.8
1.0

Table 3.7.2.3: A table displaying the concentrations of NO utilised in the NO calibrations.

3.7.2.4 Post-Implanted Calibrations

Following removal of the headpiece, calibrations were carried out using the same procedure as described in Section 3.7.2.2 for O₂ sensors and Section 3.7.2.3 for NO sensors. The headpiece was connected to the potentiostat via the pedestal (see Figure 3.8.2).

3.8 *In-Vivo* Experiments

In this Section, the procedures followed and materials utilised for the implantation of the sensors into the brain of male Wistar rats, will be described. All experiments carried out on the animals were completed under licence (B100/2205). All procedures were approved by the NUI Maynooth Ethics Committee (Animal Experimentation) in accordance with the Council of the European Parliament Directive 2010/ 63/ EU and Irish Statutory Instrument SI 543/2012. All *in-vivo* experiments were recorded continuously over a 24 hour period with animals assessed for good health according to published guidelines (*The Guide for the Care and Use of Laboratory Animals*, NIH Publication No. 85-23; and *The Handbook of Laboratory Animal Management and Welfare*, ISBN 1-4051-1159-3) immediately after recovery from anaesthesia and at the beginning of each day. All efforts were made to minimise animal suffering and the number of animals used for the study.

3.8.1 Subjects

The animals utilised throughout this project were male Wistar rats (Charles River UK Ltd., Manston Rd., Margate, Kent CT9 4 LT UK). Each animal weighed between 200 and 300 g on arrival. They were then housed in a temperature controlled (17-23 °C), humidity and light controlled (12 hr light/ 12 hr dark) environment. Access to food and water was *ad libitum* prior to surgery.

3.8.2 Surgical Protocol

All surgical procedures were carried out using aseptic techniques. The surgical bench tops and equipment were sterilised and the equipment was autoclaved prior to commencement of the surgery. The anaesthetic utilised to anaesthetize the subject was a volatile anaesthetic (Isoflurane). The animal was placed in an induction chamber for 3-4 minutes, to be anaesthetized before being transferred to the stereotaxic frame in the laminar flow hood. The nose piece was utilised for administration of the anaesthesia throughout the surgery. The head of the animal was positioned carefully in the nose piece and levelled between lambda and bregma. The anaesthesia was constantly maintained by the use of a vaporiser (Univentor). The level of anaesthetic provided to the subject in the induction chamber and in the nose piece is outlined below in Table 3.8.2 (a).

Anaesthetic	Chamber (Air)	Chamber (Isoflurane)	Nose piece (Air)	Nose piece (Isoflurane)
Isoflurane	700 – 800	4%	400 – 500	1.5 – 3%

Table 3.8.2 (a): The level of anaesthetic and air provided to the subject during surgery.

A confirmation that the subject was under anaesthetic was carried out (checking tail and paw reflexes), prior to commencing the surgery. A rectal probe was inserted into the animal and normal physiological temperature was maintained using a heating pad which the animal lay on, during the surgery. A piece of sterile gauze was used to cover the animal's eyes to prevent them drying or becoming irritated from the laminar flow hood. Sterilisation of the animals scalp was carried out using an iodine solution (Videne[®]). An incision was then made to the skin along the anterior-posterior plane. Using a cotton swab the underlying tissue was pushed back in order to expose the skull fully and to correctly identify bregma. Bregma was used as the reference point upon which the co-ordinates of various brain regions were found (Paxinos & Watson, 1998). The brain region examined during this project is summarised below in Table 3.8.2 (b).

Brain Region	(A – P)	(M – L)	(D – V)
Striatum	+ 1.0 mm	± 2.5 mm	- 5.0 mm

Table 3.8.2 (b): Stereotaxic coordinates for electrode implantation in the striatum.

Clamps were utilised in order to obtain an increased surface area for positioning and placement of the electrodes. The relevant co-ordinates were marked, along with the positions for the screws, reference and auxiliary. The holes for the support screws and electrodes were made using a hand held drill. The screws were then placed into the holes followed by the electrodes. A thin layer of cement (Dentalon[®] Plus) was applied over the skull to hold all of the electrodes in place. The cement was built up to the height of the screws and allowed to dry. Prior to the cement drying fully, it was pushed away from the skin of the animal in order to prevent sticking of the cement to the skin.

The gold clips of each electrode were placed in a Teflon[®] pedestal (Plastics One Inc.) (see Figure 3.8.2) and cemented into place. This allowed for connection between the gold clips and the potentiostat through a six-pinned cable, post-surgery. The electrodes were then carefully placed into the centre of the skull and covered with cement until no wire from the electrode was visible. The entire construct, apart from the pedestal, was cemented to create a headpiece. This alleviates the possible risk of moisture and the possibility of damage incurred by the animal to the headpiece. The surgical clamps were removed and the skin around the headpiece was sutured. The animal was then taken from the stereotaxic frame to a recovery incubator (27°C) until he had recovered. The animal was given a subcutaneous injection of Temgesic[®] (see Section 3.3.1.2) and closely monitored while recovering for 24 hours. The recovery time for each of the subjects will differ and was dependent on the volume and length of time exposed to the anaesthetic. The relevant procedures were adhered to when caring for the animal post-operatively.

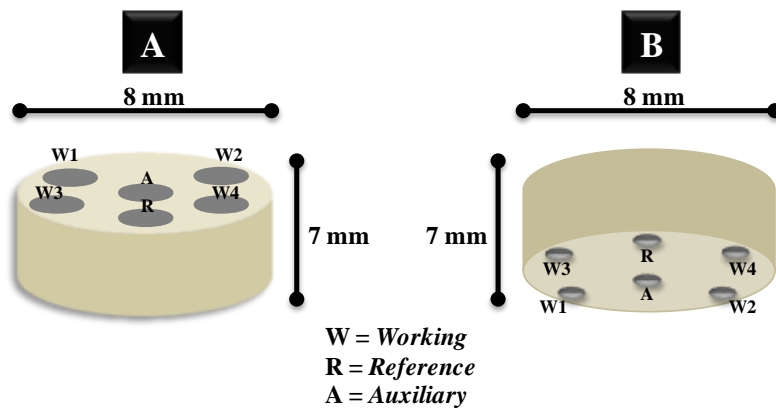


Figure 3.8.2: Images of the Teflon[®] pedestals; (A) Lower surface and (B) Upper surface

3.8.3 In-Vivo Reference and Auxiliary Electrodes

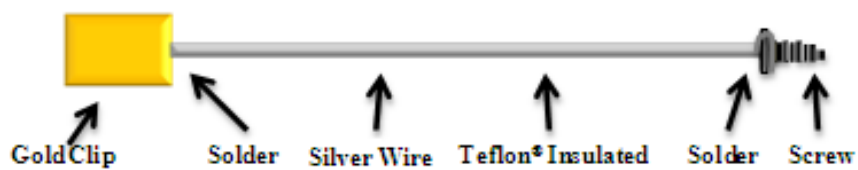


Figure 3.8.3 (a): A schematic illustrating the auxiliary electrode.

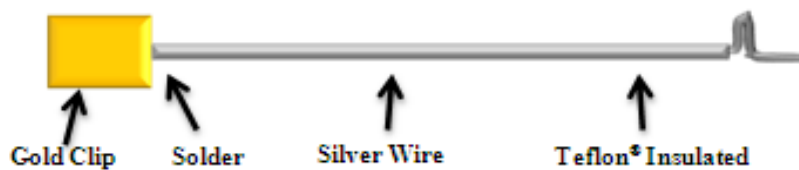


Figure 3.8.3 (b): A schematic displaying the reference electrode.

Figure 3.8.3 (a) and 3.8.3 (b), display the reference and auxiliary electrodes utilised for the *in-vivo* experiments. Both were manufactured in the same manner as the CPE (see Section 3.4.1). Once they were soldered into the gold clip, glue was applied to the exposed section of the wire, just above the clip, in order to provide the electrodes with stability when manoeuvring them during the surgery. To construct the reference electrode 3 mm of Teflon[®] was removed from the opposing end to the gold clip. The bare wire was then twisted in such a way so that it could rest against the skull of the animal and guide the vertical part of the electrode (see Figure 3.8.3 (b)) in through the reference hole in the skull of the subject. The auxiliary electrode was constructed in a similar manner as the reference electrode however; the exposed bare wire was soldered to a surgical screw (see Figure 3.8.3 (a)).

3.8.4 Physiological Stimuli

Neuronal activation was induced in the subject during the *in-vivo* experiments. These stimuli did not negatively affect the animal and the technique and results obtained were easily repeated.

3.8.4.1 Tail Pinch

A paper clip was attached to the subject's tail for a required time period of 5 minutes. This stimuli produced a behaviour pattern of gnawing, licking and eating (Stengård, 1995). The animal was distracted away from the paper clip and a piece of wood was placed in front of the animal's snout, to encourage gnawing actions. The paper clip was then removed causing little stress to the animal as possible.

3.8.4.2 Restraint Test

A restraint test was carried out for a period of 5-minutes, holding the animal in place with the aid of a towel. The towel gives comfort to the animal without any effect on the electrode response.

3.8.5 *In-Vivo* Injections

3.8.5.1 Intraperitoneal Injection (i.p)

The i.p injection was given into the body cavity at a 45 ° angle. It was usually directed in the lower left or right of the abdomen. The animal was positioned on its back and tilted so that no vital organs were present in the area that the injection was given (Wolfensohn & Lloyd, 2013).

3.8.5.2 Subcutaneous Injection (s.c)

Subcutaneous injections are seldom painful to the subject unless the substance being injected causes irritation to the animal. The injection was administered at the scruff of the neck. A fold of skin was lifted from the body using the thumb and two first fingers of one hand, the needle was then passed through, parallel to the body, avoiding tissues beneath (Wolfensohn & Lloyd, 2013).

3.9 Scanning Electron Microscopy (SEM)

This technique involved the use of a 14 Hitachi S-3200N Variable Pressure SEM. The SEM produces a high quality image created by a focused beam of high energy electrons ranging from (0 -30 kV), that have interacted with the surface of the sample. The preparation of the sample to be analysed involved, taking *ca* 1cm of the active surface end of the electrode. This was then placed on a stub that contained an area of carbon dag that prevented the electrode from moving. A thin layer of conducting material was introduced to the sample to prevent a build-up of an electrostatic charge on the sample surface. This involved the sample being sputtered with a thin layer of gold (10 nm thickness). The sample was then placed in the sample compartment of the SEM under high vacuum and the high resolution images were obtained.

3.10 NO synthesis and UV Spectroscopy

NO was synthesised in-house using an experimental method previously utilised within our research group (Brown *et al.*, 2005). Figure 3.10 (a) portrays the method used for in-house NO synthesis. The use of a commercial NO cylinder for obtaining NO was utilised also. With this method, pure NO was purged through KOH for 15 minutes and then collected for 5 minutes in the round bottom flask depicted in Figure 3.10 (a). UV spectroscopy was carried out upon collection of the NO in the same way as described by Brown *et al.*, (Brown *et al.*, 2005).

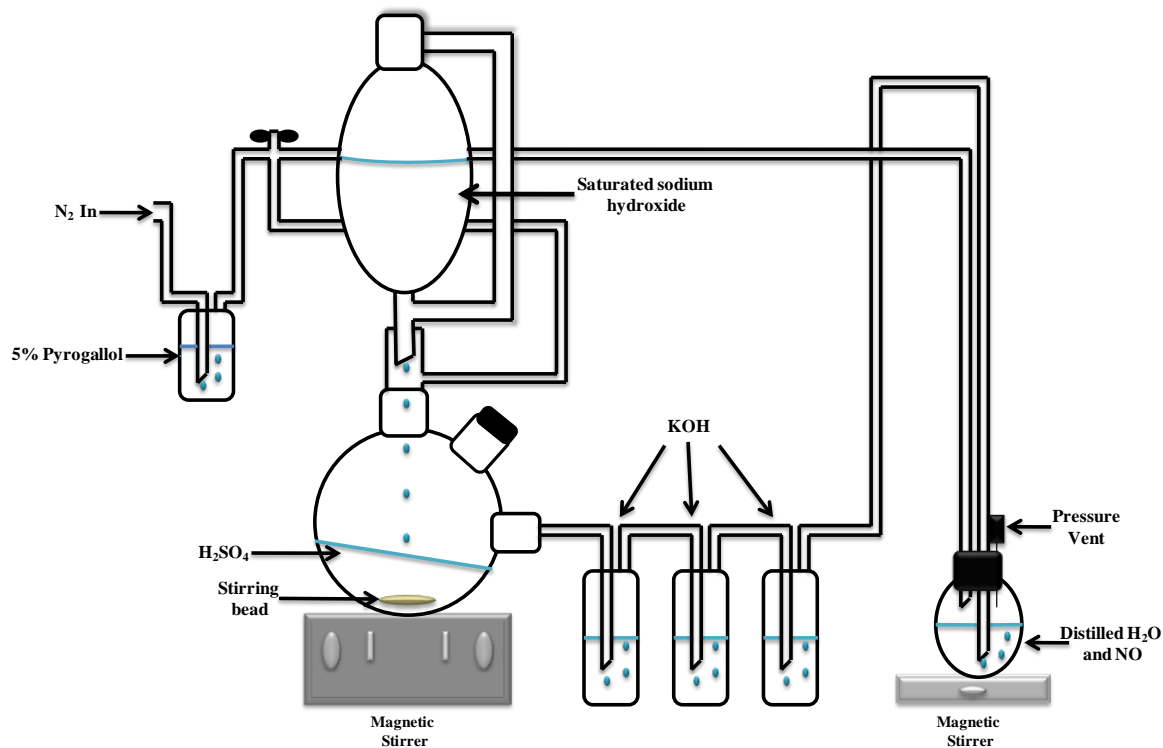


Figure 3.10 (a): A schematic illustrating the experimental set-up of the NO synthesis.

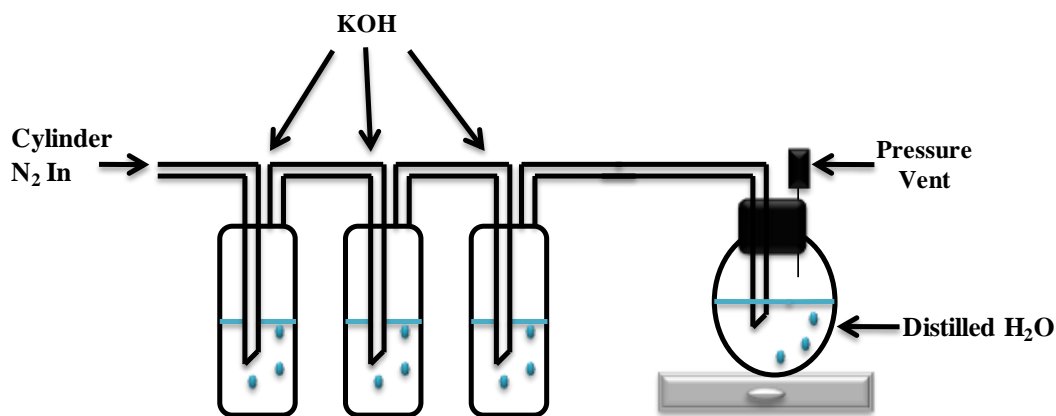


Figure 3.10 (b): A schematic illustrating the experimental set-up of the collection of NO from the cylinder.

3.11 Additional equipment

Air Pump

The air pump utilised was a Rena Air 200 (RENA[®], France) and was used during the O₂ calibrations.

Anaesthesia System

A Univentor 400 anaesthesia unit that consisted of a vaporiser for induction was utilised during the surgery. A Stellar S30 was the air pump used and the induction chamber was a 1.4 L Perspex box which were all obtained from Agnthos, Sweden. The stereotaxic frame (Kopf) allowed for the animal to be kept in an accurate position for brain coordinates to be mapped out and sensors implanted into an exact brain region. The laminar flow unit from Air Science[™] contained the entire system.

Electronic Balances

A three decimal BP 310P and a four decimal LA 2305 were the electronic balances utilised during the project. Both were from Sartorius[®] AG, Gottingen, Germany.

Incubator

The animal was placed in a heated incubator at 27 °C to recover following surgery. A Thermacage MKII from Datasand Ltd, UK, was utilised.

Magnetic Stirrer

The magnetic stirrer utilised was a Yellowline, MST mini magnetic stirrer, Lennox, Ireland.

Microscope

All *in-vitro* experiments utilised the stereomicroscope SZ51 from Olympus America Inc. and the SM 33-745-F from Hund[®] Wetzler, Germany. All *in-vivo* surgeries utilised the SZ61 microscope from Olympus.

Oven

A Binder ED 23 oven (Binder Scientific, Manchester, UK) was utilised for the production of the NO sensors.

pH Meter

The pH meter utilised was the S20 Seveneasy™ from Mettler-Toledo, Switzerland.

Sonicator

The sonicator used was a Fisherbrand FB11002, Leicestershire, UK.


Vortex

The vortex was used for the agitation and mixing of solutions (Reax Control from Heidolph).

3.12 References

- Agus DB, Gambhir SS, Pardridge WM, Spielholz C, Baselga J, Vera JC & Golde DW. (1997). Vitamin C crosses the blood-brain barrier in the oxidized form through the glucose transporters. *The Journal of Clinical Investigation* **100**, 2842-2848.
- Brown F, Finnerty N, Bolger F, Millar J & Lowry J. (2005). Calibration of NO sensors for *in-vivo* voltammetry: laboratory synthesis of NO and the use of UV-visible spectroscopy for determining stock concentrations. *Analytical and Bioanalytical Chemistry* **381**, 964-971.
- Brown FO, Finnerty NJ & Lowry JP. (2009). Nitric oxide monitoring in brain extracellular fluid: characterisation of Nafion[®]-modified platinum electrodes *in-vitro* and *in-vivo*. *Analyst* **134**, 2012-2020.
- Brown FO & Lowry JP. (2003). Microelectrochemical sensors for *in-vivo* brain analysis: an investigation of procedures for modifying Pt electrodes using Nafion[®]. *Analyst* **128**, 700-705.
- Chatzandroulis S, Goustouridis D & Raptis I. (2005). Polymeric film characterization for use in bimorph chemical sensors. *Microelectronic Engineering* **78-79**, 118-124.
- Chatzandroulis S, Tegou E, Goustouridis D, Polymenakos S & Tsoukalas D. (2004). Capacitive-type chemical sensors using thin silicon/polymer bimorph membranes. *Sensors and Actuators B: Chemical* **103**, 392-396.
- Dai H, Wu X, Wang Y, Zhou W & Chen G. (2008). An electrochemiluminescent biosensor for vitamin C based on inhibition of luminol electrochemiluminescence on graphite/poly(methylmethacrylate) composite electrode. *International Society of Electrochemistry* **53**, 5113-5117.
- Friedemann MN, Robinson SW & Gerhardt GA. (1996). o-Phenylenediamine-Modified Carbon Fiber Electrodes for the Detection of Nitric Oxide. *Analytical Chemistry* **68**, 2621-2628.
- Jiang PN. (2007). *Electroanalytical Chemistry Research Developments*. Nova Science Publishers, New York, United States of America.
- Kastek M, Sosnowski T & Piątkowski T. (2008). Passive infrared detector used for detection of very slowly moving of crawling people. *Opto-Electronics Review* **16**, 328-335.
- Khoo SB & Guo SX. (1999). Rapidly renewable and reproducible electropolymerized surface at a monomer modified carbon paste electrode. *Journal of Electroanalytical Chemistry* **465**, 102-113.

- Kuwana T & French WG. (1964). Electrooxidation or Reduction of Organic Compounds into Aqueous Solutions Using Carbon Paste Electrode. *Analytical Chemistry* **36**, 241-242.
- Lowry JP, Boutelle MG, O'Neill RD & Fillenz M. (1996). Characterisation of carbon paste electrodes *in-vitro* for simultaneous amperometric measurement of changes in oxygen and ascorbic acid concentrations *in-vivo*. *Analyst* **121**, 761-766.
- Malitesta C, Palmisano F, Torsi L & Zambonin PG. (1990). Glucose fast-response amperometric sensor based on glucose oxidase immobilized in an electropolymerized poly(o-phenylenediamine) film. *Analytical Chemistry* **62**, 2735-2740.
- Matuszewski W & Trojanowicz M. (1988). Graphite paste-based enzymatic glucose electrode for flow injection analysis. *Analyst* **113**, 735-738.
- Nayak RR, Lee KY, Shanmugaraj AM & Ryu SH. (2007). Synthesis and characterisation of styrene grafted carbon nanotube and its polystyrene nanocomposite. *European Polymer Journal* **43**, 4916-4923.
- O'Neill RD, Rocchitta G, McMahon CP, Serra PA & Lowry JP. (2008). Designing sensitive and selective polymer/enzyme composite biosensors for brain monitoring *in-vivo*. *Trends in Analytical Chemistry* **27**, 78-88.
- Ormonde DE & O'Neill RD. (1990). The oxidation of ascorbic acid at carbon paste electrodes: Modified response following contact with surfactant, lipid and brain tissue. *Journal of Electroanalytical Chemistry and Interfacial Electrochemistry* **279**, 109-121.
- Paxinos G & Watson C. (1998). *The Rat Brain: In Stereotaxic Coordinates*. Academic Press, Incorporated, United States of America.
- Porterfield DM, Laskin JD, Jung S-K, Malchow RP, Billack B, Smith PJS & Heck DE. (2001). Proteins and lipids define the diffusional field of nitric oxide. *American Journal of Physiology - Lung Cellular and Molecular Physiology* **281**, L904-L912.
- Stengård K. (1995). Tail pinch increases acetylcholine release in rat striatum even after toluene exposure. *Pharmacology Biochemistry and Behavior* **52**, 261-264.
- Wolfensohn S & Lloyd M. (2013). *Handbook of Laboratory Animal Management and Welfare*. Wiley, United Kingdom.
- Xu L, Du J, Deng Y, Li Z, Xu C & He N. (2011). Fabrication and Characterisation of Nanoporous Pseudo-Carbon Paste Electrode. *Advanced Science Letters* **4**, 104-107.



*4. In-Vitro Development of
Carbon-Based Sensors
Suitable for the Detection of
Oxygen in the Clinical
Environment*

4.1 Introduction

CPEs are the most extensively utilised electrodes in electrochemical studies. They have numerous appealing qualities like low cost, ease of construction and can be utilised to detect various analytes, for example, dopamine (O'Neill, 2005), AA (Miele & Fillenz, 1996a) and O₂ (Bolger & Lowry, 2005). The advantage of this sensor is the stability over long periods of recording time. It has been observed that interactions with lipids alter the CPEs to carbon powder electrodes through the extraction of the oil. This gives the CPEs great stability as any fouling that has occurred at the surface would be removed with the oils, by the lipids (O'Neill, 1993). CPEs are more desirable to use than metal based sensors as they do not require protective membranes to defend against surface poisoning (Bolger & Lowry, 2005). CPEs utilised for the detection of O₂ have been previously demonstrated within our research group (Lowry *et al.*, 1997; Bolger *et al.*, 2011b; Kealy *et al.*, 2013) and also for the detection of AA (Lowry *et al.*, 1996).

O₂ is an immensely important molecule that is essential for life. Determining O₂ levels is invaluable in many research fields. An example of this can be seen in the medical domain, where the evaluation of a patient's O₂ levels in the blood or in exhaled air, are key parameters in the health and welfare of that person. The brain consumes approximately 20% of the total amount of O₂ produced by the body and the tissue concentration is conditional on the blood supply and local utilisation of O₂ (Lowry *et al.*, 1997). Clark and colleagues were one of the first research groups to detect molecular O₂ voltammetrically *in-vivo* using metal electrodes. In feline experiments, they implanted insulated metal polarographic cathodes that continuously recorded O₂ availability in the animal (Clark *et al.*, 1958).

More recently, the focus of our group has concentrated on the integration of electrochemical sensors into the clinical environment. The commercially available LICOX[®] probe (see Figure 1.2.2) has been extensively characterised for measuring O₂ in brain tissue (Purins *et al.*, 2010; Dengler *et al.*, 2011; Keddie & Rohman, 2012; Morgalla *et al.*, 2012). Initial deployment of the electrochemical sensors developed in this research will focus on peripheral tissue monitoring since the regulatory hurdles associated with brain monitoring are so high. The LICOX[®] probe is electrochemical in nature and displays a lot of

similarities to our proposed device; however, the sensing component functions by diffusion of O₂ through a permeable membrane surrounding the probe and into an electrolyte solution where a signal is generated. The LICOX[®] probe is designed with brain monitoring at its core and is fixed carefully in position using a bulky housing component. The fragile membrane surrounding the probe is unsuitable for orthopaedic surgery due to risk of damage during implantation and leakage of the electrolyte into the muscle, for example. Alternative methods of measuring O₂ levels currently utilised in hospitals include Pulse Oximetry and Arterial Blood Gas (ABG) analysis.

Severe limitations exist with such techniques restricting their utility in measuring a medical emergency such as a patient with ischemia. Ischemia is defined as being a restriction in blood supply to tissues, causing a shortage of O₂ and glucose needed for cellular metabolism. O₂ is an extremely relevant real-time indicator of ischemia since it is transported to the tissue via blood supply and if the blood supply is interrupted then no O₂ can reach the tissue. ABG focuses on discrete measurements of O₂ levels in blood taken from the patient at varying time intervals and fails to address the trend in O₂ levels on a continual basis. This significant time-lag in O₂ measurements would have limited benefit to “at risk” patients since early diagnosis is critical to patient outcome. The continuous real-time characteristic of the sensor technology within our lab, will allow for millisecond changes in O₂ levels to be recorded and displayed for the clinician, significantly increasing timely intervention.

Pulse Oximetry, similar to Near Infrared Spectroscopy, measures the O₂ saturated content of haemoglobin in the blood which has been identified as being indirect in nature and having no clear threshold for measuring conditions such as ischemia (Elliott & Johnstone, 2003). Both techniques would result in false tissue readings due to its limited capability of distinguishing between O₂ levels within a tissue and those in the circulation surrounding that particular tissue. In order for an electrode to be utilised in a clinical environment, sensitivity to interfering lipophilic ions or charged surfactants should not be an issue for the electrode (Czaban, 1985). Research carried out by Ormonde and O’Neill describes how the CPEs physical and electrochemical characteristics alter, after contact with BT. The oil is removed from the carbon paste by lipids and proteins in the brain, changing the sensor from

a carbon paste to a carbon powder electrode, thus improving the sensors stability over longer periods of time (Ormonde & O'Neill, 1989, 1990).

However, the CPE would not be a reliable sensor for clinical utilisation, as there is leakage of the constituents into the environment in which it is placed. It is for this reason that the modification of the CPE is of valuable importance. In order to prevent the CPE surface alteration by interactions with the brain environment, the modification of the CPE has been detailed in this chapter. The alteration of a CPE is appealing due to the ease of manipulation and convenience of modification. The fabrication of modified CPEs began when Kuwana and French mixed electroactive organic compounds into the liquid constituent of the paste (Kuwana & French, 1964). Since that time, there has been a wide range of research carried out involving the fabrication of modified carbon based sensors (Khoo & Guo, 1999; Dai *et al.*, 2008; Melak *et al.*, 2013).

The Sty monomer has been utilised previously in the design of sensors, as an immobilisation matrix for a lactate and choline biosensor within our research group. The integration of Sty into the construction of carbon nanotube sensors with the aim of synthesising and characterising styrene grafted carbon nanotubes and its polystyrene nanocomposites has been demonstrated previously (Nayak *et al.*, 2007). MMA has been utilised as an immobilisation matrix for the fabrication of biosensors in research carried out by Perez *et al.*, (Pérez *et al.*, 2006). MMA has been incorporated into the manufacture of dental appliances, which demonstrates a compatibility with human tissue (Douglas & Bates, 1978; Murray & Darvell, 1993; Sarac *et al.*, 2006). The purpose behind the incorporation of the Sty and MMA monomer into the CPE design in this research was to try and create a more robust sensor design. The main goal was to try and produce a sensor that was not as vulnerable and as easily modified by a complex biological setting as is observed with CPEs.

This chapter describes the development of the monomer modified CPEs for the detection of O₂. Firstly, before the fabrication of these sensors was achieved, characterisation of the CPE was carried out in order to confirm accurate manufacturing capabilities and to verify that all of the parameters and characteristics of the CPE were concurrent with literature. These results are subsequently utilised for the comparison against the new monomer modified CPEs.

4.2 Experimental

The instrumentation and software utilised are described in Section 3.2. All chemicals and solutions are detailed in Section 3.3. The manufacture of a CPE, MMCPE and a SMCPE are described in Sections 3.4.1, 3.4.2 and 3.4.3 respectively. All modifications to the sensors are discussed in Section 3.5. All data was carried out in PBS (pH 7.4) unless mentioned otherwise. A working potential of -650 mV vs. SCE was applied to all working electrodes involved in the O₂ experiments. Three point calibrations were carried out by introducing varying concentrations of O₂ to the electrochemical cell (see Figure 3.7). It has been demonstrated previously that five point O₂ calibrations display a similar sensitivity slope, to three point O₂ calibrations (Bolger *et al.*, 2011a). An O₂ concentration of 0 μM was obtained by deoxygenating the buffer solution with N₂ gas. The appropriate gaseous atmosphere was maintained over the cell solution during quiescent recording for each of the O₂ concentrations (see Figure (3.7)).

The constant flushing of N₂ to achieve sub-micromolar O₂ concentrations has been demonstrated previously by Dixon *et al.*, using a similar set-up to the electrochemical cell set-up utilised in this research (Dixon *et al.*, 2002). It takes approximately ten minutes for the buffer solution to reach a new level of gaseous saturation. An O₂ concentration of 240 μM was obtained by bubbling air through the buffer solution for 30 minutes (Lowry *et al.*, 1996; Bolger & Lowry, 2005; Bolger *et al.*, 2011a). Finally, an O₂ concentration of 1200 μM was achieved, by bubbling pure O₂ gas through the buffer solution for 30 minutes (Lowry *et al.*, 1996; Bolger & Lowry, 2005; Bolger *et al.*, 2011a).

These concentrations were utilised in order to obtain regression analysis data. All data obtained is reported as mean ± SEM, *n* denotes number of electrodes, unless mentioned otherwise. The goodness of fit of the data points is measured by the R² value. The calibration plots obtained are linear, therefore the slope (nA/μM) is utilised as an indicator of sensitivity. All statistical analysis is carried out using paired, unpaired *t* tests and one way ANOVA analysis. These tests are performed using GraphPad Prism and yield a *P*-value as a result, which is a probability value that indicates if the results obtained are significantly different. How significantly different the results are, is denoted by the number of asterisks (*). Table 4.2 indicates this in more detail.

<i>P</i> value	Significance	No. of asterisks
< 0.001	Extremely significant	***
0.001 to 0.01	Very significant	**
0.01 to 0.05	Significant	*
> 0.05	Not significant	ns

Table 4.2: A table displaying a summary of the correspondence of the *P* value to the number of asterisks.

4.3 Results and Discussion

In this chapter, the development of monomer modified CPEs for the detection of O₂ is discussed. Prior to this, CPEs are manufactured, examined and analysed for comparison against the new monomer modified CPEs. CPEs have previously been characterised *in-vitro*, for simultaneous measurement of changes in O₂ and AA *in-vivo*, by Lowry *et al.*, (Lowry *et al.*, 1996). An advantage of CPEs is that they can be utilised over a wide potential window (Kalcher, 1990) and they are stable *in-vivo* for prolonged periods of time (O'Neill, 2005). The development of the SMCPE and MMCPE are subsequently described in Section 4.3.2 and 4.3.3 respectively.

4.3.1 Detection of O₂ utilising CPEs

CPEs have been extensively utilised for the detection of O₂ *in-vivo* (Lowry *et al.*, 1997; Bolger & Lowry, 2005). It has previously been demonstrated that electrodes upon encountering lipids and proteins in the brain environment cause an alteration to the morphology of the CPE. The oils within the paste are drawn out leaving a carbon powder electrode behind (Ormonde & O'Neill, 1989, 1990). This is examined in the next section using CPEs for the detection of O₂. In Figure 4.3.1 (a), a typical current vs. time response raw data trace from an O₂ calibration, utilising a CPE, is presented. The results obtained for an O₂ calibration on CPEs are displayed below in Table 4.3.1 and Figure 4.3.1 (b).

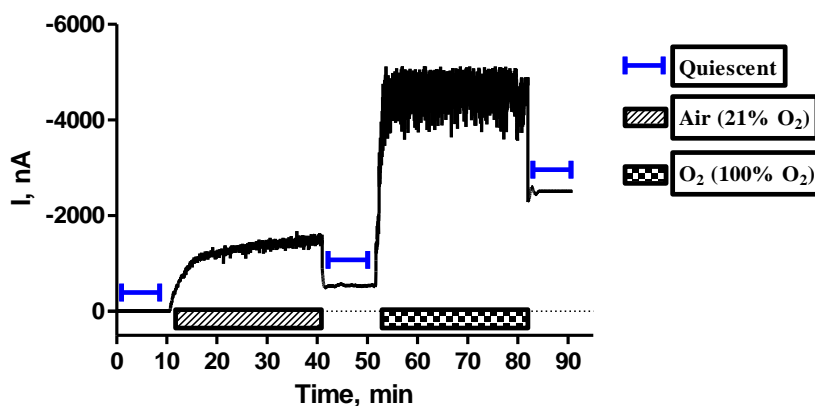


Figure 4.3.1 (a): Typical current-time response for an O_2 calibration (0-1200 μM ; N_2 , Air, O_2 -saturation) at a CPE carried out using CPA at -650 mV vs. SCE in PBS, pH 7.4.

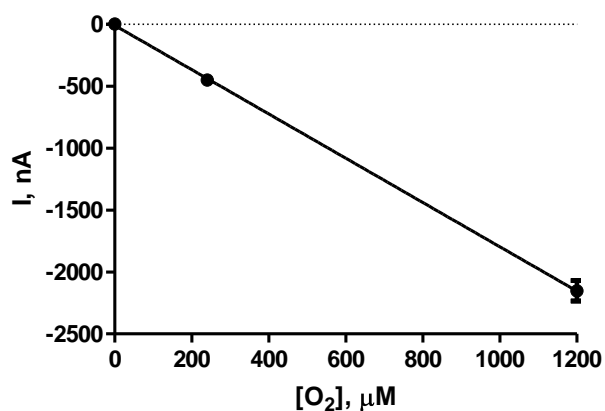


Figure 4.3.1 (b): Averaged O_2 calibrations performed with CPEs ($n = 52$) in PBS (pH 7.4) at -650 mV vs. SCE.

[O_2] μM	CPEs ($n = 52$)	
	Mean I, nA	SEM
0.0	0.0	0.0
240.0	-452.1	16.7
1200.0	-2152.2	82.6

Table 4.3.1: Table of averaged results for O_2 calibrations in PBS (pH 7.4) using CPEs ($n = 52$) at -650 mV vs. SCE. Background values subtracted. Mean background current = -1.9 ± 0.2 nA.

The results in Table 4.3.1 show the averaged currents obtained for an O₂ calibration. Linear regression analysis was performed from these results. A sensitivity of -1.8 ± 0.1 nA/ μ M, $n = 52$, was obtained. An O₂ sensitivity of -1.5 ± 0.1 nA/ μ M, $n = 8$, was achieved by Bolger *et al.*, using a five point O₂ calibration (Bolger *et al.*, 2011a) which is very similar to the sensitivity obtained in this section for the three point O₂ calibrations undertaken (-1.8 ± 0.1 nA/ μ M, $n = 52$). The response of the electrodes over the O₂ concentration range was linear with a R² value of 0.99, $n = 52$.

4.3.1.1 Biocompatibility studies

The brain environment contains a complex array of substances that may compromise the sensors performance. These interact with the electrode, changing the morphology of the surface and altering the constituents of the electrode. The CPE's sensitivity is also compromised, as proteins and lipids adsorb onto the sensor surface, reducing the active surface (Ormonde & O'Neill, 1990). To see what effect proteins and lipids had on the electrodes, experiments were carried out on the CPEs to try and replicate conditions encountered in the brain environment. BT was also utilised, as this best mimics *in-vivo* conditions and restricts mass transport to the electrode. Triton[®] X-100 was utilised by Ormonde and O'Neill as a method of removing the oil from the carbon paste *in-vitro* (Ormonde & O'Neill, 1990). Experiments in this body of work also involve the use of Triton[®] X-100 to determine the effects on the carbon paste.

The effect of the protein (BSA), see Section 4.3.1.1.1 and the lipid (PEA), see Section 4.3.1.1.2 on CPEs is examined. The results obtained from O₂ calibrations on BSA and PEA-treated CPEs are displayed in Table 4.3.1.1.1 and 4.3.1.1.2 respectively and plotted graphically in Figure 4.3.1.1.1 and 4.3.1.1.2 respectively. As the brain comprises of all of these substances that are detrimental to the workings of the electrode, BT (see Section 4.3.1.1.3 and Section 4.3.1.1.4) was also utilised. Finally, Triton[®] X-100 (see Section 4.3.1.1.5) was utilised as an added surfactant treatment against the CPEs. These studies were carried out either overnight (ON), over 3 days or after 28 days, unless otherwise stated.

4.3.1.1.1 BSA-treated CPEs

[O ₂], μM	CPE (<i>n</i> = 4)		CPE-BSA (10%) ON (<i>n</i> = 4)	
	Mean I, nA	SEM	Mean I, nA	SEM
0.0	0.0	0.0	0.0	0.0
240.0	-427.0	10.9	-286.1	6.4
1200.0	-2114.8	157.3	-1331.2	28.5

Table 4.3.1.1.1: Table of results for O₂ calibrations in PBS (pH 7.4) using CPEs (*n* = 4) pre- and post-treatment with BSA (10%) ON at -650 mV vs. SCE. Background values subtracted. Mean background current (CPEs) = -1.2 ± 0.2 nA and CPE-BSA (10%) ON = -5.2 ± 0.5 nA.

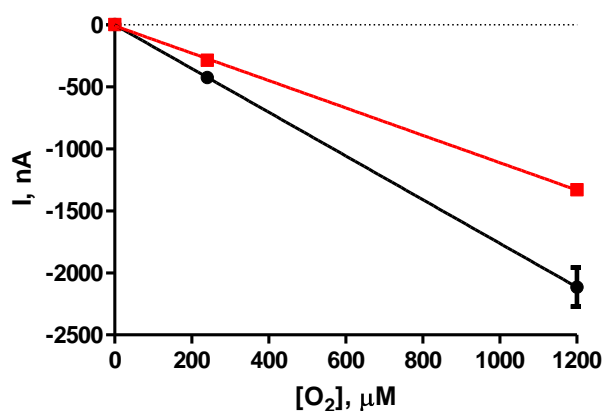


Figure 4.3.1.1.1: A current-concentration profile for O₂ calibrations in PBS (pH 7.4) using CPEs pre (black) and post (red) treatment with BSA (10%) ON at -650 mV vs. SCE.

The results obtained for O₂ calibrations using the CPEs pre- and post-treatment with BSA (10%) gave sensitivities of -1.8 ± 0.1 nA/ μM, *n* = 4 and -1.1 ± 0.1 nA/ μM, *n* = 4 respectively. The response of the electrodes was linear over the specified range with an R² value of 1.00 (pre-treatment) and 0.99 (post-treatment). The results pre- and post-treatment were significantly different (*P* = 0.0258, paired *t*-test). BSA is a large globular protein that adsorbs onto the surface of the electrodes. The decrease in sensitivity post-treatment could be indicative of the BSA (10%) blocking the active surface on the carbon paste and therefore causing a decreased detection of O₂. BSA has been utilised by other research

groups as a means of blocking the active surface on a CPE (Zhang *et al.*, 2011) and biosensors (Sun *et al.*, 2011).

The fouling of the electrode surface causing a decrease in sensitivity has been observed previously by Kane *et al.*, (A. Kane & D. O'Neill, 1998). Kane *et al.*, observed that upon treatment of the CPEs with BSA (10%) a significant positive shift ($P = 0.02$) in the peak potential and a 43 % decrease in the sensitivity was recorded. This could possibly be a reason for the decrease in sensitivity observed after treatment with BSA (10%) with the CPEs. The 10% concentration of BSA utilised is also very harsh and these levels would not be encountered *in-vivo*.

4.3.1.1.2 PEA-treated CPEs

[O ₂], μM	CPE ($n = 4$)		CPE-PEA (10%) ON ($n = 4$)	
	Mean I, nA	SEM	Mean I, nA	SEM
0.0	0.0	0.0	0.0	0.0
240.0	-395.9	16.3	-285.4	5.4
1200.0	-1942.4	34.2	-1261.8	12.1

Table 4.3.1.1.2: Table of results for O₂ calibrations in PBS (pH 7.4) using CPEs ($n = 4$) pre- and post-treatment with PEA (10%) ON carried out at -650 mV vs. SCE. Background values subtracted. Mean background current (CPE) = -0.9 ± 0.2 nA and (CPE-PEA (10%) ON) = -1.2 ± 0.3 nA.

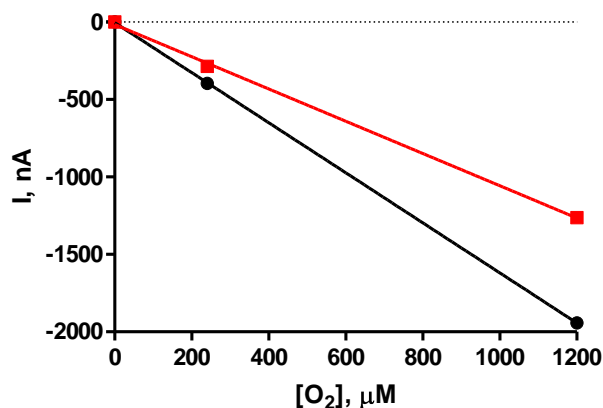


Figure 4.3.1.1.2: A current-concentration profile for O₂ calibrations in PBS (pH 7.4) using CPEs pre (black) and post (red) treatment with PEA (10%) ON carried out at -650 mV vs. SCE.

Figure 4.3.1.1.2 and Table 4.3.1.1.2 display data obtained for O₂ calibrations pre- and post-treatment with PEA (10%) ON with CPEs. Sensitivities of -1.6 ± 0.1 nA/ μ M, $n = 4$ and -1.0 ± 0.1 nA/ μ M, $n = 4$, were recorded for pre and post PEA (10%) ON treatment, respectively. Linear responses of 1.00 (pre-treatment) and 0.99 (post-treatment) over the specified range were obtained. A significant decrease in sensitivity ($P < 0.0001$, paired t -test) was recorded after treatment with PEA (10%). It has been proposed that the oil is removed from the CPE by lipids, which provides the CPEs with better stability over time but also increases the rate of electron transfer, thus increasing the sensitivity (Ormonde & O'Neill, 1989; A. Kane & D. O'Neill, 1998) however, an increase in sensitivity is not observed with this result and could be due to the adsorption of the PEA onto the surface, blocking the active surface, thus, leading to a decrease in the overall sensitivity observed. A decrease in sensitivity could also be due to restricted diffusion. As Triton[®] X causes similar effects to PEA (as PEA is also a surfactant), the SEM images in Figure 4.3.1.1.6 could suggest that the PEA is causing this leeching out of the cavity making it more difficult for the analyte to diffuse to the carbon paste. O₂ must now diffuse down the cavity as opposed to the pre-treated CPE. O₂ has a large diffusion coefficient so the restricted diffusion may not be the reasoning behind the decreased sensitivity but rather the PEA causing the paste to compact back into the cavity giving a more compact surface thus reducing the active surface area and hence the sensitivity. A combination of leeching from the cavity and a reduced active surface could be the reason for this.

4.3.1.1.3 BT treated CPEs

[O ₂], μ M	CPE ($n = 4$)		CPE-BT ON ($n = 4$)	
	Mean I, nA	SEM	Mean I, nA	SEM
0.0	0.0	0.0	0.0	0.0
240.0	-568.3	21.4	-428.2	64.4
1200.0	-2182.7	99.6	-1812.1	199.6

Table 4.3.1.1.3: Table of results for O₂ calibrations in PBS (pH 7.4) using CPEs ($n = 4$) pre- and post-treatment with BT ON carried out at -650 mV vs. SCE. Background values subtracted. Mean background currents (CPEs) = -1.9 ± 0.5 nA and (CPE-BT ON) = -2.9 ± 1.4 nA.

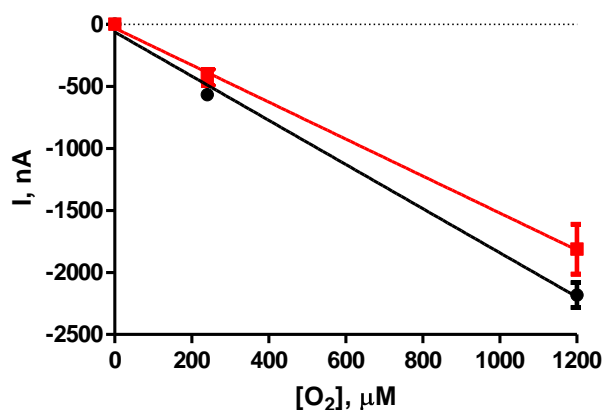


Figure 4.3.1.1.3: A current-concentration profile for O₂ calibrations in PBS (pH 7.4) using CPEs pre (black) and post (red) treatment with BT ON carried out at -650 mV vs. SCE.

The *ex-vivo* brain tissue studies are more representative of the surroundings that the sensor would have to endure, therefore, they give a better understanding as to how the sensor will behave in the *in-vivo* environment. O₂ calibrations performed on the CPEs pre and post BT ON, displayed sensitivities of -1.8 ± 0.1 nA/ μ M, $n = 4$ and -1.5 ± 0.1 nA/ μ M, $n = 4$, respectively. A linear response was obtained over the specified range with an R² value of 0.99 (pre-treatment) and 0.99 (post-treatment). The results obtained were not significantly different pre- and post-treatment ($P = 0.1864$, paired *t*-test). There was a slight reduction in sensitivity post-treatment in BT ON. This result was not unexpected, as the complex nature of BT which embodies proteins and lipids among other interferents and fouling agents would cause the sensor to be altered. Leading to the removal of the oil from the carbon paste and thus increasing the electron transfer at the electrode. This could be a reason why a significant difference is not observed pre- and post-treatment.

4.3.1.1.4 BT treated CPEs (28 days)

[O ₂], μM	CPE (n = 4)		CPE-BT 28 days (n = 4)	
	Mean I, nA	SEM	Mean I, nA	SEM
0.0	0.0	0.0	0.0	0.0
240.0	-398.4	23.6	-404.5	33.1
1200.0	-2298.6	110.3	-1892.8	141.2

Table 4.3.1.1.4: Table of results for O₂ calibrations in PBS (pH 7.4) using CPEs (n = 4) pre- and post-treatment with BT 28 days carried out at -650 mV vs. SCE. Background values subtracted. Mean background currents (CPEs) = -3.9 ± 0.3 nA and (CPE-BT 28 days) = -3.8 ± 0.6 nA.

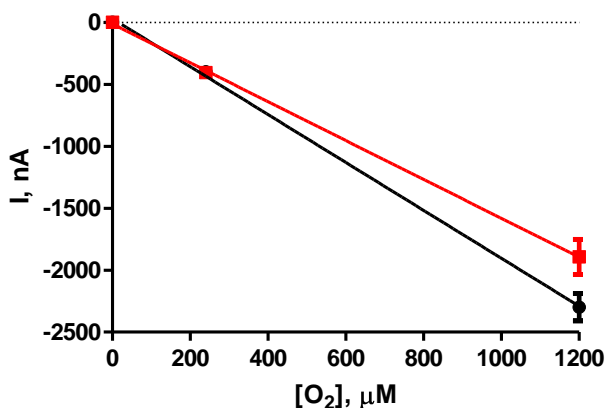


Figure 4.3.1.1.4: A current-concentration profile for O₂ calibrations in PBS (pH 7.4) using CPEs pre (black) and post (red) treatment with BT (28 days) carried out at -650 mV vs. SCE.

The results obtained for O₂ calibrations using the CPEs pre- and post-treatment with BT over 28 days yielded sensitivities of -1.9 ± 0.1 nA/μM, $n = 4$ and -1.6 ± 0.1 nA/μM, $n = 4$, respectively. This time interval chosen is more representative of how long sensors would remain implanted for. A linear response was obtained pre- and post-treatment with the BT (28 days) ($R^2 = 0.99$). A decrease in sensitivity was observed post treatment, yielding a significant difference ($P = 0.0152$). Again, this result was expected, as the *ex-vivo* brain environment would morphologically change the sensor leading to an altered response.

4.3.1.1.5 Triton[®] X-100 (10%) treated CPEs

[O ₂], μM	CPE (<i>n</i> = 8)		CPE-Triton [®] X (10%) (<i>n</i> = 8)	
	Mean I, nA	SEM	Mean I, nA	SEM
0.0	0.0	0.0	0.0	0.0
240.0	-364.3	29.6	-419.6	59.7
1200.0	-1938.8	167.4	-1665.1	246.1

Table 4.3.1.1.5: Table of results for O₂ calibrations in PBS (pH 7.4) using CPEs (*n* = 8) pre- and post-treatment with Triton[®] X-100 (10%) ON carried out at -650 mV vs. SCE. Background values subtracted. Mean background current (CPE) = -1.9 ± 0.3 nA and (CPE-Triton[®] X (10%) ON) = -4.4 ± 1.4 nA.

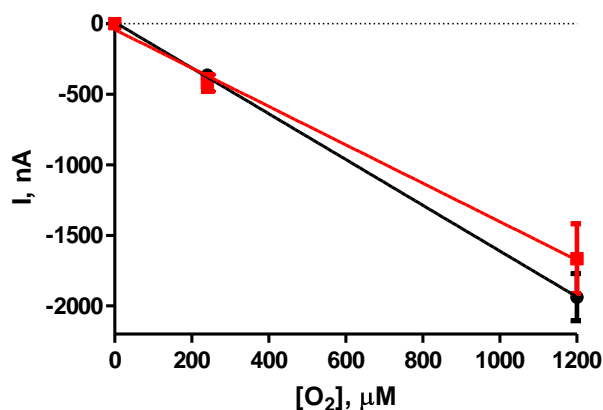


Figure 4.3.1.1.5: A current-concentration profile for O₂ calibrations in PBS (pH 7.4) using CPEs pre (black) and post (red) treatment with Triton[®] X-100 (10%) ON, carried out at -650 mV vs. SCE.

The results for the O₂ calibrations using the CPEs pre- and post-treatment with Triton[®] X (10 %) ON, yielded sensitivities of -1.6 ± 0.1 nA/ μM, *n* = 8 and -1.4 ± 0.1 nA/ μM, *n* = 8, respectively. The response of the electrodes was linear over the specified range with an R² value of 0.99 (pre-treatment) and 0.99 (post-treatment). The results pre- and post-treatment were not significantly different (*P* = 0.3270, paired *t*-test). A slight decline in sensitivity was observed, however, pre and post analysis remained similar. This could be due to the fact that some electrodes showed a greater sensitivity after treatment, which would be a consequence of the removal of the oil causing an increase in electron transfer. Whilst some

electrodes either lost connection between the surface wire and the carbon paste or decreased in sensitivity on account of the harshness of the surfactant Triton[®] X. Triton[®] X has been utilised previously as a means of removing the oil from the CPE resulting in a carbon powder electrode, which brings about faster electron transfer and greater stability over long periods of experimental recording (Ormonde & O'Neill, 1989; A. Kane & D. O'Neill, 1998). Figure 4.3.1.1.6 (A) and (B), displays the images of the CPEs pre- and post-treatment with Triton[®] X.

4.3.1.1.6 SEM images

SEM was utilised as a means of analysing the surface morphology of the CPEs more closely. Triton[®] X-100 was the harshest substance that the electrode was in contact with and has been investigated as a surfactant with CPEs previously (Ormonde & O'Neill, 1990). The images display the CPE surface pre and post Triton[®] X-100 treatment and they highlight the effect of the surfactant on the CPEs.

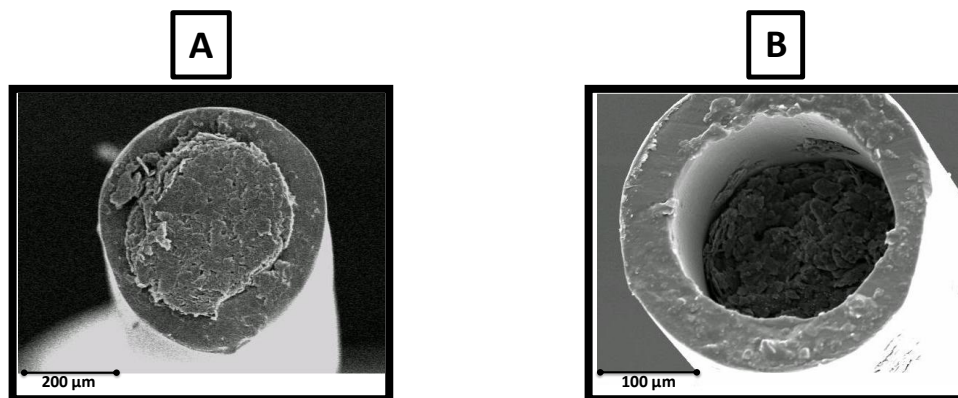


Figure 4.3.1.1.6: SEMs displaying the surface of (A); CPE prior to treatment (B); CPE post treatment with Triton[®] X-100 (10%) ON.

It is obvious from Figure 4.3.1.1.6, image B, that treating the CPEs with the surfactant Triton[®] X-100 completely alters the surface morphology. It is clear from the image that a large part of the carbon paste has been removed from the compartment of the electrode along with the silicone oil. This was evident, due to some of the carbon paste remaining in

the bottom of the enclosed container were the sensors were kept during the Triton[®] X (10%) treatment. Triton[®] X (0.1 %) was utilised by Lyne *et al.*, and O'Neill *et al.*, to mimic the outcome of implantation of the CPEs *in-vivo*, which causes the transformation of CPEs to carbon powder electrodes by removal of the oil constituent (Lyne & O'Neill, 1990; O'Neill, 1993). A 10 % solution was utilised in the experiments carried out in this thesis in order to try and elucidate whether the modified electrodes would withstand modification by such a harsh concentration of this surfactant. SEMs displaying post *in-vivo* effects on the CPEs are shown in Figure 4.4 (e).

4.3.2 Sty modified CPE (SMCPE)

The incorporation of the Sty monomer into the design of sensors has been demonstrated previously as an immobilisation matrix for a lactate and choline biosensor within our research group. Nayak *et al.*, integrated Sty into the manufacture of carbon nanotube sensors with the main goal being to synthesise and characterise styrene grafted carbon nanotubes and its polystyrene nanocomposites (Nayak *et al.*, 2007). Xu *et al.*, manufactured a nanoporous pseudo-CPE with the aid of Sty, for potential use in molecular recognition, drug and environmental detection (Xu *et al.*, 2011). Sty has also been implemented in the design of molecularly imprinted polymers for the enhanced recognition of ribonuclease A (Hsu *et al.*, 2006).

The purpose behind the implementation of the Sty monomer into the CPE design in this research, was to try and create a more robust and tough electrode. The main aim was to try and produce a sensor that was not as vulnerable and as easily modified by a complex biological milieu as is observed with the CPEs. CPEs were manufactured initially (see Section 3.4.1) and then placed in Sty ON at 4 °C in the fridge. This time frame was chosen as this is the standard protocol used within the lab. O₂ calibrations were carried out in order to examine how the electrode performed with the addition of the Sty monomer. The results for the CPEs that had been placed in Sty ON are displayed in Table 4.3.2 and Figure 4.3.2 (a).

	CPE-Sty (ON) ($n = 4$)	
[O ₂], μM	Mean I, nA	SEM
0.0	0.0	0.0
240.0	-886.8	128.0
1200.0	-2472.6	108.7

Table 4.3.2: Table of results for an O₂ calibration in PBS (pH 7.4) using CPEs placed in Sty ON, ($n = 4$), carried out at -650 mV vs. SCE. Background values subtracted. Mean background current = -4.3 ± 1.1 nA.

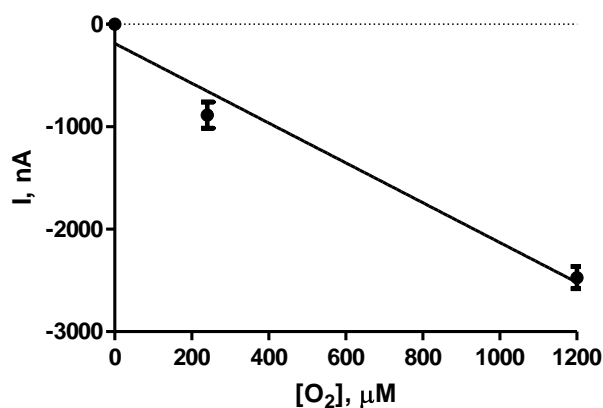


Figure 4.3.2 (a): A current-concentration profile for an O₂ calibration in PBS (pH 7.4) using CPEs placed in Sty ON ($n = 4$) carried out at -650 mV vs. SCE.

The O₂ calibration using the CPEs placed in Sty ON, gave a sensitivity of -1.9 ± 0.3 nA/ μM , $n = 4$. The response of the electrodes decreased in linearity over the specified range, mostly due to surface morphology, yielding an R^2 value of 0.97. A similar yet slightly higher sensitivity was observed for the CPEs placed in Sty ON in comparison to the unmodified CPEs. This could have been due to the greater surface area that had formed when the sensor had dried. The surface of the sensor was examined using SEM and it was clear from the image acquired that Sty was causing the surface to dip in the middle when it had desiccated, forming a concave appearance. The SEM image of the CPE incorporating the monomer Sty ON into the manufacture of the sensor is displayed below in Figure 4.3.2 (b).

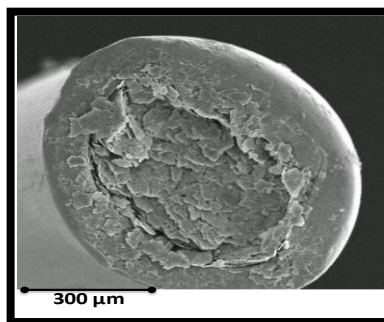


Figure 4.3.2 (b): SEM displaying the surface of the CPE placed in Sty ON.

In order to manufacture an electrode that is reproducible, a flat electrode is desirable. Prior to the development of the flat surface, O₂ calibrations pre- and post-treatment with Triton[®] X were carried out. This was deemed necessary to investigate, in order to determine if the SMCPE surface remained intact following exposure to the harsh surfactant or did a similar trend occur as was observed with the CPEs.

4.3.2.1 Treatments on SMCPE (ON) with Triton[®] X (10%)

[O ₂], μM	SMCPE (<i>n</i> = 4)		SMCPE-Triton [®] X (10%) ON (<i>n</i> = 4)	
	Mean I, nA	SEM	Mean I, nA	SEM
0.0	0.0	0.0	0.0	0.0
240.0	-886.8	128.0	-831.5	77.3
1200.0	-2472.6	108.7	-3095.5	452.9

Table 4.3.2.1: Table of results for O₂ calibrations in PBS (pH 7.4) using SMCPEs (*n* = 4) pre- and post-treatment with Triton[®] X (10%), carried out at -650 mV vs. SCE. Background values subtracted. Mean background currents (SMCPE) = -4.3 ± 1.1 nA and (SMCPE-Triton X (10%) ON) = -8.5 ± 1.0 nA.

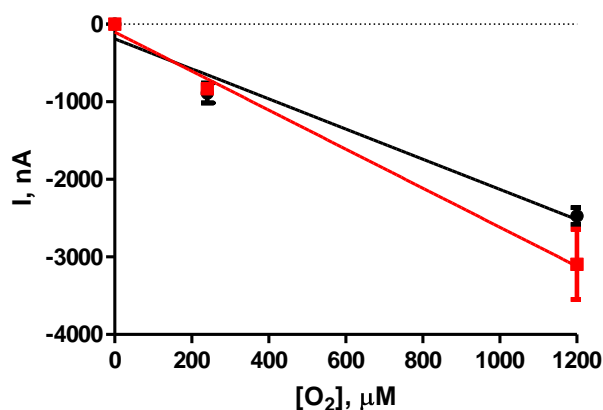


Figure 4.3.2.1: A current-concentration profile for O₂ calibrations in PBS (pH 7.4) using SMCPE pre (black) and post (red) treatment with Triton[®] X (10%) ON, carried out at -650 mV vs. SCE.

The results obtained for the O₂ calibrations using the SMCPE pre (black) and post (red) treatment with Triton[®] X (10 %) gave a sensitivity of -1.9 ± 0.3 nA/ μ M, $n = 4$ (pre-treatment) and -2.5 ± 0.2 nA/ μ M, $n = 4$ (post-treatment). The response of the electrodes decreased in linearity over the specified range with an R² value of 0.97 (pre-treatment) and increased in linearity to 0.99 (post-treatment). The results pre- and post-treatment were not significantly different ($P = 0.1742$). An increase in sensitivity after treatment with the surfactant Triton[®] X (10%) was observed, which could be as a result of the active surface being exposed due to the Triton[®] X removing the monomer from the carbon paste therefore increasing the sensitivity. The error bars were also increased after treatment with the surfactant which demonstrates that the effects on the electrodes varied.

An increase in the sensitivity may also be attributable to the increase in surface area of the electrode i.e. the concave shape that developed after the sensor had dried. After the preliminary results of treating the SMCPE with Triton[®] X-100, research was undertaken to try and obtain a flat reproducible SMCPE surface.

4.3.2.2 Optimisation of SMCPE surface

To try and eliminate the concave surface on the electrode, differing volumes of the Sty monomer ($\geq 99\%$ solution) were mixed with a consistent amount of carbon paste and repacked into the compartment of the electrode after it had been immersed in Sty ON (see Section 3.3.2.1). Once the electrodes had dried, they were tested against Triton[®] X (10%) to determine which volume of Sty, performed the best under these harsh conditions. Significant differences were observed for 16 μL ($P = 0.0021$), 20 μL ($P = 0.0005$), 24 μL ($P = 0.0139$) and 80 μL ($P = 0.0013$) Sty volumes pre and post exposure to Triton[®] X (paired t -tests). All volumes apart from 18 μL gave significant results leading to the chosen mixture of 18 μL Sty and 0.025 g carbon paste as the optimum result (shown in red).

Sensitivities of $-2.1 \pm 0.3 \text{ nA}/\mu\text{M}$, $n = 4$ and $-2.0 \pm 0.1 \text{ nA}/\mu\text{M}$, $n = 4$, pre- and post-treatment with Triton[®] X (10%) ON were recorded and the results were not significantly different ($P = 0.7783$). The result obtained from the 24 μL Sty concentration yielded an increase in the sensitivity post treatment with Triton[®] X. This was not chosen to continue on with because it showed that the electrode surface was compromised more than what was seen with the 18 μL Sty volume. From previous results, an increase in sensitivity post treatment with Triton[®] X, correlated to the leeching out of the oil, leading to greater electron transfer and an increased sensitivity. The main aim of this research was to produce an electrode that could withstand such manipulations, so therefore a volume of 18 μL of Sty was chosen.

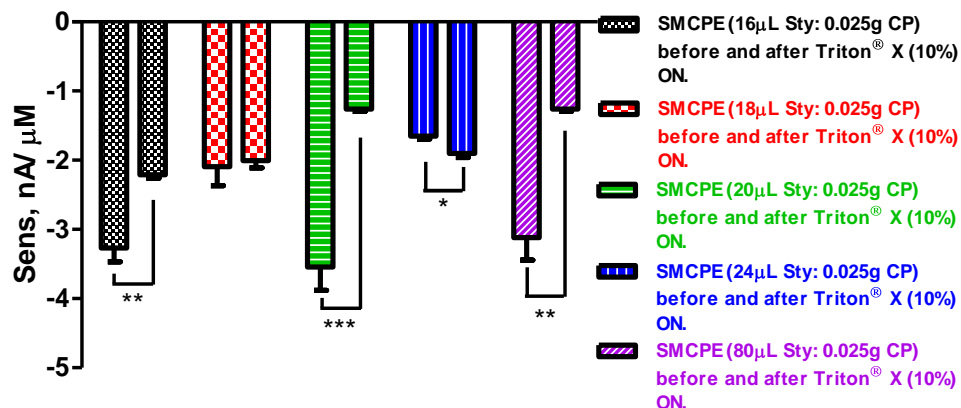


Figure 4.3.2.2 (a): A bar chart displaying the sensitivities obtained from O_2 calibrations, using SMCPE in PBS (pH 7.4) with varying volumes of the Sty mixture, pre- and post-treatment with Triton[®] X (10%), ($n = 4$) carried out at -650 mV vs. SCE.

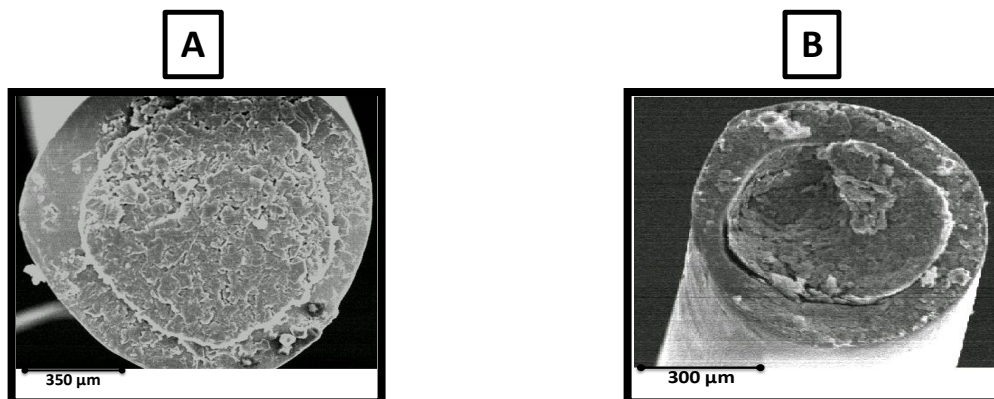


Figure 4.3.2.2 (b): SEMs displaying the surface of (A); SMCPE prior to treatment with Triton[®] X ON (B); SMCPE post treatment with Triton[®] X (10%) ON.

A flat and uniform SMCPE surface was obtained following repacking of the chosen volume of Sty mixture (see Figure (4.3.2.2 (b))). Upon treatment with Triton[®] X ON, the surface was agitated slightly on one side of the electrode, however, in comparison to the CPEs (see Figure 4.3.1.1.6), this result is dramatically improved. The SMCPE demonstrates remarkable resistance to the very harsh surfactant which is extremely encouraging for future applications of the sensor.

4.3.2.3 UV light on SMCPE

Photo-initiated polymerisations can occur with the production of radicals by UV light. Initiation by photolysis occurs with monomers (Sty and MMA) that contain a double bond linked with other groups (Oster & Yang, 1968). The polymerisation of Sty by UV light has been demonstrated by Bai *et al.*, upon which thin polystyrene films were produced on polycrystalline Pt (Bai *et al.*, 2001). Sty can also undergo thermal polymerisation and it is stated that the polymerisation occurs at a speed of 0.1 % per hour at 60 °C and 2 % per hour at 100 °C (Khuong *et al.*, 2005). Subsequent to the results obtained for the SMCPE, it was decided that UV light (which was chosen as the most suitable method of polymerisation), would be utilised to try and polymerise the Sty monomer straight after it had been repacked with the Sty/carbon paste mixture. A compact and solid mixture in the cavity was the main feature sought after by utilising this polymerisation process. The resulting electrode was then treated with Triton[®] X (10%) to determine how the electrode would perform after being immersed in a harsh milieu. The results from this are displayed in Figure 4.3.2.3 (a) and Table 4.3.2.3. Images are also shown (see Figure 4.3.2.3 (b)), to demonstrate the effect of the UV light on the electrode and the Triton[®] X treatment.

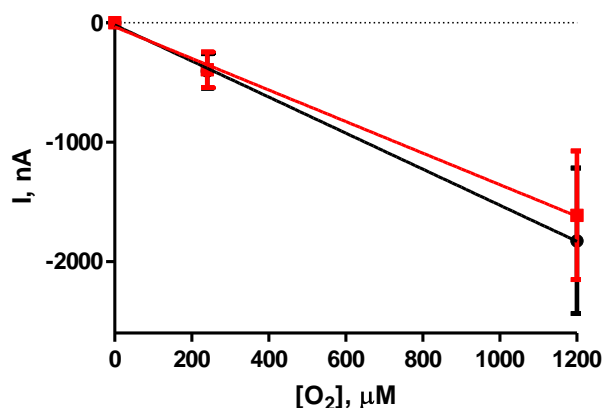


Figure 4.3.2.3 (a): A current-concentration profile for O₂ calibrations in PBS (pH 7.4) using SMCPE-UV pre (black) and post (red) treatment with Triton[®] X-100 (10%) ON, carried out at -650 mV vs. SCE.

[O ₂], μM	SMCPE-UV ($n = 4$)		SMCPE-UV-Triton [®] X ($n = 4$)	
	Mean I, nA	SEM	Mean I, nA	SEM
0.0	0.0	0.0	0.0	0.0
240.0	-403.1	144.9	-393.5	149.4
1200.0	-1826.6	610.5	-1612.8	539.5

Table 4.3.2.3: Table of results for O₂ calibrations in PBS (pH 7.4) using SMCPE-UV ($n = 4$) pre- and post-treatment with Triton[®] X-100 (10%) ON, carried out at -650 mV vs. SCE. Background values subtracted. Mean background current (SMCPE-UV-30mins) = -290.2 ± 108.9 nA and (SMCPE-UV-Triton X (10%)-ON = -175.5 ± 86.4 nA

The results obtained for the O₂ calibrations using the SMCPE-UV pre (black) and post (red) treatment with Triton[®] X-100 (10 %) ON, yielded sensitivities of -1.5 ± 0.1 nA/ μM , $n = 4$ and -1.3 ± 0.1 nA/ μM , $n = 4$, respectively. The response of the electrodes was linear over the specified range with an R² value of 0.99 (pre-treatment) and 0.99 (post-treatment). The results pre- and post-treatment were not significantly different ($P = 0.8312$, paired t -test). It was observed upon exposure to UV light that the components rose out of the cavity of some of the electrodes leading to a loss in connection between the composite and the silver wire. While other electrodes retained a connection the composite still rose from the compartment of the electrode. It is hypothesised that the polymerisation took place too quickly causing the cavity components to reduce in size and rise out of the cavity. Following treatment with Triton[®] X (10%) ON, more of the composite was removed from the cavity from some of the electrodes and the surfaces were damaged by the treatment.

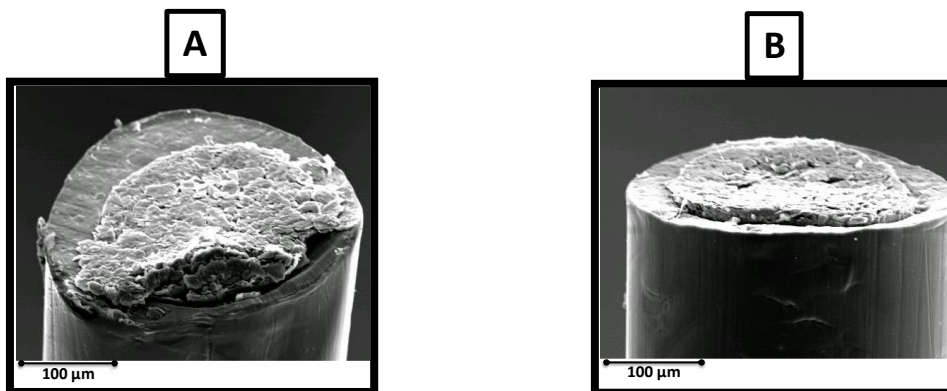


Figure 4.3.2.3 (b): SEMs displaying the surface of (A): SMCPE-UV prior to treatment with Triton[®] X (10%)-ON (B): SMCPE-UV post treatment with Triton[®] X-100 (10%) ON.

Figure 4.3.2.3 (b), displays the SMCPE post treatment with UV light. It is evident from the image that the UV light had a negative effect on the SMCPEs. The components in the compartment of the electrode had pulled up out of the cavity and some electrodes had lost connection with the silver wire surface underneath. After treatment with Triton[®] X, the loose components at the surface of the electrode were removed by the surfactant. UV appeared to compromise the sensor performance and so it was decided not to continue on with the polymerisation process for the SMCPEs.

4.3.2.4 Optimum potential profile of SMCPE

Figure 4.3.2.4, demonstrates an optimum potential profile that was carried out on the SMCPE to determine the optimum working potential to apply to the electrodes. The purpose of this was to validate that the chosen potential was indeed the correct one. Following exposure to different proteins, lipids and surfactant treatments the oxidation/reduction potentials have been shown to shift to alternative potentials. Kane *et al.*, observed this trait when treating CPEs with the different substances mentioned in Section 4.3.1.1(A. Kane & D. O'Neill, 1998).

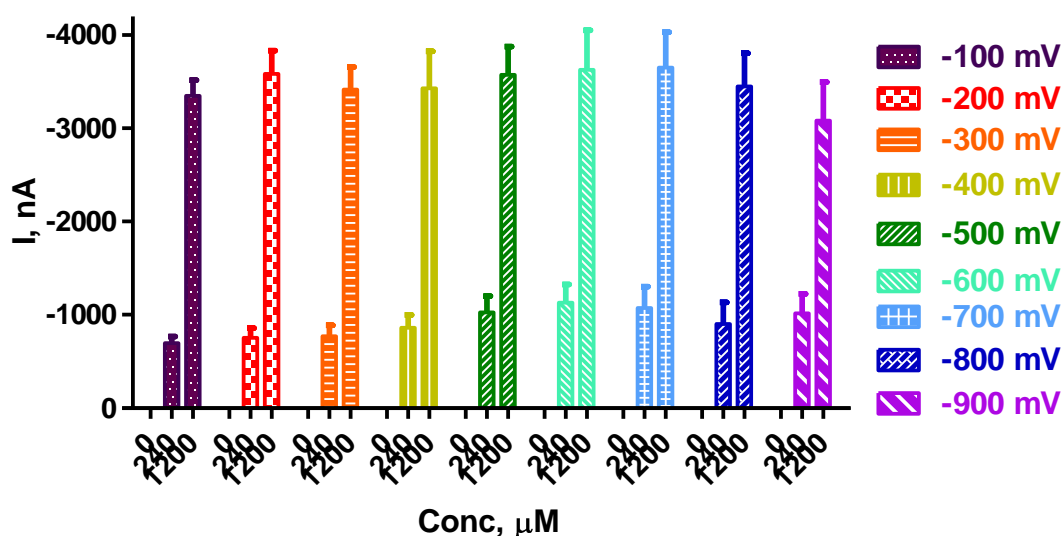


Figure 4.3.2.4: An optimum potential profile carried out on SMCPEs ($n = 4$), at a potential range of (-100 mV to -900 mV) in PBS (pH 7.4) using CPA.

There was no significant difference between all of the potentials applied to the SMCPEs ($P = 0.8706$, one-way ANOVA). It was observed that the potentials -600 mV vs. SCE and -700 mV vs. SCE gave a slightly higher sensitivity. A potential of -650 mV vs. SCE was initially suggested as the applied potential to use, as this correlated with the potential used for CPEs and other O_2 sensors in effect in the lab. To further validate that the reduction potential had not shifted, CV was performed on the sensor design to investigate this.

4.3.2.5 CV of SMCPE

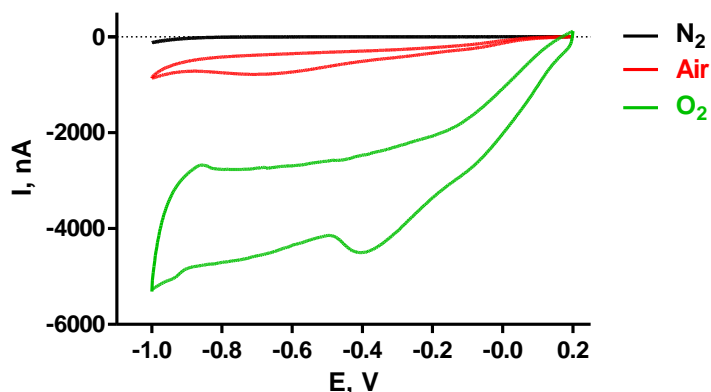


Figure 4.3.2.5: A CV from -1 to 0.2 V *vs.* SCE carried out on SMCPEs and performed in PBS (pH 7.4).

A clear O₂ reduction peak is observed at *ca.* -0.4 V in the SMCPE. The resulting O₂ wave is much larger than what can be seen in CPEs, possibly due to the different surface composition and the monomer Sty. A reduction peak is observed at *ca.* -0.6 V for CPEs which was demonstrated by Bolger *et al.*, and the O₂ peak differences in both sensors indicate that the rate constant for charge transfer is greater at SMCPEs than at CPEs (Bolger *et al.*, 2011a). It was confirmed from both the optimum potential profile and CV that a potential of -650 mV *vs.* SCE could be utilised and this was chosen for the SMCPEs, as this is in the diffusion limited region and was the potential utilised for other O₂ sensors in the lab.

4.3.2.6 Validation of the final SMCPE design

In summary, the final SMCPE design involved placing the CPEs in Sty ON and then quickly packing a mixture of the monomer and carbon paste (18 μ L and 0.025 g carbon paste) into the cavity of the electrode and allowing the electrode to dry. Following the results discussed in this section, the final method of manufacturing the SMCPE was reproduced.

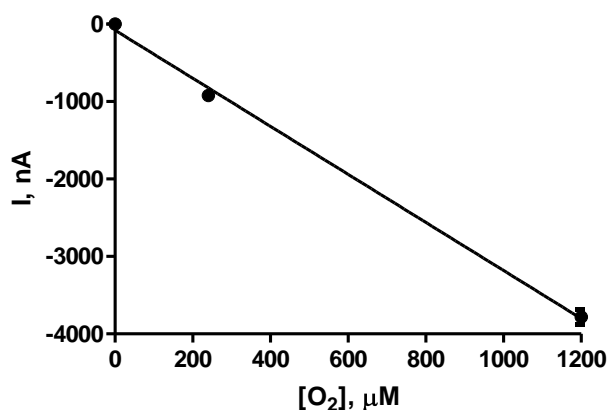


Figure 4.3.2.6: A current-concentration profile for O₂ calibrations in PBS (pH 7.4) using SMCPEs ($n = 52$), carried out at -650 mV vs. SCE.

SMCPE ($n = 52$)		
[O ₂], μM	Mean I, nA	SEM
0.0	0.0	0.0
240.0	-921.3	37.9
1200.0	-3782.5	97.5

Table 4.3.2.6: Table of results for O₂ calibrations in PBS (pH 7.4) with SMCPEs ($n = 52$), carried out at -650 mV vs. SCE. Background values subtracted. Mean background current SMCPEs = -7.8 ± 1.1 nA

Figure 4.3.2.6 and Table 4.3.2.6, display the data obtained for the O₂ calibrations with the SMCPE. A sensitivity of -3.1 ± 0.1 nA/μM, $n = 52$, was recorded and a linear response was observed over the specified range ($R^2 = 0.99$). A greater O₂ sensitivity was achieved with the new monomer modified CPE. Experiments carried out with the surfactant Triton[®] X confirmed how intact and robust the cavity components of the SMCPE were in comparison to the CPEs, which were totally destroyed by this treatment. It is hypothesised that the Sty is causing a much faster electron transfer rate, as supported by experimental data, thus creating a higher O₂ sensitivity. The next section discusses the development of the MMCPE, which was carried out in a similar manner as the SMCPE.

4.3.3 MMA modified CPE (MMCPE)

Poly (MMA) is a clear colourless polymer that has been used in optical applications. The integration of the monomer MMA with diffuser plates (which are rough reflectors that are used to scatter light and prevent glare), have been used in order to reduce irregularity and cloudiness observed in an LCD screen due to high temperatures (Kim, 2005). The incorporation of the MMA polymer as an immobilisation matrix for the fabrication of biosensors has been demonstrated in research carried out by Perez *et al.*, (Pérez *et al.*, 2006). Chatzandroulis *et al.*, describes the use of MMA for the fabrication of capacitive type chemical sensors (Chatzandroulis *et al.*, 2004b). Dai *et al.*, utilised poly(MMA) in the design of a graphite sensor for vitamin C, the characteristics that the monomer possesses, like low price and mechanical stability, were appealing for the manufacture of this sensor (Dai *et al.*, 2008).

The incorporation of MMA into the construction of dental appliances, demonstrates a compatibility with human tissue (Douglas & Bates, 1978; Murray & Darvell, 1993; Sarac *et al.*, 2006). CPEs were manufactured initially (see Section 3.4.1) and then placed in MMA ON at 4 °C in the fridge. O₂ calibrations were carried out in order to examine how the electrode performed with the addition of the MMA monomer. The results for the CPEs that were placed in MMA ON are displayed in Table 4.3.3 and Figure 4.3.3 (a).

CPE-MMA(ON) (<i>n</i> = 4)		
[O ₂], μM	Mean I, nA	SEM
0.0	0.0	0.0
240.0	-691.7	120.4
1200.0	-2998.6	107.3

Table 4.3.3: Table of results for an O₂ calibration in PBS (pH 7.4) using CPEs placed in MMA ON, *n* = 4, carried out at -650 mV vs. SCE. Background values subtracted. Mean background current of -3.8 ± 1.6 nA.

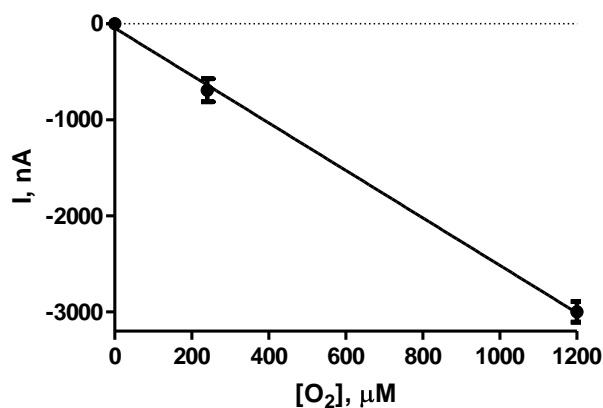


Figure 4.3.3 (a): A current-concentration profile for O₂ calibrations in PBS (pH 7.4) using CPEs placed in MMA ON, ($n = 4$), carried out at -650 mV vs. SCE.

The O₂ calibration using CPEs placed in MMA ON, displayed a sensitivity of -2.5 ± 0.1 nA/ μ M, $n = 4$. A linear response was obtained over the specified range ($R^2 = 0.99$). A slightly higher sensitivity was observed for the CPEs placed in MMA ON in comparison to the CPEs. It was noticed that the MMCPEs contained a concave shape at the surface after the composite had dried, therefore creating a greater surface area. This may be the reason for a slightly increased O₂ sensitivity. A similar occurrence was observed with the SMCPEs. The surface of the sensor was examined using SEM and it was clear from the image acquired that MMA was causing the surface to dip in the middle when it had dried, forming a concave appearance. An SEM image displaying the surface of the CPE following immersion in MMA ON is displayed in Figure 4.3.3 (b).

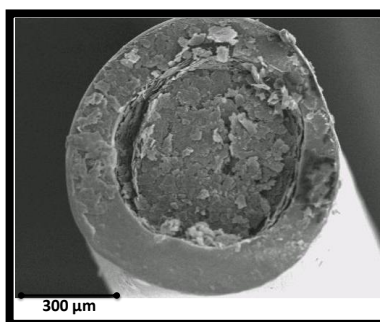


Figure 4.3.3 (b): A SEM displaying the surface of a CPE that had been immersed in MMA ON.

In Figure 4.3.3 (b), the image demonstrates how the surface had dipped in the centre, revealing a concave shape. A similar effect was displayed by the CPE that had been placed in Sty ON (see Figure 4.3.2 (b)). In order to manufacture a reproducible electrode, a flat surface must be obtained. Prior to the development of the flat surface O₂ calibrations pre- and post-treatment with Triton[®] X were carried out in order to verify if the MMCPE surface remained intact following exposure to the harsh surfactant or did a similar trend occur as was observed with the CPEs.

4.3.3.1 Treatments on MMCPE (ON) with Triton[®] X (10%)

[O ₂], μM	MMCPE (<i>n</i> = 4)		MMCPE-Triton [®] X (10%) ON, (<i>n</i> = 4)	
	Mean I, nA	SEM	Mean I, nA	SEM
0.0	0.0	0.0	0.0	0.0
240.0	-691.8	120.4	-797.1	11.9
1200.0	-2998.6	107.3	-2478.4	63.5

Table 4.3.3.1: Table of results for O₂ calibrations in PBS (pH 7.4) using MMCPEs (*n* = 4) pre- and post-treatment with Triton[®] X-100 (10%) ON, carried out at -650 mV vs. SCE. Background values subtracted. Mean background current (MMCPE) = -3.8 ± 1.6 nA and (MMCPE-Triton[®] X (10%) ON) = -10.2 ± 1.4 nA.

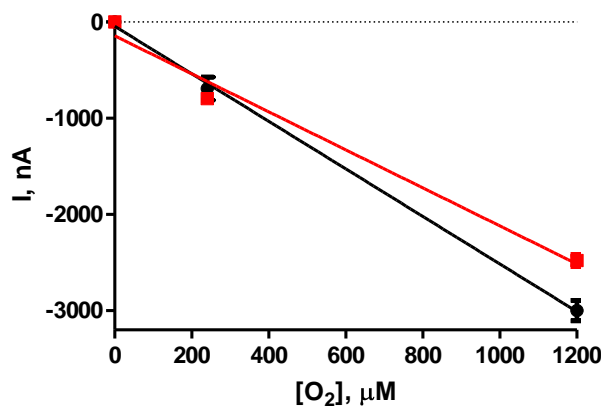


Figure 4.3.3.1: A current-concentration profile for O₂ calibrations in PBS (pH 7.4) with MMCPEs pre (black) and post (red) treatment with Triton[®] X-100 (10%) ON, carried out at -650 mV vs. SCE.

The results obtained for the O₂ calibrations using the MMCPEs pre (black) and post (red) treatment with Triton[®] X (10 %) ON, yielded sensitivities of -2.5 ± 0.3 nA/ μ M, $n = 4$ and -1.9 ± 0.3 nA/ μ M, $n = 4$, pre- and post- Triton[®] X treatment. The response of the electrodes was linear over the specified range with an R² value of 0.99 (pre-treatment) and 0.98 (post-treatment). The results pre- and post-treatment were significantly different ($P = 0.0052$, paired t -test). After the preliminary results of treating the MMCPE with Triton[®] X (10%), research was carried out in order to try and obtain a flat reproducible MMCPE surface.

4.3.3.2 Optimisation of MMCPE surface

To try and eliminate the concave surface on the electrode, differing volumes of the MMA monomer (99 % solution), were mixed with a consistent amount of carbon paste and repacked into the compartment of the electrode, after it had been immersed in MMA ON (see Section 3.4.2). Once the electrodes had dried, they were tested against Triton[®] X to determine which volume of MMA performed the best under these harsh conditions. Significant differences were observed for 16 μ L ($P = 0.0115$), 18 μ L ($P = 0.0007$) and 80 μ L ($P = 0.0180$) MMA volumes pre and post exposure to Triton[®] X (paired t -tests). There was no significant difference between the 20 μ L ($P = 0.4530$) and 24 μ L ($P = 0.5678$) MMA volumes pre- and post-treatment with Triton[®] X (10%) ON (paired t -tests). On comparison of the two MMA volumes (20 μ L vs. 24 μ L), there was no significant difference ($P = 0.2907$, unpaired t -test). The mixture of 20 μ L MMA and 0.025 g carbon paste was chosen as the optimum result (shown in green), as it utilised less of the monomer for manufacture of the sensors. The results of this volume of MMA yielded sensitivities of -2.3 ± 0.1 nA/ μ M, $n = 4$ and -2.4 ± 0.1 nA/ μ M, $n = 4$, pre- and post-treatment with Triton[®] X (10%) respectively.

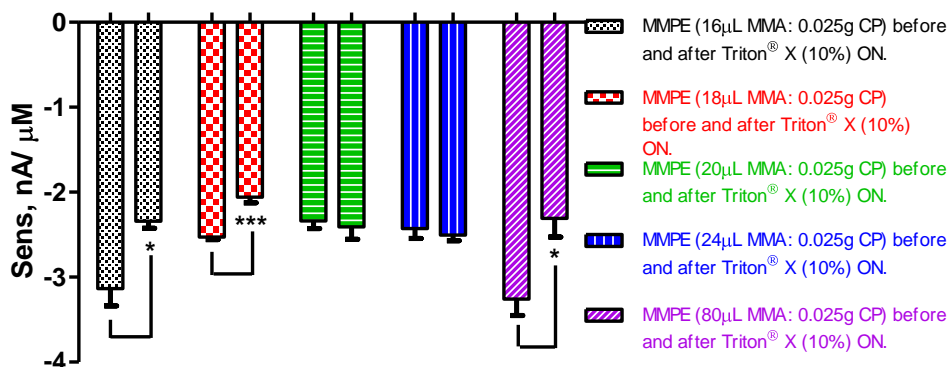


Figure 4.3.3.2 (a): A bar chart displaying the sensitivities obtained in O_2 calibrations, using MMCPE in PBS (pH 7.4) with the varying volumes of MMA mixture, and post treatment with Triton[®] X-100 (10%) ON, carried out at -650 mV vs. SCE.

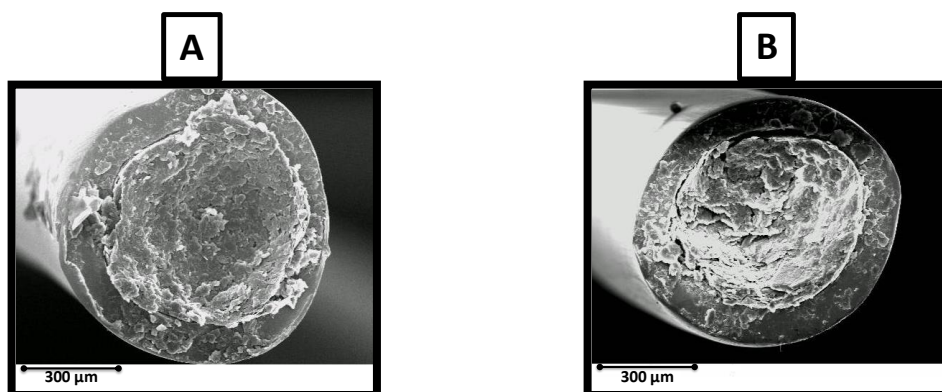


Figure 4.3.3.2 (b): SEMs displaying the surface of (A); MMCPE prior to treatment with Triton[®] X-100 ON (B); MMCPE post treatment with Triton[®] X-100 (10%) ON.

A flat uniform MMCPE surface was obtained following repacking of the optimum volume of MMA mixture (see Figure 4.3.3.2 (b)). Upon treatment with Triton[®] X ON, the surface was altered slightly, however, in comparison to the CPEs (see Figure 4.3.1.1.6), this result is considerably improved. The MMCPE demonstrates remarkable resistance to the very harsh surfactant which is extremely encouraging for future applications of the sensor.

4.3.3.3 UV light on MMCPE

Polymerisation can take place with the creation of radicals by UV light. Initiation by this UV mechanism occurs with monomers (MMA and Sty) that contain a double bond linked with other groups (Oster & Yang, 1968). An example of polymerisation of MMA at 25 °C with 5.0 % 2,2'-azobis(2-methylpropionitrile) (AIBN) initiated by UV light has been previously demonstrated by Zhu *et al.*, (Zhu *et al.*, 1990b). Another method of polymerisation has been discussed by Kruss and Patraboy who utilised intense ultrasound to initiate polymerisation of MMA (Kruus & Patraboy, 1985). In a separate study, the surface of silica nanoparticles were modified by UV induced graft polymerisation of MMA (Kim *et al.*, 2005). It was decided that UV light would be utilised to try and polymerise the monomer MMA, straight after it had been repacked with the MMA/carbon paste mixture. The resulting electrode was then treated with Triton[®] X. The results from this are displayed below in Figure 4.3.3.3 (a) and Table 4.3.3.3. SEM images are also shown (see Figure 4.3.3.3 (b)), to demonstrate the effect of the UV light on the electrode and the Triton[®] X treatment.

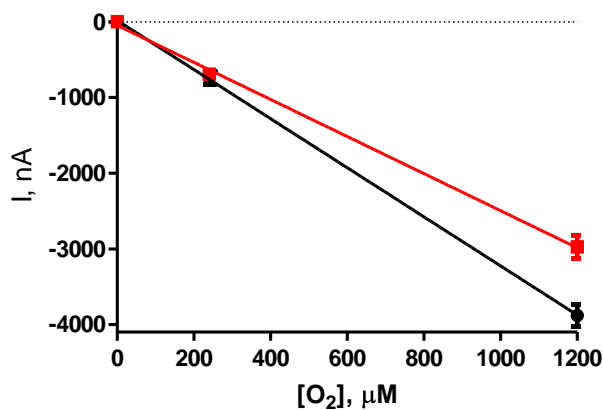


Figure 4.3.3.3 (a): A current-concentration profile for O₂ calibrations in PBS (pH 7.4) with MMCPE-UV, $n = 12$, pre (black) and post (red) treatment with Triton[®] X-100 (10%), carried out at -650 mV vs. SCE.

[O ₂], μM	MMCPE-UV (<i>n</i> = 12)		MMCPE-UV-Triton [®] X (<i>n</i> = 12)	
	Mean I, nA	SEM	Mean I, nA	SEM
0.0	0.0	0.0	0.0	0.0
240.0	-739.8	88.2	-693.2	73.5
1200.0	-3878.6	144.6	-2973.9	153.9

Table 4.3.3.3: Table of results for O₂ calibrations in PBS (pH 7.4) with MMCPE-UV (*n* = 12) pre- and post-treatment with Triton[®] X-100 (10%), carried out at -650 mV vs. SCE. Background values subtracted. Mean background current (MMCPE-UV) = -9.4 ± 1.2 nA and (MMCPE-UV-Triton[®] X ON) = -12.8 ± 1.6 nA.

O₂ calibrations using the MMCPE-UV pre (black) and post (red) treatment with Triton[®] X (10 %) displayed sensitivities of -3.2 ± 0.1 nA/ μM, *n* = 12 (pre-treatment) and -2.6 ± 0.1 nA/ μM, *n* = 12 (post-treatment). A linear response was obtained over the specified range with an R² value of 0.99 (pre-treatment) and 0.99 (post-treatment). The results pre- and post-treatment were not significantly different (*P* = 0.8735, paired *t*-test). Exposure of the electrode to UV light seemed to enhance the sensors O₂ sensitivity. The surface was much more intact and uniform on inspection after UV treatment. The experiment carried out with the surfactant Triton[®] X, slightly aggravated the surface, but in comparison to the CPEs, the electrode compartment displayed a robust and an intact characteristic.

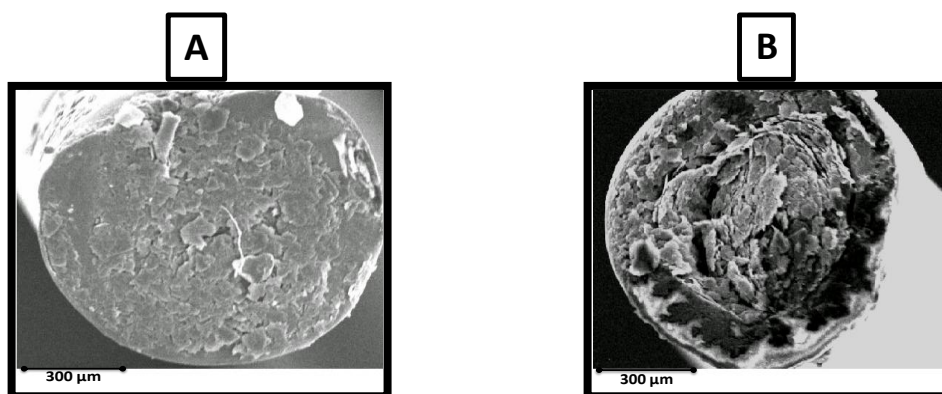


Figure 4.3.3.3 (b): SEMs displaying the surface of (A): MMCPE-UV prior to treatment with Triton[®] X (10%) ON (B): MMCPE-UV post treatment with Triton[®] X-100 (10%) ON.

Figure 4.3.3.3 (b) displays the MMCPE post treatment with UV light, it is evident from the image that a much improved electrode surface is created with placing the electrode under the UV light. After treatment with Triton[®] X ON, the surface roughness of the electrode increased, but not to the extent seen with the CPEs (see Figure 4.3.1.1.6). The final method was now fabricated for manufacture of the MMCPE.

4.3.3.4 Optimum potential profile of MMCPE

Figure 4.3.3.4, demonstrates an optimum potential profile that was carried out on the MMCPE to determine the optimum working potential at which to apply to the electrodes. The main reason for this was to validate that the chosen potential was indeed the most correct one.

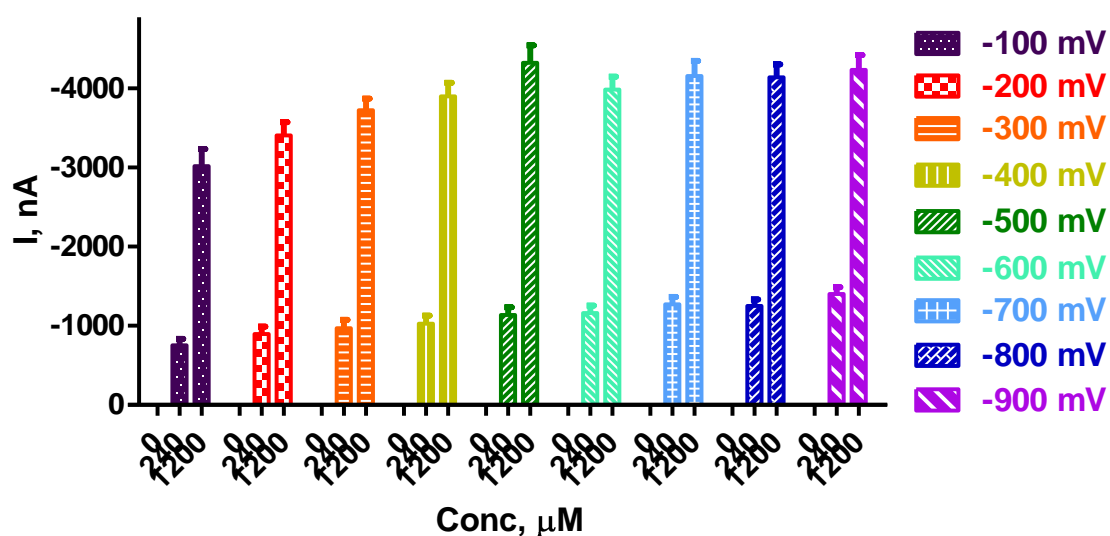


Figure 4.3.3.4: An optimum potential profile carried out on MMCPEs ($n = 8$), at a potential range of (-100 mV to -900 mV) in PBS (pH 7.4) using CPA.

There was no significant difference between any of the potentials applied to the MMCPEs ($P = 0.2818$, one-way ANOVA). It was observed that the potentials -500 mV vs. SCE displayed a slightly higher sensitivity than the rest but as there was no significance between the results, it was decided to continue with -650 mV. This will allow for direct comparison to be made against the standard CPEs, Pt O₂ sensors (Bolger *et al.*, 2011a) and also other

O₂ sensors currently utilised in our laboratory. To further confirm that the reduction potential had not shifted, cyclic voltammetry was carried out on the sensor design to examine this.

4.3.3.5 CV of MMCPE

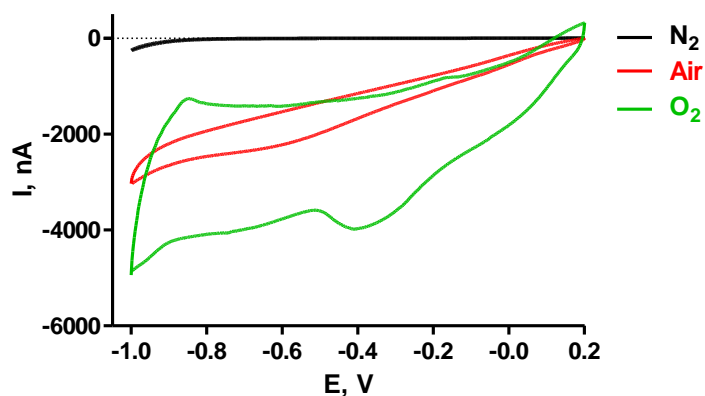


Figure 4.3.3.5: A CV from -1 to 0.2 V vs. SCE carried out on MMCPEs and performed in PBS (pH 7.4).

The O₂ wave details a reduction peak at *ca.* -0.4 V. The CPEs have been shown as having a reduction peak at *ca.* -0.6 V (Bolger *et al.*, 2011a). This reveals that the rate constant for charge transfer is higher at the MMCPEs than at CPEs. It was decided that -650 mV vs. SCE was the chosen potential to implement as this is in the diffusion limited region and all O₂ sensors employed in the lab apply this potential.

4.3.3.6 Validation of the final MMCPE design

The final MMCPE design involved placing the CPEs in MMA ON and then quickly packing a mixture of the monomer and carbon paste (20 μ L and 0.025 g carbon paste) into the compartment of the electrode, subsequent to this, UV light was utilised to initiate polymerisation of the surface of the electrode for 30 minutes. The final method for the development of the MMCPEs was now elucidated and the resulting O₂ calibrations detail

an increased sensitivity and produce a more reliable and reproducible electrode for the detection of O₂.

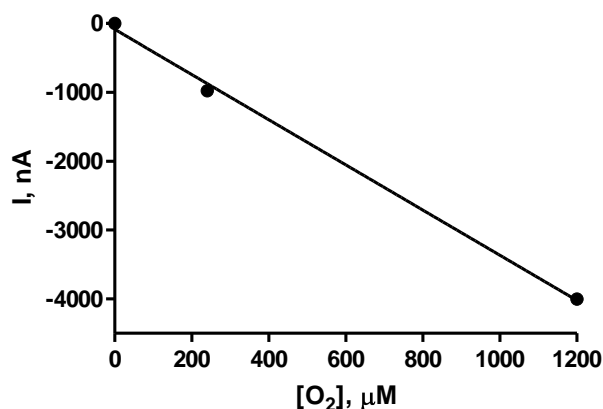


Figure 4.3.3.6: A current-concentration profile for O₂ calibrations in PBS (pH 7.4) using MMCPEs ($n = 52$), carried out at -650 mV vs. SCE.

MMCPE-UV ($n = 52$)		
[O ₂], μM	Mean I, nA	SEM
0.0	0.0	0.0
240.0	-977.5	37.7
1200.0	-4002.5	72.6

Table 4.3.3.6: Table of results for an O₂ calibration in PBS (pH 7.4) using MMCPE ($n = 52$), carried out at -650 mV vs. SCE. Background values subtracted. Mean background current = -10.21 ± 1.11 nA.

The results obtained for the O₂ calibrations on the MMCPEs exposed to UV light, $n = 52$, show a sensitivity that exceeds the sensitivity of O₂ observed at a CPE. Figure 4.3.3.6 and table 4.3.3.6, display the data. A sensitivity of -3.3 ± 0.2 nA/μM, $n = 52$, was recorded and a linear response was observed over the specified range ($R^2 = 0.99$). The monomers Sty and MMA seem to be the reason for this increased affinity for O₂.

The fabrication of an oil free carbon based sensor is discussed in the next section, in order to determine if the manufacture of the monomer-modified carbon based sensor needed to include the oil, as used in CPEs.

4.3.4 Oil free carbon based electrodes

4.3.4.1 Methyl methacrylate graphite powder electrode (MMGPE)

The exclusion of the oil from the fabrication of the monomer modified sensors was undertaken after other groups had carried out research that involved graphite powder (GP) and the monomer MMA. These studies were necessary to carry out as, utilising the GP instead of the carbon paste would alleviate some of the production time for the manufacture of the monomer modified sensor. Dai *et al.*, and Regal *et al.*, utilised graphite/poly (MMA) composite electrodes for the electrochemical detection of vitamin C and dopamine, respectively (Dai *et al.*, 2008; Regal & Lunte, 2013). In this thesis, the oil free carbon based electrode was made exactly in the same manner as the CPE, however, the carbon paste was replaced with GP leading to the results shown in Figure 4.3.4.1. A ratio of 60 %: 40 % was utilised for the MMA:GP composite, respectively (Dai *et al.*, 2008).

Varying techniques were employed to try and solidify the composite in the cavity i.e. thermal, air and UV methods. It was very difficult to pack the GP into the cavity of the electrode without the aid of the oil, as the GP was too dry, leading to the surface morphology being easily corrupted. Even with the techniques of heating, air drying and applying UV to the composite, the results obtained were not satisfactory. The ratio of the monomer was increased also to try and make the composite easier to pack but to no avail. Addition of the MMA monomer to the GP and various other methods employed to solidify the components in the cavity of the electrode, are displayed in Figure 4.3.4.1.

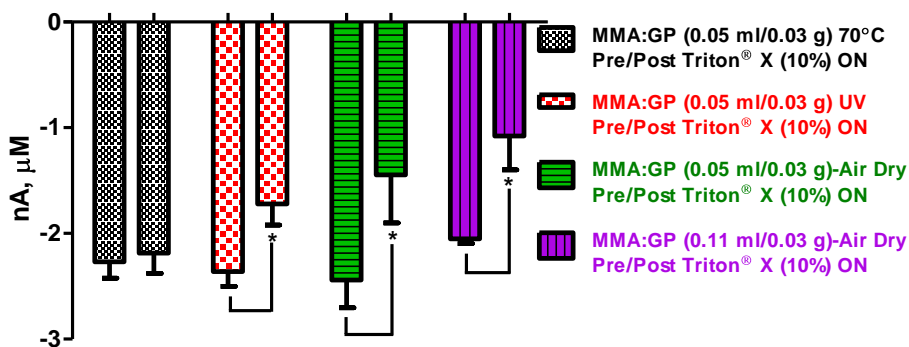


Figure 4.3.4.1: A bar chart for O₂ calibrations in PBS (pH 7.4) using an oil free carbon based monomer electrode, carried out at -650 mV vs. SCE.

Following the results shown in Figure 4.3.4.1, developing an oil free carbon based electrode was not as successful as the results attained for the MMCPEs and SMCPEs. Significant differences pre- and post-treatment with Triton[®] X were obtained for MMA:GP-UV electrodes (shown in red) ($P = 0.0401$, paired t -test), MMA:GP-Air electrodes (shown in green) ($P = 0.0486$, paired t -test) and MMA:GP-Air electrodes (shown in purple) ($P = 0.0239$, paired t -test). The best result from the graphite-monomer electrode was a sensitivity (shown in black) of -2.3 ± 0.2 pre-treatment and -2.2 ± 0.2 post-treatment with Triton[®] X. The response of the electrodes was linear over the specified range with an R^2 value of 0.99 pre-treatment and 0.99 post-treatment with Triton[®] X. The results were not significantly different pre- and post-treatment ($P = 0.7497$, paired t -test).

4.3.4.2 Styrene graphite powder electrode (SMGPE)

The same procedure was carried out for SMGPEs as was described in the previous section for MMCPEs. Replacing the carbon paste with GP and then incorporating the Sty monomer, proved to be difficult, as the graphite was too dry without the oil for packing into the cavity of the electrode. Following the addition of the Sty monomer to the GP, the electrodes were placed in an oven at 70 °C for thirty minutes. This was the optimum result achieved by the MMGPE and therefore was utilised as the method of development for the SMGPE. The results obtained for the SMGPEs are displayed in Figure 4.3.4.2.

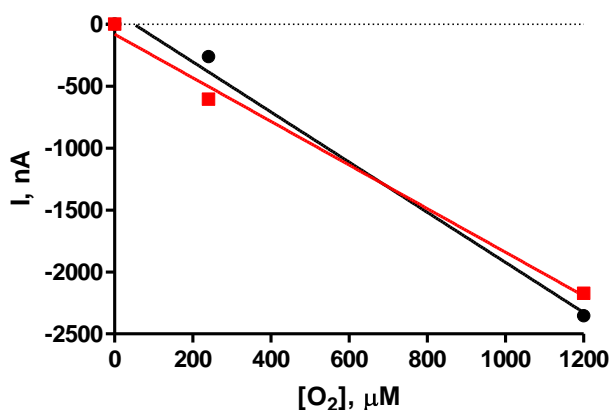


Figure 4.3.4.2: A current-concentration profile for O₂ calibrations in PBS (pH 7.4) using SMGPEs baked at 70 °C for 30 minutes ($n = 4$) pre (black) and post (red) treatment with Triton[®] X (10%) ON, carried out at -650 mV vs. SCE.

Following the results shown in Figure 4.3.4.2, developing an oil free carbon based electrode was not as successful as the results attained for the MMCPEs and SMCPEs. The best result from the SMGPE gave a sensitivity of -2.0 ± 0.2 pre-treatment (black) and -1.8 ± 0.1 post-treatment (red) with Triton[®] X (10%) ON. The response of the electrodes was linear over the specified range with an R^2 value of 0.99 pre-treatment and 0.99 post-treatment with Triton[®] X ON. The results were not significantly different pre- and post-treatment ($P = 0.1120$, paired t -test).

4.3.5 Biocompatibility studies

After the successful development of the novel monomer CPEs, experiments were undertaken to determine the effect that proteins, lipids and brain tissue would have on these new electrodes. O₂ calibrations pre- and post-treatment were initially carried out utilising the SMCPEs.

4.3.5.1 SMCPE-BSA (ON)

[O ₂], μM	SMCPE (<i>n</i> = 8)		SMCPE-BSA (10%) (<i>n</i> = 8)	
	Mean I, nA	SEM	Mean I, nA	SEM
0.0	0.0	0.0	0.0	0.0
240.0	-1153.4	79.5	-1296.1	47.9
1200.0	-3595.7	177.8	-3413.2	120.9

Table 4.3.5.1: Table of results for O₂ calibrations in PBS (pH 7.4) using SMCPEs (*n* = 8) pre- and post-treatment with BSA (10%) carried out at -650 mV vs. SCE. Background values subtracted. Mean background current (SMCPE) = -177.1 ± 58.3 nA and (SMCPE-BSA (10%)-ON) = -65.9 ± 17.2 nA.

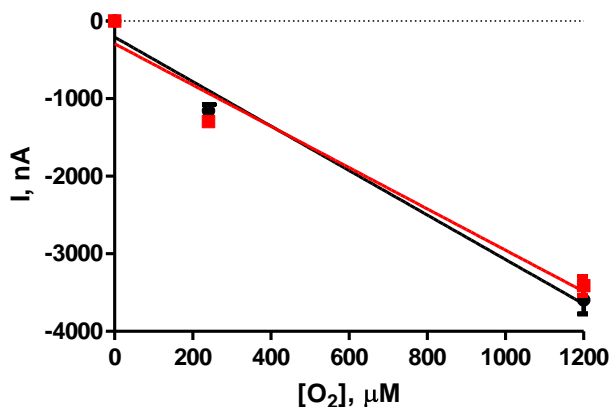


Figure 4.3.5.1: A current-concentration profile for O₂ calibrations in PBS (pH 7.4) using SMCPEs (*n* = 8) pre (black) and post (red) treatment with BSA (10%) ON, carried out at -650 mV vs. SCE.

The results obtained for the O₂ calibrations using the SMCPEs pre- and post-treatment with BSA (10%) ON, yielded sensitivities of -2.8 ± 0.4 nA/μM, *n* = 8 and -2.7 ± 0.5 nA/μM, *n* = 8, respectively. The response of the electrodes decreased in linearity over the specified range with an R² value of 0.98 (pre-treatment) and 0.96 (post-treatment). The results pre- and post-treatment were not significantly different (*P* = 0.9932, paired *t*-test). When using BSA (10%) against standard CPEs it is observed that the harsh concentration alters the morphology of the sensor and blocks the active surface on the CPEs, thus decreasing the sensitivity recorded. With these novel sensors, the BSA does not seem to hamper the ability of the sensor to detect O₂.

4.3.5.2 SMCPE-PEA (ON)

[O ₂], μM	SMCPE (<i>n</i> = 8)		SMCPE- PEA (10%) ON (<i>n</i> = 8)	
	Mean I, nA	SEM	Mean I, nA	SEM
0.0	0.0	0.0	0.0	0.0
240.0	-1019.4	69.5	-996.2	55.9
1200.0	-3256.6	68.9	-3402.2	94.2

Table 4.3.5.2: Table of results for O₂ calibrations in PBS (pH 7.4) using SMCPEs (*n* = 8) pre- and post-treatment with PEA (10%), carried out at -650 mV vs. SCE. Background values subtracted. Mean background current (SMCPEs) = -180.6 ± 11.9 nA and (SMCPE PEA (10%) ON) = -321.2 ± 25.1 nA.

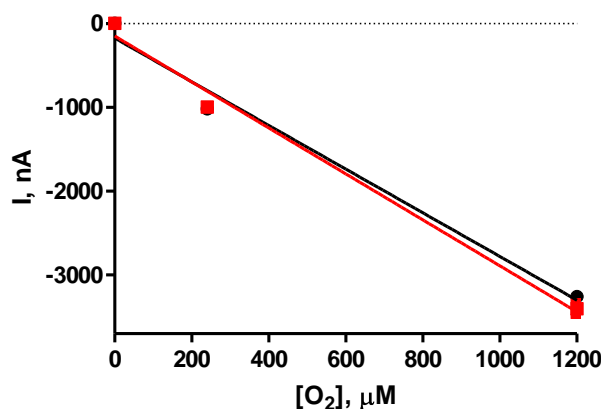


Figure 4.3.5.2: A current-concentration profile for O₂ calibrations in PBS (pH 7.4) using SMCPEs pre (black) and post (red) treatment with PEA (10%), carried out at -650 mV vs. SCE.

Figure 4.3.5.2 and Table 4.3.5.2 display data obtained for the O₂ calibration pre- and post-treatment with PEA (10%) using SMCPEs. Sensitivities of -2.6 ± 0.3 nA/μM, *n* = 8 and -2.7 ± 0.3 nA/μM, *n* = 8 pre- and post-treatment were recorded. A linear response over the specified range pre and post was attained ($R^2 = 0.98$) and ($R^2 = 0.99$) respectively. It is clear that the results show no significant difference ($P = 0.1792$, paired *t*-test). This confirms that the sensor can withstand the treatment of PEA (10%) unlike the results observed for the CPEs.

4.3.5.3 SMCPE-BT (ON)

[O ₂], μM	SMCPE (<i>n</i> = 6)		SMCPE-BT-ON (<i>n</i> = 6)	
	Mean I, nA	SEM	Mean I, nA	SEM
0.0	0.0	0.0	0.0	0.0
240.0	-843.7	95.8	-1077.1	69.2
1200.0	-3828.9	278.5	-3516.1	228.7

Table 4.3.5.3: Table of results for O₂ calibrations in PBS (pH 7.4) using SMCPEs (*n* = 6) pre- and post-treatment with BT ON, carried out at -650 mV vs. SCE. Background values subtracted. Mean background current (SMCPEs) = -94.0 ± 22.6 nA and (SMCPE-BT-ON) = -44.0 ± 16.4 nA.

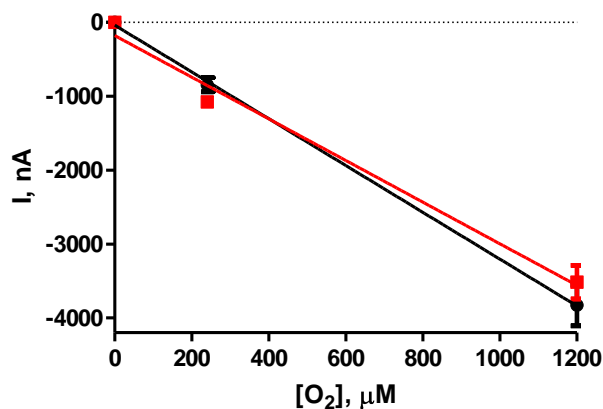


Figure 4.3.5.3: A current-concentration profile for O₂ calibrations in PBS (pH 7.4) using SMCPEs pre (black) and post (red) treatment with BT (ON), carried out at -650 mV vs. SCE.

BT encompasses all of the fouling and interfering agents that could prevent the sensor from working at its optimum capability and therefore is utilised as a necessary treatment to determine the behaviour of the electrode in the presence of these agents. O₂ calibrations using SMCPEs pre- (black) and post-treatment (red) in BT ON yielded a sensitivity of -3.2 ± 0.1 nA/μM, *n* = 6 (pre-treatment) and -2.8 ± 0.3 nA/μM, *n* = 6 (post-treatment). The response of the electrodes was linear over the specified range with an R² value of 0.99 (pre-treatment) and 0.99 (post-treatment). The results pre- and post-treatment were not significantly different (*P* = 0.1687, paired *t*-test). These results show promise that this sensor will not be affected by the harsh environment of the brain.

4.3.5.4 SMCPE-BT (3 days)

[O ₂], μM	SMCPEs (<i>n</i> = 7)		SMCPE-BT (3 days) (<i>n</i> = 7)	
	Mean I, nA	SEM	Mean I, nA	SEM
0.0	0.0	0.0	0.0	0.0
240.0	-933.7	84.2	-836.5	45.0
1200.0	-3347.6	111.3	-2887.9	209.9

Table 4.3.5.4: Table of results for O₂ calibrations in PBS (pH 7.4) with SMCPEs (*n* = 7) pre- and post-treatment with BT (3 days), carried out at -650 mV vs. SCE. Background values subtracted. Mean background currents (SMCPEs) = -14.1 ± 5.5 nA and (SMCPE-BT (3 days)) = -17.3 ± 2.4 nA.

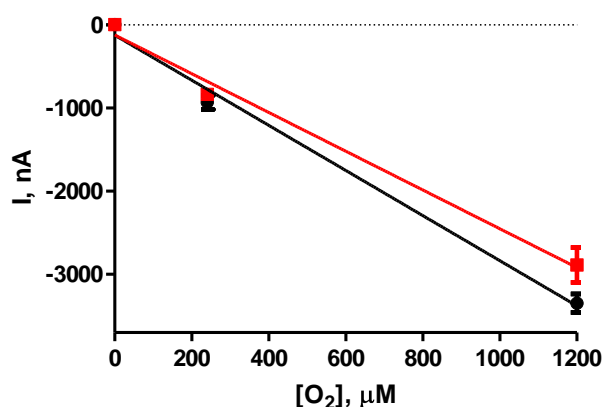


Figure 4.3.5.4: A current-concentration profile for O₂ calibrations in PBS (pH 7.4) with SMCPEs pre- (black) and post- (red) treatment with BT (3 days), carried out at -650 mV vs. SCE.

Leaving the sensors in BT for three days recorded more of an effect pre and post in comparison to the ON results. This is probably due to the BT constituents having more time to block the active surface resulting in a slight decrease in sensitivity. Pre- and post-treatment in BT (3 days) displayed sensitivities of -2.7 ± 0.2 nA/ μM, *n* = 7 and -2.3 ± 0.2 nA/ μM, *n* = 7, respectively, with no significant difference (*P* = 0.0759, paired *t*-test) observed. The response of the electrodes was linear over the specified range with an R² value of 0.99 (pre-treatment) and 0.99 (post-treatment).

4.3.5.5 SMCPE-BT (28 days)

[O ₂], μM	SMCPEs (<i>n</i> = 4)		SMCPE-BT (28 days) (<i>n</i> = 4)	
	Mean I, nA	SEM	Mean I, nA	SEM
0.0	0.0	0.0	0.0	0.0
240.0	-1129.2	97.5	-689.6	19.8
1200.0	-4295.3	116.4	-3810.5	336.0

Table 4.3.5.5: Table of results for O₂ calibrations in PBS (pH 7.4) with MMCPEs (*n* = 4) pre- and post-treatment with BT (28 days), carried out at -650 mV vs. SCE. Background values subtracted. Mean background current (MMCPEs) = -5.8 ± 0.4 nA and (MMCPE-BT (28 days)) = -4.9 ± 0.5 nA.

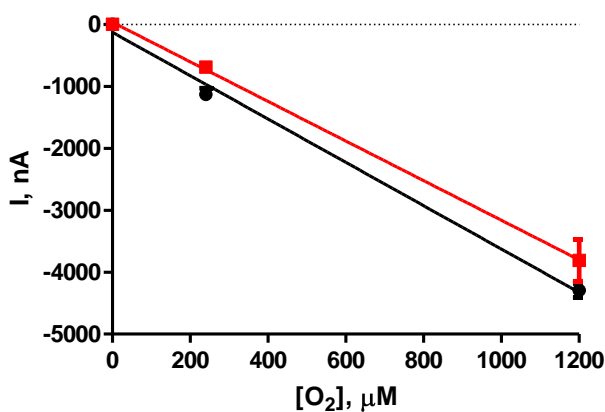


Figure 4.3.5.5: A current-concentration profile for O₂ calibrations in PBS (pH 7.4) with SMCPEs pre- (black) and post- (red) treatment with BT (28 days), carried out at -650 mV vs. SCE.

The results obtained for O₂ calibrations using the SMCPEs pre- and post-treatment with BT over 28 days yielded sensitivities of -3.5 ± 0.2 nA/μM, *n* = 4 and -3.2 ± 0.1 nA/μM, *n* = 4, respectively. A linear response was obtained pre- and post-treatment with BT (28 days) ($R^2 = 0.99$). A slight decrease in sensitivity was observed post-treatment, however, this yielded no significant difference ($P = 0.5282$, paired *t*-test) pre- and post-treatment over the 28 days. This result was excellent in comparison to the CPE sensitivity following 28 days in BT. Not only did the sensor stay fully intact and unmodified over the course of 28 days, it retained a similar sensitivity to the pre treated sensor.

4.3.5.6 MMCPE-BSA (ON)

[O ₂], μM	MMCPEs ($n = 6$)		MMCPEs-BSA (10%) ($n = 6$)	
	Mean I, nA	SEM	Mean I, nA	SEM
0.0	0.0	0.0	0.0	0.0
240.0	-940.7	49.1	-1037.9	83.9
1200.0	-4116.3	218.6	-3542.2	317.9

Table 4.3.5.6: Table of results for O₂ calibrations in PBS (pH 7.4) with MMCPEs ($n = 6$) pre- and post-treatment with BSA (10%), carried out at -650 mV vs. SCE. Background values subtracted. Mean background current (MMCPE) = -18.3 ± 10.9 nA and (MMCPE-BSA (10%) ON) = -26.4 ± 10.4 nA.

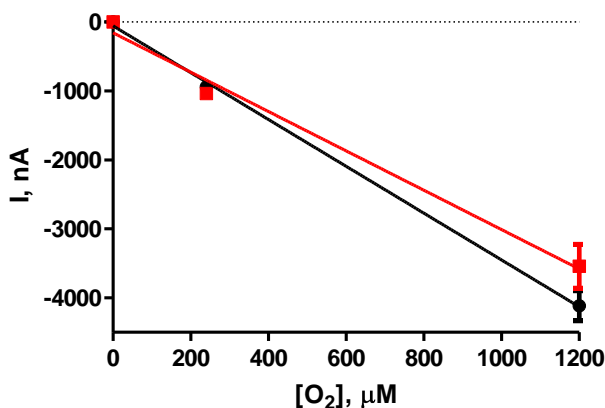


Figure 4.3.5.6: A current-concentration profile for O₂ calibrations in PBS (pH 7.4) with MMCPEs pre- (black) and post- (red) treatment with BSA (10%) ON, carried out at -650 mV vs. SCE.

There was no significant difference ($P = 0.0611$, paired t -test) recorded pre and post BSA (10%) with the MMCPEs. Sensitivities of -3.4 ± 0.1 nA/ μM , $n = 6$ (pre-treatment) and -2.9 ± 0.3 nA/ μM , $n = 6$ (post-treatment) were obtained. The response of the electrodes was linear over the specified range with an R^2 value of 0.99 (pre-treatment) and 0.99 (post-treatment). BSA (10%) treatment carried out on the MMCPEs showed a slight effect on the sensors, revealing a good capability of the sensor to retain integrity under this harsh concentration of fouling agent.

4.3.5.7 MMCPE-PEA (ON)

[O ₂], μM	MMCPE (<i>n</i> = 4)		MMCPE-PEA (10%) (<i>n</i> = 4)	
	Mean I, nA	SEM	Mean I, nA	SEM
0.0	0.0	0.0	0.0	0.0
240.0	-1116.9	98.3	-1139.1	77.7
1200.0	-3917.7	102.4	-3364.6	159.9

Table 4.3.5.7: Table of results for O₂ calibrations in PBS (pH 7.4) using MMCPEs (*n* = 4) pre- and post-treatment with PEA (10%), carried out at -650 mV vs. SCE. Background values subtracted. Mean background current (MMCPEs) = -179.6 ± 19.8 nA and (MMCPE-PEA (10%) ON) = -367.0 ± 21.0 nA.

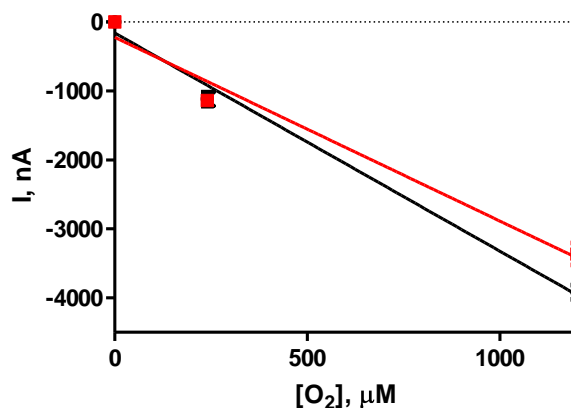


Figure 4.3.5.7: A current-concentration profile for O₂ calibrations in PBS (pH 7.4) with MMCPEs pre- (black) and post- (red) treatment with PEA (10%) ON, carried out at -650 mV vs. SCE.

Figure 4.3.5.7 and Table 4.3.5.7 display results attained for O₂ calibrations using the MMCPEs pre- and post-treatment in PEA (10%) ON. Sensitivities of -3.2 ± 0.3 nA/μM, *n* = 4 and -2.7 ± 0.4 nA/μM, *n* = 4 pre- and post-treatment, respectively, were recorded. The response of the electrodes was linear over the specified range with an R² value of 0.99 (pre-treatment) and 0.98 (post-treatment). Although there is a slight decrease in the sensitivity post treatment, the results were not significantly different (*P* = 0.0506, paired *t*-test). PEA (10%) may be causing a slight barrier at the surface as has been previously observed, thus leading to a decrease in the response.

4.3.5.8 MMCPE-BT (ON)

[O ₂], μM	MMCPE (<i>n</i> = 7)		MMCPE-BT (ON) (<i>n</i> = 7)	
	Mean I, nA	SEM	Mean I, nA	SEM
0.0	0.0	0.0	0.0	0.0
240.0	-945.7	137.7	-921.3	41.9
1200.0	-3764.9	258.7	-3340.2	149.3

Table 4.3.5.8: Table of results for O₂ calibrations in PBS (pH 7.4) with MMCPEs (*n* = 7) pre- and post-treatment with BT (ON), carried out at -650 mV vs. SCE. Background values subtracted. Mean background current (MMCPE) = -12.4 ± 2.9 nA and (MMCPE-BT (ON)) = -16.9 ± 10.2 nA.

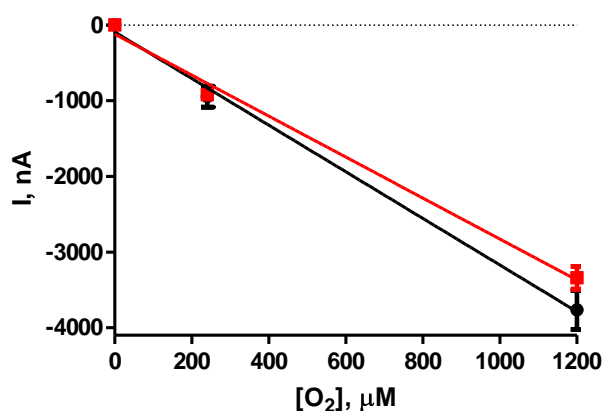


Figure 4.3.5.8: A current-concentration profile for O₂ calibrations in PBS (pH 7.4) with MMCPEs pre- (black) and post- (red) treatment with BT (ON), carried out at -650 mV vs. SCE.

O₂ calibrations on MMCPEs pre- and post-treatment in BT ON, displayed sensitivities of -3.1 ± 0.2 nA/μM, *n* = 7 (pre-treatment) and -2.7 ± 0.2 nA/μM, *n* = 7 (post-treatment). A linear response over the specified range was obtained yielding an R² value of 0.99 (pre-treatment) and 0.99 (post-treatment). The results pre- and post-treatment were not significantly different (*P* = 0.0544, paired *t*-test). BT ON did not seem to cause any considerable effect to the sensor, presenting an optimistic outlook for how this sensor will perform *in-vivo*.

4.3.5.9 MMCPE-BT (3 days)

[O ₂], μM	MMCPEs (<i>n</i> = 8)		MMCPE-BT (3 days) (<i>n</i> = 8)	
	Mean I, nA	SEM	Mean I, nA	SEM
0.0	0.0	0.0	0.0	0.0
240.0	-952.2	52.9	-1013.5	49.5
1200.0	-4019.9	27.9	-2926.9	144.8

Table 4.3.5.9: Table of results for O₂ calibrations in PBS (pH 7.4) with MMCPEs (*n* = 8) pre- and post-treatment with BT (3 days), carried out at -650 mV vs. SCE. Background values subtracted. Mean background current (MMCPEs) = -64.7 ± 18.1 nA and (MMCPE-BT (3 days)) = -78.0 ± 7.8 nA.

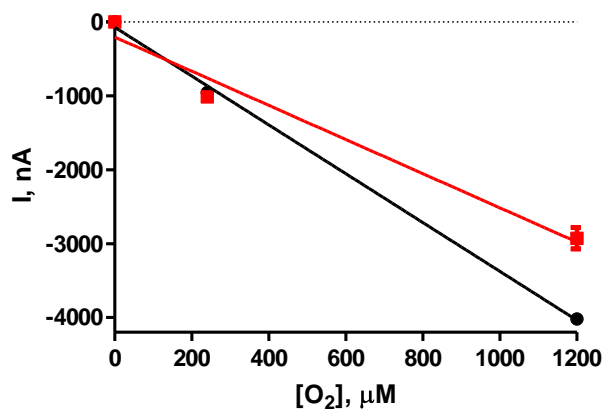


Figure 4.3.5.9: A current-concentration profile for O₂ calibrations in PBS (pH 7.4) with MMCPEs pre (black) and post (red) treatment with BT (3 days), carried out at -650 mV vs. SCE.

The results obtained for the O₂ calibrations using the MMCPEs pre- and post-treatment in BT (3 days), yielded sensitivities of -3.3 ± 0.1 nA/μM, *n* = 8 (pre-treatment) and -2.3 ± 0.4 nA/μM, *n* = 8 (post-treatment). The response of the electrodes was linear over the specified range with an R² value of 0.99 (pre-treatment) and 0.97 (post-treatment). The decrease in sensitivity resulting in a significant difference (*P* < 0.0001, paired *t*-test) could be due to the BT components having more time to adsorb to the surface causing an obstruction of the sensor face therefore decreasing the response of the electrode to O₂.

4.3.5.10 MMCPE-BT (28 days)

[O ₂], μM	MMCPEs (<i>n</i> = 4)		MMCPE-BT (28 days) (<i>n</i> = 4)	
	Mean I, nA	SEM	Mean I, nA	SEM
0.0	0.0	0.0	0.0	0.0
240.0	-1081.0	72.8	-837.9	130.7
1200.0	-4433.7	223.4	-3251.1	210.1

Table 4.3.5.10: Table of results for O₂ calibrations in PBS (pH 7.4) with MMCPEs (*n* = 4) pre- and post-treatment with BT (28 days), carried out at -650 mV vs. SCE. Background values subtracted. Mean background currents (MMCPEs) = -3.6 ± 0.3 nA and (MMCPE-BT (28 days)) = -10.2 ± 2.7 nA.

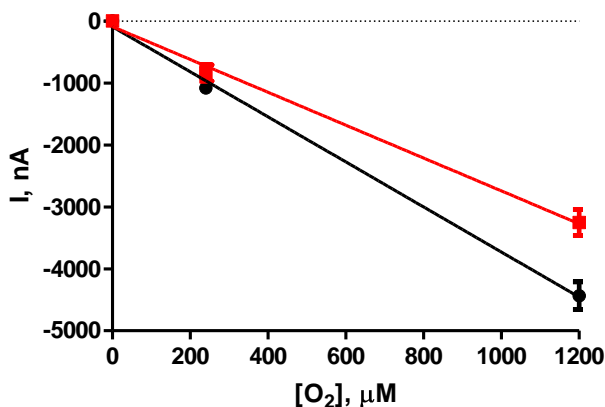


Figure 4.3.5.10: A current-concentration profile for O₂ calibrations in PBS (pH 7.4) with MMCPEs pre- (black) and post- (red) treatment with BT (28 days), carried out at -650 mV vs. SCE.

Figure 4.3.5.10 and Table 4.3.5.10 display data obtained for the O₂ calibration pre- and post-treatment with BT (28 days) using MMCPEs. Sensitivities of -3.6 ± 0.2 nA/μM, *n* = 4 and -2.6 ± 0.2 nA/μM, *n* = 4, pre- and post-treatment were recorded. A linear response over the specified range pre and post was attained ($R^2 = 0.99$) and ($R^2 = 0.99$), respectively. The results were significantly different ($P = 0.0296$, paired *t*-test). Even though there was a decrease in sensitivity observed for the MMCPEs, a greater sensitivity was achieved in comparison to the CPEs post treatment with BT after 28 days. On inspection of the MMCPEs under the microscope, a flat surface remained after removal from the BT, demonstrating that they had not been morphologically altered. It is clear that the standard

CPEs are altered from contact with any elements encountered in the *in-vivo* environment which has been demonstrated by other groups previously (Ormonde & O'Neill, 1989, 1990; A. Kane & D. O'Neill, 1998). It appears from the biocompatibility studies that both sensor types show marked improvements in comparison to the conventional sensor type, with the SMCPE displaying the most reproducible and stable sensor surface.

4.3.6 Post *In-Vivo* Comparison

In the previous sections, the effects of biological solutions, surfactants and *ex-vivo* brain tissue samples on the SMCPE and MMCPE were observed and the results showed a lot of promise. In this section an investigation into the effects of the implantation of the electrodes into the rat brain is examined and pre and post O₂ calibrations are compared. These calibrations were carried out as described in Section 3.7.2.4.

4.3.6.1 SMCPE Comparison

The effect of the living brain on the SMCPEs was investigated. The results obtained pre- and post-implantation (electrodes were implanted for an average of 15.2 ± 3.0 days in 5 animals) are presented in Table 4.3.6.1 and plotted graphically in Figure 4.3.6.1 (a).

[O ₂], μM	SMCPE (pre-implantation) ($n = 8$: 5 animals)		SMCPE (post-implantation) ($n = 8$: 5 animals)	
	Mean I, nA	SEM	Mean I, nA	SEM
0.0	0.0	0.0	0.0	0.0
240.0	-982.3	79.8	-487.6	32.8
1200.0	-4048.2	299.5	-2170.1	125.8

Table 4.3.6.1: Comparison table of mean current values for O₂ calibrations with SMCPEs ($n = 8$) in PBS (pH 7.4) pre- and post-implantation, carried out at -650 mV vs. SCE. Background values subtracted. Mean background currents (SMCPE pre-implantation) = -17.5 ± 6.0 nA and (SMCPE post-implantation) = -39.2 ± 16.2 nA.

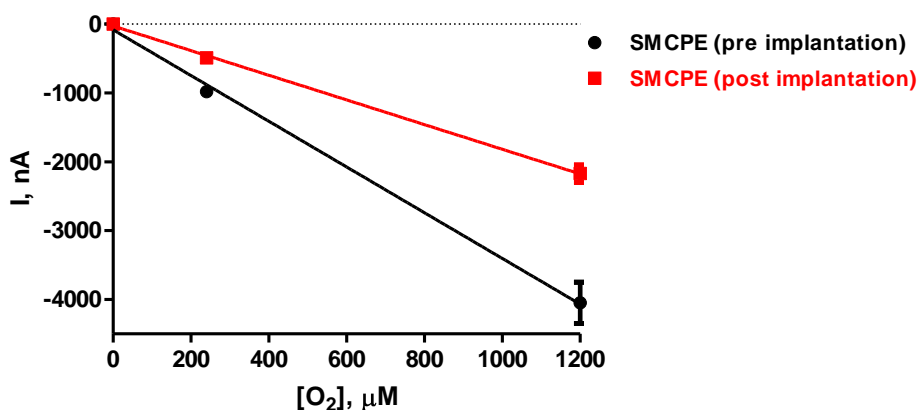


Figure 4.3.6.1 (a): A mean current-concentration profile for O₂ calibrations in PBS (pH 7.4) performed with SMCPEs, ($n = 8$: 5 animals), pre- (black) and post- (red) implantation, carried out at -650 mV.

It is observed from the comparison of the calibration slopes (nA/ μ M), -3.3 ± 0.1 nA/ μ M for pre-implantation and -1.8 ± 0.1 nA/ μ M for post-implantation, that the sensitivity of the SMCPEs decreased significantly following implantation ($P = 0.0016$, paired t -test). The response of the electrodes was linear over the specified range with an R^2 value of 0.99, $n = 8$, pre-implantation and 0.99, $n = 8$, post-implantation. Implantation of the sensor into the living brain causes a dramatic change in the sensitivity post implantation. This could be due to the harsh environment that is the brain; however, it could also be the effect of removal of the electrodes from the headpiece of the animal which may cause significant damage to the sensor. It is very difficult to perform a post *in-vivo* calibration due to these effects and also physiological effects such as gliosis. A comparison of the raw data from a typical O₂ calibration performed pre- and post-implantation is shown in Figure 4.3.6.1 (b).

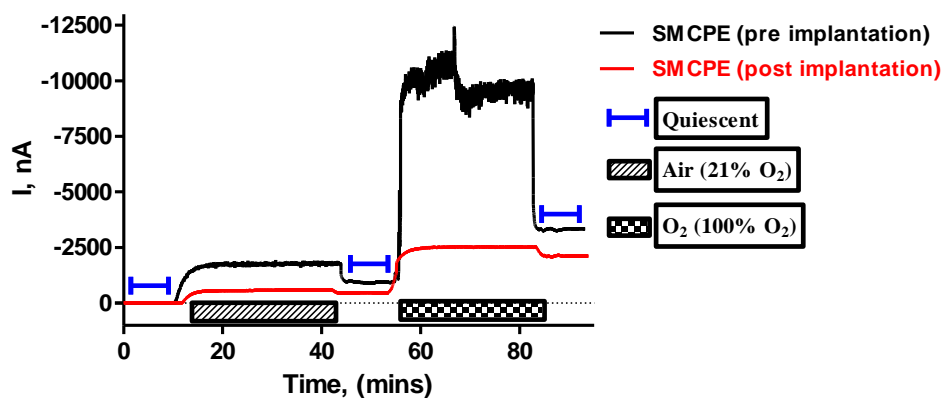


Figure 4.3.6.1 (b): A comparison of the raw data from a typical O_2 calibration performed on SMCPEs pre- and post-implantation in PBS (pH 7.4), carried out at -650 mV vs. SCE.

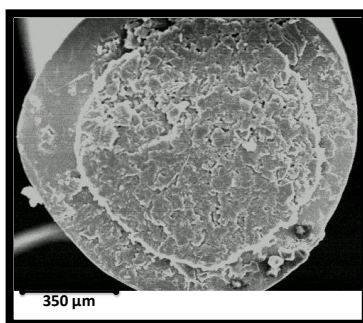


Figure 4.3.6.1 (c): An SEM displaying the surface of a SMCPE pre-implantation.

Figure 4.3.6.1 (c) displays an SEM of a pre-implanted SMCPE. This SEM can be used as a comparison when observing the SEMs in Figure 4.3.6.1 (d). Figure 4.3.6.1 (d) displays the SMCPEs post-implantation and it is clear that the surface remains flat when comparing the SEMs pre- and post-implantation.

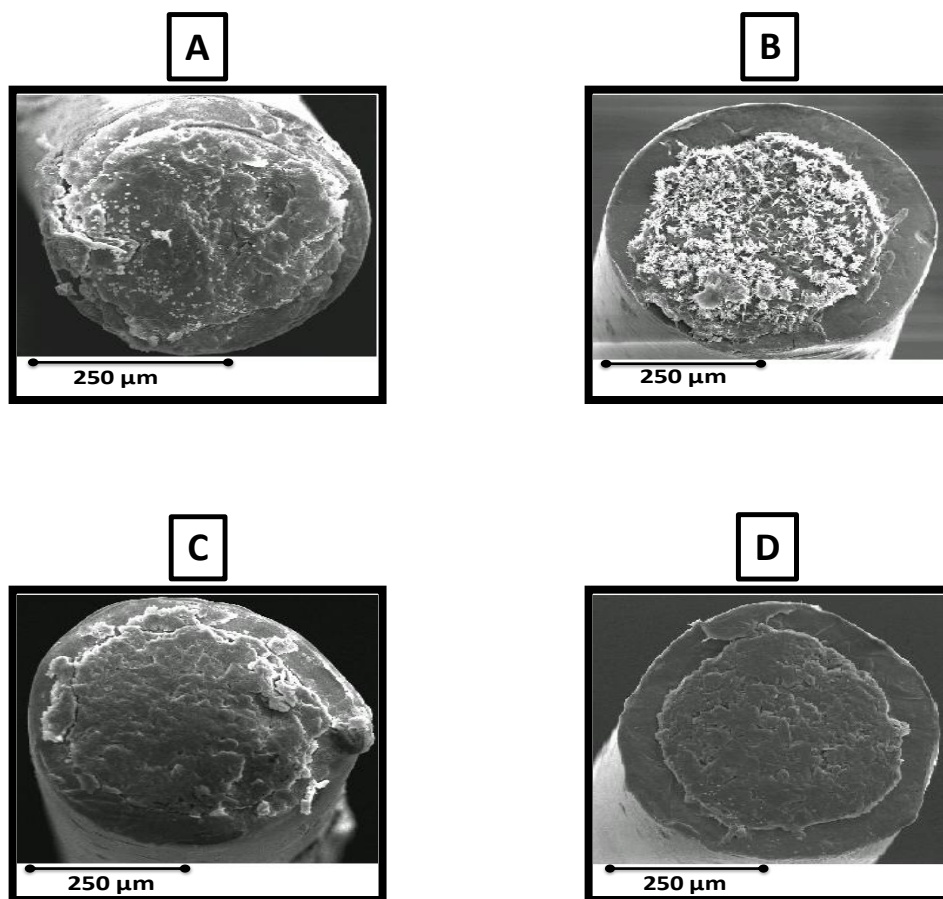


Figure 4.3.6.1 (d): (A), (B), (C) and (D); SEMs displaying the surface of different SMCPEs post-implantation.

The main aim for the implementation of the monomers into the manufacture of CPEs was to obtain a composite that was capable of withstanding morphological changes due to the *in-vivo* environment. The CPE surface is easily corrupted and therefore alters significantly by changing from a CPE to a carbon powder electrode. Although this is a positive attribute to have in a sensor as it provides the ability to record for long periods of time, by the removal of the poisons and fouling constituents from the sensor surface, it is not a great characteristic to have in a sensor for use in a clinical setting. On analysis of the SEMs pictured in Figure 4.3.6.1 (d), the surfaces remain fully intact after contact with the *in-vivo* environment. These results were outstanding, as the surfaces were clearly very capable of enduring a very complex and intricate environment. Some of the sensors contained a build

up of components from the brain environment on the surface of the sensor that had adsorbed, which can be seen very clearly in Figure 4.3.6.1 (d), image B. This observation could also be attributable to the decrease in sensitivity recorded in results from post-implantation calibrations.

4.3.6.2 MMCPE Comparison

The effect of the living brain on the MMCPEs was investigated. The results obtained pre- and post-implantation (electrodes were implanted for 14.8 ± 1.4 days) are shown in Figure 4.3.6.2 (a).

[O ₂], μM	MMCPE (pre-implantation) ($n = 8$: 5 animals)		MMCPE (post-implantation) ($n = 8$: 5 animals)	
	Mean I, nA	SEM	Mean I, nA	SEM
0.0	0.0	0.0	0.0	0.0
240.0	-906.3	96.5	-608.2	70.5
1200.0	-4075.1	444.6	-2547.5	90.5

Table 4.3.6.2: Comparison table of mean current values for O₂ calibrations with MMCPEs ($n = 8$: 5 animals) in PBS (pH 7.4) pre- and post-implantation, carried out at -650 mV vs. SCE. Background values subtracted. Mean background current (MMCPE pre-implantation) = -7.5 ± 1.7 nA and (MMCPE post implantation) = -69.9 ± 51.7 nA.

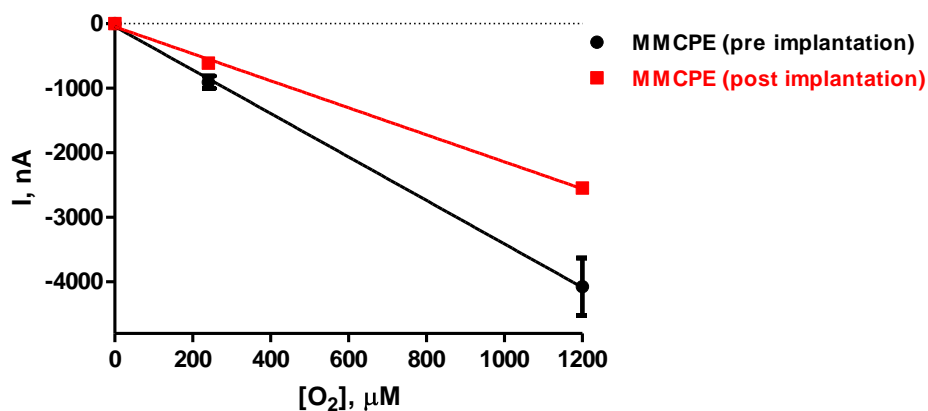


Figure 4.3.6.2 (a): A mean current-concentration profile for O₂ calibrations in PBS (pH 7.4) performed with MMCPEs, ($n = 8$), pre- (black) and post- (red) implantation, carried out at -650 mV.

It is observed from the comparison of the slopes (nA/ μM) of the electrodes, -3.4 ± 0.1 nA/ μM for pre-implantation and -2.1 ± 0.1 nA/ μM for post-implantation, that the sensitivity of the MMCPEs decreased significantly following implantation ($P = 0.0073$, paired t -test). The response of the electrodes was linear over the specified range with an R^2 value of 0.99, $n = 8$, pre-implantation and 0.99, $n = 8$, post-implantation. As the sensor remained intact and not morphologically altered (see Figure 4.3.6.2 (d)) from the brain environment, a decrease in sensitivity could be attributable to a built up of constituents from the brain on the surface of the electrode. This decrease in sensitivity has been previously observed in the lab with other sensors like Pt sensors where the decrease was attributed to a build up of species on the surface.

On examination of the *in-vivo* stability traces observed in Section 5.3.7.1 and 5.3.7.2, for the MMCPEs and SMCPEs respectively, a decrease of approximately 15.5 % (MMCPEs) and 14.4 % (SMCPEs) can be observed after day 1, respectively. After day 1 a stable current is obtained. Even though the MMCPEs and SMCPEs display a decreased post implantation sensitivity, this sensitivity observed for the two sensor designs is higher than what is obtained for a standard pre-implanted CPE, even after being implanted for approximately 15 days *in-vivo*. These results really confirm the solid structural integrity of these novel O_2 sensors. A comparison of the raw data from a typical O_2 calibration performed pre- and post-implantation is shown in Figure 4.3.6.2 (b).

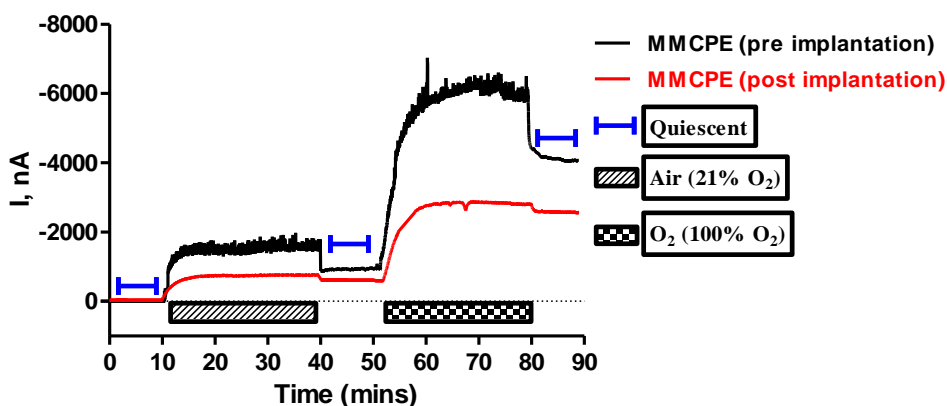


Figure 4.3.6.2 (b): A comparison of the raw data from a typical O_2 calibration performed with MMCPEs pre- and post-implantation in PBS (pH 7.4), carried out at -650 mV vs. SCE.

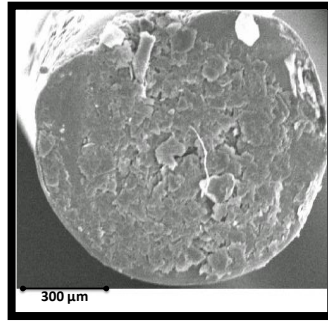


Figure 4.3.6.2 (c): An SEM displaying the surface of a MMCPE pre-implantation.

Figure 4.3.6.2 (c) displays an SEM of a pre-implanted MMCPE. This SEM can be used as a comparison when observing the SEMs in Figure 4.3.6.2 (d). Figure 4.3.6.2 (d) displays the MMCPEs post-implantation and it is clear that the surface remains flat when comparing the SEMs pre- and post-implantation.

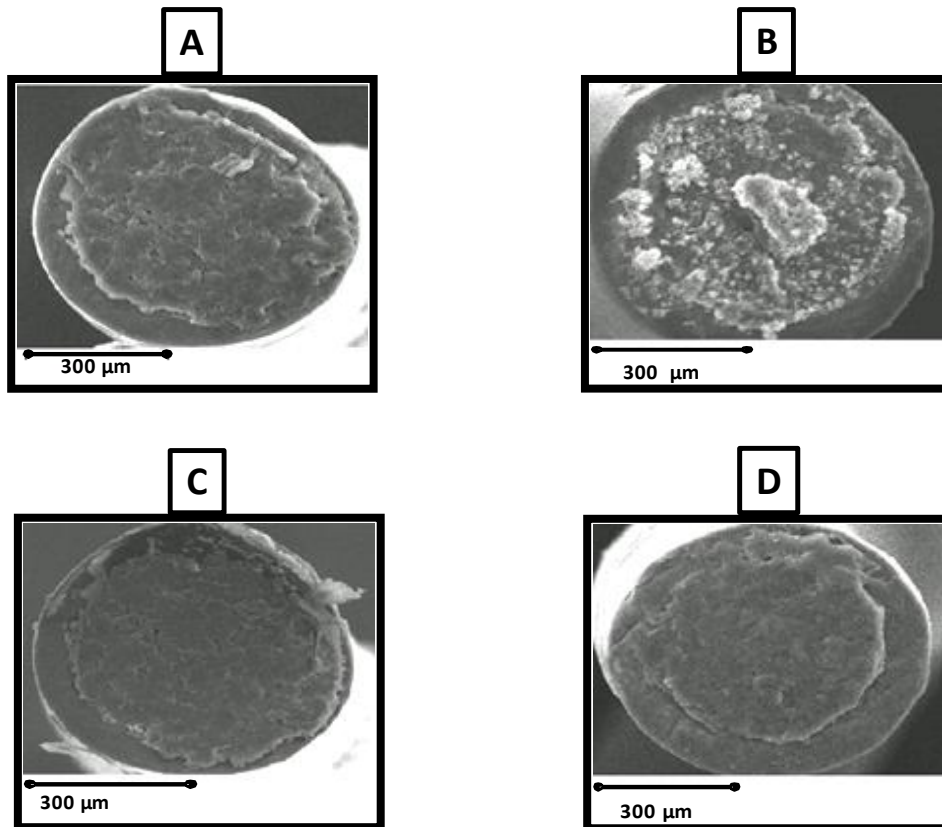


Figure 4.3.6.2 (d): (A), (B), (C) and (D); SEMs displaying the surface of different MMCPEs post implantation.

Inspection of the surface of the electrodes with SEM, confirmed that the surfaces are withstanding the *in-vivo* environment by retaining integrity and a flat uniform surface. Figure 4.3.6.2 (d), image B, shows a covering of constituents of the *in-vivo* environment on the surface of the sensor which may be giving a reason to speculate that the decrease observed in the sensitivity post implantation is due to this. On examination of the results obtained in this section, it can be seen that there is an effect on the electrodes after being implanted in the brain for 14.8 ± 1.4 days (MMCPEs, $n = 8$) and 15.2 ± 3.0 days (SMCPEs, $n = 8$).

There is a decrease in sensitivity for both the SMCPEs and the MMCPEs, pre- and post-implantation. The SEMs displayed in Figure 4.3.6.1 (d) and Figure 4.3.6.2 (d) show that the surface of the electrodes has remained intact after implantation and on removal from the animal. The SEMs also show that constituents of the brain have adsorbed onto the surface of the electrodes and it is this that is most likely causing the decrease in sensitivity.

4.3.7 Long term stability studies

4.3.7.1 Stored at Room temperature (RT)

It is well-known that the main advantage of CPEs, is their ability to sustain *in-vivo* stability over long periods of time, by altering surface morphology from a carbon paste to a carbon powder electrode in the presence of lipids (Ormonde & O'Neill, 1989). Long term stability studies were carried out on the SMCPEs and MMCPEs to compare their stability against standard CPEs. It was necessary for the sensors to retain stability over a specified time frame but to also hold surface integrity unlike the CPEs. The long term stability studies are vital to undertake. This is because in a clinical setting the optimum storage condition details would need to be known, as the sensors would not be used straight away. O₂ calibrations were performed on the SMCPEs and MMCPEs over the course of 28 days which are detailed in Figure 4.3.7.1.1 and 4.3.7.1.2. They were stored at RT and intermittently tested over the specified days.

4.3.7.1.1 SMCPEs

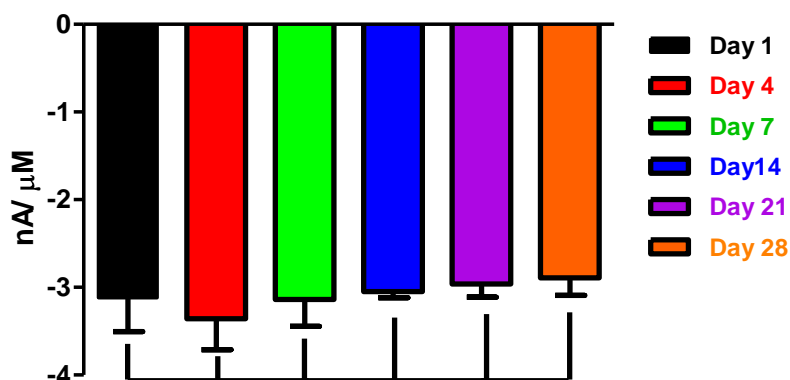


Figure 4.3.7.1.1: A bar chart for O₂ calibrations in PBS (pH 7.4) with SMCPEs ($n = 5$) over the course of 28 days, carried out at -650 mV vs. SCE.

The results obtained for the O₂ calibrations using the SMCPEs over 28 days (see Table 4.3.7.1.1), displayed excellent stability and yielded no significant difference over the course of the 28 days. Table 4.3.7.1.1 displays the P values obtained from day 1 to day 28. Paired t -tests were carried out, in order to determine if the stability of the sensors was compromised over time.

Day	P value	Significance
1 vs. 4	0.2091	ns
1 vs. 7	0.9151	ns
1 vs. 14	0.6443	ns
1 vs. 21	0.2422	ns
1 vs. 28	0.1242	ns

Table 4.3.7.1.1: A summary displaying the P values obtained for the SMCPEs over 28 days at RT.

The response of the electrodes was linear over the specified range with an R^2 value of 0.99 (day 1-28). These results signify the stability of the sensors over the 28 days of calibrations *in-vitro*, with day 28 yielding a P value that was not significantly different ($P = 0.1242$) in

comparison to day 1, demonstrating results that confirm the sensor stability over the course of a month. Repeated calibrations caused significant damage to the Pt based sensors discussed in Chapter 6, Section 6.3.8.1 and 6.3.8.2, whereas if they were only calibrated on a once off basis, a more stable result was obtained with no detrimental effect to the sensors. These results again demonstrate a more robust characteristic to the monomer modified sensors and show, that repetitive calibrations do not compromise the sensitivity and stability of the sensors.

4.3.7.1.2 MMCPEs

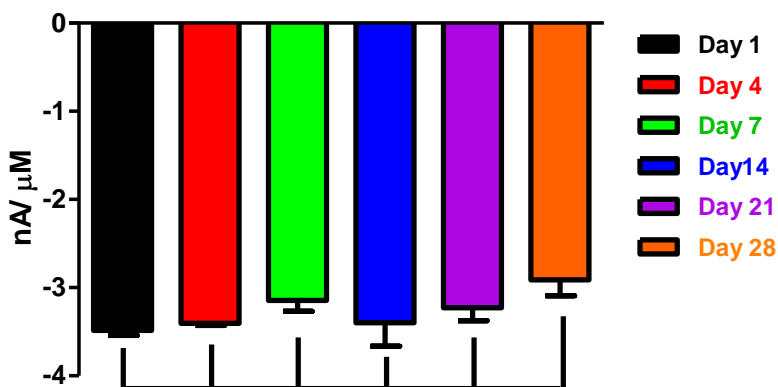


Figure 4.3.7.1.2: A bar chart for O₂ calibrations in PBS (pH 7.4) with MMCPEs ($n = 4$) over the course of 28 days, carried out at -650 mV vs. SCE.

In Figure 4.3.7.1.2, O₂ calibrations using the MMCPEs over 28 days are displayed. On analysis of the results, no significant difference was recorded over the 28 days of calibrations which is displayed in Table 4.3.7.1.2 figuratively. Paired t -tests were carried out, in order to determine if the stability of the sensors was compromised over time.

Day	<i>P</i> value	Significance
1 vs. 4	0.0862	ns
1 vs. 7	0.3034	ns
1 vs. 14	0.4912	ns
1 vs. 21	0.3377	ns
1 vs. 28	0.1747	ns

Table 4.3.7.1.2: A summary displaying the *P* values obtained for the MMCPEs over 28 days at RT

A linear response of the electrodes over the specified range yielded R^2 values of 0.99 (day 1-28). The MMCPEs demonstrate an ability to remain stable *in-vitro* over time, like the SMCPEs. Although a similar trend of a decreasing sensitivity was observed over time with both sensors, the MMCPEs at day 28 did not show a significantly different sensitivity in comparison to day 1, just like the SMCPEs. This maybe suggests that unlike the Pt based sensors discussed in Chapter 6, Section 6.3.8.1 and 6.3.8.2, there doesn't appear to be any effect of repeated calibration on the sensors which is representative of the different transducer substrates. Subsequent to these results, long term stability studies were carried out utilising differing storage conditions.

4.3.7.2 Stored in the fridge (4 °C)

The results for the SMCPE and MMCPE stored in the fridge are displayed in Figure 4.3.7.2.1 and Figure 4.3.7.2.2.

4.3.7.2.1 SMCPEs

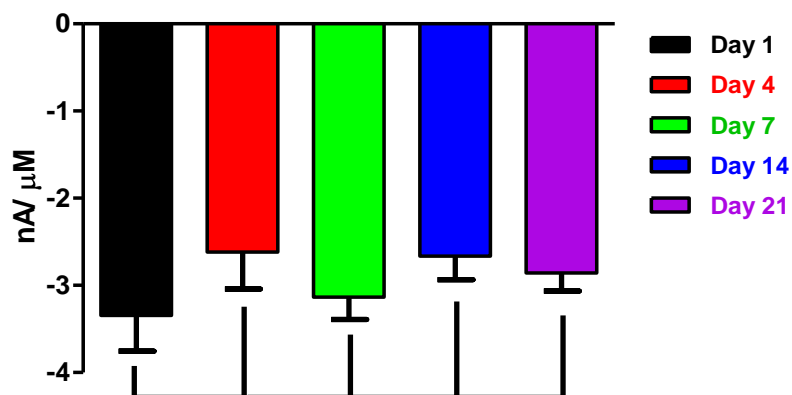


Figure 4.3.7.2.1: A bar chart for O₂ calibrations in PBS (pH 7.4) with SMCPEs, $n = 4$, over the course of 21 days that were kept in the fridge and intermittently tested and carried out at -650 mV vs. SCE.

Day	<i>P</i> value	Significance
1 vs. 4	0.0553	ns
1 vs. 7	0.3044	ns
1 vs. 14	0.0830	ns
1 vs. 21	0.1062	ns

Table 4.3.7.2.1: A summary displaying the *P* values obtained for the SMCPEs over 21 days in the fridge.

4.3.7.2.2 MMCPEs

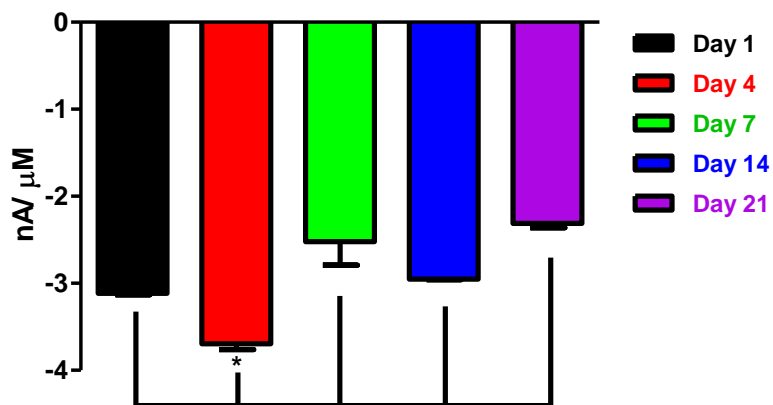


Figure 4.3.7.2.2: A bar chart for O₂ calibrations in PBS (pH 7.4) with MMCPEs, $n = 4$, over the course of 21 days that were kept in the fridge and intermittently tested and carried out at -650 mV vs. SCE.

Day	<i>P</i> value	Significance
1 vs. 4	0.0392	*
1 vs. 7	0.0576	ns
1 vs. 14	0.5866	ns
1 vs. 21	0.1166	ns

Table 4.3.7.2.2: A summary displaying the *P* values obtained for the MMCPEs over 21 days in the fridge.

The O₂ calibrations undertaken with the SMCPEs displayed sensitivities that were not significantly different over the course of the particular days. Table 4.3.7.2.2 displays these results. The MMCPEs displayed a significantly different increased sensitivity to day 4; however, the following days were not significantly different. For the SMCPEs, a linear response over the specified range was observed for Day 1 ($R^2 = 1.00$), Day 4 ($R^2 = 0.99$), Day 7 ($R^2 = 0.99$), Day 14 ($R^2 = 1.00$) and Day 21 ($R^2 = 0.99$). For the MMCPEs a linear response was also obtained, Day 1 ($R^2 = 1.00$), Day 4 ($R^2 = 0.99$), Day 7 ($R^2 = 0.98$), Day 14 ($R^2 = 1.00$) and Day 21 ($R^2 = 0.99$). The SMCPEs and MMCPEs display varying sensitivities that look unstable over the course of the 21 days; this could be due to the drop

in temperature, altering the morphology of the sensors or it could be most likely due to an effect of repetitive calibrations.

4.3.7.3 Stored in the freezer (-20 °C)

4.3.7.3.1 SMCPEs

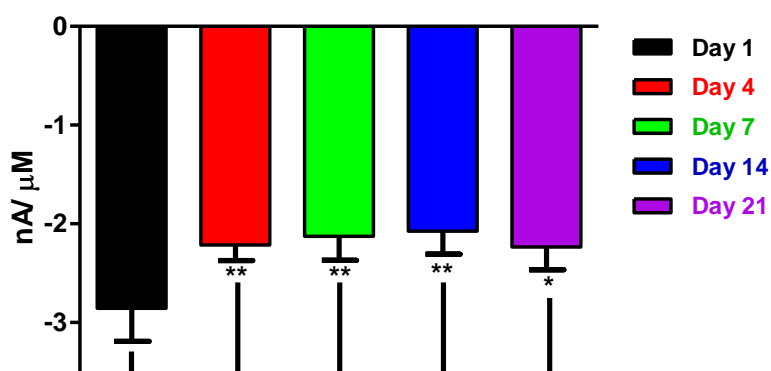


Figure 4.3.7.3.1: A bar chart for O₂ calibrations in PBS (pH 7.4) using SMCPEs over the course of 21 days that were kept in the freezer and intermittently tested and carried out at -650 mV vs. SCE.

Day	<i>P</i> value	Significance
1 vs. 4	0.0074	**
1 vs. 7	0.0085	**
1 vs. 14	0.0090	**
1 vs. 21	0.0186	*

Table 4.3.7.3.1: A summary displaying the *P* values obtained for the SMCPEs over 21 days in the freezer.

4.3.7.3.2 MMCPEs

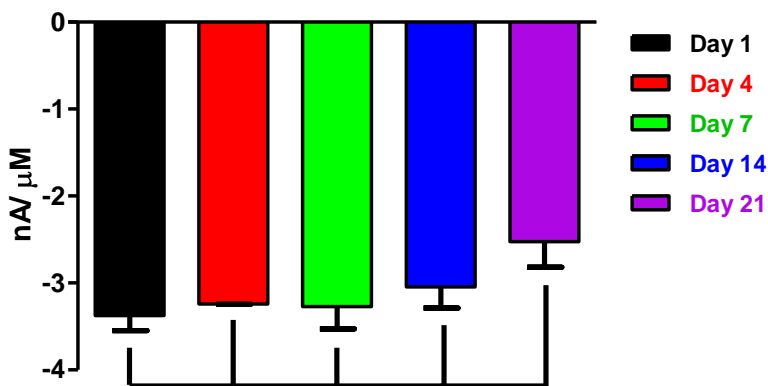


Figure 4.3.7.3.2: A bar chart for O₂ calibrations in PBS (pH 7.4) using MMCPEs over the course of 21 days that were kept in the freezer and intermittently tested and carried out at -650 mV vs. SCE.

Day	<i>P</i> value	Significance
1 vs. 4	0.7494	ns
1 vs. 7	0.8141	ns
1 vs. 14	0.4138	ns
1 vs. 21	0.0880	ns

Table 4.3.7.3.2: A summary displaying the *P* values obtained for the MMCPEs over 21 days in the freezer.

Figure 4.3.7.3.1 and 4.3.7.3.2 display O₂ calibrations using the SMCPEs and MMCPEs over 21 days. It is clear from the data that storing the sensors in the freezer causes a much greater drop in sensitivity in comparison to the results obtained at RT (see previous Section 4.3.7.1) and the fridge (see previous 4 °C Section 4.3.7.2). The MMCPEs appear to remain stable over the course of the days studied with no significant difference observed over the specified days. This is depicted in Table 4.3.7.3.2. Storing the sensors in the fridge and freezer did not seem to show sensitivities that were as stable as RT studies for both sensors. It was decided that the optimum storage conditions would be at RT.

4.3.8 Interference studies

Bolger *et al.*, carried out O_2 experiments on CPEs against a variety of potential interferents in order to fully characterise the sensor for use *in-vivo* (Bolger *et al.*, 2011b). It was decided to carry out interference studies on the SMCPE and MMCPE utilising endogenous species that would be present in the brain and that would potentially cause impairment to the sensors ability to detect the analyte of choice by the electrode. A working potential of -650 mV *vs.* SCE was utilised. Figure 4.3.8 (a) and 4.3.8 (b) detail the results obtained.

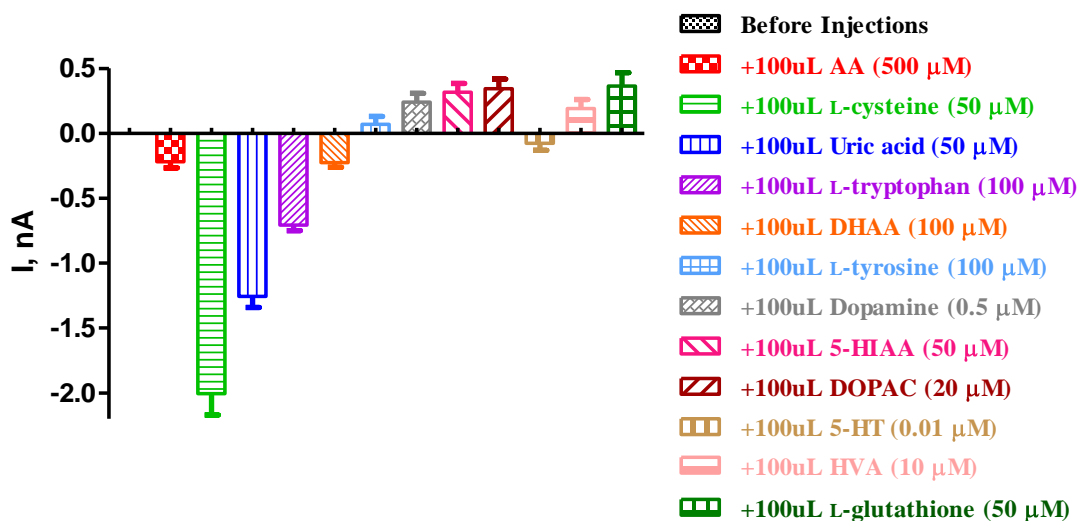


Figure 4.3.8 (a): A bar chart displaying a calibration carried out at -650 mV *vs.* SCE, $n = 4$, utilising a SMCPE in PBS (pH 7.4). Different endogenous species at their physiological concentrations were injected into the electrochemical cell and the sensitivities of each detected by the SMCPE were analysed.

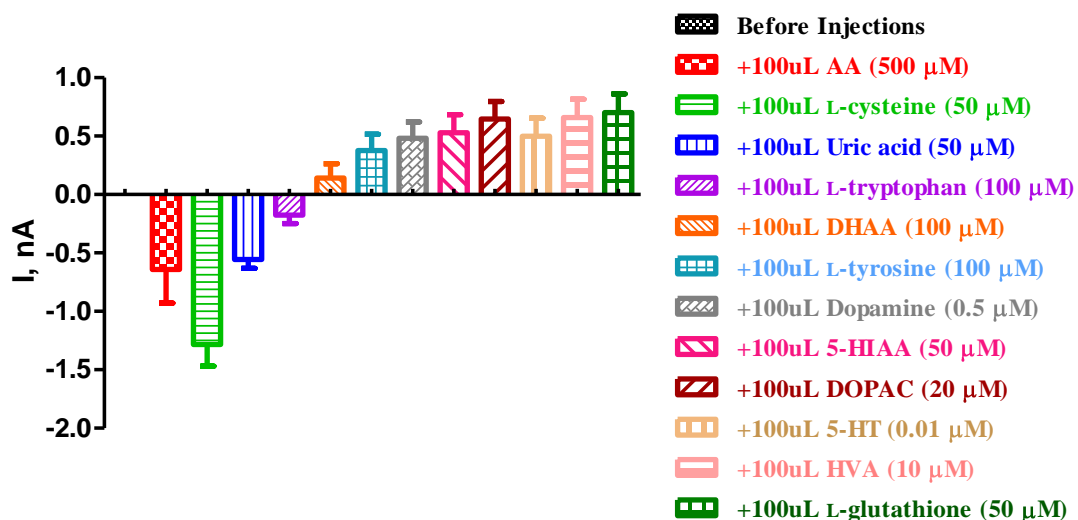


Figure 4.3.8 (b): A bar chart displaying a calibration carried out at -650 mV vs. SCE, $n = 4$, utilising a MMCPE in PBS (pH 7.4). Different endogenous species at their physiological concentrations were injected into the electrochemical cell and the sensitivities of each detected by the MMCPE were analysed.

Bolger *et al.*, found that although slightly positive changes occurred at the CPE by the interferents studied, they were deemed insignificant (Bolger *et al.*, 2011b). The sensitivities obtained by each species for both the SMCPEs and the MMCPEs were also negligible in this body of work, in comparison to the O_2 sensitivity detected at physiological concentrations.

4.3.9 pH Calibrations

The regulation of pH is very important in order for cells to function correctly. The increase or decrease of pH can compromise vital functions in the body (Chesler, 2003). *In-vivo* extracellular concentrations are constantly changing and can alter significantly with dramatic variation to normal physiology (Bolger *et al.*, 2011a). pH experiments were therefore carried out on the sensors in order to verify that even with a change in the pH, the sensor would not be affected. Two pH values were utilised (pH 6.5 and pH 8.0), however, these are extreme values that can lead to apoptosis *in-vivo*, so these values were utilised as a means to determine the capabilities of the sensor under extreme conditions.

4.3.9.1 SMCPE Repeat Calibration Experiments

Initially, the effect of repeated calibrations was determined for the SMCPE, as it was considered that carrying out repeated calibrations on the one set successively, may have a role in changing the sensitivity of the sensor each time. This could be due to the experimental set-up being changed for each calibration, therefore leading to more handling of the sensors and potential damage to the sensors.

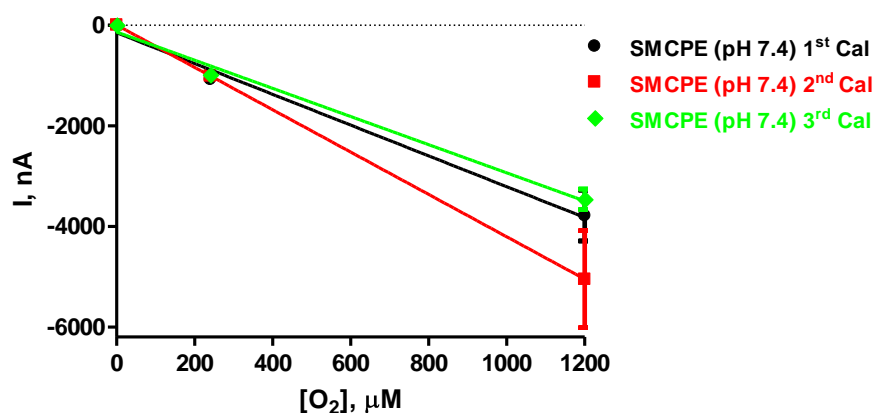


Figure 4.3.9.1 (a): A repeated O₂ calibration undertaken with the SMCPEs, $n = 4$, at -650 mV vs. SCE in PBS (pH 7.4).

Three consecutive O₂ calibrations were carried out on the SMCPE; this was to determine the effect a repeated calibration would have on the electrodes in pH 7.4. Although there was not a significant difference between the sensitivities ($P = 0.1150$, one-way ANOVA), it is clear that the sensitivities did alter between each calibration. Sensitivities of -3.1 ± 0.3 nA/μM (black) for the initial calibration, -4.2 ± 0.1 nA/μM (red) for the second and -2.8 ± 0.3 nA/μM (green) for the last calibration were obtained. The response of the electrodes was linear over the specified range, with an R^2 value of 0.99 (1st calibration), 1.00 (2nd calibration) and 0.99 (3rd calibration). The pH concentrations were varied next, in order to determine whether a change in pH resulted in a markedly different sensitivity for each pH utilised.

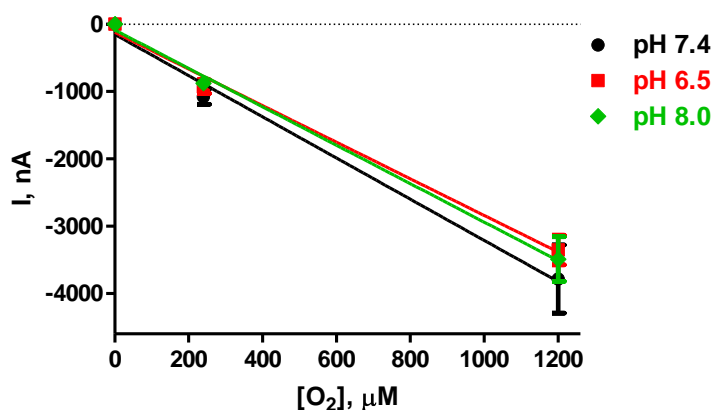


Figure 4.3.9.1 (b): O₂ calibrations undertaken with the SMCPEs, $n = 4$, at -650 mV vs. SCE in PBS (pH 7.4, 6.5 and 8.0).

No significant difference ($P = 0.9903$: one-way ANOVA) was observed for the three calibrations carried out in the different pH values. Sensitivities of -3.1 ± 0.3 nA/ μM (black) in pH 7.4, -2.7 ± 0.2 nA/ μM (red) in pH 6.5 and -2.9 ± 0.2 nA/ μM (green) in pH 8.0 were obtained. The response of the electrodes was linear over the specified range, with an R^2 value of 0.99 for each pH concentration. Succeeding the experiments carried out on the SMCPEs, experiments were undertaken on the MMCPEs in a similar manner.

4.3.9.2 MMCPE Repeat Calibration Experiments

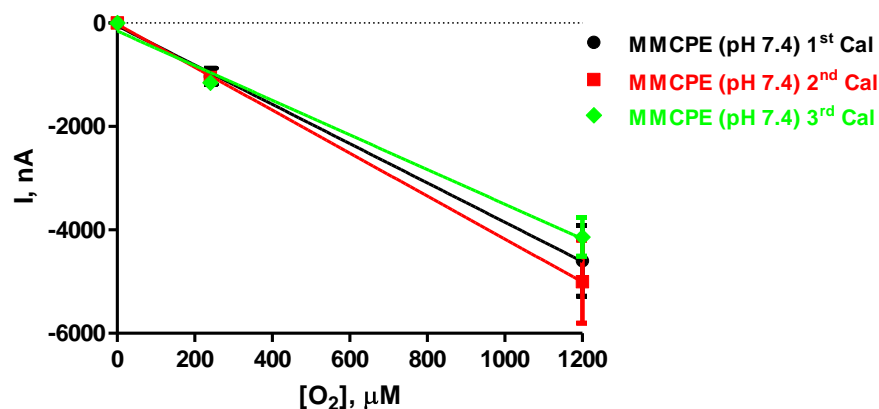


Figure 4.3.9.2 (a): A repeated O₂ calibration carried out on MMCPEs, $n = 4$, at -650 mV vs. SCE in PBS (pH7.4).

Repeated O_2 calibrations on the MMCPEs yielded sensitivities of -3.8 ± 0.1 nA/ μM (black) for the initial calibration, -4.2 ± 0.1 nA/ μM (red) for the second and -3.4 ± 0.3 nA/ μM (green) for the last calibration. The response of the electrodes was linear over the specified range, with an R^2 value of 0.99 for all calibrations undertaken. No significant difference ($P = 0.0821$) was recorded for these calibrations suggesting that repeated experimental application was not a concern. The pH values were then altered and the results are depicted in Figure 4.3.9.2 (b).

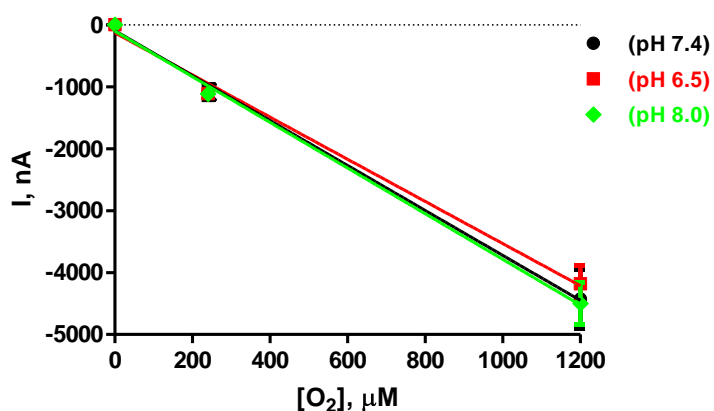


Figure 4.3.9.2 (b): O_2 calibrations carried out on MMCPEs, $n = 4$, at -650 mV vs. SCE in PBS (pH 7.4, 6.5 and 8.0).

In a similar manner to the results obtained with the SMCPEs, there was no significant difference between the sensitivities recorded ($P = 0.9982$) for the MMCPEs. The results obtained for the O_2 calibrations yielded sensitivities of -3.6 ± 0.2 nA/ μM (black) in pH 7.4, -3.4 ± 0.2 nA/ μM (red) and -3.7 ± 0.2 nA/ μM (green). The response of the electrodes was linear over the specified range, with an R^2 value of 0.99 for each pH value. This result confirms that varying the pH will not affect the sensors ability to detect O_2 .

4.3.10 Temperature studies

Metal based membrane covered O_2 sensors have a predisposition of a significant temperature dependency (Bolger *et al.*, 2011a). In order to determine that altering temperatures would not inhibit the workings of the electrode, the SMCPEs and MMCPEs were tested at 37 °C. It was necessary to test the sensors against this temperature as it was the physiological temperature of the body and therefore it was necessary to confirm that a changing temperature had no effect on the sensors. These results are shown in Figures 4.3.10.1 and 4.3.10.2 (a). A comparison of the two sensors is also displayed in Figure 4.3.10.2 (b).

4.3.10.1 SMCPEs

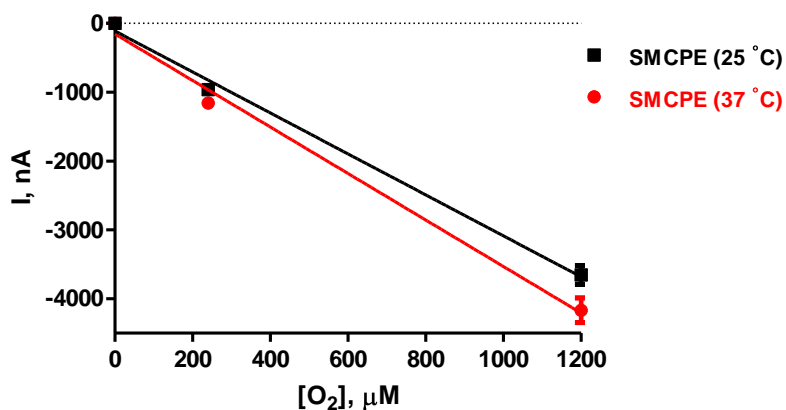


Figure 4.3.10.1: O_2 calibrations performed at 25 °C (black) and 37 °C (red) utilising SMCPEs, $n = 4$, at -650 mV vs. SCE in PBS (pH 7.4).

In Figure 4.3.10.1 the O_2 calibrations using the SMCPEs at 25 °C and 37 °C, recorded and depicted no difference pre and post altering temperature ($P = 0.8934$, paired t -test). Sensitivities of -2.9 ± 0.2 nA/ μ M, $n = 4$, (black: 25 °C) and -3.4 ± 0.3 nA/ μ M, $n = 4$, (red: 37 °C) were obtained. The response of the electrodes was linear over the specified range with an R^2 value of 0.99 (25 °C) and 0.99 (37 °C). Increasing the temperature did not hinder the sensors ability to detect O_2 and as a result, fluctuating temperatures that may be encountered *in-vivo* will have no effect on the O_2 signal.

4.3.10.2 MMCPEs

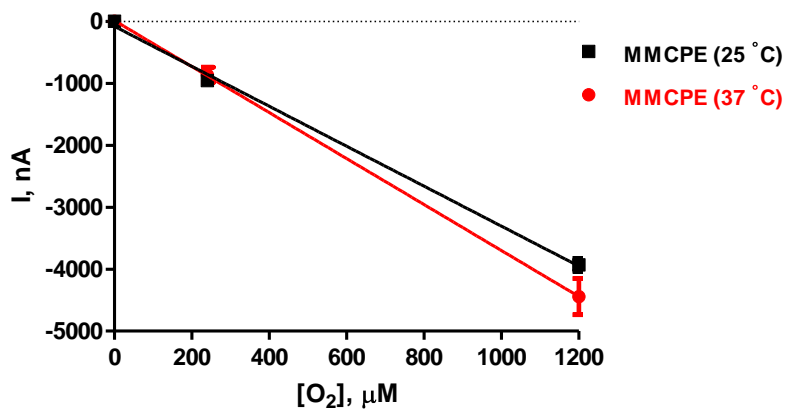


Figure 4.3.10.2 (a): O₂ calibrations performed at 25 °C (black) and 37 °C (red) utilising MMCPEs, $n = 4$, at -650 mV vs. SCE in PBS (pH 7.4).

The results obtained for the O₂ calibrations using the MMCPEs at 25 °C and 37 °C, yielded sensitivities of -3.2 ± 0.1 nA/μM, $n = 4$, (black: 25 °C) and -3.7 ± 0.1 nA/μM, $n = 4$, (red: 37 °C). The response of the electrodes was linear over the specified range with an R² value of 1.00 (37 °C) and 0.99 (25 °C). No significant difference was observed for the two calibrations ($P = 0.9415$, paired t -test), confirming no dependence of sensitivity on increasing temperature. In Figure 4.3.10.2 (b), a comparison between the SMCPE and MMCPEs is shown.

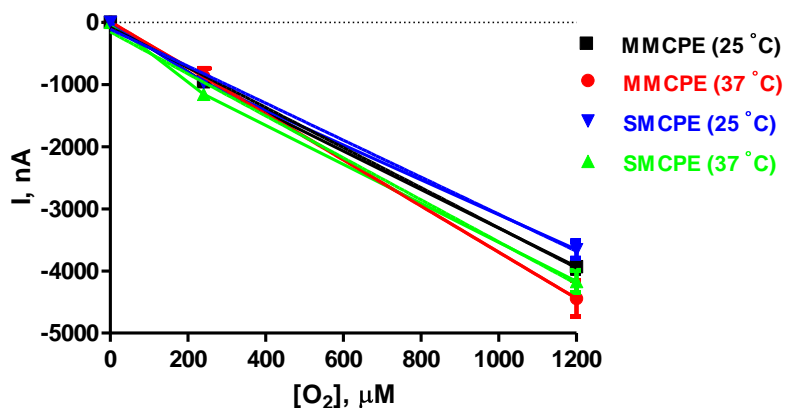


Figure 4.3.10.2 (b): An O₂ calibration comparison of MMCPEs and SMCPEs performed at 25 °C and 37 °C, $n = 4$, at -650 mV vs. SCE in PBS (pH 7.4).

The SMCPE and the MMCPE demonstrate no significant difference in the detection of O₂ with an increase in temperature ($P = 0.9988$, one-way ANOVA).

4.4 Conclusion

The results presented in this chapter are very promising for possible utilisation of the novel monomer modified CPEs in a clinical environment. An intact and solid SMCPE and MMCPE were obtained. A sensor that provided the ability to withstand morphological alterations in a very complex and hazardous environment was the aim and ambition sought when carrying out this research. The results suggested that this aim was accomplished. Initial experiments undertaken on the biocompatibility of the CPE displayed a complete breakdown of the morphology of the sensors integrity. A significant decrease in sensitivity was observed in both BSA ($P = 0.0258$) and PEA ($P < 0.0001$) studies. On examination of the results recorded for BT and Triton[®] X (10%), the sensors seemed to not be affected by these harsh treatments.

BT ON results yielded a P value that was not significant ($P = 0.1864$, $n = 4$), however leaving the CPEs in BT for 28 days caused a significant difference in the sensitivity recorded ($P = 0.0152$, $n = 4$). As stated previously in Section 4.3.1.1.4, this could be due to the components of the BT altering the surface morphology and blocking the sensor surface, thus leading to a decrease in sensitivity. The Triton[®] X results yielded a sensitivity that was

not significantly different ($P = 0.3270$, $n = 8$). On closer analysis of the CPEs, it suggests that the electrodes give a sensitivity that is similar to the sensitivities observed pre-treatment due to the extensively published alteration from a carbon paste to a carbon powder electrode, therefore leading to greater electron transfer in the ‘dry’ environment of the modified carbon electrode. This leads to a greater sensitivity obtained.

The constituents of the CPE are predisposed to modification by the environment that they are placed into, whereas the MMCPEs and SMCPEs are much more robust and remain intact. The SMCPE and MMCPE displayed the ability to endure biocompatibility tests without the integrity of the surface being compromised. Figure 4.4 (a) and Table 4.4 (a) display a summary of all of the sensors combined and the differences in the treatments observed between the varying sensors studied.

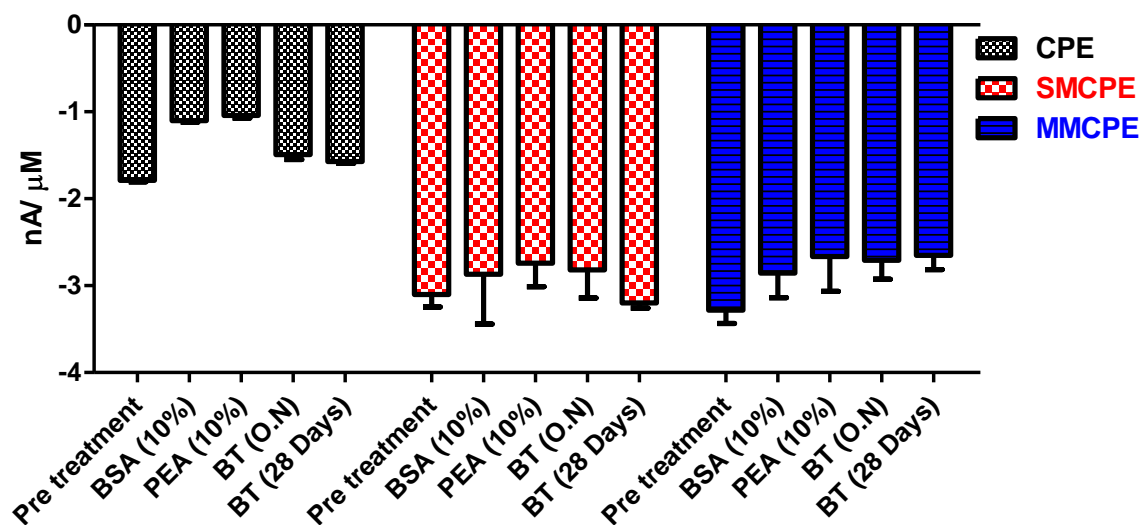


Figure 4.4 (a): A bar chart displaying a summary of the three sensors sensitivities (CPE: black), (SMCPE: red) and (MMCPE: blue) after each treatment carried out at -650 mV vs. SCE.

Treatment	CPE (nA/μM)			SMCPE (nA/μM)			MMCPE (nA/μM)		
	Mean	SEM	n	Mean	SEM	n	Mean	SEM	n
Pre	-1.8	0.1	52	-3.1	0.1	52	-3.3	0.2	52
BSA (10%)	-1.1	0.1	4	-2.7	0.5	8	-2.9	0.3	6
PEA (10%)	-1.0	0.1	4	-2.7	0.3	8	-2.7	0.4	4
BT (ON)	-1.5	0.1	4	-2.8	0.3	6	-2.7	0.2	7
BT (28 days)	-1.6	0.1	4	-3.2	0.1	4	-2.6	0.2	4

Table 4.4 (a): A table displaying a summary of the treatment results (nA/μM) for each of the sensors (CPE), (SMCPE) and (MMCPE).

It is clear that there are remarkable differences in how the sensors (CPEs, SMCPEs and MMCPEs) behave when treated with varying proteins, lipids, *ex-vivo* BT and surfactants. The SMCPEs display very stable results in terms of sensitivity, when they were treated with varying substances. All post treatment sensitivities displayed no significant difference in comparison to the pre-treatment sensitivities and the *P* values are presented in Table 4.4 (b).

Treatment	SMCPEs	
	<i>P</i> Value	<i>n</i>
BSA (10%)	0.9932	8
PEA (10%)	0.1792	8
BT (ON)	0.1687	6
BT (28 days)	0.5282	4

Table 4.4 (b): Summary of the *P* values obtained for the pre- and post-treatments carried out on the SMCPEs at -650 mV vs. SCE.

For the MMCPEs similar results were obtained with each treatment displaying no significant difference pre- and post-treatment, apart from the placement of the sensors in

BT for 28 days which yielded a significant decrease in the sensitivity ($P = 0.0296$). Even with this decrease in sensitivity it can be observed that the sensitivity obtained is much greater than the CPEs (see Figure 4.4 (a)).

Treatment	MMCPEs	
	<i>P</i> Value	<i>n</i>
BSA (10%)	0.0611	6
PEA (10%)	0.0506	4
BT (ON)	0.0544	7
BT (28 days)	0.0296	4

Table 4.4 (c): Summary of the *P* values obtained for the pre- and post-treatments carried out on the MMCPEs at -650 mV vs. SCE.

Upon removal and post calibration of the sensors from the living brain, it can be seen that the implantation of electrodes into the brain's hostile environment had an effect on the sensitivity of the SMCPEs and MMCPEs. As was observed from the SEMs pre- and post-implantation, the sensor remained undamaged and unaltered so a decrease in sensitivity was hypothesised to be a result of blockage of the surface by the many constituents of the BT environment. A decrease in sensitivity upon implantation into the brain is observed with all sensors including Pt based sensors that experience approximately a 40 % drop in sensitivity, which can be attributable to a build up of species on the surface of the sensor, as has been demonstrated by our research group. With the MMCPEs and SMCPEs a decrease of about 15.5 % and 14.4 % is observed.

Long term stability studies were then carried out on the novel developed sensors, in order to determine how stable the sensors were over the specified times detailed in Section 4.3.7. These studies were also undertaken to gain knowledge about how the sensors behave over time and where best to store them. In a clinical setting these aspects would need to be known, as the clinicians would not use these sensors straight away, they would be stored until they were needed. Different storage conditions were examined on these sensors (see Section 4.3.7). The effect of long term exposure of the SMCPEs and MMCPEs was

established in order to determine whether the sensors were suitable for long term recording *in-vivo*. The long term stability of CPEs has been demonstrated and discussed in data published by O'Neill (O'Neill, 2005). However, this stability is due to the leeching of the oil from the paste to leave a carbon powder electrode (Ormonde & O'Neill, 1989, 1990). Figure 4.4 (b) displays a summary of the results graphically, for the long term stability studies with the two monomer modified sensors from day 1 to the final day that they were calibrated in the specified storage condition.

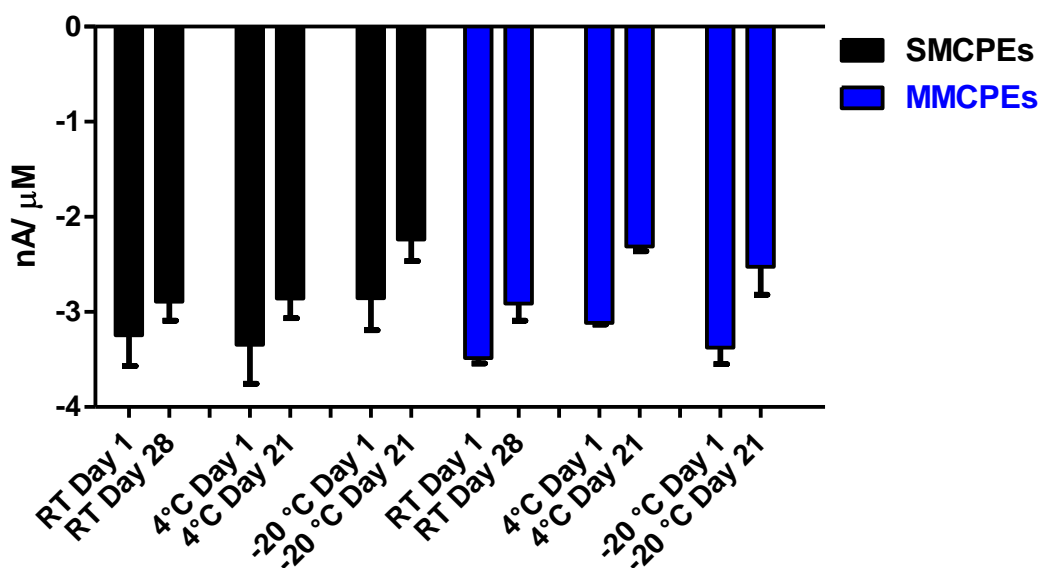


Figure 4.4 (b): A summary of the long term stability studies carried out with the SMCPEs (black) and MMCPEs (blue) under the different conditions.

It was decided that the RT storage conditions would be the chosen optimum condition to use for the two sensors, as the fridge and freezer results gave varying sensitivities on the specified days (see Section 4.3.7.2 and 4.3.7.3). As discussed previously, the lower temperatures appear to affect the sensitivity, which may be due to the morphology of the composite. The temperature and pH experiments displayed no significant differences pre and post studies undertaken with the two sensors (SMCPEs and MMCPEs). This indicates a great characteristic of the two sensors being robust and resilient under varying tests. The interference studies carried out displayed negligible sensitivities for each interferent used,

in comparison to the sensitivities obtained for O₂, for each sensor. Table 4.4 (d) displays these results with respect to percentage interference at physiological concentrations.

Analyte	MMCPE (%)	SMCPE (%)
O ₂	100.00 (<i>n</i> = 52)	100.00 (<i>n</i> = 52)
AA	0.07 (<i>n</i> = 4)	0.20 (<i>n</i> = 4)
L-cysteine	0.65 (<i>n</i> = 4)	0.39 (<i>n</i> = 4)
Uric acid	0.40 (<i>n</i> = 4)	0.17 (<i>n</i> = 4)
L-tryptophan	0.23 (<i>n</i> = 4)	0.05 (<i>n</i> = 4)
DHAA	0.07 (<i>n</i> = 4)	-0.04 (<i>n</i> = 4)
L-tyrosine	-0.02 (<i>n</i> = 4)	-0.11 (<i>n</i> = 4)
Dopamine	-0.08 (<i>n</i> = 4)	-0.15 (<i>n</i> = 4)
5-HIAA	-0.10 (<i>n</i> = 4)	-0.16 (<i>n</i> = 4)
DOPAC	-0.11 (<i>n</i> = 4)	-0.20 (<i>n</i> = 4)
5-HT	0.02 (<i>n</i> = 4)	-0.15 (<i>n</i> = 4)
HVA	-0.06 (<i>n</i> = 4)	-0.20 (<i>n</i> = 4)
L-glutathione	-0.12 (<i>n</i> = 4)	-0.21 (<i>n</i> = 4)

Table 4.4 (d): A table summarising the percentage change in sensitivity with regards to O₂ for all of the interferents studied.

On analysis of the SMCPEs and MMCPEs, a significantly higher sensitivity ($P < 0.0001$) towards O₂ was observed in comparison to the CPEs. However the sensitivities of the SMCPEs and MMCPEs themselves were not significantly different ($P = 0.3883$). Figure 4.4 (c) and Table 4.4 (e) display a comparison of the sensitivities of the sensors graphically and figuratively.

[O ₂], μM	CPEs (<i>n</i> = 52)		SMCPEs (<i>n</i> = 52)		MMCPEs (<i>n</i> = 52)	
	Mean I, nA	SEM	Mean I, nA	SEM	Mean I, nA	SEM
0.0	0.0	0.0	0.0	0.0	0.0	0.0
240.0	-452.1	16.7	-921.3	37.9	-977.5	37.7
1200.0	-2152.2	82.6	-3782.5	97.5	-4002.5	72.6

Table 4.4 (e): A comparison table comparing the sensitivities of CPEs, SMCPEs and MMCPEs, performed in PBS (pH 7.4) at -650 mV vs. SCE.

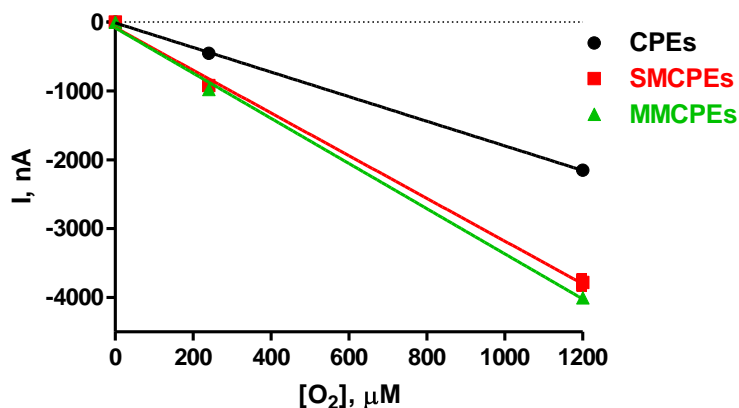


Figure 4.4 (c): A mean current concentration profile comparing the sensitivities of CPEs (black), SMCPEs (red) and MMCPEs (green) performed in PBS (pH 7.4) at -650 mV vs. SCE.

The results obtained from the O₂ calibrations yielded sensitivities of -1.8 ± 0.1 nA/ μ M, $n = 52$ (CPEs), -3.1 ± 0.1 nA/ μ M, $n = 52$ (SMCPEs) and -3.3 ± 0.2 nA/ μ M, $n = 52$ (MMCPEs). Linear regression analysis was carried out and a R^2 value of 0.99 was obtained for the CPEs, MMCPEs and SMCPEs. It is clear from the data collected for the sensors that the new monomer modified CPEs gave an enhanced sensitivity towards O₂. This characteristic is exceptional as the sensitivity is nearly double that of what can be attained with the CPEs. The SEMs displayed in Figure 4.4 (e) show the extent of the modification of the CPEs by the *in-vivo* environment. The images show that the carbon paste is being pulled away from the cavity and also that the surface of the CPEs have been aggravated. In Figure 4.4 (e), image A, the leeching of the silicone oil can be seen spilling out over the electrode.

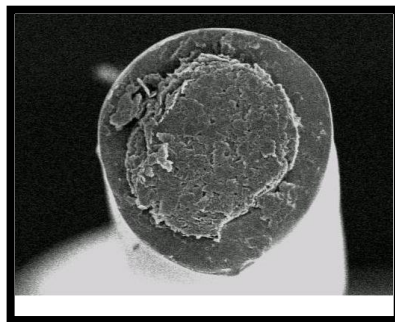


Figure 4.4 (d): SEM displaying the surface of a CPE pre-implantation.

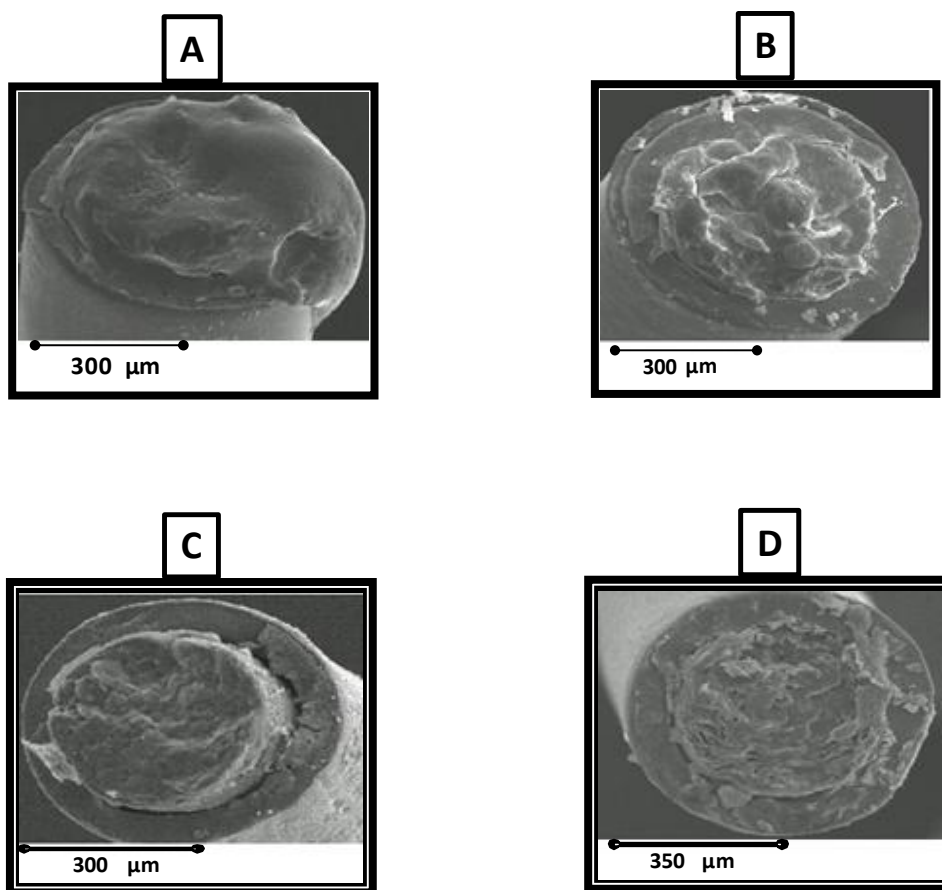


Figure 4.4 (e): (A), (B), (C) and (D); SEMs displaying the surface of different CPEs post-implantation.

With the SMCPEs and MMCPEs, all the components of the electrode remain inside the cavity, giving a surface that does not corrupt easily, unlike the CPEs. This is another very promising characteristic of the two monomer modified sensors. To have two individual sensors that perform similarly, withstand damage from a very complex environment and

that withstand the removal from that environment (which can cause detrimental harm to the sensor) whilst keeping the integrity of the electrode is a very exciting and promising result. It is critical for clinical integration that the surface remains intact to avoid unwanted leeching of carbon paste into human tissue. Strict regulatory guidelines exist when trying to get a novel medical device FDA or CE approved. Cytotoxicity testing would need to be undertaken to confirm the sensors don't have any detrimental effects on tissue cells before they could be adopted clinically.

The main aim of this chapter was to develop a new sensor that had all of the beneficial characteristics of CPEs but without the leeching of the oil (and potentially paste) from the cavity of the electrode. A CPE that incorporated the monomers Sty and MMA was successfully manufactured to detect O₂. An increase in the sensitivity of O₂ was also achieved utilising these two sensors, in comparison to the CPEs. The aim of the modified electrode was to retain good stability, without any modification to the components of the sensor. It can be seen from the results in the various sections of this chapter that the data obtained from the CPEs, SMCPEs and MMCPEs varied immensely when exposed to the different parameters tested on them. In order to fully distinguish between the CPEs and the SMCPEs and MMCPEs, their responses to the analyte O₂ *in-vivo* is examined and discussed in Chapter 5.


4.5 References

- A. Kane D & D. O'Neill R. (1998). Major differences in the behaviour of carbon paste and carbon fibre electrodes in a protein-lipid matrix: implications for voltammetry *in-vivo*. *Analyst* **123**, 2899-2903.
- Bai J, Snively C, Delgass W & Lauterbach J. (2001). Formation of ultrathin polystyrene films using a two-step deposition/polymerization process. *Macromolecules* **34**, 1214-1220.
- Bolger F & Lowry J. (2005). Brain Tissue Oxygen: *In-Vivo* Monitoring with Carbon Paste Electrodes. *Sensors* **5**, 473-487.
- Bolger FB, Bennett R & Lowry JP. (2011a). An *in-vitro* characterisation comparing carbon paste and Pt microelectrodes for real-time detection of brain tissue oxygen. *Analyst* **136**, 4028-4035.
- Bolger FB, McHugh SB, Bennett R, Li J, Ishiwari K, Francois J, Conway MW, Gilmour G, Bannerman DM, Fillenz M, Tricklebank M & Lowry JP. (2011b). Characterisation of carbon paste electrodes for real-time amperometric monitoring of brain tissue oxygen. *Journal of Neuroscience Methods* **195**, 135-142.
- Chatzandroulis S, Tegou E, Goustouridis D, Polymenakos S & Tsoukalas D. (2004). Fabrication of chemical sensors based on Si/polymer bimorphs. *Microelectronic Engineering* **73-74**, 847-851.
- Chesler M. (2003). Regulation and Modulation of pH in the Brain. *Physiological Reviews* **83**, 1183-1221.
- Clark LC, Misrahy G & Fox RP. (1958). Chronically implanted polarographic electrodes. *Journal of Applied Physiology* **13**, 85-91.
- Czaban JD. (1985). Electrochemical sensors in clinical chemistry. *Analytical Chemistry* **57**, 345A-356A.
- Dai H, Wu X, Wang Y, Zhou W & Chen G. (2008). An electrochemiluminescent biosensor for vitamin C based on inhibition of luminol electrochemiluminescence on graphite/poly(methylmethacrylate) composite electrode. *International Society of Electrochemistry* **53**, 5113-5117.
- Dengler J, Frenzel C, Vajkoczy P, Wolf S & Horn P. (2011). Cerebral tissue oxygenation measured by two different probes: challenges and interpretation. *Intensive Care Med* **37**, 1809-1815.

- Dixon BM, Lowry JP & O'Neill RD. (2002). Characterization *in-vitro* and *in-vivo* of the oxygen dependence of an enzyme/polymer biosensor for monitoring brain glucose. *Journal of Neuroscience Methods* **119**, 135-142.
- Douglas WH & Bates JF. (1978). The determination of residual monomer in polymethylmethacrylate denture-base resins. *Journal of Materials Science* **13**, 2600-2604.
- Elliott KGB & Johnstone AJ. (2003). Diagnosing acute compartment syndrome. *Journal of Bone and Joint Surgery-British Volume* **85B**, 625-632.
- Hsu C-Y, Lin H-Y, Thomas JL, Wu B-T & Chou T-C. (2006). Incorporation of styrene enhances recognition of ribonuclease A by molecularly imprinted polymers. *Biosensors and Bioelectronics* **22**, 355-363.
- Kalcher K. (1990). Chemically modified carbon paste electrodes in voltammetric analysis. *Electroanalysis* **2**, 419-433.
- Kealy J, Bennett R & Lowry JP. (2013). Simultaneous recording of hippocampal oxygen and glucose in real time using constant potential amperometry in the freely-moving rat. *Journal of Neuroscience Methods* **215**, 110-120.
- Keddie S & Rohman L. (2012). Reviewing the reliability, effectiveness and applications of Licox[®] in traumatic brain injury. *Nursing in Critical Care* **17**, 204-212.
- Khoo SB & Guo SX. (1999). Rapidly renewable and reproducible electropolymerized surface at a monomer modified carbon paste electrode. *Journal of Electroanalytical Chemistry* **465**, 102-113.
- Khuong KS, Jones WH, Pryor WA & Houk K. (2005). The mechanism of the self-initiated thermal polymerization of styrene. Theoretical solution of a classic problem. *Journal of the American Chemical Society* **127**, 1265-1277.
- Kim G. (2005). A PMMA composite as an optical diffuser in a liquid crystal display backlighting unit (BLU). *European Polymer Journal* **41**, 1729-1737.
- Kim S, Kim E, Kim S & Kim W. (2005). Surface modification of silica nanoparticles by UV-induced graft polymerization of methyl methacrylate. *Journal of Colloid and Interface Science* **292**, 93-98.
- Kruus P & Patraboy T. (1985). Initiation of polymerization with ultrasound in methyl methacrylate. *The Journal of Physical Chemistry* **89**, 3379-3384.
- Kuwana T & French WG. (1964). Electrooxidation or Reduction of Organic Compounds into Aqueous Solutions Using Carbon Paste Electrode. *Analytical Chemistry* **36**, 241-242.

- Lowry JP, Boutelle MG & Fillenz M. (1997). Measurement of brain tissue oxygen at a carbon paste electrode can serve as an index of increases in regional cerebral blood flow. *Journal of Neuroscience Methods* **71**, 177-182.
- Lowry JP, Boutelle MG, O'Neill RD & Fillenz M. (1996). Characterisation of carbon paste electrodes *in-vitro* for simultaneous amperometric measurement of changes in oxygen and ascorbic acid concentrations *in-vivo*. *Analyst* **121**, 761-766.
- Lyne PD & O'Neill RD. (1990). Stearate-modified carbon paste electrodes for detecting dopamine *in vivo*: decrease in selectivity caused by lipids and other surface-active agents. *Analytical Chemistry* **62**, 2347-2351.
- Melak F, Redi M, Tessema M & Alemayehu E. (2013). Electrochemical determination of catechol in tea samples using anthraquinone modified carbon paste electrode. *Natural Science* **5**, 888-894.
- Miele M & Fillenz M. (1996). *In-vivo* determination of extracellular brain ascorbate. *Journal of Neuroscience Methods* **70**, 15-19.
- Morgalla M, Haas R, Grözinger G, Thiel C, Thiel K, Schuhmann M & Schenk M. (2012). Experimental Comparison of the Measurement Accuracy of the Licox[®] and Raumedic[®] Neurovent-PTO Brain Tissue Oxygen Monitors. In *Intracranial Pressure and Brain Monitoring XIV*, ed. Schuhmann MU & Czosnyka M, pp. 169-172. Springer Vienna.
- Murray MD & Darvell BW. (1993). The evolution of the complete denture base. Theories of complete denture retention — A review. Part 3. *Australian Dental Journal* **38**, 389-393.
- Nayak RR, Lee KY, Shanmugaraj AM & Ryu SH. (2007). Synthesis and characterisation of styrene grafted carbon nanotube and its polystyrene nanocomposite. *European Polymer Journal* **43**, 4916-4923.
- O'Neill R. (1993). Sensor-tissue interactions in neurochemical analysis with carbon paste electrodes *in-vivo*. *The Analyst* **118**, 433.
- O'Neill R. (2005). Long-Term Monitoring of Brain Dopamine Metabolism *in-vivo* with Carbon Paste Electrodes. *Sensors* **5**, 317-342.
- Ormonde DE & O'Neill RD. (1989). Altered response of carbon paste electrodes after contact with brain tissue: Implications for modified electrode use *in-vivo*. *Journal of Electroanalytical Chemistry and Interfacial Electrochemistry* **261**, 463-469.
- Ormonde DE & O'Neill RD. (1990). The oxidation of ascorbic acid at carbon paste electrodes: Modified response following contact with surfactant, lipid and brain tissue. *Journal of Electroanalytical Chemistry and Interfacial Electrochemistry* **279**, 109-121.

- Oster G & Yang N-L. (1968). Photopolymerization of vinyl monomers. *Chemical Reviews* **68**, 125-151.
- Pérez JPH, López-Cabarcos E & López-Ruiz B. (2006). The application of methacrylate-based polymers to enzyme biosensors. *Biomolecular Engineering* **23**, 233-245.
- Purins K, Enblad P, Sandhagen B & Lewén A. (2010). Brain tissue oxygen monitoring: a study of *in-vitro* accuracy and stability of Neurovent-PTO and Licox[®] sensors. *The European Journal of Neurosurgery* **152**, 681-688.
- Regel A & Lunte S. (2013). Integration of a graphite/poly(methyl-methacrylate) composite electrode into a poly(methylmethacrylate) substrate for electrochemical detection in microchips. *Electrophoresis* **34**, 2101-2106.
- Sarac D, Sarac YS, Basoglu T, Yapici O & Yuzbasioglu E. (2006). The evaluation of microleakage and bond strength of a silicone-based resilient liner following denture base surface pretreatment. *The Journal of Prosthetic Dentistry* **95**, 143-151.
- Sun X, Zhu Y & Wang X. (2011). Amperometric immunosensor based on a protein A/deposited gold nanocrystals modified electrode for Carbofuran Detection. *Sensors* **11**, 11679-11691.
- Xu L, Du J, Deng Y, Li Z, Xu C & He N. (2011). Fabrication and Characterisation of Nanoporous Pseudo-Carbon Paste Electrode. *Advanced Science Letters* **4**, 104-107.
- Zhang J-J, Liu Y, Hu L-H, Jiang L-P & Zhu J-J. (2011). "Proof-of-principle" concept for ultrasensitive detection of cytokines based on the electrically heated carbon paste electrode. *Chemical Communications* **47**, 6551-6553.
- Zhu S, Tian Y, Hamielec AE & Eaton DR. (1990). Radical trapping and termination in free-radical polymerization of methyl methacrylate. *Macromolecules* **23**, 1144-1150.



*5. In-Vivo Characterisation
of Sensors for the
Neurochemical Detection of
Oxygen*

5.1 Introduction

Measuring and determining tissue O₂ concentration *in-vivo* is of the utmost importance, as living organisms rely on O₂ as a means of survival. It is essential that the brain along with the rest of the body obtains a continuous supply of O₂ for normal functioning, with the brain consuming about 20 % of the O₂ utilised by the body at any given time (Bolger *et al.*, 2011b). The balance between supply and utilisation is the main determinant of the tissue O₂ concentration (Lowry *et al.*, 1997). One of the first reports of changes in brain tissue was demonstrated by Clark *et al.*, using a noble metal electrode (Clark *et al.*, 1958). Since this time, detecting O₂ *in-vivo* has been widely documented in the literature (Lowry *et al.*, 1996; Lowry & Fillenz, 2001; Bolger & Lowry, 2005; Kealy *et al.*, 2013).

The reported ECF O₂ concentration ranges from 40 to 80 μM (O'Neill & Lowry, 2000). Brain tissue O₂ reacts to a range of agitations which include electrical stimulation (McCreery *et al.*, 1990) and neuromediator release (Kennedy *et al.*, 1992) and it also has a faster turnover in the cerebral cortex in contrast to other brain regions (Nair *et al.*, 1987). Different types of voltammetry can be employed to detect changes in the ECF, for example fast cyclic voltammetry (FCV), differential pulse voltammetry (DPV) and constant potential amperometry (CPA). For *in-vivo* studies, CPA is employed due to the high time resolution (Lowry & O'Neill, 2006) and has been the technique utilised for *in-vivo* experiments throughout this research and within our lab (Bolger & Lowry, 2005; Bolger *et al.*, 2011b; Kealy *et al.*, 2013).

The utilisation of CPEs for the detection of O₂ has been widely documented (Lowry *et al.*, 1996; Lowry *et al.*, 1997; Bolger & Lowry, 2005). CPEs are highly advantageous over the use of noble metal electrodes, as they are not vulnerable to surface poisoning and it is not necessary to integrate membranes onto the surface in order to protect them. Metal electrodes are hampered by this characteristic and there are many reports of ways and means of trying to avoid this by modifying the surfaces of the noble metal electrodes (Wisniewski *et al.*, 2000; Gifford *et al.*, 2006). Another advantage of CPEs is their long term stability *in-vivo*. The silicone oil is removed from the carbon paste once it interacts with the brain environment, leading to the ability of the electrode to take any proteins, lipids or constituents that have adsorbed onto the surface of the electrode from the brain

surroundings and remove them along with the oil. This leads to the overall stability of the carbon paste sensor being highly durable (Ormonde & O'Neill, 1989, 1990).

Although this is a great trait to have in a sensor when monitoring the *in-vivo* environment, it is not ideal for any constituents to leach out from the electrode compartment when monitoring in the clinical environment. For an electrode to be utilised in a clinical setting, sensitivity to impeding lipophilic ions or charged surfactants should not be an issue for the electrode (Czaban, 1985). The LICOX[®] probe (see Figure 1.2.2), is a device that is utilised in the clinical environment and is electrochemical in nature. It has a lot of similarities to our proposed device; however, the sensing component's role is to diffuse O₂ through a permeable membrane surrounding the probe and into an electrolyte solution where a signal is created. The LICOX[®] probe has a design of a bulky housing component with a fragile membrane surrounding the probe. Alternative methods of measuring O₂ levels currently utilised in hospitals include Pulse Oximetry and Arterial Blood Gas (ABG) analysis.

Severe limitations exist with such techniques restricting their utility in measuring a medical emergency such as a patient with ischemia. ABG focuses on discrete measurements of O₂ levels in blood taken from the patient at varying time intervals. It does not monitor the trend in O₂ levels on a continual basis. 'At risk' patients would therefore not benefit from this technique since early diagnosis is of the utmost importance to the patient's outcome. The continuous real-time characteristic of the sensor technology within our lab will allow for millisecond changes in O₂ levels to be recorded and presented for the clinician, significantly increasing timely intervention. It is for this reason that the CPEs were modified to produce a more robust and solid electrode that can withstand modification and morphology from a complex structure such as the living brain. This follows directly from the data presented in Chapter 4, where the MMCPEs and SMCPEs were characterised in the *in-vitro* environment.

Characterising the novel monomer modified sensors in the *in-vivo* environment is a complex procedure, due to the vast differences between the two settings. The living brain encompasses an array of endogenous substances that include proteins, lipids and electrocatalysts like AA. The brain also limits mass transport to the sensor surface and reacts to the presence of the electrode physiologically (O'Neill, 1993). The body's defence system responds to the implanted device causing the body to react as if it is responding to

an injury. This defence system includes the three stages of wound healing (inflammation and debridement, repair and maturation (Mann *et al.*, 2011)) and would therefore interact with the sensors properties. So, sensitivity, selectivity and stability of the sensor once it is placed in this *in-vivo* setting could weaken the capabilities of the electrode to perform as well as demonstrated in the *in-vitro* environment (Wisniewski *et al.*, 2000; Gifford *et al.*, 2006). Therefore, the behaviour of the electrode *in-vitro* might well be different to its behaviour in the *in-vivo* milieu.

Due to these reasons, it is clear that while *in-vitro* characterisation of the sensors is essential for determining the sensitivity and selectivity of the sensor, these parameters can alter once the sensor is placed into the biological setting as tissue components interfere with the sensor (O'Neill, 1993).

5.2 Experimental

The instrumentation and software for all experiments are described in Section 3.2. All chemicals and solutions are described in detail in Section 3.3. The sensors utilised for these experiments consist of MMCPEs and SMCPEs. The manufacture of these sensors is detailed in Section 3.4. An applied potential of -650 mV *vs.* Ag wire was applied to the electrodes involved in these experiments. All O₂ studies undertaken were performed in freely-moving animals. The surgical procedure undertaken for the implantation of the sensors is described in Section 3.8. Data is reported as mean \pm SEM. The significance of differences observed was calculated using student *t*-tests. In each of the Sections, *n* denotes the number of perturbations carried out on a given number of sensors in a given number of animals, unless stated otherwise.

5.3 Results and Discussion

It was concluded in Chapter 4, that the novel monomer modified sensors had the potential ability to remain intact and unmodified in the *in-vivo* environment while possessing a significantly increased sensitivity towards O₂. This considerable improvement to the surface integrity is pivotal to the integration of these O₂ sensors into clinical practice. It is imperative that the sensor surface remains intact and the possibility of paste leeching during implantation is negated. Since our primary area of expertise is preclinical brain monitoring, this results section comprises the data from experiments that were carried out with the objective being the *in-vivo* characterisation of the MMCPE and SMCPE for long term monitoring of brain tissue O₂. However, due to the significantly higher regulatory hurdles associated with clinical brain monitoring, identification of peripheral O₂ monitoring applications is more realistic option for the research group. Verification that the sensors responded to changing levels of oxygenation was achieved by the induction of states of mild hypoxia and hyperoxia in the subject.

5.3.1 Hypoxia

Hypoxia is defined as a decrease in the supply of O₂ to tissue below physiological levels, even though there is sufficient perfusion of the tissue by blood (Dorland, 2011). The occurrence of hypoxia can be a sign of low O₂ tension in arterial blood, the decreased ability of the blood to carry O₂ (which is caused by anaemia or carbon monoxide poisoning) or a reduced tissue perfusion, (Höckel & Vaupel, 2001), these are just a couple of examples of hypoxia induced variables. In these experiments, the production of mild hypoxia was created by the administration of a N₂/air mixture to the snout of the animal, through a plastic tube. The flow rate was kept low, in order to keep the animal at ease during the experiment.

A similar method was undertaken in previous reports (Lowry *et al.*, 1998a). The inhalation of N₂ resulted in a response at the O₂ sensors leading to a change in the O₂ current.

5.3.1.1 MMCPE

The effect of a typical 3-minute period of hypoxia recorded by the MMCPEs is displayed in Figure 5.3.1.1. The 3-minute period of hypoxia data in this section was analysed using the results from 54 perturbations with 16 sensors in 7 animals.

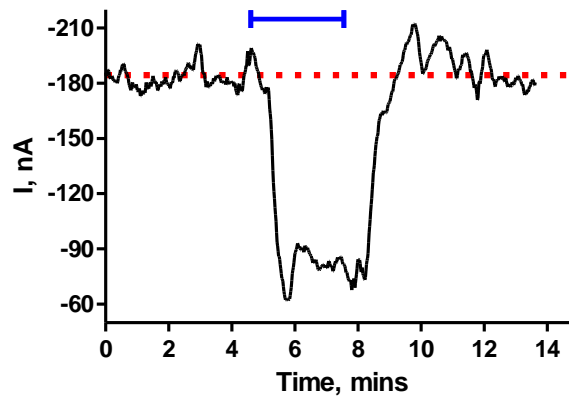


Figure 5.3.1.1: A typical example of a 3-minute period of hypoxia monitored at an MMCPE implanted in the striatum of a freely moving rat. The blue bar is indicative of the administration of a N_2 /air mixture.

Figure 5.3.1.1, demonstrates how a 3-minute period of induced hypoxia caused an immediate and significant decrease ($P < 0.0001$) in the O_2 current from a baseline level of -176.9 ± 4.7 nA, $n = 54$, to a current of -101.3 ± 3.4 nA, $n = 54$. The max response time was at 2.5 ± 0.1 minutes, $n = 54$. A maximum decrease of 75.6 ± 4.0 nA, $n = 54$, representing a mean percentage change of 41.6 ± 1.8 %, $n = 54$, was obtained. Upon cessation of inhalation of the gas, the current immediately returned to baseline currents levels of -178.6 ± 4.9 nA, $n = 54$, ($P = 0.2623$), indicating a return to normoxic conditions after 7.1 ± 0.4 minutes, $n = 54$.

Hypoxia						
	Current change (nA)	Current change (%)	Max response Time (mins)	Return Time (mins)	Baseline Pre Injection (nA)	Baseline Post Injection (nA)
MMCPEs	75.6 ± 4.0	41.6 ± 1.8	2.5 ± 0.1	7.1 ± 0.4	-176.9 ± 4.7	-178.6 ± 4.9

Table 5.3.1.1: Summary of results for the 3-minute period of hypoxia, with the MMCPEs implanted in the striatum of freely moving rats ($n = 54$, with 16 sensors in 7 animals).

5.3.1.2 SMCPE

The effect of induced hypoxia monitored with SMCPEs for 3-minutes is shown in Figure 5.3.1.2. The 3-minute period of hypoxia data in this section was analysed using the results from 66 perturbations with 13 sensors in 6 animals.

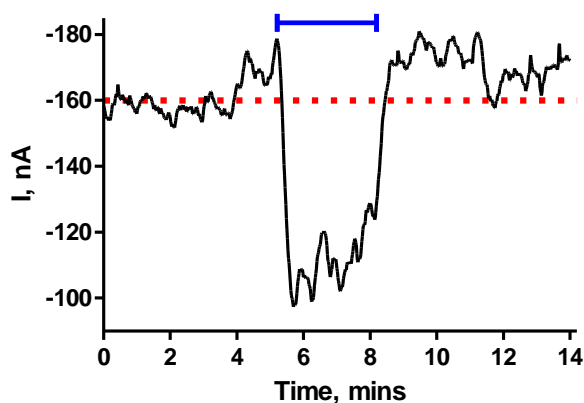


Figure 5.3.1.2: A typical example of a 3 minute period of hypoxia monitored by a SMCPE in the striatum of a freely moving rat. The blue bar is indicative of the administration of a N_2 /air mixture.

Analysis of the data confirms that the 3 minute period of hypoxia caused a decrease in the observed O_2 current that was significant ($P < 0.0001$). The O_2 level decreased by 49.9 ± 2.9 nA, $n = 66$, from a baseline of -159.8 ± 6.3 nA, $n = 66$, to a level of 110.0 ± 4.7 nA, $n = 66$, which corresponds to a mean percentage decrease of 30.9 ± 1.4 %, $n = 66$. The max response was attained after 1.7 ± 0.1 minutes, $n = 66$. Upon termination of administration of the N_2 , the current returned to similar baseline levels as before of -161.0 ± 6.6 nA, $n =$

66, ($P = 0.3064$) after 6.2 ± 0.4 nA, $n = 66$, had elapsed, which is indicative of a return back to normal O₂ conditions.

Hypoxia						
	Current change (nA)	Current change (%)	Max response Time (mins)	Return Time (mins)	Baseline Pre Injection (nA)	Baseline Post Injection (nA)
SMCPEs	49.9 ± 2.9	30.9 ± 1.4	1.7 ± 0.1	6.2 ± 0.4	-159.8 ± 6.3	-161.0 ± 6.6

Table 5.3.1.2: A table summarising the results for the 3-minute period of induced hypoxia, with the SMCPEs implanted in the striatum of freely moving rats ($n = 66$, with 13 sensors in 6 animals).

5.3.1.3 Comparison

On examination of the induced hypoxic responses obtained with the two sensors (MMCPEs and SMCPEs), it is observed that a similar O₂ trace is obtained with both sensors. Upon administration of the N₂/air mixture to the subject, the O₂ current decreases significantly by 41.6 ± 1.8 %, $n = 54$, 7 animals, ($P < 0.0001$) with the MMCPEs and 30.9 ± 1.4 %, $n = 66$, 6 animals, ($P < 0.0001$) with the SMCPEs. Although the MMCPEs detected a greater O₂ decrease, the SMCPEs still achieved a good response at the electrodes. The MMCPEs took longer to return to baseline levels (7.1 ± 0.4 minutes, $n = 54$) in comparison to the SMCPEs which took less time (6.2 ± 0.4 , $n = 66$) to achieve normal O₂ conditions, although the return time for the SMCPEs was not significantly different ($P = 0.1179$) in comparison to the MMCPEs. Bolger *et al.*, demonstrates an administration of N₂/air, using CPEs. A decrease in O₂ can be observed that yields a similar trace to what the MMCPEs and SMCPEs recorded. A decrease of 16.2 ± 4.3 nA ($n = 4$) was obtained with the CPEs for the administration of hypoxia (Bolger *et al.*, 2011b).

The MMCPEs and SMCPEs demonstrate a much greater decrease due to the administration of N₂. A significant difference can be observed between the monomer modified sensors in comparison to the CPEs (MMCPEs *vs.* CPEs: $P = 0.0004$) and (SMCPEs *vs.* CPEs: $P = 0.0061$). The increased sensitivity observed *in-vivo* correlates with the results obtained in

Chapter 4, as an increased sensitivity was observed with the sensors in comparison to the CPEs (see Section 4.4, Figure 4.4 (c)).

5.3.2 Hyperoxia

Hyperoxia is defined as a greater O_2 concentration than the normal atmospheric level (Voelkel & Rounds, 2009). Mild hyperoxia was established in the subject by the administration of an O_2 /air mixture to the snout of the subject through a plastic tube with a low flow rate. This prevents the animal from being startled or uneasy during the experiment. A similar method was reported in the literature (Lowry *et al.*, 1998a). This process was carried out on subjects that had MMCPEs and SMCPEs implanted in the striatum and the results were examined for each.

5.3.2.1 MMCPE

The effect of a typical 5-minute period of hyperoxia recorded with the MMCPE is displayed in Figure 5.3.2.1. The 5-minute period of hyperoxia data in this Section was analysed using the results from 54 perturbations with 15 sensors in 7 animals.

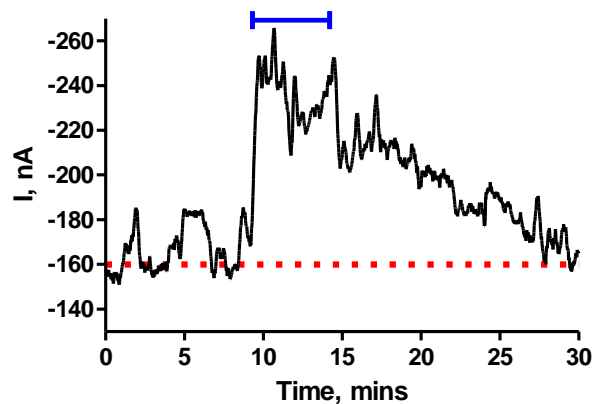


Figure 5.3.2.1: A typical example of a 5-minute period of hyperoxia monitored by an MMCPE in the striatum of a freely moving rat. The blue bar is indicative of the administration of an O_2 /air mixture.

Figure 5.3.2.1, demonstrates how a 5-minute period of induced hyperoxia caused an immediate and significant increase ($P < 0.0001$) in the O_2 current from a baseline level of -170.7 ± 5.1 nA, $n = 54$, to a current of -250.9 ± 8.9 nA, $n = 54$. This yielded a maximum increase of 80.3 ± 6.3 nA, $n = 54$, after approximately 3.0 ± 0.2 minutes, $n = 54$, representing a mean percentage change of 50.8 ± 6.0 %, $n = 54$. Upon cessation of inhalation of the gas, the current immediately returned to baseline currents of -174.3 ± 5.0 nA, $n = 54$, ($P = 0.6067$), indicating a return to normoxic conditions after 13.2 ± 0.7 minutes, $n = 54$.

	Hyperoxia					
	Current change (nA)	Current change (%)	Max response Time (mins)	Return Time (mins)	Baseline Pre Injection (nA)	Baseline Post Injection (nA)
MMCPEs	80.3 ± 6.3	50.8 ± 6.0	3.0 ± 0.2	13.2 ± 0.7	-170.7 ± 5.1	-174.3 ± 5.0

Table 5.3.2.1: Summary of results for the 5-minute period of induced hyperoxia, with the MMCPEs implanted in the striatum of freely moving rats ($n = 54$, with 15 sensors in 7 animals).

5.3.2.2 SMCPE

The effect of a typical 5-minute period of hyperoxia recorded with the SMCPE is displayed in Figure 5.3.2.2. The 5-minute period of hyperoxia data in this Section was analysed using the results from 75 perturbations with 12 sensors in 6 animals.

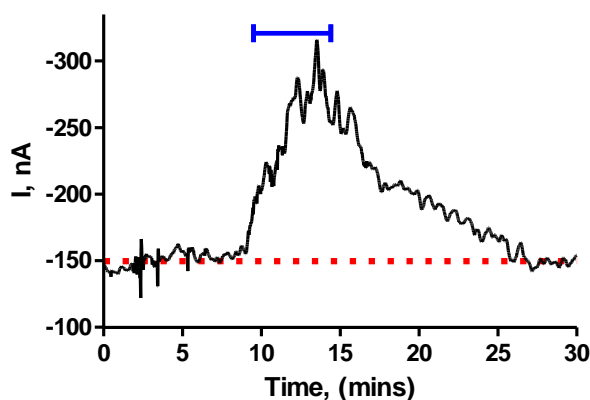


Figure 5.3.2.2: A typical example of a 5-minute period of hyperoxia monitored by an SMCPE in the striatum of freely moving rats. The blue bar is indicative of the administration of an O₂/air mixture.

Analysis of the data confirms that the 5-minute period of hyperoxia caused an increase in the observed O₂ current that was significantly different from baseline ($P < 0.0001$). The O₂ level increased by 63.6 ± 3.7 nA, $n = 75$, after 2.9 ± 0.1 minutes, $n = 75$, from a baseline of -159.8 ± 6.4 nA, $n = 75$, to a level of -223.4 ± 9.3 nA, $n = 75$, which corresponds to a mean percentage decrease of 67.4 ± 3.8 nA, $n = 75$. Upon termination of administration of the O₂, the current returned to a similar baseline levels as before of -159.3 ± 6.1 nA, $n = 75$, ($P = 0.6837$) after 12.7 ± 0.7 nA, $n = 75$, had elapsed, which is indicative of a return back to normal O₂ conditions.

Hyperoxia Administration						
	Current change (nA)	Current change (%)	Max response Time (mins)	Return Time (mins)	Baseline Pre Injection (nA)	Baseline Post Injection (nA)
SMCPEs	63.6 ± 3.7	67.4 ± 3.8	2.9 ± 0.1	12.7 ± 0.7	-159.8 ± 6.4	-159.3 ± 6.1

Table 5.3.2.2: Summary of results for the hyperoxia administration (5 minutes), with the SMCPEs implanted in the striatum of freely moving rats ($n = 75$, with 12 sensors in 6 animals).

5.3.2.3 Comparison

The hyperoxia responses attained at the two sensors both demonstrated a significant increase in the O₂ current (< 0.0001). The raw data traces for the two sensors showed similarity also. A percentage increase of $50.8 \pm 6.0 \%$, ($n = 54$, 7 animals) and $67.4 \pm 3.8 \%$, ($n = 66$, 6 animals) were obtained for the MMCPEs and SMCPEs, respectively. This shows that the two sensors have the ability to detect changes in the O₂ current. The SMCPEs returned to baseline levels at a similar time to the MMCPEs, yielding a time effect of 13.2 ± 0.7 minutes, $n = 54$, for the MMCPEs and 12.7 ± 0.7 minutes, $n = 66$, for the SMCPEs, displaying no significant difference ($P = 0.6180$) between the two time frames. On comparison to the results that Bolger *et al.*, attained with the CPEs for an administration of O₂/Air, the CPEs detected an increase in the O₂ (50.1 ± 5.9 nA, $n = 4$), that was less than what the MMCPEs and SMCPEs achieved (Bolger *et al.*, 2011b).

However, no significant difference in the O₂ sensitivity was obtained between the different sensors (MMCPEs *vs.* CPEs: $P = 0.4062$) and (SMCPEs *vs.* CPEs: $P = 0.2018$). Although no significant difference was observed, the results for the hyperoxia administration highlights how the monomer modified sensors have an increased sensitivity, as demonstrated in Chapter 4, which corresponds to the increased sensitivity achieved for the hyperoxia administration in comparison to the CPEs observed by Bolger *et al.*, (Bolger *et al.*, 2011b).

5.3.3 Neuronal Activation

Two forms of physiologically stimulated neuronal activation were utilised throughout the experiments; these were restraint stress and tail pinch. Each test was carried out for 5 minutes. These types of experiments have been demonstrated previously in our lab (Lowry *et al.*, 1997; Bolger & Lowry, 2005). The two stimuli, cause mild stress in the animal, leading to an increase in O₂ recorded by the sensors. Stress is any unpleasant stimulus, which can perturb the normal physiological homeostasis of the body (Gold & Chrousos, 2002). The capability to handle stressful stimuli plays a vital role in the determinants of health and disease (Gulati *et al.*, 2006). The application of a stress response promotes

physiological changes that include increases in heart rate and blood pressure, altered blood flow to the brain and to the stressed body site (Gold & Chrousos, 2002).

The introduction of the restraint test in order to promote a stress response has been demonstrated in the literature (Gulati *et al.*, 2006; Gulati *et al.*, 2007; Chakraborti *et al.*, 2008). The attachment of a paper clip to the tail of the subject has been demonstrated previously by Valente *et al.*, and yields a well characterised behaviour pattern of gnawing, licking, eating and a universal increase in motor activity. This physiological stimulation also increases neuronal activation in the striatum and a simultaneous elevation of cerebral blood flow and O_2 was also observed (Valente *et al.*, 2012).

5.3.3.1 Restraint

5.3.3.1.1 MMCPE

The effect of a 5-minute restraint stress recorded with an MMCPE in the striatum of a freely moving rat is shown in Figure 5.3.3.1.1. The restraint stress data in this Section was analysed using 29 perturbations with 13 sensors in 6 animals.

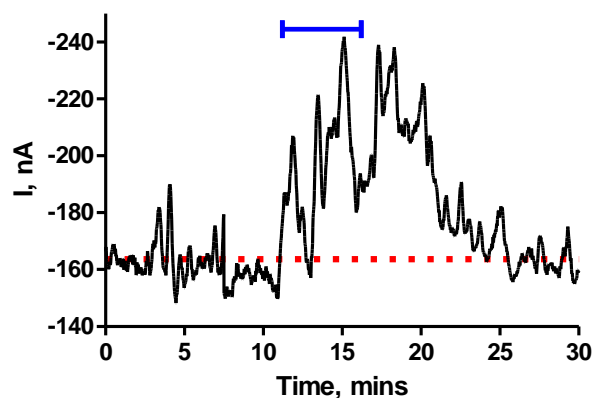


Figure 5.3.3.1.1: A typical raw data trace displaying the effects of a 5-minute restraint stress on the observed O_2 current recorded with an MMCPE in the striatum of a freely moving rat. The blue bar is indicative of the induced stress.

The application of a 5-minute restraint stress test resulted in an immediate and rapid increase in the O₂ current recorded at the MMCPEs by 26.8 ± 3.8 nA, $n = 29$, after 2.5 ± 0.3 minutes, $n = 29$, from a mean baseline of -165.9 ± 5.8 nA, $n = 29$, to a current of -192.7 ± 7.6 nA, $n = 29$. The mean percentage increase in response to the restraint test was 16.4 ± 2.2 %, $n = 29$. The resulting O₂ increase caused a significant difference in the O₂ signal obtained ($P < 0.0001$) from baseline. On cessation of the stimulus, the baseline began to fall until another increase was observed shortly afterwards. A significantly different current ($P < 0.0001$) was observed subsequent to the first max response, after 6.1 ± 0.2 minutes, $n = 29$. A current change of 33.0 ± 3.6 nA, $n = 29$, which yielded a mean percentage change of 20.1 ± 2.2 %, $n = 29$, from the mean pre baseline of -165.9 ± 5.8 nA, $n = 29$, to a current of -198.9 ± 7.4 nA, $n = 29$, was recorded.

A second O₂ increase on cessation of the stimulus was observed due to how the O₂ concentration is controlled in the body. It is based on the supply and utilisation (Lowry *et al.*, 1997), therefore once the stimulus was ceased, the supply exceeded the demand and an increase was observed, followed on by a subsequent decrease in the current. The current began to fall and returned to a baseline of -167.8 ± 5.5 nA ($P = 0.1010$) within 28.1 ± 4.3 minutes, $n = 29$.

	Restraint stress					
	Current change (nA)	Current change (%)	Max response Time (mins)	Return Time (mins)	Baseline Pre Injection (nA)	Baseline Post Injection (nA)
MMCPEs	26.8 ± 3.8	16.4 ± 2.2	2.5 ± 0.3	28.1 ± 4.3	-165.9 ± 5.8	-167.8 ± 5.5
	Restraint stress (2 nd current change)					
	(2 nd) Current change (nA)	(2 nd) Current change (%)	(2 nd) Max response Time (mins)	Return Time (mins)	Baseline Pre Injection (nA)	Baseline Post Injection (nA)
MMCPEs	33.0 ± 3.6	20.1 ± 2.2	6.1 ± 0.2	28.1 ± 4.3	-165.9 ± 5.8	-167.8 ± 5.5

Table 5.3.3.1.1: Summary of results for the first and second current change responses for a restraint stress (5-minutes), with the MMCPEs implanted in the striatum of freely moving rats ($n = 29$ with 13 sensors in 6 animals),

5.3.3.1.2 SMCPE

The effect of a typical 5-minute restraint stress monitored at a SMCPE in the striatum of a freely moving rat is depicted shown in Figure 5.3.3.1.2. The restraint stress data in this Section was analysed using 30 perturbations with 11 sensors in 5 animals.

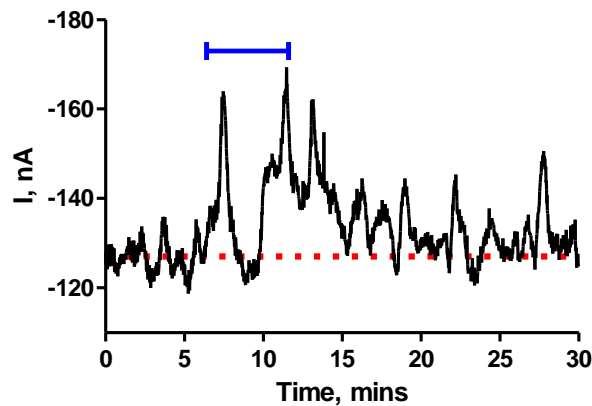


Figure 5.3.3.1.2: A typical example of the effects of a 5-minute restraint stress on the observed O_2 current recorded with an SMCPE in the striatum of a freely moving rat. The blue bar indicates the onset and duration of the restraint stress.

Figure 5.3.3.1.2, demonstrates how a 5-minute restraint test caused an immediate and significant increase ($P < 0.0001$) in the O_2 current from a baseline level of -137.0 ± 8.4 nA, $n = 30$, to a current of -159.0 ± 10.6 nA, $n = 30$, after 2.6 ± 0.3 minutes, $n = 30$. This corresponds to a maximum increase of 22.0 ± 2.8 nA, $n = 30$, representing a mean percentage change of 15.2 ± 1.3 %, $n = 30$. On release of the subject, the current began to fall and then a subsequent increase was observed similar to what was observed with the MMCPEs. A current change of 29.8 ± 4.7 nA, $n = 30$, after 6.4 ± 0.1 minutes, $n = 30$, was observed from a current of -137.0 ± 8.4 nA, $n = 30$, to a current of -166.9 ± 12.1 nA, $n = 30$. This yielded a percentage current change of 20.3 ± 2.5 % which was significantly different ($P < 0.0028$). The current began to fall and then returned to a baseline current of -143.8 ± 8.9 nA, $n = 30$ ($P < 0.0001$) which indicated that the baseline signal had altered due to the stress imposed on the subject. The new baseline was achieved after 8.9 ± 0.7 minutes, $n = 30$. The increase in the O_2 current after the subject had been released was demonstrated previously with the MMCPEs and this phenomenon occurs when the supply of O_2 surpasses

the utilisation yielding an increase until the supply and utilisation balances out which is observed in the fall of the O₂ current back to baseline levels.

Restraint stress						
	Current change (nA)	Current change (%)	Max response Time (mins)	Return Time (mins)	Baseline Pre Injection (nA)	Baseline Post Injection (nA)
SMCPEs	22.0 ± 2.8	15.2 ± 1.3	2.6 ± 0.3	8.9 ± 0.7	-137.0 ± 8.4	-143.8 ± 8.9
Restraint stress (2 nd current change)						
	(2 nd) Current change (nA)	(2 nd) Current change (%)	(2 nd) Max response Time (mins)	Return Time (mins)	Baseline Pre Injection (nA)	Baseline Post Injection (nA)
SMCPEs	29.8 ± 4.7	20.3 ± 2.5	6.4 ± 0.1	8.9 ± 0.7	-137.0 ± 8.4	-143.8 ± 8.9

Table 5.3.3.1.2: Summary of results for the first and second current change responses for a restraint stress (5-minutes), with the SMCPEs implanted in the striatum of freely moving rats ($n = 30$ with 11 sensors in 5 animals).

5.3.3.1.3 Comparison

A similar percentage increase of 16.4 ± 2.2 %, $n = 29$, 6 animals and 15.2 ± 1.3 %, $n = 30$, 5 animals, is observed at the MMCPEs and SMCPEs, respectively. Although there is a similar increase in the O₂ current for the SMCPEs the return to baseline levels are much faster than achieved with the MMCPEs. It took 28.1 ± 4.3 minutes, $n = 29$ and 8.9 ± 0.7 minutes, $n = 30$ for the MMCPEs and SMCPEs, respectively, to achieve normoxic levels. Kealy *et al.*, carried out a restraint stress on rats ($n = 13$, 5 animals) using CPEs. They achieved *ca.* 9 % increase in the O₂ current. Even though this was significantly different from the baseline levels ($P < 0.05$) (Kealy *et al.*, 2013), it can be observed that the monomer modified CPEs discussed and analysed in this section can achieve a much greater sensitivity.

5.3.3.2 Tail Pinch

5.3.3.2.1 MMCPE

The effect of a 5-minute tail pinch stress recorded with an MMCPE in the striatum of a freely moving rat is shown in Figure 5.3.3.2.1. The tail pinch data in this Section was analysed using 23 perturbations with 12 sensors in 6 animals.

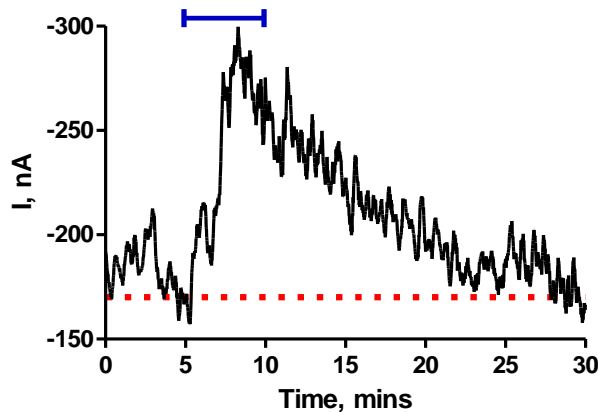


Figure 5.3.3.2.1: A typical example of the effects of a 5-minute tail pinch on the observed O₂ current recorded with an MMCPE in the striatum of a freely moving rat. The blue bar indicates the onset and duration of the tail pinch.

The application of a 5-minute tail pinch resulted in an instantaneous and rapid increase in the O₂ current observed at the MMCPEs. An immediate and significant increase ($P < 0.0001$) in the O₂ current from a baseline level of -166.9 ± 5.8 nA, $n = 23$, to a current of -198.3 ± 9.0 nA, $n = 23$, after 2.8 ± 0.3 minutes, $n = 23$. This yielded a maximum increase of 31.4 ± 6.6 nA, $n = 23$, representing a mean percentage change of 19.1 ± 4.0 %, $n = 23$. Upon removal of the stimulus, the current began to fall and returned to a new baseline of -175.0 ± 6.5 nA, $n = 23$, ($P < 0.0001$) after 28.3 ± 5.1 minutes, $n = 23$.

Tail pinch						
	Current change (nA)	Current change (%)	Max response Time (mins)	Return Time (mins)	Baseline Pre Injection (nA)	Baseline Post Injection (nA)
MMCPEs	31.4 ± 6.6	19.1 ± 4.0	2.8 ± 0.3	28.3 ± 5.1	-166.9 ± 5.8	-175.0 ± 6.5

Table 5.3.3.2.1: Summary of results for the tail pinch (5-minutes), with the MMCPEs implanted in the striatum of freely moving rats ($n = 23$ with 12 sensors in 6 animals).

5.3.3.2.2 SMCPE

The effect of a 5-minute tail pinch stress recorded with an SMCPE in the striatum of a freely moving rat is shown in Figure 5.3.3.2.2. The tail pinch data in this section was analysed using 27 perturbations with 11 sensors in 5 animals.

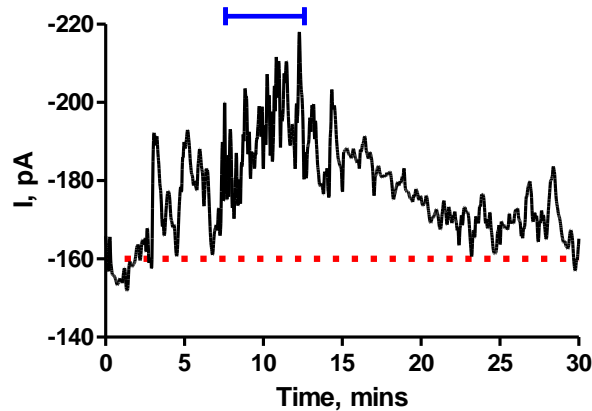


Figure 5.3.3.2.2: A typical example of the effects of a 5-minute tail pinch stress on the observed O_2 current recorded with an SMCPE in the striatum of a freely moving rat. The blue bar indicates the onset and duration of the tail pinch.

The mean percentage increase observed in response to the tail pinch was $18.7 \pm 1.8 \%$, $n = 27$. The increase in the O_2 current recorded at the SMCPEs was 30.8 ± 3.1 nA, $n = 27$, after 2.8 ± 0.2 minutes, $n = 27$, from a baseline of -162.0 ± 8.3 nA, $n = 27$, to a current of -192.7 ± 10.5 nA, $n = 27$ ($P < 0.0001$). On removal of the stimulus, the current returned to a baseline of -163.9 ± 7.8 nA, $n = 27$ ($P = 0.2024$) after 27.1 ± 3.2 minutes, $n = 27$.

Tail pinch						
	Current change (nA)	Current change (%)	Max response Time (mins)	Return Time (mins)	Baseline Pre Injection (nA)	Baseline Post Injection (nA)
SMCPEs	30.8 ± 3.1	18.7 ± 1.8	2.8 ± 0.2	27.1 ± 3.2	-162.0 ± 8.3	-163.9 ± 7.8

Table 5.3.3.2.2: Summary of results for the tail pinch (5 minutes), with the SMCPEs implanted in the striatum of freely moving rats ($n = 27$ with 11 sensors in 5 animals).

5.3.3.2.3 Comparison

Analysis of the two O₂ sensors upon application of a tail pinch yielded similar findings. The percentage increase in the O₂ current obtained for the MMCPEs and SMCPEs yielded results of $19.1 \pm 4.0 \%$, $n = 23$, 6 animals and $18.7 \pm 1.8 \%$, $n = 27$, 5 animals respectively. The time taken for the baseline to return to normoxic conditions was analogous for the two sensors 28.3 ± 5.1 minutes, $n = 23$, (MMCPEs) and 27.1 ± 3.2 minutes, $n = 27$ (SMCPEs). The results demonstrate how both sensors have the capability to detect changes in the O₂ concentration effectively. Bolger *et al.*, demonstrated an increase in the O₂ current with the application of a tail pinch in freely moving rats, $n = 8$, 2 animals. An increase of 10.8 ± 1.9 nA, $n = 8$, was achieved with the CPEs, however a much greater increase was achieved with the sensors discussed in this section. There was a significant difference between the O₂ increases, which demonstrates how the monomer modified sensors display a higher sensitivity, (MMCPEs vs. CPEs: $P = 0.0416$) and (SMCPEs vs. CPEs: $P = 0.0017$).

5.3.4 Saline Administration

The effect of an intraperitoneal (i.p.) injection of saline on the striatal O₂ current was examined as this was the route of administration for investigating the effect of drugs on the O₂ response. Using saline would demonstrate the effect of the injection stress on the subject so it would be clear for future i.p. injections what effect the drugs are having on the O₂ response. The effect of an injection of saline (NaCl, 0.9 %, i.p.) on the O₂ current was recorded with the MMCPEs and SMCPEs.

5.3.4.1 MMCPE

The effect of a typical i.p. injection of saline monitored by an MMCPE in the striatum of a freely moving rat is displayed in Figure 5.3.4.1. The saline injection data in this Section was analysed using the results from 8 perturbations with 8 sensors in 5 animals.

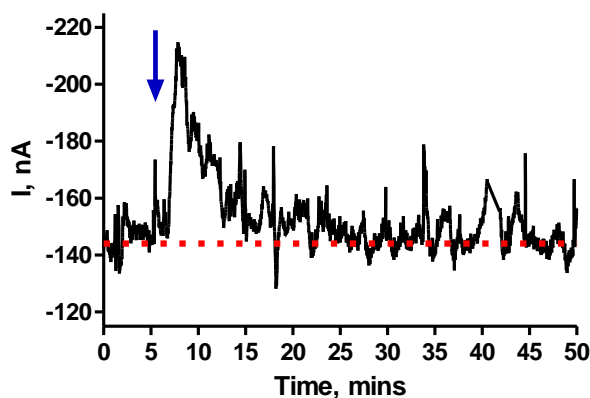


Figure 5.3.4.1: A typical raw data trace displaying the effect of an i.p. injection of saline (1.0 ml, 0.9 % NaCl) on the O₂ response, recorded with an MMCPE, in the striatum of a freely moving rat. The arrow is indicative of the injection point.

Analysis of the data shows an increase in the observed O₂ current upon injection of saline. The current increased significantly ($P = 0.0009$), by 27.2 ± 6.0 nA, $n = 8$, after 1.5 ± 0.2 minutes, $n = 8$, from a mean baseline of -153.3 ± 10.5 nA, $n = 8$ to a current of $-180.5 \pm$

10.9 nA, $n = 8$, yielding a percentage increase of $19.6 \pm 5.8 \%$, $n = 8$. The O_2 signal returned to baseline levels of -159.0 ± 10.2 , $n = 8$, ($P = 0.0026$), in 5.8 ± 1.0 minutes, $n = 8$.

Saline Injection						
	Current change (nA)	Current change (%)	Max response Time (mins)	Return Time (mins)	Baseline Pre Injection (nA)	Baseline Post Injection (nA)
MMCPEs	27.2 ± 6.0	19.6 ± 5.8	1.5 ± 0.2	5.8 ± 1.0	-153.3 ± 10.5	-159.0 ± 10.2

Table 5.3.4.1: Summary of results for a saline injection, with the MMCPEs implanted in the striatum of freely moving rats ($n = 8$ with 8 sensors in 5 animals).

5.3.4.2 SMCPE

The effect of a typical i.p. injection of saline monitored by an SMCPE in the striatum of a freely moving rat is shown in Figure 5.3.4.2. The saline injection data in this Section was analysed using the results from 11 perturbations with 8 sensors in 5 animals.

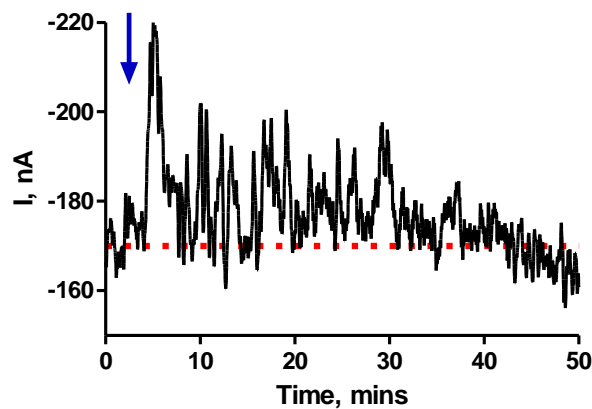


Figure 5.3.4.2: A typical raw data trace displaying the effect of an i.p injection of saline (1.0 ml, 0.9 % NaCl) on the O_2 response, monitored with an SMCPE in the striatum of a freely moving rat. The arrow indicates the point of injection.

There was an immediate and significant increase in O₂ ($P < 0.0001$) following the injection of saline from a baseline of -153.2 ± 12.2 nA, $n = 11$, to -186.2 ± 13.9 nA, $n = 11$. This yielded a current change of 33.0 ± 3.6 nA, $n = 11$, after 1.2 ± 0.2 minutes, $n = 11$, which corresponds to a percentage change of 22.4 ± 3.4 %, $n = 11$. The O₂ signal returned to a baseline of -159.1 ± 12.6 nA ($P = 0.0017$), $n = 11$, after 9.1 ± 2.0 minutes, $n = 11$.

	Saline Injection					
	Current change (nA)	Current change (%)	Max response Time (mins)	Return Time (mins)	Baseline Pre Injection (nA)	Baseline Post Injection (nA)
SMCPes	33.0 ± 3.6	22.4 ± 3.4	1.2 ± 0.2	9.1 ± 2.0	-153.2 ± 12.2	-159.1 ± 12.6

Table 5.3.4.2: Summary of results for a saline injection, with the SMCPes implanted in the striatum of freely moving rats ($n = 11$ with 8 sensors in 5 animals).

5.3.4.3 Comparison

The administration of a saline injection to the subject caused a clear stress response observed in both sensors. A percentage increase in the O₂ current of 19.6 ± 5.8 %, $n = 8$ and 22.4 ± 3.4 %, $n = 11$, for the MMCPEs and SMCPes, respectively, was obtained. The baseline current returned to new baseline currents after 5.8 ± 1.0 minutes, $n = 8$, (MMCPEs) and 9.1 ± 2.0 minutes, $n = 11$ (SMCPes), respectively. This illustrates a transient effect following the control injection. Saline injections obtained with CPEs display a similar transient response; however, a much lower response was achieved at the CPEs in comparison to the MMCPEs and SMCPes.

Bolger *et al.*, demonstrated an increase in the O₂ current of 13.5 ± 3.7 nA, $n = 4$, whereas the MMCPEs and SMCPes achieve an increase in the O₂ current of 27.2 ± 6.0 nA, $n = 8$, and 33.0 ± 3.6 nA, $n = 11$, respectively (Bolger & Lowry, 2005). Although the responses achieved at the modified sensors were greater than the CPEs, they were not significantly different (MMCPEs *vs.* CPEs: $P = 0.1607$) and (SMCPes *vs.* CPEs: $P = 0.2090$).

5.3.5 Effect of Anaesthesia

Chloral hydrate is presented as colourless translucent crystals. It depresses the cerebrum, with loss of reflex excitability. It can be provided in an oral administration dissolved in water or injected through the use of an i.p. or intravenous injection. It can cause irritation to the mucosa in the stomach which would induce vomiting so dilution in water is necessary. It has been utilised with magnesium sulphate or magnesium sulphate and sodium pentobarbital for anaesthesia in horses and cattle which is stated to induce a quicker anaesthesia state, with a smoother emergence and a greater safety margin (Tranquilli *et al.*, 2013). It has also been used previously as a method of increasing striatal O₂ levels (Lowry & Fillenz, 2001; Bolger & Lowry, 2005).

Chloral hydrate is a non-volatile anaesthetic agent commonly utilised for animal surgery. It quickly metabolises into trichloroethanol and trichloroacetic acid creating general central nervous system (CNS) depression (Kawamoto *et al.*, 1987). Trichloroethanol is alleged to be the active ingredient that induces anaesthesia (Tao & Auerbach, 1994). Figure 5.3.5.1, displays the effect of a typical administration of chloral hydrate (350 mg/kg i.p.) on the O₂ signal recorded with an MMCPE.

5.3.5.1 MMCPE

The effect of a typical i.p. injection of saline monitored by an MMCPE in the striatum of a freely moving rat is displayed in Figure 5.3.5.1. The chloral hydrate injection data in this Section was analysed using the results from 12 perturbations with 12 sensors in 7 animals.

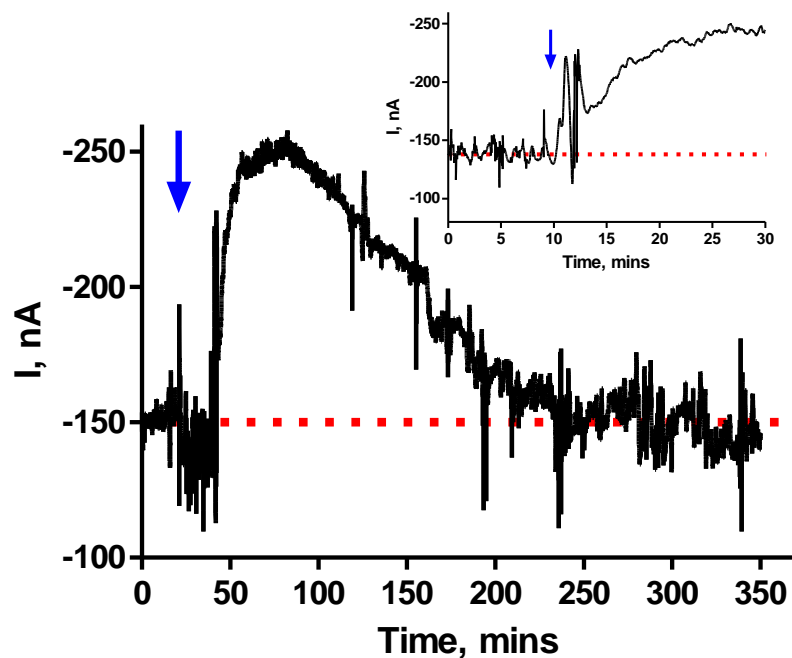


Figure 5.3.5.1: A typical example of the effect of an injection of chloral hydrate (350 mg/kg, i.p.) on the O₂ signal, monitored with an MMCPE in the striatum of a freely moving rat. *Inset:* Close-up of the signal recorded as a result of the chloral hydrate injection. The arrow is indicative of the point of injection.

The i.p. injection of chloral hydrate demonstrated the same initial response as the i.p. saline injection; a brief increase in the O₂ current (see *inset*, 5.3.5.1). However, this was followed by a much larger more long-lasting increase, which accompanied the behavioural changes associated with anaesthesia. Analysis of the data showed that the current increased significantly ($P < 0.0001$) from a baseline current of -158.1 ± 8.3 nA, $n = 12$, to a current of -264.0 ± 20.3 nA, $n = 12$, after 23.8 ± 4.4 minutes, $n = 12$, which equates to an increase of 105.9 ± 16.4 nA, $n = 12$, representing a mean percentage change of 87.8 ± 6.4 %, $n = 12$. The current then decreased to a corresponding baseline level of -162.4 ± 8.2 nA, $n = 12$, ($P = 0.0759$) after 185.8 ± 15.2 minutes and the animals began to show recovery from the anaesthesia.

Chloral Hydrate Injection						
	Current change (nA)	Current change (%)	Max response Time (mins)	Return Time (mins)	Baseline Pre Injection (nA)	Baseline Post Injection (nA)
MMCPEs	105.9 ± 16.4	87.8 ± 6.4	23.8 ± 4.4	185.8 ± 15.2	-158.1 ± 8.3	-162.4 ± 8.2

Table 5.3.5.1: Summary of results for a chloral hydrate injection, with the MMCPEs implanted in the striatum of freely moving rats ($n = 12$ with 12 sensors in 7 animals).

5.3.5.2 SMCPE

The effect of a typical administration of chloral hydrate (350 mg/kg i.p.) on the O_2 signal, monitored with an SMCPE is presented in Figure 5.3.5.2. The chloral hydrate injection data in this Section was analysed using the results from 12 perturbations with 12 sensors in 5 animals.

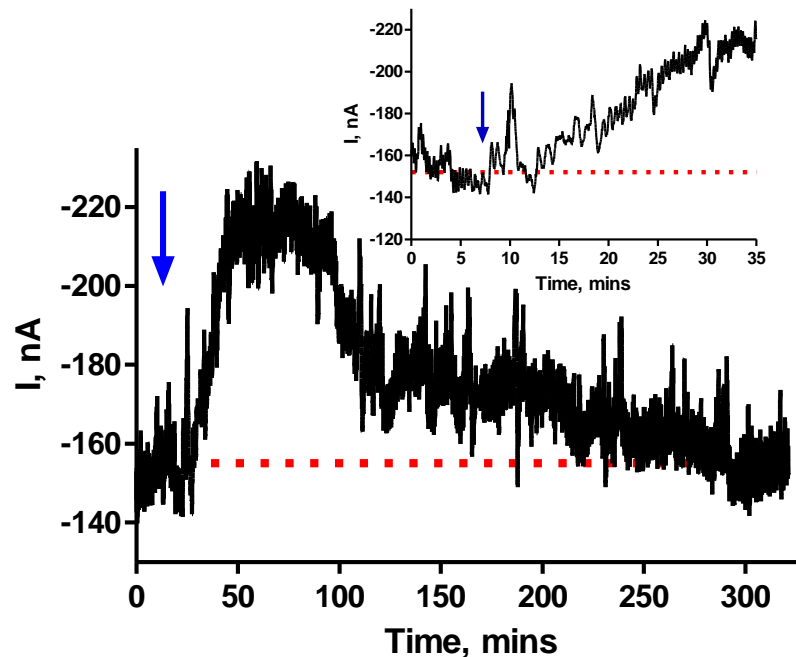


Figure 5.3.5.2: A raw data trace displaying a typical injection of chloral hydrate (350 mg/kg, i.p.) on the O_2 signal, recorded with an SMCPE in the striatum of a freely moving rat. *Inset*: Close-up of the signal recorded as a result of the chloral hydrate injection. The blue arrow indicates the point of injection.

The initial response shown in the *inset* of Figure 5.3.5.2, displays a similar response to that attained with the saline i.p. injection which is similar to the result obtained for the MMCPE. A brief increase in the O₂ current is observed, which has been shown to be due to the injection stress, followed by slower more long-lasting changes, which accompanied the behavioural changes associated with anaesthesia. Upon injection of chloral hydrate, there was a significant increase in the O₂ response ($P < 0.0001$). A current change of 92.7 ± 13.4 nA, $n = 12$, was achieved after 27.8 ± 5.3 minutes, $n = 12$, from a baseline of -158.6 ± 10.8 nA, $n = 12$, to a current of -251.3 ± 21.9 nA, $n = 12$, representing a mean percentage change of 100.4 ± 1.6 %, $n = 12$. The current returned to a baseline level of -159.2 ± 11.3 nA, $n = 12$, ($P = 0.8239$) after 215.0 ± 12.1 minutes, $n = 12$, had elapsed since the injection.

Chloral Hydrate Injection						
	Current change (nA)	Current change (%)	Max response Time (mins)	Return Time (mins)	Baseline Pre Injection (nA)	Baseline Post Injection (nA)
SMCPes	92.7 ± 13.4	100.4 ± 1.6	27.8 ± 5.3	215.0 ± 12.1	-158.6 ± 10.8	-159.2 ± 11.3

Table 5.3.5.2: Summary of results for a chloral hydrate injection, with the SMCPEs implanted in the striatum of freely moving rats ($n = 12$ with 12 sensors in 5 animals).

5.3.5.3 Comparison

Direct comparison of the responses for both sensor types (MMCPEs) and (SMCPes) reveals that for chloral hydrate administration, similar data traces are obtained. The percentage O₂ change observed for MMCPEs and SMCPEs yielded a response of 87.8 ± 6.4 %, $n = 12$ and 100.4 ± 1.6 %, $n = 12$, respectively, which depicts how the two sensors are equally capable of detecting O₂ changes but also demonstrates how chloral hydrate increases the O₂ current. A similar response was observed with CPEs as demonstrated by Bolger *et al.*, (Bolger & Lowry, 2005). They attained an O₂ current increase of 18.7 ± 3.1 nA, $n = 10$. This was a much smaller change achieved with the CPEs in comparison to the responses obtained by the MMCPEs and SMCPEs. A significant difference was therefore

recorded for the different sensors (MMCPEs vs. CPEs: $P = 0.0001$) and (SMCPEs vs. CPEs: $P < 0.0001$).

5.3.6 Acetazolamide (Diamox) Administration

Acetazolamide (Diamox) is a carbonic anhydrase inhibitor that on systematic administration has been shown to increase brain tissue O_2 (Dixon *et al.*, 2002; Bolger & Lowry, 2005). Acetazolamide is used as an exploratory tool in cerebral blood flow experiments and also for the treatment of several diseases long term (Vorstrup *et al.*, 1984). Measuring the cerebral blood flow response to diamox is a common test used to calculate the vasodilatory capacity of the cerebral circulation and is called the ACZ test (Okazawa *et al.*, 2001). The use of DMSO as a vehicle for diamox administration was utilised also. DMSO has been implemented as a vehicle for diamox in the literature (Zhou & Kost, 2006; Shinohara *et al.*, 2007; Mokhtari *et al.*, 2013).

DMSO is utilised as a solvent in many *in-vitro* and *in-vivo* studies and can cause many pharmacological effects (Yoon *et al.*, 2006). It has been demonstrated recently that the use of DMSO can cause an effect on the O_2 current (Kealy *et al.*, 2013), therefore the implementation of it as a vehicle and control with diamox, would cause inaccuracies in the results. Control studies were carried out using diamox in saline and DMSO in saline in order to determine if DMSO contributes to the current change. The effect of an administration of acetazolamide on the O_2 current was monitored with MMCPEs and SMCPEs.

5.3.6.1 MMCPEs

The effect of a typical i.p. injection of diamox/DMSO, diamox/saline and DMSO/saline monitored by an MMCPE in the striatum of a freely moving rat is displayed in Figure (5.3.6.1.1), (5.3.6.1.2) and (5.3.6.1.3), respectively.

5.3.6.1.1 Diamox (DMSO) Administration

The diamox/DMSO injection data in this Section was analysed using the results from 5 perturbations with 5 sensors in 2 animals.

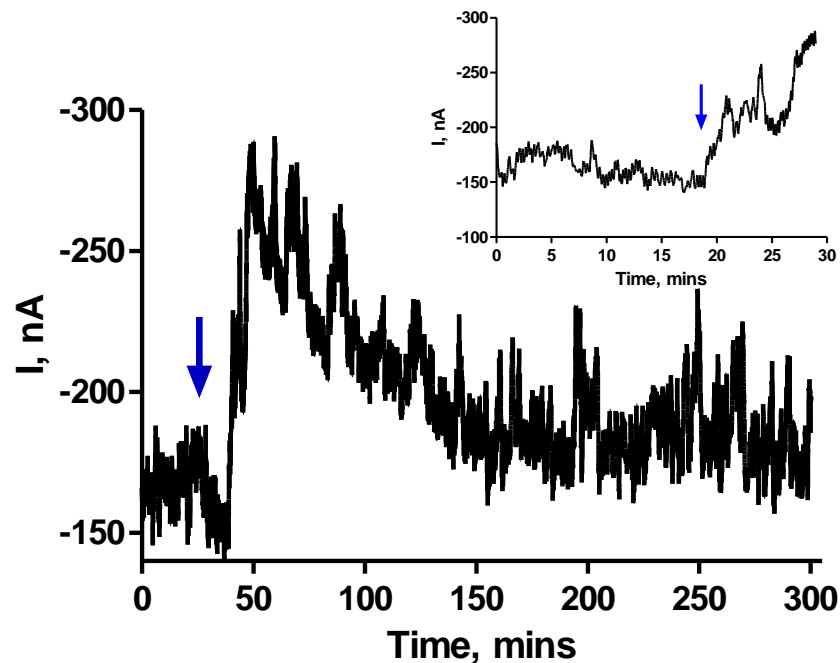


Figure 5.3.6.1.1: A typical example of the effect of an administration of diamox (50 mg/kg) in DMSO (0.5 mL) and saline (1.0 mL) on the O_2 response, recorded with an MMCPE in the striatum of a freely-moving animal. The arrow is indicative of the point of injection. *Inset*: Close-up of the signal recorded as a result of the diamox (DMSO) injection. The arrow is indicative of the point of injection.

Upon administration of diamox, initially an injection stress response is observed as was observed with the saline and chloral hydrate injections (see Figure 5.3.6.1 *inset*). Following this response, there is an increase in the O₂ current from a baseline of -163.1 ± 2.8 nA, $n = 5$ to a current of -263.0 ± 7.1 nA, $n = 5$, ($P = 0.0010$). This yielded an increase of 99.9 ± 5.6 nA, $n = 5$, after 12.0 ± 1.2 minutes, $n = 5$, representing a mean percentage increase of 61.3 ± 3.2 %, $n = 5$. A new baseline current of -176.1 ± 4.0 nA, which was significantly different ($P = 0.0010$) from pre baseline currents was achieved after 120.0 ± 1.0 minutes, $n = 5$. Previous work carried out in the lab using DMSO as a vehicle suggests an independent effect on O₂ and glucose levels recorded using electrochemical sensors (Kealy *et al.*, 2013). In order to determine if the effects observed were from the diamox alone, a solution of diamox and saline was administered.

Diamox (DMSO) Injection						
	Current change (nA)	Current change (%)	Max response Time (mins)	Return Time (mins)	Baseline Pre Injection (nA)	Baseline Post Injection (nA)
MMCPEs	99.9 ± 5.6	61.3 ± 3.2	12.0 ± 1.2	120.0 ± 1.0	-163.1 ± 2.8	-176.1 ± 4.0

Table 5.3.6.1.1: Summary of results for a diamox (DMSO) injection, with the MMCPEs implanted in the striatum of freely moving rats ($n = 5$ with 5 sensors in 2 animals).

5.3.6.1.2 Diamox (Saline) Administration

The diamox/saline injection data in this Section was analysed using the results from 3 perturbations with 3 sensors in 3 animals.

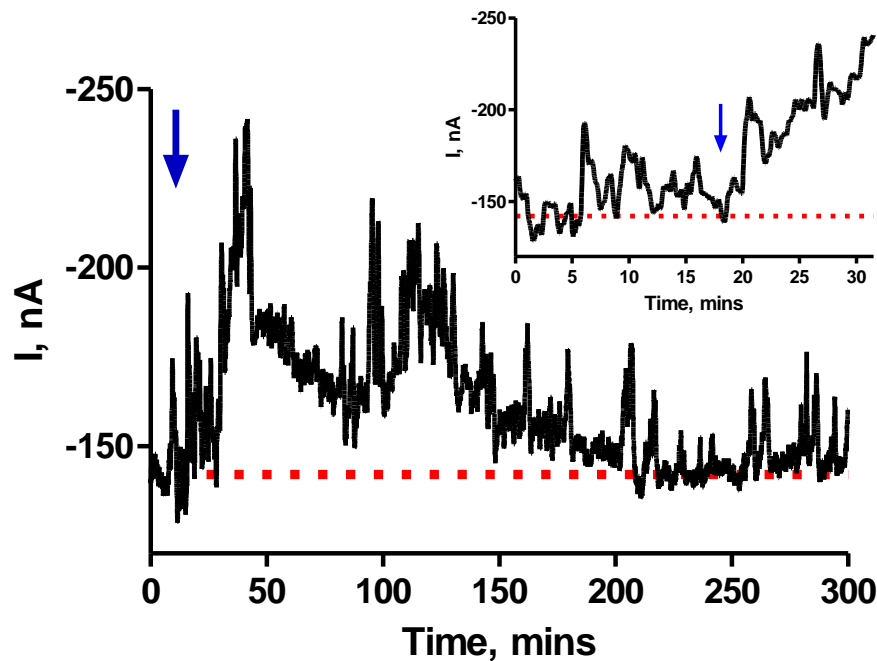


Figure 5.3.6.1.2: A typical example of the effect of an administration of diamox (50 mg/kg) in saline (1.0 mL) on the O_2 response, recorded with an MMCPE in the striatum of a freely-moving rat. The arrow is indicative of the point of injection. *Inset*: Close-up of the signal recorded as a result of the diamox (saline) injection. The arrow is indicative of the point of injection.

Figure 5.3.6.1.2, demonstrates how an injection of diamox in saline caused an increase in the O_2 current that was not significant ($P = 0.0761$), from a baseline level of -135.0 ± 18.7 nA, $n = 3$ to a current of -173.6 ± 26.8 nA, $n = 3$, after 117.5 ± 91.3 , $n = 3$. This yielded a maximum O_2 current increase of 38.6 ± 11.3 nA, $n = 3$, representing a mean percentage change of 28.1 ± 6.9 %, $n = 3$. The current returned to baseline currents of -138.4 ± 18.1 nA, $n = 3$ ($P = 0.2230$) indicating a return to normoxic conditions after 450.0 ± 229.1

minutes, $n = 3$. Subsequent to these results, a solution of DMSO and saline was administered in order to determine the effects that DMSO has on the O_2 response.

Diamox (Saline) Injection						
	Current change (nA)	Current change (%)	Max response Time (mins)	Return Time (mins)	Baseline Pre Injection (nA)	Baseline Post Injection (nA)
MMCPEs	38.6 ± 11.3	28.1 ± 6.9	117.5 ± 91.2	450.0 ± 229.1	-135.0 ± 18.7	-138.4 ± 18.1

Table 5.3.6.1.2: Summary of results for a diamox (DMSO) injection, with the MMCPEs implanted in the striatum of freely moving rats ($n = 3$ with 3 sensors in 3 animals).

5.3.6.1.3 DMSO (Saline) Administration

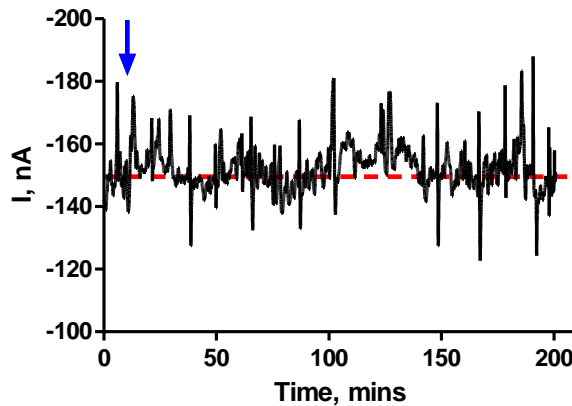


Figure 5.3.6.1.3: A typical example of the effect of an administration of DMSO in saline on the O_2 response, recorded with an MMCPE in the striatum of a freely-moving rat. The arrow is indicative of the point of injection.

The injection of a DMSO and saline mixture resulted in a slight increase in the O_2 current recorded at the MMCPEs by 5.8 ± 3.5 nA, $n = 3$, from a mean baseline of -154.8 ± 6.8 nA, $n = 3$, to a current of -160.6 ± 4.2 nA, $n = 3$ after 57.0 ± 1.0 seconds, $n = 3$. The mean percentage increase in response to the DMSO/saline injection was 3.9 ± 2.4 %, $n = 3$. The resulting O_2 increase was not significant ($P = 0.2461$). The current immediately began to fall and returned to a baseline of -156.0 ± 5.8 nA ($P = 0.4703$) within 7.0 ± 0.5 minutes, $n =$

3. This result demonstrates how an injection of DMSO/saline does not seem to have an effect on the O₂ current, an initial injection stress is observed on application of the injection which corresponds to the results obtained for the injection of saline in Figure 5.3.4.1. This validates the use of diamox/DMSO injections to increase striatal O₂ levels since a significant increase was observed compared to diamox/saline. The reason for the insignificant increase from baseline can be attributed to the insolubility of diamox in saline alone. The SMCPEs were studied using the same experiments outlined previously for the MMCPEs.

	DMSO (Saline) Injection					
	Current change (nA)	Current change (%)	Max response Time (secs)	Return Time (mins)	Baseline Pre Injection (nA)	Baseline Post Injection (nA)
MMCPEs	5.8 ± 3.5	3.9 ± 2.4	57.0 ± 1.0	7.0 ± 0.5	-154.8 ± 6.8	-156.0 ± 5.8

Table 5.3.6.1.3: Summary of results for a DMSO (saline) injection, with the MMCPEs implanted in the striatum of freely moving rats ($n = 3$ with 3 sensors in 1 animals).

5.3.6.2 SMCPEs

The effect of a typical i.p. injection of diamox/DMSO, diamox/saline and DMSO/saline monitored by an SMCPE in the striatum of a freely moving rat is displayed in Figure (5.3.6.2.1), (5.3.6.2.2) and (5.3.6.2.3), respectively.

5.3.6.2.1 Diamox (DMSO) Administration

The diamox (DMSO) injection data in this Section was analysed using the results from 7 perturbations with 7 sensors in 2 animals.

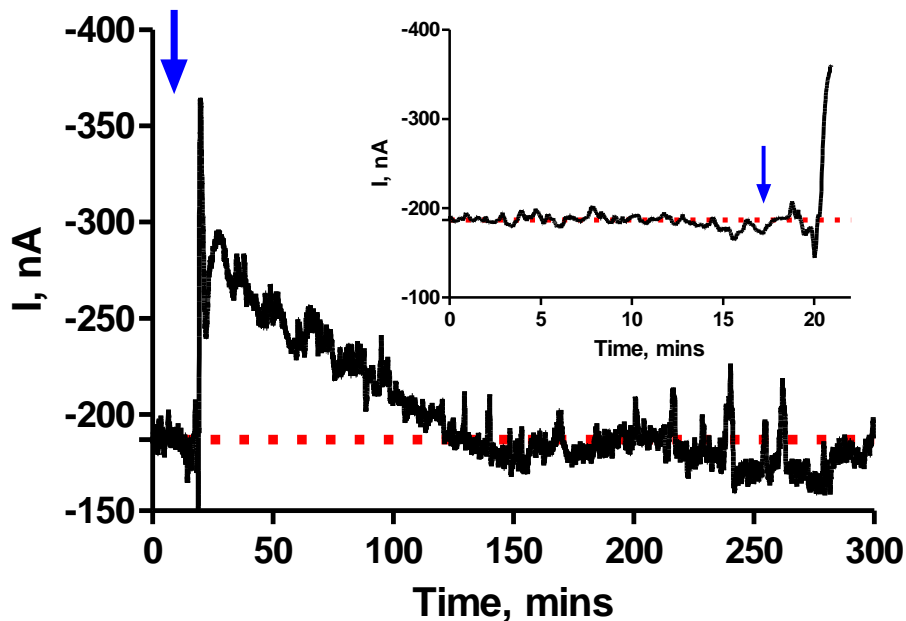


Figure 5.3.6.2.1: A typical example of the effect of an administration of diamox (50 mg/kg) in DMSO on the O_2 response, recorded with an SMCPE in the striatum of a freely-moving rat. The arrow is indicative of the point of injection. *Inset*: Close-up of the signal recorded as a result of the diamox (DMSO) injection. The arrow is indicative of the point of injection.

Upon administration of diamox, there is a significant increase ($P = 0.0003$) in the O_2 current from a baseline of -170.1 ± 16.5 nA, $n = 7$ to a current of -303.2 ± 33.3 nA, $n = 7$. This yielded an increase of 133.0 ± 17.3 nA, $n = 7$, after 7.5 ± 2.1 minutes, $n = 7$, representing a mean percentage increase of 77.2 ± 4.6 %, $n = 7$. A corresponding baseline current returned after 135.7 ± 16.2 minutes, $n = 7$, yielding a current of -175.6 ± 4.6 nA, $n = 7$, ($P = 0.0791$). Similar to the MMCPEs a solution of diamox and saline was administered in order to determine the response of diamox without DMSO at the SMCPEs and if it compares to the result attained from the MMCPEs.

Diamox (DMSO) Injection						
	Current change (nA)	Current change (%)	Max response Time (mins)	Return Time (mins)	Baseline Pre Injection (nA)	Baseline Post Injection (nA)
SMCPEs	133.0 ± 17.3	77.2 ± 4.6	7.5 ± 2.1	135.7 ± 16.2	-170.1 ± 16.5	-175.6 ± 4.6

Table 5.3.6.2.1: Summary of results for a diamox (DMSO) injection, with the SMCPEs implanted in the striatum of freely moving rats ($n = 7$ with 7 sensors in 2 animals).

5.3.6.2.2 Diamox (Saline) Administration

The diamox (saline) injection data in this section was analysed using the results from 2 perturbations with 2 sensors in 2 animals.

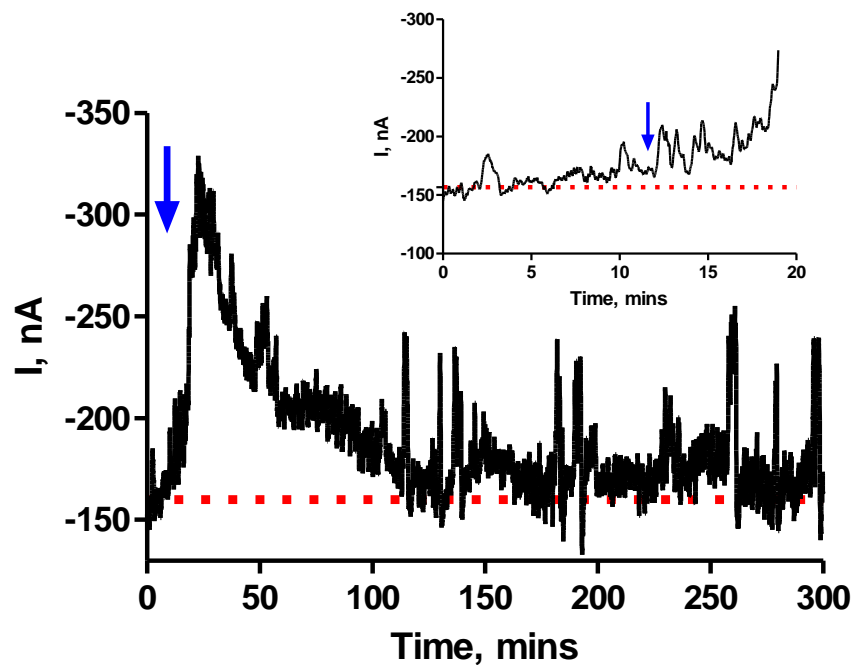


Figure 5.3.6.2.2: A typical example of the effect of an administration of Diamox (50 mg/kg) in saline (1.0 mL) on the O_2 response, recorded with an MMCPE in the striatum of a freely-moving rat. The arrow is indicative of the point of injection. *Inset*: Close-up of the signal recorded as a result of the diamox (saline) injection. The arrow is indicative of the point of injection.

Figure 5.3.6.2.2, demonstrates how an injection of diamox in saline caused an increase in the O_2 current, from a baseline level of -176.7 ± 20.1 nA, $n = 2$, to a current of -286.3 ± 14.7 nA, $n = 2$ which yielded a maximum O_2 current increase of 109.6 ± 34.7 nA, $n = 2$, after 22.0 ± 10.5 minutes, $n = 2$ and representing a mean percentage change of 65.1 ± 27.0 %, $n = 2$. The current returned to a new baseline level of -199.0 ± 24.8 nA, $n = 2$, indicating a return to normoxic conditions after 102.5 ± 2.5 minutes, $n = 2$. Subsequent to these

results, a solution of DMSO and saline was administered in order to determine the effects that DMSO has on the O₂ response.

Diamox (Saline) Injection						
	Current change (nA)	Current change (%)	Max response Time (mins)	Return Time (mins)	Baseline Pre Injection (nA)	Baseline Post Injection (nA)
SMCPEs	109.6 ± 34.7	65.1 ± 27.0	22.5 ± 10.5	102.5 ± 2.5	-176.7 ± 20.1	-199.0 ± 24.8

Table 5.3.6.2.2: Summary of results for a diamox (DMSO) injection, with the SMCPEs implanted in the striatum of freely moving rats ($n = 2$ with 2 sensors in 2 animals).

5.3.6.2.3 DMSO (Saline) Administration

The diamox/saline injection data in this section was analysed using the results from 3 perturbations with 3 sensors in 1 animal.

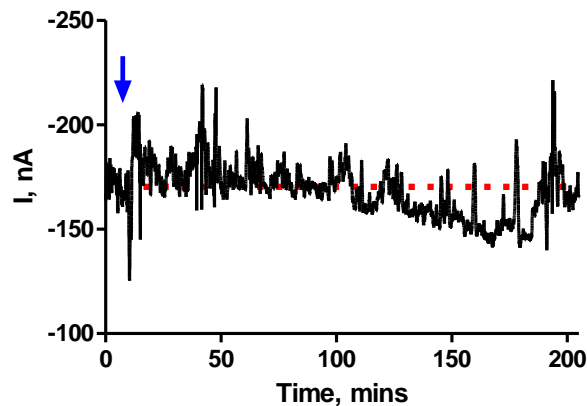


Figure 5.3.6.2.3: A typical example of the effect of an administration of DMSO in saline on the O₂ response, recorded with an SMCPE in the striatum of a freely-moving rat. The arrow is indicative of the point of injection.

Figure 5.3.6.2.3, demonstrates how an injection of DMSO in saline caused a slight increase in the O₂ current that was significant ($P = 0.0263$), from a baseline level of -153.6 ± 19.6

nA, $n = 3$ to a current of -174.5 ± 23.0 nA, $n = 3$. This yielded a maximum O₂ current increase of 20.8 ± 3.5 nA, $n = 3$, after 3.0 ± 0.5 minutes, $n = 3$, representing a mean percentage change of 13.4 ± 0.7 %, $n = 3$. The current immediately returned to baseline currents of -155.5 ± 19.8 nA, $n = 3$ ($P = 0.2504$) indicating a return to normoxic conditions after 7.0 ± 0.5 minutes, $n = 3$. The SMCPEs response attained for a DMSO and saline injection yielded a result similar to what was observed with the MMCPEs in Figure 5.3.6.1.3. It suggests that DMSO does not interfere with the increasing O₂ current obtained when using it as a vehicle for diamox administration.

DMSO (Saline) Injection						
	Current change (nA)	Current change (%)	Max response Time (mins)	Return Time (mins)	Baseline Pre Injection (nA)	Baseline Post Injection (nA)
SMCPEs	20.8 ± 3.5	13.4 ± 0.7	3.0 ± 0.5	7.0 ± 0.5	-153.6 ± 19.6	-155.5 ± 19.8

Table 5.3.6.2.3: Summary of results for a DMSO (saline) injection, with the SMCPEs implanted in the striatum of a freely moving rat ($n = 3$ with 3 sensors in 1 animal).

5.3.6.2.4 Comparison

Similar results were obtained for the two sensors (MMCPEs and SMCPEs) for the diamox and control administrations in this section. Administration of diamox in DMSO for both sensors yielded an increase in the O₂ response. Comparable percentage increases of 61.3 ± 3.2 %, $n = 5$ and 77.2 ± 4.6 %, $n = 7$, were obtained for the MMCPEs and SMCPEs respectively. On administration of the control injection of diamox and saline, a percentage increase of 28.1 ± 6.9 %, $n = 3$, was obtained for the MMCPEs and 65.1 ± 27.0 %, $n = 2$, for the SMCPEs. The result for the SMCPEs was quite similar to the administration of diamox and DMSO, however, an explanation for the MMCPEs result could have been due to the difficulty of getting diamox to dissolve into a solution of saline causing a smaller amount of diamox being injected into the subject, therefore leading to a lower increase in O₂.

Comparable results were recorded for the administration of DMSO in saline for both the MMCPEs and SMCPEs. A percentage increase of 3.9 ± 2.4 %, $n = 3$, and 13.4 ± 0.7 %, $n =$

3, were obtained for the MMCPEs and SMCPEs, respectively. A return to baseline was observed after 7.0 ± 0.5 minutes, $n = 3$ for the MMCPEs and after 7.0 ± 0.5 minutes, $n = 3$, for the SMCPEs, signifying that this increase was due to injection stress. Similar responses were also obtained for the saline injections. Previous work undertaken in the lab using DMSO as a vehicle suggested an independent effect on O_2 and glucose levels recorded using electrochemical sensors. It was confirmed in this section that DMSO does not have an effect on the O_2 signals and that it can be utilised as a vehicle without hampering the effect of diamox. Observation of the results obtained with the standard CPEs displayed a current change of 43.0 ± 10.0 nA, $n = 5$, with an i.p injection of diamox in DMSO, however, the results displayed in this section show a greater response at the monomer modified sensors.

5.3.7 Stability of O_2 sensors

In Chapter 4 the long term stability of the sensor *in-vitro* was determined over 28 days. The results demonstrated that the two sensors over the period of 28 days remained stable. When the long-term BT treatments were undertaken over 28 days the SMCPEs demonstrated no significant difference pre- and post-treatment ($P = 0.5282$). There was a slight decrease in O_2 detection recorded at the MMCPEs after the 28 days that was significant ($P = 0.0296$), however, a high O_2 sensitivity remained. The need to characterise the sensors *in-vivo* is due to the vast differences between the *in-vivo* and *in-vitro* environments. Also, the stability of the sensors needs to be examined in this harsh and complex biological milieu. In this section the stability of the sensors was determined *in-vivo* over the specified days and the results for both sensors are depicted in Figure 5.3.7.1 and 5.3.7.2. The O_2 current was taken at approximately the same time every day so that an accurate representation of the baseline could be achieved.

5.3.7.1 MMCPE

The baseline data in this section was analysed using the results from 6 animals with 12 sensors over 12 Days.

Day	MMCPE (% O ₂) decrease		
	Mean (% O ₂)	SEM	<i>n</i>
1.0	100.0	0.0	12
2.0	84.5	3.8	12
3.0	82.4	4.6	12
4.0	87.0	4.9	12
5.0	86.5	4.1	12
6.0	83.7	5.4	12
7.0	85.9	5.9	12
8.0	83.8	6.4	12
9.0	84.2	6.3	12
10.0	81.6	5.4	12
11.0	86.4	5.9	12
12.0	83.5	5.9	12

Table 5.3.7.1: The mean percentage table displaying the % decrease in O₂ after implantation with 12 sensors over 12 days in the striatum of 6 freely moving rats.

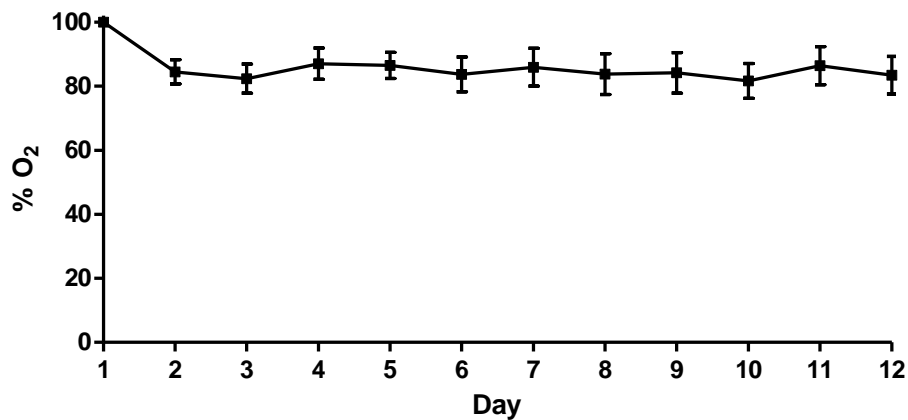


Figure 5.3.7.1: The averaged percentage O₂ decrease vs. day profile of the MMCPEs over the course of 12 days in the striatum of 6 freely moving rats with 12 sensors.

The results displayed in Table 5.3.7.1 and Figure 5.3.7.1 demonstrates how stable the MMCPEs are over the 12 days of implantation in the *in-vivo* environment. Initially there is approximately a 15.5 % decrease in the O₂ current that remains stable over the specified

days. The *in-vitro* BT results displayed a decrease of 26.7 % with 4 sensors over 28 Days (see Section 4.3.5.5). The decrease observed *in-vivo* was slightly lower than this and a shorter period of time was spent *in-vivo* in comparison to the 28 Days spent in the *ex-vivo* BT, however both of these results are comparable. One-way ANOVA analysis revealed that the results for the *in-vivo* stability were not significantly different ($P = 0.5813$) over the course of the study.

5.3.7.2 SMCPE

The baseline data in this section was analysed using the results from 6 animals with 12 sensors over 13 Days.

Day	SMCPE (% O ₂) decrease		
	Mean (% O ₂)	SEM	<i>n</i>
1.0	100.0	0.0	12
2.0	85.7	4.1	12
3.0	88.3	3.3	12
4.0	88.0	4.9	12
5.0	87.2	5.3	12
6.0	91.8	6.2	12
7.0	90.8	6.6	12
8.0	92.3	7.5	12
9.0	97.9	8.1	12
10.0	88.1	7.0	12
11.0	92.1	7.2	12
12.0	86.8	6.4	12
13.0	90.7	9.0	12

Table 5.3.7.2: The mean percentage table displaying the % decrease in O₂ after implantation over 13 days in the striatum of 6 freely moving rats with 12 sensors.

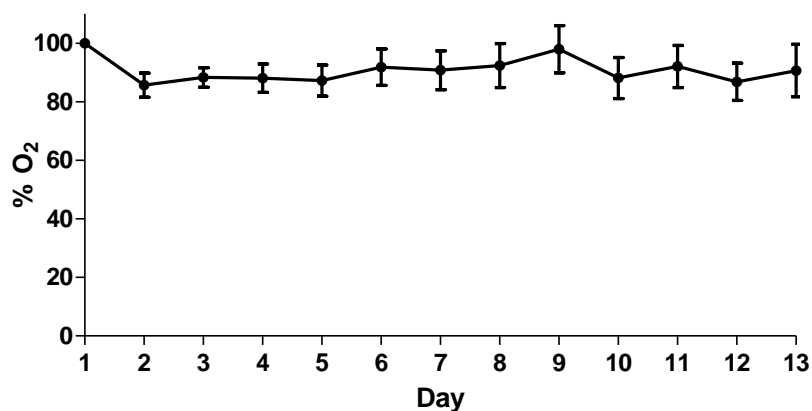


Figure 5.3.7.2: The averaged percentage O₂ decrease vs. day profile of the SMCPEs over the course of 13 days in the striatum of 6 freely moving rats with 12 sensors.

The SMCPEs displayed a similar stability result to the MMCPEs over the specified time. A percentage decrease of approximately 14.4 % occurs after day 1 and the sensitivity remains stable thereafter, which indicates that the SMCPEs are quite robust and can remain constant after the specified time implanted. The *in-vitro* BT results displayed a decrease of 11.3 % with 4 sensors over 28 days (see Section 4.3.5.10). The decrease observed *in-vivo* was slightly higher than this and a shorter period of time was spent *in-vivo* in comparison to the 28 days spent in the *ex-vivo* BT, however both of these results are comparable. One-way ANOVA analysis indicated no significant difference ($P = 0.9322$), between the currents obtained on the days specified.

5.4 Conclusion

Previously, CPEs were implanted for the detection of O₂ *in-vivo* with both DPA and CPA techniques utilised due to their great stability over long periods of time (Lowry *et al.*, 1996; Lowry *et al.*, 1997; Bolger & Lowry, 2005). However, these sensors have been studied extensively and on interaction with the *in-vivo* environment the alteration of the sensors surface is inevitable. Even though this characteristic is the reason behind how stable the CPE sensors are whilst in a biological medium, the novel monomer modified sensors utilised in this chapter were created in order to try and retain stability over long periods of

time, whilst maintaining a good sensitivity without the alteration of the surface in any way. No leeching of constituents from the sensor is paramount for integration of this sensor into the clinical environment.

Presented in this chapter are the results which confirm that both these sensors (MMCPE and SMCPE) detect changes in O_2 resulting from the introduction of periods of hypoxia and hyperoxia by the administration of N_2 /air and O_2 /air mixtures to the snout of the subject. The effects of neuronal activation, administration of saline, chloral hydrate and diamox on the O_2 sensors were also investigated. The compilation of all of these results led to the conclusion that both of these sensors would work as O_2 sensors in a clinical environment. Table 5.4 (a) and 5.4 (b), detail a summary of all of the results for the MMCPEs and SMCPEs, respectively. They possess characteristics of stability, robustness and retaining structural integrity. They are very stable over the course of the days implanted and sensitivity only decreased slightly after day 1 in both sensor types.

Due to the results attained by Kealy *et al.*, with regards to DMSO causing a change in the O_2 current upon administration, experiments were undertaken in order to replicate and confirm the results obtained by using the variety of administrations of diamox, DMSO and saline (Kealy *et al.*, 2013). However, upon administration of DMSO and saline as a control, no long-term effect was observed at both the MMCPEs and SMCPEs. An injection stress was recorded just like that obtained from the saline injections, demonstrating that DMSO could be utilised as a vehicle for diamox administration without causing anomalies in the resulting O_2 increase by diamox.

The data presented in this chapter reveals how capable these O_2 sensors are at detecting changes in O_2 without the risk of biofouling, degradation or decaying of the sensors properties. Not only are these characteristics very promising but the increased sensitivity of the MMCPEs and SMCPEs in comparison to the CPEs is a very exciting and optimistic aspect of these monomer modified sensor designs. However the key finding from this body of work is the possible adoption of these novel sensors by clinical experts. The SEMs displayed in Chapter 4, Section 4.3.6.1 and 4.3.6.2, show that the sensors remain intact and are not modified upon removal from the harsh setting of the living brain. This indicates that the two sensors are good candidates for a prospective future in a clinical setting.

Table 5.4 (a) and 5.4 (b) summarise all the results attained for the characterisation of the MMCPEs and SMCPEs, respectively, *in-vivo*.

	MMCPEs		
Administration	Current change ΔI (nA)	Max response (min)	Return to baseline (min)
Hypoxia	75.6 \pm 4.0	2.5 \pm 0.1	7.1 \pm 0.4
Hyperoxia	80.3 \pm 6.3	3.0 \pm 0.2	13.2 \pm 0.7
Restraint	26.8 \pm 3.8	2.5 \pm 0.3	28.1 \pm 4.3
Tail Pinch	31.4 \pm 6.6	2.8 \pm 0.3	28.3 \pm 5.1
Saline	27.2 \pm 6.0	1.5 \pm 0.2	5.8 \pm 1.0
Chloral hydrate	105.9 \pm 16.4	23.8 \pm 4.4	185.8 \pm 15.2
Diamox (DMSO)	99.9 \pm 5.6	12.0 \pm 1.2	120.0 \pm 1.0
Diamox (saline)	38.6 \pm 11.3	117.5 \pm 91.2	450.0 \pm 229.1
DMSO (saline)	5.8 \pm 3.5	57.0 \pm 1.0 (secs)	7.0 \pm 0.5

Table 5.4 (a): Summary of *in-vivo* characterisation data for the MMCPE O₂ sensor.

	SMCPEs		
Administration	Current change ΔI (nA)	Max response (min)	Return to baseline (min)
Hypoxia	49.9 \pm 2.9	1.7 \pm 0.1	6.2 \pm 0.4
Hyperoxia	63.6 \pm 3.7	2.9 \pm 0.1	12.7 \pm 0.7
Restraint	22.0 \pm 2.8	2.6 \pm 0.3	8.9 \pm 0.7
Tail Pinch	30.8 \pm 3.1	2.8 \pm 0.2	27.1 \pm 3.2
Saline	33.0 \pm 3.6	1.2 \pm 0.2	9.1 \pm 2.0
Chloral hydrate	92.7 \pm 13.4	27.8 \pm 5.3	215.0 \pm 12.1
Diamox (DMSO)	133.0 \pm 17.3	7.5 \pm 2.1	135.7 \pm 16.2
Diamox (saline)	109.6 \pm 34.7	22.5 \pm 10.5	102.5 \pm 2.5
DMSO (saline)	20.8 \pm 3.5	3.0 \pm 0.5	7.0 \pm 0.5

Table 5.4 (b) Summary of *in-vivo* characterisation data for the SMCPE O₂ sensor.


5.5 References

- Bolger F & Lowry J. (2005). Brain Tissue Oxygen: *In-Vivo* Monitoring with Carbon Paste Electrodes. *Sensors* **5**, 473-487.
- Bolger FB, McHugh SB, Bennett R, Li J, Ishiwari K, Francois J, Conway MW, Gilmour G, Bannerman DM, Fillenz M, Tricklebank M & Lowry JP. (2011). Characterisation of carbon paste electrodes for real-time amperometric monitoring of brain tissue oxygen. *Journal of Neuroscience Methods* **195**, 135-142.
- Chakraborti A, Gulati K & Ray A. (2008). Age related differences in stress-induced neurobehavioral responses in rats: Modulation by antioxidants and nitregeric agents. *Behavioural Brain Research* **194**, 86-91.
- Clark LC, Misrahy G & Fox RP. (1958). Chronically implanted polarographic electrodes. *Journal of Applied Physiology* **13**, 85-91.
- Czaban JD. (1985). Electrochemical sensors in clinical chemistry. *Analytical Chemistry* **57**, 345A-356A.
- Dixon BM, Lowry JP & O'Neill RD. (2002). Characterisation *in-vitro* and *in-vivo* of the oxygen dependence of an enzyme/polymer biosensor for monitoring brain glucose. *Journal of Neuroscience Methods* **119**, 135-142.
- Dorland. (2011). *Dorland's Illustrated Medical Dictionary*. Elsevier Health Sciences, New York, United States of America.
- Gifford R, Kehoe JJ, Barnes SL, Kornilayev BA, Alterman MA & Wilson GS. (2006). Protein interactions with subcutaneously implanted biosensors. *Biomaterials* **27**, 2587-2598.
- Gold P & Chrousos G. (2002). Organization of the stress system and its dysregulation in melancholic and atypical depression: high vs low CRH/NE states. *Molecular Psychiatry* **7**, 254-275.
- Gulati K, Chakraborti A & Ray A. (2007). Modulation of stress-induced neurobehavioral changes and brain oxidative injury by nitric oxide (NO) mimetics in rats. *Behavioural Brain Research* **183**, 226-230.
- Gulati K, Ray A, Masood A & Vijayan V. (2006). Involvement of nitric oxide (NO) in the regulation of stress susceptibility and adaptation in rats. *Indian Journal of Experimental Biology* **44**, 809.
- Höckel M & Vaupel P. (2001). Tumor Hypoxia: Definitions and Current Clinical, Biologic, and Molecular Aspects. *Journal of the National Cancer Institute* **93**, 266-276.

- Kawamoto T, Hobara T, Kobayashi H, Iwamoto S, Sakai T, Takano T & Miyazaki Y. (1987). The Metabolite Ratio as a Function of Chloral Hydrate Dose and Intracellular Redox State in the Perfused Rat Liver. *Pharmacology & Toxicology* **60**, 325-329.
- Kealy J, Bennett R & Lowry JP. (2013). Simultaneous recording of hippocampal oxygen and glucose in real time using constant potential amperometry in the freely-moving rat. *Journal of Neuroscience Methods* **215**, 110-120.
- Kennedy RT, Jones SR & Wightman RM. (1992). Simultaneous measurement of oxygen and dopamine: Coupling of oxygen consumption and neurotransmission. *Neuroscience* **47**, 603-612.
- Lowry J & O'Neill R. (2006). Neuroanalytical chemistry *in-vivo* using electrochemical sensors. In *Encyclopedia of Sensors*, pp. 501-524. American Scientific Publishers, United States of America.
- Lowry JP, Boutelle MG & Fillenz M. (1997). Measurement of brain tissue oxygen at a carbon paste electrode can serve as an index of increases in regional cerebral blood flow. *Journal of Neuroscience Methods* **71**, 177-182.
- Lowry JP, Boutelle MG, O'Neill RD & Fillenz M. (1996). Characterisation of carbon paste electrodes *in-vitro* for simultaneous amperometric measurement of changes in oxygen and ascorbic acid concentrations *in-vivo*. *Analyst* **121**, 761-766.
- Lowry JP, Demestre M & Fillenz M. (1998). Relation between cerebral blood flow and extracellular glucose in rat striatum during mild hypoxia and hyperoxia. *Developmental Neuroscience* **20**, 52-58.
- Lowry JP & Fillenz M. (2001). Real-time monitoring of brain energy metabolism *in-vivo* using microelectrochemical sensors: the effects of anesthesia. *Bioelectrochemistry* **54**, 39-47.
- Mann FA, Constantinescu GM & Yoon HY. (2011). *Fundamentals of Small Animal Surgery*. Wiley, United Kingdom.
- McCreery DB, Agnew WF, Bullara LA & Yuen TGH. (1990). Partial pressure of oxygen in brain and peripheral nerve during damaging electrical stimulation. *Journal of Biomedical Engineering* **12**, 309-315.
- Mokhtari RB, Kumar S, Islam SS, Yazdanpanah M, Adeli K, Cutz E & Yeger H. (2013). Combination of carbonic anhydrase inhibitor, acetazolamide, and sulforaphane, reduces the viability and growth of bronchial carcinoid cell lines. *Bmc Cancer* **13**, 1-18.
- Nair PK, Buerk DG & Halsey J. (1987). Comparisons of oxygen metabolism and tissue PO₂ in cortex and hippocampus of gerbil brain. *Stroke* **18**, 616-622.

- O'Neill R. (1993). Sensor-tissue interactions in neurochemical analysis with carbon paste electrodes *in-vivo*. *The Analyst* **118**, 433.
- O'Neill RD & Lowry JP. (2000). *Voltammetry in-vivo for chemical analysis of the living brain*. John Wiley & Sons Ltd, United Kingdom.
- Okazawa H, Yamauchi H, Sugimoto K, Toyoda H, Kishibe Y & Takahashi M. (2001). Effects of Acetazolamide on Cerebral Blood Flow, Blood Volume, and Oxygen Metabolism; A Positron Emission Tomography Study With Healthy Volunteers. *Journal of Cerebral Blood Flow & Metabolism* **21**, 1472-1479.
- Ormonde DE & O'Neill RD. (1989). Altered response of carbon paste electrodes after contact with brain tissue: Implications for modified electrode use *in-vivo*. *Journal of Electroanalytical Chemistry and Interfacial Electrochemistry* **261**, 463-469.
- Ormonde DE & O'Neill RD. (1990). The oxidation of ascorbic acid at carbon paste electrodes: Modified response following contact with surfactant, lipid and brain tissue. *Journal of Electroanalytical Chemistry and Interfacial Electrochemistry* **279**, 109-121.
- Shinohara C, Yamashita K, Matsuo T, Kitamura S & Kawano F. (2007). Effects of Carbonic Anhydrase Inhibitor Acetazolamide (AZ) on Osteoclasts and Bone Structure. *Journal of Hard Tissue Biology* **16**, 115-123.
- Tao R & Auerbach SB. (1994). Anesthetics block morphine-induced increases in serotonin release in rat CNS. *Synapse* **18**, 307-314.
- Tranquilli WJ, Thurmon JC & Grimm KA. (2013). *Lumb and Jones Veterinary Anesthesia and Analgesia*. Blackwell Publishing, Oxford, UK.
- Valente S, Ringwood J, Mangourova V & Lowry J. (2012). Investigation of events in the EEG signal correlated with changes in both oxygen and glucose in the brain. In *Signals and Systems Conference (ISSC 2012)*, pp. 1-6.
- Voelkel N & Rounds S. (2009). *The Pulmonary Endothelium: Function in Health and Disease*. Wiley, United Kingdom.
- Vorstrup S, Henriksen L & Paulson OB. (1984). Effect of acetazolamide on cerebral blood flow and cerebral metabolic rate for oxygen. *Journal of Clinical Investigation* **74**, 1634.
- Wisniewski N, Moussy F & Reichert W. (2000). Characterisation of implantable biosensor membrane biofouling. *Fresenius' Journal of Analytical Chemistry* **366**, 611-621.
- Yoon MY, Kim SJ, Lee B-H, Chung J-H & Kim YC. (2006). Effects of dimethylsulfoxide on metabolism and toxicity of acetaminophen in mice. *Biological and Pharmaceutical Bulletin* **29**, 1618-1624.

Zhou X & Kost CK. (2006). Adenosine A1 receptor antagonist blunts urinary potassium excretion, but not renal hemodynamic effects, induced by carbonic anhydrase inhibitor in rats. *Journal of Pharmacology and Experimental Therapeutics* **316**, 530-538.



*6. In-Vitro Characterisation
of Nitric Oxide Sensors*

6.1 Introduction

NO is one of the smallest molecules found in nature and is a gaseous free radical. It has been implicated in a variety of physiological and pathophysiological processes. It has a role in the regulation of vascular tone and some of the diseases that it has been linked to include hypertension, Parkinson's disease and Alzheimer's disease (Brown *et al.*, 2005). In the late 80's, NO was characterised as the endothelium derived relaxing factor (EDRF) (Ignarro *et al.*, 1987; Palmer *et al.*, 1987). The concentration of NO in physiological conditions has been established at around 0.1 μM (Hall & Garthwaite, 2009), which makes NO difficult to measure *in-vivo* but also to have the required specificity, sensitivity and speed in a sensor to detect it. It has a short half-life (typically < 10 s) due to the reactions with different molecules (Lancaster Jr, 1997).

Due to the significance of this molecule with regards to biological functions and its role in many disease states, it is important to quantify levels of NO production in both abnormal and normal tissue. A sensor for the detection of NO has previously been characterised *in-vitro* and *in-vivo* by our research group. This involved the use of Nafion[®], which was thermally annealed to the electrode surface incorporating 5 pre-coats and 2 subsequent dip-bake layers. Nafion[®] has been utilised previously in the development of carbon fibre electrodes for the detection of NO (Friedemann *et al.*, 1996; Pontié *et al.*, 1999; Patel *et al.*, 2006) and dopamine (Rice & Nicholson, 1989).

The negatively charged sulfonate groups on the Nafion[®] layers repel negatively charged species like AA and NO_2^- but facilitate neutral species like NO to pass through the membrane to the electrode surface (Yang *et al.*, 2004; Zheng *et al.*, 2009). This sensor resulted in the elimination of interferent signals like AA (which is the principal interferent in the brain), while effectively detecting NO (Brown *et al.*, 2009). A potential of +900 mV vs. SCE was utilised as the optimum applied potential for the NO sensors. The electrodes were held at this potential as it corresponds to the applied potential utilised within our research group for the sensors (Brown *et al.*, 2009). This potential has also been demonstrated in other literature (Pallini *et al.*, 1998).

In this chapter NO sensors that involve the Nafion[®] layer, while incorporating an outer o-PD layer are described. These sensors were developed by Brown *et al.*, in order to try and

improve the response time of the sensor with respect to the detection of NO (Brown *et al.*, 2009). The utilisation of less Nafion[®] layers meant that *o*-PD had to be incorporated into the design of the sensor as a permselective film against interferences. The monomer *o*-PD has previously been implemented in sensor designs as an effective barrier against electroactive species like AA (Friedemann *et al.*, 1996; Kirwan *et al.*, 2007; O'Neill *et al.*, 2008).

6.2 Experimental

The instrumentation and software utilised are described in Section 3.2. All chemicals and solutions are detailed in Section 3.3. The manufacture of the various NO sensors is described in Section 3.4. All modifications to the sensors are detailed in Section 3.5. All data was carried out in PBS (pH 7.4) unless mentioned otherwise. A potential of +900 mV vs. SCE was applied to all working electrodes involved in the NO calibrations. The experimental calibrations were carried out by introducing aliquots of stock NO (synthesised as described in Section 3.10, (Brown *et al.*, 2005) or from an NO cylinder (see Section 3.10) into the electrochemical cell (see Figure 3.7). AA calibrations were performed subsequent to NO calibrations except for those discussed in Section 6.3.8, 6.3.12 and 6.3.13. This resulted in the calibrations being performed when the NO current was returning back to baseline levels, so the drift observed below baseline is attributed to the removal of NO from solution.

The data is represented as mean \pm SEM and *n* represents the number of electrodes used unless mentioned otherwise. The slope (pA/ μ M) is used as an index of sensitivity which is defined as the change in response which results from a change in the concentration of the analyte. All statistical analysis was carried out using paired and unpaired *t*-tests which yielded a *P* value that was an indication of the significance of the results. Table 6.2 displays a summary of the *P* values and their significance.

<i>P</i> value	Significance	No. of asterisks
< 0.001	Extremely significant	***
0.001 to 0.01	Very significant	**
0.01 to 0.05	Significant	*
> 0.05	Not significant	ns

Table 6.2: A table displaying a summary of the correspondence of the *P* value to the number of asterisks.

6.3 Results and Discussion

6.3.1 Bare Pt electrodes vs. NO sensors

Initially, experiments were carried out utilising bare Pt electrodes to demonstrate how an unmodified sensor performs when calibrating with NO and AA. Although Pt electrodes detect NO, they also detect electroactive species that are present in abundance in the *in-vivo* environment owing to the lack of protective barrier layers on the sensor to block any unwanted species. AA is the main interferent that can inhibit an electrode's ability to detect a chosen analyte. AA is present in the brain at a concentration of approximately 500 μM (Miele & Fillenz, 1996a). It is a water soluble vitamin that is known for its preventative role in the disease scurvy (Terpstra & Gruetter, 2004). It is utilised in the food industry as an antioxidant, to stabilise and prolong storage of manufactured goods (Casella & Guascito, 1997).

With regards to the body, it is essential for normal physiological function and is crucial for tissue growth and the healing of wounds (Iqbal *et al.*, 2004). AA has been implemented in the health care industry where it can down-regulate cholesterol and lower blood sugar levels and insulin requirements, therefore decreasing the risk of cardiovascular disease (Rath & Pauling, 1990). The detection of AA has been demonstrated previously by Miele *et al.*, and Lowry *et al.*, utilising CPEs (Lowry *et al.*, 1996; Miele & Fillenz, 1996a). AA is used extensively as an antioxidant agent in foods and drinks. It is also utilised in the health

care sector for therapeutic purposes (Raouf *et al.*, 2001). Results recorded for AA calibrations on Pt sensors are displayed in Figure 6.3.1.1 and Table 6.3.1.1.

6.3.1.1 AA detection at Pt Sensors

[AA], μM	Pt Sensor ($n = 14$)	
	Mean I, pA	SEM
0	0	0
200	8115	683
400	15616	1233
600	22974	1770
800	30443	2484
1000	37063	2991

Table 6.3.1.1: Average 0 to 1000 μM AA response obtained from calibrations using bare Pt electrodes, $n = 14$, carried out at +900 mV vs. SCE. Background values subtracted. Mean background current = 652 ± 88 pA.

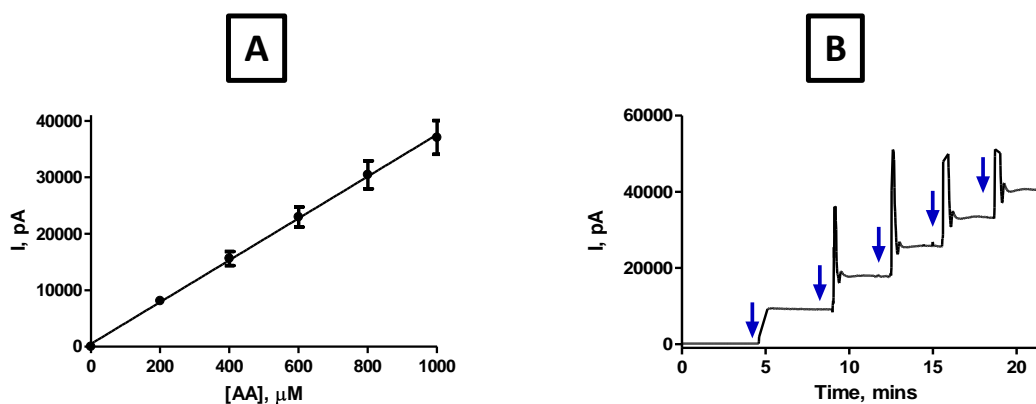


Figure 6.3.1.1: (A) A current-concentration profile for AA at bare Pt disk electrodes ($n = 14$) at +900 mV vs. SCE. (B) A typical raw data trace displaying the currents obtained using an electrode from (A). The blue arrows are indicative of an injection of AA.

Calibrating the unmodified Pt electrodes over a range of 0 - 1000 μM AA concentration range yielded a sensitivity of 37 ± 1 pA/ μM , $n = 14$. The response of the sensor was linear over the specified range with an R^2 value of 0.99. This result demonstrates how difficult it would be to detect NO at an unmodified electrode, as AA among other electroactive species

would cause substantial interference. The detection of NO with a bare Pt electrode is discussed in Figure 6.3.1.2 and Table 6.3.1.2.

6.3.1.2 NO detection at Pt Sensors

[NO], μM	Pt Sensor ($n = 14$)	
	Mean I, pA	SEM
0.0	0	0
0.2	62	7
0.4	139	9
0.6	224	14
0.8	296	19
1.0	352	25

Table 6.3.1.2: Average 0 to 1 μM NO response obtained from calibrations using bare Pt electrodes, $n = 14$, carried out at +900 mV vs. SCE. Background values subtracted. Mean background current = 445 ± 81 pA.

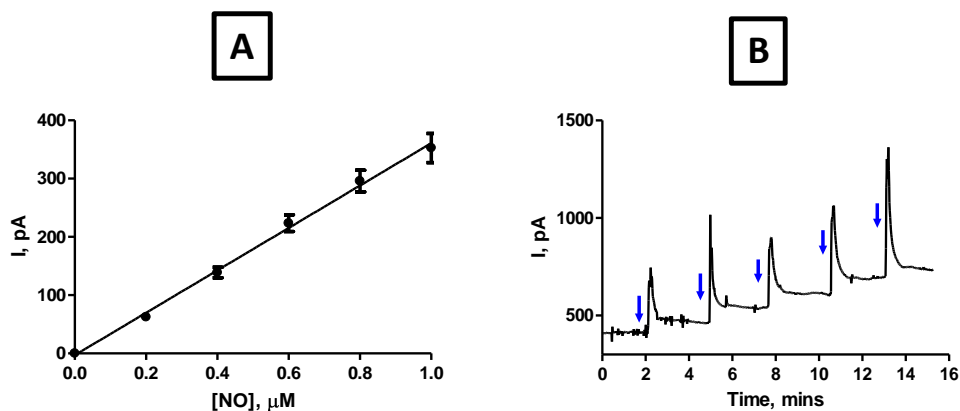


Figure 6.3.1.2 (A): A current-concentration profile for NO at bare Pt disk electrodes ($n = 14$) at +900 mV vs. SCE. (B): A typical raw data trace displaying the currents obtained using an electrode from (A). The blue arrows are indicative of an injection of NO.

The NO response attained at unmodified Pt electrodes over a range of 0 - 1 μM NO concentration range yielded a sensitivity of $364 \pm 10 \text{ pA}/\mu\text{M}$, $n = 14$. The response of the sensor was linear over the specified range ($R^2 = 0.99$). These results demonstrate that NO can be detected at an unmodified Pt electrode. The detection of NO is very low on a bare Pt electrode and with the interference from different species in the brain, working with an unmodified Pt electrode would be impossible. It is hypothesised that a possible reason for the low detection of NO at an unmodified electrode is due to adsorbed oxidation products from the oxidation of NO, decreasing the sensitivity at electrodes not modified with Nafion[®] (Brown *et al.*, 2009). The detection of AA and NO at Nafion[®] modified Pt sensors are described in the following sections.

6.3.2 Type 1 NO Sensor

The Type 1 NO Sensor involves 5 pre-coats of Nafion[®] (5 % solution in lower aliphatic alcohols/H₂O mix) and two subsequent dip-bake layers annealed at 210 °C (see Section 3.4.5.1). The extensive characterisation of this sensor *in-vitro* and *in-vivo* was carried out by Brown *et al.*, (Brown *et al.*, 2009; Finnerty *et al.*, 2012a; Finnerty *et al.*, 2012b). The results obtained during this body of work are shown in Figure 6.3.2.1 and Table 6.3.2.1 The purpose of these investigations was to determine if there was an increase in sensitivity observed with the newly developed Type 2 and Type 3 NO sensors when compared against this extensively characterised sensor type.

6.3.2.1 NO detection at Type 1 NO Sensors

Type 1 NO Sensor ($n = 17$)		
[NO], μM	Mean I, pA	SEM
0.0	0	0
0.2	232	24
0.4	498	42
0.6	728	48
0.8	927	51
1.0	1082	50

Table 6.3.2.1: Average 0 to 1 μM NO response obtained from calibrations using Type 1 NO Sensors, $n = 17$, carried out at + 900 mV vs. SCE. Background values subtracted. Mean background current = 178 ± 22 pA.

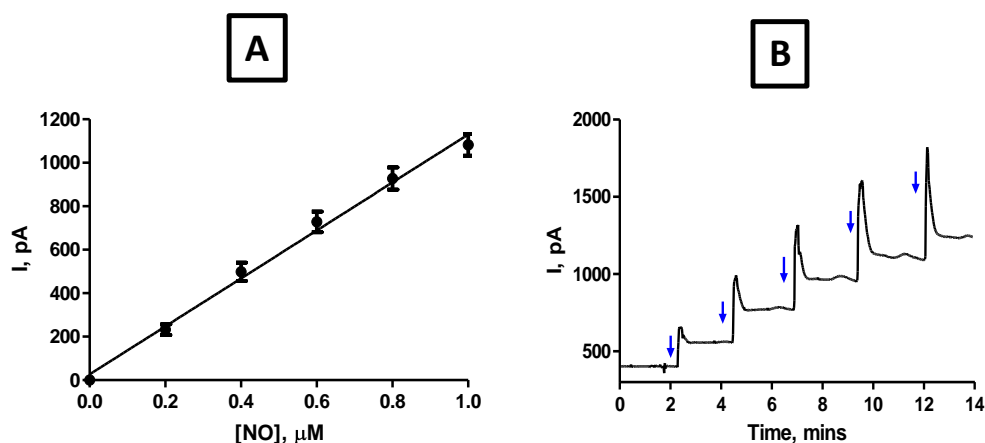


Figure 6.3.2.1: (A) A current-concentration profile for Type 1 NO Sensors ($n = 17$) at + 900 mV vs. SCE. (B) A typical raw data trace displaying the currents obtained using an electrode from (A). The blue arrows are indicative of an injection of NO.

A sensitivity of 1104 ± 46 pA/ μM , $n = 17$ was observed for the Type 1 NO sensor over a concentration range of 0 - 1 μM NO. A linear response was achieved ($R^2 = 0.99$). The results obtained, demonstrate a more sensitive sensor, with an increased detection of NO. The Nafion[®] layer that is negatively charged, is highly permeable to NO (Cadenas &

Packer, 2002). Nafion[®] contains a perfluorocarbon backbone that is hydrophobic and sulfonic groups that are hydrophilic. The hydrophobic nature of neutral NO assists hydrophobic interactions leading to permeation through the Nafion[®] layer (Brown *et al.*, 2009). The response time of the Type 1 NO sensors has been deemed slow, yielding a time of 34 ± 3 s, $n = 14$, in comparison to bare Pt electrodes that have a response time that is much quicker (6.8 ± 1.1 s, $n = 28$) (Brown *et al.*, 2009). In order to try and improve the response time, Type 2 and 3 NO sensors were manufactured. AA calibrations were carried out on the Type 1 NO sensors following the NO calibrations in order to confirm that Nafion[®] acts as a barrier against the interferent.

6.3.2.2 AA detection at Type 1 NO Sensors

Type 1 NO sensor ($n = 17$)		
[AA], μM	Mean I, pA	SEM
0	0	0
200	-1	1
400	-1	1
600	-2	1
800	-2	1
1000	-3	1

Table 6.3.2.2: Average 0 to 1000 μM AA response obtained from calibrations using Type 1 NO Sensor, $n = 17$, carried out at + 900 mV vs. SCE. Background values subtracted. Mean background current = 151 ± 13 pA.

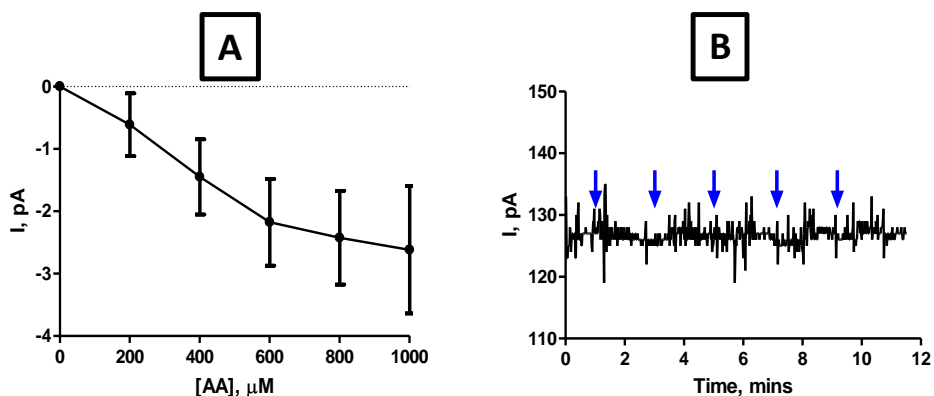


Figure 6.3.2.2: (A) A current-concentration profile for Type 1 NO Sensors ($n = 17$) at +900 mV vs. SCE. (B) A typical raw data trace displaying the currents obtained using an electrode from (A). The blue arrows are indicative of an injection of AA.

Calibrating the Type 1 NO sensors over the specified concentration range yielded a current at 1000 μM of -3 ± 1 pA, $n = 17$. The results observed exhibit how the Nafion[®] layers on the sensor repel AA from the surface. This is due to Nafion[®] consisting of sulfonate functional groups that prevent the diffusion of anions to the surface of the sensor (Cadenas & Packer, 2002). The Type 1 NO sensor completely blocked AA interference and a negative sensitivity was obtained due to the observed baseline drift described in Section 6.2. This observation can be attributed to the different NO sensors, (Type 2 NO sensors: see Section 6.3.3.2 and Type 3 NO sensors: see Section 6.3.4.2).

NO has a very short half-life (Lancaster Jr, 1997) and so to detect the analyte *in-vivo*, a sensor needs to respond very quickly to changes in the concentrations of NO. In order to develop a sensor that had a quicker response time, Brown *et al.*, reduced the thickness of the Nafion[®] layers in combination with a poly(*o*-PD) layer (Brown *et al.*, 2009). The following sections describe the different types of NO sensors that contain less layers of Nafion[®] and have an outer layer of *o*-PD.

6.3.3 Type 2 NO sensor

The Type 2 NO sensor involves 1 pre-coat, 2 applications of Nafion[®] (5 % solution in lower aliphatic alcohols/H₂O mix), annealed after each coat at 210 °C, followed by polymerisation with *o*-PD for 30 minutes (see Section 3.4.5.2). The results obtained are described in Figure 6.3.3.1 and Table 6.3.3.1.

6.3.3.1 NO detection at Type 2 NO sensors

Type 2 NO Sensor ($n = 38$)		
[NO], μM	Mean I, pA	SEM
0.0	0	0
0.2	195	10
0.4	424	19
0.6	644	24
0.8	873	29
1.0	1047	34

Table 6.3.3.1: Average 0 to 1 μM NO response obtained from calibrations using Type 2 NO Sensor, $n = 38$, carried out at +900 mV vs. SCE. Background values subtracted. Mean background current = 43 ± 19 pA.

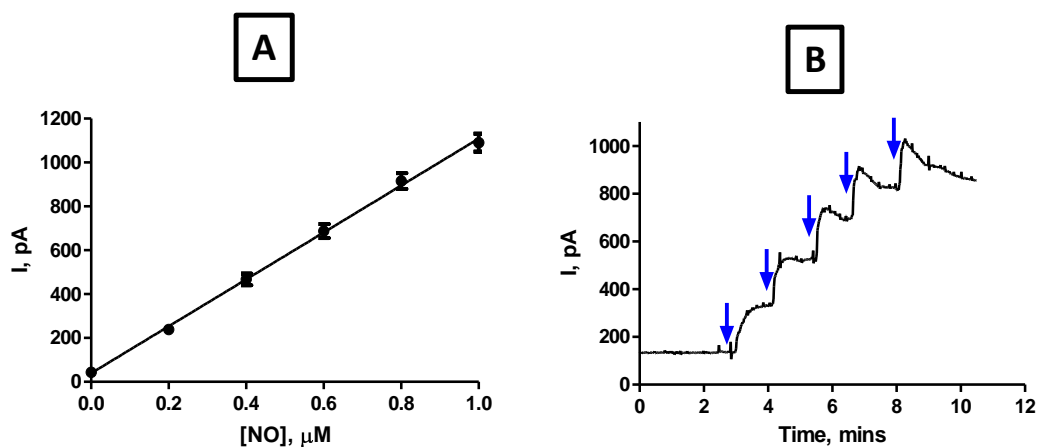


Figure 6.3.3.1: (A) A current-concentration profile for Type 2 NO Sensors ($n = 38$) at +900 mV vs. SCE. (B) A typical raw data trace displaying the currents obtained using an electrode from (A). The blue arrows are indicative of an injection of NO.

The response attained at Type 2 NO sensors over a concentration range of 0 - 1 μM NO yielded a sensitivity of 1070 ± 19 pA/ μM , $n = 38$. A linear response was observed ($R^2 = 0.99$). The results achieved demonstrate how the Nafion[®] layers on the surface of the sensor retain a good sensitivity towards NO. According to the results attained in literature for the Type 2 NO sensors, a response of 19.0 ± 3.4 seconds was obtained (Brown *et al.*, 2009). This was similar to the response achieved in this research with the Type 2 NO sensors (18 ± 2 seconds, $n = 38$). This demonstrated a much faster response time than previously observed for the Type 1 NO sensor. AA calibrations were carried out subsequent to the NO calibrations in order to confirm that Nafion[®] along with the PPD layer was an adequate barrier against the interferent.

6.3.3.2 AA detection at Type 2 NO sensors

Type 2 NO sensor ($n = 38$)		
[AA], μM	Mean I, pA	SEM
0	0	0
200	-6	4
400	-6	4
600	-7	4
800	-6	5
1000	-6	6

Table 6.3.3.2: Average 0 to 1000 μM AA response obtained from calibrations using Type 2 NO sensor, $n = 38$, carried out at + 900 mV vs. SCE. Background values subtracted. Mean background current = 199 ± 23 pA.

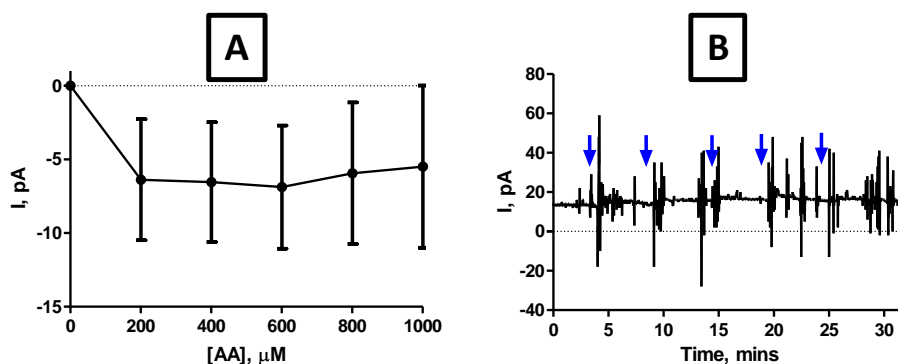


Figure 6.3.3.2 (A) A current-concentration profile for Type 2 NO Sensors ($n = 38$) at +900 mV vs. SCE. **(B)** A typical raw data trace displaying the currents obtained using an electrode from (A). The blue arrows are indicative of an injection of AA.

At a concentration of 1000 μM a current of -6 ± 6 pA, $n = 38$ was observed at the Type 2 NO sensors. The results obtained demonstrate how the Nafion[®] layers along with the PPD layer on the surface of the sensor repel AA. The Type 2 NO sensor completely blocked AA interference and a negative sensitivity was obtained due to baseline drift.

6.3.4 Type 3 NO sensor

The Type 3 NO sensor involved applying 2 pre-coats of Nafion[®] (5 % solution in lower aliphatic alcohols/ H_2O mix), followed by 1 application of Nafion[®], annealed at 210 $^{\circ}\text{C}$, then 1 dip into 5% Nafion[®] solution, annealed at 210 $^{\circ}\text{C}$ and finally polymerisation with *o*-PD for 30 minutes. The results obtained are displayed below in Figure 6.3.4.1 and Table 6.3.4.1.

6.3.4.1 NO detection at Type 3 NO Sensors

Type 3 NO Sensor ($n = 38$)		
[NO], μM	Mean I, pA	SEM
0.0	0	0
0.2	170	9
0.4	378	18
0.6	582	27
0.8	789	36
1.0	975	46

Table 6.3.4.1: Average 0 to 1 μM NO response obtained from calibrations using Type 3 NO Sensor, $n = 38$, carried out at + 900 mV vs. SCE. Background values subtracted. Mean background current = 148 ± 56 pA.

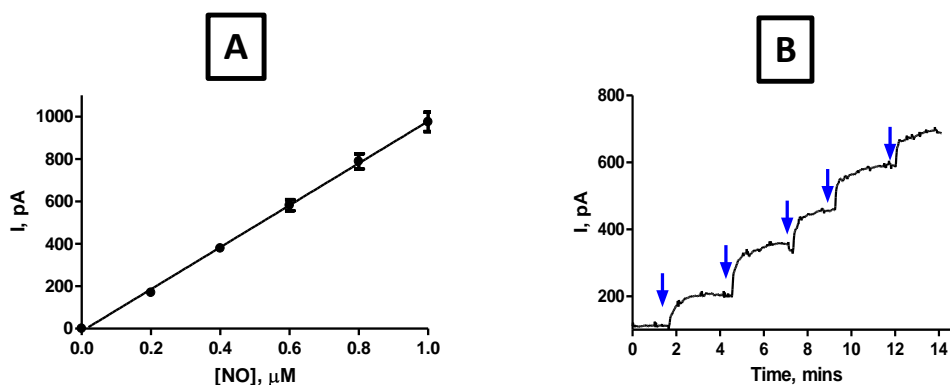


Figure 6.3.4.1: (A) A current-concentration profile for Type 3 NO Sensors ($n = 38$) at + 900 mV vs. SCE. (B) A typical raw data trace displaying the currents obtained using an electrode from (A). The blue arrows are indicative of an injection of NO.

Calibrating the Type 3 NO sensors over a range of 0 - 1 μM NO concentration yielded a sensitivity of 990 ± 14 pA/ μM , $n = 38$. A linear response over the specified range was obtained ($R^2 = 0.99$). The results achieved demonstrate how even though a different method is utilised for the manufacture of the Type 3 NO sensor with Nafion[®] and PPD, a similar sensitivity towards NO is retained. Also the response time is improved once more, displaying a much quicker reaction at the surface in comparison to the Type 1 NO sensors

(16 ± 2 seconds, $n = 38$). AA calibrations were carried out subsequent to the NO calibrations, these result are shown in Figure 6.3.4.2 and Table 6.3.4.2.

6.3.4.2 AA detection at Type 3 NO Sensors

Type 3 NO Sensor ($n = 38$)		
[AA], μM	Mean I, pA	SEM
0	0	0
200	0	2
400	-5	4
600	-7	3
800	-10	3
1000	-18	6

Table 6.3.4.2: Average 0 to 1000 μM AA response obtained from calibrations using Type 3 NO Sensor, $n = 38$, carried out at +900 mV vs. SCE. Background values subtracted. Mean background current = 226 ± 27 pA.

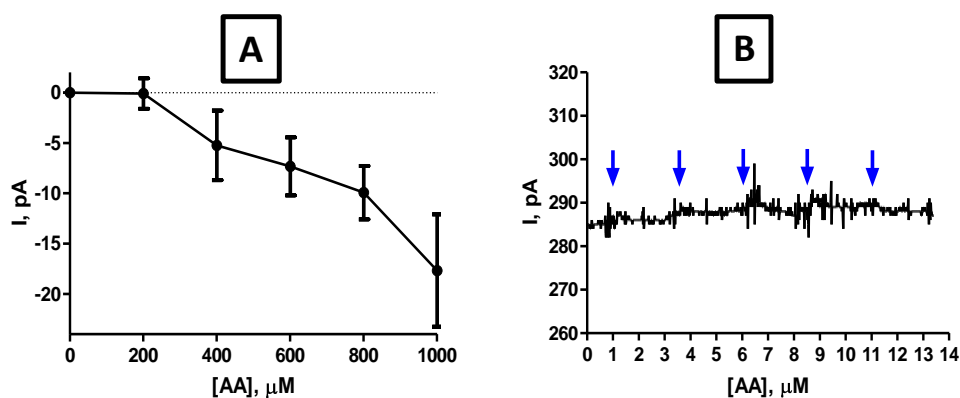


Figure 6.3.4.2: (A) A current-concentration profile for Type 3 NO Sensors ($n = 38$) at +900 mV vs. SCE. (B) A typical raw data trace displaying the currents obtained using an electrode from (A). The blue arrows are indicative of an injection of AA.

At a concentration of 1000 μM a current of -18 ± 6 pA, $n = 38$ was observed at the Type 3 NO sensors. The results obtained demonstrate how the Nafion[®] layers along with the PPD layer on the electrode prevent AA from being detected by the sensor. The Type 3 NO sensor completely blocked AA interference and a negative sensitivity was obtained due to

baseline drift. This drift in current is due to AA calibrations occurring subsequent to the NO calibrations. The PBS is purged with N₂ to remove the NO present; therefore the calibrations were performed on a decreasing current which had not settled fully. Figure 6.3.5, displays NO and AA calibration comparisons of all the sensors.

6.3.5 Comparison of Sensors

6.3.5.1 NO Detection

The detection of NO at the varying sensors is compared in Figure 6.3.5.1 (a). There is a large increase in the detection of NO at the modified sensors in comparison to the unmodified Pt sensors.

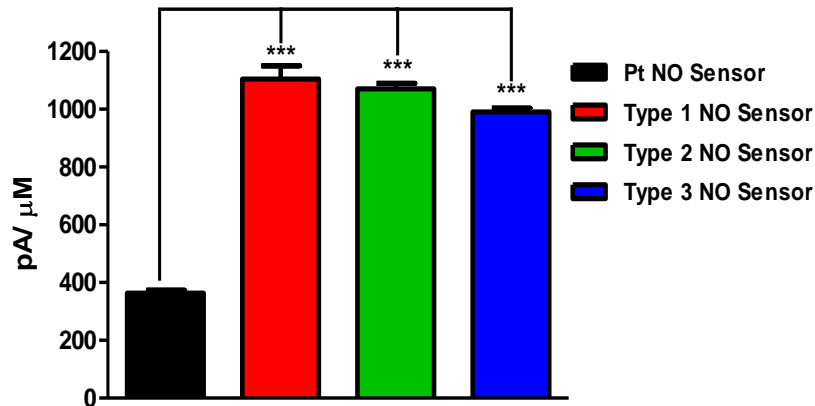


Figure 6.3.5.1 (a): A bar chart displaying a comparison of all NO sensitivities attained at each sensor, carried out at +900 mV vs. SCE.

A significant difference was observed between the unmodified Pt sensor and the modified Nafion[®] and PPD sensors ($P < 0.0001$). This is due to the negative charges of Nafion[®] that attract the NO to the surface of the sensor and prevent HNO₂ which is a product of the NO oxidation from adsorbing to the surface and thus decreasing the detection of NO (Brown *et al.*, 2009). This demonstrates the advantages of modifying the Pt sensor for detection of

NO. In Figure 6.3.5.1 (b) an AA comparison between the sensors is depicted, confirming the utmost importance of applying modifications to the sensor for preventing the detection of AA. A significant difference was recorded for all the sensors against the bare Pt sensor ($P < 0.0001$).

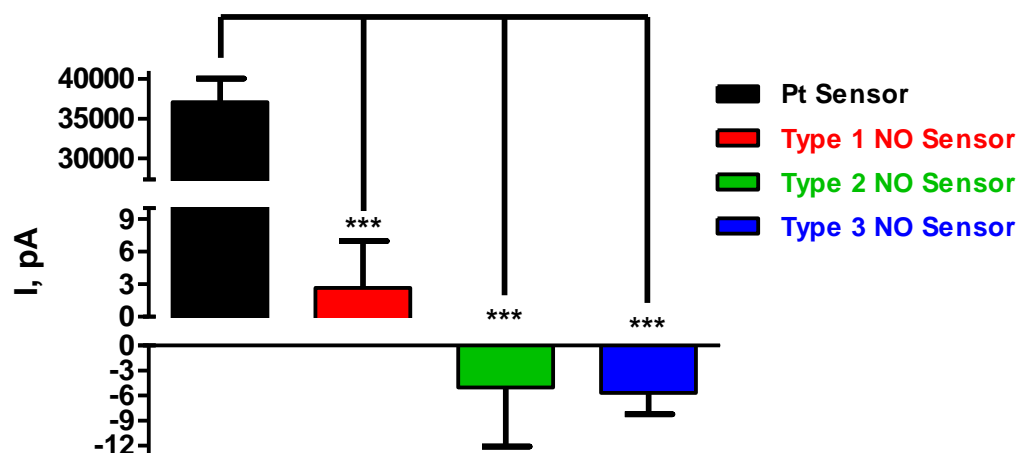


Figure 6.3.5.1 (b): A bar chart displaying a comparison of all AA sensitivities obtained at each sensor, carried out at +900 mV vs. SCE at 1000 μ M AA.

It is clear from Figure 6.3.5.1 (b) that the modified Pt sensors offer a much improved selectivity over the unmodified Pt sensor. A large AA response is detected at the Pt electrode whilst the altered Pt sensors give little or no response to AA, indicating that these sensors are sensitive and selective for detection of the analyte NO.

6.3.6 NO cylinder vs. NO synthesis

6.3.6.1 NO Synthesis

In this Section, the synthesis of NO, along with a comparison of the two types of NO sensor's sensitivity with relation to the different methods of NO collection will be discussed. In Chapter 3, Section 3.10, an illustration of the NO synthesis is portrayed. The synthesis of NO has been demonstrated by many research groups utilising varying ways of

synthesis (Mesároš *et al.*, 1997; Casero *et al.*, 2002; Zhang *et al.*, 2002b). The use of a pure NO commercial gas cylinder has been reported in the literature and is quite a common method of producing NO standard solutions (Pallini *et al.*, 1998; Casero *et al.*, 2000; Meulemans, 2002).

At the beginning of this research the synthesis of NO was produced in-house by a method previously demonstrated in our group (Brown *et al.*, 2005). Brown *et al.*, modified methods of NO production, that were previously reported in literature (Zhang *et al.*, 2002a; Zhang *et al.*, 2002b). After some issues of reproducibility had occurred, an NO cylinder was utilised thereafter, as a means of collecting NO effectively. Once the NO gas had been collected, the determination of the concentration of the NO stock solution was undertaken utilising commercially available reagents and UV-visible spectroscopy. This method of analysis was implemented by our group however it was originally demonstrated by Nims *et al.*, (Nims *et al.*, 1995).

After deciding to use the NO cylinder instead of the NO synthesis, responses attained at the sensors along with the reproducibility of the NO concentration yielded values previously achieved in our lab with these sensors. A comparison of the two sensors utilising the NO synthesis and cylinder are illustrated in Chapter 3, Figure 6.3.7.1 and Figure 6.3.7.2.

6.3.7 Comparison of NO Synthesis and NO Cylinder

During the course of the research it was noted that the in-house synthesis of NO (Brown & Lowry, 2003) demonstrated variations in response at the NO sensors. It was sometimes not reliable and yielded results that were not consistent. The NO cylinder was chosen so that a saturated concentration of NO would be attained and a more consistent NO response would occur each time the NO was collected. A comparison utilising the two different types of sensors is detailed in Figure 6.3.7.1 and Figure 6.3.7.2.

6.3.7.1 Type 2 NO sensor (synthesis vs. cylinder)

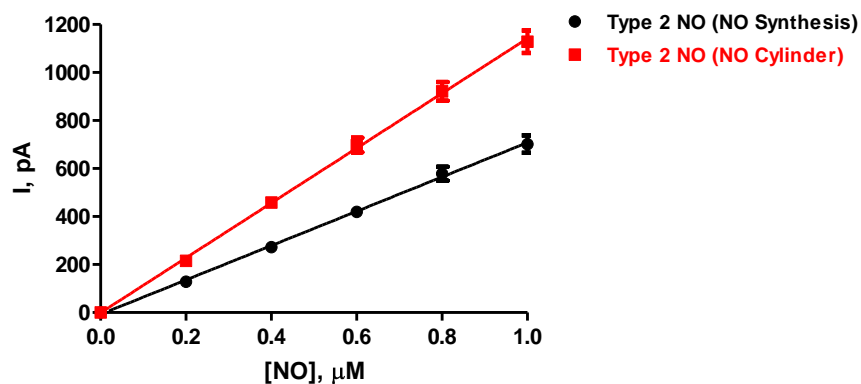


Figure 6.3.7.1: A current-concentration profile displaying a comparison between the NO synthesis and cylinder in PBS (pH 7.4), at +900 mV vs. SCE, carried out with Type 2 NO sensors.

Figure 6.3.7.1 displays the calibrations carried out on the Type 2 NO sensors using the NO synthesis ($n = 82$) and NO cylinder ($n = 32$). Sensitivities of 715 ± 11 pA/ μM (NO synthesis) and 1143 ± 14 pA/ μM (NO cylinder) were obtained. There was a very distinct difference between the NO synthesis and NO cylinder data recorded yielding a significant difference ($P < 0.0001$). In order to determine that it was the inconsistency of the NO synthesis and not just the sensors. The Type 3 NO sensors were studied in a similar manner to confirm the discrepancy in the synthesis. The results are demonstrated in Figure 6.3.7.2.

6.3.7.2 Type 3 NO sensor (synthesis vs. cylinder)

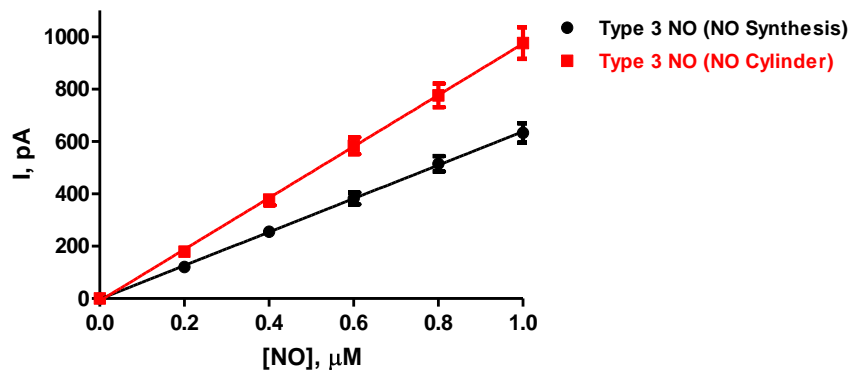


Figure 6.3.7.2: A current-concentration profile displaying a comparison between the NO synthesis and cylinder in PBS (pH 7.4), at +900 mV vs. SCE, carried out with Type 3 NO sensors.

Calibrations carried out on the Type 3 NO sensors using the NO synthesis ($n = 77$) and NO cylinder ($n = 35$) are displayed in Figure 6.3.7.2. Sensitivities of 639 ± 6 pA/ μM (NO synthesis) and 982 ± 8 pA/ μM (NO cylinder) were obtained. There was a significant difference ($P < 0.0001$) between the NO synthesis and NO cylinder data recorded. From the results obtained with the Type 2 and Type 3 NO sensors it has been established that the NO cylinder gave a more reliable NO response with each of the sensors. This way of collecting NO was utilised throughout the rest of the research as it was consistent, easy to use and did not take as long to collect the NO, in comparison to the production of the NO through the synthesis pathway.

6.3.8 Selectivity studies

6.3.8.1 Long term stability investigations on PPD layer

Stability studies were carried out on the PPD layer that is incorporated into the manufacture of Type 2 and 3 NO sensors as an outer layer against the interferent AA. Experiments were carried out utilising different storage conditions and calibrated at specified days. The days chosen varied as we wanted to confirm whether successive calibrations caused substantial damage to the interference layer on the sensor or whether it was the sensors ability to retain selectivity, deteriorating over time. The sensors were also kept in different conditions, in order to determine the optimum setting for storage.

The use of Pt (PPD) sensors for neurochemical monitoring, has been demonstrated by many research groups (Lowry & O'Neill, 1994; Kirwan *et al.*, 2007; Ariffin *et al.*, 2012; Govindarajan *et al.*, 2013). The sole purpose of the PPD layer on these sensors has been to reject interference from unwanted electroactive species. The electrodes were also stored in PBS in the fridge at 4 °C when not in use. This storage condition was utilised, along with other storage conditions to demonstrate the stability of the sensor in varying environments. Figure 6.3.8.1.1.1 and Table 6.3.8.1.1.1 (a) displays the results from the Pt (PPD) sensors stored in an enclosed dry container in the fridge at 4 °C. Repeated calibrations were carried out on these sensors and in between the calibration days the sensors were placed back in the fridge.

6.3.8.1.1 Pt (PPD) Sensor

6.3.8.1.1.1 Storage: Fridge at 4 °C (Enclosed container)

Day	[AA], 1000 μM	
	Mean I, pA	SEM
1	138	19
3	147	10
7	150	53
14	590	224
28	1847	684
56	2707	1031

Table 6.3.8.1.1.1 (a): Average AA response obtained from calibrations at 1000 μM , using Pt electrodes modified with PPD, Day 1 to Day 56 ($n = 4$), carried out at +900 mV vs. SCE. Background values subtracted. Mean background current = 300 \pm 36 pA (Day 1), 210 \pm 42 pA (Day 3), 267 \pm 46 pA (Day 7), 279 \pm 26 pA (Day 14), 359 \pm 56 pA (Day 28) and 178 \pm 24 pA (Day 56).

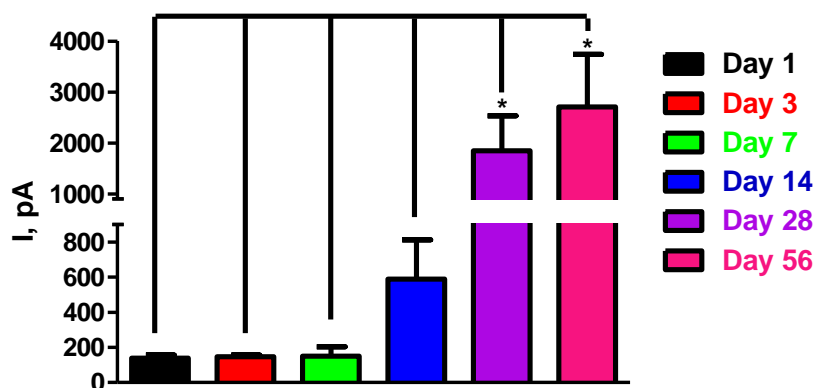


Figure 6.3.8.1.1.1: A bar chart displaying the AA sensitivity obtained at a concentration of 1000 μM with PPD modified Pt electrodes, ($n=4$), at +900 mV vs. SCE.

Figure 6.3.8.1.1.1 and Table 6.3.8.1.1.1 (a) demonstrate a rise in AA detection over the 56 days of repeated calibrations. A significant difference was observed after day 28 (see Table 6.3.8.1.1.1 (b)).

Day	<i>P</i> value	Significance
1 vs. 3	0.6749	ns
1 vs. 7	0.8343	ns
1 vs. 14	0.0905	ns
1 vs. 28	0.0466	*
1 vs. 56	0.0471	*

Table 6.3.8.1.1.1 (b): A summary displaying the *P* values obtained for the Pt (PPD) sensor over 56 Days at 4 °C in an enclosed container.

A current of 138 ± 19 pA (day 1) and 2707 ± 1031 pA (day 56) at 1000 μ M AA concentration was obtained. This shows a degradation of the PPD rejection layer over the period of days studied. In order to confirm that this was in fact the deterioration of the electrode and not the amount of repeated calibrations carried out on the sensors, fewer calibrations were carried out on another set of Pt (PPD) sensors at day 1, day 56 and day 168 utilising the same storage conditions.

6.3.8.1.1.2 Storage: Fridge at 4 °C (Enclosed container)

[AA], μ M	Day 1		Day 56		Day 168	
	Mean I, pA	SEM	Mean I, pA	SEM	Mean I, pA	SEM
1000	19	4	24	2	3490	1276

Table 6.3.8.1.1.2: Average AA responses obtained at 1000 μ M from calibrations using Pt electrodes modified with PPD ($n = 4$), on Day 1 to Day 168, carried out at +900 mV vs. SCE. Background values subtracted. Mean background current = 78 ± 3 pA (Day 1), 54 ± 2 pA (Day 56) and 3565 ± 228 pA (Day 168).

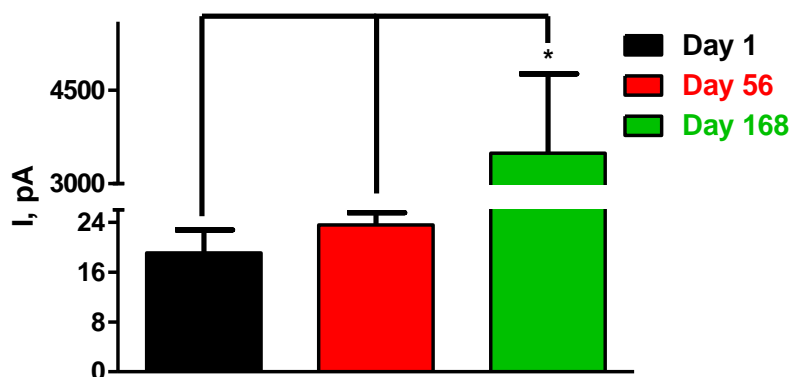


Figure 6.3.8.1.1.2: A bar chart displaying the AA sensitivity obtained at a concentration of 1000 μM with PPD modified Pt electrodes, ($n = 4$), at +900 mV vs. SCE.

At an AA concentration of 1000 μM , a current of 19 ± 4 pA (day 1) and 24 ± 2 pA (day 56) was recorded yielding no significant difference in the AA current after 56 days ($P = 0.3280$). This result demonstrates a correlation between the amount of repeated calibrations carried out on the one set of sensors over time and the degradation of the PPD layer. A significant difference ($P = 0.0471$) was observed between the repeated calibration (day 1-56) on the Pt (PPD) sensors shown in Figure 6.3.8.1.1.1, whereas these results highlight that there is no significant difference (day 1-56) on the Pt (PPD) sensors ($P = 0.3280$). The result obtained at 1000 μM AA concentration on day 168 displayed an AA response that was significantly different ($P = 0.0346$). The response was higher (3490 ± 1276 pA) than the response recorded at day 56, demonstrating a deterioration of the PPD layer after this amount of time.

As previously stated, Pt (PPD) sensors have been stored by other research groups in PBS in the fridge when not in use (Lowry & O'Neill, 1994; Kirwan *et al.*, 2007). This storage condition was then employed to see if the stability of the sensor would be improved by applying the same experimental procedures as in the previous section i.e. repeating calibrations frequently over 56 Days and repeated calibrations less frequent over 168 Days.

6.3.8.1.1.3 Storage: Fridge at 4 °C (Enclosed container with N₂ Saturated PBS)

	[AA], 1000 μM	
Day	Mean I, pA	SEM
1	201	25
3	134	20
7	406	131
14	934	218
28	1364	359
56	2319	637

Table 6.3.8.1.1.3 (a): Average AA responses observed at 1000 μM from calibrations using Pt electrodes modified with PPD ($n = 4$), on Day 1 to Day 56, carried out at +900 mV vs. SCE. Background values subtracted. Mean background current = 227 ± 54 pA (Day 1), 247 ± 60 pA (Day 3), 304 ± 80 pA (Day 7), 314 ± 48 pA, 1044 ± 17 pA (Day 28) and 278 ± 106 pA (Day 56).

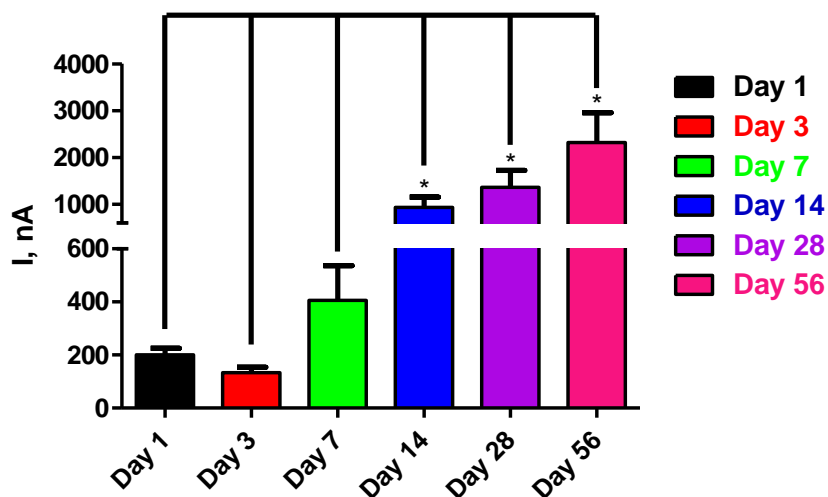


Figure 6.3.8.1.1.3: A bar chart displaying the AA sensitivity obtained at a concentration of 1000 μM with PPD modified Pt electrodes, ($n = 4$), at +900 mV vs. SCE.

The results displayed in Figure 6.3.8.1.1.3 and Table 6.3.8.1.1.3 (a), depict that over the 56 days a similar degradation of the AA rejecting PPD layer can be observed as was seen with the repeated calibrations undertaken in Figure 6.3.8.1.1.1 in the dry enclosed container. Table 6.3.8.1.1.3 (b) details the resulting P values for each of the Days.

Day	<i>P</i> value	Significance
1 vs. 3	0.0805	ns
1 vs. 7	0.1736	ns
1 vs. 14	0.0155	*
1 vs. 28	0.0179	*
1 vs. 56	0.0160	*

Table 6.3.8.1.1.3 (b): A summary displaying the *P* values obtained for the Pt (PPD) sensor over 56 Days at 4 °C in an enclosed container with N₂ saturated PBS.

A significantly different AA response from Day 14 was recorded. Subsequent to this result, fewer calibrations were undertaken utilising the same experimental conditions in Figure 6.3.8.1.1.4, to demonstrate whether the repeated calibrations are a cause of the deteriorating PPD layer or is the storage conditions playing a part in the diminishing AA barrier.

6.3.8.1.1.4 Storage: Fridge at 4 °C (Enclosed container with N₂ Saturated PBS)

[AA], μM	Day 1		Day 56		Day 168	
	Mean I, pA	SEM	Mean I, pA	SEM	Mean I, pA	SEM
1000	18	7	1123	121	4057	122

Table 6.3.8.1.1.4 (a): Average AA responses obtained at 1000 μM from calibrations using Pt electrodes modified with PPD (*n* = 4), on Day 1 to Day 168, carried out at +900 mV vs. SCE. Background values subtracted. Mean background current = 111 ± 17 pA (Day 1), 79 ± 4 pA (Day 56) and 4471 ± 158 pA (Day 168).

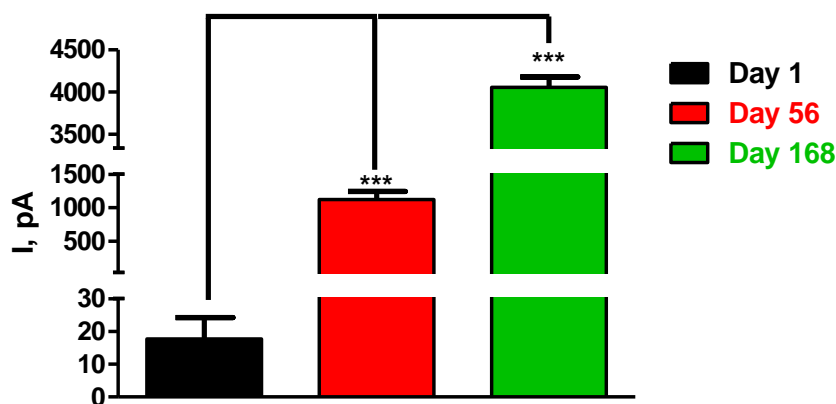


Figure 6.3.8.1.1.4: A bar chart displaying the AA sensitivity obtained at a concentration of 1000 μM with PPD modified Pt electrodes ($n = 4$), at +900 mV vs. SCE.

Figure 6.3.8.1.1.4 and Table 6.3.8.1.1.4 (a) demonstrate currents of 18 ± 7 pA (Day 1), 1123 ± 121 pA (Day 56) and 4057 ± 122 pA (Day 168). There is a significant difference from day 1 - day 56 ($P < 0.0001$) and from day 1 to day 168 ($P < 0.0001$). These results were not expected as the sensors were only calibrated once prior to day 56. It was hypothesised that keeping the sensors in PBS is not the optimum storage condition for the sensors. More studies were undertaken to try and confirm this theory. Calibrations were carried out less frequently as results recorded for repeated calibrations in Figure 6.3.8.1.1.1 and Figure 6.3.8.1.1.3 suggest that constant calibrations on the sensor diminishes the PPD layer prematurely. The sensors were placed in a N_2 saturated dry enclosed container and calibrated at day 1, day 56 and day 168, the results are illustrated in Table 6.3.8.1.1.5 and Figure 6.3.8.1.1.5.

6.3.8.1.1.5 Storage: Fridge at 4 °C (Enclosed container N_2 saturated)

[AA], μM	Day 1		Day 56		Day 168	
	Mean I, pA	SEM	Mean I, pA	SEM	Mean I, pA	SEM
1000	251	27	295	105	222	131

Table 6.3.8.1.1.5: Average AA responses obtained at 1000 μM from calibrations using Pt electrodes modified with PPD ($n = 8$), on day 1 to day 168, carried out at +900 mV vs. SCE. Background values subtracted. Mean background currents = 139 ± 31 pA (Day 1), 2029 ± 103 pA (Day 56) and 2735 ± 375 pA (Day 168).

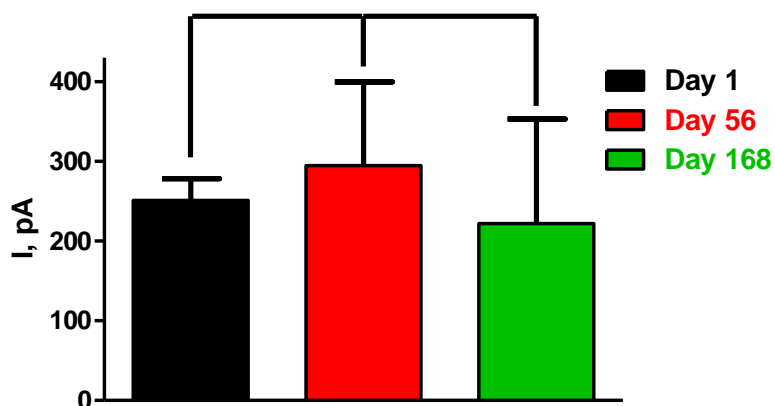


Figure 6.3.8.1.1.5: A bar chart displaying the AA sensitivity obtained at a concentration of 1000 μM with PPD modified Pt electrodes ($n = 8$), at +900 mV vs. SCE.

The response attained day 1 - day 168 at an AA concentration of 1000 μM , displayed a slight increase on day 56 that was not significant ($P = 0.6952$) and after day 168 the AA response was also not significantly different ($P = 0.8310$). This was a very promising result, as the sensors did not seem to be degrading over time and even after the three calibrations. This provides more evidence that a dry environment is the optimum condition for storing the Pt (PPD) sensors. The final place of storage for the sensors was the freezer and these results are displayed in Figure 6.3.8.1.1.6 and Table 6.3.8.1.1.6.

6.3.8.1.1.6 Storage: Freezer at $-20\text{ }^{\circ}\text{C}$ (Enclosed container)

[AA], μM	Day 1		Day 56		Day 168	
	Mean I, pA	SEM	Mean I, pA	SEM	Mean I, pA	SEM
1000	139	23	804	302	1706	615

Table 6.3.8.1.1.6: Average AA responses at 1000 μM obtained from calibrations using Pt electrodes modified with PPD ($n = 8$), on day 1 to day 168, carried out at +900 mV vs. SCE. Background values subtracted. Mean background currents = 324 ± 53 pA (Day 1), 132 ± 21 pA (Day 56) and 2049 ± 269 pA (Day 168).

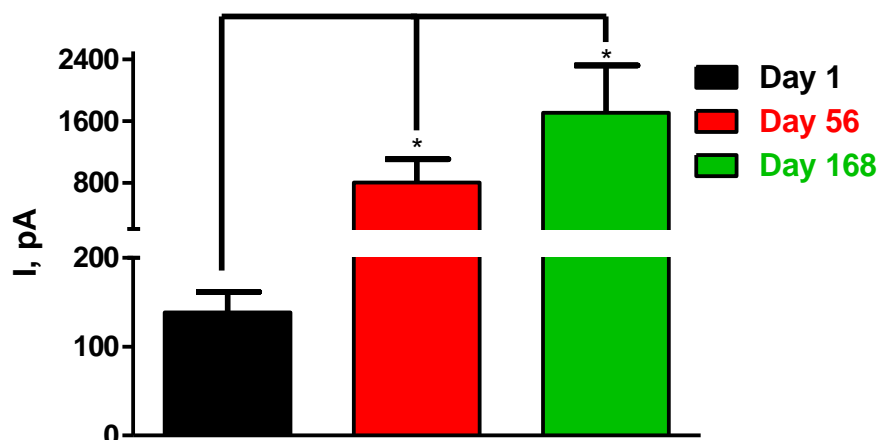


Figure 6.3.8.1.1.6: A bar chart displaying the AA sensitivity obtained at a concentration of 1000 μM with PPD modified Pt electrodes ($n = 8$), at +900 mV vs. SCE.

A current of 139 ± 23 pA (day 1), 804 ± 302 pA (day 56) and 1706 ± 615 pA (day 168) was observed for the Pt (PPD) sensors at an AA concentration of 1000 μM . The results were significantly different day 1 to day 56 ($P = 0.0451$). Day 1 to day 168 displayed a significant difference in the AA response also ($P = 0.0232$). Similar to the results observed with the Pt (PPD) sensors in N_2 saturated PBS, placing the sensors in the freezer does not offer an environment that keeps the PPD layer stable. From all of the results obtained and discussed in this section, it is confirmed that the necessary conditions for the PPD layer on the Pt (PPD) sensors to remain stable is a dry environment in the fridge at 4 °C. These studies have not been performed before and it has become more important as our group looks at commercialising these sensors. Customers will want to know what the optimum conditions are for storage and how long the sensors can be stored, without an effect on the sensors performance. Following on from this section, long term storage stability experiments were undertaken utilising the Type 1 NO Sensor which contains Nafion[®] alone as the design (see Section 3.4.5.3).

6.3.8.2 Long term stability studies on different types of NO sensors

6.3.8.2.1 Type 1 NO Sensor

6.3.8.2.1.1 Storage: Fridge at 4 °C (Enclosed container)

	[AA], 1000 μ M	
Day	Mean I, pA	SEM
1	131	29
3	260	211
7	592	328
14	1254	902
28	1598	1099
56	3239	1175

Table 6.3.8.2.1.1 (a): Average AA responses at 1000 μ M obtained from calibrations using Type 1 NO sensors ($n = 3$), on Day 1 to Day 56, carried out at +900 mV vs. SCE. Background values subtracted. Mean background current = 72 ± 4 pA (Day 1), 48 ± 6 pA (Day 3), 41 ± 6 pA (Day 7), 56 ± 3 (Day 14), 34 ± 5 pA (Day 28) and 19 ± 2 pA (Day 56).

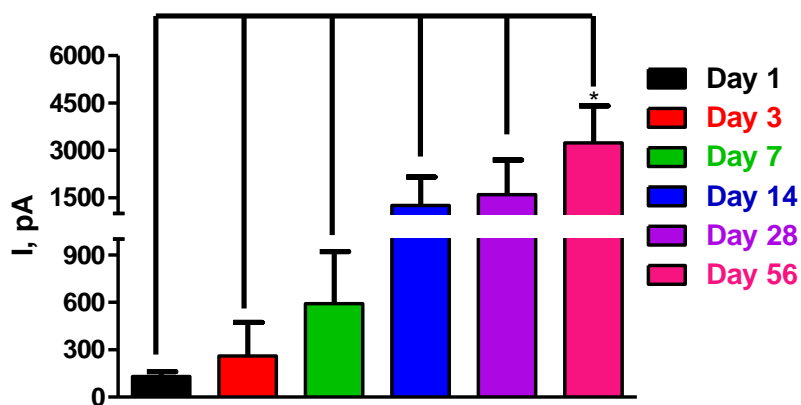


Figure 6.3.8.2.1.1: A bar chart displaying the AA sensitivity obtained at a concentration of 1000 μ M with Type 1 NO sensors ($n = 4$), at +900 mV vs. SCE.

The results recorded with the Type 1 NO sensor displays no significance from day 1 to day 28; P values are depicted in Table 6.3.8.2.1.1 (b). However, a significant increase is observed at day 56 ($P = 0.0383$). This demonstrates a trend of deterioration in the sensor with each calibration undertaken.

Day	P value	Significance
1 vs. 3	0.5650	ns
1 vs. 7	0.2119	ns
1 vs. 14	0.2597	ns
1 vs. 28	0.2306	ns
1 vs. 56	0.0383	*

Table 6.3.8.2.1.1 (b): A summary displaying the P values obtained for the Pt (PPD) sensor over 56 Days at 4 °C in an enclosed container.

A similar trend was encountered with the Pt (PPD) sensors (see Section 6.3.8.1.1). The same experiments were undertaken in order to confirm if it was an effect of repeated calibrations on the sensor or time that deteriorated the sensors ability to block AA.

6.3.8.2.1.2 Storage: Fridge at 4 °C (Enclosed container)

[AA], μM	Day 1		Day 56		Day 168	
	Mean I, pA	SEM	Mean I, pA	SEM	Mean I, pA	SEM
1000.0	-2	0	-5	1	-22	3

Table 6.3.8.2.1.2: Average AA responses obtained at 1000 μM from calibrations using Type 1 NO sensors ($n = 3$), on Day 1 to Day 68, carried out at +900 mV vs. SCE. Background values subtracted.

Mean background current = 63 \pm 6 pA (Day 1), 21 \pm 7 pA (Day 56) and 585 \pm 339 (Day 168).

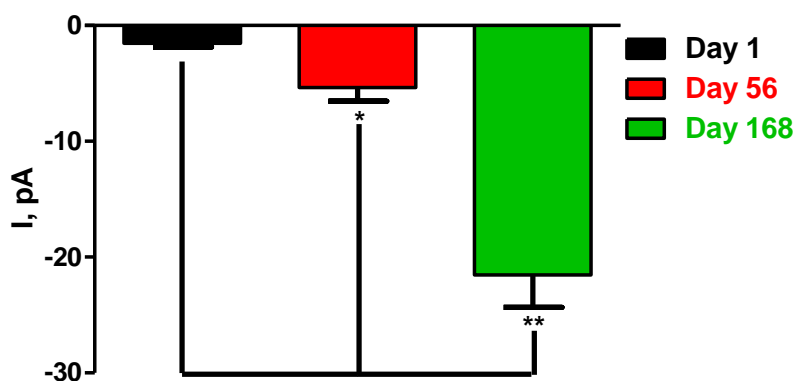


Figure 6.3.8.2.1.2: A bar chart displaying the AA sensitivity obtained at a concentration of 1000 μM with Type 1 NO Sensors ($n = 3$), at +900 mV vs. SCE.

The results were significantly different over the course of the specified days. Day 56 and day 168 displayed significantly different AA responses ($P = 0.0339$) and ($P = 0.0021$), respectively. Even though these results were significantly different in comparison to day 1, no AA had been detected at all. The Type 1 NO sensor completely blocked AA interference and a negative sensitivity was obtained due to baseline drift, which displays the current dropping slightly below the background current upon additions of AA into the electrochemical cell. This result is very encouraging, as a sensitivity of 1417 ± 743 pA at 1000 μM AA was observed at day 56 on the same sensors calibrated repeatedly, however the results here at day 56 yield a current of -5 ± 1 pA. This confirms again the theory that repetitive calibrations cause damage to the layers on the electrode that act as a barrier. Due to this result, fewer calibrations were carried out on the sensors in order to discover the required environment in which to store these sensors.

6.3.8.2.1.3 Storage: Fridge at 4 °C (Enclosed container with N₂ Saturated PBS)

[AA], μM	Day 1		Day 56		Day 168	
	Mean I, pA	SEM	Mean I, pA	SEM	Mean I, pA	SEM
1000	-14	5	-1	1	22	10

Table 6.3.8.2.1.3: Average AA response at 1000 μM obtained from calibrations using Type 1 NO sensors ($n = 4$), on Day 1 to Day 168, carried out at +900 mV vs. SCE. Background values subtracted. Mean background current = 91 ± 3 pA (Day 1), 51 ± 11 pA (Day 56) and 144 ± 26 pA (Day 168).

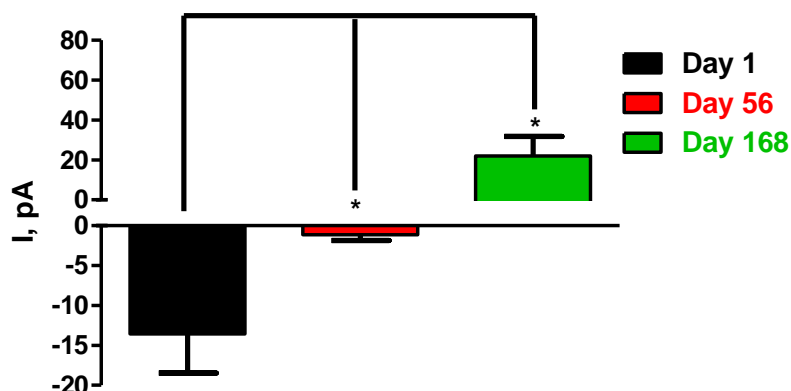


Figure 6.3.8.2.1.3: A bar chart displaying the AA sensitivity obtained at a concentration of 1000 μM with Type 1 NO Sensors ($n = 4$), at +900 mV vs. SCE.

The results recorded for the Type 1 NO Sensors in N₂ saturated PBS yielded currents of -14 ± 5 pA (day 1), -1 ± 1 pA (day 56) and 22 ± 10 pA (day 168). There was a slight detection of AA after day 168 but this detection was negligible and after 168 days is excellent. A significant difference was observed after day 56 ($P = 0.0454$) and after day 168 there was a significant difference in the AA response also ($P = 0.0176$). Nafion[®] seems to be more stable in a PBS environment, unlike Pt (PPD) sensors. Following this storage condition, a N₂ saturated enclosed container was utilised and the results are discussed in the next section.

6.3.8.2.1.4 Storage: Fridge at 4 °C (Enclosed container N₂ saturated)

[AA], μM	Day 1		Day 56		Day 168	
	Mean I, pA	SEM	Mean I, pA	SEM	Mean I, pA	SEM
1000	-17	2	48	20	259	61

Table 6.3.8.2.1.4: Average AA responses at 1000 μM obtained from calibrations using Type 1 NO sensors ($n = 3$), on Day 1 to Day 168, carried out at +900 mV vs. SCE. Background values subtracted. Mean background current = 70 ± 5 pA (Day 1), 49 ± 8 pA (Day 56) and 260 ± 40 pA (Day 168).

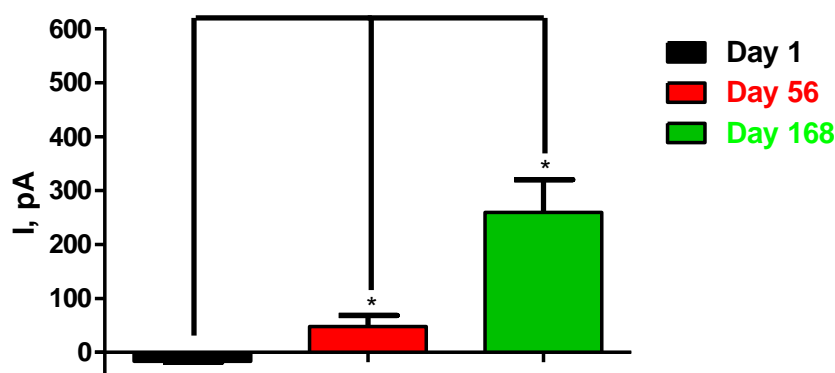


Figure 6.3.8.2.1.4: A bar chart displaying the AA sensitivity obtained at a concentration of 1000 μM with Type 1 NO sensors ($n = 3$), at +900 mV vs. SCE.

The results obtained in Figure 6.3.8.2.1.4 and Table 6.3.8.2.1.4 for the Type 1 NO sensors kept in an enclosed N₂ saturated container yielded currents of -17 ± 2 pA (day 1), 48 ± 20 pA (day 56) and 259 ± 61 pA (day 168). After day 56 and after day 168 a significant difference ($P = 0.0334$ and $P = 0.0105$) was observed, respectively. Even though the results were significantly different from day 1, day 56 and day 168 were still more stable in comparison to the repeated calibration in Figure 6.3.8.2.1.1. These results demonstrate a good stability over the course of the specified days, however, not as stable as the results observed in Figure 6.3.8.2.1.2 and Figure 6.3.8.2.1.3.

6.3.8.2.1.5 Storage: Freezer at -20°C (Enclosed container)

[AA], μM	Day 1		Day 56		Day 168	
	Mean I, pA	SEM	Mean I, pA	SEM	Mean I, pA	SEM
1000	-39	1	4	1	65	7

Table 6.3.8.2.1.5: Average AA responses at $1000\ \mu\text{M}$ obtained from calibrations using Type 1 NO sensors ($n = 4$), on day 1 to day 168, carried out at $+900\ \text{mV vs. SCE}$. Background values subtracted.

Mean background current = $57 \pm 3\ \text{pA}$ (Day 1), $32 \pm 3\ \text{pA}$ (Day 56) and $516 \pm 13\ \text{pA}$ (Day 168).

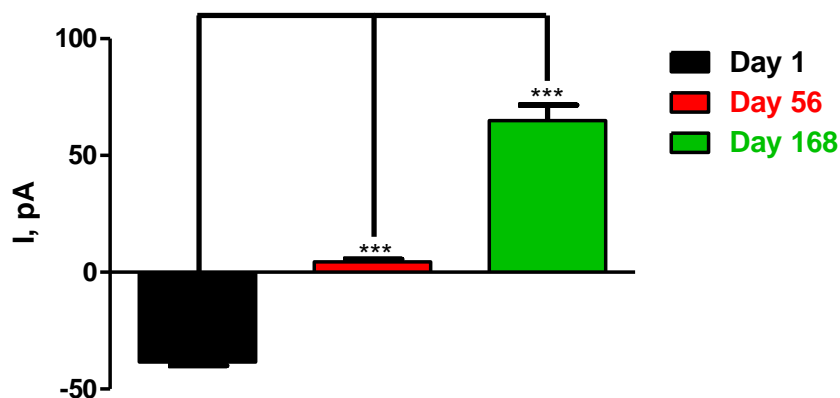


Figure 6.3.8.2.1.5: A bar chart displaying the AA sensitivity obtained at a concentration of $1000\ \mu\text{M}$ with Type 1 NO sensors ($n = 4$), at $+900\ \text{mV vs. SCE}$.

Type 1 NO sensors stored in the freezer display a good stability over the specified times. This storage environment did not seem to cause substantial degradation to the sensor until day 168, however a significant difference was observed in the AA response ($P < 0.0001$), but yet, there was still not much detection of AA at Type 1 NO sensors after that amount of time. A significant difference was observed after day 56 ($P < 0.0001$), in comparison to day 1, however the AA response was miniscule. The results exhibited in this section, yield a sensor that displays a very robust and stable characteristic in any storage environment. Over the 168 days the sensors kept in the fridge in an enclosed container displayed no AA detection (see Figure 6.3.8.2.1.2). It was also confirmed that repeatedly calibrating the sensors causes damage to the electrodes rejection layer as can be seen in Figure 6.3.8.2.1.1.

If the sensors are manufactured, calibrated and then stored immediately, they retain stability over long periods of time.

Following on from this, studies were undertaken with the two other types of NO sensors in the next section. As these sensors not only contain Nafion[®] but a PPD layer too, it was decided to utilise the storage conditions of a dry environment and N₂ saturated PBS environment to determine which condition was more suitable for these sensors. The repeated calibrations as well as the less frequent calibrations were employed in order to fully determine that the results obtained for the other sensors were transferable across all types of sensors.

6.3.8.2.2 Type 2 NO Sensor

6.3.8.2.2.1 Storage: Fridge at 4 °C (Enclosed container)

Day	[AA], 1000 μM	
	Mean I, pA	SEM
1	-59	10
3	141	107
7	2583	944
14	2910	1000
28	3299	1049
56	6539	1504

Table 6.3.8.2.2.1 (a): Average AA responses at 1000 μM obtained from calibrations using Type 2 NO sensors ($n = 4$), on day 1 to day 56, carried out at +900 mV vs. SCE. Background values subtracted. Mean background current = 191 ± 38 pA (Day 1), 285 ± 64 pA (Day 3), 585 ± 314 pA (Day 7), 84 ± 36 pA (Day 14), 115 ± 4 pA (Day 28) and 36 ± 50 pA (Day 56).

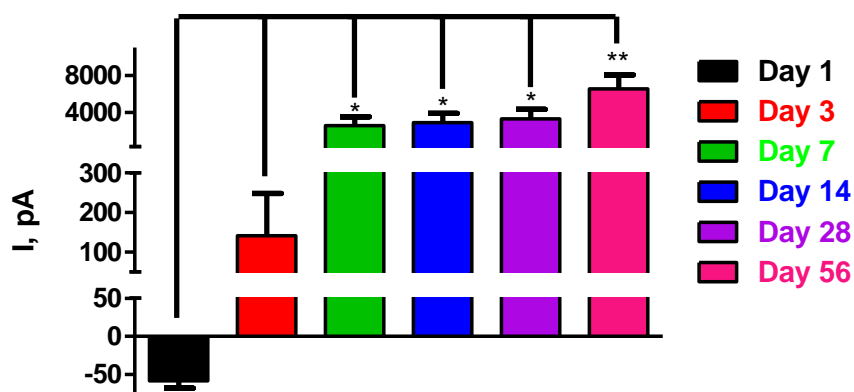


Figure 6.3.8.2.2.1: A bar chart displaying the AA current obtained at a concentration of 1000 μM with Type 2 NO sensors, ($n = 4$), at +900 mV vs. SCE.

AA calibrations carried out on Type 2 NO sensors ($n = 4$) over the specified time intervals displayed a familiar trend seen with the other sensors discussed previously. A characteristic increase in AA with continual calibration is depicted in the Figure 6.3.8.2.2.1. No significant difference was observed between day 1 and day 3 ($P = 0.1127$), however, a steady increase and significant difference in the AA response from day 3 can be observed.

Day	<i>P</i> value	Significance
1 vs. 3	0.1127	ns
1 vs. 7	0.0312	*
1 vs. 14	0.0250	*
1 vs. 28	0.0186	*
1 vs. 56	0.0046	**

Table 6.3.8.2.2.1 (b): A summary displaying the *P* values obtained for the Type 2 NO sensor over 56 Days at 4 °C in an enclosed container.

The same conditions were utilised in Figure 6.3.8.2.2.2 and the Type 2 NO sensors were calibrated less frequent to highlight the effect of repeated calibrations on the sensors.

6.3.8.2.2.2 Storage: Fridge at 4 °C (Enclosed container)

[AA], μM	Day 1		Day 56		Day 168	
	Mean I, pA	SEM	Mean I, pA	SEM	Mean I, pA	SEM
1000	6	1	60	30	117	40

Table 6.3.8.2.2.2: Average AA responses at 1000 μM obtained from calibrations using Type 2 NO sensors ($n = 4$), on day 1 to day 56, carried out at +900 mV vs. SCE. Background values subtracted.

Mean background current = 13 ± 3 pA (Day 1), 4 ± 3 pA (Day 56) and 959 ± 198 (Day 168).

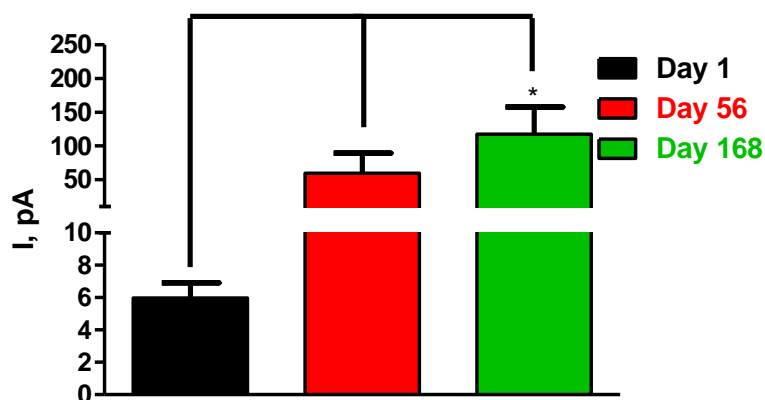


Figure 6.3.8.2.2.2: A bar chart displaying the AA current obtained at a concentration of 1000 μM with Type 2 NO sensors ($n = 4$), at +900 mV vs. SCE.

The results yielded no significant difference in the AA response after day 56 ($P = 0.1232$), however there was a significant difference ($P = 0.0324$) after 168 days. An AA current of 60 ± 30 pA on day 56 and 117 ± 40 pA on day 168 in comparison to the result obtained at day 56 with the repeated calibrations (6539 ± 1504 pA) proves that the sensors deterioration over time, is due to the repetitive calibrations causing substantial destruction to the sensors PPD layer.

6.3.8.2.2.3 Storage: Fridge at 4 °C (Enclosed container with N₂ Saturated PBS)

Day	[AA], 1000 μM	
	Mean I, pA	SEM
1	1	1
3	5	2
7	71	24
14	387	54
28	407	73
56	444	61

Table 6.3.8.2.2.3 (a): Average AA responses at 1000 μM obtained from calibrations using Type 2 NO sensors ($n = 3$), on day 1 to day 56, carried out at +900 mV vs. SCE. Background values subtracted. Mean background current = 14 ± 3 pA (Day 1), 53 ± 10 pA (Day 3), 38 ± 9 pA (Day 7), 134 ± 65 pA (Day 14), 49 ± 12 pA (Day 28) and 71 ± 12 pA (Day 168).

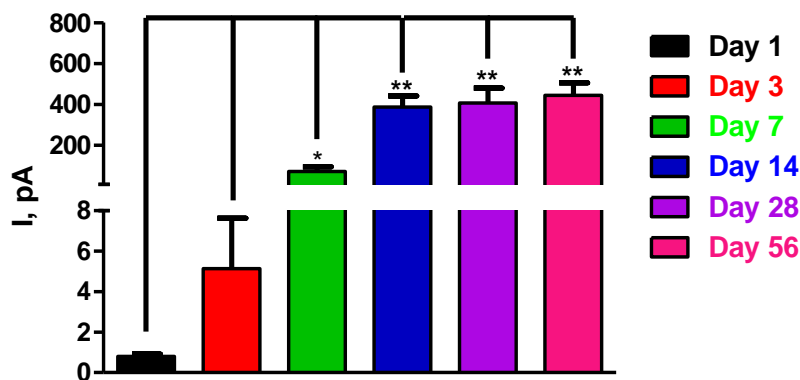


Figure 6.3.8.2.2.3: A bar chart displaying the AA current obtained at a concentration of 1000 μM with Type 2 NO sensors, ($n = 3$), at +900 mV vs. SCE.

The repeated calibrations undertaken with the Type 2 NO sensors ($n = 3$), using the storage condition of N₂ saturated PBS, yielded currents at 1000 μM AA concentration (day 56) of 444 ± 61 pA. This result depicts the deterioration of the electrode surface PPD layer due to the consecutive calibrations carried out on the sensors. From day 7 there was a significant difference (see Table 6.3.8.2.2.3 (b)) in the AA response obtained with the sensors. The characteristic trend of an increasing AA response was observed also.

Day	P value	Significance
1 vs. 3	0.1585	ns
1 vs. 7	0.0402	*
1 vs. 14	0.0020	**
1 vs. 28	0.0050	**
1 vs. 56	0.0019	**

Table 6.3.8.2.2.3 (b): A summary displaying the *P* values obtained for the Type 2 NO sensors over 56 days at 4 °C in an enclosed container with N₂ saturated PBS.

6.3.8.2.2.4 Storage: Fridge at 4 °C (Enclosed container with N₂ Saturated PBS)

[AA], μM	Day 1		Day 56		Day 168	
	Mean I, pA	SEM	Mean I, pA	SEM	Mean I, pA	SEM
1000	-1	4	85	29	780	211

Table 6.3.8.2.2.4: Average AA responses at 1000 μM obtained from calibrations using Type 2 NO sensors (*n* = 4), on day 1 to day 56, carried out at +900 mV vs. SCE. Background values subtracted. Mean background current = 62 ± 6 pA (day 1), 54 ± 5 pA (day 56) and 2578 ± 1611 pA (day 168).

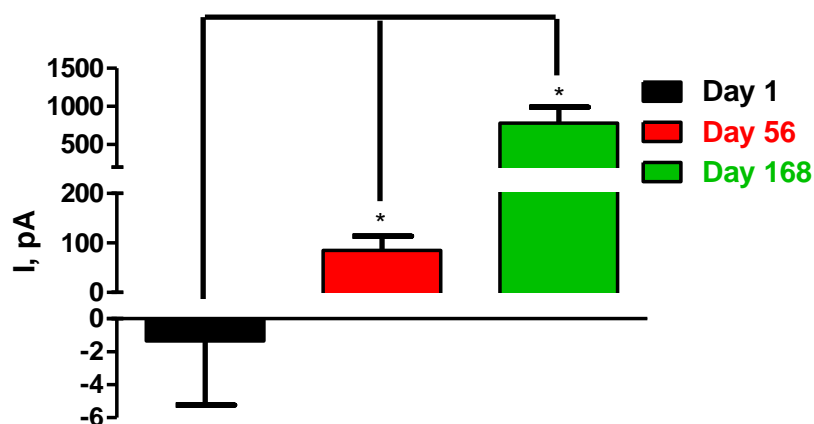


Figure 6.3.8.2.2.4: A bar chart displaying the AA current obtained at a concentration of 1000 μM with Type 2 NO sensors, (*n* = 4), at +900 mV vs. SCE.

The results recorded with the N₂ saturated PBS storage environment, showed a greater increase in the AA response that was significantly different (day 56, $P = 0.0257$) and (day 168, $P = 0.0100$), in comparison to storing the sensors dry in the fridge at 4 °C. These results obtained, still depict good stability over long periods of time. A result of 444 ± 61 pA on day 56 for the repeated calibrations in comparison to 85 ± 29 pA for the once off calibrations on day 56 really highlights the damage caused to the sensors properties when calibrated repeatedly, whilst once off calibrations show a more accurate result of degradation to the sensor. Type 3 NO sensors were subsequently studied in the same manner as the previous sensors discussed in this chapter.

6.3.8.2.3 Type 3 NO Sensor

6.3.8.2.3.1 Storage: Fridge at 4 °C (Enclosed container)

Day	[AA], 1000 μ M	
	Mean I, pA	SEM
1	2	10
3	8	1
7	473	156
14	1328	408
28	2231	594
56	4434	665

Table 6.3.8.2.3.1 (a): Average AA responses at 1000 μ M obtained from calibrations using Type 3 NO sensors ($n = 4$), on day 1 to day 56, carried out at +900 mV vs. SCE. Background values subtracted. Mean background current = 69 ± 8 pA (Day 1), 18 ± 1 pA (Day 3), 83 ± 35 pA (Day 7), 72 ± 31 pA (Day 14), 183 ± 16 pA (Day 28) and 221 ± 13 pA (Day 56).

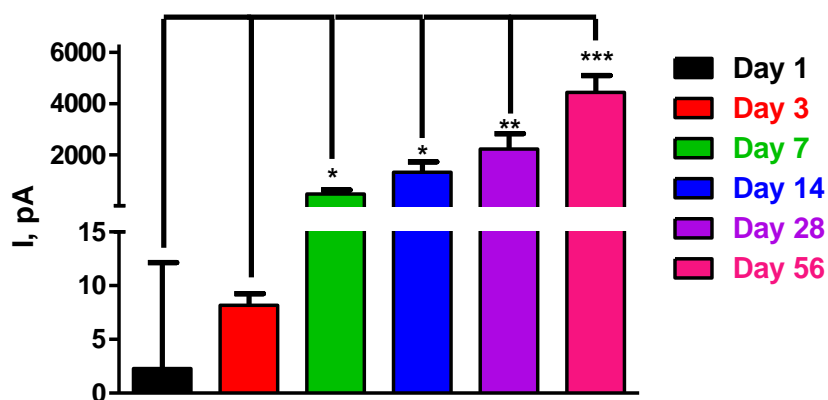


Figure 6.3.8.2.3.1: A bar chart displaying the AA currents obtained at a concentration of 1000 μM with Type 3 NO sensors, (n = 4), at +900 mV vs. SCE.

The Type 3 NO sensors displayed a current of 4434 ± 665 pA (day 56); this result was not out of the ordinary as this trend had been observed with the other sensors. Table 6.3.8.2.3.1 (b) depicts a summary of the *P* values.

Day	<i>P</i> value	Significance
1 vs. 3	0.5742	ns
1 vs. 7	0.0236	*
1 vs. 14	0.0175	*
1 vs. 28	0.0095	**
1 vs. 56	0.0006	***

Table 6.3.8.2.3.1 (b): A summary displaying the *P* values obtained for the Type 3 NO sensors over 56 days at 4 °C in an enclosed container with N₂ saturated PBS.

Less frequent calibrations are depicted in Figure 6.3.8.2.3.2 and Table 6.3.8.2.3.2 for this storage condition using the Type 3 NO sensors.

6.3.8.2.3.2 Storage: Fridge at 4 °C (Enclosed container)

[AA], μM	Day 1		Day 56		Day 168	
	Mean I, pA	SEM	Mean I, pA	SEM	Mean I, pA	SEM
1000	3	1	1	1	-32	7

Table 6.3.8.2.3.2: Average AA responses at 1000 μM obtained from calibrations using Type 3 NO sensors ($n = 4$), on day 1 to day 168, carried out at +900 mV vs. SCE. Background values subtracted.

Mean background current = 19 ± 1 pA (Day 1), 27 ± 2 pA (Day 56) and 758 ± 19 pA (Day 168).

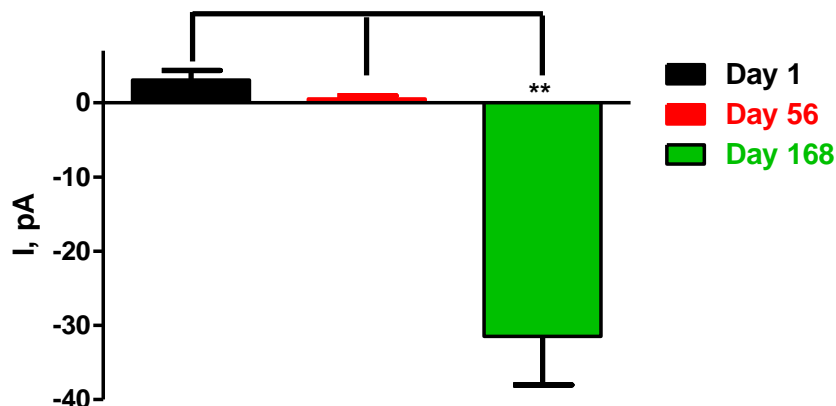


Figure 6.3.8.2.3.2: A bar chart displaying the AA sensitivity obtained at a concentration of 1000 μM with Type 3 NO sensors, ($n = 4$), at +900 mV vs. SCE.

The AA currents observed with the Type 3 NO sensors over the course of 56 days demonstrated a minuscule response that was deemed negligible ($P = 0.1435$). On day 168 a significant difference was recorded ($P = 0.0021$), however, no AA response was detected with the Type 3 NO sensors. After approximately 6 months stored in the fridge in an enclosed container, this was a remarkable result. This storage condition seemed to be the optimal state for the sensors to be stored in.

6.3.8.2.3.3 Storage: Fridge at 4 °C (Enclosed container with N₂ Saturated PBS)

Day	[AA], 1000 μ M	
	Mean I, pA	SEM
1	-6	2
3	4	28
7	4344	915
14	4303	1556
28	4642	1105
56	3937	781

Table 6.3.8.2.3.3 (a): Average AA responses at 1000 μ M obtained from calibrations using Type 3 NO sensors ($n = 4$), on day 1 to day 56, carried out at +900 mV vs. SCE. Background values subtracted. Mean background current = 74 ± 9 pA (Day 1), 87 ± 28 pA (Day 3), 168 ± 33 pA (Day 7), 71 ± 19 pA (Day 14), 502 ± 248 pA (Day 28) and 1692 ± 784 pA (Day 56).

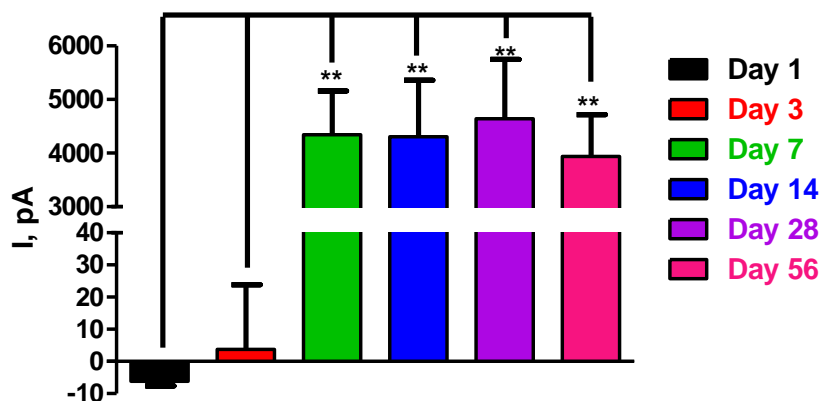


Figure 6.3.8.2.3.3: Average AA responses at 1000 μ M obtained from calibrations using Type 3 NO sensors ($n = 4$), on Day 1 to day 56, carried out at +900 mV vs. SCE.

The repeated calibrations depicted above in Figure 6.3.8.2.3.3, demonstrate that the more one calibrates the sensor, the quicker the sensor deteriorates. Table 6.3.8.2.3.3 (b), details the P values for all the days calibrated with the Type 3 NO sensor.

Day	<i>P</i> value	Significance
1 vs. 3	0.6405	ns
1 vs. 7	0.0018	**
1 vs. 14	0.0065	**
1 vs. 28	0.0056	**
1 vs. 56	0.0023	**

Table 6.3.8.2.3.3 (b): A summary displaying the *P* values obtained for the Type 3 NO sensors over 56 days at 4 °C in an enclosed container with N₂ saturated PBS.

After day 3, a greater AA detection is obvious. In Figure 6.3.8.2.3.4 fewer calibrations were carried out on the Type 3 NO sensors. An AA detection that is much lower than the observed AA response for the repeated calibrations at day 56 is obtained.

6.3.8.2.3.4 Storage: Fridge at 4 °C (Enclosed container with N₂ Saturated PBS)

[AA], μM	Day 1		Day 56		Day 168	
	Mean I, pA	SEM	Mean I, pA	SEM	Mean I, pA	SEM
1000	4	1	246	71	696	112

Table 6.3.8.2.3.4: Average AA responses at 1000 μM obtained from calibrations using Type 3 NO sensors (*n* = 4), on day 1 to day 68, carried out at +900 mV vs. SCE. Background values subtracted. Mean background current = 7 ± 1 pA (day 1), 53 ± 5 pA (day 56) and 996 ± 46 pA (day 168).

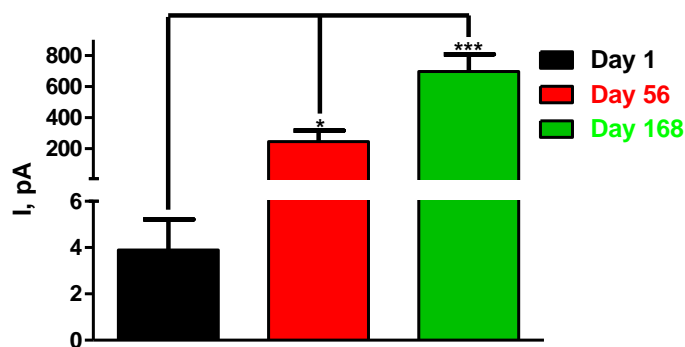


Figure 6.3.8.2.3.4: Average 1000 μM AA responses obtained from calibrations using Type 3 NO sensors ($n = 4$), on day 1 to day 56, carried out at +900 mV vs. SCE.

It is clear from the results depicted in Figure 6.3.8.2.3.4, that keeping the sensors in a N_2 saturated PBS environment does not retain the stability of the sensors, in comparison to keeping the sensors in a dry environment. A significant difference in the AA response was attained on day 56 ($P = 0.0140$) and day 168 (0.0005). A higher AA response was recorded at day 56 (246 ± 71 pA) whereas the dry environment at day 56 yielded an AA response of 1 ± 1 pA at 1000 μM . After compiling and discussing all of the results that have been illustrated for each of the sensors in these sections, it was decided that the most favourable storage for all the sensors would be enclosed in a container in the fridge at 4 °C.

6.3.9 Stability of the NO sensitivity of Type 2 NO sensors over time

Table 6.3.9 and Figure 6.3.9 display the NO sensitivities on day 1 and after 56 days for Type 2 NO sensors ($n = 10$). Sensitivities of 945 ± 12 pA/ μM (day 1) and 859 ± 18 pA/ μM (day 56) were obtained. As the optimum storage condition was chosen in the previous section to be an enclosed container at 4 °C for all the different types of NO sensors, that storage condition was therefore utilised as the one to carry on with throughout the research. There was a slight decrease in the NO sensitivity after 56 days but this did not yield a significant difference ($P = 0.7739$). A linear response was also attained at day 1 and day 56 ($R^2 = 0.99$).

[NO], μM	Type 2 NO Sensor Day 1 ($n = 10$)		Type 2 NO Sensor Day 56 ($n = 10$)	
	Mean I, pA	SEM	Mean I, pA	SEM
0.0	0	0	0	0
0.2	176	24	158	18
0.4	377	43	351	49
0.6	571	69	538	84
0.8	763	93	688	117
1.0	932	120	847	144

Table 6.3.9: Average AA responses at 0 - 1 μM obtained from calibrations using Type 2 NO sensor ($n = 4$), on day 1 to day 56, carried out at +900 mV vs. SCE. Background values subtracted. Mean background current = 204 ± 63 pA (day 1) and 425 ± 149 pA (day 56).

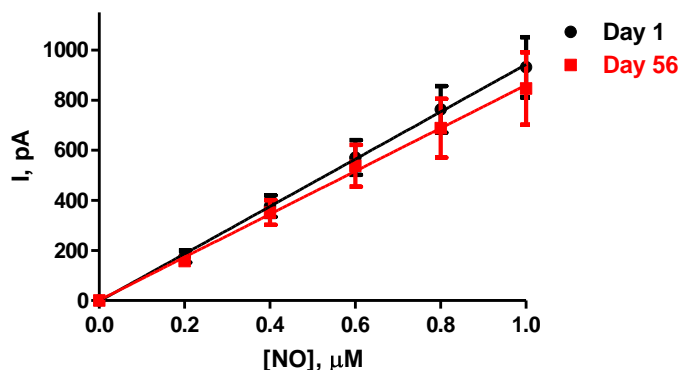


Figure 6.3.9: A current-concentration profile displaying the NO sensitivities obtained day 1 to day 56 with the Type 2 NO sensors ($n = 4$), carried out at +900 mV vs. SCE.

6.3.10 Stability of the NO sensitivity of Type 3 NO sensors over time

The NO responses recorded at the Type 3 NO sensors day 1 to day 56 are displayed in Table 6.3.10 and Figure 6.3.10. There was an increase in the NO after 56 days which demonstrates that the sensor not only can retain a stable PPD layer over time (see Section 6.3.8.2.3.2), but can retain the ability to detect NO over time also. The sensitivities were not significant day 1 to day 56 ($P = 0.1580$). A linear response was obtained at day 1 and day 56 ($R^2 = 0.99$).

[NO], μM	Type 3 NO Sensor Day 1 ($n = 11$)		Type 3 NO Sensor Day 56 ($n = 11$)	
	Mean I, pA	SEM	Mean I, pA	SEM
0.0	0	0	0	0
0.2	135	18	187	24
0.4	295	35	375	43
0.6	443	51	565	60
0.8	586	71	702	85
1.0	719	94	881	111

Table 6.3.10: Average 1 μM AA responses obtained from calibrations using Type 3 NO sensors ($n = 11$), on day 1 to day 56, carried out at +900 mV vs. SCE. Background values subtracted. Mean background current = 227 ± 33 pA (day 1) and 557 ± 157 pA (day 56).

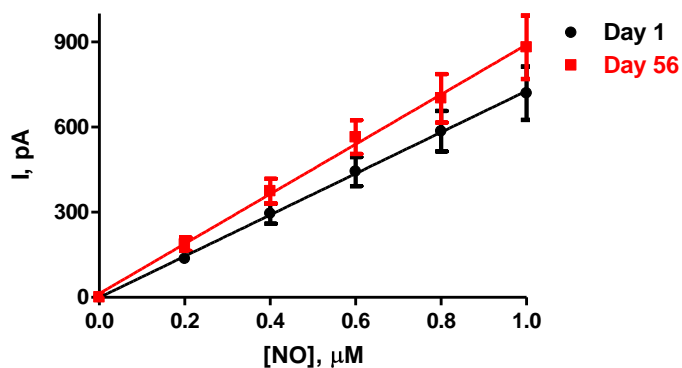


Figure 6.3.10: A current-concentration profile displaying the NO sensitivities obtained day 1 to day 56 with the Type 3 NO sensors ($n = 11$), carried out at +900 mV vs. SCE.

Following these results, interference studies were carried out in order to determine the selectivity of the sensor.

6.3.11 Interference studies Type 2 and Type 3 NO Sensor

Brown *et al.*, carried out interference studies which compared bare Pt electrodes and Type 1 NO sensors against a range of potential endogenous electroactive interferents at reported physiological concentrations (Brown *et al.*, 2009). They found that there was little or no detection of the chosen analytes at the Type 1 NO sensor; however, the bare Pt electrode detected the different analytes due to a lack of a rejection membrane to block out any of the electroactive species. The same analytes were chosen to test against the Type 2 and Type 3 NO sensors, which will be discussed in this section. A working potential of + 900 mV *vs.* SCE was utilised, as this was the potential employed for the NO sensors for the detection of NO and would be the potential required for the NO *in-vivo* studies.

6.3.11.1 [5-HT] Serotonin Type 2 and Type 3 NO sensor

[5-HT], μM	Type 2 NO Sensor ($n = 4$)		Type 3 NO Sensor ($n = 3$)	
	Mean I, pA	SEM	Mean I, pA	SEM
0.000	0	0	0	0
0.004	-3	4	9	11
0.008	-7	9	15	19
0.012	-9	11	14	19
0.016	-12	15	14	20
0.020	-16	20	12	19

Table 6.3.11.1: An averaged table of results displaying a 5-HT calibration in PBS (pH 7.4), at +900 mV *vs.* SCE, carried out on Type 2 ($n = 4$) and Type 3 NO Sensors ($n = 4$). Background values subtracted.

Mean background current of Type 2 NO and Type 3 NO Sensor = 650 ± 75 pA and 707 ± 107 pA, respectively.

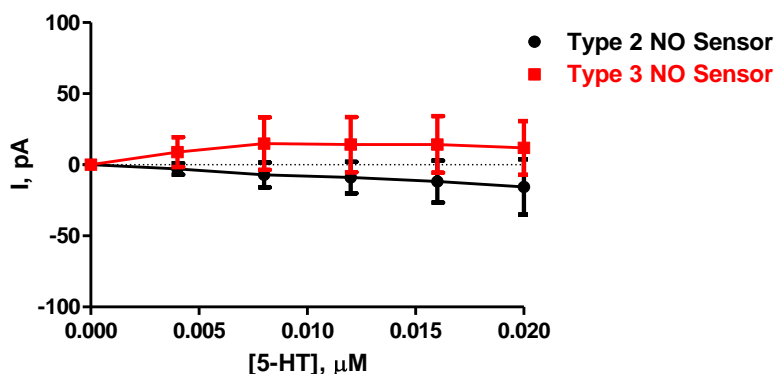


Figure 6.3.11.1: A current-concentration profile displaying a 5-HT calibration in PBS (pH 7.4), at +900 mV vs. SCE, carried out on Type 2 ($n = 4$) and Type 3 NO Sensors ($n = 4$).

5-HT (Serotonin) is an important derivative of the amino acid L-tryptophan (Sidransky, 2010). The ECF concentration of 5-HT is between 1 and 10 nM (O'Neill & Lowry, 2000). 5-HT is positively charged at pH 7 (Chattopadhyay *et al.*, 1996) which is of concern for a Nafion[®] modified sensor, as Nafion[®] possesses a negative charge which would lead to an ion exchange membrane accommodating species that encompass a positive charge. Since the two NO sensors described in this section contain not only Nafion[®] but a PPD layer, this concern is diminished. At a concentration of 0.020 μM , negligible currents of -15.6 ± 19.5 pA and 54.0 ± 43.2 pA for Type 2 and Type 3 NO sensors were obtained. This suggests that this interferent would not prove problematic for the NO sensors described in this body of work. Subsequent to this, DOPAC calibrations were carried out.

6.3.11.2[DOPAC] Type 2 and Type 3 NO sensor

[Dopac], μM	Type 2 NO Sensor ($n = 4$)		Type 3 NO Sensor ($n = 4$)	
	Mean I, pA	SEM	Mean I, pA	SEM
0	0	0	0	0
10	-10	23	5	4
20	-10	29	4	8
30	-7	30	1	10
40	-7	31	-4	10
50	-6	32	-5	12

Table 6.3.11.2: An averaged table of results displaying a DOPAC calibration in PBS (pH 7.4), at +900 mV vs. SCE, carried out on Type 2 ($n = 4$) and Type 3 NO Sensors ($n = 4$). Background values subtracted. Mean background current of Type 2 NO and Type 3 NO Sensor = 675 ± 138 pA and 575 ± 60 pA, respectively.

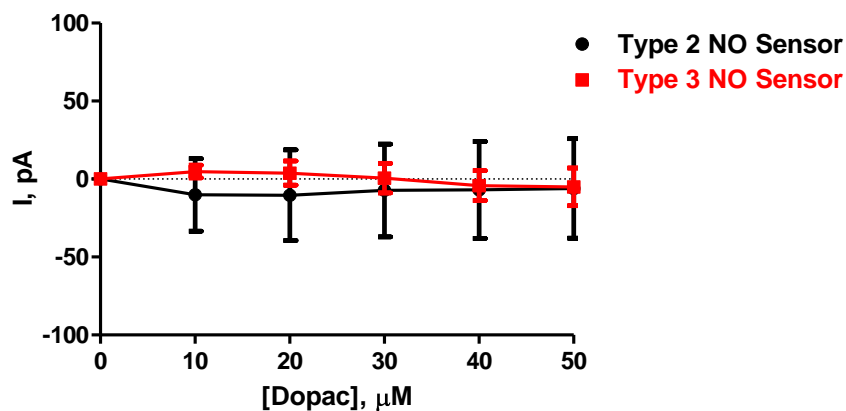


Figure 6.3.11.2: A current-concentration profile displaying a DOPAC calibration in PBS (pH 7.4), at +900 mV vs. SCE, carried out on Type 2 ($n = 4$) and Type 3 NO Sensors ($n = 4$).

DOPAC is a metabolite of dopamine (Wallace & Traeger, 2012). The ECF concentration of DOPAC is approximately 1 to 20 μM (O'Neill & Lowry, 2000). It contains a negative charge (Lowry *et al.*, 1996; O'Neill *et al.*, 1998) and so should be repelled by the negatively charged Nafion[®] layer. The DOPAC currents obtained were insignificant. At a

concentration of 50 μM , currents of -6 ± 32 pA (Type 2 NO sensor) and -5 ± 12 pA (Type 3 NO sensor) were observed, highlighting how capable the sensor is at blocking this interferent from being detected. A negative current is obtained due to a slight drift in current below the background current.

6.3.11.3[Dopamine] Type 2 and Type 3 NO sensor

Dopamine is a very important neurotransmitter that is implicated in Parkinson's disease (Wightman *et al.*, 1988). The brain ECF concentration of dopamine is around 1 to 50 nM (O'Neill & Lowry, 2000). Table 6.3.11.3 and Figure 6.3.11.3 display the currents obtained at a concentration of 1.0 μM for the two sensors.

[Dopamine], μM	Type 2 NO Sensor ($n = 4$)		Type 3 NO Sensor ($n = 6$)	
	Mean I, pA	SEM	Mean I, pA	SEM
0.0	0	0	0	0
0.2	-3	1	-6	8
0.4	-6	3	-1	6
0.6	-6	4	5	5
0.8	-2	4	5	6
1.0	5	3	8	7

Table 6.3.11.3: An averaged table of results displaying a dopamine calibration in PBS (pH 7.4), at +900 mV vs. SCE, carried out on Type 2 ($n = 4$) and Type 3 NO Sensors ($n = 6$). Background values subtracted. Mean background current of Type 2 NO and Type 3 NO Sensor = 564 ± 132 pA and 396 ± 58 pA, respectively.

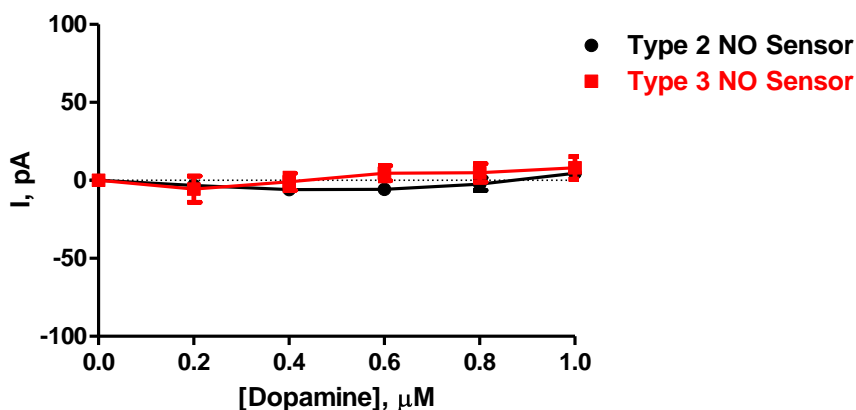


Figure 6.3.11.3: A current-concentration profile displaying a dopamine calibration in PBS (pH 7.4), at +900 mV vs. SCE, carried out on Type 2 ($n = 4$) and Type 3 NO Sensors ($n = 6$).

It can be seen from Figure 6.3.11.3 that there was a slight dopamine response from the sensors after injecting a concentration of 1.0 μM into the electrochemical cell. The dopamine results achieved for Type 2 and Type 3 NO sensors would not cause a problem for the detection of the chosen analyte NO as the detection is miniscule.

6.3.11.4 [Glutathione] Type 2 and Type 3 NO sensor

Glutathione is a key substance found to play a role in antioxidant defence, nutrient metabolism and the regulation of cellular events. It has an ECF concentration of approximately 50 μM . Insufficient glutathione contributes to oxidative stress which in turn has a role in the pathogenesis of some diseases (Wu *et al.*, 2004). It also partakes in the transport of some amino acids across membranes in the kidneys (Chailapakul *et al.*, 2001). Table 6.3.11.4 and Figure 6.3.11.4 illustrate the currents recorded for the two sensors.

[Glutathione], μM	Type 2 NO Sensor ($n = 4$)		Type 3 NO Sensor ($n = 4$)	
	Mean I, pA	SEM	Mean I, pA	SEM
0	0	0	0	0
20	-2	1	-1	2
40	-2	2	-6	4
60	-1	4	-6	6
80	1	5	-5	8
100	2	6	9	14

Table 6.3.11.4: An averaged table of results displaying a glutathione calibration in PBS (pH 7.4), at +900 mV vs. SCE, carried out on Type 2 ($n = 4$) and Type 3 NO Sensors ($n = 4$). Background values subtracted. Mean background current of Type 2 NO and Type 3 NO Sensor = 467 ± 47 pA and 434 ± 71 pA, respectively.

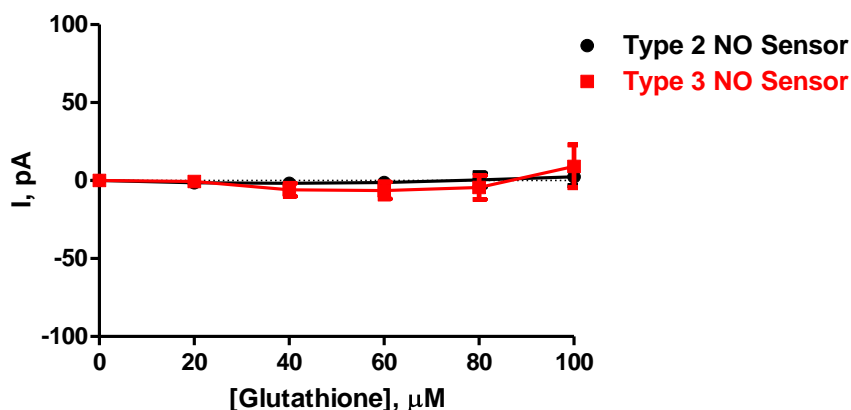


Figure 6.3.11.4: A current-concentration profile displaying a glutathione calibration in PBS (pH 7.4), at +900 mV vs. SCE, carried out on Type 2 ($n = 4$) and Type 3 NO Sensors ($n=4$).

The results displayed a slight change in the observed current upon additions of glutathione into the cell. A current of 2 ± 6 pA and 9 ± 14 pA was recorded at 100 μM for the Type 2 and Type 3 NO sensors, respectively. Therefore, glutathione would not hamper the sensors ability to detect the analyte NO.

6.3.11.5 [H₂O₂] Type 2 and Type 3 NO sensor

H₂O₂ is an important species that plays a role in cell signalling pathways that are essential for a living organism's development, growth and well being. However, disparity of H₂O₂ production can lead to oxidative stress which can initiate damage to tissues and organs (Van de Bittner *et al.*, 2010). H₂O₂ is a neutral molecule that can be oxidised at a similar potential to NO (Zhang *et al.*, 2002a) and has an ECF concentration of approximately 1.0 μM, however this could be an over estimation of the H₂O₂ concentration, due to excess levels being produced following tissue damage caused by the large size of the probe.

[H ₂ O ₂], μM	Type 2 NO Sensor (n = 4)		Type 3 NO Sensor (n = 4)	
	Mean I, pA	SEM	Mean I, pA	SEM
0	0	0	0	0
1	8	2	-6	7
2	14	2	37	20
5	36	5	94	57
10	69	6	161	77
20	153	12	212	82
50	428	25	341	90
100	848	53	562	98

Table 6.3.11.5: An averaged table of results displaying a H₂O₂ calibration in PBS (pH 7.4), at +900 mV vs. SCE, carried out on Type 2 (n = 4) and Type 3 NO Sensors (n = 4). Background values subtracted.

Mean background current of Type 2 NO and Type 3 NO Sensor = 538 ± 42 pA and 231 ± 21 pA, respectively.

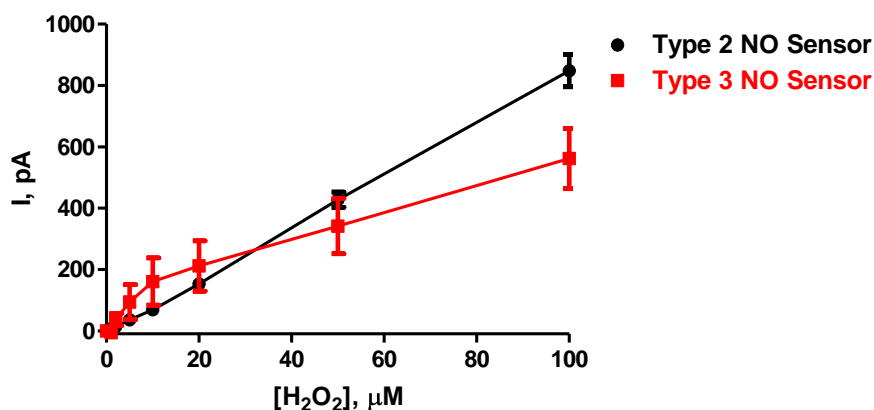


Figure 6.3.11.5: A current-concentration profile displaying a H₂O₂ calibration in PBS (pH 7.4), at +900 mV vs. SCE, carried out on Type 2 ($n = 4$) and Type 3 NO Sensors ($n = 4$).

The maximum current detected by the Type 2 and Type 3 NO sensor was 848 ± 53 pA and 562 ± 98 pA, respectively at 100 μM concentration of H₂O₂. This is a very high detection and would cause problems if this was the concentration found in the brain, however, since the H₂O₂ concentration in the brain is around 1 to 3 μM (Bedioui & Griveau, 2013) and this concentration value could be an overestimation due to tissue damage causing an increased H₂O₂ concentration, H₂O₂ would not hamper the electrodes ability to detect NO successfully.

6.3.11.6[5-HIAA] Type 2 and Type 3 NO sensor

5-HIAA is the main metabolite of 5-HT and has been utilised as a measurement tool in order to determine if a patient has carcinoid syndrome (Lee *et al.*, 2000). 5-HIAA possesses a much greater ECF concentration than NO and therefore could potentially become a problem. At an estimated range of 1 to 10 μM , it would be a cause of concern for the NO sensor (Lowry *et al.*, 1996; O'Neill *et al.*, 1998).

[5-HIAA], μM	Type 2 NO Sensor ($n = 4$)		Type 3 NO Sensor ($n = 4$)	
	Mean I, pA	SEM	Mean I, pA	SEM
0	0	0	0	0
20	-8e-01	3	0	4
40	-3	7	-1	5
60	-5	9	-1	4
80	-2	16	-4	5
100	-6	16	-2	6

Table 6.3.11.6: An averaged table of results displaying 5-HIAA calibrations in PBS (pH 7.4), at +900 mV vs. SCE, carried out on Type 2 ($n = 4$) and Type 3 NO Sensors ($n = 4$). Background values subtracted. Mean background current of Type 2 NO and Type 3 NO Sensor = 627 ± 65 pA and 458 ± 75 pA, respectively.

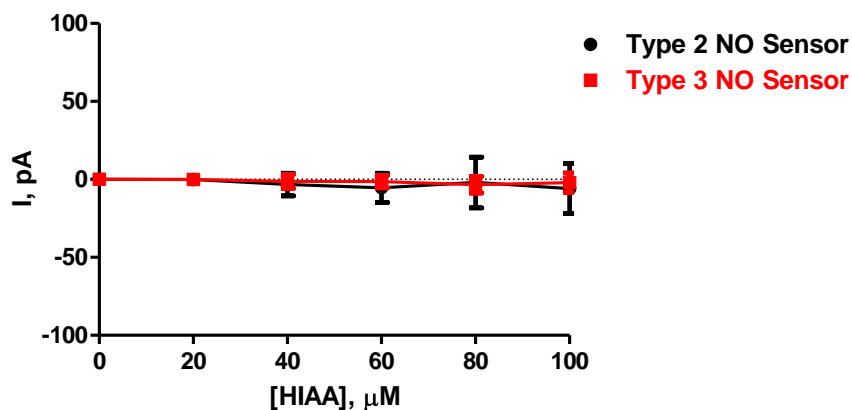


Figure 6.3.11.6: A current-concentration profile displaying a HIAA calibration in PBS (pH 7.4), at +900 mV vs. SCE, carried out on Type 2 ($n = 4$) and Type 3 NO Sensors ($n = 4$).

The design of the Type 2 and Type 3 NO sensors demonstrated a great ability to block interferences from this analyte. Currents of -6 ± 16 pA and -2 ± 6 pA for the Type 2 and Type 3 NO sensors, respectively, were obtained. Negative currents were achieved due to baseline drift.

6.3.11.7[HVA] Type 2 and Type 3 NO sensor

HVA is a metabolite of dopamine (Kopin *et al.*, 1988). Monitoring urinary levels of HVA has been utilised as a means of neuroblastoma tumour detection (Jones, 2010). The ECF concentration of HVA is approximately 1 to 10 μM which is greater than the concentrations observed for NO which could increase the risk of potential interference of the NO signal.

[HVA], μM	Type 2 NO Sensor ($n = 3$)		Type 3 NO Sensor ($n = 4$)	
	Mean I, pA	SEM	Mean I, pA	SEM
0	0	0	0	0
5	-21	17	-1	13
10	-27	18	2	21
15	-28	19	7	30
20	-30	20	7	32
25	-13	7	6	33

Table 6.3.11.7: An averaged table of results displaying a HVA calibration in PBS (pH 7.4), at +900 mV vs. SCE, carried out on Type 2 ($n = 4$) and Type 3 NO Sensors ($n = 4$). Background values subtracted. Mean background current of Type 2 NO and Type 3 NO Sensor = 580 ± 151 pA and 725 ± 249 pA, respectively.

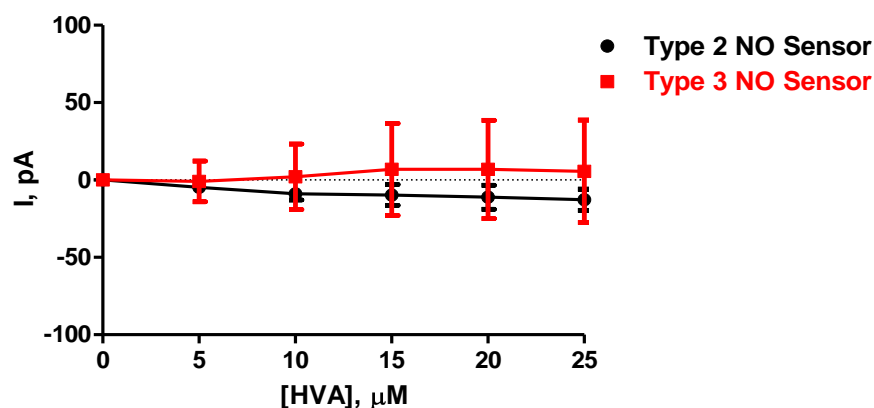


Figure 6.3.11.7: A current-concentration profile displaying a HVA calibration in PBS (pH 7.4), at +900 mV vs. SCE, carried out on Type 2 ($n = 4$) and Type 3 NO Sensors ($n = 4$).

The results recorded at the Type 2 and Type 3 NO sensors for the HVA calibration would not prove problematic as they are negligible. A negative current of -33 ± 21 pA was observed from the Type 2 NO sensors ($n = 4$) and 6 ± 33 pA was attained by the Type 3 NO sensors ($n = 4$).

6.3.11.8 [NO₂⁻] Type 2 and Type 3 NO sensor

NO₂⁻ is an interferent that causes great concern for the detection of NO at an electrochemical sensor. However, due to the negatively charged attribute of Nafion[®], the NO₂⁻ is repelled making NO detection possible (Katrлік & Zálešáková, 2002). Linear regression was carried out on the Type 2 and Type 3 NO sensors yielding sensitivities of 0.072 ± 0.002 pA/ μ M and 0.032 ± 0.005 pA/ μ M, respectively. With an ECF concentration in the brain of 100 μ M, this would yield miniscule interference from NO₂⁻.

	Type 2 NO Sensor ($n = 4$)		Type 3 NO Sensor ($n = 6$)	
[NO ₂ ⁻], μ M	Mean I, pA	SEM	Mean I, pA	SEM
0	0	0	0	0
200	12	5	1	2
400	30	8	6	3
600	41	12	12	6
800	59	15	20	8
1000	71	20	33	14

Table 6.3.11.8: An averaged table of results displaying an NO₂⁻ calibration in PBS (pH 7.4), at +900 mV vs. SCE, carried out on Type 2 ($n = 4$) and Type 3 NO Sensors ($n = 6$). Background values subtracted.

Mean background current of Type 2 NO and Type 3 NO Sensor = 394 ± 38 pA and 482 ± 125 pA, respectively.

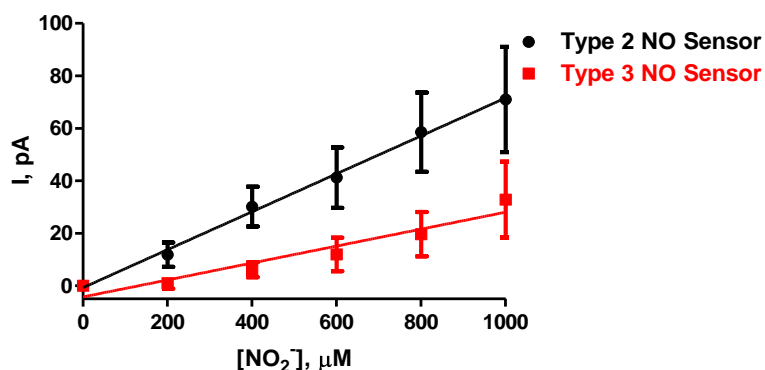


Figure 6.3.11.8: A current-concentration profile displaying a NO_2^- calibration in PBS (pH 7.4), at +900 mV vs. SCE, carried out on Type 2 ($n = 4$) and Type 3 NO Sensors ($n = 4$).

The currents observed after injecting 1000 μM concentration of NO_2^- into the electrochemical cell were very small and would not cause any issues to arise when detecting NO. Linear regression analysis was carried out on the Type 2 and Type 3 NO sensors to reveal sensitivities of 0.07 ± 0.002 pA/ μM and 0.03 ± 0.005 pA/ μM , respectively. The response was linear for Type 2 NO sensors ($R^2 = 0.99$) and Type 3 NO sensors ($R^2 = 0.92$). These sensitivities are very small and negligible.

6.3.11.9[Uric acid] Type 2 and Type 3 NO sensor

Uric acid is a weak acid that is created during the metabolism of purines. It is also produced by the degradation of xanthine by the enzyme xanthine oxidase (Schrier, 2007). The quantification and determination of uric acid *in-vivo* has been of great importance as an increased urate level has been implicated in medical conditions like leukaemia and pneumonia (Miland *et al.*, 1996). Uric acid is found at much higher concentrations than NO in the ECF of the brain and has an approximate concentration of around 5 to 50 μM (Bedioui & Griveau, 2013). Its presence is due to tissue damage (Duff & O'Neill, 1994).

[Uric Acid], μM	Type 2 NO Sensor ($n = 4$)		Type 3 NO Sensor ($n = 4$)	
	Mean I, pA	SEM	Mean I, pA	SEM
0	0	0	0	0
10	0	2	-6	4
20	0	7	-9	4
30	-6	6	-20	5
40	-10	2	-27	8
50	4	3	-20	6
60	5	2	-11	6

Table 6.3.11.9 (a): An averaged table of results displaying a uric acid calibration in PBS (pH 7.4), at +900 mV vs. SCE, carried out on Type 2 ($n = 3$) and Type 3 NO Sensors ($n = 4$). Background values subtracted. Mean background current of Type 2 NO ($n = 3$) and Type 3 NO Sensor ($n = 4$) = 748 ± 90 pA and 2835 ± 791 pA, respectively.

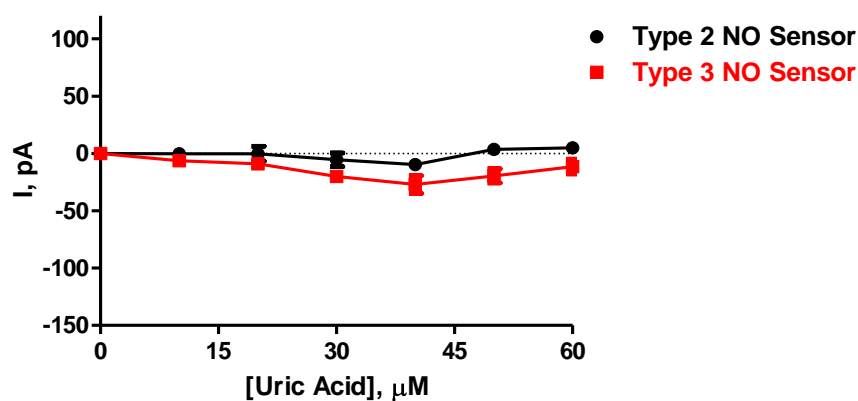


Figure 6.3.11.9: A current-concentration profile displaying a uric acid calibration in PBS (pH 7.4), at +900 mV vs. SCE, carried out on Type 2 ($n = 4$) and Type 3 NO Sensors ($n = 4$).

There was limited or no detection of uric acid at the two sensors (see Figure 6.3.11.9). With this being the last interferent studied, it can be hypothesised that the sensors presented and discussed in this section would be free from interference from other analytes and that the sensor can be deemed selective to NO without concern of interference from other electroactive species.

Analyte	NO Response (pA)		% of NO signal	
	Type 2	Type 3	Type 2	Type 3
NO	1047 ± 34	975 ± 46	100	100
5-HT	-6 ± 6	-18 ± 6	≤ 1	≤ 1
Dopac	-16 ± 20	12 ± 19	≤ 1	≤ 1
Dopamine	-6 ± 32	-5 ± 12	≤ 1	≤ 1
Glutathione	5 ± 3	8 ± 7	≤ 1	≤ 1
H₂O₂	2 ± 6	9 ± 14	≤ 1	≤ 1
5-HIAA	8 ± 2	-6 ± 7	≤ 1	≤ 1
HVA	-6 ± 16	-2 ± 6	≤ 1	≤ 1
NO₂⁻	-13 ± 7	6 ± 33	≤ 1	≤ 1
UA	5 ± 2	-11 ± 6	≤ 1	≤ 1

Table 6.3.11.9 (b): A summary of all the sensitivities of the interferents and their percentage effect on the NO signal.

6.3.12 Biocompatibility

6.3.12.1 Type 2 NO Sensor

In this section the sensors ability to refrain from fouling and modification by interactions in the brain was assessed, as a stable sensor *in-vivo* is of the utmost importance. The environment of the brain contains many harsh variables that may interact with the sensor causing the sensor to underperform under the harsh conditions. Calibrations were undertaken to determine the effect that proteins, lipids and other variables would have on the sensors. The sensors were placed in enclosed containers that included each of the treatments and calibrated approximately one month after placement in each of the solutions. As the PPD layer is the most vulnerable component of the sensor and is essential for the rejection of interferences, AA calibrations were carried out at +900 mV vs. SCE.

AA was chosen as the analyte to utilise because a much clearer result would be obtained from the AA calibrations in comparison to NO calibrations. It has been demonstrated that a similar NO sensitivity is obtained post *in-vivo* studies, however, on analysis of the AA

detection on the same set of sensors post *in-vivo* studies a degradation of the rejection layer on the sensor can be observed (see Section 6.3.15.1 and 6.3.15.2). This confirms the reason to use AA instead of NO as the analyte of choice when determining the biocompatibility of these sensors.

6.3.12.1.1 BSA (10%)

[AA], μM	Type 2 NO Sensor ($n=4$)		Type 2 NO Post BSA (10%) (28 Days) ($n = 4$)	
	Mean I, pA	SEM	Mean I, pA	SEM
0	0	0	0	0
200	40	9	84	15
400	80	10	164	30
600	88	4	239	45
800	91	4	305	60
1000	99	6	369	74

Table 6.3.12.1.1: An averaged table of results displaying AA calibrations in PBS (pH 7.4), at +900 mV vs. SCE, carried out on Type 2 NO Sensors prior to treatment with BSA (10%) and the results obtained post treatment with BSA (10%). Background values subtracted. Mean background current (Type 2 NO Sensor) and Type 2 NO Sensor BSA (10%) = 718 ± 48 pA and 589 ± 88 pA, respectively.

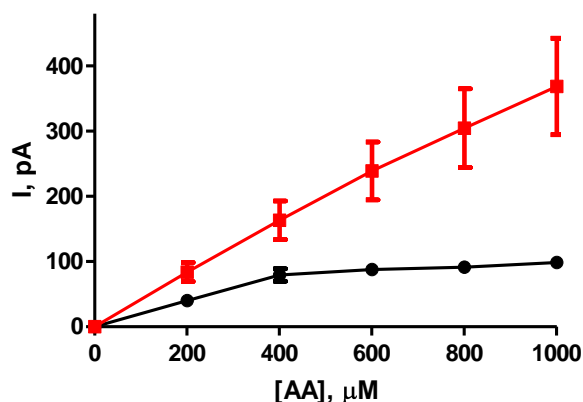


Figure 6.3.12.1.1 (a): Mean current-concentration profile for AA calibrations in PBS at +900 mV vs. SCE using Type 2 NO Sensor pre (black) and post treatment (red) with BSA (10%) (28 Days).

AA calibrations on Type 2 NO sensors ($n = 4$) pre- and post-BSA (10%) (28 days) yielded currents of 99 ± 6 pA and 369 ± 6 pA, respectively at $1000 \mu\text{M}$. The results observed highlighted a significant increase in the detection of AA at the electrodes post BSA (10%) treatment ($P = 0.0297$). This displays a degradation of the PPD layer on the surface of the sensor as more AA is gaining access through the layer to be detected. SEMs are displayed in Figure 6.3.12.1.1 (b) to illustrate the effect that BSA (10%) had on the Type 2 NO sensors.

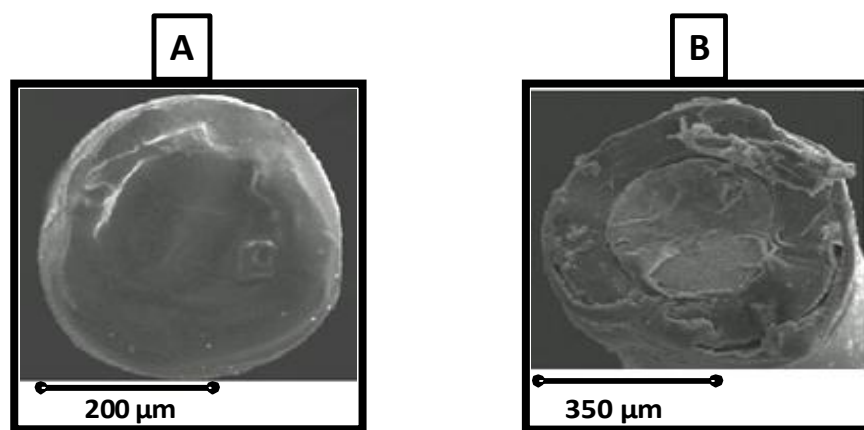


Figure 6.3.12.1.1 (b): An SEM displaying the surface of a Type 2 NO sensor (A) pre BSA (10%) treatment and (B) post treatment with BSA (10%) 28 Days.

It is clear from the image that BSA (10%) caused the PPD layer to be damaged slightly, revealing some of the Pt surface. BSA (10%) is a very harsh concentration to use and would not be encountered in the environment of the brain. One month is also a long time to keep the sensors in this harsh solution.

6.3.12.1.2 PEA (10%)

[AA], μM	Type 2 NO Sensor ($n = 8$)		Type 2 NO Post PEA (10%) (28 Days) ($n = 8$)	
	Mean I, pA	SEM	Mean I, pA	SEM
0	0	0	0	0
200	14	4	66	25
400	24	6	128	59
600	27	9	185	53
800	27	10	243	72
1000	29	13	299	95

Table 6.3.12.1.2: An averaged table of results displaying AA calibrations in PBS (pH 7.4), at +900 mV vs. SCE, carried out on Type 2 NO Sensors prior to treatment with PEA (10%) (28 days) and the results obtained post treatment with PEA (10%) (28 days). Background values subtracted. Mean background current (Type 2 NO Sensor) and (Type 2 NO Sensor PEA (10%) 28 Days) = 610 ± 138 pA and 934 ± 213 pA, respectively.

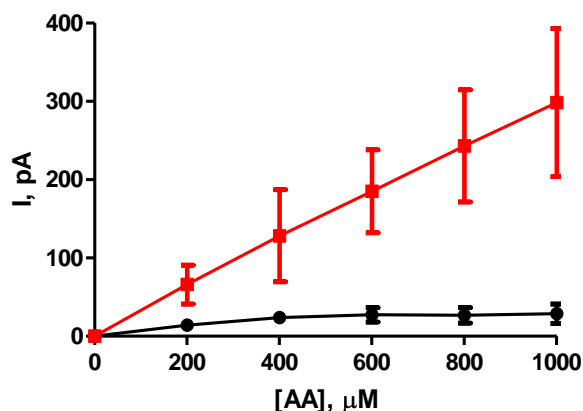


Figure 6.3.12.1.2 (a): Mean current concentration profile for an AA calibration in PBS at +900 mV vs. SCE using Type 2 NO Sensor pre (black) and post treatment (red) with PEA (10%) 28 days.

Currents pre and post PEA (10%) of 29 ± 13 pA and 299 ± 95 pA, respectively, was recorded at the Type 2 NO sensors ($n = 8$). Similar to the BSA (10%) results, a higher detection of AA was obtained at the sensors, yielding a significant increase in AA detection ($P = 0.0234$). Figure 6.3.12.1.2 (b) displays an SEM of the Type 2 NO sensor pre and post treatment with PEA (10%). The surface has been distorted demonstrating the damaging

effect that PEA (10%) had on the sensor over the 28 days. PEA (10%) is a very harsh concentration utilised and would not be found in the *in-vivo* environment. The brain ECF would not contain such high levels of protein and lipids.

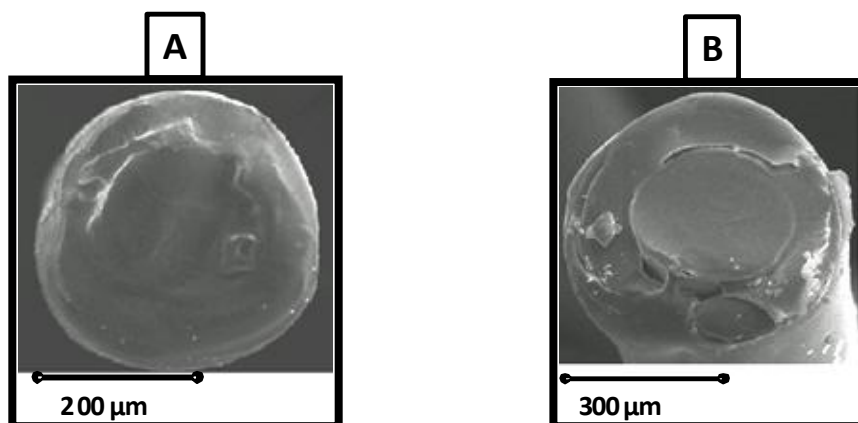


Figure 6.3.12.1.2 (b): An SEM displaying the surface of a Type 2 NO sensor (A) pre PEA (10%) treatment and (B) post PEA (10%) 28 days treatment.

Subsequent to the results obtained with BSA and PEA, it was decided to treat the sensors with *ex-vivo* BT as this treatment encompasses all variables that could potentially harm the sensors ability to detect the chosen analyte NO, and so has the capability to mimic the *in-vivo* environment to a greater extent than just the proteins and lipids.

6.3.12.1.3 BT (28 Days)

[AA], μM	Type 2 NO Sensor ($n = 4$)		Type 2 NO Post BT (28 Days) ($n = 4$)	
	Mean I, pA	SEM	Mean I, pA	SEM
0	0	0	0	0
200	74	55	78	96
400	81	58	213	117
600	87	58	349	127
800	91	60	452	139
1000	103	60	540	152

Table 6.3.12.1.3: An averaged table of results displaying AA calibrations in PBS (pH 7.4), at +900 mV vs. SCE, carried out on Type 2 NO Sensors prior to treatment with BT (28 days) and the results obtained post treatment with BT (28 days). Background values subtracted. Mean background current Type 2 NO Sensor and Type 2 NO Sensor BT (28 days) = 610 ± 138 pA and 934 ± 213 pA, respectively.

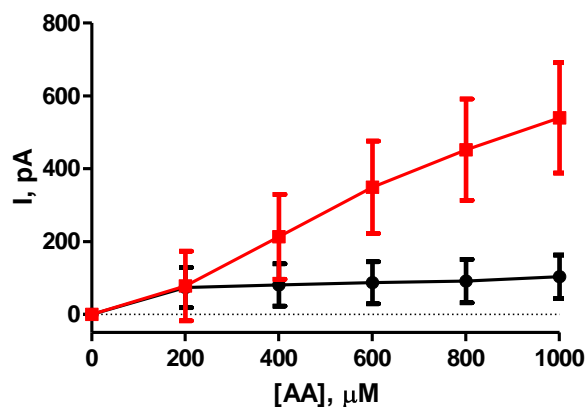


Figure 6.3.12.1.3 (a): Mean current-concentration profile for an AA calibration in PBS at +900 mV vs. SCE using Type 2 NO Sensor pre (black) and post treatment (red) with BT (28 days).

The results obtained for the Type 2 NO sensors post BT (28 days), displayed a much greater detection of AA, which was significantly different from the results observed pre BT ($P = 0.0450$). The PPD rejection layer has been compromised by placing the sensors in BT for a month. The SEM displayed in Figure 6.3.12.1.3 (b), image B, shows a sensor with the

Pt surface showing more, due to the removal of the polymer, leading to a much greater detection of AA.

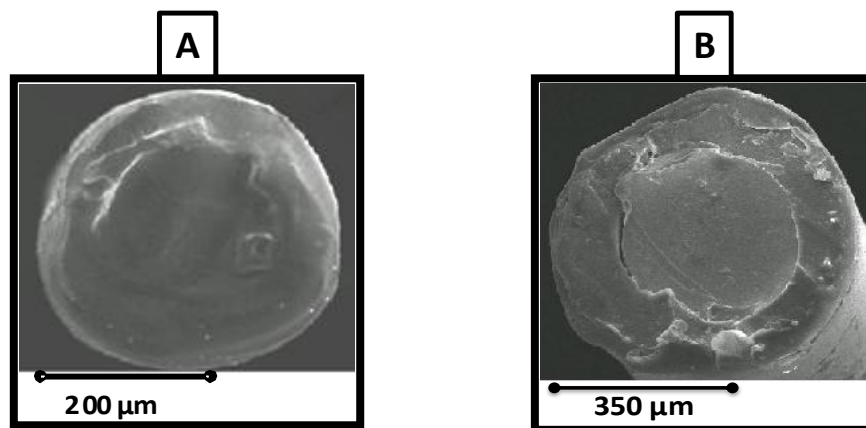


Figure 6.3.12.1.3 (b): An SEM displaying the surface of the Type 2 NO sensor (A) pre BT and (B) post BT (28 Days).

After the results obtained from the Type 2 NO sensors, the same experiments were undertaken with the Type 3 NO sensors, in order to validate how stable the sensors were when being tested against these harsh conditions.

6.3.13 Biocompatibility

6.3.13.1 Type 3 NO Sensor

6.3.13.1.1 BSA (10%)

[AA], μM	Type 3 NO Sensor ($n = 4$)		Type 3 NO Post BSA (10%) (28 Days) ($n = 4$)	
	Mean I, pA	SEM	Mean I, pA	SEM
0	0	0	0	0
200	-11	10	48	13
400	-17	13	101	22
600	-21	15	155	31
800	-25	16	204	40
1000	-29	18	271	48

Table 6.3.13.1.1: An averaged table of results displaying AA calibrations in PBS (pH 7.4), at +900 mV vs. SCE, carried out on Type 3 NO Sensors prior to treatment with BSA (10%) (28 days) and the results obtained post treatment with BSA (10%) (28 days). Background values subtracted. Mean background current (Type 3 NO Sensor) and (Type 3 NO Sensor BSA (10%) (28 days)) = 520 ± 36 pA and 1260 ± 131 pA, respectively.

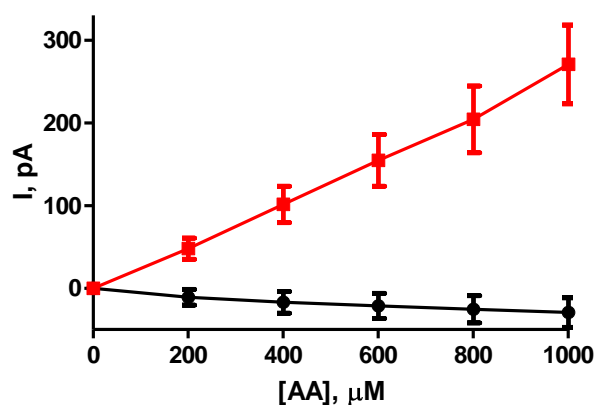


Figure 6.3.13.1.1 (a): Mean current concentration profile for an AA calibration in PBS at +900 mV vs. SCE using Type 3 NO Sensor ($n = 4$) pre (black) and post treatment (red) with BSA (10%) 28 days.

Similar to the results obtained for the Type 2 NO sensors an increase in AA detection was observed at the Type 3 NO sensor. Currents of -29 ± 18 pA and 271 ± 48 pA pre and post treatment with BSA (10%), respectively, was obtained at an AA concentration of $1000 \mu\text{M}$. A significant difference pre and post was obtained ($P = 0.0226$). The SEM in Figure 6.3.13.1.1 (b), image B displays damage to the right side of the sensor which leads to a greater detection of AA.

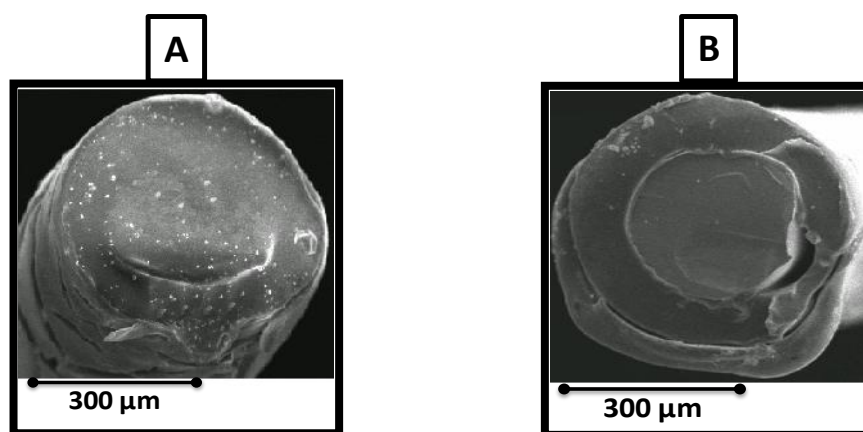


Figure 6.3.13.1.1 (b): An SEM displaying the surface of the Type 3 NO sensor pre- and post-treatment with BSA (10%) 28 days.

6.3.13.1.2 PEA (10%)

[AA], μM	Type 3 NO Sensor ($n = 8$)		Type 3 NO Post PEA (10%) 28 Days ($n = 8$)	
	Mean I, pA	SEM	Mean I, pA	SEM
0	0	0	0	0
200	37	16	101	35
400	27	8	193	64
600	17	9	274	86
800	22	16	338	106
1000	45	43	396	124

Table 6.3.13.1.2: An averaged table of results displaying AA calibrations in PBS (pH 7.4), at +900 mV vs. SCE, carried out on Type 3 NO Sensors ($n = 8$) prior to treatment with PEA (10%) (28 days) and the results obtained post treatment with PEA (10%) (28 days). Background values subtracted. Mean background current (Type 3 NO Sensor) and (Type 3 NO Sensor PEA (10%) 28 days) = 648 ± 206 pA and 776 ± 178 pA, respectively.

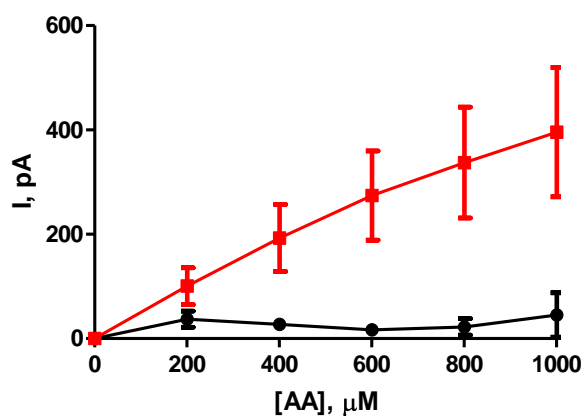


Figure 6.3.13.1.2 (a): Mean current concentration profile for an AA calibration in PBS at +900 mV vs. SCE using Type 3 NO Sensor ($n = 8$) pre- (black) and post-treatment (red) with PEA (10%) 28 days.

Again, analogous results were obtained for the Type 3 NO sensors ($n = 8$) pre and post PEA (10%), as was seen with the Type 2 NO sensors ($n = 8$). An increase in AA detection was seen post PEA treatment yielding a sensitivity of 395.7 ± 123.9 pA and a significant difference ($P = 0.0204$). Figure 6.3.13.1.2 (b), image B, displays the SEM post PEA treatment and it is clear that this treatment alters the surface leading to part of the Pt wire being revealed.

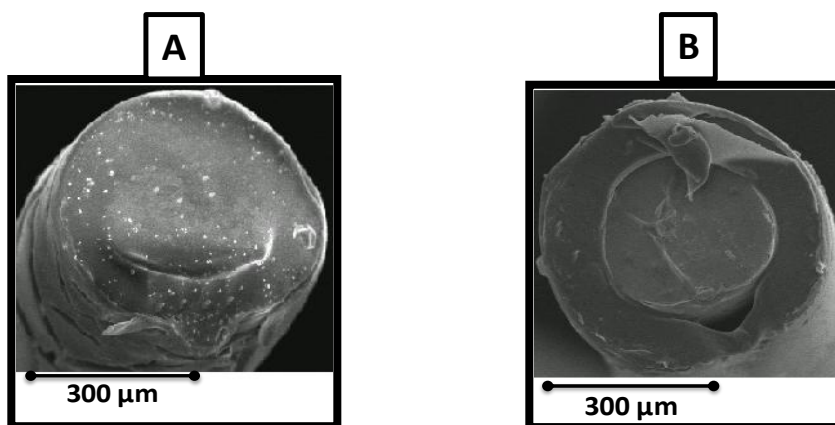


Figure 6.3.13.1.2 (b): An SEM displaying the surface of a Type 3 NO sensor (A) pre PEA (10%) treatment an (B) post PEA (10%) treatment.

6.3.13.1.3 *BT (28 Days)*

[AA], μM	Type 3 NO Sensor ($n = 8$)		Type 3 NO Post BT (28 Days) ($n = 8$)	
	Mean I, pA	SEM	Mean I, pA	SEM
0	0	0	0	0
200	32	12	116	28
400	27	6	226	52
600	21	8	324	71
800	25	13	404	89
1000	42	32	480	106

Table 6.3.13.1.3: An averaged table of results displaying AA calibrations in PBS (pH 7.4), at +900 mV vs. SCE, carried out on Type 3 NO Sensors ($n = 8$) prior to treatment with BT (28 days) and the results obtained post treatment with BT (28 days). Background values subtracted. Mean background current Type 3 NO Sensor and Type 3 NO Sensor BT (28 Days) = 650 ± 75 pA and 707 ± 107 pA, respectively.

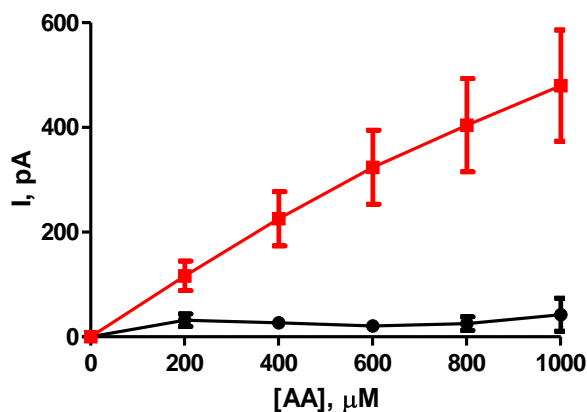


Figure 6.3.13.1.3 (a): Mean current concentration profile for an AA calibration in PBS at +900 mV vs. SCE using Type 3 NO Sensor ($n = 8$) pre (black) and post treatment (red) with BT (28 days).

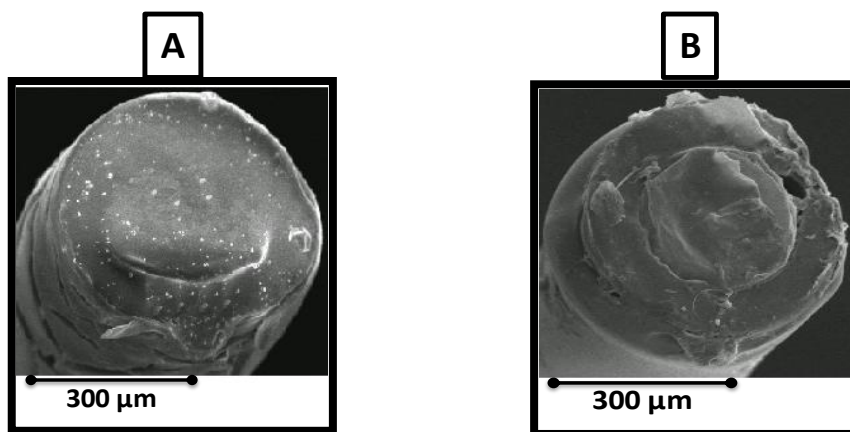


Figure 6.3.13.1.3 (b): An SEM displaying the surface of the Type 3 NO sensor (A) pre BT and (B) post BT (28 Days).

AA calibrations carried out on the Type 3 NO sensors in BT pre- and post-treatment yielded currents of 42 ± 32 pA and 480 ± 106 pA, respectively at a $1000 \mu\text{M}$ AA concentration. A significant difference was observed ($P = 0.0202$). The BT treatment caused the PPD layer to be altered and change, which is clear from the SEM demonstrated in Figure 6.3.13.1.3 (b), image B.

6.3.14 Temperature studies on Type 2 Sensor and Type 3 NO Sensor

Temperature studies were undertaken on Type 2 and Type 3 NO sensors in this section to determine if a changing temperature would cause an alteration in the sensitivity of NO. Similar studies were carried out by Brown *et al.*, on Type 1 NO sensors. They achieved an analogous sensitivity at 37 °C which yielded no significant difference to the sensitivity they attained at 25 °C ($P = 0.5002$) (Brown *et al.*, 2009). It is necessary to verify how the sensor works at an elevated temperature of 37 °C in order to mimic the temperature experienced by NO sensors *in-vivo*.

[NO], μM	Type 2 NO (Temp 37°C) ($n = 6$)		Type 3 NO (Temp 37°C) ($n = 6$)	
	Mean I, pA	SEM	Mean I, pA	SEM
0.0	0	0	0	0
0.2	207	33	106	34
0.4	493	54	353	42
0.6	699	47	453	61
0.8	1057	36	602	73
1.0	1251	79	790	111

Table 6.3.14: An averaged table of results displaying an NO calibration in PBS (pH 7.4), at +900 mV vs. SCE, carried out on Type 2 ($n = 6$) and Type 3 NO Sensors ($n = 6$) at 37 °C. Background values subtracted. Mean background current of Type 2 NO and Type 3 NO Sensor = 1405 \pm 156 pA and 1037 \pm 239 pA, respectively.

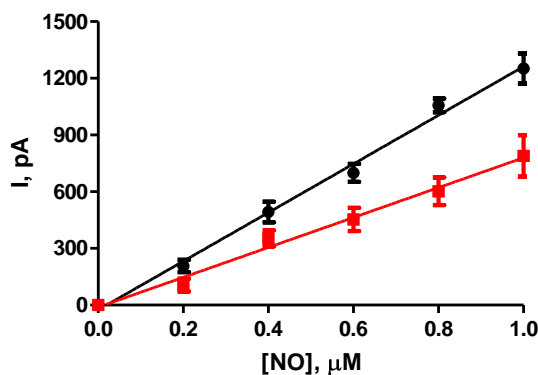


Figure 6.3.14: A current-concentration profile displaying an NO calibration in PBS (pH 7.4), at +900 mV vs. SCE (37 °C), carried out on Type 2 ($n = 6$) and Type 3 NO Sensors ($n = 6$).

Calibrating the two types of NO sensors at a temperature of 37 °C yielded sensitivities of 1287.0 ± 47.7 pA/ μ M ($R^2 = 0.99$) and 790.9 ± 40.6 pA/ μ M ($R^2 = 0.99$) for the Type 2 NO and Type 3 NO sensors respectively. There was no significant difference between the sensitivities obtained for the Type 2 NO sensors at 25 °C and 37 °C ($P = 0.7400$) and the Type 3 NO sensors at 25 °C and 37 °C ($P = 0.6231$). Although there was no disparity observed between the sensitivities at 25 °C and 37 °C for the two sensor types, a difference in the response time was achieved for the two sensors at 37 °C. Brown *et al.*, achieved a very promising result of an improved response time in an altered temperature setting of 37 °C with Type 1 NO sensors. They identified a significant decrease ($P = 0.0029$) in the response time from 33.7 ± 3.7 seconds, $n = 14$, at 25 °C to 14.0 ± 2.5 seconds, $n = 5$, at 37 °C (Brown *et al.*, 2009).

Just like the result obtained by Brown *et al.*, for the Type 1 NO sensor, a similar outcome was achieved with the Type 2 and 3 NO sensors. A response time of 18.1 ± 1.7 seconds, $n = 38$, at 25 °C, to 14.4 ± 0.2 seconds, $n = 6$, at 37 °C was obtained with the Type 2 NO sensors. For the Type 3 NO sensors, a response time of 15.9 ± 2.2 seconds, $n = 38$, at 25 °C to 10.3 ± 1.0 seconds, $n = 6$, at 37 °C was attained. Although both of these results do not yield significant decreases ($P = 0.3968$ and $P = 0.3234$) for Type 2 and Type 3 NO sensors, respectively, the characteristic decrease in response time upon placement into an elevated temperature is observed.

6.3.15 Post Calibrations *in-vivo* Type 2 NO Sensor

In this section an investigation into the effects of the implantation of the electrodes into the *in-vivo* brain is examined, pre and post NO and AA calibrations are compared ($n = 7$, 6 animals implanted for 11 days). These calibrations were carried out as described in Section 3.7.2.4.

6.3.15.1 Pre and post *in-vivo* NO calibrations

[NO], μM	Type 2 NO Sensor Pre <i>In-Vivo</i> ($n = 7$)		Type 2 NO Sensor Post <i>In-Vivo</i> ($n = 7$)	
	Mean I, pA	SEM	Mean I, pA	SEM
0.0	0	0	0	0
0.2	228	20	168	16
0.4	467	41	388	42
0.6	689	64	594	66
0.8	898	84	780	91
1.0	1094	98	955	117

Table 6.3.15.1: An averaged table displaying the results pre and post *in-vivo* calibrations for Type 2 NO sensors at +900 mV vs. SCE. Background values subtracted. Mean background current for Type 2 NO sensor ($n = 7$) pre and post *in-vivo* calibrations = 205 ± 69 pA and 257 ± 85 pA, respectively.

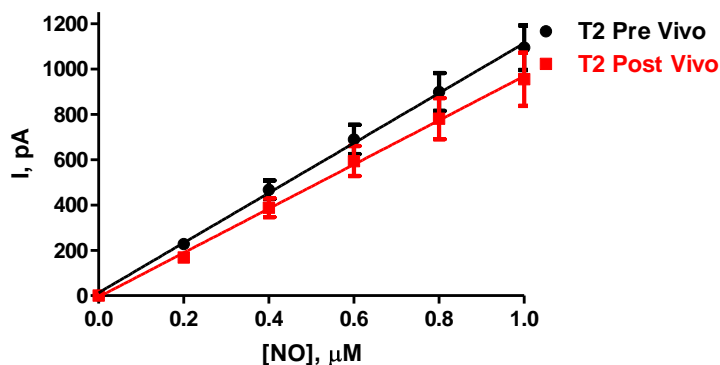


Figure 6.3.15.1: A current-concentration profile displaying a pre and post *in-vivo* NO calibration in PBS (pH 7.4), at +900 mV vs. SCE, carried out on Type 2 NO Sensors ($n = 7$).

It is observed from the comparison of the slopes (pA/ μM) of the electrodes, 1100 ± 19 pA/ μM for pre implantation and 974 ± 18 pA/ μM for post implantation, that the sensitivity of the Type 2 NO sensors did not alter dramatically. No significant difference was observed ($P = 0.7229$). The response of the electrodes was linear over the specified range with an R^2 value of 0.99, $n = 7$, pre implantation and 0.99, $n = 7$, post implantation. Following this, AA calibrations were carried out on the same sensors as detailed in Section 3.7.2.1.

6.3.15.2 Pre and post in-vivo AA calibrations

	Type 2 NO Sensor Pre <i>In-Vivo</i> ($n = 7$)		Type 2 NO Sensor Post <i>In-Vivo</i> ($n = 7$)	
[AA], μM	Mean I, pA	SEM	Mean I, pA	SEM
0	0	0	0	0
200	4	2	1196	467
400	3	3	2339	963
600	15	13	2458	960
800	19	16	3081	1261
1000	27	21	2691	923

Table 6.3.15.2: An averaged table displaying the results pre and post *in-vivo* AA calibrations for Type 2 NO sensors ($n = 7$) at +900 mV vs. SCE. Background values subtracted. Mean background current for Type 2 NO Sensor pre and post *in-vivo* calibrations = 183 ± 67 pA and 622 ± 31 pA, respectively.

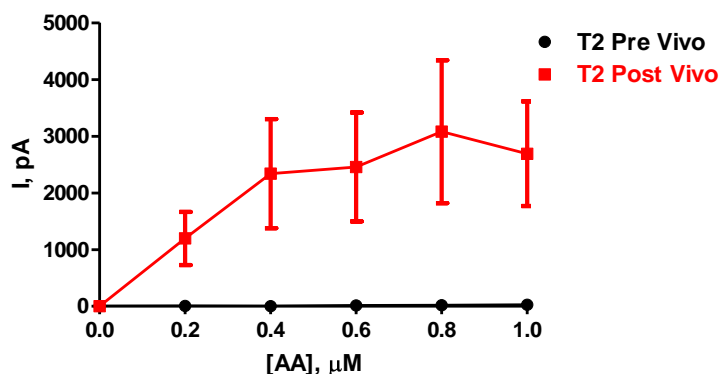


Figure 6.3.15.2 (a): A current-concentration profile displaying a pre and post *in-vivo* AA calibration in PBS (pH 7.4), at +900 mV vs. SCE, carried out on Type 2 NO Sensors ($n = 7$).

There is a large increase in the AA response at the electrodes post implantation that yields a significant difference pre and post ($P = 0.0020$). Although there is a large increase, the AA response remains relatively stable between 0.4 and 1.0 μM . Implantation of the sensor into the living brain causes a dramatic change in the sensitivity post-implantation. This could be due to the harsh environment that is the brain; however, it could also be the effect of removal of the electrodes from the headpiece of the animal which may cause significant damage to the sensors PPD layer. This has been observed with other PPD coated sensors in our group. Gliosis results in glial cells adhering to implanted sensors and a strong grip is formed around the mesh like structure of PPD. Upon removal of the sensors from the brain,

part of the membrane is removed as a result of this affect of gliosis. It is very difficult to post calibrate *in-vivo* sensors for this reason.

In Figure 6.3.15.2 (b), SEMs display the surface of the Type 2 NO sensor pre- and post-implantation. It is evident from the images that a smooth surface is obtained initially prior to insertion into the brain environment, conversely on analysis of the surface of the sensor post implantation, it is apparent that the PPD layer had been aggravated and distorted, therefore allowing an enhanced detection of AA.

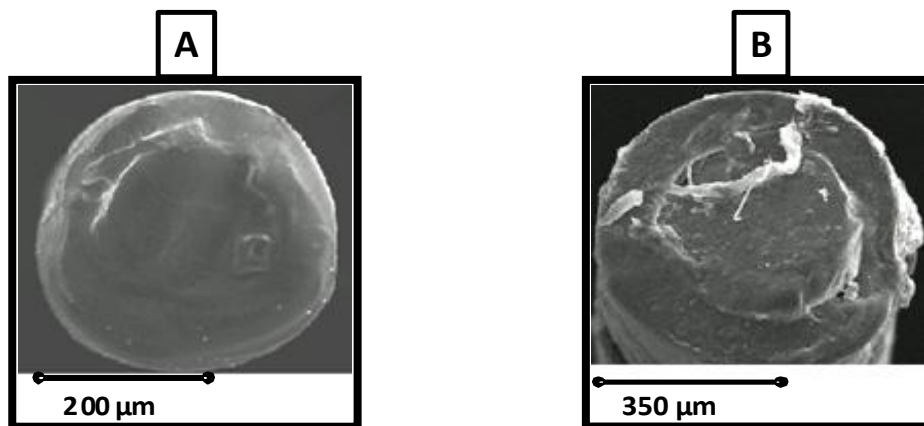


Figure 6.3.15.2 (b): SEMs displaying the surface of (A); Type 2 NO sensor prior to implantation (B); Type 2 NO sensor post implantation.

6.3.16 Post Calibrations *in-vivo* Type 3 NO Sensor

In this section the effect of implanting the electrodes into the *in-vivo* brain is examined, pre and post NO and AA calibrations are compared ($n = 6$, 6 animals implanted for 10 days). These calibrations were carried out as described in Section 3.7.2.4.

6.3.16.1 Pre and post in-vivo NO calibrations

	Type 3 NO Sensor pre <i>In-Vivo</i> ($n = 6$)		Type 3 NO Sensor post <i>In-Vivo</i> ($n = 6$)	
[NO], μM	Mean I, pA	SEM	Mean I, pA	SEM
0.0	0	0	0	0
0.2	216	28	184	22
0.4	448	53	468	43
0.6	689	69	746	69
0.8	908	92	999	94
1.0	1115	107	1238	125

Table 6.3.16.1: An averaged table displaying the results pre and post *in-vivo* NO calibrations for Type 3 NO sensors ($n = 6$) at +900 mV vs. SCE. Background values subtracted. Mean background current for Type 3 NO sensor pre and post *in-vivo* calibrations = 322 ± 94 pA and 247 ± 208 pA, respectively.

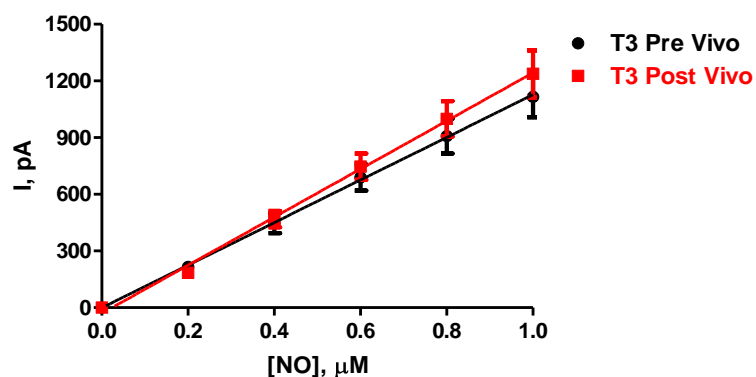


Figure 6.3.16.1 (a): A current-concentration profile displaying a pre and post *in-vivo* NO calibration in PBS (pH 7.4), at +900 mV vs. SCE, carried out on Type 3 NO Sensors ($n = 6$).

It is observed from the comparison of the slopes (pA/ μM) of the electrodes, 1128 ± 13 pA/ μM for pre-implantation and 1273 ± 32 pA/ μM for post-implantation, that the sensitivity of the Type 3 NO sensors did not alter. No significant difference was observed ($P = 0.8709$). The response of the electrodes was linear over the specified range with an R^2 value of 0.99, $n = 6$, pre-implantation and 0.99, $n = 6$, post-implantation. Following this, AA calibrations were carried out on the same sensors as detailed in Section 3.7.2.1.

6.3.16.2 Pre and post in-vivo AA calibrations

[AA], μM	Type 3 NO Sensor pre <i>In-Vivo</i> ($n = 6$)		Type 3 NO Sensor post <i>In-Vivo</i> ($n = 6$)	
	Mean I, pA	SEM	Mean I, pA	SEM
0.0	0	0	0	0
200.0	18	6	1027	651
400.0	24	10	1987	1239
600.0	33	17	3555	2295
800.0	50	25	4398	2779
1000.0	66	33	4893	3050

Table 6.3.16.2: An averaged table displaying the results pre and post *in-vivo* AA calibrations for Type 3 NO sensors at +900 mV vs. SCE. Background values subtracted. Mean background current for Type 3 NO sensor pre and post *in-vivo* calibrations = 367 ± 60 pA and 482 ± 201 pA, respectively.

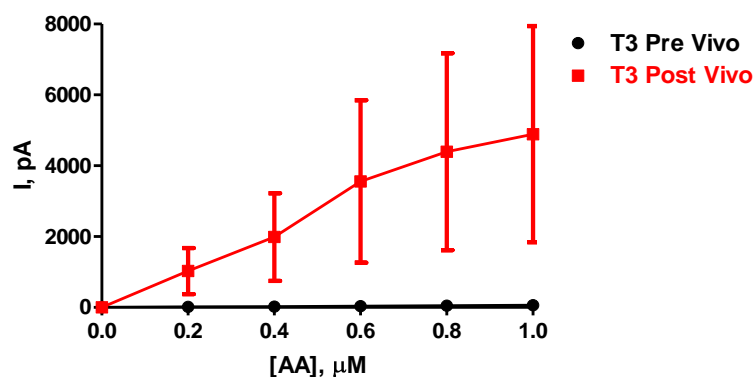


Figure 6.3.16.2: A current-concentration profile displaying a pre and post *in-vivo* AA calibration in PBS (pH 7.4), at +900 mV vs. SCE, carried out on Type 3 NO Sensors ($n = 6$).

There is a large increase in the AA response at the electrodes post-implantation that yields a significant difference pre and post ($P = 0.0083$). This could be as a result of the ruthless environment that is the brain; alternatively, it could also be the effect of removal of the electrodes from the headpiece of the animal which may cause significant damage to the sensors PPD layer. In Figure 6.3.16.2 (b), SEMs display the surface of the Type 3 NO sensor pre- and post-implantation.

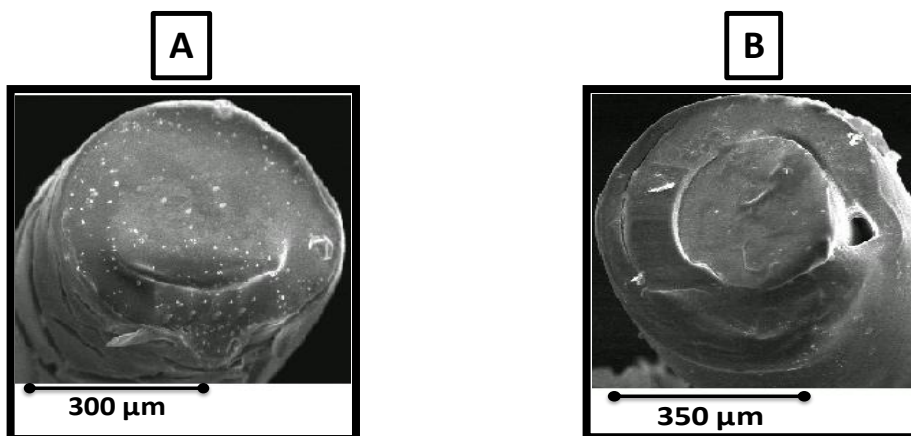


Figure 6.3.16.2 (b): SEMs displaying the surface of (A); Type 3 NO sensor prior to implantation (B); Type 3 NO sensor post-implantation.

It is evident from the images in Figure 6.3.16.2 (b), that an even and uniform surface is attained prior to introduction into the brain environment, conversely on analysis of the surface of the sensor post-implantation, it is clear that the PPD layer had been damaged and deformed, therefore allowing some detection of AA.

6.4 Conclusion

The main focus of this chapter was to extensively characterise the Type 2 and Type 3 NO sensors *in-vitro* for their potential use *in-vivo*. A determination of the sensitivity and selectivity of the Type 2 and Type 3 NO sensors was undertaken, to observe whether these sensors were on par with the NO sensor already utilised in our lab and reported in the literature (Brown & Lowry, 2003; Brown *et al.*, 2005; Brown *et al.*, 2009; Finnerty *et al.*, 2012a; Finnerty *et al.*, 2012b). A comparison of the Type 1, Type 2 and Type 3 NO sensor sensitivities to NO are detailed in Figure 6.4 (a).

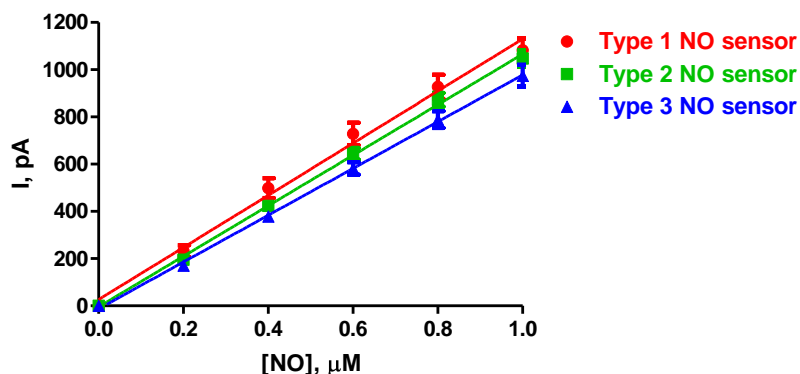


Figure 6.4 (a): A current-concentration profile displaying the NO sensitivities obtained in PBS (pH 7.4), at +900 mV vs. SCE, with the Type 1 ($n = 17$), Type 2 ($n = 38$) and Type 3 NO sensors ($n = 38$).

Although the Type 1 NO sensor produced a greater NO sensitivity, the Type 2 and 3 NO sensors displayed sensitivities that were not significantly different. Type 1 vs. Type 2 ($P = 0.8440$), Type 1 vs. Type 3 ($P = 0.6823$) and Type 2 vs. Type 3 ($P = 0.8332$). A bar chart comparing the NO sensitivities of the three types of NO sensors against the Pt sensor highlights the vast differences in the detection of NO and the advantages of modifying the NO sensors to make detecting NO more efficient is displayed in Figure 6.4 (b).

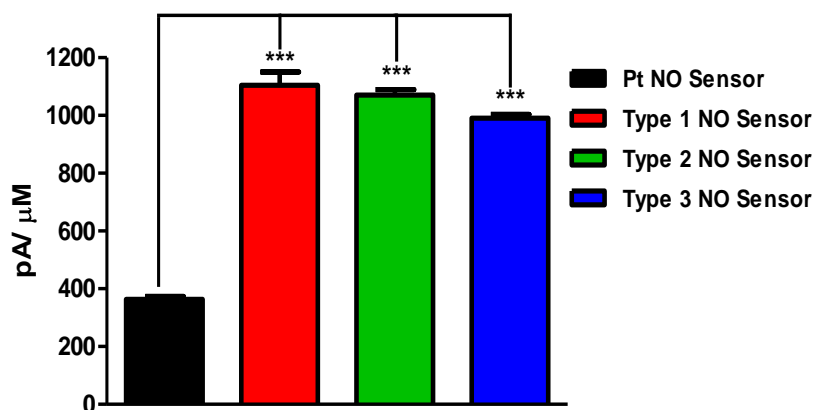


Figure 6.4 (b): A bar chart displaying a comparison of all NO sensitivities attained at each sensor, carried out at +900 mV vs. SCE.

There is a significant difference between the sensitivities obtained for the Pt sensors against the other types of NO sensor, which is very evident in the bar chart displayed in Figure 6.4 (b). On comparison of the individual NO sensors against the bare Pt sensor, a P value of < 0.0001 was recorded, signifying the observed distinction between the sensors.

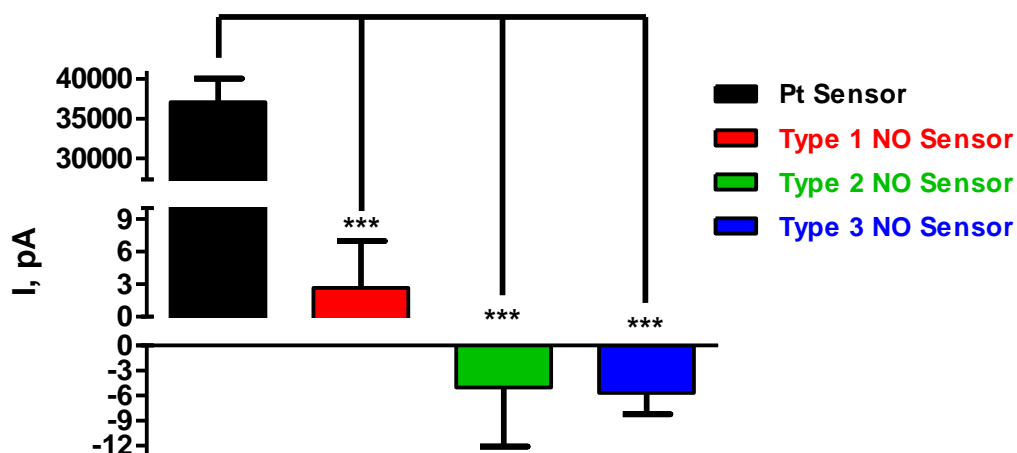


Figure 6.4 (c): A bar chart displaying the AA currents obtained at $1000 \mu\text{M}$ AA in PBS (pH 7.4), at $+900 \text{ mV vs. SCE}$, with the Pt ($n = 14$), Type 1 ($n = 17$), Type 2 ($n = 38$) and Type 3 NO sensors ($n = 38$).

The AA calibration displayed in Figure 6.4 (c), achieved no AA detection with all of the NO sensors yielding no significant difference between them, Type 1 vs. Type 2 ($P = 0.6264$), Type 2 vs. Type 3 ($P = 0.0772$) and Type 2 vs. Type 3 ($P = 0.2553$). However, a significant difference was recorded between the Pt sensor and all of the different types of NO sensor, Pt vs. Type 1 ($P < 0.0001$), Pt vs. Type 2 ($P < 0.0001$) and Pt vs. Type 3 ($P < 0.0001$). The long-term stability research carried out on these sensors revealed information that would change the way studies over extended periods of time were carried out in the lab. It was observed that on repeated calibration of the sensors, that the surface of each sensor was altered and modified more extensively than when the sensors were calibrated less frequently. Negligible results were presented after 56 days of storage and in comparison to the repeated calibrations displayed in this chapter, these results were very promising. The storage conditions were the same for all three sensors (enclosed container at 4°C) and a summary is presented in Table 6.4 (a) of all of these results.

<i>Sensor Type</i>	<i>Day 1 (pA)</i>		<i>Day 56 (pA)</i>		<i>Day 168 (pA)</i>	
	Mean (1000 μ M)	SEM	Mean (1000 μ M)	SEM	Mean (1000 μ M)	SEM
Pt-PPD (n = 4)	19	4	24	2.	3490	1276
Type 1 NO (n = 3)	-2	0	-5	1	-22	3
Type 2 NO (n = 4)	6	1	60	40	117	113
Type 3 NO (n = 4)	3	1	1	1	-32	7

Table 6.4 (a): A table summarising the responses attained with the individual sensors from day 1 to day 168 utilising the chosen storage condition of enclosed in a container dry at 4 °C in the fridge.

As the full characterisation of the Type 1 NO sensor had already been completed by Brown *et al.*, and Finnerty *et al.*, (Brown *et al.*, 2009; Finnerty *et al.*, 2012a; Finnerty *et al.*, 2012b), biocompatibility studies of the Type 2 and Type 3 NO sensors were undertaken. An effect was observed at the two sensors when treated with the proteins and lipids. Placement into BT yielded the most dramatic increase in AA detection on both sensors. Brown *et al.*, detailed a drop in NO sensitivity at the Type 1 NO sensor after treatment with BSA (10%) and PEA (10%) for a period of 72 hours in either solution (Brown *et al.*, 2009). They did not determine if there was any degradation of the sensor's layers after this time in each treatment. Reports utilising amperometric biosensors have observed between 20 and 50 % decreases in sensitivity after exposure to BT (Garguilo & Michael, 1994; Hu *et al.*, 1994). The sensors studied in this thesis were placed in the treatments for a month. This is an extensive time for the sensors to be immersed in treatments in comparison to what Brown *et al.*, completed (Brown *et al.*, 2009).

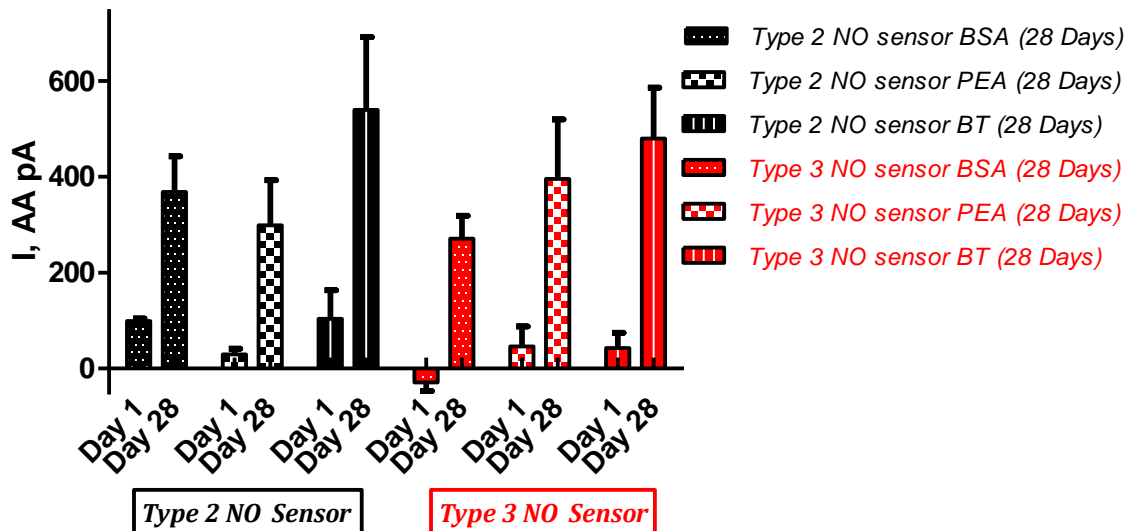


Figure 6.4 (d): A bar chart summarising the biocompatibility studies for each sensor described above over the course of 28 days.

Interference studies carried out on the sensors yielded no possibility for detection of any analyte other than NO, due to insignificant currents obtained for different interferents. Table 6.4 (b) depicts a summary of all the analytes and the percentage contribution to the overall NO signal. Subsequent to this Table, a summary of the *in-vitro* response attained with the potential interferents utilising bare Pt electrodes courtesy of Brown, F.O. (Brown, F.O. 2003) is depicted. This highlights the need for modification of the sensor with Nafion[®], as the interferents can cause a substantial influence on the NO signal.

Analyte	NO Response (pA)		% of NO signal	
	Type 2	Type 3	Type 2	Type 3
NO	1047 ± 34	974 ± 46	100	100
AA	-6 ± 6	-18 ± 6	≤ 1	≤ 1
5-HT	-16 ± 20	12 ± 19	≤ 1	≤ 1
Dopac	-6 ± 32	-5 ± 12	≤ 1	≤ 1
Dopamine	5 ± 3	8 ± 7	≤ 1	≤ 1
Glutathione	2 ± 6	9 ± 14	≤ 1	≤ 1
H ₂ O ₂	8 ± 2	-6 ± 7	≤ 1	≤ 1
5-HIAA	-6 ± 16	-2 ± 6	≤ 1	≤ 1
HVA	-13 ± 7	6 ± 33	≤ 1	≤ 1
NO ₂ ⁻	7 ± 0	3 ± 1	≤ 1	≤ 1
UA	5 ± 2	-11 ± 6	≤ 1	≤ 1

Table 6.4 (b): A summary of all the sensitivities of the interferents and their percentage effect on the NO signal with Type 2 and Type 3 NO sensors.

Analyte	NO Response (pA)
	Bare Pt electrode
NO	352 ± 25 (<i>n</i> = 14)
AA	37063 ± 2992 (<i>n</i> = 14)
5-HT	≤ 1 (<i>n</i> = 4)
Dopac	940 ± 170 (<i>n</i> = 4)
Dopamine	9 ± 1 (<i>n</i> = 4)
Glutathione	9 ± 1 (<i>n</i> = 4)
H ₂ O ₂	4 ± 1 (<i>n</i> = 3)
5-HIAA	990 ± 100 (<i>n</i> = 4)
HVA	100 ± 10 (<i>n</i> = 4)
NO ₂ ⁻	560 ± 110 (<i>n</i> = 3)
UA	1530 ± 50 (<i>n</i> = 4)

Table 6.4 (c): A summary of all the sensitivities of the interferents obtained with Pt electrodes (Brown, F.O. 2003).

Temperature studies undertaken with the Type 2 and Type 3 NO sensors displayed no significant difference ($P = 0.7400$ and $P = 0.6231$), respectively, on elevation of the temperature to 37°C . Figure 6.4 (e) displays a summary of the results obtained for the two sensors.

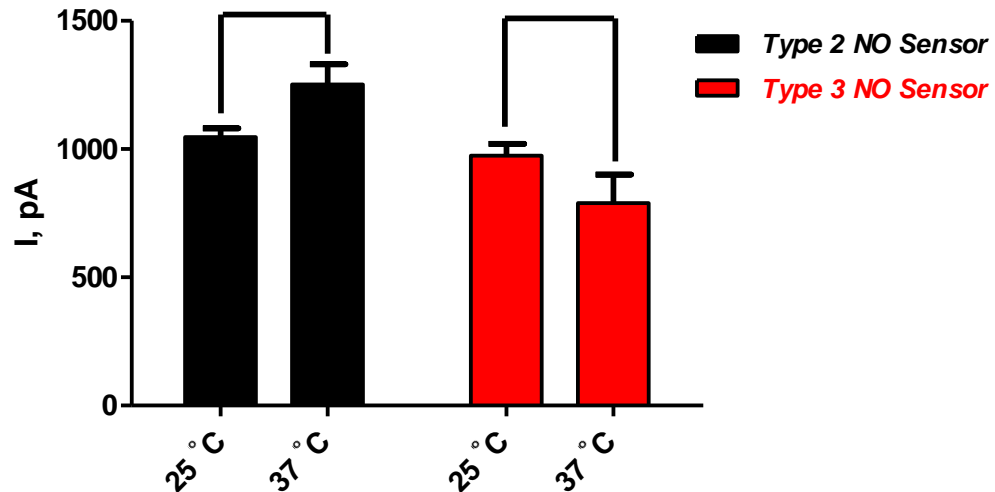


Figure 6.4 (e): A bar chart depicting the temperature elevation NO sensitivity results for Type 2 and Type 3 NO sensors at 25°C and 37°C .

As a slow response time was a major hindrance of the Type 1 NO sensor (34 ± 3 s, $n = 14$), the two NO sensors (Type 2 and Type 3) were manufactured in order to try and alleviate this problem, while retaining the sensitivity and selectivity of the sensor. This was accomplished, yielding response times of 18 ± 2 s, $n = 38$ and 16 ± 2 s, $n = 38$, for Type 2 and Type 3 NO sensors, respectively. When the temperature was elevated to 37°C , which is the temperature found *in-vivo*, the response times for the two sensor types decreased, which was also demonstrated previously with the Type 1 NO sensor by Brown *et al.*, (Brown *et al.*, 2009). The response times were found to have decreased to 14 ± 1 seconds, $n = 6$ and 10 ± 1 seconds, $n = 6$, for the Type 2 and Type 3 NO sensors respectively.

Figure 6.4 (f), details the NO sensitivities obtained for the Type 2 and Type 3 NO sensors pre- and post-implantation. There was no significant difference recorded for the Type 2 NO sensor ($P = 0.7229$) and Type 3 NO sensor ($P = 0.8709$). However, with regards to the AA response pre- and post-implantation a significant difference was observed for the Type 2

NO sensor ($P = 0.0020$) and Type 3 NO sensor ($P = 0.0083$) (see Section 6.3.15 and 6.3.16). As previously stated, this could be due to the complex and harsh environment of the brain, however, it could also be the effect of removal of the sensors from the headpiece of the animal which can cause significant damage to the PPD layer of the sensor. Overall, the results observed for these two sensors indicate a potential use *in-vivo*.

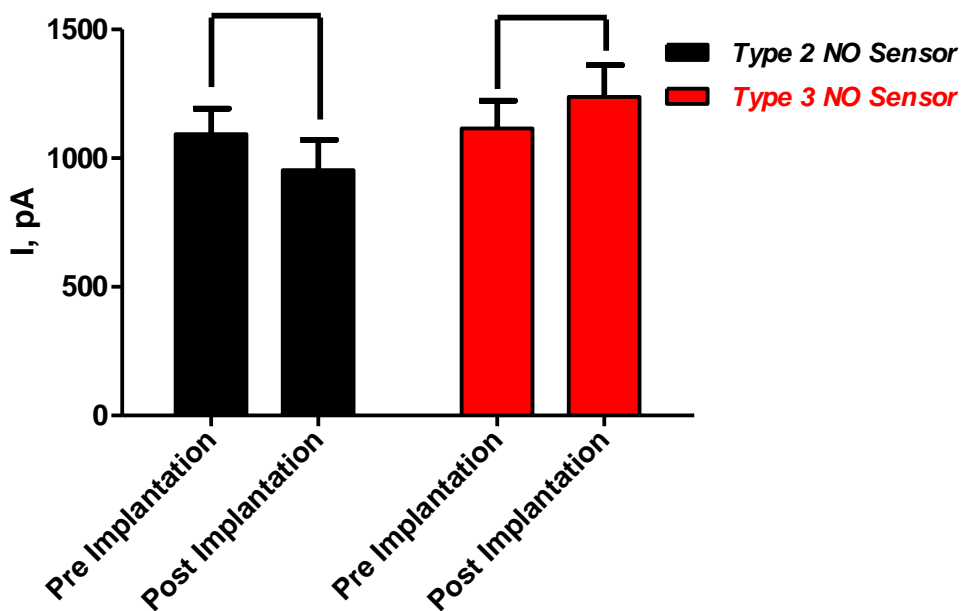


Figure 6.4 (f): A bar chart illustrating the NO sensitivities obtained pre and post implantation for the Type 2 and 3 NO sensor.

6.5 References


- Ariffin AA, O'Neill RD, Yahya M & Zain ZM. (2012). Electropolymerization of *o*-Phenylenediamine and its Use for Detection on Hydrogen Peroxide and Ascorbic Acid by Electrochemical Impedance Spectroscopy. *International Journal of Electrochemical Science* **7**, 10154-10163.
- Bedioui F & Griveau S. (2013). Electrochemical Detection of Nitric Oxide: Assessment of Twenty Years of Strategies. *Electroanalysis* **25**, 587-600.
- Brown F, Finnerty N, Bolger F, Millar J & Lowry J. (2005). Calibration of NO sensors for *in-vivo* voltammetry: laboratory synthesis of NO and the use of UV-visible spectroscopy for determining stock concentrations. *Analytical and Bioanalytical Chemistry* **381**, 964-971.
- Brown FO, Finnerty NJ & Lowry JP. (2009). Nitric oxide monitoring in brain extracellular fluid: characterisation of Nafion[®]-modified platinum electrodes *in-vitro* and *in-vivo*. *Analyst* **134**, 2012-2020.
- Brown FO & Lowry JP. (2003). Microelectrochemical sensors for *in-vivo* brain analysis: an investigation of procedures for modifying Pt electrodes using Nafion[®]. *Analyst* **128**, 700-705.
- Cadenas E & Packer L. (2002). *Nitric Oxide*. Elsevier Science, New York, United States of America.
- Casella IG & Guascito MR. (1997). Electrocatalysis of ascorbic acid on the glassy carbon electrode chemically modified with polyaniline films. *Electroanalysis* **9**, 1381-1386.
- Casero E, Alonso C, Martín-Gago JA, Borgatti F, Felici R, Renner F, Lee TL & Zegenhagen J. (2002). Nitric-oxide adsorption and oxidation on Pt(111) in electrolyte solution under potential control. *Surface Science* **507-510**, 688-694.
- Casero E, Darder M, Pariente F & Lorenzo E. (2000). Peroxidase enzyme electrodes as nitric oxide biosensors. *Analytica Chimica Acta* **403**, 1-9.
- Chailapakul O, Fujishima A, Tiphara P & Siritwongchai H. (2001). Electroanalysis of glutathione and cefalexin using the boron-doped diamond thin-film electrode applied to flow-injection analysis. *Analytical Sciences* **17**, i417-i422.
- Chattopadhyay A, Rukmini R & Mukherjee S. (1996). Photophysics of a neurotransmitter: ionization and spectroscopic properties of serotonin. *Biophysical journal* **71**, 1952-1960.

- Duff A & O'Neill RD. (1994). Effect of Probe Size on the Concentration of Brain Extracellular Uric Acid Monitored with Carbon Paste Electrodes. *Journal of Neurochemistry* **62**, 1496-1502.
- Finnerty NJ, O'Riordan SL, Brown FO, Serra PA, O'Neill RD & Lowry JP. (2012a). *In-vivo* characterisation of a Nafion[®]-modified Pt electrode for real-time nitric oxide monitoring in brain extracellular fluid. *Analytical Methods* **4**, 550-557.
- Finnerty NJ, O'Riordan SL, Palsson E & Lowry JP. (2012b). Brain nitric oxide: Regional characterisation of a real-time microelectrochemical sensor. *Journal of Neuroscience Methods* **209**, 13-21.
- Friedemann MN, Robinson SW & Gerhardt GA. (1996). o-Phenylenediamine-Modified Carbon Fiber Electrodes for the Detection of Nitric Oxide. *Analytical Chemistry* **68**, 2621-2628.
- Garguilo MG & Michael AC. (1994). Quantitation of choline in the extracellular fluid of brain tissue with amperometric microsensors. *Analytical Chemistry* **66**, 2621-2629.
- Govindarajan S, McNeil CJ, Lowry JP, McMahon CP & O'Neill RD. (2013). Highly selective and stable microdisc biosensors for l-glutamate monitoring. *Sensors and Actuators B: Chemical* **178**, 606-614.
- Hall CN & Garthwaite J. (2009). What is the real physiological NO concentration *in-vivo*? *Nitric Oxide* **21**, 92-103.
- Hu Y, Mitchell KM, Albahadily FN, Michaelis EK & Wilson GS. (1994). Direct measurement of glutamate release in the brain using a dual enzyme-based electrochemical sensor. *Brain Research* **659**, 117-125.
- Ignarro LJ, Buga GM, Wood KS, Byrns RE & Chaudhuri G. (1987). Endothelium-derived relaxing factor produced and released from artery and vein is nitric oxide. *Proceedings of the National Academy of Sciences* **84**, 9265-9269.
- Iqbal K, Khan A & Khattak M. (2004). Biological significance of ascorbic acid (vitamin C) in human health—a review. *Pakistan Journal of Nutrition* **3**, 5-13.
- Jones DP. (2010). *Biomedical Sensors*. Momentum Press, New York, United States of America.
- Katrlík J & Zálešáková Pn. (2002). Nitric oxide determination by amperometric carbon fiber microelectrode. *Bioelectrochemistry* **56**, 73-76.
- Kirwan S, Rocchitta G, McMahon C, Craig J, Killoran S, O'Brien K, Serra P, Lowry J & O'Neill R. (2007). Modifications of Poly(o-phenylenediamine) Permeable Layer on Pt-Ir for Biosensor Application in Neurochemical Monitoring. *Sensors* **7**, 420-437.

- Kopin I, White JH & Bankiewicz K. (1988). A new approach to biochemical evaluation of brain dopamine metabolism. *Cellular and Molecular Neurobiology* **8**, 171-179.
- Lancaster Jr JR. (1997). A Tutorial on the Diffusibility and Reactivity of Free Nitric Oxide. *Nitric Oxide* **1**, 18-30.
- Lee M-S, Cheng F-C, Yeh H-Z, Liou T-Y & Liu J-H. (2000). Determination of Plasma Serotonin and 5-Hydroxyindoleacetic Acid in Healthy Subjects and Cancer Patients. *Clinical Chemistry* **46**, 422-423.
- Lowry JP, Boutelle MG, O'Neill RD & Fillenz M. (1996). Characterisation of carbon paste electrodes *in-vitro* for simultaneous amperometric measurement of changes in oxygen and ascorbic acid concentrations *in-vivo*. *Analyst* **121**, 761-766.
- Lowry JP & O'Neill RD. (1994). Partial characterization *in-vitro* of glucose oxidase-modified poly(phenylenediamine)-coated electrodes for neurochemical analysis *in-vivo*. *Electroanalysis* **6**, 369-379.
- Mesároš Š, Grunfeld S, Mesárošová A, Bustin D & Malinski T. (1997). Determination of nitric oxide saturated (stock) solution by chronoamperometry on a porphyrine microelectrode. *Analytica Chimica Acta* **339**, 265-270.
- Meulemans A. (2002). A brain nitric oxide synthase study in the rat: production of a nitroso-compound NA and absence of nitric oxide synthesis. *Neuroscience Letters* **321**, 115-119.
- Miele M & Fillenz M. (1996). *In-vivo* determination of extracellular brain ascorbate. *Journal of Neuroscience Methods* **70**, 15-19.
- Miland E, Miranda Ordieres AJ, Tuñón Blanco P, Smyth MR & Fágáin CÓ. (1996). Poly(o-aminophenol)-modified bienzyme carbon paste electrode for the detection of uric acid. *Talanta* **43**, 785-796.
- Nims RW, Darbyshire JF, Saavedra JE, Christodoulou D, Hanbauer I, Cox GW, Grisham MB, Laval F, Cook JA, Krishna MC & Wink DA. (1995). Colorimetric Methods for the Determination of Nitric Oxide Concentration in Neutral Aqueous Solutions. *Methods* **7**, 48-54.
- O'Neill RD & Lowry JP. (2000). *Voltammetry in-vivo for chemical analysis of the living brain*. John Wiley & Sons Ltd, United Kingdom.
- O'Neill RD, Lowry JP & Mas M. (1998). Monitoring Brain Chemistry *in-vivo*: Voltammetric Techniques, Sensors, and Behavioral Applications. *Critical Reviews™ in Neurobiology* **12**, 69-127.

- O'Neill RD, Rocchitta G, McMahon CP, Serra PA & Lowry JP. (2008). Designing sensitive and selective polymer/enzyme composite biosensors for brain monitoring *in-vivo*. *Trends in Analytical Chemistry* **27**, 78-88.
- Pallini M, Curulli A, Amine A & Palleschi G. (1998). Amperometric Nitric Oxide Sensors: a Comparative Study. *Electroanalysis* **10**, 1010-1016.
- Palmer RM, Ferrige AG & Moncada S. (1987). Nitric oxide release accounts for the biological activity of endothelium-derived relaxing factor. *Nature* **327**, 524-526.
- Patel BA, Arundell M, Parker KH, Yeoman MS & O'Hare D. (2006). Detection of Nitric Oxide Release from Single Neurons in the Pond Snail, *Lymnaea stagnalis*. *Analytical Chemistry* **78**, 7643-7648.
- Pontié M, Bedioui F & Devynck J. (1999). New Composite Modified Carbon Microfibers for Sensitive and Selective Determination of Physiologically Relevant Concentrations of Nitric Oxide in Solution. *Electroanalysis* **11**, 845-850.
- Raof J-B, Ojani R & Kiani A. (2001). Carbon paste electrode spiked with ferrocene carboxylic acid and its application to the electrocatalytic determination of ascorbic acid. *Journal of Electroanalytical Chemistry* **515**, 45-51.
- Rath M & Pauling L. (1990). Hypothesis: lipoprotein(a) is a surrogate for ascorbate. *Proceedings of the National Academy of Sciences* **87**, 6204-6207.
- Rice ME & Nicholson C. (1989). Measurement of nanomolar dopamine diffusion using low-noise perfluorinated ionomer-coated carbon fiber microelectrodes and high-speed cyclic voltammetry. *Analytical Chemistry* **61**, 1805-1810.
- Schrier RW. (2007). *Diseases of the Kidney and Urinary Tract*. Wolters Kluwer Health/Lippincott Williams & Wilkins, United States of America.
- Sidransky H. (2010). *Tryptophan: Biochemical and Health Implications*. Taylor & Francis, United States of America.
- Terpstra M & Gruetter R. (2004). ¹H NMR detection of vitamin C in human brain *in-vivo*. *Magnetic resonance in medicine* **51**, 225-229.
- Van de Bittner GC, Dubikovskaya EA, Bertozzi CR & Chang CJ. (2010). *In-vivo* imaging of hydrogen peroxide production in a murine tumor model with a chemoselective bioluminescent reporter. *Proceedings of the National Academy of Sciences* **107**, 21316-21321.
- Wallace LJ & Traeger JS. (2012). Dopac distribution and regulation in striatal dopaminergic varicosities and extracellular space. *Synapse* **66**, 160-173.

- Wightman RM, May LJ & Michael AC. (1988). Detection of dopamine dynamics in the brain. *Analytical Chemistry* **60**, 769A-793A.
- Wu G, Fang Y-Z, Yang S, Lupton JR & Turner ND. (2004). Glutathione Metabolism and its Implications for Health. *The Journal of Nutrition* **134**, 489-492.
- Yang Y, Yang H, Yang M, Liu Y, Shen G & Yu R. (2004). Amperometric glucose biosensor based on a surface treated nanoporous ZrO₂/Chitosan composite film as immobilization matrix. *Analytica Chimica Acta* **525**, 213-220.
- Zhang X, Kislyak Y, Lin J, Dickson A, Cardosa L, Broderick M & Fein H. (2002a). Nanometer size electrode for nitric oxide and S-nitrosothiols measurement. *Electrochemistry Communications* **4**, 11-16.
- Zhang X, Wang H, Liang S-C & Zhang H-S. (2002b). Spectrofluorimetric determination of nitric oxide at trace levels with 5,6-diamino-1,3-naphthalene disulfonic acid. *Talanta* **56**, 499-504.
- Zheng D, Ye J, Zhou L, Zhang Y & Yu C. (2009). Simultaneous determination of dopamine, ascorbic acid and uric acid on ordered mesoporous carbon/Nafion composite film. *Journal of Electroanalytical Chemistry* **625**, 82-87.



*7. In-Vivo Characterisation
of Sensors for the
Neurochemical Detection of
Nitric Oxide*

7.1 Introduction

Subsequent to the *in-vitro* characterisation of the Type 2 and Type 3 NO sensors in Chapter 6, an investigation into the performance of the sensors under physiological conditions was undertaken. While the results obtained from the *in-vitro* characterisation specify that the Type 2 and Type 3 NO sensors have the necessary properties with regards to selectivity, sensitivity and stability for the neurochemical monitoring of NO *in-vivo*, it is important to perform an *in-vivo* characterisation of the sensors to ensure that the results obtained *in-vitro* can be sustained in the more complex target biological setting. A challenge that is facing science today is the comprehension of the living brain, how it works and what happens at any given moment upon initiation of a stimulus or a drug. The brain comprises of neurons and glial cells that interact through chemicals released into the extracellular space and it is due to this fact that monitoring these chemical messengers is of great importance (Kennedy *et al.*, 2002). The incorporation of electrochemistry *in-vivo* entails the use of amperometric electrodes and voltammetry techniques in order to detect electroactive species (O'Neill *et al.*, 1998).

Although the *in-vitro* setting is ideal for sensor development and can give a valuable insight into how a sensor might perform under certain conditions, detecting NO in the *in-vivo* environment yields a more complex and difficult environment for a sensor to withstand. In addition to being very diverse and complicated, BT comprises of surfactants (lipids), poisons (proteins), and electrocatalysts (AA) along with other species that may be detrimental to the sensors performance. Another concern is the restricted mass transport of the particular analyte to the surface of the sensor (O'Neill, 1993). This can give rise to very difficult conditions when trying to detect a very small molecule like NO, that is short-lived and highly reactive (Finnerty *et al.*, 2012a). NO is a gaseous free radical and one of the smallest molecules found in nature. It has been found to play a role in a range of physiological and pathophysiological processes. The regulation of vascular tone and some diseases have been found to be linked to NO, some of which include hypertension, Parkinson's disease and Alzheimer's disease (Brown *et al.*, 2005). In addition to all of these factors, the NO concentration in the brain extracellular fluid has been established as

approximately 0.1 μM (Hall & Garthwaite, 2009), making NO a very difficult molecule to detect.

The characterisation of the NO sensors in this chapter involved the systemic administration of the NO precursor L-arginine, the nitric oxide synthase (NOS) inhibitor L-NAME, a control injection of saline and an interference test injection of sodium L-ascorbate. This characterisation protocol of NO sensors has previously been demonstrated by Finnerty *et al.*, (Finnerty *et al.*, 2012a; Finnerty *et al.*, 2012b). The main aim of this chapter was to follow on from the previous NO characterisation *in-vitro* chapter and confirm the sustainability and viability of the Type 2 and Type 3 NO sensors *in-vivo*, by administration of potential interferents, inducers and inhibitors of NO.

7.2 Experimental

The instrumentation and software utilised are described in Section 3.2. All chemicals and solutions are detailed in Section 3.3. The manufacture of the different NO sensors is described in Sections 3.4. All modifications to the sensors are detailed in Section 3.5. A potential of +900 mV *vs.* Ag wire was applied to all working electrodes involved in the NO calibrations. The surgical procedure undertaken for the implantation of the sensors is detailed in Section 3.8.2. All *i.p.* injections were prepared in normal saline or otherwise stated. All *in-vivo* experiments were undertaken as described in Section 3.8. All experiments were carried out in freely moving animals.

Data is reported as mean \pm S.E.M. All statistical analysis was carried out using student *t*-tests. These tests were performed using GraphPad prism and yielded a *P*-value result, which is the probability value that specifies if the results observed are significantly different. In each of the Sections, *n* denotes the number of perturbations carried out on a given number of sensors in a given number of animals, unless stated otherwise.

7.3 Results and Discussion

This results section comprises the data from experiments undertaken to characterise the Type 2 and Type 3 NO sensors *in-vivo*. As the route of administration for investigating the effect of drugs on the NO response was through an i.p injection, the effect of an i.p. injection of saline on the NO current was examined. Using saline, demonstrates the effect of the injection stress on the NO response. An injection of saline (NaCl, 0.9 %, i.p.) on the NO current was recorded with the Type 2 and Type 3 NO sensors and is demonstrated in Figure 7.3.1.1 and 7.3.1.2. A significant change in the baseline levels in NO sensors implanted in the striatum of rats have been demonstrated previously, however it is short lived and a corresponding return to baseline is observed (Finnerty *et al.*, 2012a). A similar observation was obtained by Bolger *et al.*, for tissue O₂ (Bolger *et al.*, 2011b) and Lowry *et al.*, for glucose (Lowry *et al.*, 1998b).

7.3.1 Saline Administration

A typical example of the effect of a saline administration (NaCl, 0.9 %, i.p.) on the NO current for Type 2 and Type 3 NO sensors is depicted in Figure 7.3.1.1 and 7.3.1.2.

7.3.1.1 Type 2 NO sensor

The saline injection data in this Section was analysed using the results from 8 perturbations with 8 sensors in 6 animals.

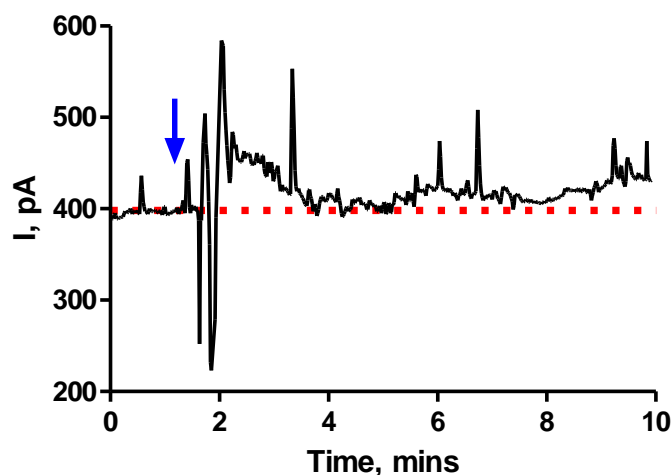


Figure 7.3.1.1: A typical example of an i.p. injection of saline (1 mL (NaCl) 0.9 %) monitored by a Type 2 NO sensor implanted in the striatum of a rat. The arrow is indicative of the point of injection.

The results in Figure 7.3.1.1 demonstrate how the NO sensor reacts to an i.p. injection of saline. A transient increase occurred in the oxidation current that was not significantly different ($P = 0.0819$) from baseline levels. The increase occurred after approximately 3 ± 1 minutes, $n = 8$, from a baseline of 378 ± 169 pA, $n = 8$, to a current of 405 ± 181 pA, $n = 8$, yielding a current change of 27 ± 13 pA, $n = 8$. This corresponded to a percentage change of 7 ± 3 %, $n = 8$. The increase returned to a post injection baseline level (388 ± 179 pA, $n = 8$), that was not significantly different ($P = 0.4642$) from the pre-injection baseline after 18 ± 5 minutes, $n = 8$. These results demonstrate that an initial increase in the oxidation current was recorded, due to the injection stress which causes an increase in the NO current very briefly, and an analogous NO baseline return.

Saline (i.p. injection)					
Current change (pA)	Current change (%)	Max response Time (mins)	Return Time (mins)	Baseline Pre Injection (pA)	Baseline Post Injection (pA)
27 ± 13	7 ± 3	3 ± 1	18 ± 5	378 ± 169	388 ± 179

Table 7.3.1.1: Summary of results for saline administration (1 mL (NaCl) 0.9 %), on Type 2 NO sensors, implanted in the striatum of freely moving rats ($n = 8$ with 8 sensors in 6 animals).

7.3.1.2 Type 3 NO sensor

The saline injection data in this Section was analysed using the results from 8 perturbations with 8 sensors in 5 animals.

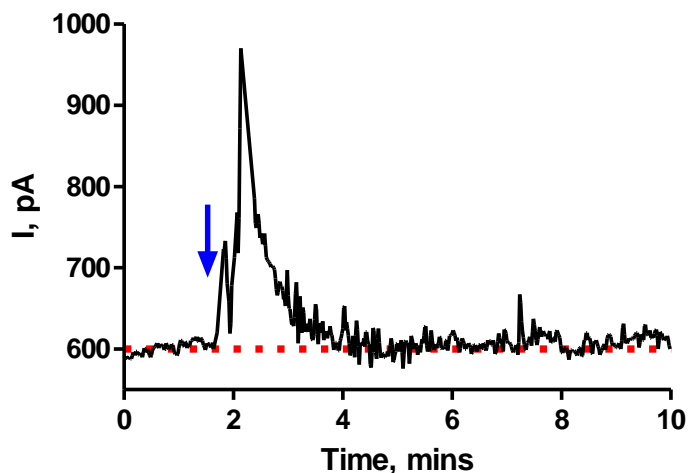


Figure 7.3.1.2: A typical example of an i.p. injection of saline (1 mL (NaCl) 0.9 %) monitored by a Type 3 NO sensor implanted in the striatum of a rat. The arrow is indicative of the point of injection.

On analysis of the results, a short-lived increase occurred in the NO signal that was not significantly different ($P = 0.0768$) from baseline levels, after approximately 3 ± 1 minutes, $n = 8$. A current change of 43 ± 21 pA, $n = 8$, from a baseline of 621 ± 202 pA, $n = 8$, to a current of 663 ± 220 pA, $n = 8$, was obtained which corresponded to a percentage change of 4 ± 2 %, $n = 8$. These increases returned to corresponding baseline levels that were not significantly different ($P = 0.1155$) from baseline levels, after 9 ± 2 minutes, $n = 8$, to currents of 645 ± 212 pA, $n = 8$. These results demonstrate that an initial increase in the NO current was recorded, but this was very short-lived and due to this being the route for all injections, it shows that the injection stress itself causes an increase in the NO current, however, an analogous NO baseline returns quite quickly.

Saline (i.p. injection)					
Current change (pA)	Current change (%)	Max response Time (mins)	Return Time (mins)	Baseline Pre Injection (pA)	Baseline Post Injection (pA)
43 ± 21	4 ± 2	3 ± 1	9 ± 2	621 ± 202	645 ± 212

Table 7.3.1.2: Summary of results for saline administration (1 mL (NaCl) 0.9 %), on Type 3 NO sensors, implanted in the striatum of freely moving rats ($n = 8$ with 8 sensors in 5 animals).

7.3.2 L-NAME Administration

There are many NOS inhibitors in the literature that are widely utilised as pharmacological agents to inhibit NOS in varying biological systems (Alderton *et al.*, 2001). L-NAME has been identified as contending with arginine, the pre-cursor for NO production, for its binding site (Lajoix *et al.*, 2004) on the NOS isozyme. N^G-nitro-L-arginine (L-NOARG) and L-NAME were found to be effective inhibitors of endothelial and neuronal NOS in the 1990's (Miilsch & Busse, 1990; Rees *et al.*, 1990b), however, despite having analogous structures, L-NAME was observed as being less potent than L-NOARG (Pfeiffer *et al.*, 1996). The use of L-NAME as an NO synthesis inhibitor has been demonstrated by many research groups (Rees *et al.*, 1990b; Miller *et al.*, 1993; Losonczy *et al.*, 1996).

The involvement of NO in the migration, invasiveness and carcinogenesis of tumors has been hypothesised by a number of *in-vitro* and *in-vivo* investigations that have been undertaken (Yu *et al.*, 2005). The utilisation of L-NAME in applying anti-cancer effects to human head and neck cancer as well as mammary tumors has been demonstrated *in-vitro* (Gallo *et al.*, 1998; Jadeski & Lala, 1999). Phencyclidine (PCP) administration has been incorporated into studies to yield a pharmacological animal model for schizophrenia (Javitt & Zukin, 1991; Johansson *et al.*, 1997; Pålsson *et al.*, 2009). It was demonstrated that NO levels were increased upon administration of the drug PCP; conversely upon pre-treatment with the NOS inhibitor L-NAME, this increase was counteracted. This suggested that L-NAME could block the effects of PCP-induced characteristics.

The main aim of this section was to provide real-time confirmation that L-NAME decreases NO concentrations when administered systemically. Figures 7.3.2.1 and 7.3.2.2 demonstrate the responses attained at a Type 2 and 3 NO sensor upon administration of an i.p. injection of L-NAME.

7.3.2.1 Type 2 NO Sensor

The L-NAME injection data in this Section was analysed using the results from 8 perturbations with 8 sensors in 6 animals.

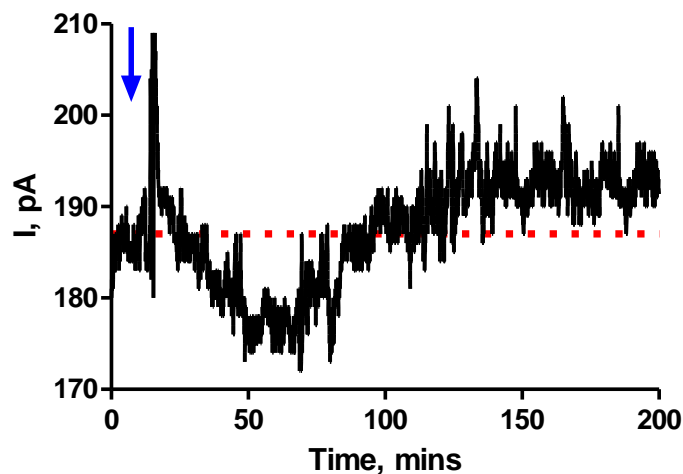


Figure 7.3.2.1: A typical example of an i.p. injection of L-NAME (30 mg/kg in 1 ml saline) monitored at a Type 2 NO sensor implanted in the striatum of a rat. The arrow is indicative of the point of injection.

An immediate and short-lived increase in the oxidation current can be seen upon injection of L-NAME which is similar to the response observed upon injection of saline shown in Figure 7.3.1.1, demonstrating the initial stress response following injection. This response is brief and has been demonstrated previously in the literature (Finnerty *et al.*, 2012a). Subsequent to this stress response, is the response attained from the L-NAME injection. As L-NAME is a NOS inhibitor, the expected result is to observe a decrease in the NO signal. In Figure 7.3.2.1, a typical NO response to L-NAME demonstrates this decrease. The overall decrease in oxidation current (32 ± 13 pA, $n = 8$), was significantly different ($P =$

0.0388) from pre-baseline levels. The current decreased from a baseline level of 465 ± 174 pA, $n = 8$, to a current of 434 ± 164 pA, $n = 8$, yielding a percentage change of $7 \pm 2\%$, $n = 8$. The maximum decrease was reached after approximately 58 ± 10 minutes, $n = 8$ and a corresponding baseline occurred after 134 ± 21 minutes, $n = 8$, that was not significantly different ($P = 0.6480$) from the baseline level prior to the injection.

L-NAME (i.p. injection)					
Current change (pA)	Current change (%)	Max response Time (mins)	Return Time (mins)	Baseline Pre Injection (pA)	Baseline Post Injection (pA)
32 ± 13	7 ± 2	58 ± 10	134 ± 21	465 ± 174	420 ± 171

Table 7.3.2.1: Summary of results for L-NAME administration on Type 2 NO sensors, implanted in the striatum of freely moving rats ($n = 8$ with 8 sensors in 6 animals).

7.3.2.2 Type 3 NO Sensor

The L-NAME injection data in this Section was analysed using the results from 6 perturbations with 6 sensors in 4 animals.

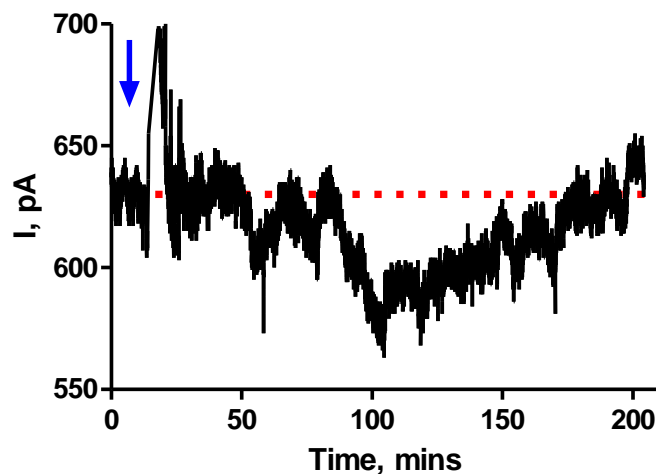


Figure 7.3.2.2: A typical example of an i.p. injection of L-NAME (30 mg/kg in 1 ml saline) monitored by a Type 3 NO sensor implanted in the striatum of a rat. The arrow is indicative of the point of injection.

Upon initial injection of L-NAME, a sharp increase in the baseline can be seen which corresponds to the injection stress observed previously for saline administrations. After 83 ± 16 minutes, $n = 6$, a decrease in the NO response was observed from a baseline of 583 ± 45 pA, $n = 6$, to an NO current of 531 ± 38 pA, $n = 6$, yielding a current change of 52 ± 15 pA, $n = 6$, and a corresponding percentage change of $9 \pm 2\%$, $n = 6$. The decrease attained on the NO current was significantly different ($P = 0.0161$) from baseline and a return to an equivalent baseline (532 ± 46 , $n = 6$), occurred after 142 ± 25 , $n = 6$, to a baseline that was not significantly different ($P = 0.0764$) from pre-injection levels.

L-NAME (i.p. injection)					
Current change (pA)	Current change (%)	Max response Time (mins)	Return Time (mins)	Baseline Pre Injection (pA)	Baseline Post Injection (pA)
52 ± 15	9 ± 2	83 ± 16	142 ± 25	583 ± 45	532 ± 46

Table 7.3.2.2: Summary of results for L-NAME administrations on Type 3 NO sensors, implanted in the striatum of freely moving rats ($n = 6$ with 6 sensors in 4 animals).

7.3.3 L-Arginine Administration

The synthesis of NO involves a two step process, one of which L-arginine plays a vital role. The NO precursor L-arginine is transformed to arginine-hydroxide in a reaction that is catalysed by NOS. Subsequent to this, arginine-hydroxide is then transformed to NO and citrulline, the synthesis involves cofactors also, which include calcium/calmodulin, O_2 and nicotinamide adenine dinucleotide phosphate (Bredt & Snyder, 1992). Previous publications have discussed the use of an amperometric sensor to detect the NO response to L-arginine administration in the prefrontal cortex, nucleus accumbens and the striatum of a freely moving rat, with results displaying an increase in NO levels (Brown *et al.*, 2009; Finnerty *et al.*, 2012a; Finnerty *et al.*, 2012b).

In other animal studies the antioxidant effects of L-arginine in brain ischemia were confirmed. After administration of L-arginine, decreases in the concentrations of lipid peroxidation products and increases in the concentrations of the antioxidant effects were observed (Maksimovich *et al.*, 2006). L-arginine has been utilised in order to improve disorders where NO is hypothesised as playing a part. For example, Creager *et al.*, demonstrated that the introduction of L-arginine improved the endothelium-dependent vasodilation in the disorder hypercholesterolemia in humans, by possibly enhancing the synthesis of NO (Creager *et al.*, 1992). Another study undertaken by Drexler *et al.*, demonstrated how administration of L-arginine partially restored the endothelium-dependent vasodilation in the disorder hypercholesterolemia (Drexler *et al.*, 1991).

Measurements of NO production in erythrocytes during stimulation by L-arginine has been demonstrated by Carvalho *et al.*, using a commercial NO sensor (Carvalho *et al.*, 2004). Research carried out which involved the long term oral supplementation of L-arginine for 6 months was found to improve coronary small vessel endothelial function. This significantly improved the symptoms associated with the disorder coronary endothelial dysfunction (Lerman *et al.*, 1998). Contradictory studies undertaken that incorporate the supplementation of L-arginine demonstrate that L-arginine does not increase NO synthesis or improve vascular reactivity and also could potentially do more damage to patients with peripheral arterial disease (Wilson *et al.*, 2007). In this section, data is presented that outlines the NO response to systemic administration of L-arginine in the striatum of a freely moving rat.

7.3.3.1 Type 2 NO Sensor

The L-arginine injection data in this Section was analysed using the results from 7 perturbations with 6 sensors in 5 animals.

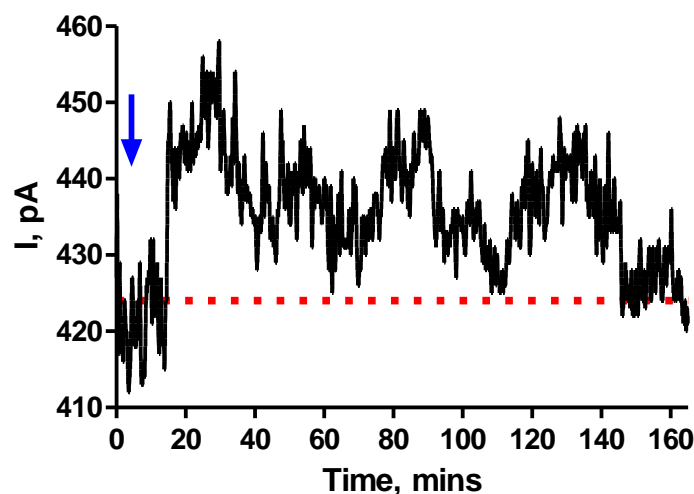


Figure 7.3.3.1: A typical example of an i.p. injection of L-arginine (300 mg/kg in 1 ml saline) monitored by a Type 2 NO sensor implanted in the striatum of a rat. The arrow is indicative of the point of injection.

It can be seen from Figure 7.3.3.1, that following the systemic administration of L-arginine, the oxidation current increases. Following the injection of L-arginine, a stress signal is observed which was demonstrated previously for the other i.p. injections, as a transient increase in the NO current before a rapid return to baseline. Following this, a maximum current change of 25 ± 7 pA, $n = 7$, was observed after 19 ± 4 minutes, $n = 7$, from a baseline of 380 ± 185 pA, $n = 7$, to a current of 404 ± 186 pA, $n = 7$. This yielded a percentage change of 12 ± 5 %, $n = 7$. The increase recorded was significantly different ($P = 0.0160$) from baseline and a corresponding baseline returned after 98 ± 12 minutes, $n = 7$, that was not significantly different ($P = 0.1889$) from pre-injection baseline levels.

L-Arginine (i.p. injection)					
Current change (pA)	Current change (%)	Max response Time (mins)	Return Time (mins)	Baseline Pre Injection (pA)	Baseline Post Injection (pA)
25 ± 7	12 ± 5	19 ± 4	98 ± 12	380 ± 185	407 ± 202

Table 7.3.3.1: Summary of results for L-NAME administration on Type 2 NO sensors, implanted in the striatum of freely moving rats ($n = 7$ with 6 sensors in 5 animals).

7.3.3.2 Type 3 NO Sensor

The L-arginine injection data in this Section was analysed using the results from 7 perturbations with 5 sensors in 3 animals.

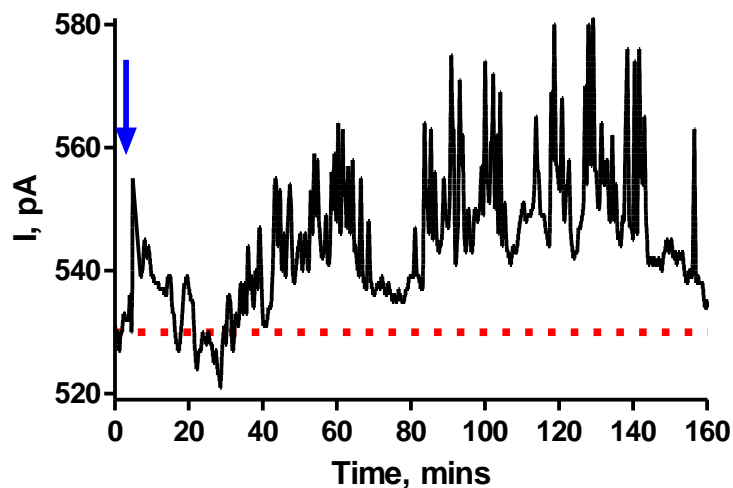


Figure 7.3.3.2: A typical example of an i.p. injection of L-arginine (300 mg/kg in 1 ml saline) monitored by a Type 3 NO sensor implanted in the striatum of a rat. The arrow is indicative of the point of injection.

For the Type 3 NO sensors, an increase in the NO current after administration of L-arginine was recorded. Injection stress can be seen initially by the transient increase in the NO current. Subsequent to this, a larger increase is observed in the NO signal yielding a current change of 28 ± 12 pA, $n = 7$, from a baseline level of 462 ± 39 pA, $n = 7$, to a new current of 490 ± 35 pA, $n = 7$. This increase was significantly different ($P = 0.0069$) from baseline with a percentage change of 7 ± 4 % occurring after 32 ± 4 minutes, $n = 7$. The signal returned to a new baseline level of 465 ± 43 pA, $n = 7$, after 103 ± 23 minutes, $n = 7$, which was significantly different ($P = 0.8878$) from pre-injection baseline levels.

L-Arginine (i.p. injection)					
Current change (pA)	Current change (%)	Max response Time (mins)	Return Time (mins)	Baseline Pre Injection (pA)	Baseline Post Injection (pA)
28 ± 12	7 ± 4	32 ± 4	103 ± 23	462 ± 39	465 ± 43

Table 7.3.3.2: Summary of results for the L-arginine administration from Type 3 NO sensors, implanted in the striatum of freely moving rats ($n = 7$ with 5 sensors in 3 animals).

7.3.4 Sodium Ascorbate Administration

In Chapter 6, the Type 2 and 3 NO sensors demonstrated excellent selectivity towards NO *in-vitro* against a wide range of electroactive interferents (e.g. ascorbic acid, dopamine, DOPAC, NO₂⁻, serotonin) found in the brain ECF (see Figure 6.3.11). Ascorbic acid or in this case its mineral salt sodium ascorbate was chosen as the main interferent to test the selectivity of the NO sensors against *in-vivo*, as it is the primary endogenous interferent present in the brain (Brown *et al.*, 2009). It is ubiquitous, with a concentration in the ECF stated as approximately 500 μM (Miele & Fillenz, 1996a). In order to characterise any sensor thoroughly, it is necessary to characterise the selectivity of sensor designs prior to implantation. This has been demonstrated with many sensors including glucose sensors (Lowry & O'Neill, 1992; Lowry *et al.*, 1998a; Kealy *et al.*, 2013) or in this case NO sensors (Brown & Lowry, 2003; Ferreira *et al.*, 2005; Brown *et al.*, 2009).

Sodium ascorbate is one of a number of mineral salts of ascorbic acid also referred to as vitamin C. Ascorbic acid has been known to be more acidic than its mineral salts, due to the fact that these mineral salts are buffered (Higdon & Drake, 2011). Ascorbic acid can cause the animal discomfort and aggravation around the injection site due to the acidity, so an i.p. injection of sodium ascorbate, which is milder, was chosen. This will confirm that the sensor design was still intact and the rejection layer had not been compromised during the implantation of the sensors. It is imperative to confirm that the two Types of NO sensors reported in this chapter have not degraded and that the sensors still exhibit similar selectivity characteristics to those recorded *in-vitro*. In Figure 7.3.4.1 (a) and 7.3.4.2, the

responses acquired with the Type 2 and 3 NO sensors from the injection of sodium ascorbate are depicted.

7.3.4.1 Type 2 NO Sensor

The sodium ascorbate injection data in this Section was analysed using the results from 9 perturbations with 9 sensors in 6 animals.

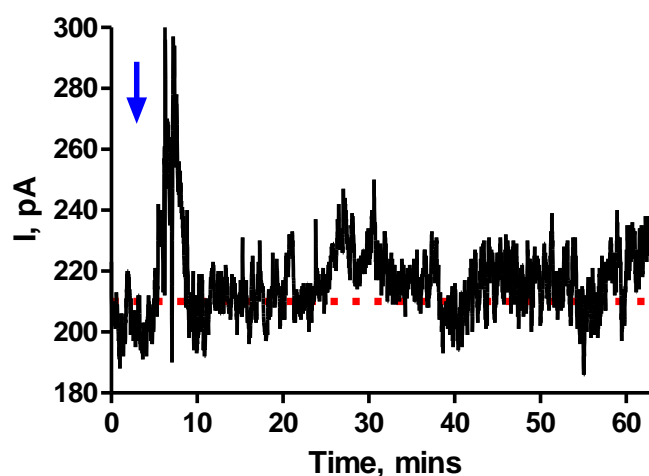


Figure 7.3.4.1 (a): A typical example of an i.p. injection of sodium ascorbate (1g/kg in 1 ml of saline) monitored by a Type 2 NO sensor implanted in the striatum of a rat. The arrow is indicative of the point of injection.

The Type 2 NO sensor response to an i.p. injection of sodium ascorbate demonstrates a brief increase in the NO response which corresponds to injection stress. This response has been observed throughout each of the injections carried out on the animals. An initial rapid increase occurs, however, returns back to a steady baseline quite quickly and the NO current remains relatively stable, demonstrating no detection of AA. This leads to the confirmation that the structural design of the sensor has not been damaged from the implantation protocol or aggravated from being situated in a harsh and complex environment that is the living brain. It has been previously illustrated with CPEs, that if any response to sodium ascorbate was to occur it would do so within a time range of 60 minutes (Finnerty *et al.*, 2012a). Figure 7.3.4.1 (c), displays the response to a sodium ascorbate

injection using CPEs, taken from Finnerty *et al.*, 2012. It can be observed that there has been a response at the CPEs and it is clear from the Type 2 NO sensor data that there is no significant change ($P = 0.2052$) in the oxidation current (-44 ± 30 pA, $n = 9$), over the 60 minutes post ascorbate injection. The decrease in the current can be attributed to fluctuations in NO levels associated with circadian rhythms. Figure 7.3.4.1 (b) demonstrates these fluctuations recorded over a 3 hour period which further validates the selectivity of the sensor towards NO over ascorbate. A summary table of the results obtained for 6 animals is displayed in Table 7.3.4.1.

Sodium ascorbate (i.p. injection)		
Current change (pA)	Current change (%)	Significance
-44 ± 30	8 ± 10	$P = 0.2052$

Table 7.3.4.1: Summary of results for sodium ascorbate administration on Type 2 NO sensors, implanted in the striatum of freely moving rats ($n = 9$ with 9 sensors in 6 animals).

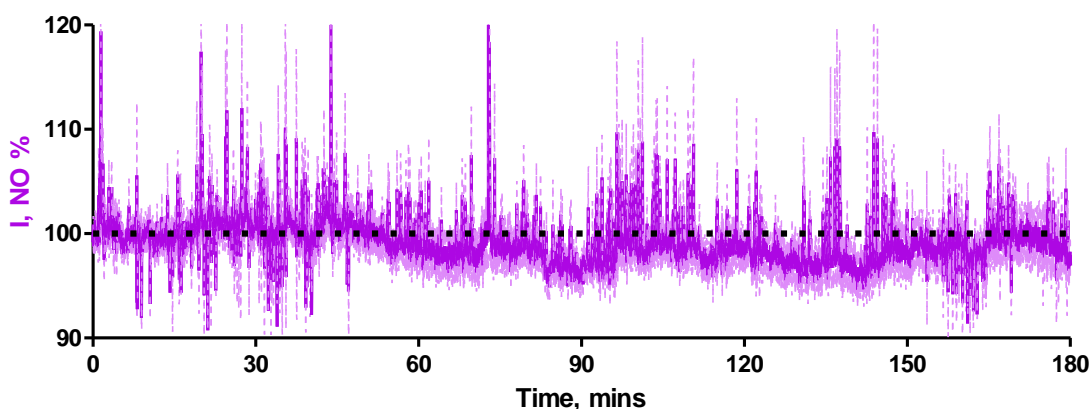


Figure 7.3.4.1 (b): A time vs. percentage change graph of baseline NO currents monitored by NO sensors (Type 2 and Type 3 NO sensors), displaying a stable baseline over the course of three hours *in-vivo* (15 sensors in 5 animals)

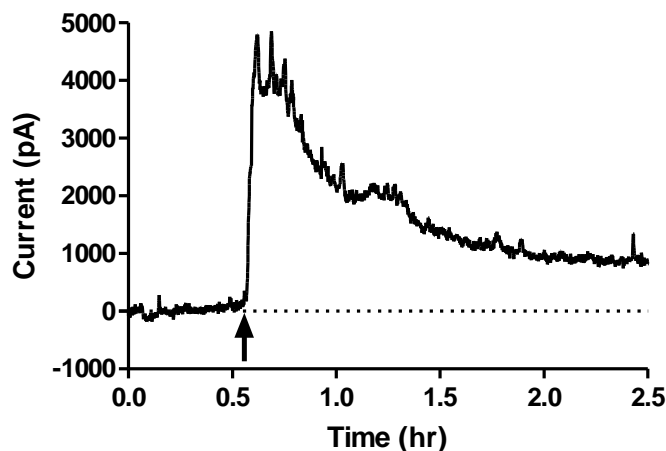


Figure 7.3.4.1 (c): A typical example of the effect of an i.p injection of sodium ascorbate on the response of a CPE implanted in rat striatum (Finnerty *et al.*, 2012a).

7.3.4.2 Type 3 NO Sensor

The sodium ascorbate injection data in this Section was analysed using the results from 9 perturbations with 8 sensors in 5 animals.

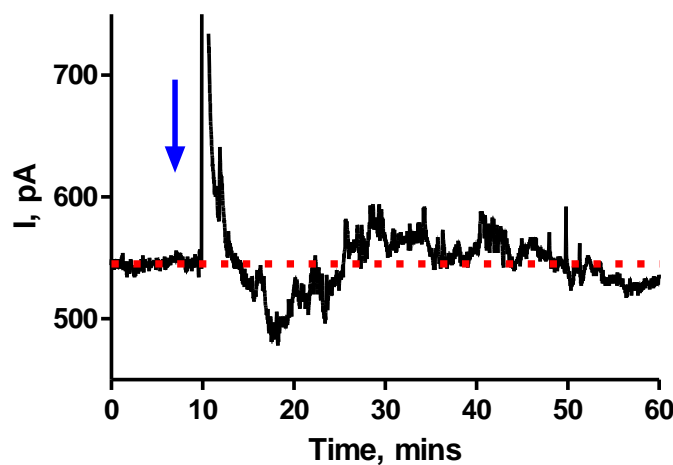


Figure 7.3.4.2: A typical example of an i.p. injection of sodium ascorbate (1g/kg in 1 ml of saline) monitored by a Type 3 NO sensor implanted in the striatum of a rat. The arrow is indicative of the point of injection.

The sodium ascorbate i.p. injection for the Type 3 NO sensor displayed a similar response attained by the Type 2 NO sensors. An initial increase in the NO current related to the stress of the injection and a return to baseline was observed. If any change in the oxidation current was to occur from this ascorbate injection, it would take place within 60 minutes (see Figure 7.3.4.1 (c)). An overall current change of -21 ± 14 pA, $n = 9$, was obtained. There was no significant difference ($P = 0.2214$) between the initial pre-injection baseline (696 ± 274 pA, $n = 9$) and the new recorded level of 674 ± 262 , $n = 9$. A slight decrease in current was observed which can be attributed to the fluctuation in the NO current (see Figure 7.3.4.1 (b)) recorded over the 60 minutes. A similar trend has been reported by Brown *et al.*, during *in-vitro* investigations (Brown & Lowry, 2003). This confirms that the Type 3 NO sensors once implanted retained their integrity and the surface of the sensor remained intact which blocked the detection of sodium ascorbate.

Sodium ascorbate (i.p. injection)		
Current change (pA)	Current change (%)	Significance
-21 ± 14	-0.3 ± 1.5	$P = 0.2214$

Table 7.3.4.2: Summary of results for sodium ascorbate administration on Type 3 NO sensors, implanted in the striatum of freely moving rats ($n = 9$ with 8 sensors in 5 animals)

7.3.5 Stability of the NO sensors

In Chapter 6 the long term stability of the sensors *in-vitro* was determined over 56 days and for the calibrations that were carried out less frequently, a calibration at day 168 was tested also (see Section 6.3.8.2). The results demonstrated that the two NO sensors over the period of 56 days remained stable, when calibrated once prior to day 56. The chosen optimum storage condition (4 °C, enclosed container) displayed an AA response at a concentration of 1000 µM, of 60 ± 30 pA for the Type 2 NO sensors and 1 ± 1 pA for the Type 3 NO sensors after 56 days. When the long-term BT treatments were undertaken over 28 days the Type 2 and Type 3 NO sensors demonstrated a significant difference pre- and post-treatment ($P = 0.0450$ and $P = 0.0202$), respectively. The need to characterise the sensors *in-vivo* is due to the vast differences between the *in-vivo* and *in-vitro* environments. In this Section the stability of the sensors was determined *in-vivo* over the specified days and the results for both sensors are depicted in Figure 7.3.5.1 and 7.3.5.2. The NO current was taken at approximately the same time every day so that an accurate representation of the baseline could be achieved.

7.3.5.1 Type 2 NO sensor

The baseline data in this section was analysed using the results from 5 animals with 8 sensors over 11 Days.

Day	Type 2 NO sensor (% NO) decrease		
	Mean (% O ₂)	SEM	<i>n</i>
1	100	0	8
2	71	11	8
3	65	12	8
4	66	12	8
5	67	13	8
6	65	14	8
7	66	13	8
8	66	14	8
9	68	15	8
10	72	11	8
11	72	15	8

Table 7.3.5.1: The mean percentage table displaying the % decrease in NO after implantation with 8 Type 2 NO sensors over 11 days in the striatum of 5 freely moving rats.

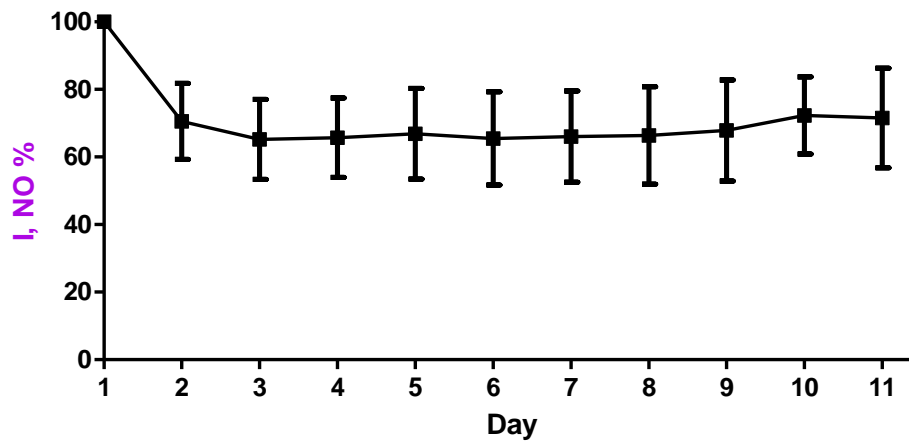


Figure 7.3.5.1: The averaged percentage NO decrease vs. day profile of the Type 2 NO sensors over the course of 11 days in the striatum of 5 freely moving rat with 8 sensors

The results displayed in Table 7.3.5.1 and Figure 7.3.5.1 demonstrates how stable the Type 2 NO sensors are over the 11 days of implantation in the *in-vivo* environment. Initially there is approximately a 29 % decrease in the NO current that remains stable over the specified days. One-way ANOVA analysis revealed that the results for the *in-vivo* stability were not significantly different ($P = 0.7763$) over the course of the study. The Type 3 NO sensor stability data is displayed in Section 7.3.5.2.

7.3.5.2 Type 3 NO Sensor

The baseline data in this section was analysed using the results from 5 animals with 8 sensors over 10 Days.

Type 3 NO sensor (% NO) decrease			
Day	Mean (% O ₂)	SEM	<i>n</i>
1	100	0	8
2	75	10	8
3	78	9	8
4	78	6	8
5	84	5	8
6	85	4	8
7	87	3	8
8	72	7	8
9	73	9	8
10	86	12	8

Table 7.3.5.2: The mean percentage table displaying the % decrease in NO after implantation with 8 Type 3 NO sensors over 10 days in the striatum of 5 freely moving rats.

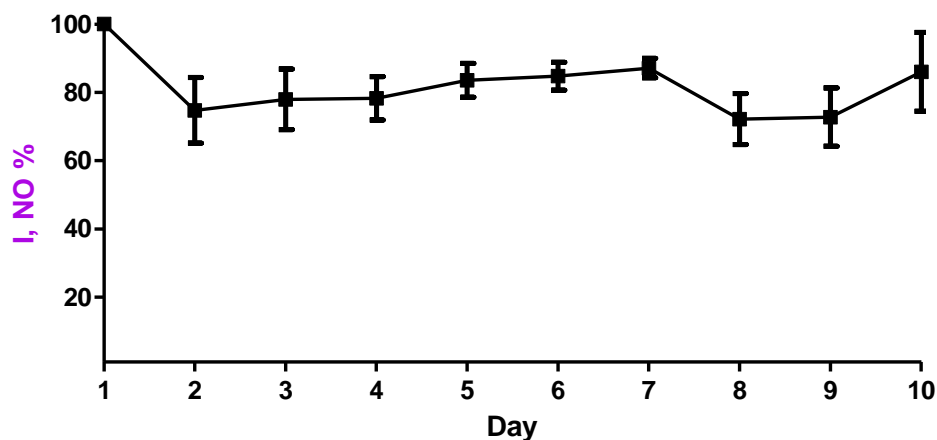


Figure 7.3.5.2: The averaged percentage NO decrease vs. day profile of the Type 3 NO sensors over the course of 10 days in the striatum of 5 freely moving rat with 8 sensors

The Type 3 NO sensors displayed a similar stability result to the Type 2 NO sensors over the specified time. A percentage decrease of approximately 25 % occurs after day 1 and the sensitivity remains relatively stable thereafter. One-way ANOVA analysis indicated no significant difference ($P = 0.2457$), between the currents obtained on the days specified. Overall the two sensors behaved quite stable in the *in-vivo* environment over the days specified.

7.4 Conclusion

Reported in this chapter is the *in-vivo* characterisation of the Type 2 and Type 3 NO sensor in the striatum of freely moving rats. The characterisation of the Type 1 NO sensor has been demonstrated previously in the literature by Finnerty *et al.*, in the striatum using local and systemic administrations (Finnerty *et al.*, 2012a). To characterise the two sensors *in-vivo*, systemic administrations of known inducers and inhibitors of NO production and the corresponding changes in the NO current were investigated. The first experiments carried out were control saline injections. Since all administrations were by i.p. injection it was important to validate the response attained by the injection itself, therefore utilising saline to verify this. The response recorded by the Type 2 NO sensor demonstrated that the injection caused a sharp increase with a quick return to baseline revealing no effect from the saline itself. An increase that was not significant ($P = 0.0819$), of 27 ± 13 pA, $n = 8$, after 3 ± 1 minutes, $n = 8$, with a return to an analogous baseline after 18 ± 5 minutes, $n = 8$, was very short-lived.

A similar saline administration response was obtained with the Type 3 NO sensor. A current change of 43 ± 21 pA, $n = 8$, after 3 ± 1 minutes, $n = 8$, that was not significant ($P = 0.0768$) was attained. The baseline returned quicker in comparison to the Type 2 NO sensor with a steady baseline observed after 9 ± 2 minutes, $n = 8$. The NO signal traces observed for the two sensors were quite similar, demonstrating the ability of the two different designs to detect rapid changes in the NO response. As the injection responses were now verified, the next step was to try and perturb the NO signalling pathway by introducing inducers or inhibitors of NO through systemic injections. The first i.p. injection utilised was L-NAME which is a non-selective NOS inhibitor. The expected result to observe from this injection was a decrease in the NO signal. In the literature an observation of a decrease in the NO after administration of L-NAME has been demonstrated (Kurose *et al.*, 1993; Jones *et al.*, 2004; Finnerty *et al.*, 2012a; Finnerty *et al.*, 2012b).

It has been hypothesised that L-NAME is in competition with the NO pre-cursor L-arginine to bind with the NOS enzyme (Da Cunha *et al.*, 2005), decreasing the enzymes availability for NO synthesis thus reducing the production of NO. For the Type 2 NO sensors a significant change ($P = 0.0388$) in the NO response was observed after the L-NAME

administration. A clear decrease was observed with all of the Type 2 NO sensors after 58 ± 10 minutes, $n = 8$. The results for the Type 3 NO sensors yielded a significant decrease in the observed NO current ($P = 0.0161$) after approximately 83 ± 16 minutes, $n = 6$. This confirms that L-NAME causes an effect on the NO, which was recorded as a decrease in both sensors studied.

L-arginine, which is the precursor for NO production in the body, was administered systemically by i.p. injection. As expected, this administration produced a significant increase in the NO signal for the Type 2 ($P = 0.0160$), $n = 7$ and Type 3 NO sensors ($P = 0.0069$), $n = 7$. A similar trace was obtained for both sensors shown in Figure 7.3.3.1 and 7.3.3.2. This corresponds to results obtained within our group by Brown *et al.*, and Finnerty *et al.*, (Brown *et al.*, 2009; Finnerty *et al.*, 2012a; Finnerty *et al.*, 2012b). Also these results corroborate previous indirect results postulated by various groups (Ashab *et al.*, 1995; Carvalho *et al.*, 2004; Maksimovich *et al.*, 2006). Following confirmation that the two sensors were detecting changes in NO production, it was important to investigate if the sensors had lost their selectivity following implantation or from being placed into the complex environment of proteins, lipids and other biofouling agents. An investigation of this was undertaken by ascorbate administration, as it is the most abundant interferent present in the brain (Miele & Fillenz, 1996a).

The administration of sodium ascorbate resulted in an NO response that was similar to that which was attained by the administration of saline. A transient increase in the NO current was observed, followed by a quick return to baseline levels after a short amount of time. It has been previously illustrated with CPEs, that if any response to sodium ascorbate was to occur it would do so within a time range of 60 minutes (Finnerty *et al.*, 2012a). The result obtained by the Type 2 and Type 3 NO sensors displayed no significant difference ($P = 0.2052$) and ($P = 0.2214$), respectively, between the pre- and post-baseline levels over the 60 minutes analysed. These results show how the initial stress of the injection causes a brief increase in the NO response followed shortly by a return to baseline levels, which corresponds to the results obtained from the saline injections. This leads to the confirmation that the sensors have in fact remained intact and the sensor design has not been compromised which would allow the detection of the interferent. In Section 7.3.5, the stability of the NO sensors can be observed during the days implanted in the *in-vivo*

environment. A decrease of 29 % and 25 % was observed for the Type 2 and Type 3 NO sensors, respectively, after day 1 *in-vivo*. However, the two sensors remained relatively stable for the rest of the days implanted thereafter.

In summary, this chapter presents results of investigations into the systemic effects of well documented inhibitors and inducers of NO production. It details the changes observed in the NO current recorded by each of the NO sensors implanted. The results demonstrate how capable the Type 2 and Type 3 NO sensors are at detecting a molecule that is so small and short-lived in an environment that is so intricate and complicated. Table 7.4 (a) and 7.4 (b), display a summary of the characterisation data for the Type 2 and Type 3 NO sensors respectively.

Type 2 NO Sensor	Current change (ΔI , pA)	Max response time (mins)	Return to baseline time (mins)
Administrations			
Saline	27 ± 13 ($n = 8$)	3 ± 1 ($n = 8$)	18 ± 5 ($n = 8$)
L-NAME	32 ± 13 ($n = 9$)	58 ± 10 ($n = 9$)	134 ± 21 ($n = 9$)
L-Arginine	25 ± 7 ($n = 7$)	19 ± 4 ($n = 7$)	98 ± 12 ($n = 7$)
Ascorbate	-44 ± 30 ($n = 8$)	n/a	n/a

Table 7.4 (a): A summary of the *in-vivo* characterisation data for the Type 2 NO sensor.

Type 3 NO Sensor	Current change (ΔI , pA)	Max response time (mins)	Return to baseline time (mins)
Administrations			
Saline	43 ± 21 ($n = 8$)	3 ± 1 ($n = 8$)	9 ± 2 ($n = 8$)
L-NAME	52 ± 15 ($n = 9$)	83 ± 16 ($n = 9$)	142 ± 25 ($n = 9$)
L-Arginine	28 ± 12 ($n = 7$)	32 ± 4 ($n = 7$)	103 ± 23 ($n = 7$)
Ascorbate	-21 ± 14 ($n = 6$)	n/a	n/a

Table 7.4 (b): A summary of the *in-vivo* characterisation data for the Type 3 NO sensor.


7.5 References

- Alderton W, Cooper C & Knowles R. (2001). Nitric oxide synthases: structure, function and inhibition. *Journal of Biochemistry* **357**, 593-615.
- Ashab I, Peer G, Blum M, Wollman Y, Chernihovsky T, Hassner A, Schwartz D, Cabili S, Silverberg D & Iaina A. (1995). Oral administration of L-arginine and captopril in rats prevents chronic renal failure by nitric oxide production. *Kidney International* **47**, 1515-1521.
- Bolger FB, McHugh SB, Bennett R, Li J, Ishiwari K, Francois J, Conway MW, Gilmour G, Bannerman DM, Fillenz M, Tricklebank M & Lowry JP. (2011). Characterisation of carbon paste electrodes for real-time amperometric monitoring of brain tissue oxygen. *Journal of Neuroscience Methods* **195**, 135-142.
- Bredt DS & Snyder SH. (1992). Nitric oxide, a novel neuronal messenger. *Neuron* **8**, 3-11.
- Brown F, Finnerty N, Bolger F, Millar J & Lowry J. (2005). Calibration of NO sensors for *in-vivo* voltammetry: laboratory synthesis of NO and the use of UV-visible spectroscopy for determining stock concentrations. *Analytical and Bioanalytical Chemistry* **381**, 964-971.
- Brown FO, Finnerty NJ & Lowry JP. (2009). Nitric oxide monitoring in brain extracellular fluid: characterisation of Nafion[®]-modified platinum electrodes *in-vitro* and *in-vivo*. *Analyst* **134**, 2012-2020.
- Brown FO & Lowry JP. (2003). Microelectrochemical sensors for *in-vivo* brain analysis: an investigation of procedures for modifying Pt electrodes using Nafion[®]. *Analyst* **128**, 700-705.
- Carvalho FA, Martins-Silva J & Saldanha C. (2004). Amperometric measurements of nitric oxide in erythrocytes. *Biosensors and Bioelectronics* **20**, 505-508.
- Creager MA, Gallagher SJ, Girerd XJ, Coleman SM, Dzau VJ & Cooke JP. (1992). L-arginine improves endothelium-dependent vasodilation in hypercholesterolemic humans. *Journal of Clinical Investigation* **90**, 1248.
- Da Cunha IC, José RF, Orlandi Pereira L, Pimenta JA, Oliveira de Souza IA, Reiser R, Moreno Júnior H, Marino Neto J, Paschoalini MA & Faria MS. (2005). The role of nitric oxide in the emotional learning of rats in the plus-maze. *Physiology & Behavior* **84**, 351-358.
- Drexler H, Zeiher A, Meinzer K & Just H. (1991). Correction of endothelial dysfunction in coronary microcirculation of hypercholesterolaemic patients by L-arginine. *The Lancet* **338**, 1546-1550.

- Ferreira NR, Ledo A, Frade JG, Gerhardt GA, Laranjinha J & Barbosa RM. (2005). Electrochemical measurement of endogenously produced nitric oxide in brain slices using Nafion/*o*-phenylenediamine modified carbon fiber microelectrodes. *Analytica Chimica Acta* **535**, 1-7.
- Finnerty NJ, O'Riordan SL, Brown FO, Serra PA, O'Neill RD & Lowry JP. (2012a). *In-vivo* characterisation of a Nafion[®]-modified Pt electrode for real-time nitric oxide monitoring in brain extracellular fluid. *Analytical Methods* **4**, 550-557.
- Finnerty NJ, O'Riordan SL, Palsson E & Lowry JP. (2012b). Brain nitric oxide: Regional characterisation of a real-time microelectrochemical sensor. *Journal of Neuroscience Methods* **209**, 13-21.
- Gallo O, Fini-Storchi I, Vergari WA, Masini E, Morbidelli L, Ziche M & Franchi A. (1998). Role of nitric oxide in angiogenesis and tumor progression in head and neck cancer. *Journal of the National Cancer Institute* **90**, 587-596.
- Hall CN & Garthwaite J. (2009). What is the real physiological NO concentration *in-vivo*? *Nitric Oxide* **21**, 92-103.
- Higdon J & Drake V. (2011). *An Evidence-Based Approach to Vitamins and Minerals: Health Benefits and Intake Recommendations*. Thieme International, New York, United States of America.
- Jadeski LC & Lala PK. (1999). Nitric Oxide Synthase Inhibition by *N*^G-Nitro-L-Arginine Methyl Ester Inhibits Tumor-Induced Angiogenesis in Mammary Tumors. *The American Journal of Pathology* **155**, 1381-1390.
- Javitt DC & Zukin SR. (1991). Recent advances in the phencyclidine model of schizophrenia. *The American Journal of Psychiatry* **148**, 1301-1308.
- Johansson C, Jackson DM & Svensson L. (1997). Nitric oxide synthase inhibition blocks phencyclidine-induced behavioural effects on prepulse inhibition and locomotor activity in the rat. *Psychopharmacology* **131**, 167-173.
- Jones AM, Wilkerson DP & Campbell IT. (2004). Nitric oxide synthase inhibition with L-NAME reduces maximal oxygen uptake but not gas exchange threshold during incremental cycle exercise in man. *The Journal of Physiology* **560**, 329-338.
- Kealy J, Bennett R & Lowry JP. (2013). Simultaneous recording of hippocampal oxygen and glucose in real time using constant potential amperometry in the freely-moving rat. *Journal of Neuroscience Methods* **215**, 110-120.
- Kennedy RT, Watson CJ, Haskins WE, Powell DH & Strecker RE. (2002). *In-vivo* neurochemical monitoring by microdialysis and capillary separations. *Current Opinion in Chemical Biology* **6**, 659-665.

- Kurose I, Kubes P, Wolf R, Anderson DC, Paulson J, Miyasaka M & Granger DN. (1993). Inhibition of nitric oxide production. Mechanisms of vascular albumin leakage. *Circulation Research* **73**, 164-171.
- Lajoix A-D, Pugnère M, Roquet F, Mani J-C, Dietz S, Linck N, Faurie F, Ribes G, Petit P & Gross R. (2004). Changes in the dimeric state of neuronal nitric oxide synthase affect the kinetics of secretagogue-induced insulin response. *Diabetes* **53**, 1467-1474.
- Lerman A, Burnett JC, Higano ST, McKinley LJ & Holmes DR. (1998). Long-term L-Arginine Supplementation Improves Small-Vessel Coronary Endothelial Function in Humans. *Circulation* **97**, 2123-2128.
- Losonczy G, Mucha I, Müller V, Kriston T, Ungvári Z, Tornoci L, Rosivall L & Venuto R. (1996). The vasoconstrictor effects of L-NAME, a nitric oxide synthase inhibitor, in pregnant rabbits. *British Journal of Pharmacology* **118**, 1012-1018.
- Lowry JP, Demestre M & Fillenz M. (1998a). Relation between cerebral blood flow and extracellular glucose in rat striatum during mild hypoxia and hyperoxia. *Developmental Neuroscience* **20**, 52-58.
- Lowry JP, Miele M, O'Neill RD, Boutelle MG & Fillenz M. (1998b). An amperometric glucose-oxidase/poly(*o*-phenylenediamine) biosensor for monitoring brain extracellular glucose: in vivo characterisation in the striatum of freely-moving rats. *Journal of Neuroscience Methods* **79**, 65-74.
- Lowry JP & O'Neill RD. (1992). Homogeneous mechanism of ascorbic acid interference in hydrogen peroxide detection at enzyme-modified electrodes. *Analytical Chemistry* **64**, 453-456.
- Maksimovich NE, Zinchuk VV & Maslakov DA. (2006). The degree of oxidative stress in the rat brain during ischemia and reperfusion in conditions of correction of the L-arginine-NO system. *Neuroscience and Behavioral Physiology* **36**, 373-378.
- Miele M & Fillenz M. (1996). *In-vivo* determination of extracellular brain ascorbate. *Journal of Neuroscience Methods* **70**, 15-19.
- Miilsch A & Busse R. (1990). NG-nitro-L-arginine (N5-[imino (nitroamino) methyl]-L-ornithine) impairs endothelium-dependent dilations by inhibiting cytosolic nitric oxide synthesis from L-arginine. *Naunyn-Schmiedeberg's Archives of Pharmacology* **341**, 143-147.
- Miller MJ, Sadowska-Krowicka H, Chotinaruemol S, Kakkis JL & Clark DA. (1993). Amelioration of chronic ileitis by nitric oxide synthase inhibition. *Journal of Pharmacology and Experimental Therapeutics* **264**, 11-16.

- O'Neill R. (1993). Sensor-tissue interactions in neurochemical analysis with carbon paste electrodes *in-vivo*. *The Analyst* **118**, 433.
- O'Neill RD, Lowry JP & Mas M. (1998). Monitoring Brain Chemistry *in-vivo*: Voltammetric Techniques, Sensors, and Behavioral Applications. *Critical Reviews™ in Neurobiology* **12**, 69-127.
- Pålsson E, Finnerty N, Fejgin K, Klamer D, Wass C, Svensson L & Lowry J. (2009). Increased cortical nitric oxide release after phencyclidine administration. *Synapse* **63**, 1083-1088.
- Pfeiffer S, Leopold E, Schmidt K, Brunner F & Mayer B. (1996). Inhibition of nitric oxide synthesis by N^G nitro-L-arginine methyl ester (L-NAME): requirement for bioactivation to the free acid, N^G-nitro-L-arginine. *British Journal of Pharmacology* **118**, 1433-1440.
- Rees DD, Palmer RMJ, Schulz R, Hodson HF & Moncada S. (1990). Characterization of three inhibitors of endothelial nitric oxide synthase *in-vitro* and *in-vivo*. *British Journal of Pharmacology* **101**, 746-752.
- Wilson AM, Harada R, Nair N, Balasubramanian N & Cooke JP. (2007). l-Arginine Supplementation in Peripheral Arterial Disease: No Benefit and Possible Harm. *Circulation* **116**, 188-195.
- Yu L-B, Dong X-S, Sun W-Z, Zhao D-L & Yang Y. (2005). Effect of a nitric oxide synthase inhibitor N^G-nitro-L-arginine methyl ester on invasion of human colorectal cancer cell line SL-174T. *World Journal of Gastroenterology* **11**, 6385.



*8. Simultaneous Recording
of Nitric Oxide and Oxygen
In-Vivo*

8.1 Introduction

NO is a small molecule that possesses an unpaired electron. Due to this fact, NO is a highly reactive free radical with a short half-life. It has been linked to a wide range of physiological and pathophysiological processes. It regulates vascular tone and is hypothesised in playing a part in hypertension, Parkinson's disease and Alzheimer's disease (Brown *et al.*, 2005). It is biosynthesised from L-arginine yielding a co-product of L-citrulline and catalysed by one of three NOS isoenzymes. It requires nicotinamide adenine dinucleotide phosphate (NADPH), flavin adenine dinucleotide (FAD), flavin mononucleotide (FMN), tetrahydrobiopterin (BH₄), calmodulin, O₂ and heme in order for the reaction to take place (Dinerman *et al.*, 1993; Schmidt *et al.*, 1993). The various NOS enzymes responsible for the synthesis of NO are of, neuronal (nNOS), endothelium (eNOS) and inducible NOS (iNOS) forms (Alderton *et al.*, 2001). The nNOS and eNOS are calcium and calmodulin dependent (Mungrue *et al.*, 2003), whereas, iNOS is calcium and calmodulin independent. The latter is expressed in response to immunological or an inflammatory stimulation in macrophages, astrocytes, microglia and other cells producing NO that last for hours or even days (Iadecola *et al.*, 1995).

In 1988, Garthwaite *et al.*, observed that upon activation of the NMDA receptors, the release of NO occurred (Garthwaite *et al.*, 1988). It has been stated that nNOS is the main source of NO in neurons and localises to synaptic spines (Zhou & Zhu, 2009). It has also been demonstrated that in the striatum, NO is mainly produced via the nNOS enzyme (Bredt *et al.*, 1990; Bredt *et al.*, 1991). Upon binding of glutamate to the NMDA receptors, the calcium channels open. An influx of calcium causes the activation of the nNOS inside the neurons and the subsequent production of NO is triggered (Piknova *et al.*, 2011). Ignarro *et al.*, reported that the EDRF is an unstable substance that is released from the endothelium to promote smooth muscle relaxation (Ignarro *et al.*, 1987). In the late 1980's, there were three main groups that independently reported that the EDRF might be NO. All three found that NO and the EDRF possessed identical biological and chemical characteristics and each established substantial evidence that made this claim plausible (Ignarro *et al.*, 1987; Palmer *et al.*, 1987; Furchgott, 1988).

The eNOS enzyme is the major isoform expressed in the cardiovascular system (Mungrue *et al.*, 2003). The release of NO from endothelial cells is believed to be an essential vasodilator mechanism responsible for the maintenance of vasomotor function. In both the cerebral and peripheral blood vessels, the decrease in NO concentration results in a major change of vascular function which includes vasoconstriction and increases in arteriole blood pressure (Katusic & Austin, 2013). It has been demonstrated by Macrae *et al.*, that inhibition of the synthesis of NO resulted in a long lasting decrease in CBF in rats (Macrae *et al.*, 1993). It is evident that NO plays a role in the regulation of CBF and this statement has been widely accepted (Lindauer *et al.*, 1999).

It has been shown that the direct real-time measurement of brain tissue O₂ can act as an indicator for increases in CBF (Lowry *et al.*, 1997). Further to this, the hydrogen clearance technique has also been utilised previously as a measurement tool for local blood flow (Aukland *et al.*, 1964; Aukland, 1965). This technique is inexpensive and involves the inhalation of hydrogen gas. Once the administration of hydrogen has ceased the rate of clearance which is proportional to local blood flow is monitored by a Pt electrode. However, this technique has some downfalls with difficulty of administration in freely moving animals. It is believed that an alternative measurement demonstrated by Lowry *et al.*, which measures changes in the concentration of the substance delivered to the tissue by the blood stream i.e. O₂, can accurately and reliably give an indication of changes in CBF. O₂ concentration has been described as the balance between its supply as a result of blood flow from the capillaries and its utilisation which occurs as a result of metabolism in cells. Upon the rise in CBF under physiological stimulation, the supply of O₂ will surpass the utilisation, ensuing in a net increase in O₂ (Lowry *et al.*, 1997).

CBF is fundamental to the living brain and there is an increase in the need for more blood flow upon the rise in neuronal activity (Liao *et al.*, 2013). Neurovascular coupling describes the relationship between local neural activity and the subsequent changes that occur in CBF (Zheng *et al.*, 2010). Understanding how neurovascular coupling works is important for many reasons, one of which is brain imaging. Brain imaging relies on this coupling in order to map brain activity. Non-invasive imaging of the brain involves techniques that utilise this coupling, provide an insight into how the brain works in extraordinary detail and has been established by Raichle *et al.*, (Raichle, 1998). One such brain imaging technique is

functional magnetic resonance imaging (fMRI). Functional MRI is the main neuroimaging technique for research carried out in humans (Moreno *et al.*, 2013). It is non-invasive and a quick technique, however, despite the advantages that it possesses, it faces challenges especially in the clinical environment. This technique does not directly determine neuronal activation, but the related signals that are associated with neuronal activity. It also has the drawback of exclusion of certain patients that don't fulfil the necessary requirements for the imaging protocols in the clinical setting. Patients with movement disorders and patients that have difficulty with completing the tasks needed for fMRI analysis due to cognitive impairments are excluded and this can be a significant limitation of fMRI (Faro & Mohamed, 2010).

In some brain pathologies the communication between the cerebral blood vessels and neuronal activity are disturbed and the ensuing imbalance could contribute to the dysfunction of the brain. This can be observed in disorders like hypertension and Alzheimer's disease (Girouard & Iadecola, 2006). Hypertension changes the construction of cerebral blood vessels and weakens how they function (Faraci *et al.*, 1990; Dickinson, 2001). The alteration of neurovascular coupling from hypertension has been hypothesised by Kasama *et al.*, (Kazama *et al.*, 2003). Alzheimer's disease demonstrates an alteration in cerebrovascular structure, cerebral micro vessels decrease in number, endothelial cells are compressed and there is a degeneration in the smooth muscle cells (Farkas & Luiten, 2001). In 2010, Lowry *et al.*, demonstrated the real time simultaneous monitoring of blood oxygenation level dependant (BOLD) fMRI and brain tissue O₂. The findings demonstrated the possibility of achieving real-time metabolite information during fMRI acquirement and that the O₂ sensor could provide an indicator for alterations of the BOLD response, leading to a substitute for brain imaging in rodents which facilitates behavioural testing (Lowry *et al.*, 2010).

The importance of NO in the brain is determined by its involvement in neurodegenerative diseases and neuronal, glial and vascular physiological effects. This gives rise to the potential pharmacological treatments concentrating on the NO metabolic pathways. Figure 8.1, depicts a scheme that defines physiological changes that link neural responses and vascular responses. In this chapter the simultaneous real-time monitoring of NO and O₂ is explored during periods of hypoxia and hyperoxia, neuronal activation and i.p. injections of

chloral hydrate, diamox, L-NAME and L-arginine. Interesting and unpredicted results were obtained and are discussed fully in the subsequent sections.

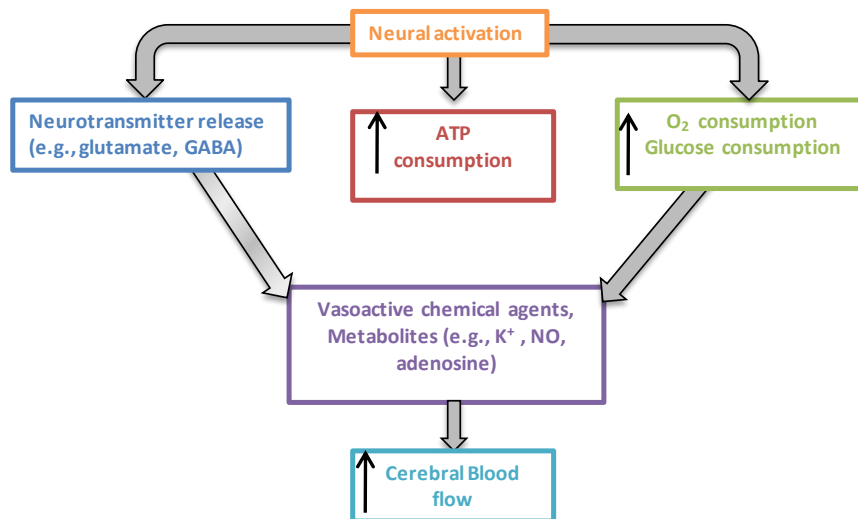


Figure 8.1: A summary of physiological changes linking neural responses and vascular responses. Redrawn from http://www.scholarpedia.org/article/Neurovascular_coupling.

8.2 Experimental

The instrumentation and software utilised are described in Section 3.2. All chemicals and solutions are detailed in Section 3.3. The manufacture of the varying NO and O₂ sensors are described in Section 3.4. O₂ sensors were co-implanted with NO sensors in the striatum of rats. A potential of +900 mV *vs.* Ag wire was applied to all the NO working electrodes and a potential of -650 mV *vs.* Ag wire was applied to all the O₂ working electrodes. All *i.p.* injections were prepared in normal saline or otherwise stated. All *in-vivo* experiments were undertaken as described in Section 3.8. All experiments were carried out in freely moving animals. The surgical procedure undertaken for the implantation of the sensors is detailed in Section 3.8.2. Data is reported as mean \pm S.E.M. All statistical analysis was carried out using student *t*-tests. These tests were performed using GraphPad prism and yielded a *P*-value result, which is the probability value that specifies if the results observed are significantly different.

In each of the sections, n denotes the number of perturbations carried out on a number of sensors in a certain amount of animals, unless stated otherwise. The NO currents are presented in pA and NO sensitivity in pA/ μ M. The O₂ currents are presented in nA and O₂ sensitivity in nA/ μ M. All data presented had baselines normalised to 100 % illustrating the overall change in current as % of the pre-perturbation baseline level. This removes both inter-electrode and inter-animal variability by ensuring that the presented NO changes are representative of the data from all animals utilised in each study undertaken. All max response times and return to baseline times are taken from post administration/perturbations and not from time zero.

8.3 Results and Discussion

This results section comprises the data from experiments undertaken to monitor the changes in NO and O₂ *in-vivo*, simultaneously. The NO and O₂ results within this chapter are from the monitoring of the NO and O₂ molecules with the combined sensors (Type 2 and Type 3 NO sensors) and (SMCPEs and MMCPEs). There was little difference between the SMCPEs and MMCPEs for the monitoring of O₂ and the Type 2 and Type 3 sensors for the monitoring of NO, with regards to sensitivity and overall behaviour *in-vivo* (see Chapter 5 and Chapter 7, respectively), so it was deemed appropriate to collate the sensors for this chapter. In Figure 8.3.1 (a) and 8.3.1 (b), baseline recordings are displayed over a three hour period for NO and O₂ which demonstrate how baseline levels remain stable whilst the animal is in a state of ease.

8.3.1 Baseline recordings

The baseline recordings data in this section was analysed using the results from 15 sensors in 5 animals for the NO sensors and 5 sensors in 5 animals for the O₂ sensors.

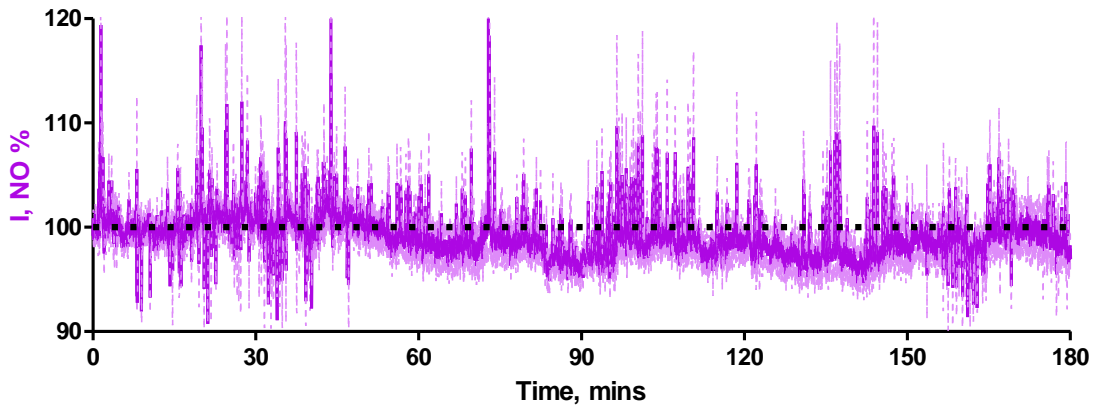


Figure 8.3.1 (a): A time vs. percentage change graph of baseline NO currents monitored by NO sensors (Type 2 and Type 3 NO sensors), displaying a stable baseline over the course of three hours *in-vivo* (15 sensors in 5 animals)

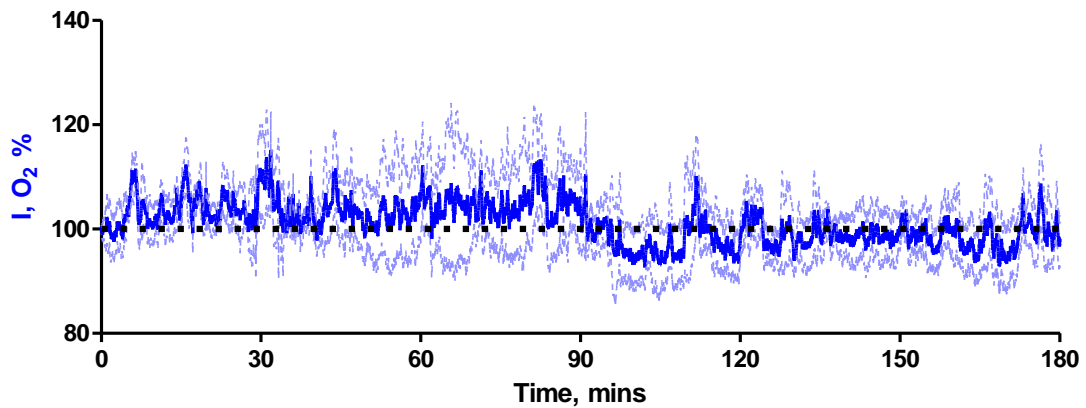


Figure 8.3.1 (b): A time vs. percentage change graph of baseline O₂ currents monitored by O₂ sensors (MMCPEs and SMCPEs), displaying a stable baseline over the course of three hours *in-vivo*, (5 sensors in 5 animals).

Figure 8.3.1 (a) and 8.3.1 (b) display baseline levels for NO and O₂ respectively, over the course of three hours. The data demonstrates how the levels remain stable whilst the animal is in a state of rest. The results in this Chapter demonstrate how different experiments undertaken with these sensors, cause a distinct change from stable baselines levels, which are discussed in more detail in the subsequent sections.

8.3.2 Hypoxia

In these experiments, the production of mild hypoxia was created by the administration of a N_2 /air mixture to the snout of the animal, through a plastic tube. The flow rate was kept low, in order to keep the animal as comfortable as possible, during the experiment. The effect of a 3-minute period of hypoxia recorded by the NO and O_2 sensors simultaneously, is displayed in Figure 8.3.2. The 3-minute period of hypoxia data in this section was analysed using the results from 17 perturbations with 12 sensors in 5 animals for the NO data and 17 perturbations with 8 sensors in 5 animals for the O_2 data.

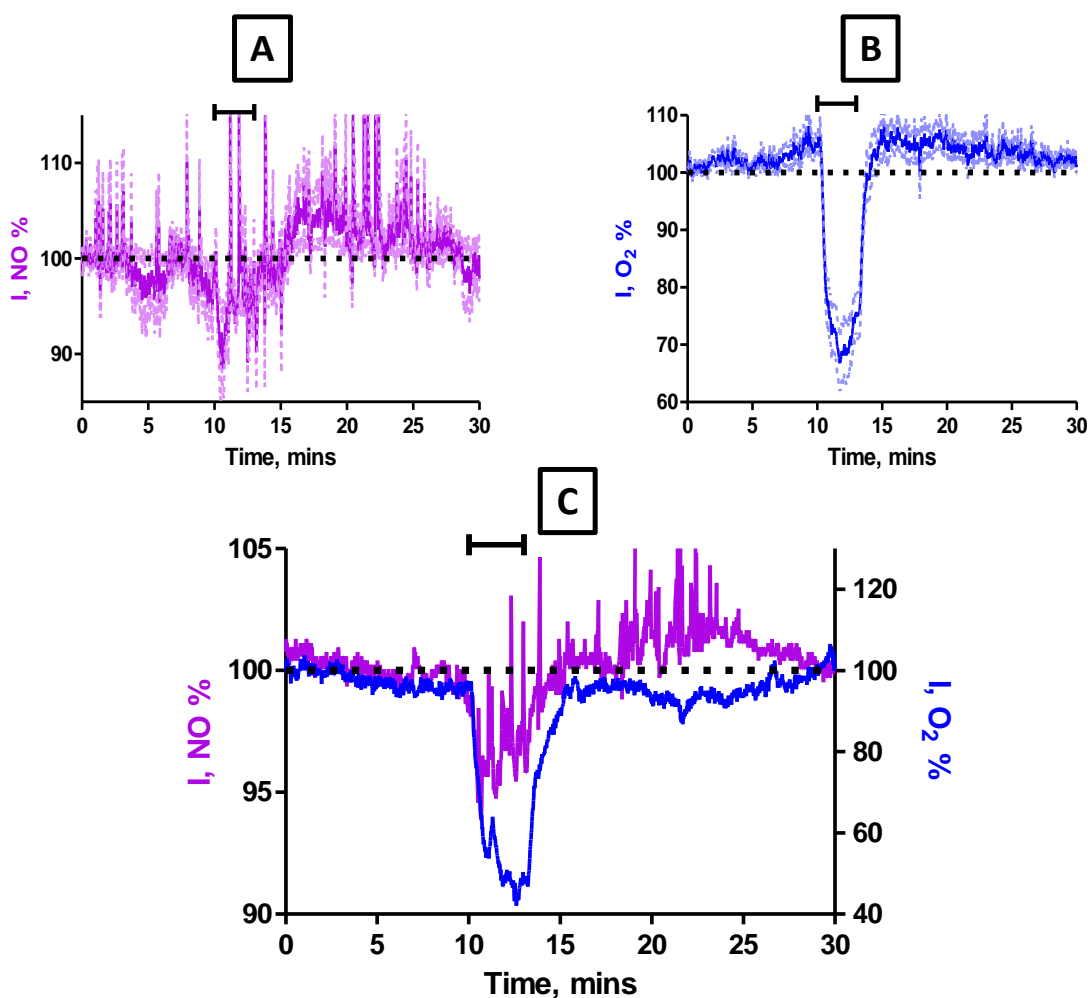


Figure 8.3.2: Time vs. percentage change graphs during a 3-minute period of hypoxia monitoring (A) NO (Type 2 and Type 3 NO sensors, $n = 17$: 5 animals) and (B) O_2 (MMCPes and SMCPEs, $n = 17$: 5 animals). (C) A typical raw data example displaying the combined data of the percentage change in NO and O_2 . The black bar is indicative of the duration of the administration.

Figure 8.3.2, demonstrates how a 3-minute period of induced hypoxia caused an immediate decrease in both O₂ and NO currents from baseline levels. The decrease in the O₂ levels achieved, were significantly different ($P < 0.0001$) from pre-hypoxia baseline levels. A decrease was observed in the NO currents, that was also significantly different ($P < 0.0001$) from the pre-baseline levels obtained. A percentage change of $6.3 \pm 1.5 \%$, $n = 17$ and $35.7 \pm 1.2 \%$, $n = 17$, was achieved for NO and O₂, respectively. The maximum response time for O₂ and NO was 2.5 ± 0.1 mins, $n = 17$ and 2.0 ± 0.1 mins, $n = 17$, respectively. Upon cessation of inhalation of the gas, the O₂ and NO levels returned to corresponding baseline currents of -168.9 ± 4.3 nA, $n = 17$, ($P = 0.8315$) and 628.2 ± 149.1 pA, $n = 17$, ($P = 0.7440$), after 6.6 ± 0.3 mins, $n = 17$ and 7.0 ± 0.6 mins, $n = 17$, respectively.

A summary of the results for the 3-minute period of hypoxia on the O₂ and NO currents is given in Table 8.3.2 (a) and 8.3.2 (b).

Hypoxia (NO Sensors)					
Current change (pA)	Current change (%)	Max response Time (mins)	Return Time (mins)	Baseline Pre Injection (pA)	Baseline Post Injection (pA)
20.1 ± 3.4	6.3 ± 1.5	2.0 ± 0.1	7.0 ± 0.6	631.1 ± 145.2	628.2 ± 149.1

Table 8.3.2 (a): Averaged results table for a 3-minute period of hypoxia, recorded with NO sensors (Type 2 and Type 3 NO Sensor, implanted in the striatum of 5 freely moving rats ($n = 17$ with 12 sensors)).

Hypoxia (O ₂ Sensors)					
Current change (nA)	Current change (%)	Max response Time (mins)	Return Time (mins)	Baseline Pre Injection (nA)	Baseline Post Injection (nA)
-167.5 ± 4.1	35.7 ± 1.2	2.5 ± 0.1	6.6 ± 0.3	-167.5 ± 4.1	-168.9 ± 4.3

Table 8.3.2 (b): Averaged results table for a 3-minute period of hypoxia, recorded with O₂ sensors (MMCPes and SMCPEs), implanted in the striatum of 5 freely moving rats ($n = 17$ with 8 sensors)).

In the literature it has been suggested that eNOS activity is enhanced by hypoxia (Pearce *et al.*, 1989; Pearce *et al.*, 1990). So if we were observing a current change by which eNOS had been activated then this statement suggests an increase in NO would have occurred. Studies have also suggested that O₂ is required for NOS activity and that NO production would decrease under low O₂ tension (Coggins & Bloch, 2007). As O₂ is one of the substrates required for the production of NO, a lack of O₂ during hypoxia would cause inhibition of the enzyme activity even if intracellular calcium increases (Leone *et al.*, 1991). Pelligrino *et al.*, reported that a reduction in O₂ supply in rats may decrease the NO generating capacity in the brain (Pelligrino *et al.*, 1993). The observation of a decrease in the NO response after a N₂/air administration suggests that the decrease in NO production is directly due to a decrease in the O₂ supply. It has to be noted also, that the majority of literature studies are based on indirect measurements of NO, however, in this body of research the direct real-time measurement of NO is achieved. The slight over shoot in NO after the administration had ceased suggests a return of reoxygenation back into the system and the subsequent NO/NMDA pathway trying to re-establish an NO baseline.

8.3.3 Hyperoxia

Mild hyperoxia was established in the subject by the administration of O₂/air to the snout of the animal through a plastic tube with a low flow rate. This prevents the animal from being startled or uneasy during this procedure. The effects of a typical 5-minute period of hyperoxia recorded with the NO and O₂ sensors are displayed in Figure 8.3.3. The 5-minute period of hypoxia data in this section was analysed using the results from 18 perturbations with 12 sensors in 4 animals for the NO data and 18 perturbations with 4 sensors in 4 animals for the O₂ data.

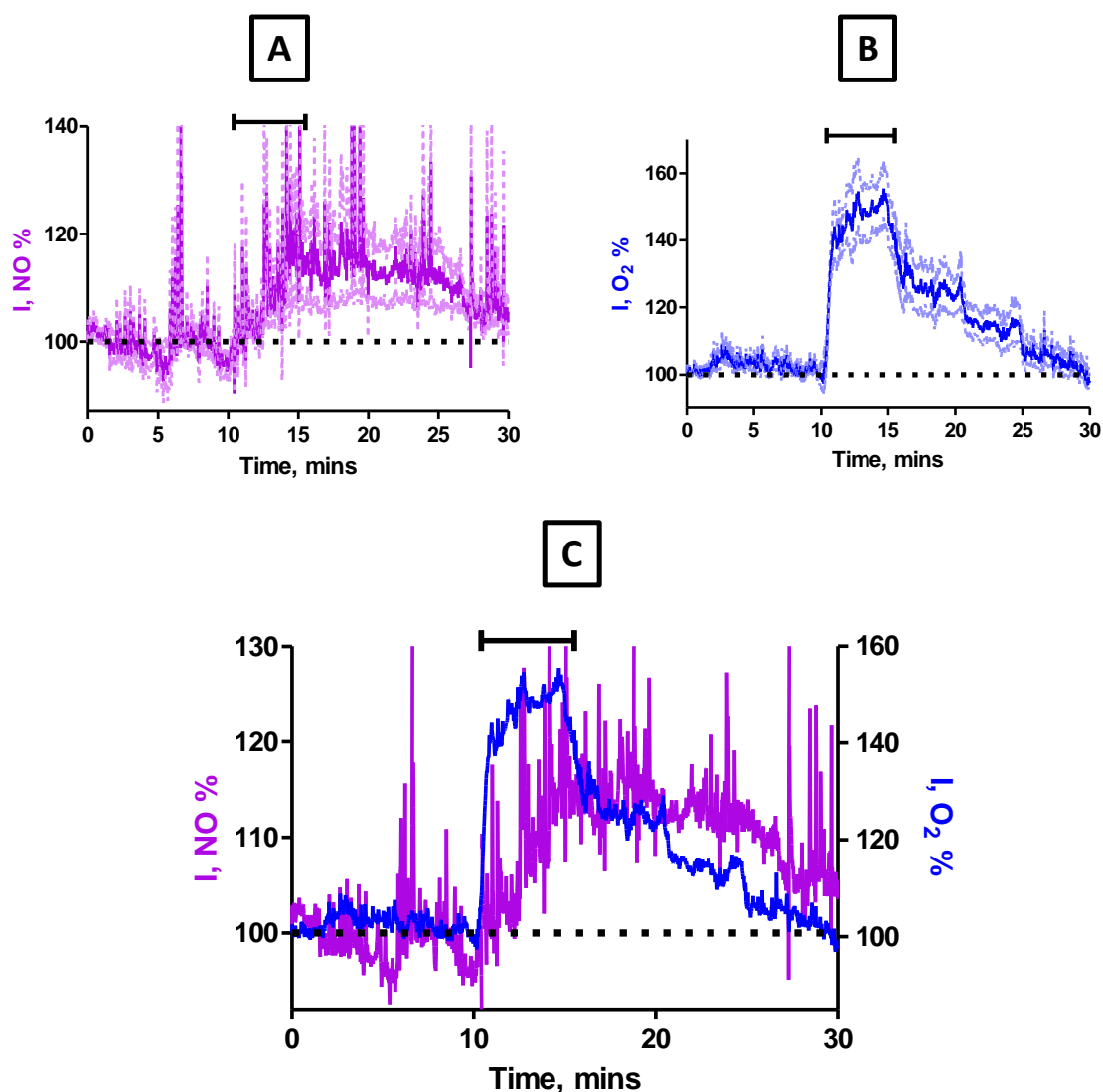


Figure 8.3.3: Time vs. percentage change graphs during a 5-minute period of hyperoxia monitoring (A) NO (Type 2 and Type 3 NO sensors, $n = 18$: 4 animals) and (B) O₂ (MMCPes and SMCPEs, $n = 18$: 4 animals). (C) A typical raw data example displaying the combined data of the percentage change in NO and O₂. The black bar is indicative of the duration of the administration.

Figure 8.3.3, demonstrates how a 5 minute period of induced hyperoxia caused an immediate and significant increase ($P < 0.0001$) in the O₂ current, however, although an increase in the NO signal was observed, it was not significantly different ($P < 0.0001$) from pre-baseline levels. A percentage change of $44.5 \pm 2.8 \%$, $n = 18$, after approximately 2.9 ± 0.1 mins, $n = 18$, was achieved with the O₂ sensors. The NO signal yielded a percentage change of $5.7 \pm 1.0 \%$, $n = 18$, after approximately 3.6 ± 0.2 mins, $n = 18$. Upon cessation

of inhalation of the gas, the O₂ and NO currents returned to baseline levels of -165.6 ± 4.2 nA, $n = 18$, ($P = 0.8307$) and 352.2 ± 41.2 pA, $n = 18$, ($P = 0.1932$), respectively. Table 8.3.3 (a) and 8.3.3 (b), detail a summary of the results from the administration of O₂/air.

It is observed that it takes slightly longer for the NO currents to return to corresponding baseline levels (NO: 14.5 ± 1.9 mins, $n = 18$ and O₂: 12.9 ± 0.5 mins, $n = 18$), however not significantly different ($P = 0.4211$).

Hyperoxia (NO Sensors)					
Current change (pA)	Current change (%)	Max response Time (mins)	Return Time (mins)	Baseline Pre Injection (pA)	Baseline Post Injection (pA)
17.3 ± 2.7	5.7 ± 1.0	3.6 ± 0.2	14.5 ± 1.9	341.3 ± 38.8	352.2 ± 41.2

Table 8.3.3 (a): Averaged results table for a 5-minute period of hyperoxia, recorded with NO sensors (Type 2 and Type 3 NO Sensor), implanted in the striatum of 4 freely moving rats ($n = 18$ with 12 sensors).

Hyperoxia (O₂ Sensors)					
Current change (nA)	Current change (%)	Max response Time (mins)	Return Time (mins)	Baseline Pre Injection (nA)	Baseline Post Injection (nA)
70.6 ± 3.5	44.5 ± 2.8	2.9 ± 0.1	12.9 ± 0.5	-164.3 ± 4.3	-165.6 ± 4.2

Table 8.3.3 (b): Averaged results table for a 5-minute period of hyperoxia, recorded with O₂ sensors (MMCPEs and SMCPEs), implanted in the striatum of 4 freely moving rats ($n = 18$ with 4 sensors).

The increase in NO after the period of hyperoxia could be due to the increased availability of O₂, therefore causing a rise in the production of NO. *In-vitro* studies demonstrated that O₂ can affect the expression of NOS and NO production in cultured cells exposed to hyperoxia (Liao *et al.*, 1995). It has also been demonstrated by Vacchiano *et al.*, that macrophages obtained from the bronchoalveolar lavage of animals exposed to O₂, have been shown to produce NO (Vacchiano & Tempel, 1994). Again, the indirect measurements of these molecules can only provide a certain amount of information

whereas, the hyperoxia results shown in this body of research demonstrate real time *in-vivo* detection of changes in O₂ and NO.

8.3.4 Restraint stress

Two forms of physiological stimulation were utilised throughout the experiments; these were restraint stress and tail pinch. Tail pinch results are presented in the next section (see Section 8.3.5). Each test was carried out for 5-minutes. The two stimuli, cause neuronal activation in the animal, leading to changes in the currents recorded by the sensors. The 5-minute period of a restraint stress data in this section was analysed using the results from 12 perturbations with 12 sensors in 5 animals for the NO data and 12 perturbations with 5 sensors in 5 animals for the O₂ data.

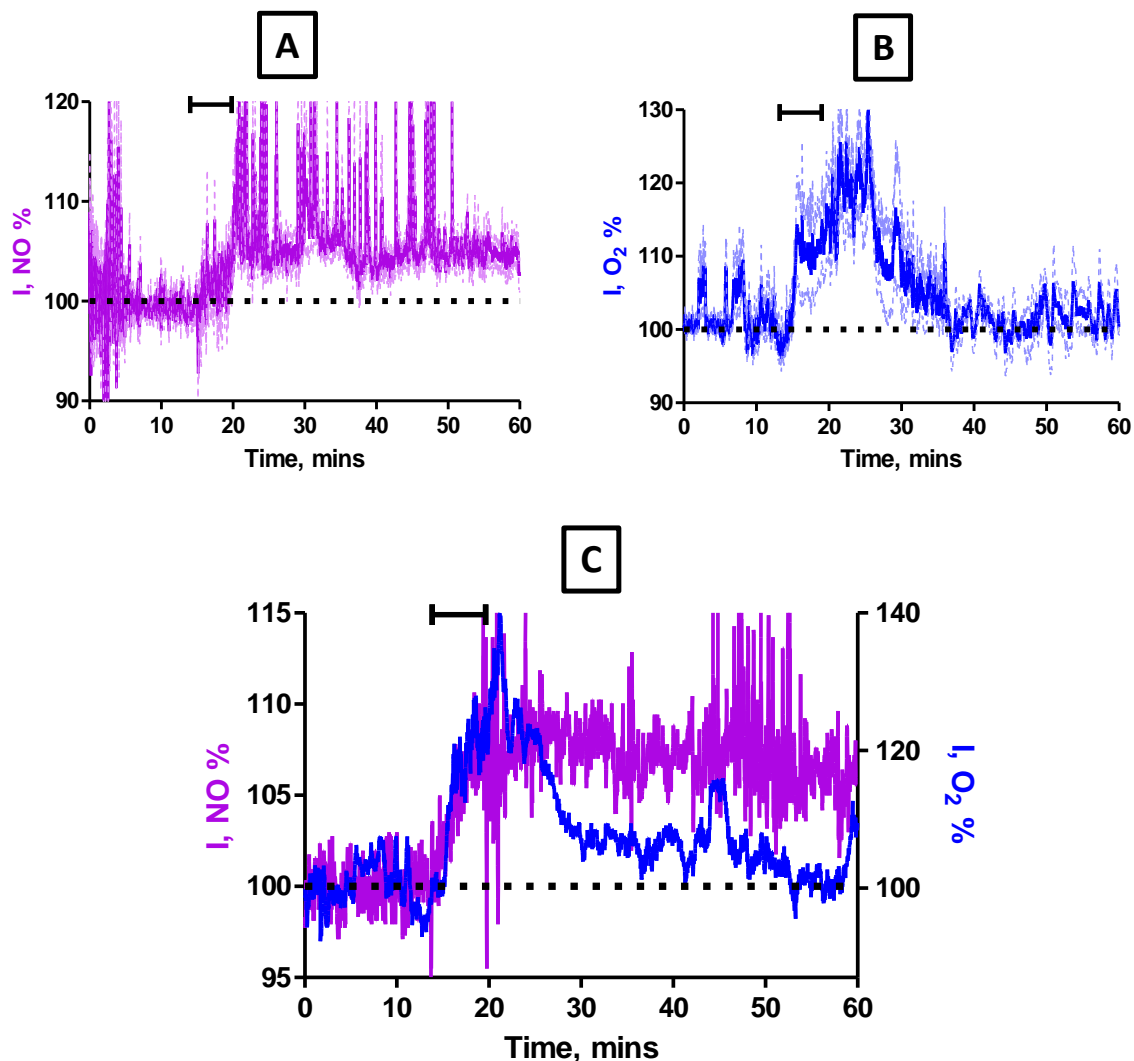


Figure 8.3.4 (a): Time vs. percentage change graphs during a restraint stress monitoring (A) NO (Type 2 and Type 3 NO sensors, $n = 12$: 5 animals) and (B) O₂ (MMCPEs and SMCPEs, $n = 12$: 5 animals). (C) A typical raw data example displaying the combined data of the percentage change in NO and O₂. The black bar is indicative of the duration of the stimulus.

The application of a 5-minute restraint stress resulted in a rapid increase in the O₂ current recorded at the O₂ sensors. A percentage change of $15.8 \pm 1.3\%$, $n = 12$ after 2.6 ± 0.2 mins, $n = 12$, that was significantly different ($P = 0.0088$) from pre-baseline levels was achieved by the O₂ sensors. The NO sensors displayed a percentage change of $3.9 \pm 2.0\%$, $n = 12$, that was significantly different ($P = 0.0271$) from pre-baseline levels. Upon cessation of the stimulus, the O₂ baseline currents began to fall until another increase in the O₂ current was observed shortly afterwards. A second O₂ increase on cessation of the

stimulus was observed most likely due to O₂ concentration regulation in the body. It is based on supply and utilisation (Lowry *et al.*, 1997), therefore once the stimulus was ceased, the supply exceeded the demand and an increase was observed, followed on by a subsequent decrease in the current.

A significantly different ($P = 0.0017$) baseline O₂ current was observed, subsequent to the first maximum response, after 6.1 ± 0.1 mins, $n = 12$. A percentage change of 20.2 ± 1.6 %, $n = 12$, was recorded from the second maximum response. The O₂ current returned to corresponding baseline levels of -155.6 ± 5.5 nA, $n = 12$, after 18.4 ± 2.5 mins, $n = 12$, ($P = 0.5750$), however the NO current remained at a new recorded level of 447.4 ± 91.3 pA, $n = 12$, ($P = 0.0122$). The O₂ returned back to pre-baseline levels, whereas, the NO failed to do so within that time frame. The de-synchronisation between the NO and O₂ currents suggests that the NO that we are detecting is not endothelial, since O₂ returns to baseline levels, but instead it remains elevated more than likely due to the NMDA receptor activity brought about by the neuronal activation. Table 8.3.4 (a) and 8.3.4 (b) display a summary of all the results obtained by the NO and O₂ sensors.

Restraint Stress (NO Sensors)					
Current Change (pA)	Current Change (%)	Max Response Time (mins)	Return Time (mins)	Baseline Pre Injection (pA)	New Recorded Baseline Level (pA)
14.2 ± 5.9	3.9 ± 2.0	2.2 ± 0.3	-----	432.4 ± 87.1	447.4 ± 91.3

Table 8.3.4 (a): Averaged results table for restraint stress, recorded with NO sensors (Type 2 and Type 3 NO Sensor), implanted in the striatum of 5 freely moving rats ($n = 12$ with 12 sensors). The dashed line (under return time), corresponds to the NO response remaining elevated and not returning back to baseline levels, during the time frame specified in the graph.

Restraint stress O ₂ Sensors					
Current change (nA)	Current change (%)	Max response Time (mins)	Return Time (mins)	Baseline Pre Injection (nA)	Baseline Post Injection (nA)
24.3 ± 2.3	15.8 ± 1.3	2.6 ± 0.2	18.4 ± 2.5	-151.2 ± 5.4	-155.6 ± 5.5
Restraint stress (2 nd current change)					
(2 nd) Current change (nA)	(2 nd) Current change (%)	(2 nd) Max response Time (mins)	Return Time (mins)	Baseline Pre Injection (nA)	Baseline Post Injection (nA)
31.4 ± 3.0	20.2 ± 1.6	6.1 ± 0.1	18.4 ± 2.5	-151.2 ± 5.4	-155.6 ± 5.5

Table 8.3.4 (b): Summary of results for the first and second current change responses for a restraint stress (5-minutes), with the O₂ sensors implanted in the striatum of freely moving rats ($n = 12$ with 5 sensors in 5 animals).

A similar response from NO after a restraint stress was observed within our group with the Type 1 NO sensor. There was an increase in the NO signal upon initiation of the restraint and it remained elevated after the restraint stress had ceased. Figure 8.3.4 (b) displays the Type 1 NO sensor trace in response to the restraint stress (courtesy of Dr. Niall Finnerty). The Type 1 NO sensor has been fully characterised *in-vitro* and *in-vivo* within our research group (Brown *et al.*, 2009; Finnerty *et al.*, 2012a; Finnerty *et al.*, 2012b). These results demonstrate that the NO signal that was observed is not sensor specific and has been observed utilising other sensor designs. Figure 8.3.4 (c), displays the result of a restraint stress recorded by a glutamate sensor courtesy of Dr. Fiachra Bolger.

An elevated response of glutamate that does not return back to baseline levels after the stimulus had ceased, yielded a very similar elevated response obtained by the NO sensors. As glutamate is linked to the activation of the NMDA receptors (VanDongen, 2008), it can be postulated that the glutamate response observed by Dr. Fiachra Bolger, after a 5-minute restraint stress, is strongly linked to the increase in NO observed in this section after a 5-minute restraint stress. An increase in glutamate could possibly cause the activation of the NMDA receptor and thus an increase in NO.

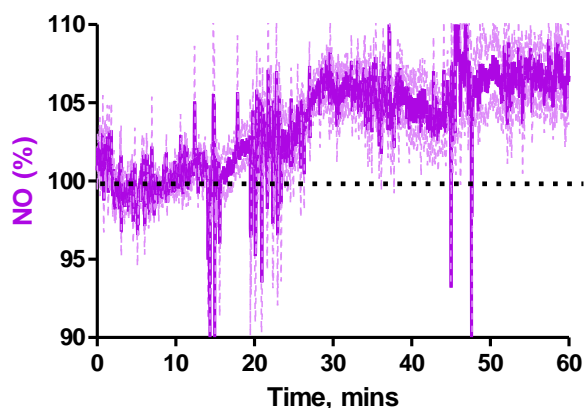


Figure 8.3.4 (b): A time vs. percentage graph displaying the NO percentage change response attained from a 5-minute period of restraint stress with Type 1 NO sensors, $n = 9$, in 3 animals (Courtesy of Dr. Niall Finnerty).

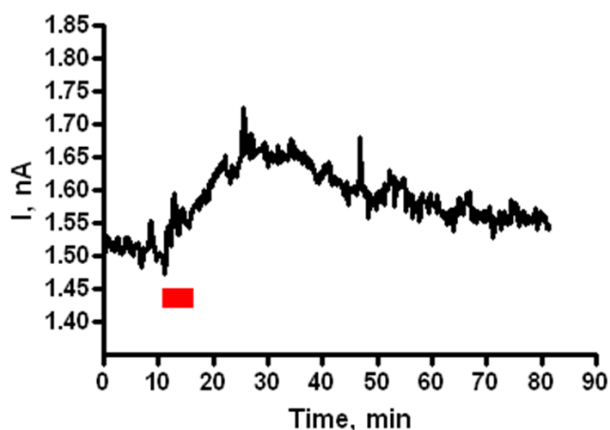


Figure 8.3.4 (c): A typical example of a time vs. current response graph, displaying the increase in the glutamate response detected with a glutamate sensor, in the striatum of a freely moving rat after a 5-minute period of a restraint stress administration (Courtesy of Dr. Fiachra Bolger).

Since NMDA-glutamate receptors are coupled to nNOS (Buerk *et al.*, 2003), it is possible that the increase in neuronal activity and subsequent NO production in the striatum that was observed, is from nNOS, although eNOS contribution cannot be ruled out. The interesting observation was the elevated NO response after the restraint stress had ceased. This result was shown not only in the Type 2 and Type 3 NO sensors but also in the Type 1 NO sensor (courtesy of Dr. Niall Finnerty). As the O_2 current returned to baseline levels and O_2 can be utilised as a reliable index of cerebral blood flow (Lowry *et al.*, 1997), it is suggested that if

the eNOS enzyme was the main NO producing enzyme signal observed for the restraint stress, then a return to pre-baseline levels would have been observed. Therefore, the eNOS enzyme is not causing this increase and therefore it is believed the NMDA/receptor nNOS pathway is the main contributor to this production of NO.

8.3.5 Tail Pinch

The application of a 5-minute tail pinch causes physiological stimulation that increases neuronal activation in the striatum and a simultaneous elevation of CBF and O₂ (Valente *et al.*, 2012). The 5-minute period of a tail pinch stress data in this section was analysed using the results from 18 perturbations with 13 sensors in 5 animals for the NO data and 18 perturbations with 5 sensors in 5 animals for the O₂ data. Figure 8.3.5 (a) displays the results achieved for both NO and O₂.

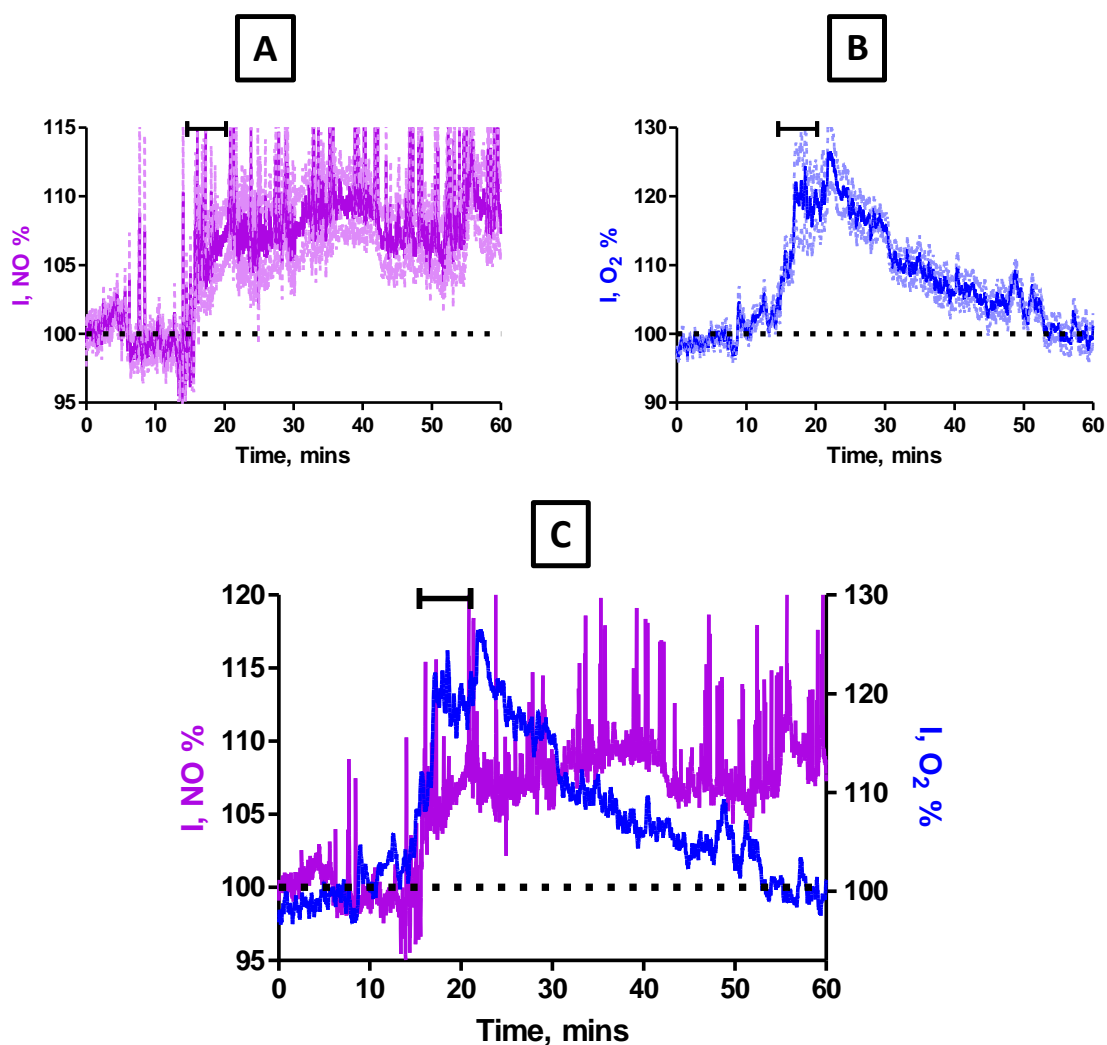


Figure 8.3.5 (a): Time vs. percentage change graphs during a restraint stress monitoring (A) NO (Type 2 and Type 3 NO sensors, $n = 18$: 5 animals) and (B) O₂ (MMCPEs and SMCPEs, $n = 18$: 5 animals). (C) A typical raw data example displaying the combined data of the percentage change in NO and O₂.

The black bar is indicative of the duration of the stimulus.

The application of a 5-minute tail pinch resulted in an instantaneous and rapid increase in the O₂ and NO current observed at the O₂ and NO sensors. An immediate and significant increase ($P = 0.0010$) in the O₂ current was observed. The NO sensors displayed an increase in the NO current that remained elevated after the stimulus had ceased, displaying a current that was significantly different ($P = 0.0387$) from pre-baseline levels. The NO and O₂ currents achieved a maximum response after 2.3 ± 0.4 mins, $n = 18$ and 2.8 ± 0.2 mins, $n = 18$, that corresponded to a percentage change of 9.4 ± 2.2 %, $n = 18$ and 18.9 ± 2.1 %, $n = 18$.

= 18, respectively. A return to baseline levels of -168.9 ± 5.2 pA, $n = 18$, ($P = 0.5212$) for the O₂ was achieved after 27.7 ± 2.9 mins, $n = 18$, however the NO response remained elevated at a baseline of 589.0 ± 140 pA, $n = 18$, ($P = 0.0098$). A similar observation was demonstrated with the application of the restraint stress (see Section 8.3.4).

Tail Pinch (NO Sensors)					
Current Change (pA)	Current Change (%)	Max Response Time (mins)	Return Time (mins)	Baseline Pre Injection (pA)	New Recorded Baseline Level (pA)
60.5 ± 27.0	9.4 ± 2.2	2.3 ± 0.4	-----	533.5 ± 126.8	589.0 ± 140.0

Table 8.3.5 (a): Averaged results for tail pinch, recorded with NO sensors (Type 2 and Type 3 NO Sensor), implanted in the striatum of 5 freely moving rats ($n = 18$ with 13 sensors). The dashed line (under return time), corresponds to the NO response remaining elevated and not returning back to baseline levels, during the time frame specified in the graph.

Tail Pinch (O₂ Sensors)					
Current change (nA)	Current change (%)	Max response Time (mins)	Return Time (mins)	Baseline Pre Injection (nA)	Baseline Post Injection (nA)
31.1 ± 3.4	18.9 ± 2.1	2.8 ± 0.2	27.7 ± 2.9	-164.2 ± 5.2	-168.9 ± 5.2

Table 8.3.5 (b) Averaged results for tail pinch, with O₂ sensors (MMCPEs and SMCPEs), implanted in the striatum of 5 freely moving rats ($n = 18$ with 5 sensors).

The NO response obtained from the tail pinch with the Type 2 and Type 3 NO sensors in this section, has been previously observed within our laboratory utilising other NO sensor designs. A lack of a return back to pre-administration NO baseline levels was demonstrated previously utilising the Type 1 NO sensor, showing that the response again was not sensor specific. Figure 8.3.5 (b), displays the result of a tail pinch recorded by the Type 1 NO sensor courtesy of Dr. Niall Finnerty. Figure 8.3.5 (c), displays the result of a tail pinch recorded by a glutamate sensor courtesy of Dr. Fiachra Bolger. An elevated response of glutamate that does not return back to baseline levels after the stimulus had ceased, yielded

a very similar elevated response obtained by the NO sensors for the tail pinch stress. An identical hypothesis is proposed for this elevated glutamate and NO response with reference to the response obtained for the restraint stress (see Section 8.3.4).

NO has been demonstrated to regulate CBF since its establishment as the EDRF in the 1980's (Ignarro *et al.*, 1987; Furchgott, 1988). As the O₂ levels return to normoxic conditions, the NO current remains elevated. It is postulated that if there had been a contribution from eNOS then the NO would have returned to corresponding baseline levels along with the O₂. O₂ can be utilised as a reliable index of cerebral blood flow (Lowry *et al.*, 1997) under these circumstances and therefore, it appears that the eNOS enzyme is not causing this increase and therefore it is believed the NMDA/receptor nNOS pathway is the main contributor to this production of NO.

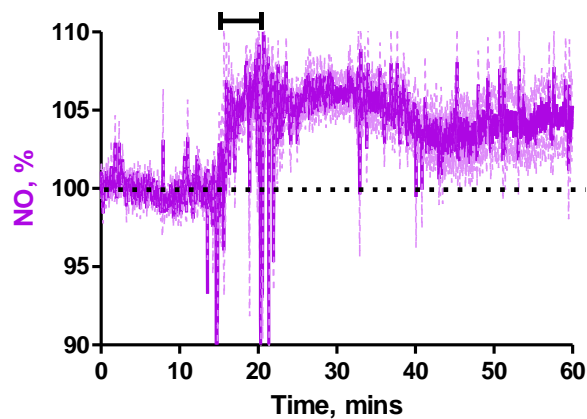


Figure 8.3.5 (b): A time vs. percentage graph displaying the NO percentage change response attained from a 5-minute period of tail pinch stress with Type 1 NO sensors, $n = 14$, in 4 animals. The bar is indicative of the duration of the tail pinch (Courtesy of Dr. Niall Finnerty).

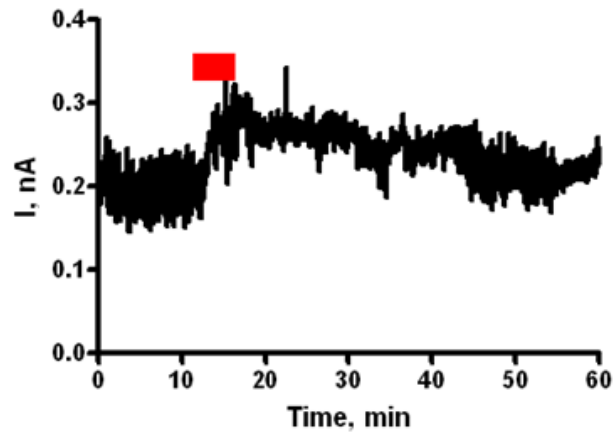


Figure 8.3.5 (c): A typical example of a time vs. current response graph, displaying the increase in the glutamate response detected with a glutamate sensor after a 5-minute period of a tail pinch administration in the striatum of a freely moving rat (Courtesy of Dr. Fiachra Bolger).

8.3.6 Chloral Hydrate

Chloral hydrate depresses the cerebrum, with loss of reflex excitability. It has been used previously as a method of increasing the striatal O₂ levels in rats (Lowry & Fillenz, 2001; Bolger & Lowry, 2005). Figure 8.3.6, displays results attained from the administration of chloral hydrate (350 mg/kg i.p.) on the O₂ and NO signals recorded with the O₂ (MMCPEs and SMCPEs) and NO (Type 2 and Type 3) sensors. The chloral hydrate injection data in this section was analysed using the results from 17 perturbations with 15 sensors in 5 animals for the NO data and 6 perturbations with 5 sensors in 5 animals for the O₂ data.

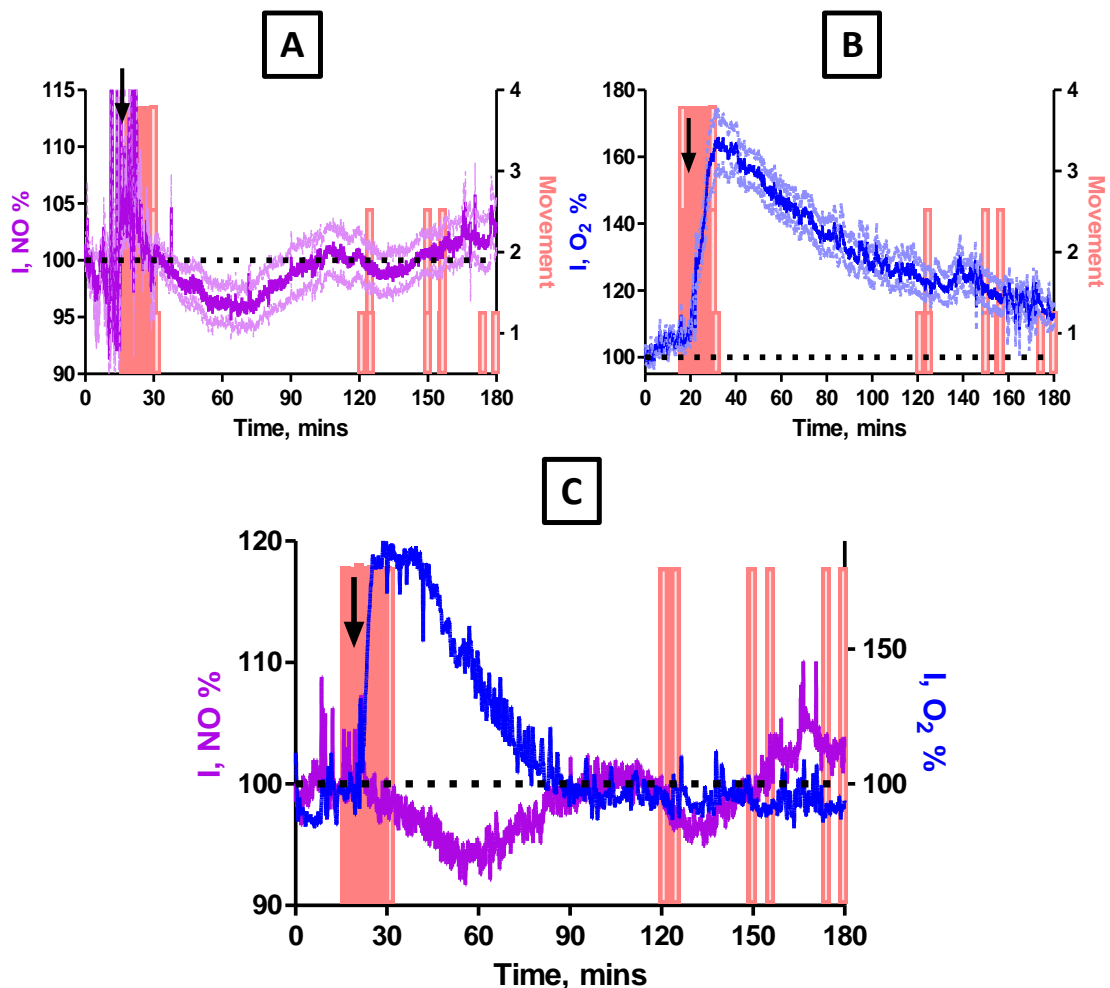


Figure 8.3.6: Time vs. percentage change graphs for an i.p. injection of chloral hydrate (350mg/kg in 1ml of saline) for (A) NO (Type 2 and Type 3 NO sensors, $n = 17$: 6 animals) and (B) O₂ (MMCPs and SMCPEs, $n = 17$: 6 animals). (C) A typical raw data example displaying the combined data of the percentage change in NO and O₂. The arrow is indicative of the point of injection and the pink bars are indicative of the movement of the animal.

The chloral hydrate injection yielded an increase in the O₂ current that was significantly different ($P = 0.0009$) from pre-baseline O₂ currents. A contrasting result was obtained from the NO sensors upon the injection of chloral hydrate. A decrease in the NO signal was observed, displaying no correlation between the O₂ and NO behaviour. Analysis of the data showed that the NO current decrease was significantly different ($P = 0.0007$) from pre-baseline levels, however, a clear decrease can be observed, especially in comparison to baseline NO data taken over the period of three hours (see Section 8.3.1). The maximum

response time observed for the NO sensors was 75.7 ± 18.6 mins, $n = 17$ and 14.0 ± 2.6 mins, $n = 17$ for the O₂ sensors response time. These response time results signify the extent of the different effects on the two molecules by the chloral hydrate injection. The O₂ response time is much quicker than the response time observed by the NO sensors ($P = 0.0025$).

The chloral hydrate effect on suppressing neuronal activity is quick, resulting in the increase in O₂ due to the supply of O₂ exceeding the utilisation of O₂. However, the NMDA mediated effect is much slower and occurs over a longer time frame. This also shows the advantage of real-time *in-vivo* monitoring with sensors, instead of conventional indirect methods, as the time disparity between these two molecules would not be noticed. O₂ and NO currents returned to corresponding baseline levels after 198.7 ± 16.7 mins, $n = 17$, ($P = 0.8108$) and 181.1 ± 52.5 mins, $n = 17$, ($P = 0.9666$), respectively and the animals began to show recovery from the anaesthesia. The pink bars display the movement data for the animals. The animals began to move at approximately 120 minutes; however, they displayed signs of waking up prior to this, but did not begin to move until the time indicated on the graphs by the movement data. Table 8.3.6 (a) and 8.3.6 (b) give a summary of the response attained at both the NO and O₂ sensor.

Chloral Hydrate Injection (NO Sensors)					
Current change (pA)	Current change (%)	Max response Time (mins)	Return Time (mins)	Baseline Pre Injection (pA)	Baseline Post Injection (pA)
37.7 ± 8.5	13.8 ± 3.8	75.7 ± 18.6	181.1 ± 52.5	317.5 ± 51.9	314.8 ± 91.4

Table 8.3.6 (a): Averaged table of results for an i.p. injection of chloral hydrate with NO sensors (Type 2 and Type 3 NO sensor, implanted in the striatum of 6 freely moving rats ($n = 17$ with 15 sensors)).

Chloral Hydrate Injection (O ₂ Sensors)					
Current change (nA)	Current change (%)	Max response Time (mins)	Return Time (mins)	Baseline Pre Injection (nA)	Baseline Post Injection (nA)
111.2 ± 19.2	67.6 ± 10.4	14.0 ± 2.6	198.7 ± 16.7	-163.9 ± 11.5	-167.9 ± 11.7

Table 8.3.6 (b): Averaged table of results for an injection of chloral hydrate with O₂ sensors (MMCPEs and SMCPEs, implanted in the striatum of 5 freely moving rats (*n* = 6 with 5 sensors)).

The results observed for the chloral hydrate injection were very interesting. An increase in the O₂ current was obtained which should have meant an increase in NO, as more O₂ would suggest an increased production of NO, however the complete opposite occurred. Evidence has suggested that the NMDA receptors are targets of anaesthetic agents in the central nervous system and that some of the biological actions created by the anaesthetics effect the NMDA receptors. It was demonstrated in a study undertaken by LacKamp *et al.*, that chloral hydrate caused the loss of surface expressed NMDA receptors (LacKamp *et al.*, 2009). So if there is an inhibition of chloral hydrate on the NMDA receptors, NO production would therefore be reduced leading to a decrease in the NO signal observed at the NO sensors.

In another study carried out by Kreuter *et al.*, they found that chloral hydrate seemed to reduce glutamate release and decrease activation of glutamate receptors (Kreuter *et al.*, 2004). The results obtained in this section strongly suggest that the production of NO throughout the results obtained has been from the nNOS enzyme as opposed to the eNOS enzyme. Further clarifying what other research groups have suggested, that nNOS is more ubiquitous in the brain. If the NMDA receptors are activated, calcium channels open and there is an influx of calcium causing activation of nNOS and therefore NO production (Santos *et al.*, 2012). However, when NMDA receptors are inhibited, as in this case, calcium influx cannot be achieved, which is a prerequisite for the production of NO to occur. The decrease in NO current observed can be attributed to this hypothesised NMDA receptor inhibition.

8.3.7 Diamox

Acetazolamide (Diamox) is a carbonic anhydrase inhibitor that has been shown to increase brain tissue O_2 (Dixon *et al.*, 2002; Bolger & Lowry, 2005). It has been used as an exploratory tool in cerebral blood flow experiments and also for the treatment of several diseases long term (Vorstrup *et al.*, 1984). It has been demonstrated that extracellular pH decreases after diamox induced carbonic anhydrase inhibition (Severinghaus & Cotev, 1968; Bickler *et al.*, 1988). It is also known that pH is an inhibitor of NMDA receptor activation (Tang *et al.*, 1990; Traynelis & Cull-Candy, 1990). The frequency by which the NMDA receptor channel opens is decreased by protons above the physiological range and at pH 6.0, receptor activation is suppressed (Traynelis *et al.*, 1995). Diamox has an effect on the NMDA receptors and any shift in the pH sensitivity can up regulate or down regulate the receptor function (Low *et al.*, 2003). The effect of an administration of acetazolamide on the O_2 and NO current was monitored with the O_2 (MMCPEs and SMCPEs) and NO (Type 2 and Type 3) sensors, simultaneously. The diamox injection data in this section was analysed using the results from 15 perturbations with 15 sensors in 5 animals for the NO data and 5 perturbations with 5 sensors in 5 animals for the O_2 data.

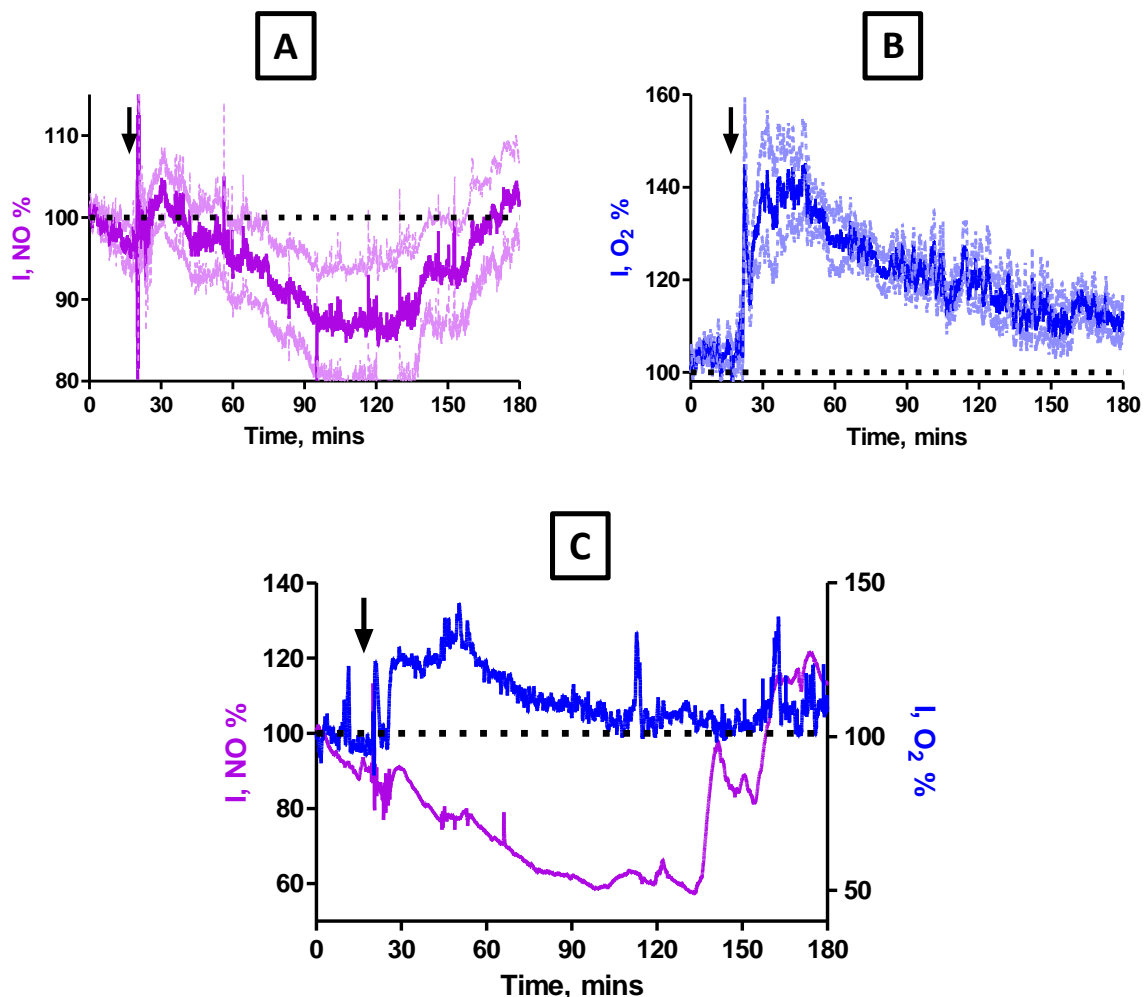


Figure 8.3.7: Time vs. percentage change graphs for an i.p. injection of diamox (50mg/kg in 1ml of saline) for (A) NO (Type 2 and Type 3 NO sensors, $n = 15$: 5 animals) and (B) O₂ (MMCPEs and SMCPEs, $n = 5$: 5 animals). (C) A typical raw data example displaying the combined data of the percentage change in NO and O₂. The arrow is indicative of the point of injection.

Figure 8.3.7 demonstrates the results obtained by the NO and O₂ sensors after an i.p. injection of diamox. A characteristic increase in the O₂ current was observed which was significantly different ($P = 0.0356$) from pre-baseline currents. However, similar to the chloral hydrate injection, NO displayed a decrease in the NO current after the injection of diamox which was significantly different ($P = 0.0010$) from pre-baseline levels. It is clear from the graphs that there has been a change in the two currents, similar to what was observed by the chloral hydrate injection. On comparison of the baseline recordings obtained in Section 8.3.1 for NO and O₂ over the course of three hours, a clear indication of

a change in the NO and O₂ current can be observed. Table 8.3.7 (a) and 8.3.7 (b) display a summary of the results.

Diamox Injection (NO Sensors)					
Current change (pA)	Current change (%)	Max response Time (mins)	Return Time (mins)	Baseline Pre Injection (pA)	Baseline Post Injection (pA)
89.4 ± 42.3	23.3 ± 10	92.0 ± 6.6	153.6 ± 8.8	397.6 ± 77.1	423.5 ± 91.6

Table 8.3.7 (a): Averaged table of results for an injection of diamox with NO sensors (Type 2 and Type 3 NO sensor, implanted in the striatum of 5 freely moving rats ($n = 14$ with 14 sensors)).

Diamox Injection (O₂ Sensors)					
Current change (nA)	Current change (%)	Max response Time (mins)	Return Time (mins)	Baseline Pre Injection (nA)	Baseline Post Injection (nA)
67.0 ± 21.5	42.9 ± 1.5	30.0 ± 6.7	167.8 ± 36.0	-151.7 ± 15.8	-162.6 ± 1.7

Table 8.3.7 (b): Averaged table of results for an injection of diamox with O₂ sensors (MMCPEs and SMCPEs, implanted in the striatum of 5 freely moving rats ($n = 5$ with 5 sensors)).

The maximum response time observed for the NO sensors was 92.0 ± 6.6 mins, $n = 14$ and 30.0 ± 1.5 mins, $n = 5$ for the O₂ sensors. These response time results demonstrate the extent of the varying effects on the two molecules following diamox injection. The O₂ response time is much quicker than that observed for the NO sensors ($P < 0.0001$). The effect of the diamox on the O₂ response is quick and a resulting increase is observed, validating its choice as a method of increasing tissue O₂ and a subsequent increase in cerebral blood flow. The increase in cerebral blood flow is caused by a decrease in the pH levels which induces the dilation of blood vessels (Bolger & Lowry, 2005). The NO response is much slower and occurs over a longer period of time suggesting that alternative pathways are involved.

pH is reported to be an inhibitor of NMDA function and it has been shown to decrease the expression of the NMDA receptors thus decreasing the production of NO (Tang *et al.*,

1990; Traynelis & Cull-Candy, 1990). Therefore, the observed NO decrease, suggests that the NO production is inhibited, due to the suppression of the NMDA receptor by the diamox induced decrease in pH. O₂ and NO currents returned to corresponding baseline levels after 167.8 ± 36.0 mins, $n = 5$ ($P = 0.0929$) and 153.6 ± 8.8 mins, $n = 14$, ($P = 0.2460$), respectively. It would be of great interest to monitor concurrently pH, NO and O₂ in the diamox drug model, to investigate the effect of NMDA receptor protonation.

8.3.8 L-NAME

L-NAME is a non-selective inhibitor of the NOS enzyme and causes a decrease in the production of NO. It has been identified as competing with arginine, the pre-cursor for NO production, for its binding site (Lajoix *et al.*, 2004) on the NOS isozyme. The injection of L-NAME data in this section was analysed using the results from 15 perturbations with 15 sensors in 5 animals for the NO data and 5 perturbations with 5 sensors in 5 animals for the O₂ data. Figure 8.3.8 displays the results recorded at the NO and O₂ sensors after an i.p injection of L-NAME.

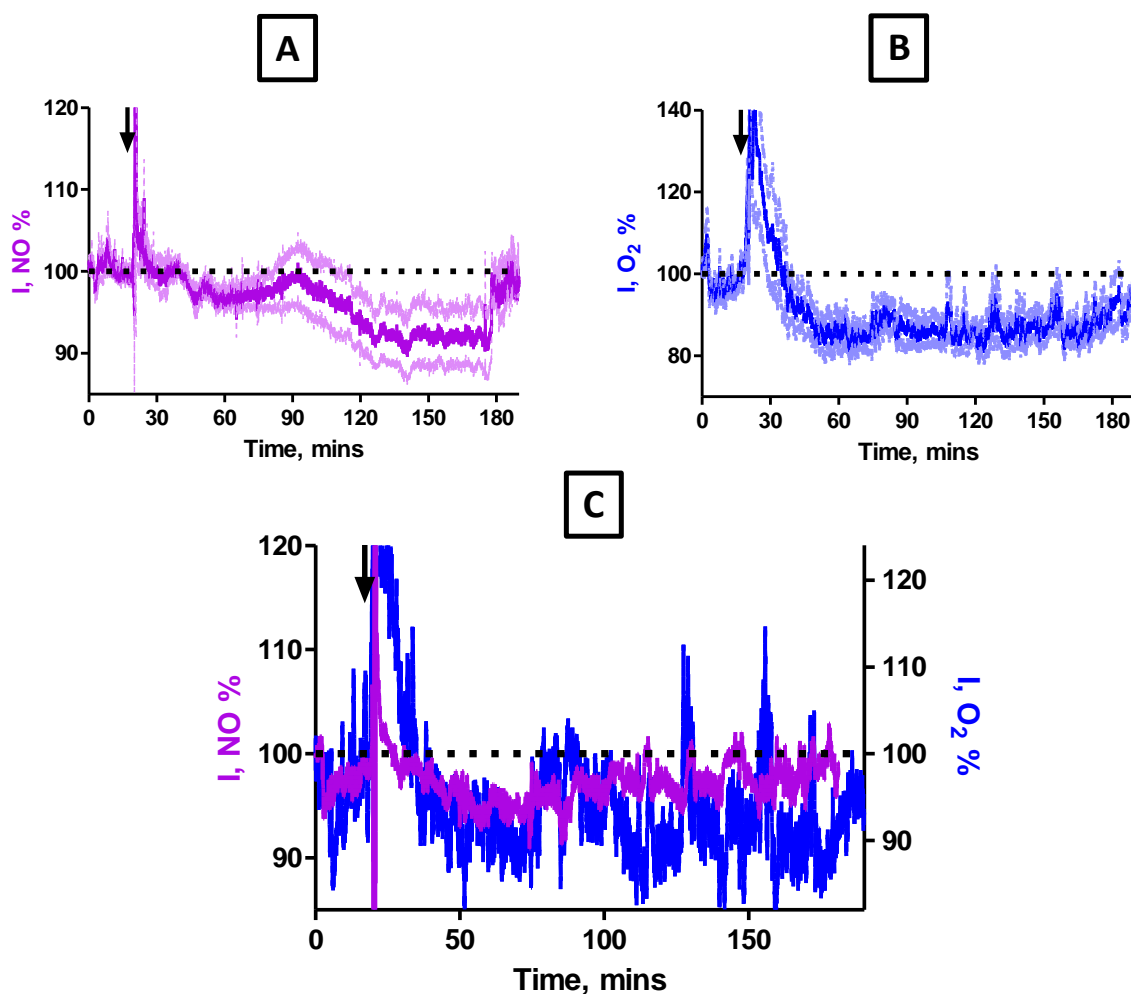


Figure 8.3.8: Time vs. percentage change graphs for an i.p. injection of L-NAME (30mg/kg in 1ml of saline) for (A) NO (Type 2 and Type 3 NO sensors, $n = 15$: 5 animals) and (B) O₂ (MMCPEs and SMCPEs, $n = 5$: 5 animals). (C) A typical raw data example displaying the combined data of the percentage change in NO and O₂. The arrow is indicative of the point of injection.

As L-NAME is a NOS inhibitor, the expected result is to observe a decrease in the NO signal. In Figure 8.3.8, a typical NO response to L-NAME demonstrates this decrease which was significantly different ($P = 0.0010$) from pre-baseline currents. The O₂ signal also displayed a decrease in the current of approximately $17.3 \pm 3.2\%$, $n = 15$, after 48.9 ± 11.2 mins, $n = 15$, which was significantly different ($P = 0.0045$) from pre-baseline levels. New baseline levels for NO and O₂ were obtained after 142.4 ± 17.1 mins, $n = 14$, ($P = 0.0186$) and 93.3 ± 23.7 mins, $n = 14$, ($P = 0.0044$), respectively. L-NAME inhibits all of the NOS enzymes. There is also a decrease in vasculature conductance, arterial pressure

and a reduction in heart rate (Jones *et al.*, 2004). The observed O₂ decrease would be due to a decrease in the cerebral blood flow therefore a decrease in the O₂ supply, which was detected by the O₂ sensors.

The inhibition of the NOS enzymes by L-NAME causes the decrease in the NO production and therefore the constriction of the blood vessels causes the subsequent decrease in the O₂ response recorded at the O₂ sensors. Table 8.3.8 (a) and 8.3.8 (b) display a summary of the results.

L-NAME Injection (NO Sensors)					
Current change (pA)	Current change (%)	Max response Time (mins)	Return Time (mins)	Baseline Pre Injection (pA)	Baseline Post Injection (pA)
40.5 ± 10.3	7.7 ± 1.5	68.4 ± 10.0	142.4 ± 17.1	515.9 ± 107.2	467.6 ± 105.5

Table 8.3.8 (a): Averaged table of results for an injection of L-NAME with NO sensors (Type 2 and Type 3 NO sensor, implanted in the striatum of 5 freely moving rats (*n* = 15 with 15 sensors)).

L-NAME Injection (O₂ Sensors)					
Current change (nA)	Current change (%)	Max response Time (mins)	Return Time (mins)	Baseline Pre Injection (nA)	Baseline Post Injection (nA)
28.2 ± 6.4	17.3 ± 3.2	48.9 ± 11.2	93.3 ± 23.7	-153.8 ± 16.3	-130.5 ± 13.7

Table 8.3.8 (b): Averaged table of results for an injection of L-NAME with O₂ sensors (MMCPEs and SMCPEs, implanted in the striatum of 5 freely moving rats (*n* = 5 with 5 sensors)).

8.3.9 L-Arginine

The NO precursor L-arginine is transformed to arginine-hydroxide in a reaction that is catalysed by NOS. Subsequent to this, arginine-hydroxide is then transformed to NO and L-citrulline, the synthesis involves cofactors also, which include calcium/calmodulin, O₂ and nicotinamide adenine dinucleotide phosphate (Bredt & Snyder, 1992) thus, L-arginine plays

a vital role in the production of NO. In this section, data is presented that outlines the NO and O₂ responses to systemic administration of L-arginine. The injection of L-arginine data in this section was analysed using the results from 12 perturbations with 10 sensors in 5 animals for the NO data and 5 perturbations with 4 sensors in 5 animals for the O₂ data.

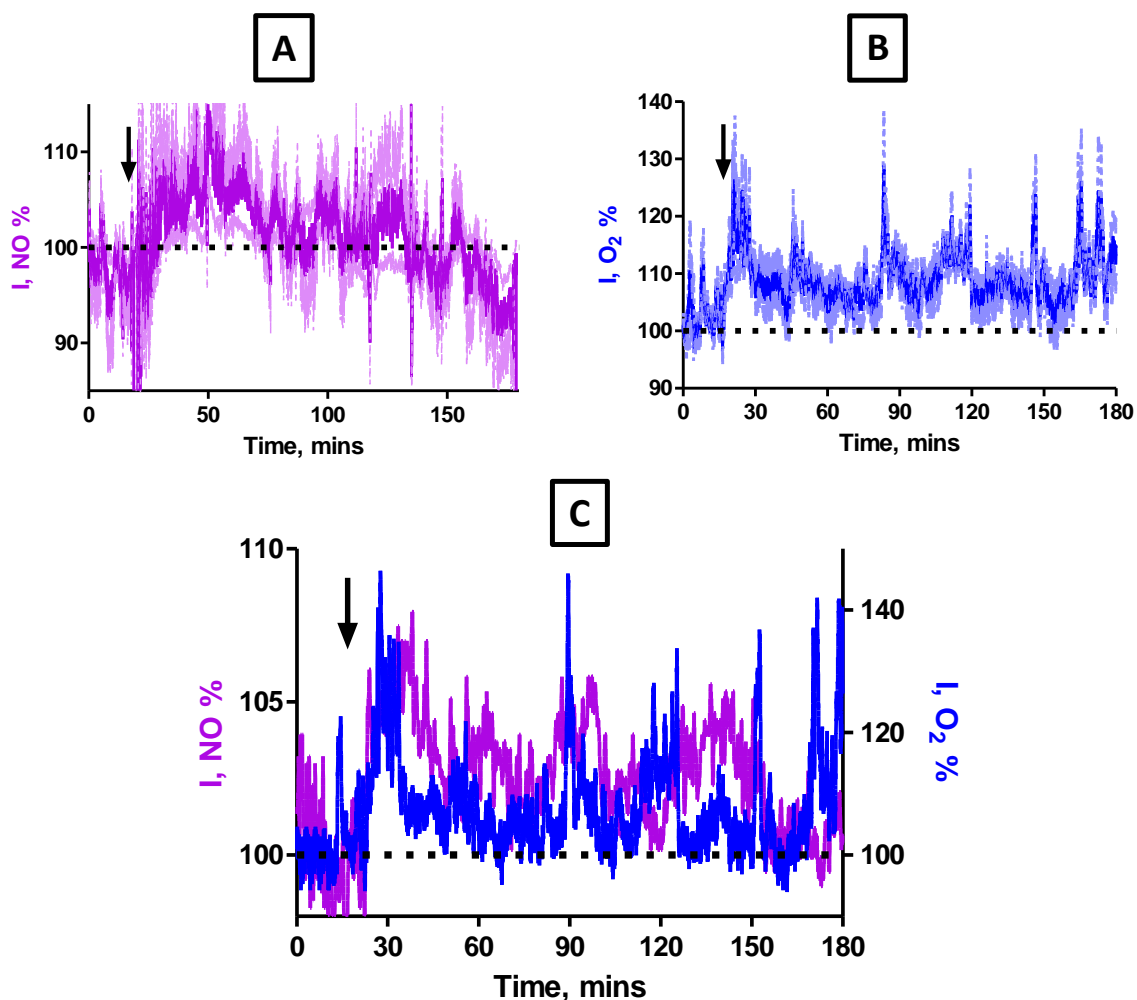


Figure 8.3.9: Time vs. percentage change graphs for an i.p. injection of L-arginine (300mg/kg in 1ml of saline) for (A) NO (Type 2 and Type 3 NO sensors, $n = 12$: 5 animals) and (B) O₂ (MMCPEs and SMCPEs, $n = 5$: 5 animals). (C) A typical raw data example displaying the combined data of the percentage change in NO and O₂. The arrow is indicative of the point of injection.

The injection of L-arginine produced an increase in both the O₂ and NO signal. A percentage change of 9.4 ± 3.1 %, $n = 12$ and 10.6 ± 2.2 %, $n = 5$, was obtained for NO and O₂, respectively. The percentage increase of NO and O₂ was significantly different ($P =$

0.0018 and 0.0193) from pre-baseline levels, respectively, after the injection of L-arginine. The NO and O₂ baseline levels returned after 100.4 ± 12.5 mins, $n = 12$, ($P = 0.1511$) and 146.6 ± 44.2 mins, $n = 5$, ($P = 0.4318$), respectively. This result was expected, as an increase in NO would cause an increase in O₂ due to the increased blood supply. As L-arginine is vital for the production of NO, having an increased level of L-arginine available for the production of NO would suggest an increased amount of NO being synthesised through the nNOS and eNOS pathways with the latter causing an increase in the cerebral blood flow thus showing an increased O₂ response at the O₂ sensors. Table 8.3.9 (a) and 8.3.9 (b), display a summary of the results attained at the NO and O₂ sensors.

L-Arginine Injection (NO Sensors)					
Current change (pA)	Current change (%)	Max response Time (mins)	Return Time (mins)	Baseline Pre Injection (pA)	Baseline Post Injection (pA)
26.1 ± 6.6	9.4 ± 3.1	25.2 ± 3.0	100.4 ± 12.5	421.0 ± 91.6	436.2 ± 99.7

Table 8.3.9 (a): Averaged table of results for an injection of L-Arginine with NO sensors (Type 2 and Type 3 NO sensor, implanted in the striatum of 5 freely moving rats ($n = 10$ with 5 sensors)).

L-Arginine Injection (O₂ Sensors)					
Current change (nA)	Current change (%)	Max response Time (mins)	Return Time (mins)	Baseline Pre Injection (nA)	Baseline Post Injection (nA)
15.6 ± 3.3	10.6 ± 2.2	60.0 ± 20.7	146.6 ± 44.2	-162.3 ± 34.6	-170.0 ± 37.6

Table 8.3.9 (b): Averaged table of results for an injection of L-Arginine with O₂ sensors (MMCPEs and SMCPEs, implanted in the striatum of 5 freely moving rats ($n = 5$ with 4 sensors)).

8.3.10 Day vs. night study

Preliminary work displayed in Figure 8.3.10 (a) and 8.3.10 (b), identifies the NO and O₂ percentage change over the course of 6 hours during night (Figure 8.3.10 (a)) and day (Figure 8.3.10 (b)). Movement data was added to the graph in order to observe how the signals changed over the course of the 6 hours and if the movement of the animal caused any significant changes observed in the currents. The data observed in this section was analysed using sensors that were simultaneously recording NO and O₂, along with the movement in the one animal over the course of a day and night.

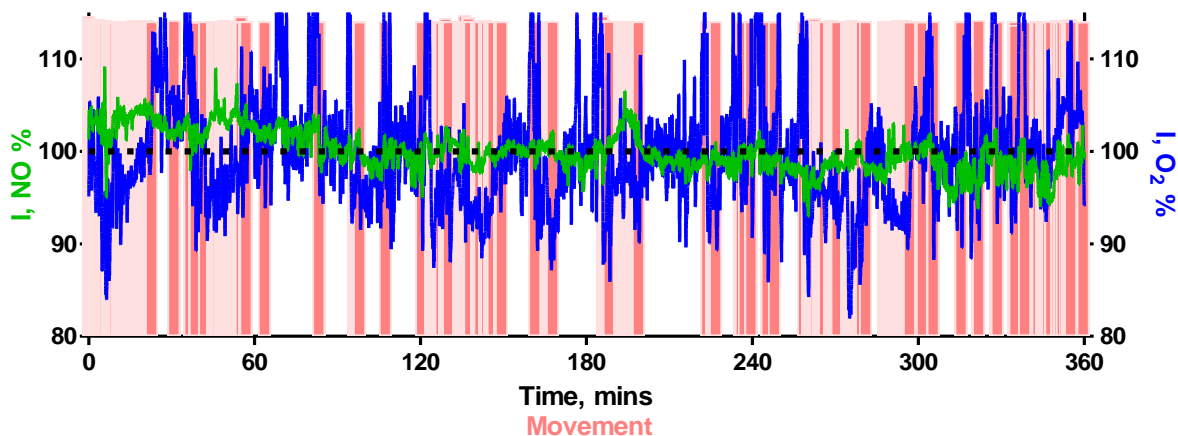


Figure 8.2.10 (a): A time vs. percentage change profile over the course of 6 hours (8pm to 2am) recorded with O₂ (1 sensor) and NO (3 sensors) in the striatum of a freely moving rat. The pink bars are indicative of movement.

The NO and O₂ baselines remained stable over the course of the 6 hours, however, there was more deviation in the O₂ trace. It is known that the supply and utilisation of O₂ will cause slight variations in the O₂ signal over time (Lowry *et al.*, 1997). The movement data also demonstrates how active the animal is during the night. This suggests that NO fluctuations are not associated with the movement of the animal.

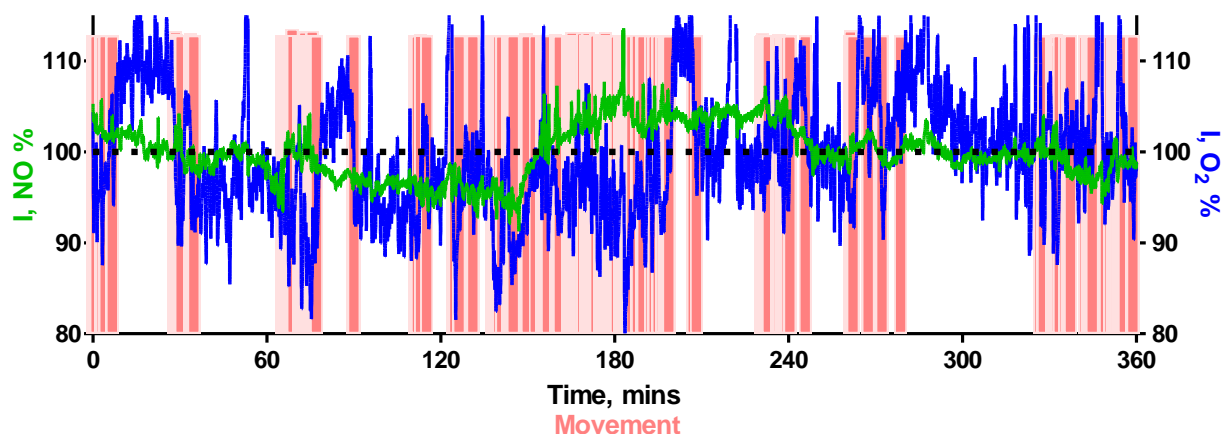


Figure 8.3.10 (b): A time vs. percentage change profile over the course of 6 hours (8am to 2pm) recorded with O₂ (1 sensor) and NO (3 sensors) in the striatum of a freely moving rat. The pink bars are indicative of movement.

The NO and O₂ trace observed in Figure 8.3.10 (b), seems to deviate much more than was observed with the baselines recorded during the night (8pm to 2am). In general, when experiments are not being carried out on the animals during the day, the activity of the animal is less frequent than the activity during the night. A clearer display of this can be observed in Figure 8.3.10 (c), where the NO and O₂ baseline along with the movement data from one animal was recorded over two Days continuously. NO has been implicated in the regulation of sleep (Obal Jr & Krueger, 2003; Calabrese *et al.*, 2007; Wisor *et al.*, 2011; Kostin *et al.*, 2013). In a study undertaken by Kostin *et al.*, with the use of the Type 1 NO sensor extensively developed within our lab (Brown *et al.*, 2009; Finnerty *et al.*, 2012a; Finnerty *et al.*, 2012b), extracellular levels of NO across a spontaneous sleep-wake cycle in response to sleep deprivation and during light *vs.* dark phases in freely moving animals was monitored (Kostin *et al.*, 2013).

The main findings from the research carried out by Kostin *et al.*, was that endogenous NO levels were at their highest during waking, intermediate in the deepest stage of sleep that is rapid eye movement (REM) sleep and lowest during non-REM sleep. They also reported data which demonstrated that NO levels exhibit diurnal modulation (Kostin *et al.*, 2013). The fluctuating NO response during the day (see Figure 8.3.10 (b)) in comparison to the stable NO baseline observed during the night (see Figure 8.3.10 (a)) when the rat is most

active, suggests that what is being observed here is the diurnal modulation of NO, which was observed by Kostin *et al.*, (Kostin *et al.*, 2013).

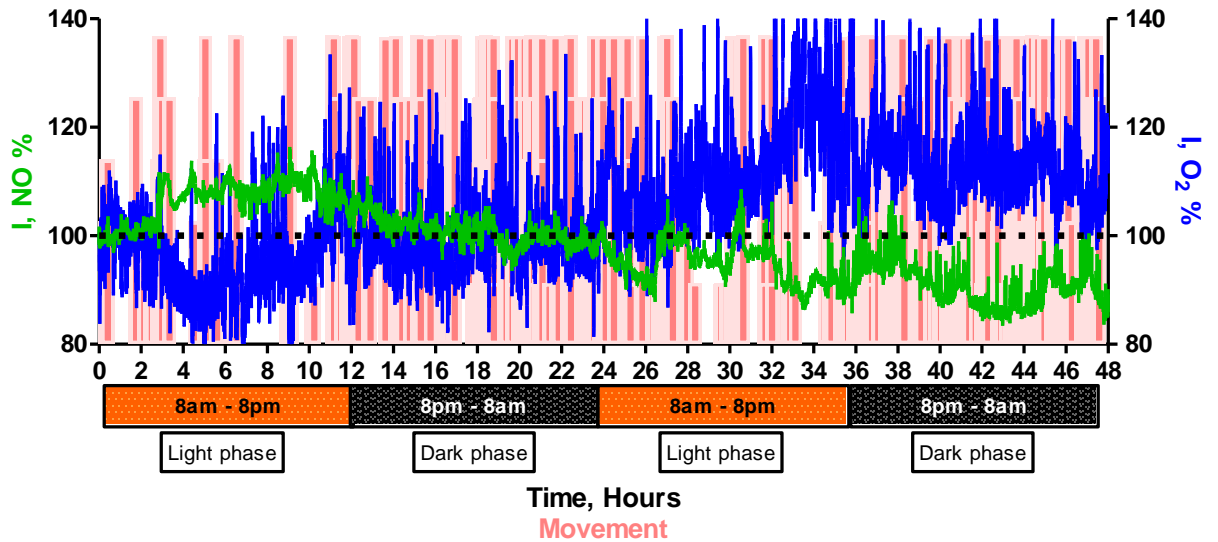


Figure 8.3.10 (c): A time vs. percentage change profile over the course of 2 days recorded with O₂ (1 sensor) and NO (3 sensors) in the striatum of a freely moving rat. The pink bars are indicative of movement.

The animal displays a more active persona during the dark phase in comparison to the light phase. During the day is when the animal would try to sleep as they are naturally nocturnal. It is clear from Figure 8.3.10 (c), that NO is much more dynamic during the day i.e. sleep.

8.4 Conclusion

Reported in this chapter is the simultaneous monitoring of NO and O₂ in the striatum of freely moving rats. The coupling of the O₂ (SMCPes and MMCPes) and NO (Type 2 and Type 3 NO) sensors was deemed applicable, as the results attained in the preceding characterisation chapters displayed little difference between the sensors, with regards to their capabilities of detecting NO and O₂ in the *in-vivo* environment. Various experiments were undertaken to try and determine the relationship between the two molecules in an *in-vivo* setting. The simultaneous NO and O₂ baseline recordings displayed in Figure 8.4 (a), demonstrate how stable the sensors are *in-vivo*. The currents did not deviate much from baseline levels over the course of three hours. This data is utilised as a control to demonstrate the effects of the different perturbations which can be attributed to the particular procedure/administration.

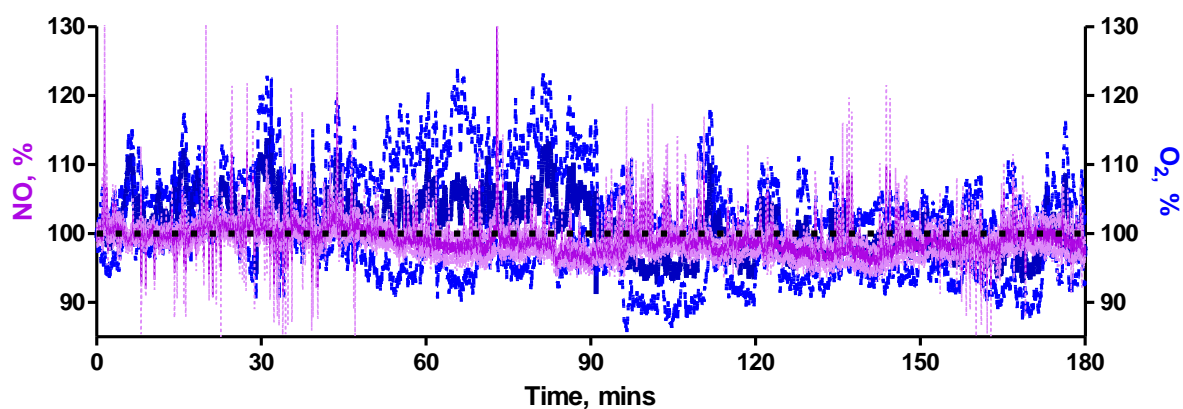


Figure 8.4 (a): A time vs. percentage change graph of baseline NO and O₂ currents monitored by NO sensors (Type 2 and Type 3 NO sensors, 15 sensors in 5 animals) and O₂ sensors (MMCPes and SMCPEs, 5 sensors in 5 animals) displaying a stable baseline over the course of three hours *in-vivo*.

Subsequent to this, 3- and 5-minute periods of hypoxia and hyperoxia were performed, respectively. The results suggested a correlation between the two molecules. Upon the decrease in the O₂ levels, there was a decrease in NO and a similar occurrence was observed after the 5 minute period of hyperoxia (an increase in O₂ yielded an increase in

NO). Figure 8.4 (b), displays the percentage changes observed from the two sensors after the 3- and 5-minute periods of hypoxia and hyperoxia, respectively.

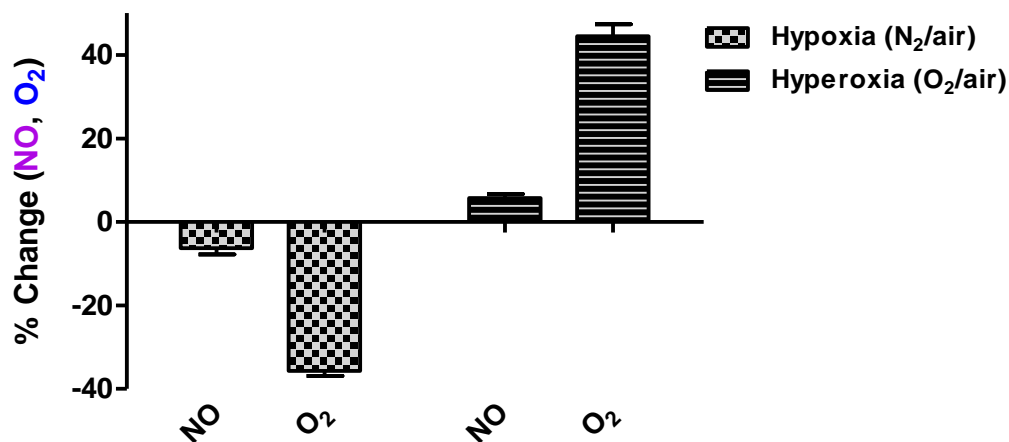


Figure 8.4 (b): A graph displaying the percentage changes observed with the NO (Type 2 and Type 3 NO sensors) and O₂ sensors (MMCPEs and SMCPEs) after hypoxia and hyperoxia was induced in the animals.

After the exogenous perturbations had ceased the return to corresponding baseline levels were similar for the NO and O₂ responses. A return time of 7.0 ± 0.6 mins, $n = 17$, 5 animals and 6.6 ± 0.3 mins, $n = 17$, 5 animals was observed for NO and O₂ during an administration of N₂/air, respectively. A return time of 14.5 ± 1.9 mins, $n = 18$, 4 animals and 12.9 ± 0.5 mins, $n = 18$, 4 animals was recorded for the NO and O₂ during an administration of O₂/air, respectively. As stated previously, research undertaken by Pearce *et al.*, suggests that eNOS activity is enhanced by hypoxia (Pearce *et al.*, 1989; Pearce *et al.*, 1990). If this was the case then it is postulated that if we were observing an NO current change by an eNOS induced pathway, then a resulting NO increase would have been observed. However, a decrease in NO was observed, which suggests that the decrease in O₂ that is needed for the synthesis of NO contributed to the decrease in NO monitored at the NO sensors. It is hypothesised that this NO production that is observed is in fact occurring through an NMDA receptor/ nNOS pathway, however it cannot be ruled out at present that eNOS could be contributing also. The increase in NO after the period of hyperoxia could be due to the increased availability of O₂, thus, causing a rise in the production of NO. O₂ is a

vital component of the synthesis of NO (see Figure 1.4) and Liao *et al.*, have demonstrated that hyperoxia can affect the expression of NOS and NO production in cultured cells (Liao *et al.*, 1995).

Neuronal activation experiments were then undertaken to try and achieve more information about the association between NO and O₂. The restraint stress and tail pinch would yield more information about endogenous perturbations that may cause changes in NO and O₂. In Figure 8.4 (c), a graph displays the percentage change that occurred in O₂ and NO simultaneously.

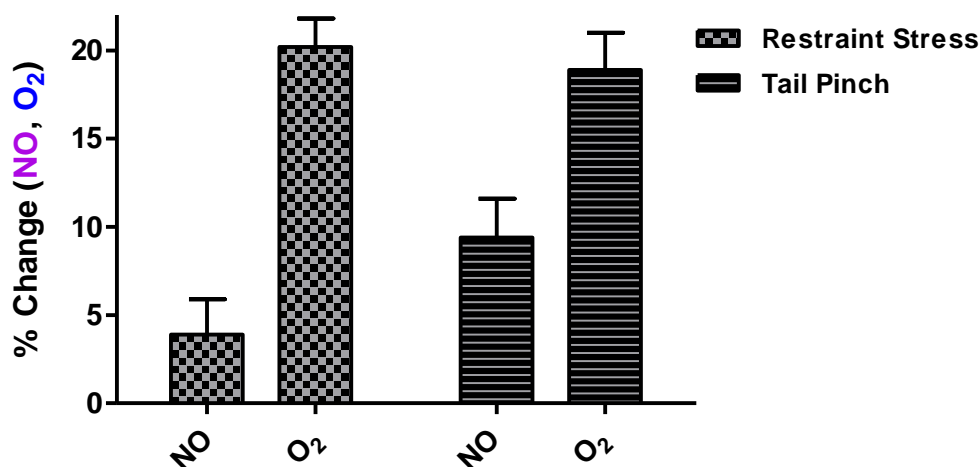


Figure 8.4 (c): A graph displaying the percentage changes observed with the NO (Type 2 and Type 3 NO sensors) and O₂ sensors (MMCPEs and SMCPEs) after restraint stress and tail pinch studies.

The results obtained with the restraint stress and tail pinch displayed a concurrent increase in NO and O₂, as was seen with the hypoxia and hyperoxia induced states. Again this would seem like a correlation between NO and O₂ is occurring, however, what was interesting about these results was the elevated NO response after the stimulus had ceased. The NO current remained high after the O₂ had returned to corresponding baseline levels. These results again suggest that there is another mechanism of NO production responsible and not the production of NO through the eNOS enzyme which is known to act on the dilation and constriction of blood vessels (see Figure 8.3.4 (a) and 8.3.5 (a)).

Following on from this, i.p. injections of chloral hydrate and diamox were performed. The recorded currents obtained for NO after the two i.p. injections were fascinating results, as both injections displayed no association with O₂. The O₂ increase observed for both injections were expected, however from the results obtained prior to this we were also expecting an increase in NO. However, we observed a decrease in NO for both i.p. injections. Figure 8.4 (d) displays the percentage change in both the O₂ and NO.

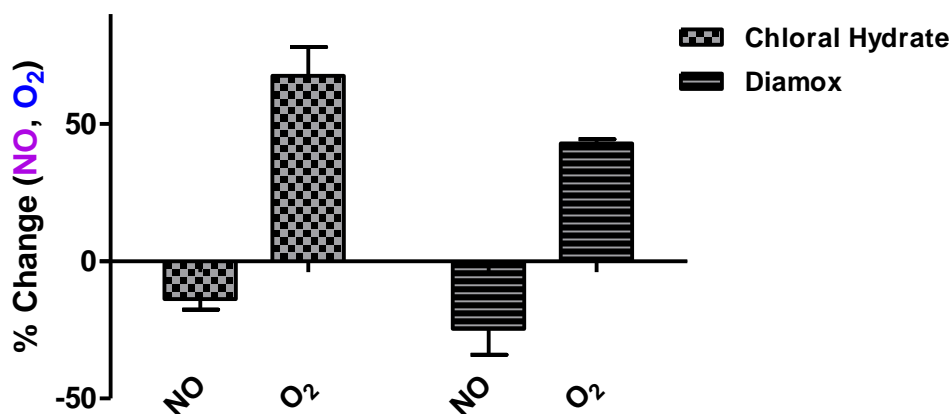


Figure 8.4 (d): A graph displaying the percentage changes observed with the NO (Type 2 and Type 3 NO sensors) and O₂ sensors (MMCPEs and SMCPEs) after an i.p. injection of chloral hydrate (350mg/kg) and diamox (50mg/kg).

Evidence has suggested that the NMDA receptors are targets of anaesthetic agents in the central nervous system and that some of the biological actions created by the anaesthetics affect the NMDA receptors. So, if there is a loss of surface expressed NMDA receptors, this would lead to a decreased NO production. Chloral hydrate increases striatal O₂ and that is why an increase in observed in the O₂ current. If eNOS was the enzyme producing the NO and causing an increase in cerebral blood flow an increase in NO would have been observed, however we did not observe this, which suggests that it is the nNOS enzyme that is producing the NO through the activation of the NMDA receptors.

The diamox result yielded a similar conclusion. Diamox is a carbonic anhydrase inhibitor that is known to increase O₂ and it is also known that it induces a decrease in pH. The NMDA receptors are inhibited by a decreased pH and it has been shown that the frequency

by which the NMDA receptor channel opens is decreased by protons above the physiological range and at pH 6.0, receptor activation is suppressed. These results lead to a hypothesis that the NO being detected is from the NMDA-receptor pathway involving nNOS, however, it cannot be ruled out that some contribution may be occurring from other sources of NO. Following on from this result, i.p. injections of L-NAME and L-arginine were administered. Figure 8.4 (e) displays the percentage change observed from the NO and O₂ sensors after the injections.

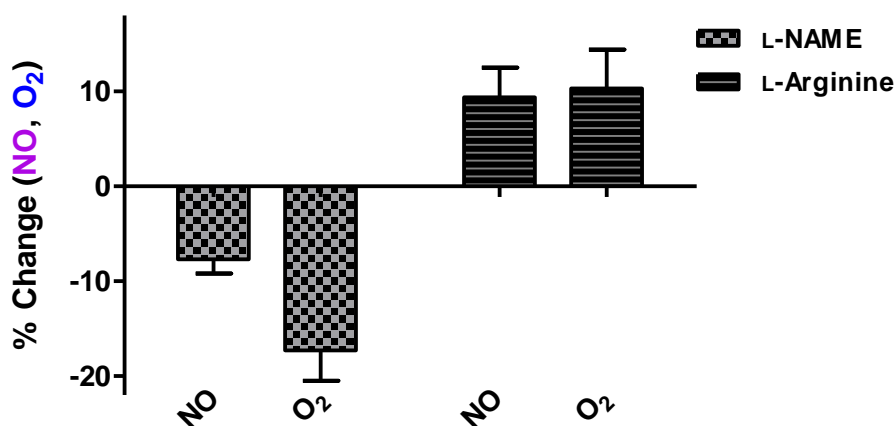


Figure 8.4 (e): A graph displaying the percentage changes observed with the NO (Type 2 and Type 3 NO sensors) and O₂ sensors (MMCPEs and SMCPEs) after an i.p. injection of L-NAME (30mg/kg) and L-arginine (300mg/kg).

The results obtained for the L-NAME injection were as expected as it is known that L-NAME inhibits eNOS, nNOS and iNOS. This would therefore lead to a decreased NO production and a reduction in cerebral blood flow which would yield a decrease in O₂. The L-arginine result was the opposite of this. L-arginine produces a greater amount of NO, which increases blood supply and thus increases O₂.

In Figure 8.3.10 (a), (b) and (c), the data observed for the NO, O₂ baseline and movement data highlight the activity of the rat during different times over a 6 hour period (Figure 8.3.10 (a) and (b)) and over the course of a 2 day period (8.3.10 (c)). The fluctuation in the NO current observed during the day is suggested to be an effect of diurnal modulation which has been reported in the literature (Kostin *et al.*, 2013). A clear difference can be observed between the two graphs (during the day and during the night). Due to the

nocturnal nature of the rat, they are more active during the night and we observe a more stable NO current during this time.

It can be observed from the results in this chapter, that the NO molecule did not behave the way we anticipated. It has been suggested that there is a correlation between NO and O₂ and this is due to the connection the two molecules have with CBF. O₂ is known to reliably act as an index of CBF (Lowry *et al.*, 1997) and NO is known to cause vasodilation or constriction of cerebral blood vessels by the production of NO derived from endothelial cells i.e. eNOS (Moncada *et al.*, 1991). It would suggest from the results obtained for the hypoxia and hyperoxia studies, that there was a correlation between the O₂ and NO signal obtained, as the increases and decreases observed seemed to behave the same (Park *et al.*, 2010). However, the more studies that were completed, the more contradicting the findings became. The restraint stress and tail pinch studies displayed a different NO behaviour. The two studies showed an elevation in the NO current upon initiation of the stimulus and upon cessation of the stimulus, an elevated NO response remained, whilst the O₂ current was observed to have returned to pre-baseline currents. However, it is imperative to mention that the NO did return to pre-baseline levels a short time after. Thus, suggesting an involvement of the NMDA receptor and the nNOS enzyme contributing to the NO response that we were observing with the sensors. Studies carried out involving rodents and primates have shown that nNOS is ubiquitous in the brain (Calabrese *et al.*, 2007).

The chloral hydrate and diamox studies displayed results that were not foreseen. These results showed a total separation in the correlation of the two molecules. It was very interesting to observe how both of these drugs, caused two different behaviours in the molecules, thus validating an independent function of NO that is not correlated to O₂. From all of the results studied in this Chapter, it would suggest that the NO in which we are detecting is from the NMDA receptor/nNOS mediated synthesis of NO and it would confirm many hypothesis in literature that suggest that nNOS is the enzyme in abundance in the brain.

8.5 References

- Alderton W, Cooper C & Knowles R. (2001). Nitric oxide synthases: structure, function and inhibition. *Journal of Biochemistry* **357**, 593-615.
- Aukland K. (1965). Hydrogen polarography in measurement of local blood flow; theoretical and empirical basis. *Acta Neurologica Scandinavica* **41**, 42-45.
- Aukland K, Bower BF & Berliner RW. (1964). Measurement of Local Blood Flow with Hydrogen Gas. *Circulation Research* **14**, 164-187.
- Bickler PE, Litt L, Banville DL & Severinghaus JW. (1988). Effects of acetazolamide on cerebral acid-base balance. *Journal of Applied Physiology* **65**, 422-427.
- Bolger F & Lowry J. (2005). Brain Tissue Oxygen: *In-Vivo* Monitoring with Carbon Paste Electrodes. *Sensors* **5**, 473-487.
- Bredt DS, Glatt CE, Hwang PM, Fotuhi M, Dawson TM & Snyder SH. (1991). Nitric oxide synthase protein and mRNA are discretely localized in neuronal populations of the mammalian CNS together with NADPH diaphorase. *Neuron* **7**, 615-624.
- Bredt DS, Hwang PM & Snyder SH. (1990). Localization of nitric oxide synthase indicating a neural role for nitric oxide. *Nature* **347**, 768-770.
- Bredt DS & Snyder SH. (1992). Nitric oxide, a novel neuronal messenger. *Neuron* **8**, 3-11.
- Brown F, Finnerty N, Bolger F, Millar J & Lowry J. (2005). Calibration of NO sensors for *in-vivo* voltammetry: laboratory synthesis of NO and the use of UV-visible spectroscopy for determining stock concentrations. *Analytical and Bioanalytical Chemistry* **381**, 964-971.
- Brown FO, Finnerty NJ & Lowry JP. (2009). Nitric oxide monitoring in brain extracellular fluid: characterisation of Nafion[®]-modified platinum electrodes *in-vitro* and *in-vivo*. *Analyst* **134**, 2012-2020.
- Buerk DG, Ances BM, Greenberg JH & Detre JA. (2003). Temporal dynamics of brain tissue nitric oxide during functional forepaw stimulation in rats. *Neuroimage* **18**, 1-9.
- Calabrese V, Mancuso C, Calvani M, Rizzarelli E, Butterfield DA & Stella AM. (2007). Nitric oxide in the central nervous system: neuroprotection versus neurotoxicity. *Nature Reviews Neuroscience* **8**, 766-775.
- Coggins MP & Bloch KD. (2007). Nitric Oxide in the Pulmonary Vasculature. *Arteriosclerosis, Thrombosis, and Vascular Biology* **27**, 1877-1885.

- Dickinson CJ. (2001). Why are strokes related to hypertension? Classic studies and hypotheses revisited. *Journal of Hypertension* **19**, 1515-1521.
- Dinerman JL, Lowenstein CJ & Snyder SH. (1993). Molecular mechanisms of nitric oxide regulation. Potential relevance to cardiovascular disease. *Circulation Research* **73**, 217-222.
- Dixon BM, Lowry JP & O'Neill RD. (2002). Characterisation *in-vitro* and *in-vivo* of the oxygen dependence of an enzyme/polymer biosensor for monitoring brain glucose. *Journal of Neuroscience Methods* **119**, 135-142.
- Faraci FM, Baumbach GL & Heistad DD. (1990). Cerebral circulation: humoral regulation and effects of chronic hypertension. *Journal of the American Society of Nephrology* **1**, 53-57.
- Farkas E & Luiten PG. (2001). Cerebral microvascular pathology in aging and Alzheimer's disease. *Progress in Neurobiology* **64**, 575-611.
- Faro SH & Mohamed FB. (2010). *BOLD fMRI: A Guide to Functional Imaging for Neuroscientists*. Springer, New York, United States of America.
- Finnerty NJ, O'Riordan SL, Brown FO, Serra PA, O'Neill RD & Lowry JP. (2012a). *In-vivo* characterisation of a Nafion[®]-modified Pt electrode for real-time nitric oxide monitoring in brain extracellular fluid. *Analytical Methods* **4**, 550-557.
- Finnerty NJ, O'Riordan SL, Palsson E & Lowry JP. (2012b). Brain nitric oxide: Regional characterisation of a real-time microelectrochemical sensor. *Journal of Neuroscience Methods* **209**, 13-21.
- Furchgott RF. (1988). *Studies on relaxation of rabbit aorta by sodium nitrite: the basis for the proposal that acid-activable inhibitory factor from bovine retractor penis is inorganic nitrite and the endothelium derived relaxing factor is nitric oxide*. Raven Press, New York, United States of America.
- Garthwaite J, Charles SL & Chess-Williams R. (1988). Endothelium-derived relaxing factor release on activation of NMDA receptors suggests role as intercellular messenger in the brain. *Nature* **336**, 385-388.
- Girouard H & Iadecola C. (2006). Neurovascular coupling in the normal brain and in hypertension, stroke, and Alzheimer disease. *Journal of Applied Physiology* **100**, 328-335.
- Iadecola C, Zhang F, Xu S, Casey R & Ross ME. (1995). Inducible nitric oxide synthase gene expression in brain following cerebral ischemia. *Journal of Cerebral Blood Flow & Metabolism* **15**, 378-384.

- Ignarro LJ, Buga GM, Wood KS, Byrns RE & Chaudhuri G. (1987). Endothelium-derived relaxing factor produced and released from artery and vein is nitric oxide. *Proceedings of the National Academy of Sciences* **84**, 9265-9269.
- Jones AM, Wilkerson DP & Campbell IT. (2004). Nitric oxide synthase inhibition with L-NAME reduces maximal oxygen uptake but not gas exchange threshold during incremental cycle exercise in man. *The Journal of Physiology* **560**, 329-338.
- Katusic ZS & Austin SA. (2013). Endothelial nitric oxide: protector of a healthy mind. *European Heart Journal* **10**, 1-7.
- Kazama K, Wang G, Frys K, Anrather J & Iadecola C. (2003). Angiotensin II attenuates functional hyperemia in the mouse somatosensory cortex. *American Journal of Physiology - Heart and Circulatory Physiology* **285**, H1890-H1899.
- Kostin A, McGinty D, Szymusiak R & Alam MN. (2013). Sleep-wake and diurnal modulation of nitric oxide in the perifornical-lateral hypothalamic area: Real-time detection in freely behaving rats. *Neuroscience* **254**, 275-284.
- Kreuter J, Mattson B, Wang B, You Z-B & Hope B. (2004). Cocaine-induced Fos expression in rat striatum is blocked by chloral hydrate or urethane. *Neuroscience* **127**, 233-242.
- LacKamp A, Zhang G-C, Mao L-M, Fibuch E & Wang J. (2009). Loss of surface N-methyl-D-aspartate receptor proteins in mouse cortical neurones during anaesthesia induced by chloral hydrate *in-vivo*. *British Journal of Anaesthesia* **102**, 515-522.
- Lajoix A-D, Pugnère M, Roquet F, Mani J-C, Dietz S, Linck N, Faurie F, Ribes G, Petit P & Gross R. (2004). Changes in the dimeric state of neuronal nitric oxide synthase affect the kinetics of secretagogue-induced insulin response. *Diabetes* **53**, 1467-1474.
- Leone A, Palmer R, Knowles R, Francis P, Ashton D & Moncada S. (1991). Constitutive and inducible nitric oxide synthases incorporate molecular oxygen into both nitric oxide and citrulline. *Journal of Biological Chemistry* **266**, 23790-23795.
- Liao JK, Zulueta JJ, Yu F-S, Peng H-B, Cote CG & Hassoun PM. (1995). Regulation of bovine endothelial constitutive nitric oxide synthase by oxygen. *Journal of Clinical Investigation* **96**, 2661-2666.
- Liao L-D, Tsytsarev V, Delgado-Martínez I, Li M-L, Erzurumlu R, Vipin A, Orellana J, Lin Y-R, Lai H-Y & Chen Y-Y. (2013). Neurovascular coupling: *in-vivo* optical techniques for functional brain imaging. *Biomedical Engineering Online* **12**, 38-57.
- Lindauer U, Megow D, Matsuda H & Dirnagl U. (1999). Nitric oxide: a modulator, but not a mediator, of neurovascular coupling in rat somatosensory cortex. *American Journal of Physiology - Heart and Circulatory Physiology* **277**, H799-H811.

- Low C-M, Lyuboslavsky P, French A, Le P, Wyatte K, Thiel WH, Marchan EM, Igarashi K, Kashiwagi K & Gernert K. (2003). Molecular determinants of proton-sensitive N-methyl-D-aspartate receptor gating. *Molecular pharmacology* **63**, 1212-1222.
- Lowry JP, Boutelle MG & Fillenz M. (1997). Measurement of brain tissue oxygen at a carbon paste electrode can serve as an index of increases in regional cerebral blood flow. *Journal of Neuroscience Methods* **71**, 177-182.
- Lowry JP & Fillenz M. (2001). Real-time monitoring of brain energy metabolism *in-vivo* using microelectrochemical sensors: the effects of anesthesia. *Bioelectrochemistry* **54**, 39-47.
- Lowry JP, Griffin K, McHugh SB, Lowe AS, Tricklebank M & Sibson NR. (2010). Real-time electrochemical monitoring of brain tissue oxygen: A surrogate for functional magnetic resonance imaging in rodents. *Neuroimage* **52**, 549-555.
- Macrae I, Dawson D, Norrie J & McCulloch J. (1993). Inhibition of nitric oxide synthesis: effects on cerebral blood flow and glucose utilisation in the rat. *Journal of Cerebral Blood Flow & Metabolism* **13**, 985-992.
- Moncada S, Palmer RM & Higgs EA. (1991). Nitric oxide: physiology, pathophysiology, and pharmacology. *Pharmacological Reviews* **43**, 109-142.
- Moreno A, Jegou P, de la Cruz F & Canals S. (2013). Neurophysiological, metabolic and cellular compartments that drive neurovascular coupling and neuroimaging signals. *Frontiers in Neuroenergetics* **5**, 1-7.
- Mungrue IN, Bredt DS, Stewart DJ & Husain M. (2003). From molecules to mammals: what's NOS got to do with it? *Acta Physiologica Scandinavica* **179**, 123-135.
- Obal Jr F & Krueger JM. (2003). Biochemical regulation of non-rapid-eye-movement sleep. *Frontiers in Bioscience: A Journal and Virtual Library* **8**, 520-550.
- Palmer RM, Ferrige AG & Moncada S. (1987). Nitric oxide release accounts for the biological activity of endothelium-derived relaxing factor. *Nature* **327**, 524-526.
- Park SS, Hong M, Song C-K, Jhon G-J, Lee Y & Suh M. (2010). Real-time in vivo simultaneous measurements of nitric oxide and oxygen using an amperometric dual microsensor. *Analytical Chemistry* **82**, 7618-7624.
- Pearce W, Ashwal S & Cuevas J. (1989). Direct effects of graded hypoxia on intact and denuded rabbit cranial arteries. *American Journal of Physiology-Heart and Circulatory Physiology* **257**, H824-H833.
- Pearce WJ, Reynier-Rebuffel A-M, Lee J, Aubineau P, Ignarro L & Seylaz J. (1990). Effects of methylene blue on hypoxic cerebral vasodilatation in the rabbit. *Journal of Pharmacology and Experimental Therapeutics* **254**, 616-625.

- Pelligrino D, Koenig H & Albrecht R. (1993). Nitric oxide synthesis and regional cerebral blood flow responses to hypercapnia and hypoxia in the rat. *Journal of Cerebral Blood Flow & Metabolism* **13**, 80-87.
- Piknova B, Kocharyan A, Schechter AN & Silva AC. (2011). The role of nitrite in neurovascular coupling. *Brain Research* **1407**, 62-68.
- Raichle ME. (1998). Behind the scenes of functional brain imaging: A historical and physiological perspective. *Proceedings of the National Academy of Sciences* **95**, 765-772.
- Santos RM, Lourenço CF, Ledo A, Barbosa RM & Laranjinha J. (2012). Nitric Oxide Inactivation Mechanisms in the Brain: Role in Bioenergetics and Neurodegeneration. *International Journal of Cell Biology* **2012**, 1-13.
- Schmidt HHHW, Lohmann SM & Walter U. (1993). The nitric oxide and cGMP signal transduction system: regulation and mechanism of action. *Biochimica et Biophysica Acta (BBA) - Molecular Cell Research* **1178**, 153-175.
- Severinghaus JW & Cotev S. (1968). Carbonic acidosis and cerebral vasodilation after diamox. *Scandinavian Journal of Clinical & Laboratory Investigation* **21**, 1E.
- Tang C-M, Dichter M & Morad M. (1990). Modulation of the N-methyl-D-aspartate channel by extracellular H⁺. *Proceedings of the National Academy of Sciences* **87**, 6445-6449.
- Traynelis SF & Cull-Candy SG. (1990). Proton inhibition of N-methyl-D-aspartate receptors in cerebellar neurons. *Nature* **345**, 347-350.
- Traynelis SF, Hartley M & Heinemann SF. (1995). Control of proton sensitivity of the NMDA receptor by RNA splicing and polyamines. *Science* **268**, 873-876.
- Vacchiano CA & Tempel GE. (1994). Role of nonenzymatically generated prostanoid, 8-iso-PGF₂ alpha, in pulmonary oxygen toxicity. *Journal of Applied Physiology* **77**, 2912-2917.
- Valente S, Ringwood J, Mangourova V & Lowry J. (2012). Investigation of events in the EEG signal correlated with changes in both oxygen and glucose in the brain. In *Signals and Systems Conference (ISSC 2012)*, pp. 1-6.
- VanDongen AM. (2008). *Biology of the NMDA Receptor*. Taylor & Francis, United States of America.
- Vorstrup S, Henriksen L & Paulson OB. (1984). Effect of acetazolamide on cerebral blood flow and cerebral metabolic rate for oxygen. *Journal of Clinical Investigation* **74**, 1634.

- Wisor JP, Gerashchenko D & Kilduff TS. (2011). Sleep-active neuronal nitric oxide synthase-positive cells of the cerebral cortex: a local regulator of sleep? *Current Topics in Medicinal Chemistry* **11**, 2483-2489.
- Zheng Y, Pan Y, Harris S, Billings S, Coca D, Berwick J, Jones M, Kennerley A, Johnston D & Martin C. (2010). A dynamic model of neurovascular coupling: Implications for blood vessel dilation and constriction. *Neuroimage* **52**, 1135-1147.
- Zhou L & Zhu D-Y. (2009). Neuronal nitric oxide synthase: structure, subcellular localization, regulation, and clinical implications. *Nitric Oxide* **20**, 223-230.



9. Conclusion

One of the greatest challenges facing science today is the understanding of the brain. How does it control behaviour, how does it malfunction in brain disorders, such as schizophrenia, Parkinson's disease, Alzheimers disease and many more. The rectification of such malfunctions by gaining knowledge about the mechanisms of the brain is a challenging objective undertaken by many scientists. The brain comprises of a very complex network of neurons and glial cells that interact with each other producing different chemical messengers into the ECF and it is these chemicals that are of interest to monitor (Kennedy *et al.*, 2002). The measurement of real-time *in-vivo* recordings is a supreme technique that allows the researcher to observe instantaneous chemical changes in the living brain with the use of the specific analyte monitoring sensors. Investigating the functions and roles of certain neurochemicals in neuronal signalling, drug action and behaviour with these sensors provides a lot of interesting and exciting information about the inner workings of the body.

This thesis attempts to further the area of neurochemical monitoring by developing novel O₂ sensors that could potentially be utilised in a clinical setting, specifically sensors that can withstand morphological changes in a harsh environment, such as the human body. Also the characterisation of novel Type 2 and Type 3 NO sensors for faster detection of NO *in-vivo* was undertaken in order to try and discover more about the inner workings of the NO molecule in the *in-vivo* environment. There has been much research into the detection of O₂, owing to the fact that it is a vital biological substrate that is involved in the many mechanisms that maintain the functioning of our bodies. Previous methods of detection include the use of carbon-based sensors such as CPEs (Lowry *et al.*, 1996; Lowry *et al.*, 1997; Bolger & Lowry, 2005; Bolger *et al.*, 2011b) and carbon fibre electrodes (Zimmerman & Wightman, 1991).

CPEs are very efficient for the detection of O₂ due to the great stability observed over extended periods of time. The only problem associated with this sensor, especially with the hope of integrating it into a clinical environment, is the surface alteration it undergoes when in the presence of lipids and proteins. The CPE changes to a carbon powder electrode upon the interaction with BT, due to the leeching of the silicone oil from the paste (Ormonde & O'Neill, 1989, 1990). Therefore, the removal of the oil into the central or peripheral compartment of the human body would not be considered ideal. It was for this reason that

the monomer modification of the CPEs was undertaken. In order to achieve a composite electrode that was very robust and that was not easily modified by whatever environment it was placed into.

Presented in the first of the results chapters (Chapter 4) is the *in-vitro* characterisation of the MMCPEs and SMCPEs. The main goal of this chapter was to obtain an electrode with a composite surface that was not as prone to leeching by whatever physiological environment it was placed into (Dai *et al.*, 2008), whilst retaining sensitivity and stability. The results suggest that this aim was achieved. Biocompatibility experiments were carried out on the CPEs to directly compare differences between the monomer modified sensors and the CPEs. There were very distinguishable differences observed from the effects of the biocompatibility experiments between the CPEs, SMCPEs and MMCPEs.

	CPEs (nA/ μ M)			SMCPEs (nA/ μ M)			MMCPEs (nA/ μ M)		
	Mean	SEM	<i>n</i>	Mean	SEM	<i>n</i>	Mean	SEM	<i>n</i>
Pre treatment	-1.8	0.1	52	-3.1	0.1	52	-3.3	0.2	52
BSA (10%)	-1.1	0.1	4	-2.7	0.5	8	-2.9	0.3	6
PEA (10%)	-1.0	0.1	4	-2.7	0.3	8	-2.7	0.4	4
BT (0.N)	-1.5	0.1	4	-2.8	0.3	6	-2.7	0.2	7
BT (28 Days)	-1.6	0.1	4	-3.2	0.1	4	-2.7	0.2	4

Table 9 (a): A table displaying a summary of the treatment results (nA/ μ M) for each of the sensors (CPE), (SMCPE) and (MMCPE).

Table 9 (a) displays a summary of the results for each of the sensors and each of the main treatments undertaken with them. It can clearly be observed that there is an increase in the sensitivity obtained with the SMCPEs and MMCPEs in comparison to the CPEs. This has been hypothesised as being due to the increase in the rate of electron transfer due to the Sty and MMA within the carbon paste. The SMCPE and MMCPE sensitivities observed yielded a significantly different sensitivity ($P < 0.0001$) in comparison to the CPEs. During the biocompatibility studies the CPE surface was easily altered by the different treatments undertaken, whilst the SMCPEs and MMCPEs surfaces remained intact and unaltered by these harsh conditions. As the CPEs are known for their great stability characteristic *in-vivo*

(O'Neill, 2005), it was attempted to try and achieve a similar stability with the monomer modified sensors without alteration of the composite surface.

The long term stability studies would provide information, especially for clinicians, on the storage and stability life of the sensors, as they would not use the sensors straight away. The long term stability studies of the SMCPEs and MMCPEs were very promising. The RT storage condition was chosen as the optimum storage condition. The results from the SMCPEs over the 28 days showed no significant difference from day 1 to day 28 ($P = 0.1242$) and likewise with the MMCPEs ($P = 0.1747$). The ECF of the brain contains a wide array of endogenous species that could potentially interfere with the sensors sensitivity (O'Neill & Lowry, 2006). Interference tests carried out on the SMCPEs and MMCPEs all displayed negligible results with all interferents studied contributing $< 1\%$ to the overall signal (see Section 4.3.8). Temperature and pH changes did not affect the ability of the SMCPEs and MMCPEs to detect O_2 (see Section 4.3.9 and 4.3.10). Sensors need to be able to withstand temperature and pH changes *in-vivo*, especially since the temperature of the body is 37°C . Changes in pH also occur *in-vivo*, however, they are tightly regulated by mechanisms in the body (Chesler, 2003). It has also been shown that pH can be altered in disorders such as depression and ischemia (Mutch & Hansen, 1984). Table 9 (b) displays the P values (one-way ANOVA and a paired t -test) obtained for the temperature and pH data respectively, all results showed no significant difference.

One-way ANOVA	SMCPEs	MMCPEs	Paired t -tests	SMCPEs	MMCPEs
pH	P value		Temperature	P value	
7.4/6.5/8.0	0.9903	0.9982	$25^\circ\text{C}/37^\circ\text{C}$	0.8934	0.9415

Table 9 (b): A table displaying a summary of the pH and temperature P value results obtained with the MMCPEs and SMCPEs.

To further validate how these sensors would behave in a very complex environment such as the living brain, they were implanted in the striatum of freely moving rats over the course of 12 and 13 days using the MMCPEs and SMCPEs respectively. Chapter 5 details the *in-vivo* characterisation of the SMCPEs and MMCPEs. Upon examination of the results presented in Chapter 5, it can be seen that the response obtained by the SMCPEs and

MMCPEs after various perturbations such as hypoxia, hyperoxia, neuronal activation, exposure to anaesthesia and the carbonic anhydrase inhibitor acetazolamide, yielded a better sensitivity than the CPEs. This corroborates the *in-vitro* studies undertaken and the higher sensitivity achieved. The MMCPEs and SMPCEs were much more effective in detecting the subtle changes in the O₂ concentration as opposed to the CPEs (Bolger *et al.*, 2011b).

Pre- and post-implantation results displayed a decrease in the O₂ sensitivity that yielded significantly different sensitivities for the MMCPEs ($P = 0.0073$) and SMCPEs ($P = 0.0016$), however, the sensitivity remained higher than that of the untreated CPEs (see Section 4.3.6.1 and 4.3.6.2). The CPEs are susceptible to alteration by the *in-vivo* environment, so it was vital that this did not occur with the MMCPEs and SMCPEs, as clinical integration necessitates a robust composite that does not leech out into the surrounding tissue. The results obtained were very promising with regards to the structural integrity of the two monomer modified sensors. SEM data (shown in Section 4.3.6.1 (d) and 4.3.6.2 (d)) displayed the SMCPEs and MMCPEs post implantation, where the surface remained intact with deposits of the *in-vivo* environment left behind on the surface. However, the morphology of the sensor did not alter, which was the main goal of this research and one that we feel was very successful, thus, concluding that these sensors could potentially be utilised in the clinical setting.

The other major aspect of this thesis was the characterisation of the sensors (Type 2 and Type 3 NO sensor) for the amperometric detection of brain extracellular NO. Described in Chapter 6 is the research carried out into the characterisation of the novel Type 2 and Type 3 NO sensors. Initially, studies were carried out with the more commonly utilised Type 1 NO sensor that has been extensively characterised within our lab (Brown *et al.*, 2009; Finnerty *et al.*, 2012a; Finnerty *et al.*, 2012b). The sensitivities achieved with the Type 1, Type 2 and Type 3 NO sensors displayed no significant difference between each of the sensors. Table 9 (c), displays the P values obtained.

	Type 1 vs. Type 2	Type 1 vs. Type 3	Type 2 vs. Type 3
<i>P</i> value	0.8440	0.6823	0.8332

Table 9 (c): A table summarising the *P* values obtained for the sensitivities of the Type 1, Type 2 and Type 3 NO sensors

Long term stability tests gave very promising results. It was observed that on repeated calibration of the sensors, the surface was altered and modified more extensively than when the sensors were calibrated less frequently. Negligible results were presented after 56 Days of storage for all the sensors and in comparison to the repeated calibrations displayed in Section 6.3.8, it was confirmed that the repetitive calibrations were the cause of the degradation of the sensor and not the sensors composition deteriorating over time. Biocompatibility studies were undertaken that displayed an effect on the sensors after 28 days immersed in each of the treatments. AA calibrations were carried out in order to determine the extent of the damage caused by the different treatments to the sensors. It has been observed that NO calibrations would not give any information on the damage done to the sensors, as a similar sensitivity to pre implanted sensors is obtained with post implanted sensors (see Section 6.3.15 and 6.3.16). The amount of AA being detected by the sensors would yield information about the condition of the rejection layer, in this case the *o*-PD layer.

The BT results displayed the most damage to the sensor surface with 540.0 ± 151.6 pA for the Type 2 NO sensors and 479.9 ± 106.1 pA for the Type 3 NO sensors being detected at an AA concentration of 1000 μ M. Interference tests undertaken with the Type 2 and Type 3 NO sensors yielded negligible results detected with the sensors (see Section 6.3.11) for some of the principle endogenous species found in the ECF of the brain. The temperature studies undertaken with the Type 2 and Type 3 NO sensors displayed no significant difference ($P = 0.7400$) and ($P = 0.6231$), respectively, on elevation of the temperature to 37 °C. It has been observed previously by Brown *et al.*, that on alteration of the temperature to 37 °C the response of the Type 1 NO sensor became quicker (Brown *et al.*, 2009). A quicker response time was also achieved with the Type 2 and Type 3 NO sensors (see Section 6.3.14). Pre- and post-implantation results for the NO sensitivities obtained for the Type 2 and Type 3 NO sensors displayed no significant difference ($P = 0.7229$) and (P

= 0.8709), respectively. However, with regards to the AA response pre- and post-implantation, a significant difference was observed for the Type 2 NO sensor ($P = 0.0020$) and Type 3 NO sensor ($P = 0.0083$) (see Section 6.3.15 and 6.3.16), showing a breakdown of the rejection layer.

Chapter 7 details the *in-vivo* characterisation of the Type 2 and Type 3 NO sensor, subsequent to the *in-vitro* characterisation. To characterise the two sensors *in-vivo*, systemic administrations of known inducers and inhibitors of NO production and the corresponding changes in the NO current were investigated. The first experiments carried out were control saline injections, since all administrations were by i.p. injection it was important to validate the response attained by the injection itself, therefore utilising saline to verify this. Following on from this, L-NAME, L-arginine and finally sodium ascorbate was administered. The saline injections displayed a short lived change in the NO current for the Type 2 NO sensor and Type 3 NO sensor that was not significantly different ($P = 0.0819$) and ($P = 0.0768$) from pre baseline levels, respectively. The L-arginine injections caused an increase in the NO current that was significantly different ($P = 0.0819$) and ($P = 0.0768$) from pre baseline currents for Type 2 and Type 3 NO sensors respectively.

The ascorbate injection which is undertaken to determine if the rejection layer on the sensors is still intact, displayed no change in the observed oxidation current. It has previously been illustrated with CPEs, that if any response to sodium ascorbate was to occur it would do so within a time range of 60 minutes (Lowry *et al.*, 1996). The result obtained by the Type 2 and Type 3 NO sensors displayed no significant difference ($P = 0.2052$) and ($P = 0.2214$), respectively, between the pre and post baseline levels over the 60 minutes analysed. The final results chapter (Chapter 8), demonstrates the versatility of the sensors as analytical tools in the field of neurochemistry. The O₂ (SMCPEs and MMCPEs) and NO (Type 2 and Type 3) sensors for this chapter were implanted in the striatum of freely moving rats, simultaneously. There were no differences in how the MMCPEs and SMCPEs behaved in the *in-vivo* environment (see Chapter 5) so it was deemed satisfactory to combine them. This was the same for the Type 2 and Type 3 NO sensors (see Chapter 7). Various experiments were undertaken to try and determine the relationship between the two molecules (NO and O₂) in an *in-vivo* setting. The initial experiments carried out were periods of induced hypoxia and hyperoxia. The results suggested a correlation between NO

and O₂ as the two molecules behaved in the same manner. The following experiments carried out displayed an NO response that caused us to reconsider whether NO and O₂ were actually behaving in correlation or whether there was a desynchronisation of the two molecules. Firstly during periods of neuronal activation, it was observed that although NO and O₂ displayed an increase in their response simultaneously, the NO response was slightly longer and remained elevated (see Figure 8.3.4 (a) and 8.3.5 (a)). This was observed with the restraint stress and tail pinch experiments undertaken.

These results suggest that NO is behaving independently through the NMDA receptor/nNOS pathway (see Section 8.3.5). The O₂ levels return to normoxic conditions after cessation of the two stimuli and the NO current remains elevated. It is postulated that if the NO that we were detecting was from eNOS then the NO would have returned to corresponding baseline levels along with the O₂ current. However, we did not observe this and so it is hypothesised from these experiments that the synthesis of NO from the nNOS enzyme through the NMDA receptors pathway is the NO we are mostly detecting. The next results displayed total desynchronisation of the NO and O₂ currents after the same perturbation. Chloral hydrate and diamox results displayed a decrease in the NO current, whilst the O₂ current increased. The increase in the O₂ current was expected as chloral hydrate and diamox both increase the levels of O₂ (see Figure 8.3.6 and 8.3.7). However, the NO decreases observed in both cases were unexpected.

It has always been thought that a correlation between NO and O₂ exists, which means we should have observed an increase with NO upon an increase of O₂. It is known that the NMDA receptors are suppressed upon administration of chloral hydrate (LacKamp *et al.*, 2009). Diamox is also known to induce a decrease in pH, which suppresses activity of the NMDA receptors (Bickler *et al.*, 1988; Tang *et al.*, 1990). It is therefore strongly postulated that the decrease in the NMDA receptor activity would cause a decrease in the production of NO, which is what we observed with the chloral hydrate and diamox results (see Figure 8.3.6 and 8.3.7). All of the results observed in Chapter 8, strongly suggest that the NO in which we are detecting is from the NMDA receptor/nNOS mediated synthesis of NO, however the contribution from eNOS cannot be ruled out. Continuation of this body of work would initially require the use of specific selective inhibitors to try and determine if the NO being produced in the brain is in fact from the nNOS enzyme. This would also

determine if nNOS is the enzyme that is in abundance in the brain, which has previously been stated in the literature (Calabrese *et al.*, 2007; Zhou & Zhu, 2009).

9.1 References

- Bickler PE, Litt L, Banville DL & Severinghaus JW. (1988). Effects of acetazolamide on cerebral acid-base balance. *Journal of Applied Physiology* **65**, 422-427.
- Bolger F & Lowry J. (2005). Brain Tissue Oxygen: *In-Vivo* Monitoring with Carbon Paste Electrodes. *Sensors* **5**, 473-487.
- Bolger FB, McHugh SB, Bennett R, Li J, Ishiwari K, Francois J, Conway MW, Gilmour G, Bannerman DM, Fillenz M, Tricklebank M & Lowry JP. (2011b). Characterisation of carbon paste electrodes for real-time amperometric monitoring of brain tissue oxygen. *Journal of Neuroscience Methods* **195**, 135-142.
- Brown FO, Finnerty NJ & Lowry JP. (2009). Nitric oxide monitoring in brain extracellular fluid: characterisation of Nafion[®]-modified platinum electrodes *in-vitro* and *in-vivo*. *Analyst* **134**, 2012-2020.
- Calabrese V, Mancuso C, Calvani M, Rizzarelli E, Butterfield DA & Stella AM. (2007). Nitric oxide in the central nervous system: neuroprotection versus neurotoxicity. *Nature Reviews Neuroscience* **8**, 766-775.
- Chesler M. (2003). Regulation and Modulation of pH in the Brain. *Physiological Reviews* **83**, 1183-1221.
- Dai H, Wu X, Wang Y, Zhou W & Chen G. (2008). An electrochemiluminescent biosensor for vitamin C based on inhibition of luminol electrochemiluminescence on graphite/poly(methylmethacrylate) composite electrode. *International Society of Electrochemistry* **53**, 5113-5117.
- Finnerty NJ, O'Riordan SL, Brown FO, Serra PA, O'Neill RD & Lowry JP. (2012a). *In-vivo* characterisation of a Nafion[®]-modified Pt electrode for real-time nitric oxide monitoring in brain extracellular fluid. *Analytical Methods* **4**, 550-557.
- Finnerty NJ, O'Riordan SL, Palsson E & Lowry JP. (2012b). Brain nitric oxide: Regional characterisation of a real-time microelectrochemical sensor. *Journal of Neuroscience Methods* **209**, 13-21.
- Kennedy RT, Watson CJ, Haskins WE, Powell DH & Strecker RE. (2002). *In-vivo* neurochemical monitoring by microdialysis and capillary separations. *Current Opinion in Chemical Biology* **6**, 659-665.
- LacKamp A, Zhang G-C, Mao L-M, Fibuch E & Wang J. (2009). Loss of surface N-methyl-D-aspartate receptor proteins in mouse cortical neurones during anaesthesia induced by chloral hydrate *in-vivo*. *British Journal of Anaesthesia* **102**, 515-522.

- Lowry JP, Boutelle MG & Fillenz M. (1997). Measurement of brain tissue oxygen at a carbon paste electrode can serve as an index of increases in regional cerebral blood flow. *Journal of Neuroscience Methods* **71**, 177-182.
- Lowry JP, Boutelle MG, O'Neill RD & Fillenz M. (1996). Characterisation of carbon paste electrodes *in-vitro* for simultaneous amperometric measurement of changes in oxygen and ascorbic acid concentrations *in-vivo*. *Analyst* **121**, 761-766.
- Mutch W & Hansen A. (1984). Extracellular pH changes during spreading depression and cerebral ischemia: mechanisms of brain pH regulation. *Journal of Cerebral Blood Flow & Metabolism* **4**, 17-27.
- O'Neill RD & Lowry JP. (2006). Voltammetry *In-Vivo* for Chemical Analysis of the Living Brain. In *Encyclopedia of Analytical Chemistry*. John Wiley & Sons, Ltd, United Kingdom.
- O'Neill R. (2005). Long-Term Monitoring of Brain Dopamine Metabolism *in-vivo* with Carbon Paste Electrodes. *Sensors* **5**, 317-342.
- Ormonde DE & O'Neill RD. (1989). Altered response of carbon paste electrodes after contact with brain tissue: Implications for modified electrode use *in-vivo*. *Journal of Electroanalytical Chemistry and Interfacial Electrochemistry* **261**, 463-469.
- Ormonde DE & O'Neill RD. (1990). The oxidation of ascorbic acid at carbon paste electrodes: Modified response following contact with surfactant, lipid and brain tissue. *Journal of Electroanalytical Chemistry and Interfacial Electrochemistry* **279**, 109-121.
- Tang C-M, Dichter M & Morad M. (1990). Modulation of the N-methyl-D-aspartate channel by extracellular H⁺. *Proceedings of the National Academy of Sciences* **87**, 6445-6449.
- Zhou L & Zhu D-Y. (2009). Neuronal nitric oxide synthase: structure, subcellular localization, regulation, and clinical implications. *Nitric Oxide* **20**, 223-230.
- Zimmerman JB & Wightman RM. (1991). Simultaneous electrochemical measurements of oxygen and dopamine *in-vivo*. *Analytical Chemistry* **63**, 24-28.